Abou el Kacem Qaiss
Rachid Bouhfid
Mohammad Jawaid   *Editors*

Graphene and Nanoparticles Hybrid Nanocomposites

From Preparation to Applications

Springer

Composites Science and Technology

Series Editor

Mohammad Jawaid, Laboratory of Biocomposite Technology, Universiti Putra
Malaysia, INTROP, Serdang, Malaysia

Composites Science and Technology (CST) book series publishes the latest developments in the field of composite science and technology. It aims to publish cutting edge research monographs (both edited and authored volumes) comprehensively covering topics shown below:

- Composites from agricultural biomass/natural fibres include conventional composites-Plywood/MDF/Fiberboard
- Fabrication of Composites/conventional composites from biomass and natural fibers
- Utilization of biomass in polymer composites
- Wood, and Wood based materials
- Chemistry and biology of Composites and Biocomposites
- Modelling of damage of Composites and Biocomposites
- Failure Analysis of Composites and Biocomposites
- Structural Health Monitoring of Composites and Biocomposites
- Durability of Composites and Biocomposites
- Biodegradability of Composites and Biocomposites
- Thermal properties of Composites and Biocomposites
- Flammability of Composites and Biocomposites
- Tribology of Composites and Biocomposites
- Bionanocomposites and Nanocomposites
- Applications of Composites, and Biocomposites

To submit a proposal for a research monograph or have further inquries, please contact springer editor, Ramesh Premnath (ramesh.premnath@springer.com).

More information about this series at http://www.springer.com/series/16333

Abou el Kacem Qaiss · Rachid Bouhfid ·
Mohammad Jawaid
Editors

Graphene and Nanoparticles Hybrid Nanocomposites

From Preparation to Applications

Springer

Editors
Abou el Kacem Qaiss 🆔
Laboratory of Polymer Processing
Moroccan Foundation for Advanced
Science, Rabat, Morocco

Rachid Bouhfid 🆔
Rabat Design Center, Moroccan Foundation
for Advanced Science, Rabat, Morocco

Mohammad Jawaid
Laboratory of Biocomposite Technology
INTROP, Universiti Putra Malaysia
Serdang, Selangor, Malaysia

Contents

Generality of Hybridization of Graphene: From Design to Applications

Khadija El Bourakadi, Mohamed El Mehdi Mekhzoum, Abou el kacem Qaiss, and Rachid Bouhfid

Abstract Currently, the research and development in the field of graphene, graphene oxide and reduced graphene oxide and its combination with several nanoparticles has accrued an extensive attention in scientific research field in both academic and industrial. The hybridization is considered as a best process which is incorporating graphene nanosheets with various nanoparticles such as nanoclays, silver nanoparticles, carbon nanotubes and many others. The obtained materials are well-known as a hybride nanocomposites that characterized by their excellent properties and high performances which are related to the properties of both graphene and nanoparticles. These outstanding properties make hydride nanocomposite a great candidate for potential applications in different areas including, materials science and engineering, medicine and biology, energy storage and environmental remediation. Herein, this chapter gives you an idea about the various derivatives of graphene and their functional hybride materials, followed by the detailed introduction on graphene- nanostructures hybrids. The present chapter reveals the interest from the hybridization of graphene derivatives with different nanoparticles. After a brief introduction about graphene and its importance in nontechnology field. In the second part, we give you some basic information about graphene its preparation, characterization and the nanocomposites made from graphene. The third part concerns the hybride nanocomposites made up from graphene with various nanostructures. It also includes industrial and practical application of graphene-nanoparticles hybrids.

Keywords Graphene · Graphene oxide · Reduced graphene oxide · Hybridization · Nanoparticles · Hybride nanocomposites · Preparation routes · Functional applications

K. El Bourakadi · M. E. M. Mekhzoum · A. Qaiss · R. Bouhfid (✉)
Moroccan Foundation for Advanced Science, Innovation and Research (MAScIR), Composites Et Nanocomposites Center, Rabat Design Center, Rue Mohamed El Jazouli, Madinat El Irfane, 10100 Rabat, Morocco
e-mail: r.bouhfid@mascir.com

1   Introduction

In front of the continuous evolution of our society, the technological, energy and environmental challenges are frequently being redefined. Companies are looking for ever more efficient materials to better answer the market demand and to improve its performance. Biodegradability, resistance, lightness and even flexibility are all new parameters that must now be considered when designing high-performance manufactured nanocomposite materials.

In recent years, the development progresses in science and technologies guided to an enormous number of composites materials which are characterized by several advantages and also some drawbacks related mostly to its non-biodegradability and high toxicity which are responsible to their limitation in the market. For that reason, it is necessary to find new renewable and environmentally friendly new material alternatives to responding to market and owner demands. Hybride materials made up from graphene and its derivatives combined with several nanoparticles have been found to be the best alternative solution to this issue.

Graphene was then presented as the "material of the future" or the "miracle material" and was very studied to identify its properties and their origin [1]. Outstanding to its exceptional and remarkable properties for example high thermal conductivity, brilliant electrical conductivity, and significant optical transmittance, this new discovered material has implicated in several applications alone or combined with other nanostructures.

Since its discovery, a great interest has been paid to graphene by several researchers and scientists from different field and different discipline. This material was found to be as a promising reinforcing agent for multivarious nanoparticles such as nanoclays, silver nanoparticles, gold particles, ferrite nanoparticles and many more. The hybridization of these materials can be done by employing several methods, each method related to the nanoparticles used and the conditions could be changed from nanoparticles to other [2]. The fabricated hybrid nanocomposite obtained from this combination has been characterized by several advantages namely, biocompatibility, biodegradability, non-toxicity, high mechanical properties, excellent biological activities, especially, antibacterial and anticancer, also they great electrochemical properties [3].

More specifically, these hybride materials are used to make probes to detect activity inside cells, as transporters for the controlled release of drugs and as contrast agents for medical imaging. In addition, these materials are used also to fabricate capacitive electrodes for lithium batteries, supercapacitors, photocatalysts, electrocatalysts [4], absorbent materials [5], transparent conductive films [6], devices for chemical or biological detection, antibacterial and anticancer.

Here, we are going to report the current advances in the properties, characterizations, and applications of graphene-nanostructures hybrids for several application. This chapter may help a wide range of students, professors, and scientific researchers in different areas of materials science and technology. Also, we will present the latest research works reported in the field of nanocomposite-based graphene and their

main properties and characterization showing their combination to various types of nanoparticles, as well, we will demonstrate some major applications in attractive areas.

2   Graphene: Preparation, Characterization, Nano and Bio-Composites-Based Graphene

Since its discovery, graphene and its derivatives continue to arouse great interest because of their exceptional physicochemical and high thermomechanical properties, including, high theoretical specific surface area [7], elevated intrinsic mobility, high Young's modulus, breaking strength [8], mechanical stiffness [9], good thermal conductivity [10], high electrical conductivity [11], and high optical transmittance [12]. Graphene is a sp2 hybridized carbon nanostructure which has high electronic and optical properties. These advantages render it an appealing material especially in the conception and development of a novel generation of devices and materials for several applications, in particular in the field of batteries [13], electrochemical supercapacitors [14], solar cells [15], fuel cells [16], hydrogen storage[17], capturing and storing CO_2 [18], recovering metals [19], desalinating water [20], sensors and biosensors [21] and also in the design and development of systems and devices for photodetection, spintronics and optoelectronics [22].

Interestingly, the research on graphene has progressively increasing since its discovered in 2004 [23]. Increasingly, researchers are interested in producing graphene on a large scale with fewer defects. Thus, in order to prepare graphene with high quality and better performances, several methods have been reported such as mechanical exfoliation [7], growth by epitaxy on silicon carbide [24], chemical vapor deposition [25], liquid phase exfoliation [26], chemical oxidation / exfoliation followed by reduction [27], electrochemical exfoliation [28], the electric arc method [29] and other forms of graphene preparation such as industrial production methods [30] have been developed and continue to emerge. Each synthesis method has advantages and disadvantages.

Once the graphene nanosheets and its derivatives were synthesized and purified, numerous characterization techniques can be used to identify their physicochemical properties, morphological, thermal as well as their chemical structures. The standard methods mostly used in this case are optical microscope, scanning electron microscopy (SEM), Transmission Electron Microscopy (TEM), Atomic Force Microscope (AFM), Raman spectroscopy, Fourier transform infrared spectroscopy (FTIR), X-ray diffraction etc.

The graphene sheets's identification, on a thick layer, maybe done per optical microscopy through the color contrast chatted via the light interference effect on the SiO_2 substrate, which is regulated via the graphene layer [31]. while, in a recent study, the researchers were reported the utility of the three microscopic techniques mostly used to identify graphene nanosheets [1], mainly, AFM is generally used for

the measurement of lateral dimensions and thickness, topography, structural defects and bending properties of exfoliated graphene nanosheets. TEM is also used for the determination of the size of nanosheets as well as from electron diffraction we can differentiate if the sheets are individual or multiple. SEM be able to provide a qualitative overview of the three-dimensional structure of graphene sheet. In an another work, Wang et al. [32], were reported that the confirmation of the intercalation of graphite or graphite oxide and also the confirmation of the total exfoliation of graphene nanosheets is usually investigated by X-ray diffraction. Whereas, Raman spectroscopy can be used to quantify the transformation from hybridization sp^3 to that sp^2 in the case of the reduction of graphene oxide to graphene.

After its preparation and characterization, graphene can therefore be combined with other elements namely polymers, metals, ceramic, metal oxides as well as gas, in very small quantities to produce different types of materials including composite materials, nanocomposite materials and bio-composite materials with superior and very interesting properties [33]. Research on graphene-based composite materials, mainly, graphene/polymer, graphene/carbon fibers, graphene/poly-epoxides and graphene/nanoparticles is growing rapidly with a view to using it very soon in industry applications and academic research [34]. These materials become lighter, stronger and more resistant to erosion [35] and corrosion [36] due to the properties it acquires by combining with graphene, even in very small quantities [37]. For instance, when 0.9% by weight of graphene was added to the polystyrene, the researchers showed that the breaking strength and Young's modulus increased by 70 and 57% respectively [38]. More recently, the Vorbeck company has been capable to pick up the properties of thermoplastics, elastomers and epoxies by making them more solid, more conductive and more efficient by adding less than 1% of graphene [39]. By decorating graphene with nanoparticles such as Ag, Pt and Au or metallic oxides such as MoS_2, Co, CoO, it is possible to increase the electrocatalytic activity for the reduction of the oxygen [40]. The best and only solution to overcome certain challenges such as the non-conductivity and the rigidity of certain materials (S, Si) is either to develop a sulfur composite based on graphene capable of absorbing polysulfide, increasing the electrical conductivity and adapting to structural change, when these elements are used in lithium batteries [41].

In these days, several research investigations have been focused on the enlargement of a huge number of nanocomposite materials based on polymer as a matrix reinforced by graphene oxide using the solution mixing procedure. In this, divers kinds of nanocomposites have been developed with graphene oxide and water-soluble polymers such as polyvinyl alcohol (PVA) [42] and chitosan [43]. This approach for the preparation of polymer nanocomposites/ graphene oxide, using the mixture's solution, as well is acted as an effective way for the manufacturing of nanocomposites-based polymer with the graphene chemically reduced. Since, following the experimental discovery of graphene, a group of researchers have been developed the polymer/graphene-based nanocomposites by mixing the graphene oxide with polystyrene (PS) followed by an in situ chemical reduction of graphene oxide to graphene using hydrate hydrazine [44]. On other hand, the nanocomposite materials based on graphene as well as another derivative of graphene can also be

elaborated by the *in-situ* polymerization process. Several polymer nanocomposites were prepared using this method by employing various kinds of graphene-based nanofillers [45].

Through the use of twin-screw micro-extruders, several strategies and studies have been developed to fabricate a new generation of nanocomposite systems by incorporating reduced graphene nanosheets into a diversity of polymer matrices as poly(ethylene naphthalate) (PEN) [46], polycarbonate (PC) [47], polyurethane (PU) [45] and polyethylene (PE) [48]. The authors highlighted that the properties of these nanocomposites were significantly enhanced even if with a small fraction of graphene which is added.

3 Hybrid Nanocomposite Materials-Based Graphene

With the aim to increase the performance of carbon-based materials and to orient towards a tailor-made application, hybrid materials were developed to gain, for example, graphene oxide (GO) -allotropic carbon, GO-molecule composites organic, GO-living organism and GO- nanoparticle. The new trend in the field of carbon chemistry research is to develop new carbon-based structures mixing two allotropes as carbon nanotube and fullerene [49], graphene and carbon nanotube [50], or graphene and diamond [51]. In addition, it is possible to graft bioactive molecules on the surface of allotropes such as aptamers [52], a drug, a protein, a peptide, or a nucleic acid [53], and also living organisms like a bacteria, cell, or virus [54]. Recently, hybrid materials of the graphene-metallic nanoparticles have been specially developed for the emerging field of nanoelectronics [55].

The discussion below briefly overviews the principal nanoparticles mostly used with graphene and its derivatives for the preparation of new generation of hybride materials for functional applications.

4 Silver Nanoparticles

In the field of nanotechnology, silver (Ag) nanoparticle nanocomposites with graphene or graphene oxide have considered a promising hybrid material for several potential applications. There are many reports concerning the effect of the combination between silver nanoparticles and graphene on the final properties of fabricated materials have been reported in the literature. For instance, Ma et al. [56] were developed a new hybride nanocomposite for biomedical application by employing Silver-modified graphene oxide nanosheets. The prepared materials were found to be used as a potential antibacterial agent, especially against *Escherichia coli*. There are two main objectives of the deposition of Ag nanoparticles on the surface of graphene oxide nanosheets are:

- Content of Ag nanoparticles well dispersed in an aqueous solution by means of graphite nanoparticles,
- Improve the antibacterial properties by the synergistic effect of silver nanoparticles and graphene oxide.

In the same context, it has been reviewed [2] that the hybridization of graphene and graphene oxide with diverse aspects of silver nanoparticle are extremely studies and show great promise as they can provide the necessary constancy and processability for important antibacterial applications [57]. In general, the nanocomposite based on silver nanoparticles/graphene have been synthesized by various techniques, the figure below (Fig. 1) demonstrates the different synthesis methods of silver-graphene nanocomposite.

Similarly, Gurunathan et al. [21] were prepared a novel hybride nanocomposite by combining on reduced graphene oxide (RGO) with silver nanoparticle (AgNPs). The corresponding composite were characterized with several techniques such as FTIR, Raman spectroscopy, XRD and TEM. For example, The SEM images (Fig. 2) of the hybrid nanocomposite (RGO-AgNPs) showed that AgNPs with diameters of around 20 nm were deposited homogeneously and efficiently on the surface of
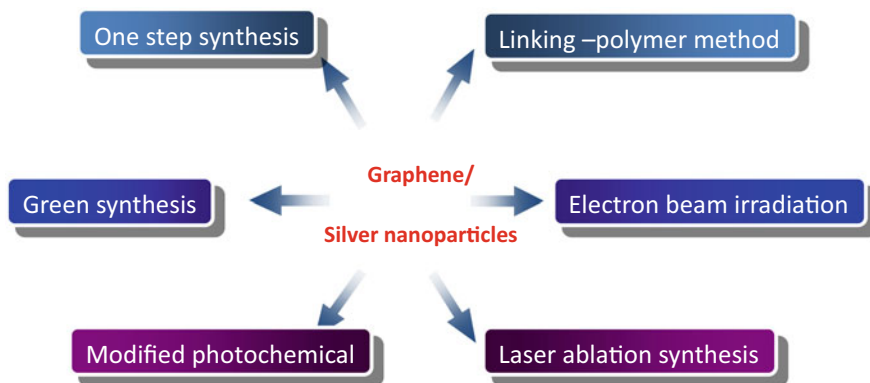
Fig. 1 Synthesis methods of silver nanoparticle/graphene hybride materials
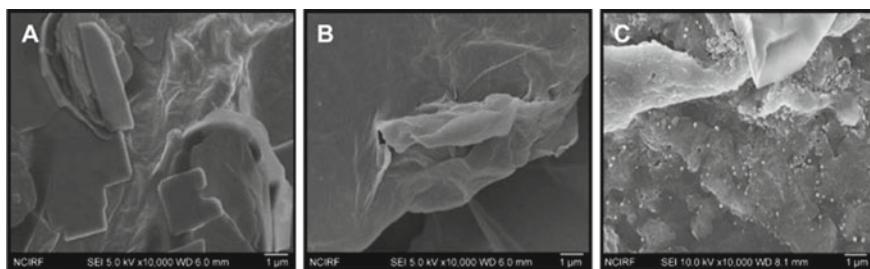
Fig. 2 SEM images of GO (A), ROG (B) and RGO–Ag nanocomposite (C)[21]

RGO. As a result of this investigation, it has been remarked that the prepared RGO–Ag nanocomposite exhibited an important cytotoxicity and demonstrated extremely effective apoptotic activity against human ovarian cancer cells.

In another field, Li et al. [58] were reported a novel invention of hydride nanocomposite by combining silver nanoparticles/graphene oxide using a simple and easy synthesis approach employing glucose as a reducing and stabilizing agent. The synthesized materials could be used as to produce a novel electrochemical sensor which are characterized by their exceptional repeatability and long-term constancy. The results obtained here confirms that the silver nanoparticles/ graphene oxide obsessed synergetic catalytic effect on the oxidation of tryptophan.

More recently, there are several studies mentioned in the literature demonstrated the great potential effect of silver nanoparticles on graphene, graphene oxide and reduced graphene oxide[59]. This combination has paying a great of interest owing to its importance of creating new kind of hybride materials used in different field [60].

5   Carbon Nanotubes

To extend the scope of application of graphene slight by means of agglomeration of graphene plates due to its strong van der Waals influence. Accordingly, the most excellent solution to render graphene more suitable for a variety of utilizations is add some spaces between its sheets to save similar repackaging and agglomerate formation, also, the spacer must be greatest add to the whole surface area and electrical conductivity of the composite [61]. Thus, According to several research studies, carbon nanotubes (CNT) was found to be as an ideal candidate owing to their unique properties in terms of high conductivity, large specific surface, also, their good similarity of carbon structure, resulted in special interaction with graphene sheets [62]. Consequently, graphene and CNT hybride materials have attracted huge interest in both scientific and academic research because of its outstanding physical properties mainly elevated electronic conductivity, excellent thermal stability, and exceptional mechanical strength. For instance, Sheka and Chernozatonskii [63] were developed a series of composites based on single-walled CNTs and graphene.

In order to develop to a variety of nanostructured hybrid materials with diverse topological architectures, Zhang et al.[64]. were used the hybridization approach between 1D CNTs and 2D graphene. According to the authors, the hybrids materials based on CNTs and graphene are classified on three types (Fig. 3):

Type 1: CNTs adsorbed horizontally to the graphene surface,

Type 2: CNTs adsorbed perpendicularly to the graphene surface,

Type 3: Wrapped with graphene.

According to the literature, Hybridization of graphene with CNTs is typically carried out via two different techniques:

Assembly technique basically co-assembles graphene and CNTs jointly.
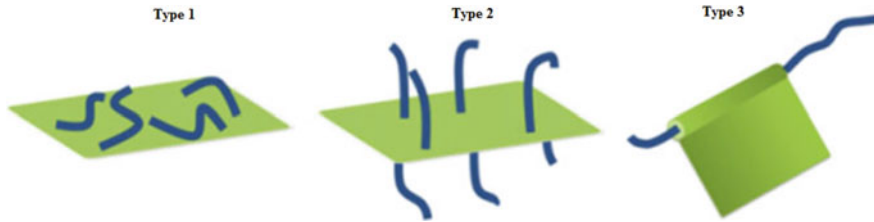
Fig. 3 Hybride materials of graphene/CNTs [65]
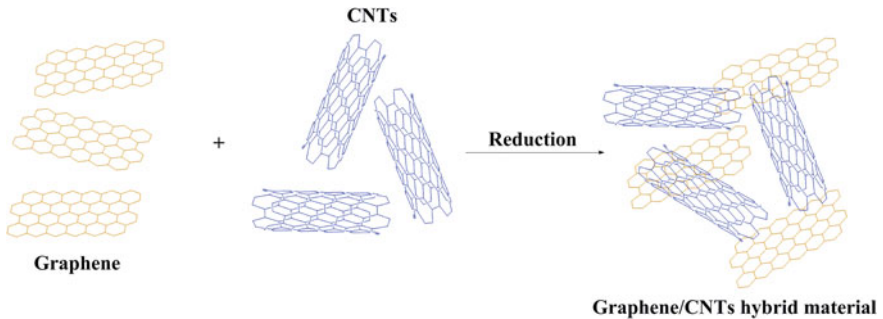
Fig. 4 Processing of preparation of graphene/CNTs hybride materials

The in-situ process requires unzipping CNTs into CNT/GNR hybrids or increasing CNTs on graphene sheets.

With aim to develop a new generation of hybride materials based on graphene/CNT and their polyvinyl alcohol nanocomposite, Zhou et al. [66] were used a too easy and green approach to prepare graphene-CNT aerogels using a one-step hydrothermal redox reaction (Fig. 4). The obtained aerogels have very low densities. In relation with the density of the adsorbed organics, adsorption abilities of their weight can be attained with optimized Graphene-oxide/CNT mass ratios. Particularly, the prepared graphene-CNT aerogels showed exceptional reusability and constancy after incessant absorption–combustion and adsorption–squeezing experiments.

On other hand, Xianfu Chen et al. [67] were reported the creation of new hybrid nanofiltration membranes with high permeability using reduced graphene oxide which is intercalated with carbon nanotubes. The obtained hybrid materials were fabricated through a simplistic vacuum-assisted filtration process and then were used in treatment and purification of water to eliminate the nanoparticles, proteins, dyes, organophosphates, and mostly humic acid as of drinking water.

6 Cellulose Nanocrystals/nanofibrils

The use of cellulose as an additive to get better both physical and mechanical properties of hybride nanocomposites has recently generated a lot of concern, and a promise potential for application in the field of paper and packaging technology is provide in the future[68]. In this context, many researchers are interested in the grafting of cellulose on the surface of graphite oxide [69], to improve physical, chemical and thermal properties by different grafting methods [70]. For example, Ouyang et al. [69] have adsorbed cellulose on the surface of oxidized graphite via hydrogen bonds between the oxygen atom of the carboxylic acid function of graphene oxide and the hydrogen atom of the function cellulose hydroxyl (Fig. 5).

Similarly, Zhang et al. [6] prepared nanocomposite films containing graphene and cellulose in a DMAC/LiCl solution. The morphology of these prepared hybride composites was investigated through scanning electron microscopy (SEM) and transmission electron microscopy. The images SEM (Fig. 6) exposed that the graphene was dispersed in nano-scale way into the cellulose matrix.
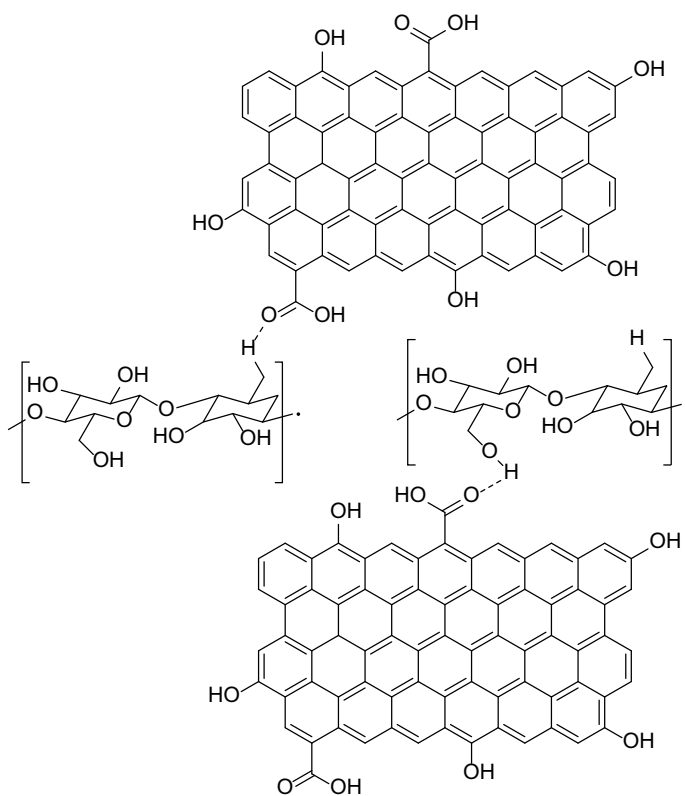
Fig. 5 Adsorption of cellulose on the surface of graphene oxide by hydrogen bonds
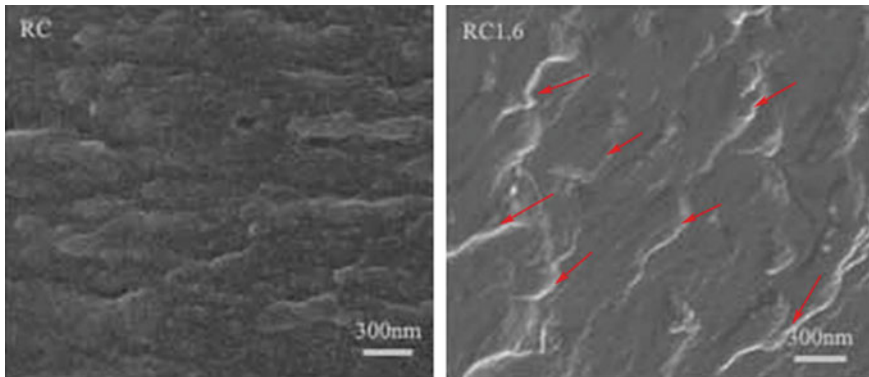
Fig. 6 SEM images of regenerated cellulose and composite with 1.6 wt.% graphene [6]

The preparation of films by surface chemical modification of graphene oxide with cellulose has also been studied by Peng et al.[71] by the use of an ionic liquid solution (1-Butyl-3-methylimidazolium chloride ([Bmim] Cl). This chemical modification has been characterized by UV–visible spectroscopy, IR spectroscopy, X-ray diffraction and Raman spectroscopy. As a result, the analysis by UV–Visible shows that the graphene oxide shows a characteristic peak at 231 nm, which corresponds to the π-π * transition of the carbon–carbon bond, and a shoulder at about 300 nm, which is due to the n-π * transition of the carboxyl bond. Nevertheless, after the reduction, the peak at 231 nm is shifted towards red at 269 nm, with the disappearance of the absorption peak at 300 nm. This disappearance has been associated with the restoration of electronic conjugation in graphene oxide. Also, the results of X-ray diffraction, the diffractogram shows the appearance of peaks at 15.1, 16.8, and 22.5°, may attributed to the crystalline phase of cellulose, which confirms the adsorption of cellulose on graphene oxide.

In another interesting work, Yun and Kim [72] have shown that the direct grafting of cellulose on graphene oxide or on carbon nanotubes (NTC) can also be carried out with a covalent bond and more precisely by a chemical reaction called esterification between the carboxylic acid functions of graphene oxide and the hydroxyl functions of cellulose. The composite prepared was used to elaborate electroactive paper with high mechanical properties and good performances.

More recently, Kafy et al. [73] prepared various nanocomposites based on graphene grafted cellulose (CFG) for several applications, especially in the storage of energy and electronic procedure. From this study, the researchers have proved that these nanocomposites have a behavior ferroelectric related with an integrated polarization which is able to change with the temperature. Thus, grafting has been analyzed by diverse characterization tools including X-ray diffraction.

7 Gold Nanoparticles

Charging of metallic nanoparticles in recovered graphene oxide (RGO) sheets can be active to increase the space between them, create a large remaining surface area and restore the electrochemical capacity on both sides of RGO. [74]. Therefore, Gold nanoparticles (AuNPs) were found to be an outstanding composites for separation of re-stacked RGO sheets [75]. In this context, Zhihao Yu et al. [13] were reported the preparation and characterization of new nanocomposite materials based on electrodeposition of AuNPs nanoparticles on the electrochemically RGO. The synthesized RGO-AuNPs nanocomposite was characterized by several characterization tools. For example, the morphology of this composite was characterized by scanning electron microscopy (SEM) which is confirms the presence of gold nanoparticles on the sheets surface and inter-space of RGO as reported in the figure below (Fig. 7). According to the results obtained in this study, RGO-AuNPs nanocomposite was found to be a great candidate for super-capacitive application.

More recently, A novel printed electrochemical sensor having into them cubic gold nanoparticles associated with 2-aminoethanethiol,functionalized graphene oxide and modified glassy carbon electrode has been developed for determination of tyrosine in milk [76].

In another interesting work, Wang et al. [77] were prepared a reinforced nanohybrid nanocomposite by employing gold nanoparticles (Au NPs) with chemically reduced graphene oxide nanosheets and carried out the self-assembling of cholinesterase using poly(diallyldimethylammonium chloride) as a linker. This design idea of nanohybrid and nano-assembly has exhibited its interesting applications in the field of stabilization of enzyme and the detection of paraoxon. In the same field, for in vitro diagnostics, several proteins may detected by bio-sensor using decorating thermally-reduced graphene oxide sheets with chosen gold nanoparticle (Au NP)-antibody conjugate [78].

For another domain, the combination between gold nanoparticles of controlled size and shape with graphene oxide nanosheets dispersed in water, can be used
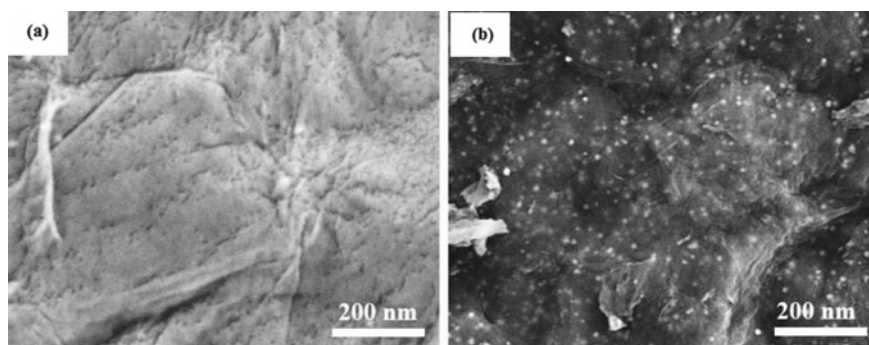
Fig. 7 SEM images of (a) RGO and (b) RGO-AuNPs nanocomposite[13]

as a great approach to fabricate ultra-small gold/graphene nanocomposites which is considered as novel photothermal energy convertors for a diversity of thermo-chemical and thermomechanical applications, including:

- In the medicine field, especially in photo-thermal therapy,
- Heating and evaporating some liquids through solar energy,
- Explosion of solid fuels, and joining of composites

8 Ferrite Nanoparticles

Among the nanoparticles mostly used with graphene to develop a new hybride materials for several applications, ferrite nanoparticles with excellent properties such as bio-compatibility, constancy, non-toxicity, easily synthesized, it has been found that a slight band gap and absorption in the visible part of light are more commonly used with graphene oxide for the production of photocatalytic materials. [79]. In this sense, Javed et al. [80] were used $Ni_{0.65}Zn_{0.35}Fe_2O_4$ nanoparticles with reduced graphene oxide (RGO) to prepare the composites with ferrite nanoparticles. These hybride nanocomposites were characterized by scanning electron microscopic (SEM) to confirm division of ferrites nanoparticles into the graphene sheets (Fig. 8). The formation of spinel ferrite nanoparticles and their nanocomposites from RGO was confirmed by characterization methods. Therefore, these nanohybrids will become a potential candidate for the photodegradation of the often-visible light of organic pollutants in wastewater in the future.

Similarly, in order to remove trace sulfonamide antibiotics from waste-water by adsorption method, Jianrong Wu et al. [81]. were used graphite oxide and metal ions as starting materials to develop reduced graphene oxide (RGO) supported ferrite hybrid materials. The prepared materials were characterized via several techniques such as transmission electron microscopy (TEM), Fourier transform infrared spectrophotometer (FTIR) and X-ray powder diffraction pattern (XRD). Prominently, the
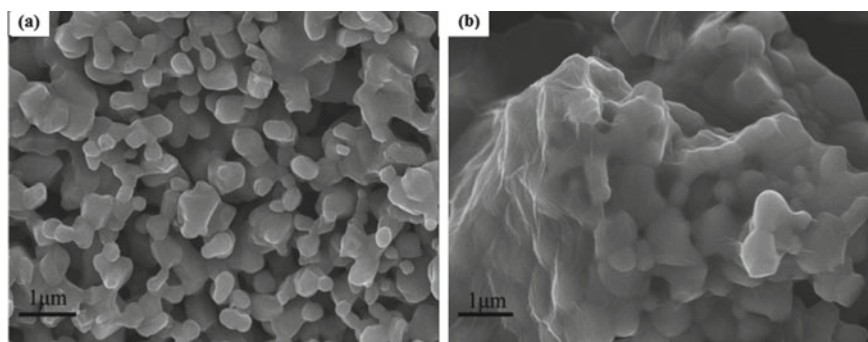
Fig. 8 SEM images of **a** ferrite nanoparticles **b** ferrite particules/RGO nano-hybrids [80]

fabricated nanocomposite hybride are effectual adsorbents for the determination and removal of three sulfonamides in wastewater. A number of parameters were taken into consideration during the extraction of these pollutants in efficiency manner, mainly:

- Quantity of adsorbent,
- Removal time,
- pH and desorption parameters.

Currently, Qiu et al. [82] were mentioned in their paper that, three-dimensional hierarchical compounds of cobalt ferrite-graphene have been prepared using crystalline $CoFe_2O_4$ stones growing in situ on graphene oxide, followed by a hydrothermal procedure. in addition to the promising application in Photo-Fenton reaction, the nano-hybride exhibit a good lithium storage performance with elevated reversible capability and outstanding cyclic retention at each actual density as used the anode material in Lithium-ion batteries. These data proved a broad choice of perspectives for the application of 3D graphene-based hybrids in wastewater treatment and energy storage.

9 Nano-Clays

Recently, several studies have been reported on the assembly of graphene nano platelets with minerals clay. This approach was to operate under a mechanical sound treatment, the aim was to compare the dispersions of graphene with and without clay. The results showed that the absence of clay created a quick decantation of the product in water, whereas the presence of clay causes the resulting dispersion to stay put constant for several months, without synergistic effects [83]. This research opened the doors to advanced conductive materials based on small amounts of graphene nano platelets due to the interactions of molecules for example organic dyes and polymers in certain types of clay such as sepiolite.

In fact, using very small quantities of graphene-nanoclays can obtain a new generation of hybrid composites with high electrical conductivity, while retaining improved mechanical properties, at a low cost. In other hand, the mixtures of montmorillonite/graphene or organo-montmorillonite/graphene nanofillers are mostly used in the design processing of nanocomposite materials. In this context, Fukushima et al. [84] have been studied the effect of the association of two nanofillers, namely, expanded graphite (GE) and organophilic montmorillonite C30B on the properties of the poly (lactic acid) matrix. The authors explain the enhancement of thermal stability, blaze properties and mechanical tensile properties to the excellent co-dispersion and the significant reinforcement obtained with GE/C30B mixtures.

The advantage of mixing graphene with different types of clays has also been observed for other non-biodegradable matrices. Indeed, Longun et al. [85] have been showed significant improvements in the viscoelastic and thermal properties of the polyimide matrix (PI) in the presence of organo-montmorillonite (OMMT)/ graphene
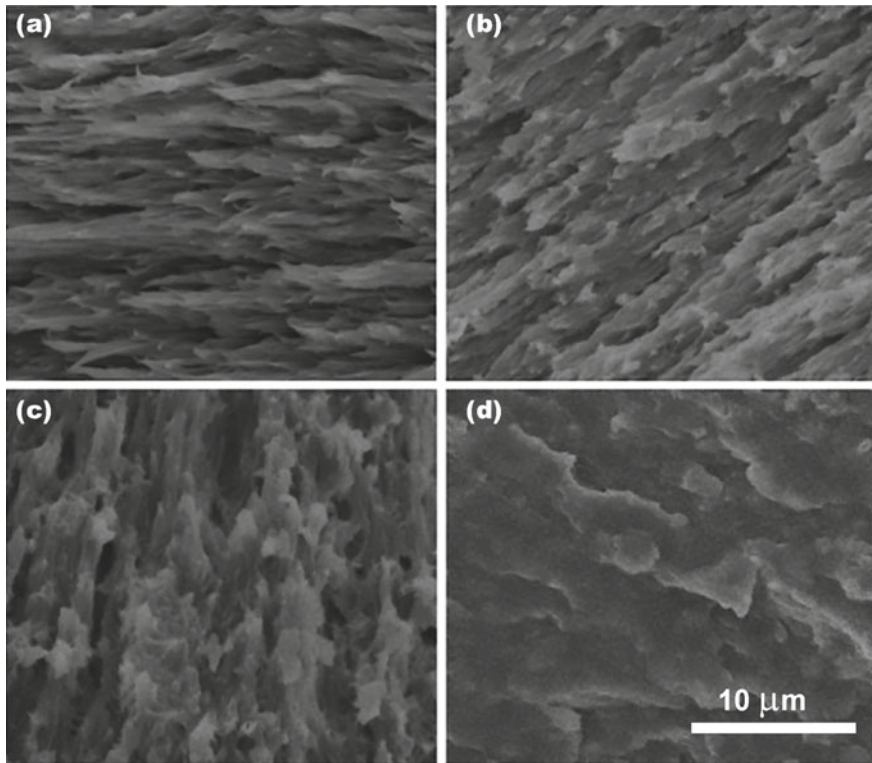
Fig. 9 SEM images of tensile fracture surface of **a** PVA, **b** PVA-Gr-0.3, **c** PVA-Gr-0.6 and **d** PVA-Gr-0.9-MMT-0.3[86]

(Gr) blends compared to binary blends PI/Gr and PI/OMMT. Greater reinforcement has been obtained for hybrid nanocomposites polyvinyl alcohol (PVA)/clay/graphene corresponding to the excellent dispersion of the charge mixtures and to the presence of strong interfacial interactions confirmed by the morphological and thermal characterizations [86]. Figure below illustrates the SEM images of prepared hybride composites (Fig. 9).

10 Titanium Oxides

Titanium dioxide (TiO_2) is the most attractive photocatalyst, owing to its non-toxicity, chemical stability, commercially available, relatively cheap, and indeed widely used in composites preparation, especially combined with graphene. The manufacturing and application of hybrid nanocomposite materials using titanium dioxide as starting material, which was reinforced with graphene nanosheets was done. In this, a novel nanocomposite based on TiO_2/graphene by using a suspension of graphene

nanosheets combined with titania peroxo complex as starting materials through one-pot thermal hydrolysis approach. The prepared materials can be considered as an excellent photocatalytic. The results showed that the TiO2-graphene nanocomposite exhibited the maximum mineralization under UV and visible light, and the sample called TiPC0100 with the optimum ratio of TiO_2 and graphene displayed the highest mineralization. [87].

Another study was reported a green one-step hydrothermal preparation of ultra-fine TiO_2 nanocrystals consistently dispersed on the whole surface of graphene nanosheets. The high photocatalytic activity and excellent stability of the prepared nanocomposites are mainly due to the beneficial nanostructure including the super-dispersed and ultrafine properties of TiO2 nanocrystals, in addition to the intimate and best contact interface connecting TiO2 and graphene. It supports a very high surface area, excellent charge separation, and enhanced visible light absorption created by the structure. [88].

A hybrid material using TiO2 reinforced with graphene was applied to some applications, and its application to a high-performance lithium-ion secondary battery was investigated [89], oxygen reduction reaction [90].

11   Zinc Oxides

Metal nanoparticles have attracted attention in various research fields centering on biological fields such as antibacterial research and are used in various applications such as the production of new hybrid materials as reinforcing agents. In recent years, zinc oxide (ZnO) has attracted attention because of its characteristic properties such as low cost, abundant availability, nontoxicity, and electrochemical activity [3]. ZnO is considered as a battery active material.

With the aim to mix the excellent individual properties of both graphene and zinc oxide. Several techniques used in preparing graphene–zinc oxide hybrid nanocomposites for different applications have been reported. E.R. Ezeigwe et al. [4] were adopted a simple, green and competent technique by utilizing a novel liquid phase exfoliation and solvothermal to develop graphene-ZnO hybrid materials. The prepared nanocomposites were found to be a great candidate for electrochemical capacitors as electrode material. In the same context, ZnO is combined with graphene nanosheets via a green and simple approach to prepare a new kind of hybride materials. From this study, Jun Wang et al. [91] were confirmed the good effect of adding small among of ZnO particles inside of graphene sheet on the final properties of the materials ZnO-graphene, especially for energy storage application in supercapacitors.

Very recently, a group of researchers from Zhejiang Normal University of china [92] were developed a series of hybride nanocomposite based on zinc oxide (ZnO) nanoparticles with reduced graphene oxide (RGO) by employing a facile, simple and green approach in one-step to pick up the photocatalytic properties of these materials. From the whole results obtained in this study, the authors concluded that

the ZnO-RGO composites are found to be a promising candidate for functional use in pollutant decomposition as efficient photocatalysts.

Currently, the hybride nanocomposite materials based on zinc oxides and graphene nanosheets have gained a great interest in both scientific and academic research. These kind of materials with their unique properties such as improved photocatalytic activity and anti-photo-corrosion [93], high-sensitive flexible gas sensors [94] and excellent photo-catalytic performances [95], have been found multivarious applications in different field.

12 Application of Hybride Materials Based on Graphene

Due to their remarkable properties i.e. mechanical, electrical, optical, and thermal, various carbon derivatives including, graphene, graphene oxide and fullerene with canted geometric shapes have attracted enormous interest from two points of view, scientists, and engineering. These new discovering composites have found a great potential application in the different fields of electronics, sensors, actuators, solar cells, data storage, optics and photonics, medical and biological applications. In recent years, hybrid materials made of graphene with several nanoparticles have elaborated by different route and have expanded a lot of interest because of their high performances compared with traditional materials. These materials were subjected to several applications, they were used to inhibit the growth of several bacteria stains. These materials were also screened to investigate their anticancer activity [21].

Generally, the type of application of the hybride nanocomposite is frequently related to the nature of nanostructures and its among used during the hybridization process, also the method used in the fabrication can be affected the results and oriented the application of the obtained materials. The figure below illustrated the major functional applications of hybride materials made up from graphene with different nanoparticles (Fig. 10).

13 Conclusion

The hybridization of graphene derivatives with nanoparticles represents a promising process, as it enhances the overall properties of the nanocomposite hybride materials. Owing to its unique properties and characteristic chemical structure, graphene and its derivatives could be combined with various nanoparticles (zinc oxide, cellulose nanocrystals/nanofibrils and titanium oxides …). The hybride materials resulted from this combination are characterized by excellent properties which are related to the properties of graphene as reinforcing agent and the properties of the nanostructures used even a small among. The exceptional performances of these hybride nanocomposite make them more suitable for several functional and practical application in
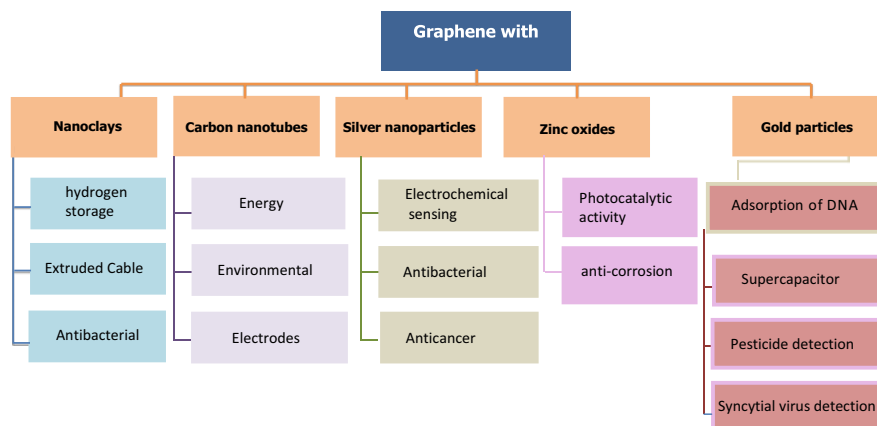
Fig. 10 Major functional applications of hydride nanocomposites based on graphene-nanoparticles

different domains, including, biology and medicine, energy and green chemistry, electronics, and electrochemical field.

References

1. Dong L, Chen Q (2010) Properties, synthesis, and characterization of graphene. Front Mater Sci China 2010(4):45–51
2. Liu M, Zhong H, Yun L, Samal K (2016) Synthesis, characterization, and antibacterial properties of Silver Nanoparticles-Graphene and Graphene Oxide Composites, Biotechnol. Bioprocess Eng 18:1–18
3. Selvakumar G, Krishna Bhat M, Manish Aggarwal D, Prahladh Iyer A, Sravani S (2010) Nano ZnO-activated carbon composite electrodes for supercapacitors, Phys B Phys Condens Matter 405:2286–2289
4. Raphael E, Tan MTT, Sim P, Wee C (2014) One-step green synthesis of graphene / ZnO nanocomposites for electrochemical capacitors. Ceram Int 41:715–724
5. Liu J (2012) Adsorption of DNA onto gold nanoparticles and graphene oxide : surface science and applications. Phys Chem C Hem P Hys 14:10485–10496
6. Zhang X, Liu X, Zheng W, Zhu J (2012) Regenerated cellulose / graphene nanocomposite films prepared in DMAC / LiCl solution. Carbohydr Polym 88:26–30
7. Alam S, Nizam B, Maksudul U (2016) Synthesis of graphene. Int Nano Lett 6:65–83
8. Bipasha FA (2015) A review of functionalized Graphene properties and its application a review of functionalized Graphene properties and its application 2
9. Ions D, Mechanical E, Cross-linking PC, Park S, Lee K, Bozoklu G, Cai W, Nguyen ḰST, Ruoff RS (2008) Graphene Oxide papers modified by divalent Ions—enhancing mechanical properties via chemical cross-linking. ACS Nano 2:578–578
10. Zhu BY, Murali S, Cai W, Li X, Suk JW, Potts JR, Ruoff RS (2010) Graphene and Graphene Oxide: synthesis, properties, and applications. Adv Mater 22:3906–3924
11. Zheng W, Wong S, Sue H (2002) Transport behavior of PMMA / expanded graphite nanocomposites. Polyhedron 73:6767–6773

12. Georgakilas V, Tiwari JN, Kemp KC, Perman JA, Bourlinos AB, Kim KS, Zboril R (2016) Noncovalent functionalization of Graphene and Graphene Oxide for Energy Materials, Biosensing, Catalytic, and Biomedical Applications. Chem Rev 116:5464–5519

13. Yu Z, Sun S, Huang M (2016) Electrodeposition of Gold Nanoparticles on Electrochemically Reduced Graphene Oxide for High Performance Supercapacitor Electrode Materials. Int J Electrochem Sci 11:3643–3650

14. Jing Y, Lin Y, Su E, Liu X, Li Y, Yuan H, … Fan X (2016) Electrodeposition of Au nanoparticles on poly (diallyldimethylammonium chloride) functionalized reduced graphene oxide sheets for voltammetric determination of nicotine in tobacco products and anti-smoking pharmaceuticals. RSC Adv 0:1–3

15. Rajendra Prasad N, Munichandraiah K (2002) Electrooxidation of methanol on polyaniline without dispersed catalyst particles. J Power Sources 103:300–304

16. Moradi Golsheikh CY, Huang A, Lim NM, Zakaria HN, Yin R (2016) One-step electrodeposition synthesis of silver-nanoparticle-decorated graphene on indium-tin-oxide for enzymeless hydrogen peroxide detection, Carbon NY 62:405–412

17. Eredia P, Bertolazzi M, Leydecker S, El Garah T, Janica M, Melinte I, Samorì G (2017) Morphology and electronic properties of electrochemically exfoliated Graphene. Physiccal Chem Lett 8:3347–3355

18. Munuera JMD, Paredes JM, Enterría JI, Pagán M, Villar-Rodil A, Pereira S, … Tascón MFR (2017) Electrochemical Exfoliation of Graphite in Aqueous Sodium Halide Electrolytes toward Low Oxygen Content Graphene for Energy and Environmental Applications. ACS Appl Mater Interfaces 9:24085–24099

19. Song H, Xu J, Xing L, Li R, Zhou Q, Liu C, Song S (2014) Synthesis of Au / Graphene Oxide composites for selective and sensitive electrochemical detection of Ascorbic. Sci Rep 4:1–7

20. Yin Z, Tang H, Wang H, Gao D, Tang Y (2012) Facile synthesis of surfactant-free Au Cluster/Graphene Hybrids for high- performance Oxygen reduction reaction. ACS Nano 6:8288–8297

21. Gurunathan JH, Han S, Park JW, Kim JH, Choi JS, Kwon YJ, Kim DN (2015) Reduced graphene oxide—silver nanoparticle nanocomposite : a potential anticancer nanotherapy. Int J Nanomedicine 10:6257–6276

22. Nethravathi C, Anumol EA, Rajamathi M, Ravishankar N (2011) Highly dispersed ultrafine Pt and PtRu nanoparticles on graphene : formation mechanism and electrocatalytic activity †. Nanoscale 3:569–571

23. Sutter PW, Flege J, Sutter ELIA (2008) Epitaxial graphene on ruthenium. Nat Mater 7:406–411

24. Norimatsu W, Kusunok M (2014) Epitaxial graphene on SiC{0001}: advances and perspectives., Chem Chem Phys 16:3501–3511

25. Guermoune M, Chari A, Popescu T, Sabri F, Guillemette SS, Skulason J, … Siaj S (2011) Chemical vapor deposition synthesis of graphene on copper with methanol , ethanol , and propanol precursors, Carbon N. Y 49:4204–4210

26. Parvez K, Yang S, Feng X, Müllen K (2015) Exfoliation of graphene via wet chemical routes. Synth Met 210:123–132

27. Khan JN, O'Neill U, Lotya A, De M, Coleman S (2010) High-concentration solvent Exfoliation of Graphene. Small 6:864–871

28. Zhong YL, Swager TM (2012) Enhanced electrochemical expansion of Graphite for in situ electrochemical functionalization. J Am Chem Soc 134:17896–17899

29. Cai HC, Thorpe M, Adamson D, Schniepp DH (2012) Methods of graphite exfoliation. J Mater Chem 22:24992–25002

30. Gautham Krishnaiah VV (2012) Process for the preparation of Graphite Oxde and Graphene sheets, US 2012/0128570 A1

31. Gao HM, Ren L, Li W, Cheng F (2008) Total color difference for rapid and accurate identification of Graphene. ACS Nano 2:1625–1633

32. Wang G, Yang J, Park J, Gou X, Wang B, Liu H, Yao J (2008) Facile synthesis and characterization of Graphene Nanosheets. J Phys Chem C 112:8192–8195

33. Ichinokura S, Sugawara S, Takayama K, Takahashi A, Hasegawa T (2016) Superconducting Calcium-Intercalated Bilayer Graphene. ACS Nano 10:2761–2765
34. Monetta T, Acquesta A, Bellucci F (2015) Graphene/Epoxy Coating as multifunctional material for aircraft structures. Aerospace 2:423–434
35. Zhang W, Yi M, Shen Z (2013) Graphene-reinforced epoxy resin with enhanced atomic oxygen erosion resistance. J Mater Sci 48:2416–2423
36. Zhang Z, Zhang W, Li D, Sun Y, Wang Z, Hou C (2015) Mechanical and anticorrosive properties of Graphene / Epoxy Resin composites coating prepared by in-situ method. Int J Mol Sci 16:2239–2251
37. Shen W, Zhai B, Lu W, Wang D, Zheng J (2012) Ultrasonication-assisted direct functionalization of graphene with macromolecules. RSC Adv 2:4713–4719
38. Fang S, Wang M, Lu K, Yang H, Nutt Y (2009) Covalent polymer functionalization of graphene nanosheets and mechanical properties of composites. J Mater Chem 19:7098–7105
39. John KR, Crain M, Lettow JS (2017) Fuel system components. US 9,625,062 B2
40. Alam SN, Sharma N, Kumar L (2017) Synthesis of Graphene Oxide (GO) by modified hummers method and its thermal reduction to obtain Reduced Graphene Oxide (rGO) *. Sci Res Publ 6:1–18
41. Park RS, An S, Potts J, Velamakanni JR, Murali A, Ruoff S (2011) Hydrazine-reduction of graphite- and graphene oxide, Carbon NY 49:3019–3023
42. Xu G, Hong Y, Bai W, Li H, Shi C (2009) Strong and ductile poly (vinyl alcohol)/ graphene oxide composite films with a layered structure, Carbon NY 47:3538–3543
43. Yang X, Tu X, Li Y, Shang L, Tao S (2010) Well-dispersed Chitosan/Graphene Oxide Nanocomposites. ACS Appl Mater Interfaces 2:1707–1713
44. Stankovich RS, Dikin S, Dommett DA, Kohlhaas GHB, Zimney KM, Stach EJ, … Ruoff EA (2006) Graphene-based composite materials. Nat Lett 442:282–286
45. Kim CW, Miura H, Macosko Y (2010) Graphene / Polyurethane Nanocomposites for improved gas barrier and electrical conductivity. Chem Mater 22:3441–3450
46. Kim H, Macosko CW (2008) Morphology and properties of Polyester / Exfoliated Graphite Nanocomposites. Macromolecules 41:3317–3327
47. Kim H, Macosko CW (2009) Processing-property relationships of polycarbonate / graphene composites. Polymer (Guildf) 50:3797–3809
48. Kim CW, Kobayashi H, AbdurRahim S, Zhang MA, Khusainova MJ, Hillmyer A, … Macosko MA (2011) Graphene / polyethylene nanocomposites : Effect of polyethylene functionalization and blending methods, Polymer (Guildf) 52:1837–1846
49. Nasibulin AG, Nasibulin EI, Pikhitsa AG, Jiang PV, Brown H, Krasheninnikov DP, Anisimov AV, … Kauppinen AS (2007) A novel hybrid carbon material, Letters 2:156–161
50. Parker JT, Raut CB, Brown AS, Stoner B, Glass BR (2012) Three-dimensional arrays of graphenated carbon nanotubes. J Mater Res 27:1046–1053
51. Varshney G, Venkateswara Rao D, Guinel C, Ishikawa MJF, Weiner Y, Morell BR (2013) Free standing graphene-diamond hybrid films and their electron emission properties. J Appl Phys 110:44324
52. Contreras Jiménez M, Eissa G, Ng S, Alhadrami A, Zourob H, Siaj M (2014) Aptamer-based label-free impedimetric biosensor for the detection of Progesterone. Anal Chem 87:1075–1082
53. Krueger BA (2008) Diamond nanoparticles : jewels for chemistry and physics. Adv Mater 20:2445–2449
54. Liu X, Yin M, Ulin-Avila X, Geng E, Zentgraf B, Ju T, … Zhang L (2011) A graphene-based broadband optical modulator. Nature 474:64–67
55. Wang W, Cui Q, Chen X, Zheng J, Liu X, Xue C, … Zheng T (2012) Well-dispersed palladium nanoparticles on graphene oxide as a non-enzymatic glucose sensor. RSC Adv 2:6245–6249
56. Yong Y, Ma J, Zhao XS, Zhang J, Xiong Z (2011) Preparation, characterization and antibacterial properties of silver-modified graphene oxide. Chem J Mater 21:3350–3352
57. Marta S, Potara B, Iliut M, Jakab M, Radu E, Imre-Lucaci T, … Astilean F (2015) Designing chitosan–silver nanoparticles-graphene oxide nanohybrids with enhanced antibacterial activity against Staphylococcus aureus, Elsevier B.V. 487:113–120

58. Li D, Kuang J, Feng D, Zhang Y, Xu F, Liu Z, Wang M (2013) Green synthesis of silver nanoparticles—graphene oxide nanocomposite and its application in electrochemical sensing of tryptophan. Biosens Bioelectron 42:198–206

59. Wang Z, Zhao C, Li M, Yu J, Sun J, Ge S, … Guo S (2017) Silver nanoparticles/graphene oxide decorated carbon fiber synergistic reinforcement in epoxy-based composites. Polymer (Guildf) 131:263–271

60. Han Y, Miao K, Tong P, Liu H, Cheng T, Zhu W, Tang X (2014) Preparation of silver nanoparticles / graphene nanosheets as a catalyst for electrochemical oxidation of methanol. Appl Phys Lett 104:53101

61. Badhulika A, Terse-Thakoor S, Villarreal T, Mulchandani C (2015) Graphene hybrids : synthesis strategies and applications in sensors and sensitized solar cells. Front Chem 3:38

62. Lee SO, Maiti WJ, Lee UN, Lim JM, Han J, Kim TH (2014) Nitrogen-doped carbon nanotubes and graphene composite structures for energy and catalytic applications. Chem Commun 50:6818–6830

63. Sheka EF, Chernozatonskii LA (2010) Graphene-carbon nanotube composites. J Comput Theor Nanosci 7:1814–1824

64. Chao Z, Tianxi LIU (2012) A review on hybridization modification of graphene and its polymer nanocomposites. Chin Sci Bull 57:3010–3021

65. Fan T (2017) Wei, Zhang. Longsheng, Liu, Graphene-Carbon nanotube hybrids for energy and environmental applications, Springer Nature

66. Fan W, Liu T, Zhang C, Huang S, Tjiu WW (2012) Facile preparation of water-dispersible graphene sheets stabilized by. J Mater Chem 22:2427–2434

67. Chen Y, Qiu X, Ding M, Fu H, Fan K (2016) A reduced graphene oxide nanofiltration membrane intercalated by well-dispersed carbon nanotubes for drinking water purification. Nanoscale 8:5696–5705

68. Cooper HD, Ravich CA, Lips D, Mayer D, Wagner J (2002) Distribution and alignment of carbon nanotubes and nanofibrils in a polymer matrix. Compos Sci Technol 62

69. Ouyang Y, Sun W, Memon J, Wang J, Geng C, Huang J (2013) Scalable preparation of three-dimensional porous structures of reduced graphene oxide / cellulose composites and their application in supercapacitors, Carbon N. Y. 62:501–509

70. Soheilmoghaddam RT, Pasbakhsh M, Wahit P, Bidsorkhi MU, Pour HC, Whye RH, De Silva WT (2014) Regenerated cellulose nanocomposites reinforced with exfoliated graphite nanosheets using BMIMCL ionic liquid, Polymer (Guildf) 55:3130–3138

71. Peng Q, Meng H, Niu L, Lu L (2012) Simultaneous reduction and surface functionalization of Graphene Oxide by natural cellulose with the assistance of the Ionic Liquid. J Phys Chem C 116:16294–16299

72. Yun S, Kim J (2009) Sensors and Actuators a : physical covalently bonded multi-walled carbon nanotubes-cellulose electro-active paper actuator. Sensors Actuators A 154:73–78

73. Kafy J, Sadasivuni A, Kim KK, Akther HC, Kim A (2015) Designing flexible energy and memory storage materials using cellulose modified graphene oxide nanocomposites. Phys Chem Chem Phys 17:5923–5931

74. Scott CL, Pumera M (2011) Nanogold spacing of stacked Graphene Nanofibers for Supercapacitors. Electroanalysis 23:858–861

75. Güneş YH, Shin F, Biswas HJ, Han C, Kim GH, Chae ES, … Lee SJ (2010) Layer-by-layer doping of few-layer. ACS Nano 4:4595–4600

76. Lütfi M, Eren T, Atar N (2015) A sensitive molecular imprinted electrochemical sensor based on gold nanoparticles decorated graphene oxide : Application to selective determination of tyrosine in milk. Sensors Actuators B Chem 210:149–157

77. Wang Y, Zhang Y, Du S, Shao D, Li Y, Wang Z, … Lin J (2011) Self assembly of acetylcholinesterase on a gold nanoparticles—graphene nanosheet hybrid for organophosphate pesticide detection using polyelectrolyte as a linker †. J Mater Chem 21:5319–5325

78. Mao J, Lu S, Yu G, Bo K, Chen Z (2010) Specifi c Protein detection using thermally reduced Graphene Oxide sheet decorated with gold nanoparticle-antibody conjugates. Adv Mater 22:3521–3526

79. Nazim MF, Kousar S, Shahid T, Khan M, Nasar MA, Sher G, Warsi M (2016) New graphene-Co x Zn 1 À x Fe 2 O 4 nano-heterostructures : magnetically separable visible light photocatalytic materials. Ceram Int 42:1–8

80. Javed MF, Rehman H, Mussadiq A, Shahid S, Khan M, Shakir MA, … Warsi I (2019) Reduced graphene oxide-spinel ferrite nano-hybrids as magnetically separable and recyclable visible light driven photocatalyst. Synth Met 254:1–9

81. Wu H, Zhao J, Chen H, Pham-Huy R, Hui C, He X (2016) Adsorptive removal of trace sulfonamide antibiotics by water-dispersible magnetic reduced graphene oxide-ferrite hybrids from wastewater. J Chromatogr B 1029–1030:106–112

82. Qiu J, Deng B, Du Y, Xing M, Zhang M (2016) Ultradispersed Cobalt Ferrite nanoparticles assembled in Graphene Aerogel for continuous Photo-Fenton reaction and enhanced Lithium storage performance. Nat Publ Gr 6:29099

83. Ruiz-Hitzky E, Sobral MM, Gómez-Avilés A, Nunes C, Ruiz-García C, Ferreira P, Aranda P (2016) Clay-Graphene Nanoplatelets functional conducting composites. Adv Funct Mater 26:7394–7405

84. Fukushima P, Murariu K, Camino M, Dubois G (2010) Effect of expanded graphite / layered-silicate clay on thermal , mechanical and fire retardant properties of poly (lactic acid). Polym Degrad Stab 95:1063–1076

85. Longun J, Walker G, Iroh JO (2013) Surface and mechanical properties of graphene—clay / polyimide composites and thin films. Carbon N. Y. 63:9–22

86. Li L, Li C, She Y, Vongsvivut X, Li J, She J, … Kong F (2015) Reinforcement and deformation behaviors of polyvinyl alcohol / graphene / montmorillonite clay composites. Compos Sci Technol 118:1–8

87. Václav Štengl PV, Popelková D (2011) TiO_2 À Graphene Nanocomposite as high performace Photocatalysts. J Phys Chem 115:25209–25218

88. Shao F, Tian P, Shi J, Gao W, Cui S (2015) Eco-friendly one-pot synthesis of ultradispersed TiO_2 nanocrystals/graphene nanocomposites with high photocatalytic activity for dye degradation. Mater Chem A 3:19913–19919

89. Zhang M, Cao F, Yue H, Zhang D, Qu J (2012) Enhanced Anode Performances of Polyani-line—TiO_2—reduced Graphene Oxide Nanocomposites for Lithium Ion Batteries. Inorg Chem 54:9544−9551

90. Sun J, Liu M, Liu H, Qu Y, Li J (2015) Graphene-based transition metal oxide nanocomposites for the oxygen reduction reaction. Nanoscale 7:1250–1269

91. Wang Z, Gao J, Li Z, Wang Z, Yan B, Liu Y, … Jiang Q (2011) Green thesis of graphene nanosheets / ZnO composites and electrochemical properties. J Solid State Chem 184:1421–1427

92. Zhao W, Liu Y, Cui L, Tong T, Wu G (2017) Enhanced photocatalytic properties of ZnO/reduced graphene oxide sheets (rGO) composites with controllable morphology and composition. Appl Surf Sci 412:58–68

93. Peng D, Ji Y, Chen J (2015) Ultrasound assisted synthesis of ZnO/reduced graphene oxide composites with enhanced photocatalytic activity and anti-photocorrosion. Appl Surf Sci 356:762–768

94. Yi J, Lee JM, Il Park W (2011) Vertically aligned ZnO nanorods and graphene hybrid architectures for high-sensitive flexible gas sensors. Sens Act B Chem 155:264–269

95. Li H, Wang X, Zhao Q, Wu Y, Chen W, Meng J (2013) Green synthesis and photo-catalytic performances for ZnO-Reduced Graphene Oxide Nanocomposites. J Colloid Interface Sci 411:69–75

Characterization Techniques for Hybrid Nanocomposites Based on Graphene and Nanoparticles

Check for updates

Mohamed Hamid Salim, Zineb Kassab, Ihsane Kassem, Houssine Sehaqui, Rachid Bouhfid, Johan Jacquemin, Abou El Kacem Qaiss, Jones Alami, and Mounir El Achaby

Abstract Hybrid nanocomposites have appealing chemical and physical properties and are used on a large scale worldwide. Graphene-nanoparticles (G-NP) hybrid fillers and their composites have particularly gained attention among researchers in recent times, as the incorporation of nanoparticles (NP) into the chemically derived graphene (G) in hybrid fillers open for new applications. This is as a result of the synergetic properties of the obtained materials, such as biodegradability, low density, physical and chemical structure, etc. The novelty of this chapter is to present a review of the recent studies of G-NP hybrid filler's characteristics and their composites using the most fundamental characterization techniques. Our literature review examines various published findings regarding, among others, surface, mechanical and thermal properties in order to determine the performance of the fillers. Therefore, we briefly reviewed their basic structure and surface modifications of G-NP hybrid fillers and nanocomposites. The main output is to study and review techniques frequently reported in the literature to examine their structure and properties, we exemplified and discussed in this chapter key results collected from SEM, AFM, TEM, HRTEM, FTIR, UV-vis, Raman, XRD, XPS, SEM, TGA-DTA, DMA and tensile analyses. To help the readers, this chapter is subdivided into three sections covering a state-of-the-art of the most recent hybrid fillers, their preparation and characterization. The overall objective of this chapter is to dress a relationship between their structure and property to provide key indicators and future directions for their efficient large-scale

M. H. Salim · Z. Kassab · I. Kassem · H. Sehaqui · J. Jacquemin · J. Alami · M. El Achaby (✉)
Materials Science and Nano-engineering (MSN) Department, Mohammed VI Polytechnic University (UM6P), Lot 660 – Hay Moulay Rachid, 43150 Benguerir, Morocco
e-mail: mounir.elachaby@um6p.ma

R. Bouhfid · A. E. K. Qaiss
Composites and Nanocomposites Center (CNC), Moroccan Foundation for Advanced Science, Innovation and Research (MAScIR), Rabat Design Center, Rue Mohamed El Jazouli, Madinat El Irfane, 10100 Rabat, Morocco

J. Jacquemin
Laboratoire PCM2E, Faculté des Sciences, Université de Tours, Parc Grandmont, 37200 Tours, France

production of G-NP hybrid nanocomposite with unique characteristics for different applications.

1   Introduction

Research on nanomaterials characteristics and properties has seen a strong increase thanks to the ever-increasing industrial needs [1], and the limited performance of conventional materials [2, 3]. The hybridization of different materials at the nanometer scale has been shown to bring about new and improved materials properties [4]. Among those, graphene (G) with its derivatives (graphene oxide (GO), reduced graphene oxide (rGO) and graphene oxide nanosheets (GON)) combined with nanoparticles (NP) have been developed as novel hybrid nanomaterials with excellent properties [5, 6].

Since its discovery, G is at the forefront of research in various fields of application because of its excellent chemical, electrical, optical and mechanical properties. It was proposed for applications such as a nanofiller in hybrid nanocomposites [7, 8], consisting of functional inorganic nanoparticles or aggregates incorporated in a polymer matrix. These materials exhibit several distinctive properties that are not achievable with organic polymers or inorganic materials individually. The G-NP based polymeric composites have excellent properties like mechanical, thermal, optical, and structural which are not observed in bulk materials [9–11]. Additionally, the performance of hybrid polymer nanocomposite is dependent on the characteristics of hybrid nanofillers, the filler dispersion in the matrix, the interlinkages linking the matrix and the arrangement of fillers within the matrix [12–14]. In recently published works, it has been demonstrated that G-NP based hybrid composite nanomaterials are ideal for use in different applications, such as food packaging, energy storage, sensors technology, water treatment, and transparent-flexible electrodes [15–17].

Hence, there is a need to understand the characteristics of the different G-NP hybrids like their morphology, the choice to incorporate organic or inorganic materials dispersed in the polymer matrix, which can lead to several changes in properties of the neat material. Therefore, in order to facilitate a better understanding of the characteristics of the G-NP based materials, for the first time, this chapter reviewed and classified the G-NP hybrids into five categories: (1) G-metal and metal oxide, (2) G-metal alloy, (3) G-carbon nanotubes, (4) G-nanocellulose and v) G-nanoclays.

Metal or metal oxide nanoparticles are commonly used to produce the G-based hybrid nanofillers [18]. G hybrids incorporated with different metal nanoparticles have been reported like, for example, G-Au [19], G-Ag [20], G-Cu [18], G-Ni [21], G-Pd [22], G-Zn [23], etc. Besides, there are numerous G-metal and G-metal-oxide nanohybrid synthesis methods. Similarly, various nanometal alloys were integrated by appropriate synthetic approaches on the G surface to ensure a high degree of morphological and structural properties and minimizing the possibility of their fragmentation and agglomeration in the matrix [18, 24, 25]. Currently, researchers have developed different synthetic methods for the preparation of the G-metal alloy

nanohybrids, such as reduction, solvothermal, microwave-assisted, electrochemical and chemical vapor deposition [25–28].

Recently, carbon nanomaterials, such as carbon nanotubes (CNT), were introduced to the carbon family. Carbon nanotubes (both single- and multi-walled CNT) with G are commonly used as nanofillers of polymer composite materials [29, 30]. Various processes including chemical vapor deposition, physical vapor deposition, chemical processing, pyrolysis, 3D printing and more assembly-based techniques were developed to produce 3D G-CNT materials [10, 31–33]. G and CNT have remarkable mechanical strength, high thermal and chemical stability and wide surface area, and are therefore used for the production of hybrid composite materials [32, 34–36].

A fourth category of NP is cellulose nanomaterials. They are derived from abundant renewable organic biomaterials, and have been attracting much interest because of their high crystallinity, chemical versatility, low density and renewable 'green' nature [2, 3, 37], and in particular for the fabrication of hybrid G-nanocellulose nanocomposite [38–40].

The last category of nanoparticles depicts nanoclays (NC). These are some of the most abundant nanosized materials, normally available in hundreds of tons and broadly used in different applications [41]. NC are organically modified layered silicates with applications as a reinforcement filler in hybrid nanocomposite [12, 42]. In the preparation of hybrid nanocomposites, many NC (montmorillonite, kaolin, halloysite and bentonite) along with silica and GO nanoparticles are used.

In this chapter, key findings of the characterization techniques for hybrid nanocomposites, whereby G and NP are distributed into a matrix, are reviewed. This chapter also explains that the synthesis of these nanocomposites varies depending on the nanofillers' properties; i.e., the G and NP, its dispersion and alignment as reinforcements within the polymer matrix, as well as the interaction of the polymer matrix with the reinforcement. Examples of morphology, structure and property, including the relationship between structure and property, are explored upon characterization. This perspective on the properties of G-NP hybrid materials will provide a detailed view of the current stage of characterization techniques, highlighting the obstacles and new directions for the future production of G-NP hybrid materials.

2   Hybrid Nanocomposite Based on Graphene and Nanoparticles as Advanced Materials

2.1   Graphene and Nanoparticles as Hybrid Nanomaterials

2.1.1   Graphene-Metal and Metal Oxide

G and its derivatives could be obtained by following a top-down (mechanical cleavage or liquid phase exfoliation) or a bottom-up (such as chemical vapor deposition, arc-discharge, chemical conversion, unzipping carbon nanotubes, and epitaxial growth on SiC) preparation method [43].

G-metal and metal oxide hybrids have excellent properties, with promising applications in electronics, sensors, solar cells, batteries, and supercapacitors [11, 19, 20]. Their synthesis could be achieved by using various preparation methods based on microwave-assisted synthesis, thermal evaporation, chemical reduction, photochemical synthesis and electroless metallization [13, 44, 45].

In the case of metals, nanoparticles precursors, *i.e.* metal salts, are generally reduced in a solvent containing GO and rGO [47]. Due to the weak van der Walls interactions, these graphene derivatives tend then to aggregate and even stack to form graphite in the solution [47]. Hence, by attaching metal NP, it is, in fact, possible to prepare individual G sheets and to reduce their agglomeration [47]. In many instances, researchers use this direct chemical reduction approach in order to prepare a large variety of G-metal nanohybrids by combining metal precursors with G or its derivatives, GO and rGO [20, 22, 48]. Among the many deposition approaches of G-NP fillers onto polymers, G and metal hybrid nanostructures are some of the most effective platforms for various applications [9, 45, 49]. For instance, in order to obtain a homogeneous suspension of exfoliated GO, Feng et al. prepared G-TiO$_2$ by dispersing GO in an ethanol solution under ultrasonication and by adding then Ti(OPr)$_4$ [46]. The resulting solution was then moved to an autoclave and placed in the oven for 12 h at 150 °C [46]. The desired product was thus isolated by centrifugation, thoroughly rinsed with deionized water and ethanol prior to be vacuum-dried [46]. The development procedure as shown in Fig. 1 resulted in a G-TiO$_2$ hybrid in the form of black, gray powder [46]. The G-TiO$_2$ hybrids (2 wt%) was used as filler for PVC films, with a glass transition temperature that increased by 3.5 °C and a storage modulus that increased by 50% relative to a pure PVC film [46].

2.1.2   Graphene-Metal Alloy

Owing to the great synergetic performance and long-term working stability of hybrids, the G hybridization with nanometal alloys has shown high potential for various applications [25, 50]. Synthetic methods have integrated various metal alloys on the G surface to reach a perfect control of their morphological and structural properties, by enhancing the adhesion and by limiting the possibility of their dissolution
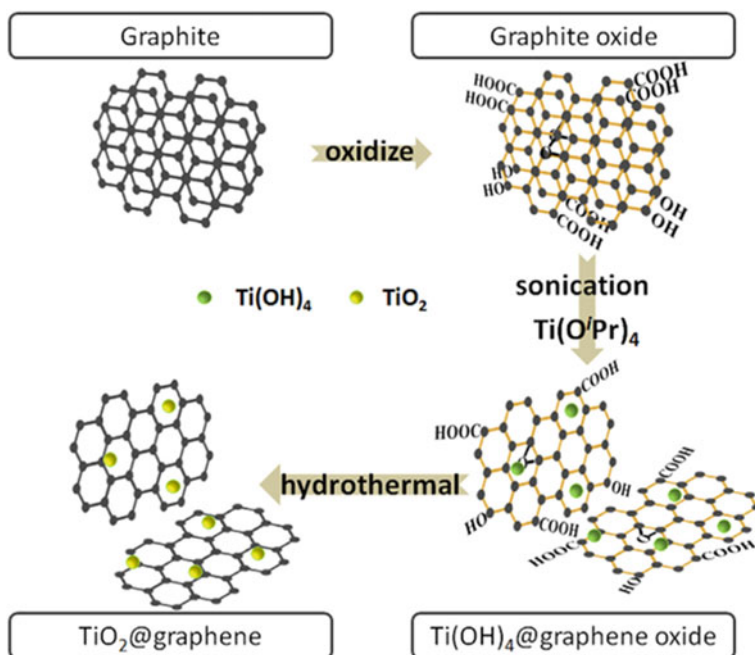
Fig. 1 G-TiO$_2$ hybrid preparation and structure schematic presentation [46]

and aggregation [22, 28, 50]. To date, numerous novel metal alloy nanostructures integrated on G nanosheets have been widely produced simply by changing the conditions of the reaction, such as the concentration of the precursor, the temperature of the reaction and introduction of the dispersion agent. The nanohybrids obtained displayed very interesting morphologies that were compatible with unique chemical and physical properties [25, 27, 28]. For example, in order to produce G-nanoalloy (Palladium-Copper) hybrid, precursors (Na$_2$PdCl$_4$ and CuSO$_4$ of molar ratio 1:3) were mixed together with a suspension containing G. As shown in in Fig. 2, during this preparation method, metal ions from precursors such as PdCl$_4^{2-}$ and Cu^{2+} were adsorbed onto the surface of G nanosheet thanks to a coordination effect between its remaining oxygen moieties and each ion [28].

2.1.3 Graphene-Carbon Nanotubes

In recent years, carbon-based nanofillers such as G and carbon nanotubes (CNT) in nanocomposites have been shown to have better structure and functional properties and a broad range of applications [51, 52]. CNT are prepared using various process techniques including chemical vapor deposition, laser ablation, arc evaporation, electrolysis, flame synthesis, etc. [53, 54]. The CNT are generally used as a filler due to their excellent filler properties including a high conductivity and a superior aspect
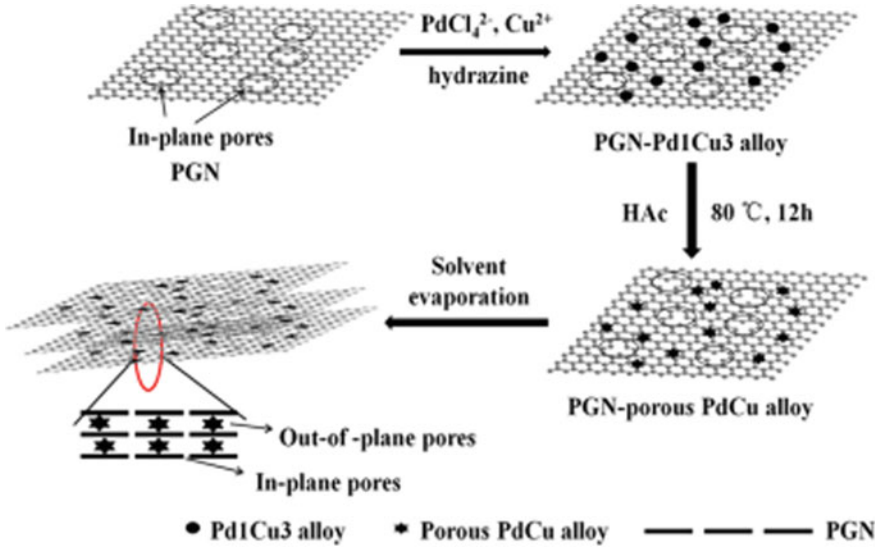
Fig. 2 Hybrid processing design of 3D G-nano alloy (G-PdCu) [28]

ratio and tensile strength. G fillers have also the potential to adjust or fine-tune the properties of targeted materials, which attracted various interests of several scientists working in different research fields [55–57]. Furthermore, a homogenous dispersion could be achieved during the early stages of processing of nanocomposites by incorporating CNT into the polymeric matrix limiting in fact their aggregation [30, 58]. For this reason, several research groups reported on the successful preparation and utilization of G-CNT hybrid fillers in diverse applications such as energy storage, sensing, water treatment, capacitors, etc. [34, 59–61].

The characteristics of G, CNT or hybrid fillers depend upon many parameters such as the type of CNT, the type of G, the purity, the size of CNT, the aspect ratio of the nanotubes, the loading, the interactions, the alignment, and the anti-agglomeration of G and CNT [63]. Three techniques are used for processing G-CNT hybrids: solution mixing, chemical vapor deposition and in situ polymerization [64–66]. In a study by Kong et al., a two-stage method for G-CNT hybrid synthesis was developed. This is shown in Fig. 3 [62], where it was reported that the CNT growth uniformly on the G surface followed that of the modification agent, resulting in the creation of a complex interface driven by a covalent C–C bonding connection between the G and CNT [62]. Similar observations were made by various studies on G-CNT hybrid [67–69].
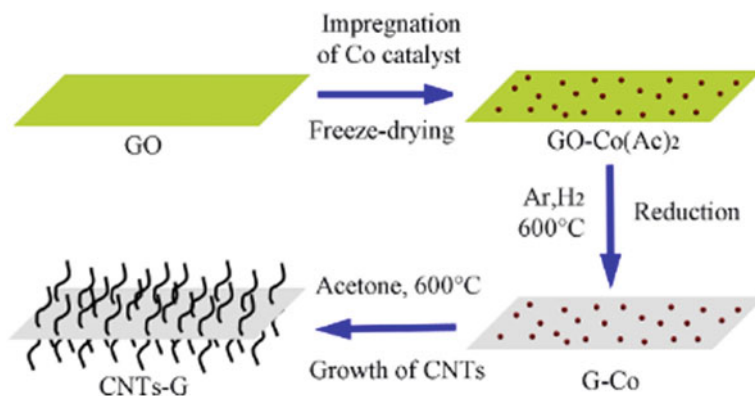
Fig. 3 Schematic diagram of the G-CNT hybrid synthetic method [62]

2.1.4 Graphene-Nanocelluloses

Nanocellulose, an organic compound extracted from natural resources, is biodegradable, biocompatible, and can demonstrate interesting properties when used as a filler in composites [70, 71]. Nanocellulose has unique characteristics including a large aspect ratio, good mechanical properties, good flexibility and hydrophilicity, explaining why it is therefore used as a filler to form nanocomposite [72]. The hierarchical structure and the presence of rigid chains on its molecular structure allow the formation of composite containing nanocellulose with flexible substrates and other materials [73]. Nanocellulose is found in the form of crystals (CNC) or fibrils (CNF), which can be dispersed and self-assembled easily in a solution under the ultrasonication process [72, 74]. Graphene, on the other hand, is a two-dimensional carbon nanostructure that has drawn considerable attention in the development of composites because of its excellent thermal properties, large surface area, high strength and young's modulus [75]. However, due to the presence of strong intermolecular π-π stacking attraction forces and van der Waals interaction, G has the tendency to aggregate irreversibly even in water or in organic solutions [75].

Researchers have suggested a new strategy to hybridize G with amphipathic nanocellulose during GO reduction, acting as a stabilizer or a supporting agent [15, 38, 40]. Depending on the G-nanocellulose ratio, the resulting hybrid material is made up of G layers surrounded by nanocellulose to a greater or lesser limit [76]. The G-nanocellulose hybrid was demonstrated to have a covalent chemical structure and an excellent aqueous suspension stability, which greatly facilitated G dispersion [77]. Studies have reported that the abundance of oxygen-containing groups decorated with G can combine with nanocellulose hydroxyl groups and oxygen atoms, which are advantageous for the homogeneous dispersion of G and nanocellulose in the shaped hybrid nanofiller [40, 76, 78]. Hence, the preparation of covalent cross-linked G-nanocellulose hybrids was realized by esterification between hydroxyl groups [79].
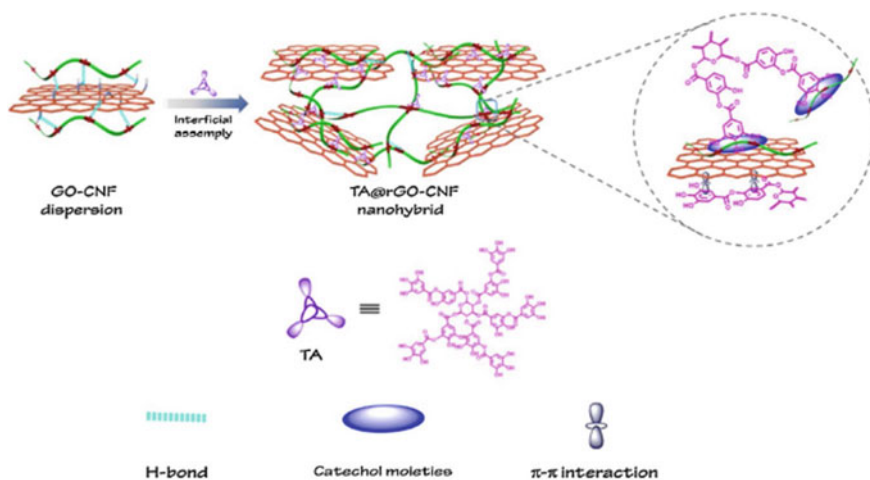
Fig. 4 Schematic diagram and nanohybrid structure of rGO-CNF [76]

Montes et al. prepared fillers based on G-CNC by assisting the graphite exfoliation in a liquid-phase containing CNC. By following this novel approach, graphene flakes seem to be stabilized in aqueous dispersions [80]. Similarly, as shown in Fig. 4, Wang et al. produced rGO-CNF hybrid with rGO and CNF aqueous suspension by using a one-step synthesis combining a chemical reduction and an induced materials assembly, which was facilitated by the addition of the tannic acid [76]. Due to the functional catechol chemistry of tannic acid, the interfacial interactions between rGO nanosheets and CNF (which includes π-π and hydrogen bonding) improved; this created a strong adherent coating acting as a capping layer to stabilize and decorate the obtained rGO-CNF hybrid [76].

2.1.5 Graphene-Nanoclays

Natural occurring nanoclays (NC) like montmorillonite, bentonite, laponite, halloysite and kaolin were used as nanofillers for the production of composites in a variety of industrial applications [81]. The NC platelet structure allows it to form a protective barrier once a high degree of exfoliation with a good dispersion has been achieved, resulting in an improved mechanical performance of materials [82]. Similarly, G is a member of the family of monolayer carbon atoms, fully compacted into a 2D honeycomb network, which acts as a fundamental structural block for graphite-based materials [83–86]. A high-performance material is thus obtained by producing, a hybrid composed of GO and NC [82, 83, 86].

In different studies, GO hybrids reduced by halloysite nanotubes were prepared by simultaneous reduction and hybridization of GO with halloysite nanotubes [84, 87, 88]. It was observed that the hybrids had a perfect coverage structure and that the
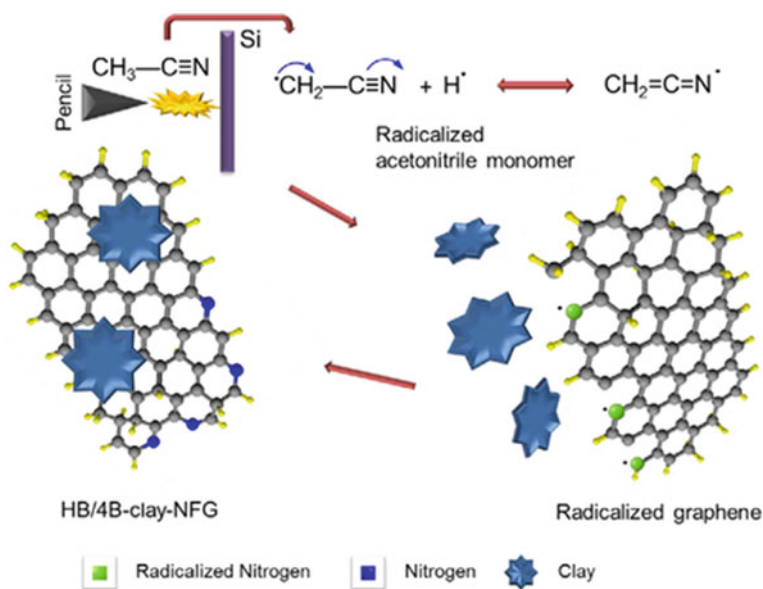
Fig. 5 Proposed framework for G-NC hybrid formation [90]

intercalation of halloysite nanotubes within the GO sheet interlayers was likely due to the excellent compatibility between G and halloysite nanotubes [87]. Research on GO-montmorillonite hybrid has shown that the hybrid material's d-spacing is observed between that of the GO-montmorillonite and the structure of the GO flake-pillared montmorillonite [89].

NC's role in the manufacture of G-based hybrids was thus explored due to its high chemical stability, specific swelling capability and ability to exchange ions [41]. As seen in the Fig. 5, the scattered nanoclay particles are physically or chemically absorbed at the ionized sites of the G layers in the hybrid [90]. The particles of NC do not attract or interact with the sites of radicalized G as they are effectively surrounded by the radicals of hydrogen [90]. The distributed radicalized G has a high affinity with H and CH2-CN radicals and generates, as a result, G-NC hybrid pyridinic and pyrrolic systems [90].

2.2 Hybrid Nanocomposites Based on Graphene and Nanoparticles

2.2.1 Hybrid Polymer Nanocomposites Based on Graphene and Metal/metal Oxide

Hybrid G-nanometal polymer composite materials is a subject that gained much attention recently [6, 91, 92]. In particular the design and preparation methods of polymer nanocomposites reinforced by G-nanometal have become common practice, since these hybrid fillers provide unique properties to the polymer matrix [92, 93]. The hybrid G-nanometal/metal oxide in the polymer matrix has the advantage that the G sheets serve as a loader for regulated metal NP production and can prevent the self-assembly of small metal NP during the preparation of the composite nanomaterials [6, 18, 94]. Metal oxides play here a significant role in improving the polymer's immobilization and thus the enzyme stability [95].

For instance, the polyvinyl chloride (PVC's) glass transition temperature reinforced with G-TiO_2 hybrid increased from 71.3 to 74.8 °C compared with neat PVC, indicating that the segmental chain mobility is limited by the intense interfacial interactions between the nanohybrids and the polymer matrix [46]. Kumar et al. prepared a multifunctional biodegradable material where hybrid graphene-silver (rGO-Ag) nanoparticles were used to enhance poly-caprolactone (PCL) matrix, as demonstrated in Fig. 6 [6]. Comparing with rGO or Ag nanoparticles alone, rGO-Ag hybrid nanoparticles were found to be well dispersed in the polymer matrix due to enhanced exfoliation [6]. In addition, it was noted that uniformly scattered rGO-Ag hybrid nanoparticles resulted in a 77% increase in the PCL Youngs' modulus at 5 wt% filler, which exceeded significantly the improvements achieved with the addition
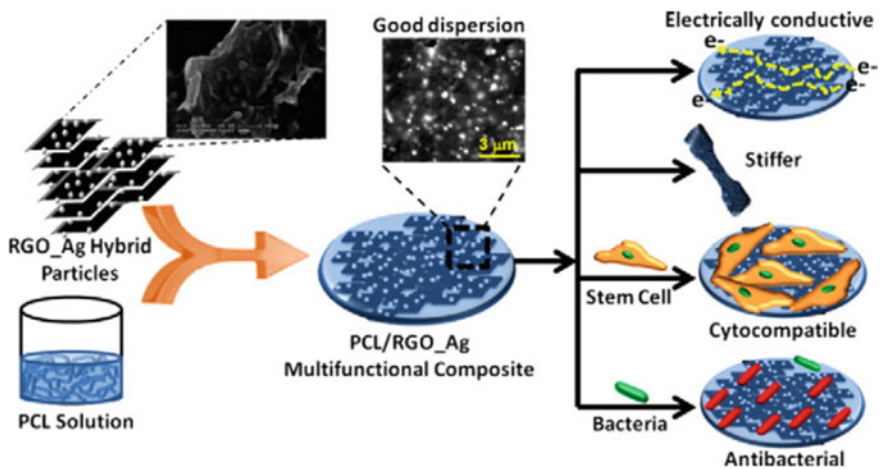
Fig. 6 Schema polymer nanocomposite incorporated with rGO-Ag hybrid [6]

of rGO or Ag nanoparticles alone in the PCL [6]. Other improved properties include conductivity, stiffness, antibacterial property and cytocompatibility [6]. Likewise, by adding 0.25 phr rGO—Fe_2O_3 in the epoxy matrix, tensile strength, flexural strength and impact strength improved by 56%, 81% and 112% respectively [92].

2.2.2 Hybrid Polymer Nanocomposites Based on Graphene and Metal Alloy

Metals' scarcity, mass interaction and stability have become the critical limiting factors that hinder the commercial applications of metal-based materials, in recent years [96, 97]. A number of strategies have been adapted to enhance those properties, two of which are: i. reducing the size of metals to a nanoscale, which can provide more active sites and increases the use of metals per mass, ii. alloying with earth-abundant transition metals (Cu, Zn, Ni, and Fe), which may improve the metal-based hybrid's mass activity and stability due to the synergetic effects resulting from changes in the nano-alloy surface physical and chemical natures [26]. These approaches and others have helped the rapid advancement of G-based nanocomposites, highlighting the nanometal alloys strong mechanical reinforcement strength, large specific surface area, excellent biocompatibility and good thermal properties [48, 98, 99].

Hong et al. prepared poly(methyl methacrylate) (PMMA) nanocomposite as shown in Fig. 7, reinforced by rGO-NiAl hybrid, using a simple solution blending method, in order to investigate its effect on increasing the composite's thermal stability [48]. It was observed in the thermal studies that a greater residue of 3.7 wt% was obtained, which was attributable to the combination of the physical barrier effect of rGO and the NiAl alloy nanoparticles, hence confirming enhanced thermal stability of the PMMA hybrid nanocomposite [48]. Physical characterization demonstrated that poly (triazine imide) (PTI) nanosheets hindered G nanosheets restacking and allowed the even-scattering of the 2.5 nm PtSn alloy nanoparticles on the PTI graphene support materials [99].
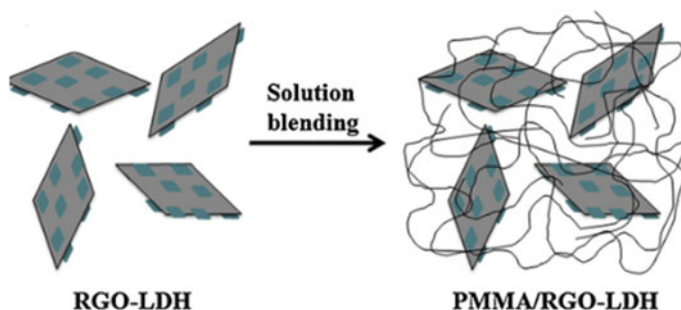
Fig. 7 Schema of the formation of poly(methyl methacrylate) composite reinforced with rGO/NiAl-layered double hydroxide hybrid (presented as rGO-LDH) [48]

2.2.3 Hybrid Polymer Nanocomposites Based on Graphene and Carbon Nanotubes

The improvement of the nanocomposite materials properties could be achieved by using CNT as fillers since the CNT have a high Young's modulus, a high tensile strength, a high aspect ratio, a low density, etc. [29, 100]. These exceptional properties make CNT ideal as a reinforcement additive in hybrid nanocomposites. On the other side, G and its derivatives can be used to modify the inherent properties or induce new properties to the matrix [101, 102]. G based-polymer composites show improved mechanical, thermal, and barrier properties compared to the neat polymeric materials [103]. However, difficulties lie in transforming or imparting the unique properties of G or CNT alone to the polymer [104, 105]. The homogeneous dispersion of the filler in the matrix is crucial in ensuring a good interfacial interaction and adhesion between the phases [106].

The incorporation of the G-CNT hybrid filler to the polymer matrix has more attractive properties compared to the neat polymer [108]. Hybrid polymer nanocomposite based on G and CNT can be used for diverse applications like conduction, coating and films, electromagnetic interference shielding materials for electronic devices, thermal interface materials, etc. [35, 36, 64]. As an illustration, Liu et al. prepared hybrid polyethylene polymer composites based on graphene and carbon nanotubes [109]. They demonstrated an impressive synergetic effect between the G and CNT leading to a clear improvement of the interfacial mechanical properties of the polyethylene matrix [109]. Furthermore, they showed that the reinforcement effect on the covalent bond of the G-CNT hybrid is directly related to the CNT length and radius, and also to the choice of CNT as the use of multi-walled CNT seems to lead to more efficient materials than those made using single-walled CNT [109]. By the addition of GO-CNT hybrid charges to the polymer matrix, it was observed that the composite's storage modulus was the main thermal response speed factor [63]. This observation could be attributed by the presence of specific molecular interactions occurring within the G-CNT hybrid and the polymeric structure.

In another study, Bagotia et al. successfully prepared polycarbonate/ethylene methyl acrylate nanocomposites by following a melt-blending method using different ratios of the G-CNT hybrid filler, as shown in Fig. 8 [107]. Among the tested materials, hybrid filler composites with 10 phr loading (G:CNT ratio 1:3) have a highest tensile strength and tensile modulus than G or CNT based composites at the same loading [107]. In summary, the G-CNT hybrid nanostructure exhibited a synergistic effect improving thus the structural, mechanical and thermal properties of the composite even by selecting a large variety of polymeric matrix, like, exemplified using the poly(vinylidene fluoride) [67], epoxy [63], poly(methyl methacrylate) [110], poly(ether sulfone) [32], poly(vinyl alcohol) [69, 111], poly(dimethylsiloxane) [62], poly(ether-ether-ketone) [112], poly(styrene-b-butadiene-b-styrene) [112], etc.
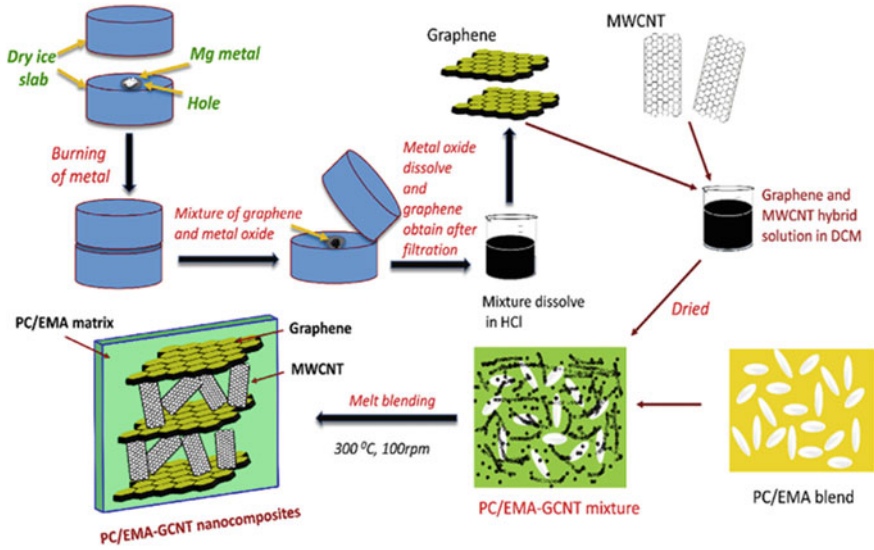
Fig. 8 Graphical description for manufacturing of G-CNT hybrid reinforced polymer composite [107]

2.2.4 Hybrid Polymer Nanocomposites Based on Graphene and Nanocelluloses

Nanocellulose (CNC or CNF) was used individually as an efficient reinforcing fillers on many kinds of polymers [73, 113]. Driven by unique properties (high specific strength, biocompatibility, biodegradability, low weight, abundance, barrier properties and capacity for reinforcement) nanocellulose is recognized as an ideal candidate for the development of polymer nanocomposites [71, 114]. On the other hand, G and its derivatives are also well-known to be potentially the best options leading to high enhancement of polymeric nanomaterials due to their favorable scalability, high mechanical/thermal conductivity, and chemical flexibility [103]. However, as with most nanocomposites, several crucial challenges, such as incomplete G exfoliation, uneven dispersion of fillers, high hydrophilicity of nanocellulose and weak G-matrix adhesion, present limited the full functionality of most described nanomaterials containing G or nanocellulose alone [78, 103, 115].

The development of sustainable and biodegradable nanocellulose aligns with an environmentally friendly approach to mediate G dispersion in aqueous media and its integrated morphology in polymeric matrices such as polyvinyl alcohol [15, 79, 80], polyethylene [40], poly-lactic [38, 78], polyphenol [76], rubber [77], etc. Recent studies have therefore explored the use of sustainable carbohydrate polymers (i.e. cellulose), as they are biocompatible and environmentally friendly, thus achieving

Fig. 9 Schematic presentation of poly (vinyl alcohol) nanocomposites with G-CNC hybrid [80]
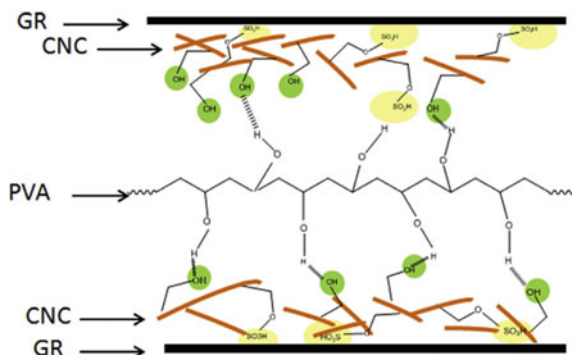
the functionalized biopolymer G-nanocellulose hybrids to reinforce the nanocomposites [40]. The obtained G-nanocellulose hybrids have excellent aqueous suspension stability, which greatly facilitated their dispersion into polymer matrix [15].

In many cases, it was noted that the G-cellulose nanohybrids are selectively located in the interfaces between the polymer microspheres and are assembled into a 3D hierarchical conductive network structure during co-coagulation [77, 79, 116]. Interestingly, the use of G-nanocellulose hybrid was considered a simple approach not only to prevent the use of chemicals modifying agents, but also to enhance the conductivity and mechanical properties of G-based composites prepared with randomly scattered G, through traditional production procedures [39, 77, 79].

For instance, the G-CNC hybrid was combined with poly(vinyl alcohol) (PVA) aqueous solutions to prepare PVA-based nanocomposites (PVA/G-CNC), using a simple and environmentally friendly casting process [80]. It was stated that the synergistic reinforcing effect of G-CNC was obtained through the presence of strong H-bonds between -OH groups of the PVA and CNC enhancing thus their interfacial interaction. This was also achieved thanks to the presence of CNG, promoting the dispersion of graphene in the PVA matrix, as shown in Fig. 9 [80]. Similarly, owing to the synergistic reinforcement of G-CNC, it was noticed that Young's modulus, tensile strength and resilience of the PVA nanocomposite containing 5 wt% hybrid nanofiller (G:CNC ratio 1:2) increased substantially by 320%, 124% and 159% respectively; and the break elongation remained substantial compared to the pure PVA matrix [15].

2.2.5 Hybrid Polymer Nanocomposites Based on Graphene and Nanoclays

Nanocomposites made of clay-based polymers have gained significant interest from the scientific community over the past decade [81]. Researchers studied particularly the potential for reinforcement of polymeric matrix with modified nanoclays (montmorillonite, bentonite, laponite, halloysite and kaolin), so as to improve its properties such as thermal, barrier, mechanical and resistance to flammability [84, 117, 118]. Compatibilizers such as G are also used in the preparation of nanocomposites as well

as modifying the nanoclays (NC) to enhance the dispersion of the filler particles [86]. Hence, the synergetic effect of dispersion and flame retardancy was the key element to the introduction of G-NC hybrid fillers in the polymer matrix [119].

In addition to flame retardants, G-NC hybrids have been used in various polymer matrices for various other applications such as nylon thermomechanical properties enhancement [82], supercapacitors electrode materials [41, 85], superabsorbent [88], water treatment [84, 118], thermoplastics manufacture [120], etc.

Figure 10 shows graphene oxide-halloysite nanotubes hybrids (HRGO) prepared by simultaneous reduction and hybridization of GO with halloysite nanotubes. The HRGO have been integrated into an epoxy matrix to improve its thermal and the mechanical properties [87]. In fact, the Halloysite nanotubes effectively impeded the accumulation of GO sheets in the epoxy matrix [87]. Similarly, the epoxy nanocomposites showed improvements of 36, 16, 27 and 19% in Young's modulus, tensile power, critical stress intensity factor (KIC) and critical energy release rate (GIC) were achieved using GO-attapulgite hybrids, respectively [121]. In a different study where hybrids with different montmorillonite/GO ratios were examined, the 5:1 mass-ratio hybrid offered better dispersibility and more effectively, while the mechanical strength of epoxy-based composites was enhanced [89].
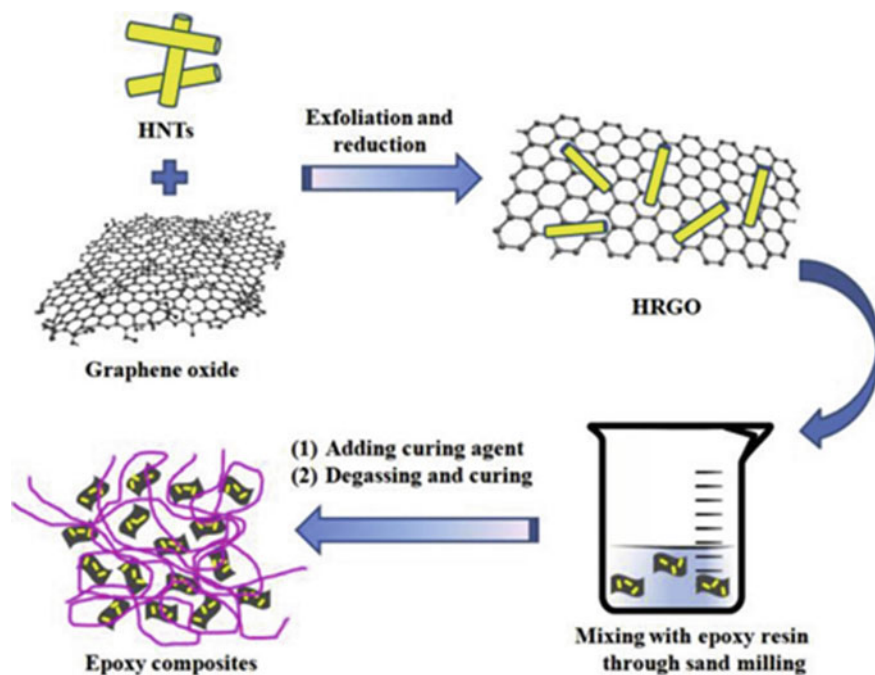
Fig. 10 Schematic overview of GO-halloysite nanotubes hybrid (HRGO) preparations and HRGO-reinforced epoxy composites [87]

3 Characterization Techniques

In materials science, material properties are fundamentally linked to microstructure, which necessitates knowledge of the recent characterization approaches [122, 123]. This is because materials such as thermoplastics, composites and hybrid films have several elementary constituents dispersed in more than one process of fabrication. Characterization is, otherwise, essential for the systematic production of these different materials and for determining their functionality in practical uses. Several commercially available techniques are used to study materials, e.g., microscopy, spectroscopy, and thermal analysis. Each of these techniques is typically used for a define type of materials or for the retrieval specific information. This presents a technical challenge in choosing the adequate characterization technique when dealing with a specific sample. Researchers or engineers must therefore specify which information is required to thoroughly describe each substance and use that data to understand its behavior, create new and advanced materials, minimize costs, or comply with regulatory standards. The following sub-chapter provides all the contexts required to understand the, as characterization technologies of graphene-based nanohybrid and its composite materials, with particular attention to the current and most commonly used techniques as presented in Fig. 11.
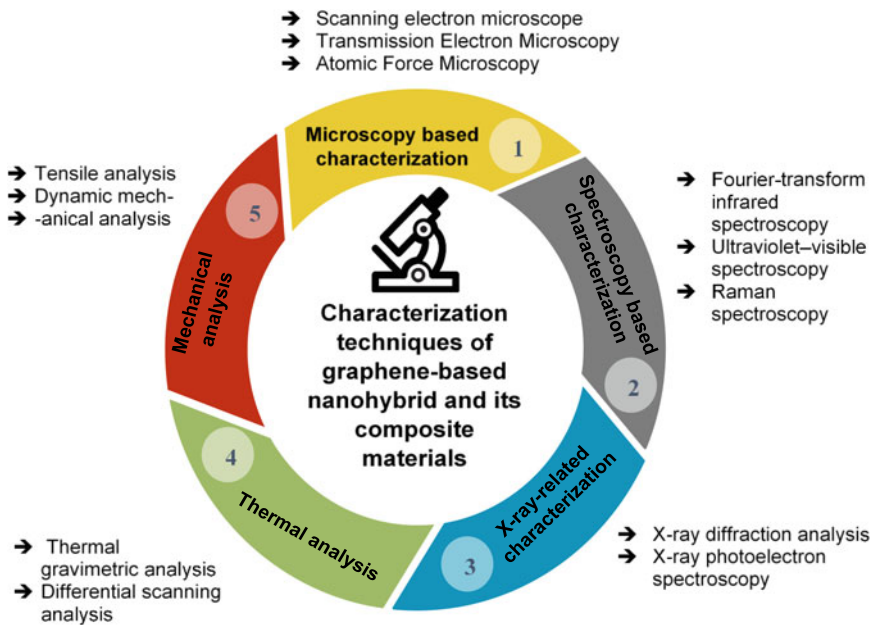
Fig. 11 Categories of the characterization techniques used to study G-NP based hybrid composites

3.1 Microscopy-Based Characterization

3.1.1 Scanning Electron Microscope, SEM

Roughness, morphology, size and state of dispersion of particles in a material can be measured using several microscopy techniques at various length scales. Scanning electron microscopy (SEM), transmission electron microscopy (TEM) and atomic force microscopy (AFM) can provide a straightforward way of observing and analyzing the dispersion of particles at various lengths qualitatively [124]. SEM used a focused electron beam to scan a surface and subsequently present an image [125]. SEM has been used in several works in order to study the dispersion of the graphene-based hybrid nanofillers and examine the surfaces of their composites [23, 32, 45, 80, 126].

With the help of SEM images it was possible to confirm that SnO_2 nanocrystals are attached to the surface of rGO sheets, where the presence of SnO_2 nanocrystals proved that GO and $SnCl_4$ hydrothermal treatment is an effective preparation method of the rGO-SnO_2 hybrid [127]. Similarly, the GO-TiO_2 hybrid SEM images proved that dense TiO_2 nanocrystals were tightly attached to GO sheets and did not separate under sonication [128]. Furthermore, from the analysis of the SEM images of the GO-TiO_2 hybrid, it was possible to conclude that the coating of TiO_2 nanocrystals on graphene is denser with increasing the Ti $(BuO)_4$/GO feed ratio [128]. Further analysis of the dispersion of nanoparticles in the hybrids shows that the SEM images (Fig. 12a) exhibit the presence of individually large Cu or copper oxide particles in the hybrid rGO-Cu (ratio: 1–2) [21]. The rGO-Cu hybrid SEM image (ratio: 1–1) shown in Fig. 12b also clearly indicates the size of the non-uniform nanoparticles in the hybrid [21]. An increase of the mass ratio of rGO-Cu to 2:1 leads to highly dispersed metallic Cu nanoparticles with a small size distribution of 50–100 nm within the GO structure, as shown by SEM image in Fig. 12c. Further increase of the mass ratio of GO-Cu to 5:1 leads to even smaller Cu nanoparticles on the surface of rGO nanosheets with a size distribution of 5–15 nm, as shown in Fig. 12d [21].

SEM analysis was also used to investigate the fracture surfaces of epoxy composites reinforced with G-CNT nanofillers [106]. For the composite with the G-CNT hybrid filler structure, the dispersion of the CNT within the matrix is improved with no rich CNT domains on the surface [106]. The analysis showed that a small amount of G has greatly modified the dispersion and state of aggregation of CNT. In fact, there were no voids or gaps found on the surface of the fracture [106]. Yang et al. demonstrated that the SEM images demonstrated a better dispersion and homogeneity of G and CNT within the epoxy matrix for composites which contain the G-CNT hybrid nanofillers [126]. The SEM images proved that adding CNT significantly affected the dispersion of graphene and the state of aggregation in the epoxy matrix [126], and confirmed the impact that the synergetic effects that CNT and G have on the mechanical properties and composite thermal conductivity [126].

The SEM images (Fig. 13) of the cryogenically broken cross-section of the nanocomposite films obtained in the polyimide (PI) matrix brings to light details
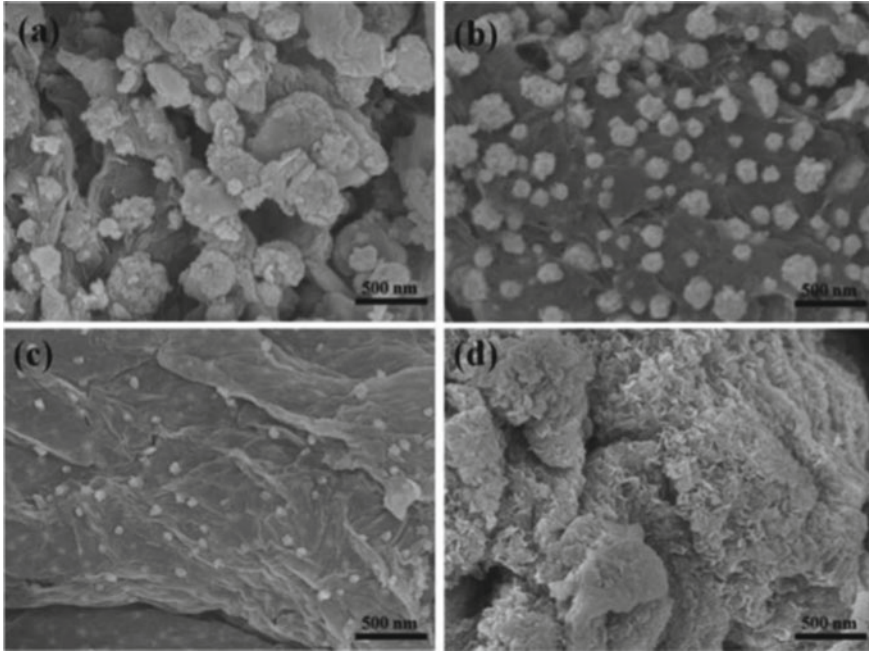
Fig. 12 SEM images of rGO-Cu hybrid at different ratios [21]
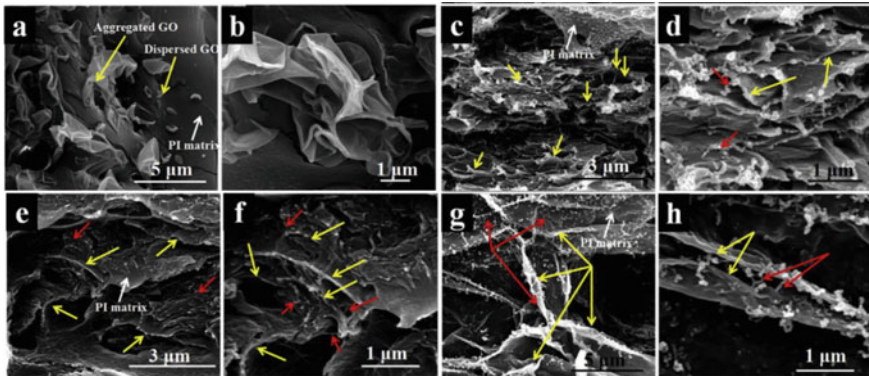
Fig. 13 SEM observations of hybrid polyimide (PI) polymer nanocomposites based on GO-CNT fillers [129]. The yellow arrows indicate the GO nanosheets and the red arrows indicate the CNT

of these nanofillers [129]. For example, many of the GO nanosheets were aggregated together in the PI/GO nanocomposites (Fig. 13a), aside from some scattered GO nanosheets. In addition, the zone magnified in Fig. 13b suggests that the GO nanosheets were poorly compatible with the PI matrix and formed an extreme aggregation, resulting from the wide surface area of GO, which easily stacks to

form agglomerates [129]. The GO agglomeration decreases the area of interaction between GO and PI, leading to low-efficiency GO-reinforcing. Figure 13c, d show the PI nanocomposites packed with the GO-CNT hybrid. It is seen that the introduction of CNT prevents the aggregation of nanosheets of GO and increases the area of interaction between matrix GO and PI. For PI nanocomposites filled with the GO-CNT hybrid (shown in Fig. 13e, f), GO is firmly embedded in the PI matrix, which suggests an excellent stability of hybrid GO-CNT nanofillers in the PI matrix, due to the creation of hybrid nanostructure bound by the hydrogen bond interaction [129]. Additionally, 3D hybrid networks were formed between GO and CNT and well distributed in the PI matrix containing GO-crosslinked and oxidized CNT nanofillers (Fig. 13g, h), which is regarded to be of great advantage in increasing the performance of PI matrix [129].

3.1.2 Transmission Electron Microscopy, TEM

Besides SEM analysis, TEM is a technique that also uses an electron beam to image a sample, offering a much better resolution than light- imaging techniques [130]. TEM is the best tool for calculating the scale of the NP, the grain scale, the size distribution and the morphology of hybrid nanofillers [129]. For example, analysis of the TEM images allows the confirmation of the morphology structure of nanohybrid based on exfoliated G and CNF [131]. Using a TEM image of the G-CNF hybrid, it was observed that graphene had a crumpled geometry and that CNF were found on the G surface [131]. The selected area electron diffraction pattern (SAED) from the TEM analysis showed that standard six-fold symmetry diffraction spots with the outer hexagon spots appear slightly weaker than those of the inner hexagon, which also confirms the obtained monolayer graphene, as shown in Fig. 14.

TEM images were also used by Taj et al. to confirm the existence of gold nanostructures on the 2D layer of a G hybrid [132]. The images demonstrated that it is possible to obtain a uniform distribution of gold nanostructures (2–8 nm diameters) anchored on nanosheets of G by in-situ synthesis [132]. Besides, the corrugated structure of the
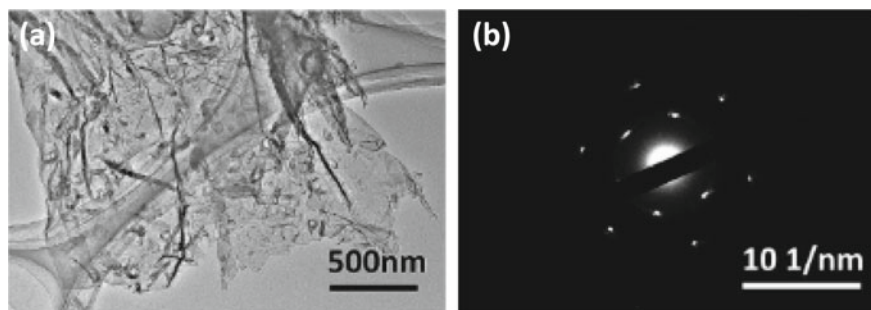
Fig. 14 a TEM images and **b** SAED pattern of graphene-chitin nanofibers (G-CNF) hybrid nanomaterial [131]
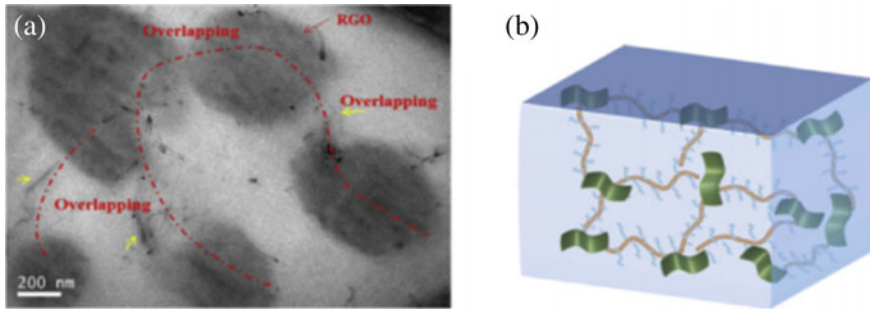
Fig. 15 TEM images of the styrene-butadiene rubber composites containing 3% rGO-CNT. **a** The red lines illustrate the pathways of heat transfer. **b** Schematic diagram of the proposed thermal conduction [133]

G sheets was possible to demonstrate [132], and it was observed that approximately 75% of the particle size distribution was with a dimension of 2–4 ± 1.2 nm, while the remainder occurs within a range of 4–8 nm [132]. Similarly, typical G-PtAu hybrid TEM images were obtained with various magnifications, showing that PtAu bimetallic nanoparticles with an average diameter of 3.3 nm are spread evenly on G nanosheets [50]. Furthermore, Taj et al. confirmed that the results of microscopy obtained by SEM and TEM are in agreement and define the novel morphology of the hybrid G-NP [132].

Yue et al. analyzed TEM images of microtomed samples at an average filler concentration of 0.1 wt% in order to examine the filler dispersion in the epoxy composites with G-CNT hybrid nanofillers [106]. For the nanohybrid epoxy composite network, the dispersion of the filler significantly increased [106]. The nanoplatelets of 2D graphene were intercalated between the nanotubes of 1D carbon, which could contribute to the creation of a network of 3D fillers, and lead to better mechanical and electrical properties [106].

Through TEM analysis, the rGO-CNT hybrid has shown a good dispersion in the rubber matrix [133]. Song et al. confirmed the introduction of CNT bridges into the isolated rGO nanosheets, which resulted in reduced interfacial thermal resistance from the filler-filler interface and the filler/rubber interface (Fig. 15a) [133]. Thus, the ultimate thermal energy of the rubber composites is transferred to strictly defined 3D channels, as demonstrated with the normal red arrows in the model shown in Fig. 15b.

3.1.3 High-Resolution Transmission Electron Microscopy

In the same way as TEM analysis technique, HRTEM is a developed transmission electron microscope imaging mode that allows direct imagery of the graphene-based nanohybrid material's atomic structure [11, 48, 62, 134]. For instance, Chouhan et al. obtained the high resolution transmission electron microscopy (HRTEM) image of

GO-Laponite nanohybrid, which indicated that the GO and Laponite layers are overlapped with each other [134]. The overlapping is a clear indicator of the interactions between the GO and Laponite layers at nanoscale [134]. The hexagonal sequence of bright spots in the selected region electron diffraction (SAED) pattern, obtained from the HRTEM analysis, showed a bright spot, identifying the group of {1100} plane perpendicular to the basal plane (0001). This indicates clearly the presence of GO sheets. Whereas in the SAED pattern, the amorphous ring pattern suggest the existence of Laponite [134].

Similarly, Fig. 16 displays TEM, HRTEM images of a silica and G-silica nanohybrid, as well as the associated select area electron diffraction (SAED) patterns [135]. It is seen that the size of the silica particles is very uniform (Fig. 16a) [135], and that the silica aerogel sample is primarily composed of amorphous and disordered structures, as disclosed in the HRTEM image in Fig. 16b [135]. Furthermore, the silica aerogel SAED pattern (Fig. 16c) reveals diffraction rings without any diffraction dots, which validates the existence of an amorphous structure of the silica aerogel [135]. Figure 16d shows a TEM image of a G-silica nanohybrid, in which many small-layered graphene layers wrinkled on a silica aerogel can be identified [135]. The HRTEM image of G-silica nanohybrid analysis revealed that thin walls as shown in Fig. 16e, usually consist of just a certain layer of graphene sheets formed from silica aerogel. As further confirmation, selected area electron diffraction (SAED)
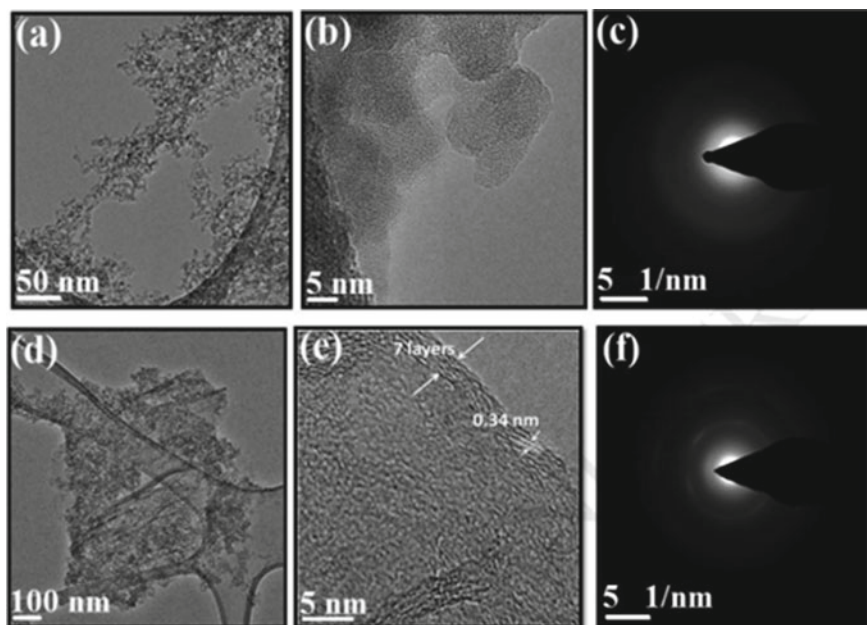
Fig. 16 TEM images of **a** silica, and **d** G-silica hybrids, HRTEM images of **b** silica, and **e** G-silica nanohybrids and equivalent SAED patterns of **c** silica, and **f** G-silica hybrids [135]

was used to uncover the crystal structure of G on silica, as can be seen in Fig. 16f [135].

3.1.4 Atomic Force Microscopy

AFM is another advanced micro-based technology used to analyze a surface in its complete, three-dimensional space, down to the nanometer size [37, 71]. The AFM techniques have been commonly used to study the G-based hybrid filler structure's physical behavior and its effect on a polymer matrix [15, 129, 136, 137]. Illustratively, AFM studies were used to investigate the morphology and measurements of the nanomaterials GO, CNC and their hybrid nanofillers GO-CNC [15]. For CNC, the AFM image demonstrated that there were needle-like nanoparticles for the as-extracted CNC, indicating that their isolation from the treated sugarcane bagasse was productive [15]. On the other hand, the GO's AFM images showed the presence of individual irregularly shaped nanosheets with identical thicknesses and different lateral sizes [15]. AFM characterization of the GO-CNC nanofiller hybrid (GO: CNC-1:2) revealed that the GO surface had become fully and densely covered with randomly arranged CNC [15].

In another study (Fig. 17), the AFM morphology of GO-CNF and rGO-CNF revealed an ultrathin GO surface (~1.0 nm thickness, ~0.6 μm size) [76]. As shown in Fig. 17a, the CNF nanofibers were partially absorbed on the GO surface; the thinness of GO-CNF hybrids was approximately 2.42 nm [76]. In comparison, the thickness of rGO-CNF nanohybrid layer was about 5.245 nm (Fig. 17b), which was much thicker than the GO-CNF specimen [76]. Xiong et al. noted that the AFM images analyses helped realize that the combination of cellulose nanofibers CNF and GO nanosheets resulted in the spontaneous creation of stable 2D hybrid nanostructures with planar GO nanosheets uniformly encapsulated in a dense network of 1D nanofibers [138]. Furthermore, it was also noticed the thick CNF coating
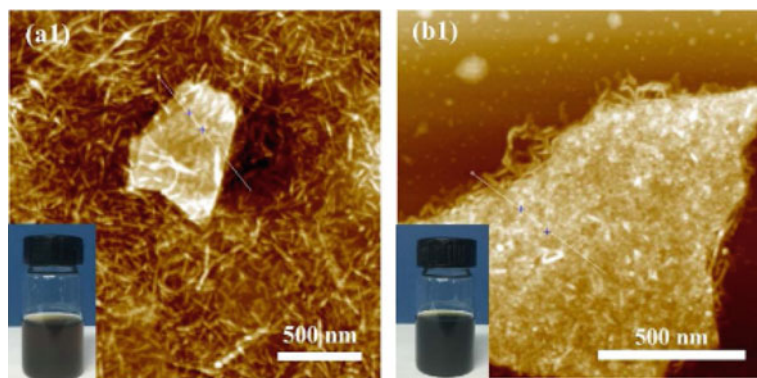
Fig. 17 AFM images of **a** GO-CNF hybrid, and **b** rGO-CNF hybrid [76]

renders them extended from the sides of GO, like long hairs produced around the sides of GO [138].

AFM was also utilized to investigate the surface morphology of the polyimide reinforced with hybrid GO-CNT [129]. It was noted that the surface roughness of the polyimide matrix increased considerably with the addition of either GO or CNT compared to that of pure PI [129]. Compared to all other polyimide-based nanocomposites, the surface roughness value decreased when incorporating the hybrid GO-CNT, and almost identical to that of neat polyimide [129].

For further illustration, Fig. 18 portrays AFM 3D topography images of pure polysulfone (PSf) and composite membranes filled with CNT, rGO and rGO-CNT nanofiller hybrids [136]. The pure PSf film micrograph was found to be coarser with a roughness of 19.89 nm, which showed that an amorphous network is built on the surface [136], While the PSf reinforced with the CNT film exhibited a roughness of 18.12 nm, it addressed improved compatibility of CNT within the PSf matrix. This is illustrated in the topographic image, which shows homogeneously scattered bright patches on the surface [136]. The PSf-rGO film micrograph showed, on the other hand, the presence of a thicker area with a layered and firmer structure, with a roughness of 21.5 nm [136]. The hybrid composite film AFM micrograph showed the presence of several convex hills and walls on the surface with a roughness of
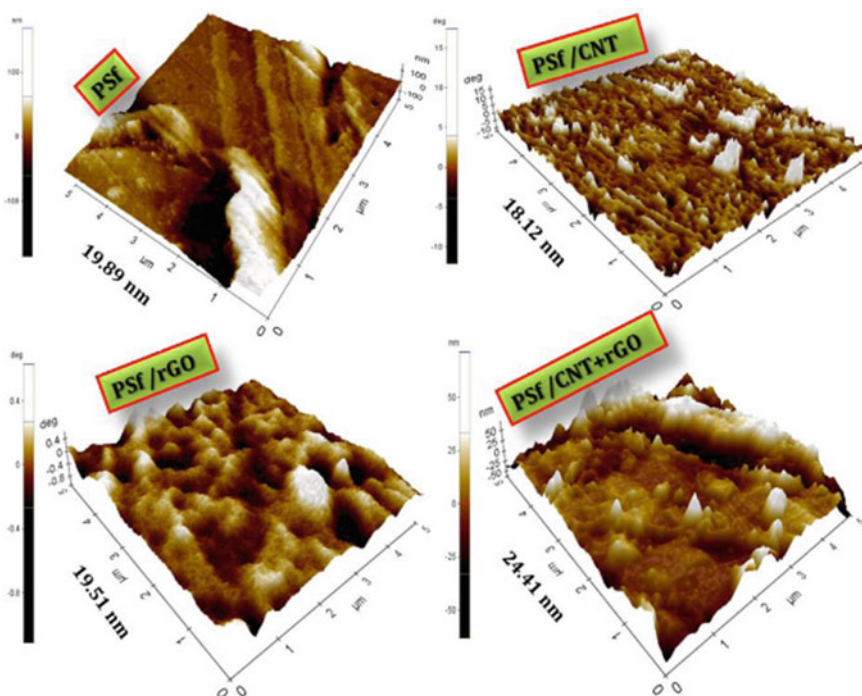
Fig. 18 AFM 3D composite samples topographical micrographs [136]

22.86 nm, which is higher than for the matrix reinforced with G and CNT alone [136].

3.2 Spectroscopy-Based Characterization

Spectroscopy characterization is the study of the interaction between material and electromagnetic radiation by means of electron and atomic energy [139–142]. Many such interactions include spectroscopy of absorption, elastic, resonance, emission and inelastic scattering [143–145]. Spectroscopic studies were essential to the development of nanohybrids and composites based on G [15, 46, 80]. There are several types of spectroscopy, though the most common types used for GF-NP based hybrid composite analysis include Fourier transform infrared spectroscopy, ultraviolet and visible spectroscopy and Raman spectroscopy.

3.2.1 Fourier Transform Infrared Spectroscopy

Fourier Transform Infrared Spectroscopy (FTIR) spectroscopy is used to demonstrate what kinds of bonds are present in a composite material by measuring at various frequencies different forms of interatomic bond vibrations [70, 146]. The FTIR spectra create a sample profile, a distinctive molecular fingerprint that can be used for screening and scanning nanofiller samples for different components based on G [12]. From an analytical point of view, by measuring the impact of molecular vibrations at the polymer and nanofiller interaction, the fraction of the interfacial polymer composite can be determined via FTIR spectroscopy [18, 147].

For instance, Pu et al. observed the characteristic FTIR spectra of GO and GO-TiO_2 nanohybrids (shown in Fig. 19) [148]. Both GO and GO-TiO_2 displayed spectra that have a large peak above 3000 cm^{-1}, resulting from the OH stretching vibrations of the H_2O and the C–OH groups [148]. GO displays the peaks for C=O at 1110 cm^{-1}, C–O–C at 1250 cm^{-1}, C–H at 1387 cm^{-1}, and C=O at 1720 cm^{-1} [148]. As for the hybrid GO-TiO_2 nanohybrid, the spectra for C=O disappeared completely, confirming the decomposition of partial oxygen comprising functional groups under microwave irradiation [148]. In addition, it was observed that the absorption edge of GO-TiO_2, relative to pure TiO_2, displayed an apparent shift [148]. This result indicated the narrowing of TiO_2's bandgap, which also supports the development of Ti–O–C bonds between GO and TiO_2 [148].

Figure 20 displays FTIR results for the main GO-SiO_2 hybrid filler (Fig. 20a) and the hybrid PLA composites (Fig. 20b) [12]. In addition to the predicted FTIR peaks for each filler in Fig. 20a, it was predicted that the peak at approximately 1420 cm^{-1} in the GO-SiO_2 nanohybrid originates from the -COOSi-group, which confirmed the desired connection between GO and silica [12]. Terzopoulou et al. used the FTIR results to compare a poly-lactic acid (PLA) composite structure when filled with hybrid fillers based on graphene and silica nanoparticles [12]. Figure 20b, particularly

Fig. 19 FTIR spectra of raw GO and GO-TiO$_2$ nanohybrid [148]
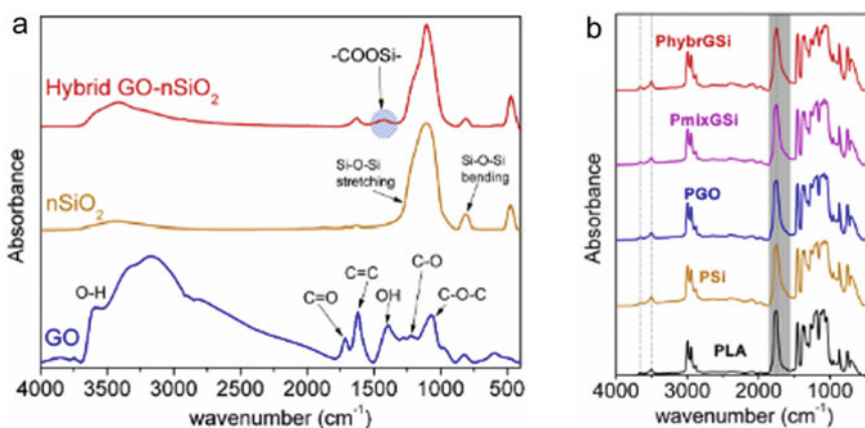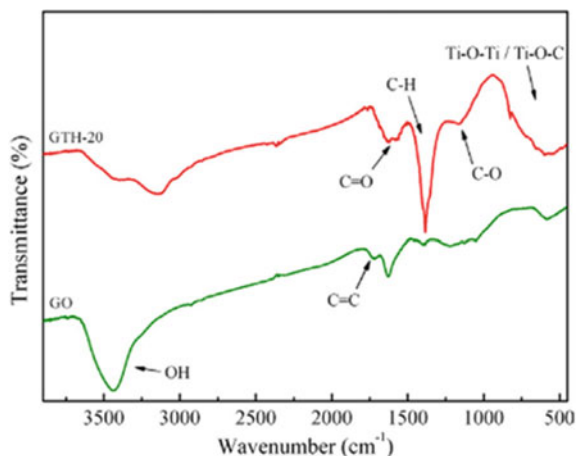
Fig. 20 Comparative FTIR spectra for **a** hybrid fillers GO-SiO$_2$ and **b** hybrid filler-based PLA composites. The major molecular vibrating groups leading to the spectra are colored grey [12]

the spectra around 1750 cm^{-1}, provided interesting information regarding the interactions between the polymer-fillers. The key sources of the peaks are the stretching and vibration of the PLA free carbonyl –C=O groups. The peak was clearly absent in the smooth GO and SiO$_2$ hybrid spectra (Fig. 20a), which affirms the polymer-filler interaction [12].

3.2.2 Ultraviolet-Visible Spectroscopy

In the same manner, as FTIR, Ultraviolet–visible spectroscopy (UV-Vis) technique applies to spectroscopy of absorption and reflectance within the section of

the ultraviolet and the complete, adjacent visible spectral region [149]. UV-vis-spectrophotometry was used as a function of light wavelength for determining light transmittance through graphene-based hybrid nanocomposite films [44, 150]. Furthermore, UV spectroscopy is an important method for the quantitative detection of various analytes in G based hybrid materials, such as transition metal ions (Cu, Au, Ag, Pb, Fe, Zn etc.) and conjugated organic compounds [22, 24, 151]. Such in the case of Wang et al. who analyzed the UV vis-à-vis spectra of rGO-TiO$_2$, rGO-Ag–TiO$_2$ and rGO-Pt–TiO$_2$ hybrids and found that all had a wide absorption range of 300–350 nm due to the TiO$_2$ absorption [151]. It was reported that the absorption in the rGO-Ag–TiO$_2$ nanohybrid spectrum at around 431 nm resulted from the excitation of a surface plasmon in noble metal nanoparticles and further confirmed the formation of Ag particles on the rGO-TiO$_2$ surface [151]. No apparent surface plasmon absorption was observed for the rGO-Pt–TiO$_2$ nanohybrid in the visible area [151].

UV-Vis spectrometry analysis was performed to investigate the electronic interaction of the G and nanometals (silver (Au) and gold (Ag)) [24]. Compared to the G spectra, additional peaks were observed for all the hybrids due to metal nanoparticles insertion [24]. Characteristic peaks at 545 and 410 nm were attributed respectively to Au and Ag surface plasmon resonance (SPR) [24], indicated the presence of Ag and Au nanoparticles on the surfaces of graphene. The G-AuAg's UV-Vis spectrum showed a strong absorption peak at 477 nm, which is noticeably different from G-Ag and G-Au hybrids peaks positions [24]. In order to study the conjugated structure of exfoliated graphene in G-CNF hybrid nanomaterials, UV-vis absorption spectra were analyzed for GO, rGO, and G-CNF [131]. As illustrated in Fig. 21, The UV-vis hybrid spectrum shows a high absorption peak of about 267 nm, close to that of rGO, whose conjugated graphic structure has been restored by chemical reduction, relative to that of GO [131].

UV-Visible spectrometry measured the anti-UV properties of polylactic acid (PLA) and nanocomposite films [44]. The pure PLA film absorbed strongly ultraviolet light (200–400 nm) and visible light (400–800 nm), by 92% transmittance [44]. Because of the combination of GO and ZnO nanoparticles, which increases the light

Fig. 21 UV-vis spectra of GO, rGO, G-CNF and exfoliated graphene obtained in N-Methyl-2-pyrrolidone (NMP) or in Sodium dodecyl sulfate (SDS) aqueous solution (presented in the graph as GO, RGO, GE (NMP) and GE (SDS), respectively) [131]
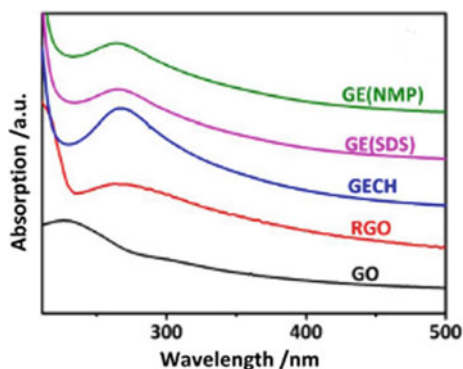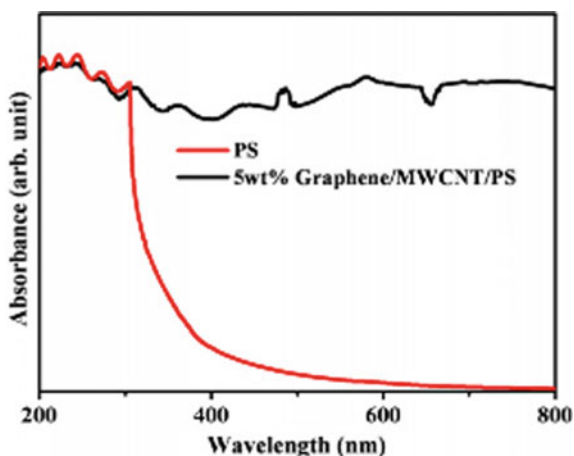
absorption spectrum, the film displayed good anti-UV safety and good transmission of visible light when combined with GO-ZnO nanohybrid [44]. It was noticed that when the GO-ZnO content increases, the nanocomposite films obtain excellent absorption properties both in the UV region and in the visible region [44]. Similarly, in a study, Patole et al. presented UV-visible spectra of the polystyrene (PS) hybrid nanocomposite at wavelengths from 200 to 800 nm as shown in Fig. 22. PS spectra displayed peaks from lower to higher at approx. 200–400 nm led by associative interactions between the phenyl groups [35]. Similar peaks, less intense, appeared in the hybrid nanocomposite caused by addition of G-CNT hybrid, where the PS chains get tangled and trigger a screen effect limiting the absorption of the light beam [35].

3.2.3 Raman Spectroscopy

Raman spectroscopy is a valuable tool for performing carbon nanomaterials characterization, especially for identifying the order of graphene particles layers [75, 152]. Raman Spectroscopy was done to analyze the efficiency of the graphene nanosheets before and after a hybrid nanocomposite preparation [59]. Much information like grain boundaries, edge, disorder, doping, thickness, thermal conductivity and strain of graphene, can be obtained from the Raman spectrum and its characteristic s under various physical conditions [62, 68].

Considering the example in Fig. 23, Raman characterization that showed D band intensity ratios to G band (ID/IG) of GO, rGO, and G-CNT hybrid, which was around 0.97, 0.82, and 1.10, respectively [62]. These results confirmed that the amorphous carbon layer is formed during the CNT growth process [62]. In a different study, Das et al. analyzed the G-CNT hybrid's Raman spectrum, where all the typical carbon nanostructure bands (G, D, and 2D/2 G) were shown [153]. The full-width half maxima (FWHM) of 2D band were 30 for mono and bilayer graphene and 69.14 for

Fig. 23 Raman spectra of GO, RGO and G-CNT hybrid [62]
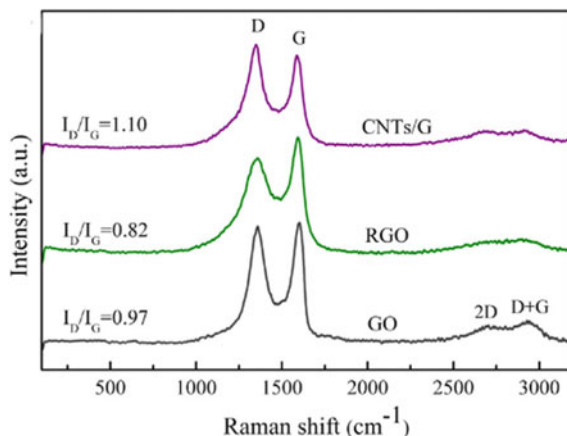
G-CNT [153]. It has been noted that the 2D peak enlargement can be attributed to the layer increase in the G architecture [153]. Likewise, the blue shift in the G-CNT hybrid band positions also suggested a relatively stronger bond between the G and CNT [153].

Xu et al. reported that G-metal contact, together with physisorption and chemisorption, cause the deviations of the G-band responses and the shifts of 2D-band frequency [154]. Furthermore, it was noted that the Cr, Ag and Al's interaction with G lead to a blueshift of the G peak, while Ni and Ti result in a redshift for the G peak [154]. The interactions of G and electrode metals like Ni, Ti, Al, Cr, and Ag introduced shifts in the peak G and the peak 2D [154]. Ni and Ti contributed to the peak G redshifts. Raman spectroscopy was reported to be an effective method for graphene studies, even if it interacts strongly with transition nanometal surfaces [154].

In another study, Raman analysis spectrum of GO displayed a D band at $1359 \, cm^{-1}$ as well as a G band at $1602 \, cm^{-1}$, while the rGO-Co_3O_4 nanohybrid D and G bands were at $1330 \, cm^{-1}$ and $1596 \, cm^{-1}$, respectively [9]. It was further noted that the redshift of the G band from 1602 to $1596 \, cm^{-1}$ for the rGO-Co_3O_4 nanohybrid was attributable to the recovery of the carbon atom's hexagonal network [9]. The nanohybrid rGO-Co_3O_4 exhibited a comparatively higher D-to-G-band intensity ratio (1.16) compared to the GO (0.96) [9]. Similarly, with regards to pure graphene D-to-G intensity ratio (0.497), the graphene-titanium dioxide hybrid D-to-G intensity ratio increased by 1.5 times (0.7) [155]. These results confirmed that after the chemical reduction of GO, there was the creation of a new graphitic domain [9, 155].

Research has been done using Raman spectroscopy to study the poly(pyronin Y) and the impact of rGO-silver (Ag) nanohybrid on the polymer [20]. It was observed that the rGO-Ag nanohybrid Raman spectrum resembles that of rGO sheet [20]. Furthermore, it was noticed that the ID/IG ratio for the rGO-Ag nanohybrid was 0.91, which was lower than that the rGO sheet, which may be an indication of Ag nanoparticles doping by filling the gaps left after extracting oxygen and iodine
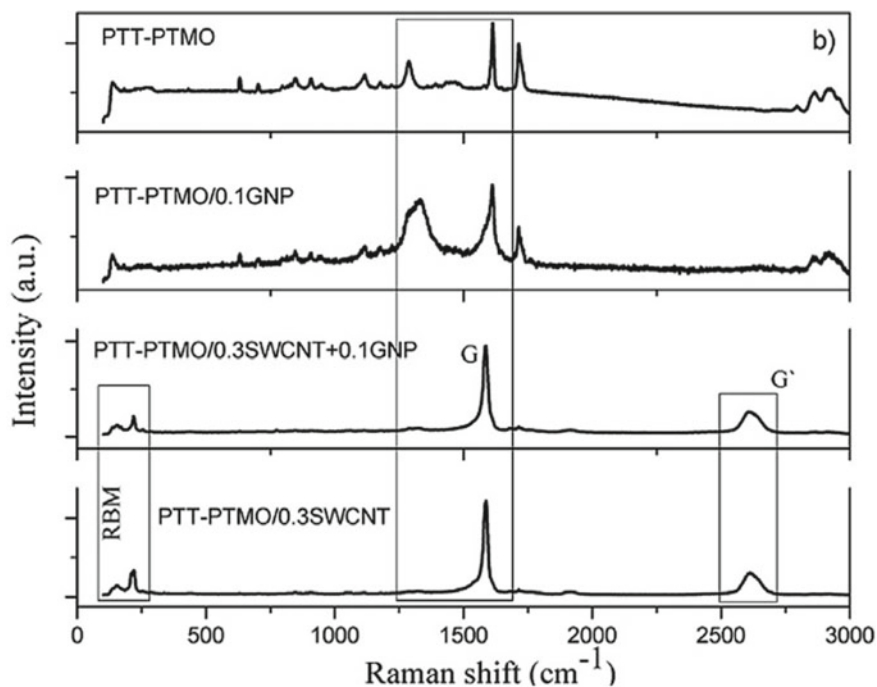
Fig. 24 Raman spectra of pure and hybrid PTT-PTMO [68]

molecules, decreasing the defect density [20]. Moreover, it was noted that for the poly(pyronin Y)/rGO-Ag hybrid nanocomposite Raman spectrum was considerably different than that of the fillers, due to the presence of poly (pyronin Y) as a matrix [20].

Raman spectroscopy was also performed for hybrid composites based on poly (trimethylene terephthalate-block-poly (Tetramethylene oxide) (PTT-PTMO) and G-CNT nanofillers as shown in Fig. 24 [68]. It was noted that the Raman spectrum corresponding to the hybrid nanocomposite with G-CNT hybrid nanofiller was almost similar to the nanocomposite with the CNT filler alone [68]. Therefore, CNT were proposed to be an indicator in deciding the properties of the hybrid nanocomposites [68]. In a different study, the structural study of the rGO, CNT, G-CNT, Polymethyl-methacrylate (PMMA), and PMMA/G-CNT hybrid composite was performed using Raman spectroscopy [16]. It was noted that PMMA Raman spectra display all of the typical PMMA peaks, except D and G bands [16]. After the G-CNT nanohybrid filler was integrated into the PMMA polymer matrix, D and G bands began to appear [16]. Furthermore, it was found that as the content of the G-CNT nanofiller increased, the intensity of the bands increased and showed a slight shift in peak position of the D and G bands, independent of the PMMA polymer peaks. This was related to chemical interactions between the PMMA polymer particles and the G-CNT nanohybrid filler particles [16].

3.3 X-Ray-Related Characterization

3.3.1 X-Ray Diffraction

X-ray methods are instrumental in providing data on the chemical composition and crystalline and amorphous structures of materials [40]. The X-ray Diffraction (XRD) and X-ray photoelectron spectroscopy (XPS) analysis are the most commonly used methods for characterizing composite hybrid materials [19, 151, 156]. XRD operates on the concept of diffraction from various planes of the atom generating a pattern of diffraction (diffractogram), that contains data of the atomic structure of the crystal. XRD is also used to detect a polymorph phase and determine the abundance of a phase to classify the hybrids and compare the compositional efficiency of composites [12, 151, 155].

Using XRD analysis of rGO-CNC nanohybrid, it was possible to confirm that the CNC were decorated on the rGO surface [40]. It was confirmed by noticing that after reduction, the strong (002) GO diffraction peak at $2\theta = 11.8°$ disappeared in the rGO and rGO-CNC hybrid [40]. Four defined diffraction peaks at 14.9, 16.6, 22.7 and 34.5° were reported, related to the presence of the crystalline region in the CNC and rGO-CNC nanohybrid, which suggests that the rGO-CNC crystalline structure is undamaged after GO reduction [40].

In another example, XRD was used to analyze and characterize the crystal structure patterns of the GO, rGO, Ni–Al alloy nanoparticles and an rGO-Ni–Al hybrid nanofiller (Fig. 25) [48]. It was observed that the GO's XRD pattern (Fig. 25) displayed a sharp peak at 10.48, suggesting the interplanar spacing of the (002) is around 0.85 nm, which is explained by the turbostratic structure of the stacked graphene plates [48]. The diffraction peaks (Fig. 25) of 11.48°, 23.18°, 35.28°, 39.38° and 46.58° correspond to the respective planes (003), (006), (012), (015) and (018), which is typical for a Ni–Al alloy hydrotalcite [48]. Furthermore, the XRD pattern

Fig. 25 XRD patterns of the obtained GO, rGO, Ni–Al layered double hydroxide and rGO-Ni–Al (rGO-LDH) [48]
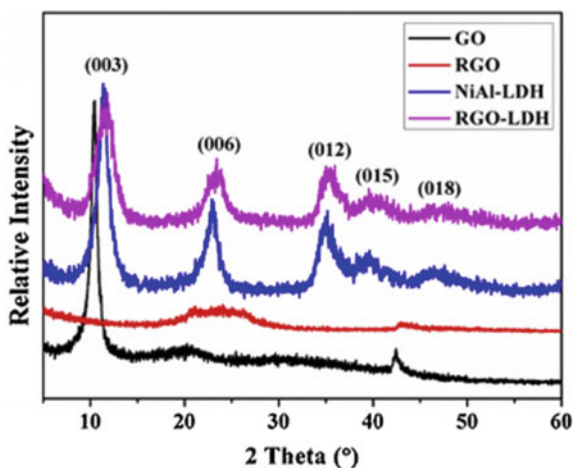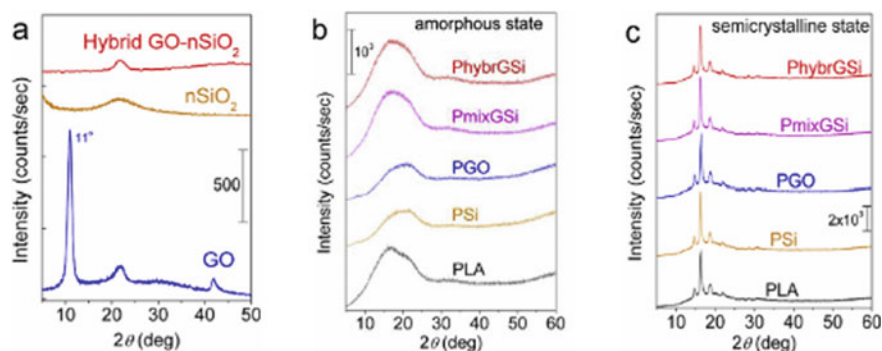
Fig. 26 XRD spectra for **a** the nanofiller particles (GO and SiO$_2$), and **b**, **c** pure polylactic acid (PLA) and PLA hybrid nanocomposite **b** amorphous and **c** semicrystalline nanocomposites [12]

of rGO-Ni–Al hybrid nanofiller is almost similar to that of pure Ni–Al alloy, and no characteristic peaks of the rGO are observed. These findings suggested that the Ni–Al alloy nanoparticles were well anchored on the rGO nanosheets, effectively preventing the graphene from being restacked [48].

In order to investigate the impact of integrating rGO and CNC on the crystallinity of the polylactic acid (PLA) matrix, the structure of CNC, the rGO filler and the neat PLA and rGO-CNC reinforced PLA nanocomposite were characterized by broad angle XRD analysis [78]. A broad diffraction band at $2\theta = 16.5°$ was depicted from the XRD spectra of the neat PLA polymer, suggesting a PLA's XRD-amorphous structure [78]. The XRD curves of the nanocomposite reinforced with rGO-CNC showed no peak of CNC and rGO at low filler contents, other than the wide prominent peak at $2\theta = 16.5°$, confirming a typical amorphous material [78].

In a different study, a polymer hybrid nanocomposite in its amorphous (melt-quenched) and semicrystalline (annealed) structures were investigated. Figure 26a displays the XRD spectrometers for the fillers separately and (Fig. 26b, c) for the nanocomposite [12]. Compared to the stuck-formed GO, it was confirmed that the complete exfoliation of the hybrid GO-SiO$_2$ was achieved [12]. This was confirmed by the absence of XRD peaks in the nanohybrid GO-SiO$_2$ at $2\theta \sim 10°$ in Fig. 26a. [12]. For the polymer hybrid nanocomposites, the XRD findings from Fig. 26b, c showed no observable alternations between the polymer matrix and the polymer hybrid nanocomposites in the reported XRD spectra [12]. Therefore, no significant alteration is observed in the crystalline structure of the neat polymer, nor in the polymer hybrid nanocomposites [12].

3.3.2　X-Ray Photoelectron Spectroscopy

X-ray photoelectron spectroscopy (XPS) is another method for the study of composite material's surface chemistry [157, 158]. The basic XPS principle is to irradiate

the surface of the studied material with X-rays to eject electrons from its surface [158]. The energy of these electrons, which is used to determine the surface chemical composition, is then measured [158]. XPS was used to analyze the elementary composition and the chemical state of a wide variety of solid samples from hybrids to composite materials [19, 49]. Besides, XPS was used in this study to determine the oxidation states of metal atoms, and the nitrogen bonding configuration of a G-$MnCo_2O_4$ nanohybrid [49]. It has been demonstrated that the observed characteristic peaks suggested that the hybrids contain carbon (C 1 s peak), oxygen (O 1 s peak), nitrogen (N 1 s peak), cobalt (Co 2p peak) and manganese (Mn 2p peak) elements and that the Co-to-Mn ratio is approximately 2 which was a close match to the modeled ratio [49]. Similarly, the chemical composition of rGO and rGO-Au nanohybrid was analyzed using XPS spectra of C1s and O1s [19]. XPS spectra of C1s and O1s, which confirmed the effective chemical reduction of GO and Au nanoparticles were present in the rGO-Au nanohybrid [19].

The XPS measurements confirmed the efficiency of the surface functionalization and the reduction of the hybrid nanofiller rGO-CNF [76]. Figure 27 shows that the intensity of the oxygen-containing group peaks for C1s binding region of rGO-CNF clearly decreased compared with that of the GO-CNF nanohybrid, indicating an efficient GO reduction [76].

Similarly, the surface chemical composition of the soy protein (SPI) hybrid nanocomposite films reinforced with GO-CNF and rGO-CNF were surveyed by XPS measurements [76]. The effective application of tannic acid coating on the SPI/GO-CNF structure was demonstrated in the SPI/rGO-CNF nanocomposite film spectrum by an increase in C1s and O1s peaks [76]. In addition, it was noted that the peak corresponding to the C=OH groups with rGO-CNF integration was significantly increased in the SPI/rGO-CNF nanocomposite film, which indicated the reaction potential of rGO-CNF with SPI matrix [76].

Fig. 27 Full XPS spectra **a** GO, CNFs, GO-CNFs and rGO-CNFs [76]
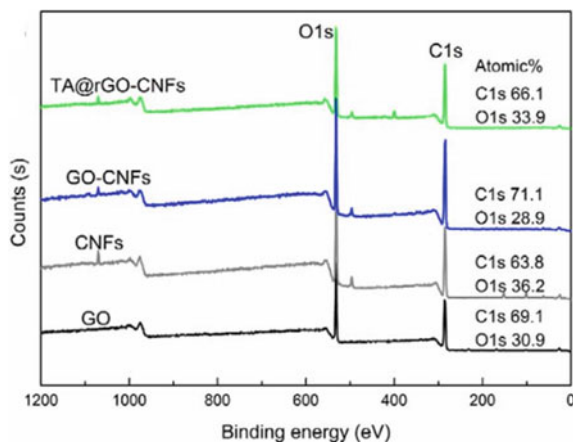
3.4 Thermal Analysis

3.4.1 Thermal Stability Analysis

Thermal analysis techniques are essential for a wide range of materials such as polymers, composites, pharmaceutical products, food packaging, fuels, energy, chemicals, and many more [70, 72]. These techniques, such as thermogravimetric analysis (TGA) and differential scanning calorimetry (DSC), usually measure heat transfer, weight loss, difference in size, or mechanical properties, as a function of change in temperature [156]. The thermogravimetric analysis (TGA) or derivative thermogravimetry (DTG) is an important laboratory tool used for the characterization of composite material. It measures the mass of material as temperature changes over time [159]. The TGA/DTG technique was used through the desired temperature range to provide insight into mass changes of G-NP hybrid and its nanocomposites [12, 31, 48, 159, 160]. In the case of the GO-CNT-CNF hybrid's, thermal stability was evaluated and two weight-loss mechanisms were demonstrated using TGA analysis [160]. It was found that a weight loss occurred in the temperature range 144−226 °C, due to the removal of oxygen-containing groups from the GO nanosheets [160]. Moreover, another weight loss was observed over the temperature range 233 − 413 °C, which agreed with the decomposition of the CNF in the GO-CNT-CNF hybrid [160]. In comparison, it was noted that in the TGA study of the rGO-CNT-CNF hybrid, there was only one weight loss phase, and it was correlated with the CNF decomposition. Such findings led to the interpretation that a successful reduction of the GO nanosheets to rGO [160].

Similarly, Tajik et al. examined the G-silica nanohybrid using TGA and DTG. They showed that there existed three thermally stable regions [159]. Due to its high percentage of silica phase, an effective thermal stability can be observed up to 549.06 °C at the first region [159]. Then, the second region was relevant to the abrupt reduction of sample weight from 549.06 to 629.78 °C likening it to the complete loss of G [159]. Therefore, the amount of G in the G-silica nanohybrid was roughly evaluated by the TGA and DTG analysis and was determined to be 16 wt% [159]. Hence, the TGA and DTG measurements have approved the formation of G nanosheet in the nanohybrid [159].

The TGA analysis was also used to characterize the thermal properties of the neat PVA film and the G-CNT hybrid nanofiller-reinforced PVA films at different hybrid filler ratio [31]. Both the neat PVA and the PVA hybrid composite films have been found to decompose through a two-step process [31]. First, a weight loss phase resulting from a thermal decomposition of PVA was estimated to take place at around 220–350 °C and a second step related to the thermal decomposition of the residue was considered to be at around 400–500 °C [31]. The TGA curve of the PVA hybrid nanocomposite film was shifted to a slightly higher temperature in comparison with that of the pure PVA film [31]. The PVA hybrid nanocomposite film peak temperatures at 314.4 and 440.3 °C, were approximately at 19.8 and 7.4 °C slightly higher than those of the neat PVA, which suggested to be due to enhanced compatibility

Table 1 TGA analysis data of PMMA neat polymer and PMMA reinforced with rGO, and Ni–Al alloy nanoparticles and rGo-NiAl hybrid nanofiller [48]

Sample	$T_{-5\%}$ (°C)	T_{max} (°C)	Residue at 750 °C (wt%)
PMMA	332	382	0.6
PMMA/rGO	320	384	1.4
PMMA/NiAl	326	386	2.2
PMMA/rGO-NiAl	330	380	3.7

between the PVA and the G-CNT hybrid nanofillers [31]. Similar findings were reported for the G-CNT as a hybrid reinforcement of poly(ether-ether-ketone) and poly(styrene-b-butadiene-b-styrene) [35, 112, 161].

TGA has further been used to analyze the effect of a rGO-Ni–Al hybrid on the thermal stability of the polymethyl methacrylate (PMMA) matrix as shown in the Table 1 [48]. Neat PMMA's thermal degradation demonstrated a single phase, and no residues were left [48]. It was remarked when rGO was added in the polymer matrix, the $T_{-5\%}$ (defined as the temperature where 5% of weight loss occurs) decreased by 12 °C because of the high thermal conductivity of rGO [48]. It was found that the maximum rate of decomposition decreases significantly, with the little residue possibly remaining because of the rGO that prevents the final thermal degradation of the polymer PMMA [48]. In the case of PMMA polymer reinforced with Ni–Al alloy, more char residue (2.2 wt%) remained, due to the catalytic carbonization effect of layered double hydroxide [48]. An improved thermal resilience of the PMMA polymer was achieved as demonstrated by a higher residue of 3.7 wt%, attributable to the combination of the rGO's physical barrier effect and the Ni–Al alloy's catalytic carbonization [48]. The TGA summary data of the PMMA neat polymer and the PMMA hybrid nanocomposite are given in Table 1.

3.4.2 Differential Scanning Analysis

Differential Scanning Calorimetry (DSC) is another thermal analysis method in which the heat flow in or out of a material is determined as a variable of temperature or time. In contrast, the material is exposed to a temperature-regulated system [35, 112]. DSC analysis was performed to evaluate the degree of crystallinity (X_c), the fusion heat (ΔHf) and the melting temperature (T_m) of graphene based nanohybrid composites [12, 15, 35, 40]. The degree of crystallinity (χ_c) is determined as follows: $\chi_c = \Delta H_m / \Delta H_0$ where ΔH_m is the evaluated melting enthalpy from DSC curves, and $\Delta H0$ is the 100% crystalline melting enthalpy. In a study by Patole et al., DSC analysis were done to examined the impact of G-CNT hybrid filler in the thermal transformation of a segmental motion of the polystyrene (PS) polymeric chain [35]. It was observed that the existence of such a carbonaceous kind of filler enhanced thermal effect since the temperature needed to modify the behavior of the PS chains in hybrid nanocomposite from the glassy to the rubbery state was raised by 70 °C in comparison with the pure PS [35]. Furthermore, a high shoulder peak between 150

Table 2 Glass transition temperature (T_g) and melting conditions of PVA and its hybrid nanocomposite with a 0.5, 0.75 and 1.0 wt% reinforced G-CNT filler material [31]

	T_g (°C)	ΔH_m (J/g)	X_c (%)	T_m (°C)
PVA	77.3	67.24	48.5	221.24
PVA/0.5 wt% G-CNT	79.2	67.76	48.9	223.10
PVA/0.75 wt% G-CNT	80.3	67.68	48.8	223.92
PVA/1 wt% G-CNT	81.5	67.71	48.9	221.68

and 170 °C was also observed [35]. It was proposed that the thermal transformation started to become flexible from 150 °C due to the PS polymer chain at the edge of G, which was not fully covered by the carbonaceous fillers [35]. The shielding effect was caused by the presence of CNT, which is sandwiched between two graphene flakes and surrounded by the polymer chain PS [35].

Similarly, DSC analysis was used to evaluate the temperature of the glass transition (Tg) of pure PVA and its nanocomposite film, as summarized in Table 2 [31]. It was noted that PVA with 1 wt% G-CNT composite film exhibited 81.5 °C higher T_g than the pure PVA film (77.3 °C) [31]. The rise in T_g showed that PVA's successful attachment to graphene nanosheets limited the PVA chains' segmental motion [31]. It was further noted that there is a strong interfacial interaction between the G-CNT matrix and the PVA matrix, which benefits the successful transfer of load [31]. Correspondingly, For the GO-CNC hybrid nanofiller containing the high amount of GO (GO:CNC-2:1), the impact of nanofillers on the PVA's glass transition (T_g) and melting (T_m) temperatures from DSC is more significant because the (PVA-GO:CNC-2:1) exhibited a higher T_g and T_m compared to (PVA-GO:CNC-1:1) and (PVA-GO:CNC-1:2) [15].

3.5 Mechanical Characterization

3.5.1 Tensile Analysis

Polymer composites' mechanical properties rely on their structure at the nano- and micro-scales [31, 33, 109]. Generally, a good dispersion and a strong interfacial interaction between particles and the selected polymeric matrix induce superior mechanical properties of the polymer composite materials [30, 33, 106]. This was well attested by comparing the tensile stress–strain curves, highlighting that the compressive strength, Young's modulus and breaking elongation of well-dispersed G-NP hybrid composites are significantly higher than those observed for composites based on G or NP alone [11, 112, 161].

For instance, Fig. 28 demonstrates the tensile strength and the Young's modulus of polyvinyl chloride (PVC) film. It was noted that the Young's modulus with rGO-ZnO fillers varying from 5 to 20 wt% and PVC films with G-Zno hybrid fillers [11].
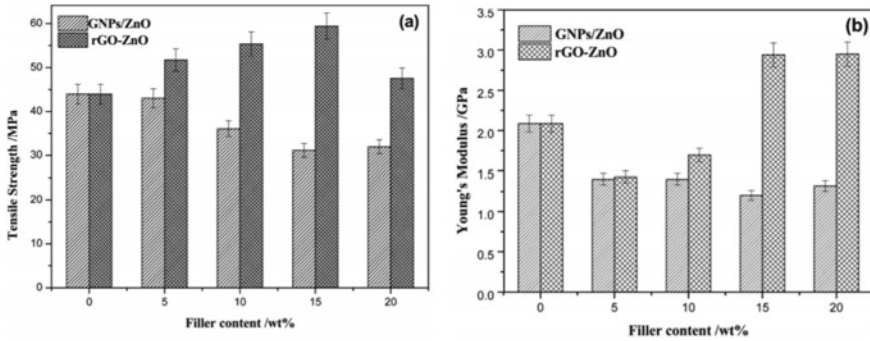
Fig. 28 **a** Tensile strength and **b** Young modulus of polyvinyl chloride (PVC) film incorporated with the specific ratio of G-ZnO and rGO-ZnO fillers [11]

Indeed, because of the poor interaction and aggregation of fillers, the tensile strength of PVC with G-ZnO fillers decreased with the increase of the filler material [11]. In comparison, it was found that PVC's tensile strength was obviously enhanced by adding rGO-ZnO hybrids, even at a high fillers content (20 wt%) [11]. It was also observed that the addition of G-ZnO hybrid particles had a negligible impact on the PVC's young modulus [11]. These results suggested that strong interfacial interaction occurred between rGO-ZnO hybrid particles and PVC chains but the interfacial interaction between G-ZnO hybrid particles and PVC chains were weak [11].

Several studies show that mechanical properties increased after reaching a critical GO-CNT content added into hybrid nanocomposites [129, 133]. Better mechanical properties could be achieved by using a homogenous dispersion and alignment, preventing the particles agglomeration and a better load transfer to filler material. For example, a uniaxial tensile measurement was used to investigate the mechanical properties of neat polyimide and its nanocomposites [129]. The tensile strength, Young modulus, toughness of fracture and strain at break of pure PI were found to be 74.3 MPa, 2.47 GPa, 12.71 MPa and 21.4%, respectively [129]. The strength and Young's modulus of the polyimide matrix were increased with the addition of GO, while the resilience of the strain at break and fracture significantly decreased [129]. However, by adding a small amount of CNT, the reinforcing efficiency of GO on polyimide was enhanced by 86%, 56%, 220% and 78% on the tensile strength, modulus, toughness and strain at break respectively, compared with those of the neat polyimide [129].

3.5.2 Dynamic Mechanical Analysis

Dynamic mechanical analysis (DMA) is the most useful tool for studying the viscoelastic condition of polymers and their composites [21, 30]. DMA analysis is defined as a function of temperature by the bending elastic modulus and damping
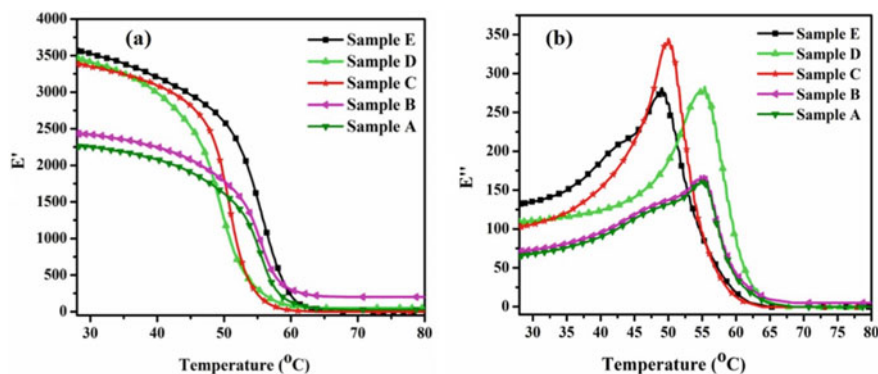
Fig. 29 E' and E'' values obtained for the fabricated hybrid films obtained by DMA (Sample A: pure PLA and Sample B-E: PLA nanocomposite with G-CNC hybrid filler with ratio of 1:2, 1:4, 1:6 and 1:10 respectively) [38]

properties of the G-NP based hybrid composites. DMA analysis was used to study mechanical behaviors of polymers with different hybrid nanofillers such as G-CNT [161], G-SiC [162], G-TiO$_2$ [46], GO-CNT [112], rGO-CNC [38], etc. As a function of temperature in tensile mode, the dynamic mechanical behavior of the produced polylactic acid (PLA) hybrid nanocomposite films was calculated by DMA in terms of storage modulus (E') and loss modulus (E'') as shown in Fig. 29 [38]. By adding modified rGO-CNC hybrid in the PLA, it was observed that the E' values were enhanced by approximately 1.6 times for rGO-CNC based PLA compared to the neat PLA at 28 °C [38]. It was noted that the increase in E' values with increasing CNC concentration in the rGO-CNC hybrid could be related to the cross-related structure formation, enhancement of crystallinity (more organized regions formed) and better dispersion of rGO-CNC in the PLA matrix, resulting in improved adhesion between hybrid and polymer [38].

Similarly, the E' and loss factor (tanδ) of the studied G and CNC based natural rubber composites were investigated using DMA as a function of temperature (-30 to 80 °C) [39]. It was observed that the natural rubber composite filled with G, displayed the highest E' when the temperature was lower than the temperature of the glass transition [39]. It was also noted that natural rubber composites filled with CNC displayed a similar storage modules above the glass transition temperature (T_g) in comparison with the pure natural rubber [39]. It was concluded that the addition of G-CNC hybrid had no influence on the composites' glass transition temperature [39].

In other research works, the DMA findings showed a major enhancement of the E' and T_g in the GO-ZnO based poly-lactic acid (PLA) hybrid nanocomposite films [44]. The tanδ specified as the ratio of the loss module to the storage module displayed a peak around 60–80 °C corresponding to the glass transition of the PLA polymer chains [44]. The T_g values for pure PLA increased from 65.45 to 70.90 °C for the PLA nanocomposite reinforced with 0.5 wt% GO-ZnO filler [44]. Furthermore,

it was reported that this effect was caused by the large specific surface area of the GO sheets and the reinforcement effect of loaded ZnO nanoparticles on the GO surfaces, strong interfacial action was effectively created and the mobility of PLA chains was reduced [44].

4   Conclusion

The characterization of hybrid nanocomposites is fundamental to obtain important information on these materials, such as: (1) the hybrid filler distribution in the polymer matrix, (2) the effect of the filler surface modification on the filler dispersion and composite properties, (3) interactions of the hybrid filler with the polymer chains, (4) changes in the process parameters on the resulting morphology and properties, (5) broad range of properties to establish potential applications of nanocomposites. This chapter has provided the advances on recent characterization techniques for the nanocomposites specifically prepared by the incorporation of G-NP as hybrid fillers.

Major categories of hybrid fillers and nanocomposites based on G and NP were also briefly summarized in their preparation and proposed chemical structures. The exceptional morphological, chemical, thermal, and mechanical properties demonstrated for hybrids of G-NP make of them an excellent candidate for strengthening nanocomposites. It is also worth noting that different G-NP hybrid fillers influence high specific properties such as mechanical and thermal properties of the polymeric matrix, but how effective the influence is based solely on their degree of dispersion within the matrix because agglomeration of the hybrid nanofillers significantly reduces or causes more detrimental impact on the hybrid nanocomposite.

The most significant characterization techniques in this field of research were reviewed and the relevant literature existing for G-NP based polymer nanocomposites was highlighted. Hence, attention was given to the numerous methods of analysis in the available literature such as the microscopy techniques SEM, TEM, HRTEM and AFM, spectroscope technologies (FTIR, UV-vis and Raman), X-ray related analysis (XRD and XPS), Thermal analysis (TGA/DTG and DSC) and mechanical characterization methods.

Recent studies of fillers and nanocomposite based on G-NP have been represented using various microscopic techniques, such as SEM, TEM, and AFM. The capabilities of each microscopy technique allow for analysis of various aspects of hybrid fillers and nanocomposites. It was also highlighted that the information obtained by the spectroscopic techniques (FTIR, UV-vis and Raman) involves a number of aspects, such as the chemical composition of the samples, the binding of the surfactants to the surface of the nanoparticles, the intercalation of the modifiers in the basal spacing of the hybrid fillers and the presence of an intermolecular interaction between the hybrid nanofillers and the polymer matrix. In the case where the optical behavior of nanocomposites is defined, UV-vis analysis is performed, which shows the peak wavelength.

For the X-ray based characterization, XRD was used to measure the effectiveness of the filler on crystallization and lamella thickness. In contrast, XPS was used to investigate a wide variety of surface modifications on graph fillers and polymeric materials. Thermal analysis is essential to the design of materials for heat management services: because thermal properties of a composite material boost and guarantee a system's service life as well as reduce hazard. At the same time, mechanical characterization is important to understand hybrid nanocomposite characteristics in advanced applications such as packaging, automotive, sensor technology and other thermomechanical facilities. All of these techniques will be suitable and essential to understanding the better formulation of G-NP based hybrid composites for a wide range of different technological applications. The developments in the above methods will provide more knowledge in this field in the near future, as well as greater insight into G-NP based hybrid fillers and composites structures.

References

1. Khin MM, Nair AS, Babu VJ, Murugan R, Ramakrishna S (2012) A review on nanomaterials for environmental remediation. Energy Environ Sci 5(8):8075–8109
2. Kassab Z, Abdellaoui Y, Salim MH, El Achaby M (2020) Cellulosic materials from pea (Pisum Sativum) and broad beans (Vicia Faba) pods agro-industrial residues. Mater Lett 280:128539
3. Kassab Z, Abdellaoui Y, Salim MH, Bouhfid R, Qaiss AEK, El Achaby M (2020) Micro- and nano-celluloses derived from hemp stalks and their effect as polymer reinforcing materials. Carbohydr Polym 245:116506
4. Gunjakar JL, Kim IY, Lee JM, Jo YK, Hwang SJ (2014) Exploration of nanostructured functional materials based on hybridization of inorganic 2D nanosheets. J Phys Chem C 118(8):3847–3863
5. Devi MM, Sahu SR, Mukherjee P, Sen P, Biswas K (2015) Graphene: a self-reducing template for synthesis of graphene-nanoparticles hybrids. RSC Adv 5(76):62284–62289
6. Kumar S, Raj S, Jain S, Chatterjee K (2016) Multifunctional biodegradable polymer nanocomposite incorporating graphene-silver hybrid for biomedical applications. Mater Des 108:319–332
7. Mittal G, Dhand V, Rhee KY, Park SJ, Lee WR (2015) A review on carbon nanotubes and graphene as fillers in reinforced polymer nanocomposites. J Ind Eng Chem 21:11–25 (Korean Society of Industrial Engineering Chemistry)
8. Tabandeh-Khorshid M, Kumar A, Omrani E, Kim C, Rohatgi P (2020) Synthesis, characterization, and properties of graphene reinforced metal-matrix nanocomposites. Compos Part B: Eng 183:107664 (Elsevier Ltd.)
9. Wang GS et al (2014) Fabrication of reduced graphene oxide (RGO)/Co_3O_4 nanohybrid particles and a RGO/Co_3O_4/poly(vinylidene fluoride) composite with enhanced wave-absorption properties. ChemPlusChem 79(3):375–381
10. Cho BG, Lee S, Hwang SH, Han JH, Chae HG, Bin Park Y (2018) Influence of hybrid graphene oxide-carbon nanotube as a nano-filler on the interfacial interaction in nylon composites prepared by in situ interfacial polymerization. Carbon NY 140:324–337
11. Li P, Chen X, Zeng JB, Gan L, Wang M (2016) Enhancement of the interfacial interaction between poly(vinyl chloride) and zinc oxide modified reduced graphene oxide. RSC Adv 6(7):5784–5791
12. Terzopoulou Z et al (2019) Interfacial interactions, crystallization and molecular mobility in nanocomposites of Poly(lactic acid) filled with new hybrid inclusions based on graphene oxide and silica nanoparticles. Polymer (Guildf) 166:1–12

13. Zhang J et al (2014) Magnetic and mechanical properties of polyvinyl alcohol (PVA) nanocomposites with hybrid nanofillers—Graphene oxide tethered with magnetic Fe_3O_4 nanoparticles. Chem Eng J 237:462–468

14. Chatterjee S, Nafezarefi F, Tai NH, Schlagenhauf L, Nüesch FA, Chu BTT (2012) Size and synergy effects of nanofiller hybrids including graphene nanoplatelets and carbon nanotubes in mechanical properties of epoxy composites. Carbon NY 50(15):5380–5386

15. El Miri N et al (2016) Synergistic effect of cellulose nanocrystals/graphene oxide nanosheets as functional hybrid nanofiller for enhancing properties of PVA nanocomposites. Carbohydr Polym 137:239–248

16. Mishra SK, Tripathi SN, Choudhary V, Gupta BD (2015) Surface Plasmon resonance-based fiber optic methane gas sensor utilizing graphene-carbon nanotubes-poly(methyl methacrylate) hybrid nanocomposite. Plasmonics 10(5):1147–1157

17. Du X, Zhou M, Deng S, Du Z, Cheng X, Wang H. Poly(ethylene glycol)-grafted nanofibrillated cellulose/graphene hybrid aerogels supported phase change composites with superior energy storage capacity and solar-thermal conversion efficiency. Cellulose 27

18. Fakhri P, Mahmood H, Jaleh B, Pegoretti A (2016) Improved electroactive phase content and dielectric properties of flexible PVDF nanocomposite films filled with Au- and Cu-doped graphene oxide hybrid nanofiller. Synth Met 220:653–660

19. Wang Y et al (2011) Self assembly of acetylcholinesterase on a gold nanoparticles-graphene nanosheet hybrid for organophosphate pesticide detection using polyelectrolyte as a linker. J Mater Chem 21(14):5319–5325

20. Daşcıl K, Alanyalıoğlu M (2016) Preparation of free-standing and flexible graphene/Ag nanoparticles/poly(pyronin Y) hybrid paper electrode for amperometric determination of nitrite. ACS Appl Mater Interfaces 8(4):2713–2722

21. Huang X, Zhao G, Wang X (2015) Fabrication of reduced graphene oxide/metal (Cu, Ni, Co) nanoparticle hybrid composites via a facile thermal reduction method. RSC Adv. 5(62):49973–49978

22. Li J et al (2015) Bimetallic Ag–Pd nanoparticles-decorated graphene oxide: A fascinating three-dimensional nanohybrid as an efficient electrochemical sensing platform for vanillin determination. Electrochim Acta 176:827–835

23. Gao T, Chen L, Li Z, Yu L, Wu Z, Zhang Z (2016) Preparation of zinc hydroxystannate-decorated graphene oxide nanohybrids and their synergistic reinforcement on reducing fire hazards of flexible poly (vinyl chloride). Nanoscale Res Lett 11(1):1–10

24. Manolata Devi M, Sahu SR, Mukherjee P, Sen P, Biswas K (2016) Graphene–metal nanoparticle hybrids: electronic interaction between graphene and nanoparticles. Trans Ind Inst Met 69(4):839–844

25. Sun Y, Zheng H, Wang C, Yang M, Zhou A, Duan H (2016) Ultrasonic-electrodeposition of PtPd alloy nanoparticles on ionic liquid-functionalized graphene paper: towards a flexible and versatile nanohybrid electrode. Nanoscale 8(3):1523–1534

26. Liu T, Li C, Yuan Q (2018) Facile synthesis of PtCu alloy/graphene oxide hybrids as improved electrocatalysts for alkaline fuel cells. ACS Omega 3(8):8724–8732

27. Ren F et al (2018) Synergistic effect of graphene nanosheets and carbonyl iron-nickel alloy hybrid filler on electromagnetic interference shielding and thermal conductivity of cyanate ester composites. J Mater Chem C 6(6):1476–1486

28. Shang L, Zhao F, Zeng B (2014) 3D porous graphene-porous PdCu alloy nanoparticles-molecularly imprinted poly(para-aminobenzoic acid) composite for the electrocatalytic assay of melamine. ACS Appl Mater Interfaces 6(21):18721–18727

29. Jiang Q, Wang X, Zhu Y, Hui D, Qiu Y (2014) Mechanical, electrical and thermal properties of aligned carbon nanotube/polyimide composites. Compos Part B Eng. 56:408–412

30. Yang Z, Li Q, Tong Y, Wu T, Feng Y (2019) Homogeneous dispersion of multiwalled carbon nanotubes via in situ bubble stretching and synergistic cyclic volume stretching for conductive LDPE/MWCNTs nanocomposites. Polym Eng Sci 59(10):2072–2081

31. Ma HL et al (2014) Radiation preparation of graphene/carbon nanotubes hybrid fillers for mechanical reinforcement of poly(vinyl alcohol) films. Radiat Phys Chem 118:21–26

32. Zhang S, Yin S, Rong C, Huo P, Jiang Z, Wang G (2013) Synergistic effects of functionalized graphene and functionalized multi-walled carbon nanotubes on the electrical and mechanical properties of poly(ether sulfone) composites. Eur Polym J 49(10):3125–3134

33. Qian Z, Song J, Liu Z, Peng Z (2019) Improving mechanical properties and thermal conductivity of styrene-butadiene rubber via enhancing interfacial interaction between rubber and graphene oxide/carbon nanotubes hybrid. Macromol Res 27(11):1136–1143

34. Zhu Z (2017) An overview of carbon nanotubes and graphene for biosensing applications. Nano-Micro Lett. 9(3):1–24

35. Patole AS, Patole SP, Jung SY, Yoo JB, An JH, Kim TH (2012) Self assembled graphene/carbon nanotube/polystyrene hybrid nanocomposite by in situ microemulsion polymerization. Eur Polym J 48(2):252–259

36. David L, Feldman A, Mansfield E, Lehman J, Singh G (2014) Evaluating the thermal damage resistance of graphene/carbon nanotube hybrid composite coatings. Sci Rep 4:1–6

37. Kassab Z, Aziz F, Hannache H, Ben Youcef H, El Achaby M (2019) Improved mechanical properties of k-carrageenan-based nanocomposite films reinforced with cellulose nanocrystals. Int J Biol Macromol 123:1248–1256

38. Pal N, Banerjee S, Roy P, Pal K (2019) Reduced graphene oxide and PEG-grafted TEMPO-oxidized cellulose nanocrystal reinforced poly-lactic acid nanocomposite film for biomedical application. Mater Sci Eng C 104:109956

39. Lin L et al (2018) Study on the impact of graphene and cellulose nanocrystal on the friction and wear properties of SBR/NR composites under dry sliding conditions. Wear 414–415:43–49

40. Ye YS et al (2016) Biocompatible reduced graphene oxide sheets with superior water dispersibility stabilized by cellulose nanocrystals and their polyethylene oxide composites. Green Chem 18(6):1674–1683

41. Oraon R, De Adhikari A, Tiwari SK, Nayak GC (2015) Nanoclay based graphene polyaniline hybrid nanocomposites: promising electrode materials for supercapacitors. RSC Adv 5(84):68334–68344

42. Trifol J, Plackett D, Sillard C, Szabo P, Bras J, Daugaard AE (2016) Hybrid poly(lactic acid)/nanocellulose/nanoclay composites with synergistically enhanced barrier properties and improved thermomechanical resistance. Polym Int 65(8):988–995

43. Walimbe P, Chaudhari M (2019) State-of-the-art advancements in studies and applications of graphene: a comprehensive review. Mater Today Sustain 6:100026 (Elsevier Ltd.)

44. Huang Y et al (2015) Poly(lactic acid)/graphene oxide-ZnO nanocomposite films with good mechanical, dynamic mechanical, anti-UV and antibacterial properties. J Chem Technol Biotechnol 90(9):1677–1684

45. Wang C et al (2017) Silver nanoparticles/graphene oxide decorated carbon fiber synergistic reinforcement in epoxy-based composites. Polymer (Guildf) 131:263–271

46. Feng X, Xing W, Song L, Hu Y, Liew KM (2015) TiO_2 loaded on graphene nanosheet as reinforcer and its effect on the thermal behaviors of poly(vinyl chloride) composites. Chem Eng J 260:524–531

47. Wang S et al (2013) Ionic-liquid-assisted facile synthesis of silver nanoparticle-reduced graphene oxide hybrids by gamma irradiation. Carbon NY 55:245–252

48. Hong N et al (2014) Co-precipitation synthesis of reduced graphene oxide/NiAl-layered double hydroxide hybrid and its application in flame retarding poly(methyl methacrylate). Mater Res Bull 49(1):657–664

49. Wang D, Zhang Q, Zhou K, Yang W, Hu Y, Gong X (2014) The influence of manganese-cobalt oxide/graphene on reducing fire hazards of poly(butylene terephthalate). vol 278. Elsevier B.V.

50. Zhang S et al (2011) Graphene decorated with PtAu alloy nanoparticles: Facile synthesis and promising application for formic acid oxidation. Chem Mater 23(5):1079–1081

51. Chen Q, Liu P, Sheng C, Zhou L, Duan Y, Zhang J (2014) Tunable self-assembly structure of graphene oxide/cellulose nanocrystal hybrid films fabricated by vacuum filtration technique. RSC Adv 4(74):39301–39304

52. Mani V, Govindasamy M, Chen SM, Karthik R, Huang ST (2016) Determination of dopamine using a glassy carbon electrode modified with a graphene and carbon nanotube hybrid decorated with molybdenum disulfide flowers. Microchim Acta 183(7):2267–2275

53. Mwafy EA, Mostafa AM (2019) Multi walled carbon nanotube decorated cadmium oxide nanoparticles via pulsed laser ablation in liquid media. Opt Laser Technol 111(September 2018):249–254

54. Venkatesan S, Visvalingam B, Mannathusamy G, Viswanathan V, Rao AG (2018) Effect of chemical vapor deposition parameters on the diameter of multi-walled carbon nanotubes. Int Nano Lett 8(4):297–308

55. Che J, Jing M, Liu D, Wang K, Fu Q (2018) Largely enhanced thermal conductivity of HDPE/boron nitride/carbon nanotubes ternary composites via filler network-network synergy and orientation. Compos Part A Appl Sci Manuf 112:32–39

56. Che J, Wu K, Lin Y, Wang K, Fu Q (2017) Largely improved thermal conductivity of HDPE/expanded graphite/carbon nanotubes ternary composites via filler network-network synergy. Compos Part A Appl Sci Manuf 99:32–40

57. Belmonte M, Nistal A, Boutbien P, Román-Manso B, Osendi MI, Miranzo P (2016) Toughened and strengthened silicon carbide ceramics by adding graphene-based fillers. Scr Mater 113:127–130

58. Fatemi SM, Foroutan M (2016) Recent developments concerning the dispersion of carbon nanotubes in surfactant/polymer systems by MD simulation. J Nanostructure Chem 6(1):29–40

59. Xu J et al (2018a) A review of functionalized carbon nanotubes and graphene for heavy metal adsorption from water: preparation, application, and mechanism. Chemosphere 195:351–364

60. Wen L, Li F, Cheng HM (2016) Carbon nanotubes and graphene for flexible electrochemical energy storage: from materials to devices. Adv Mater 28(22):4306–4337

61. Deng L, Gu Y, Gao Y, Ma Z, Fan G (2017) Carbon nanotubes/holey graphene hybrid film as binder-free electrode for flexible supercapacitors. J Colloid Interface Sci 494:355–362

62. Kong L et al (2014) Electromagnetic wave absorption properties of graphene modified with carbon nanotube/poly(dimethyl siloxane) composites. Carbon NY 73:185–193

63. Wang E et al (2019) Effect of graphene oxide-carbon nanotube hybrid filler on the mechanical property and thermal response speed of shape memory epoxy composites. Compos Sci Technol 169:209–216

64. Verma M, Chauhan SS, Dhawan SK, Choudhary V (2017) Graphene nanoplatelets/carbon nanotubes/polyurethane composites as efficient shield against electromagnetic polluting radiations. Compos Part B Eng 120:118–127

65. Wang C, Yang S, Ma Q, Jia X, Ma PC (2017) Preparation of carbon nanotubes/graphene hybrid aerogel and its application for the adsorption of organic compounds. Carbon NY 118:765–771

66. Dasgupta A, Rajukumar LP, Rotella C, Lei Y, Terrones M (2017) Covalent three-dimensional networks of graphene and carbon nanotubes: synthesis and environmental applications. Nano Today 12:116–135

67. Jun Xiao Y et al (2016) Hybrid network structure and thermal conductive properties in poly(vinylidene fluoride) composites based on carbon nanotubes and graphene nanoplatelets. Compos Part A Appl Sci Manuf 90:614–625

68. Paszkiewicz S et al (2015) Synergetic effect of single-walled carbon nanotubes (SWCNT) and graphene nanoplatelets (GNP) in electrically conductive PTT-block-PTMO hybrid nanocomposites prepared by in situ polymerization. Compos Sci Technol 118:72–77

69. Zhang C, Huang S, Tjiu WW, Fan W, Liu T (2012) Facile preparation of water-dispersible graphene sheets stabilized by acid-treated multi-walled carbon nanotubes and their poly(vinyl alcohol) composites. J Mater Chem 22(6):2427–2434

70. Kassab Z, Syafri E, Tamraoui Y, Hannache H, Qaiss AEK, El Achaby M (2019) Characteristics of sulfated and carboxylated cellulose nanocrystals extracted from Juncus plant stems. Int J Biol Macromol

71. El Achaby M, Kassab Z, Barakat A, Aboulkas A (2018) Alfa fibers as viable sustainable source for cellulose nanocrystals extraction: application for improving the tensile properties of biopolymer nanocomposite films. Ind Crops Prod 112:499–510

72. El Achaby M, Kassab Z, Aboulkas A, Gaillard C, Barakat A (2018) Reuse of red algae waste for the production of cellulose nanocrystals and its application in polymer nanocomposites. Int J Biol Macromol 106:681–691

73. Kassab Z et al (2020) Identifying Juncus plant as viable source for the production of micro- and nano-cellulose fibers: application for PVA composite materials development. Ind Crops Prod 144(December 2019):112035

74. Kassab Z, Kassem I, Hannache H, Bouhfid R, Qaiss AEK, El Achaby M (2020) Tomato plant residue as new renewable source for cellulose production: extraction of cellulose nanocrystals with different surface functionalities. Cellulose 7:1–17

75. Terrones M et al (2010) Graphene and graphite nanoribbons: morphology, properties, synthesis, defects and applications. Nano Today 5(4):351–372 (Elsevier B.V.)

76. Wang Z, Kang H, Zhao S, Zhang W, Zhang S, Li J (2018) Polyphenol-induced cellulose nanofibrils anchored graphene oxide as nanohybrids for strong yet tough soy protein nanocomposites. Carbohydr Polym 180:354–364

77. Cao J, Zhang X, Wu X, Wang S, Lu C (2016) Cellulose nanocrystals mediated assembly of graphene in rubber composites for chemical sensing applications. Carbohydr Polym 140:88–95

78. Pal N, Dubey P, Gopinath P, Pal K (2017) Combined effect of cellulose nanocrystal and reduced graphene oxide into poly-lactic acid matrix nanocomposite as a scaffold and its anti-bacterial activity. Int J Biol Macromol 95:94–105

79. Xu S, Yu W, Yao X, Zhang Q, Fu Q (2016) Nanocellulose-assisted dispersion of graphene to fabricate poly(vinyl alcohol)/graphene nanocomposite for humidity sensing. Compos Sci Technol 131:67–76

80. Montes S et al (2015) Synergistic reinforcement of poly(vinyl alcohol) nanocomposites with cellulose nanocrystal-stabilized graphene. Compos Sci Technol 117:26–31

81. Zabihi O, Ahmadi M, Nikafshar S, Chandrakumar Preyeswary K, Naebe M (2018) A technical review on epoxy-clay nanocomposites: Structure, properties, and their applications in fiber reinforced composites. Compos Part B: Eng 135:1–24 (Elsevier Ltd.)

82. Panwar V, Chattree A, Pal K (2017) Effect of nanoclay on thermomechanical behaviour of graphene oxide/polymer composites. Procedia Eng 216:101–110

83. Adrar S, Habi A, Ajji A, Grohens Y (2018) Synergistic effects in epoxy functionalized graphene and modified organo-montmorillonite PLA/PBAT blends. Appl Clay Sci 157(February):65–75

84. Zhan Y, He S, Wan X, Zhao S, Bai Y (2018) Thermally and chemically stable poly(arylene ether nitrile)/halloysite nanotubes intercalated graphene oxide nanofibrous composite membranes for highly efficient oil/water emulsion separation in harsh environment. 567 (Elsevier B.V.)

85. Oraon R, De Adhikari A, Tiwari SK, Sahu TS, Nayak GC (2015) Fabrication of nanoclay based graphene/polypyrrole nanocomposite: An efficient ternary electrode material for high performance supercapacitor. Appl Clay Sci 118:231–238

86. Bouakaz BS, Pillin I, Habi A, Grohens Y (2015) Synergy between fillers in organomontmorillonite/graphene-PLA nanocomposites. Appl Clay Sci 116–117:69–77

87. Mia X et al (2019) Fabrication of halloysite nanotubes/reduced graphene oxide hybrids for epoxy composites with improved thermal and mechanical properties. Polym Test 76(April):473–480

88. Liu C, Yu L, Zhang Y, Zhang B, Liu J, Zhang H (2013) Preparation of poly(sodium acrylate-acrylamide) superabsorbent nanocomposites incorporating graphene oxide and halloysite nanotubes. RSC Adv 3(33):13756–13763

89. Li S, Yang Z, Xu J, Xie J (2018) Montmorillonite–graphene oxide hybrids and montmorillonite–graphene oxide/epoxy composite: synthesis, characterization, and properties. Polym Compos 39:E2084–E2095

90. Senthilnathan J, Sanjeeva Rao K, Lin WH, Der Liao J, Yoshimura M (2014) Low energy synthesis of nitrogen functionalized graphene/nanoclay hybrid via submerged liquid plasma approach. Carbon NY 78:446–454

91. Zhao C, Lv J, Xu X, Zhang G, Yang Y, Yang F (2017) Highly antifouling and antibacterial performance of poly (vinylidene fluoride) ultrafiltration membranes blending with copper oxide and graphene oxide nanofillers for effective wastewater treatment. J Colloid Interface Sci 505:341–351

92. Bindu Sharmila TK, Antony JV, Jayakrishnan MP, Sabura Beegum PM Thachil ET (2016) Mechanical, thermal and dielectric properties of hybrid composites of epoxy and reduced graphene oxide/iron oxide. Mater Des 90:66–75

93. Huang YL et al (2012) Self-assembly of silver-graphene hybrid on electrospun polyurethane nanofibers as flexible transparent conductive thin films. Carbon NY 50(10):3473–3481

94. Zhang L, Han G, Liu Y, Tang J, Tang W (2014) Immobilizing haemoglobin on gold/graphene-chitosan nanocomposite as efficient hydrogen peroxide biosensor. Sens Actuat B Chem 197:164–171

95. He F, Lam K, Ma D, Fan J, Chan LH, Zhang L (2013) Fabrication of graphene nanosheet (GNS)-Fe$_3$O$_4$ hybrids and GNS- Fe$_3$O$_4$/syndiotactic polystyrene composites with high dielectric permittivity. Carbon NY 58:175–184

96. Xia BY, Yan Y, Li N, Bin H, Wu B, Lou XWD, Wang X (2016) A metal-organic framework-derived bifunctional oxygen electrocatalyst. Nat Energy 1(1):1–8

97. Fernandes R, Patel N, Miotello A, Jaiswal R, Kothari DC (2011) Stability, durability, and reusability studies on transition metal-doped Co–B alloy catalysts for hydrogen production. Int J Hydrogen Energy 36(21):13379–13391

98. Vinayan BP, Ramaprabhu S (2013) Platinum-TM (TM=Fe,Co) alloy nanoparticles dispersed nitrogen doped (reduced graphene oxide-multiwalled carbon nanotube) hybrid structure cathode electrocatalysts for high performance PEMFC applications. Nanoscale 5(11):5109–5118

99. Jia X, Guan Q, Chen Y, Wang Y, Zhao Q, Li J (2019) Poly (triazine imide) (PTI) and graphene hybrids supported Pt[sbnd]Sn catalysts for enhanced electrocatalytic oxidation of ethanol. Appl Surf Sci 492(June):879–885

100. Nan X, Ma J, Liu J, Zhao J, Zhu W (2016) Effect of surfactant functionalization of multi-walled carbon nanotubes on mechanical, electrical and thermal properties of epoxy nanocomposites. Fibers Polym 17(11):1866–1874

101. Cai D, Song M (2010) Recent advance in functionalized graphene/polymer nanocomposites. J Mater Chem 20(37):7906–7915

102. Cui Y, Kundalwal SI, Kumar S (2016) Gas barrier performance of graphene/polymer nanocomposites. Carbon NY 98:313–333

103. Kim H, Abdala AA, MacOsko CW (2010) Graphene/polymer nanocomposites. Macromolecules 43(16):6515–6530

104. Kurapati R, Kostarelos K, Prato M, Bianco A (2016) Biomedical uses for 2D materials beyond graphene: current advances and challenges ahead. Adv Mater 28(29):6052–6074

105. Byrne MT, Guin'Ko YK (2010) Recent advances in research on carbon nanotube-polymer composites. Adv Mater 22(15):1672–1688

106. Yue L, Pircheraghi G, Monemian SA, Manas-Zloczower I (2014) Epoxy composites with carbon nanotubes and graphene nanoplatelets—Dispersion and synergy effects. Carbon NY 78:268–278

107. Bagotia N, Choudhary V, Sharma DK (2019) Synergistic effect of graphene/multiwalled carbon nanotube hybrid fillers on mechanical, electrical and EMI shielding properties of polycarbonate/ethylene methyl acrylate nanocomposites. Compos Part B Eng 159:378–388

108. Chen L et al (2014) Electron field emission characteristics of graphene/carbon nanotubes hybrid field emitter. J Alloys Compd 610:659–664

109. Liu F et al (2017) Investigation on the interfacial mechanical properties of hybrid graphene-carbon nanotube/polymer nanocomposites. Carbon NY 115:694–700

110. Zhang H et al (2018) Synergistic effect of carbon nanotube and graphene nanoplates on the mechanical, electrical and electromagnetic interference shielding properties of polymer composites and polymer composite foams. Chem Eng J 353:381–393

111. Li Y, Yang T, Yu T, Zheng L, Liao K (2011) Synergistic effect of hybrid carbon nantube-graphene oxide as a nanofiller in enhancing the mechanical properties of PVA composites. J Mater Chem 21(29):10844–10851

112. Hwang Y, Kim M, Kim J (2013) Improvement of the mechanical properties and thermal conductivity of poly(ether-ether-ketone) with the addition of graphene oxide-carbon nanotube hybrid fillers. Compos Part A Appl Sci Manuf 55:195–202

113. Kassab Z, El Achaby M, Tamraoui Y, Sehaqui H, Bouhfid R, Qaiss AEK (2019) Sunflower oil cake-derived cellulose nanocrystals: Extraction, physico-chemical characteristics and potential application. Int J Biol Macromol 136:241–252

114. Kassab Z, Boujemaoui A, Ben Youcef H, Hajlane A, Hannache H, El Achaby M (2019), Production of cellulose nanofibrils from alfa fibers and its nanoreinforcement potential in polymer nanocomposites. Cellulose 26(18):9567–9581

115. Calvino C, Macke N, Kato R, Rowan SJ (2020) Development, processing and applications of bio-sourced cellulose nanocrystal composites. Progr Polym Sci 103:101221 (Elsevier Ltd.)

116. Akindoyo JO, Ismail NH, Mariatti M (2019) Performance of poly(vinyl alcohol) nanocomposite reinforced with hybrid TEMPO mediated cellulose-graphene filler. Polym Test 80:106140

117. Ganjaee Sari M, Shamshiri M, Ramezanzadeh B (2017) Fabricating an epoxy composite coating with enhanced corrosion resistance through impregnation of functionalized graphene oxide-co-montmorillonite nanoplatelet. Corros Sci 129(September):38–53

118. He K et al (2019) Graphene hybridized polydopamine-kaolin composite as effective adsorbent for methylene blue removal. Compos Part B Eng 161:141–149

119. Zuo L et al (2017) Graphene/montmorillonite hybrid synergistically reinforced polyimide composite aerogels with enhanced flame-retardant performance. Compos Sci Technol 139:57–63

120. Zhou X et al (2018) Morphology and properties of shape memory thermoplastic polyurethane composites incorporating graphene-montmorillonite hybrids. J Appl Polym Sci 135(15):1–9

121. Wang R, Li Z, Liu W, Jiao W, Hao L, Yang F (2013) Attapulgite-graphene oxide hybrids as thermal and mechanical reinforcements for epoxy composites. Compos Sci Technol 87:29–35

122. Haase C, Tang F, Wilms MB, Weisheit A, Hallstedt B (2017) Combining thermodynamic modeling and 3D printing of elemental powder blends for high-throughput investigation of high-entropy alloys—Towards rapid alloy screening and design. Mater Sci Eng A 688:180–189

123. Huang K, Marthinsen K, Zhao Q, Logé RE (2018) The double-edge effect of second-phase particles on the recrystallization behaviour and associated mechanical properties of metallic materials. Progr Mater Sci 92:284–359 (Elsevier Ltd.)

124. Eaton P et al (2017) A direct comparison of experimental methods to measure dimensions of synthetic nanoparticles. Ultramicroscopy 182:179–190

125. Dudkiewicz A et al (2011) Characterization of nanomaterials in food by electron microscopy. TrAC Trends Anal Chem 30(1):28–43 (Elsevier)

126. Yang SY et al (2011) Synergetic effects of graphene platelets and carbon nanotubes on the mechanical and thermal properties of epoxy composites. Carbon NY 49(3):793–803

127. Zhang D, Chang H, Li P, Liu R, Xue Q (2016) Fabrication and characterization of an ultra-sensitive humidity sensor based on metal oxide/graphene hybrid nanocomposite. Sens Actuat B Chem 225:233–240

128. Liang Y, Wang H, Casalongue HS, Chen Z, Dai H (2010) TiO_2 Nanocrystals grown on graphene as advanced photocatalytic hybrid materials. Nano Res 3(10):701–705

129. Wang J, Jin X, Wu H, Guo S (2017) Polyimide reinforced with hybrid graphene oxide @ carbon nanotube: toward high strength, toughness, electrical conductivity. Carbon NY 123:502–513

130. Kelly DJ et al (2018) Nanometer resolution elemental mapping in graphene-based TEM liquid cells. Nano Lett 18(2):1168–1174

131. Wang K, Ma Q, Pang K, Ding B, Zhang J, Duan Y (2018) One-pot synthesis of graphene/chitin nanofibers hybrids and their remarkable reinforcement on Poly(vinyl alcohol). Carbohydr Polym 194:146–153

132. Taj A et al (2019) In-situ synthesis of 3D ultra-small gold augmented graphene hybrid for highly sensitive electrochemical binding capability. J Colloid Interface Sci 553:289–297

133. Song S, Zhang Y (2017) Carbon nanotube/reduced graphene oxide hybrid for simultaneously enhancing the thermal conductivity and mechanical properties of styrene -butadiene rubber. Carbon NY 123:158–167

134. Chouhan DK et al (2016) Graphene oxide-Laponite hybrid from highly stable aqueous dispersion. Appl Clay Sci 132–133:105–113
135. Tajik S, Shahrabadi A, Rashidi A, Jalilian M, Yadegari A (2018) Application of functionalized silica-graphene nanohybrid for the enhanced oil recovery performance. Colloids Surfaces Physicochem Eng Asp 556:253–265
136. Swain SS, Unnikrishnan L, Mohanty S, Nayak SK (2019) Synergistic influence of anisotropic 3D carbon nanotube-graphene hybrid mixed matrix membranes on stability and gas permeation characteristics. J Taiwan Inst Chem Eng 105:150–165
137. Maya MG et al (2020) A comprehensive study on the impact of RGO/MWCNT hybrid filler reinforced polychloroprene rubber multifunctional nanocomposites. Polym Test 87:106525
138. Xiong R et al (2018) Wrapping nanocellulose nets around graphene oxide sheets. Angew Chemie Int Ed 57(28):8508–8513
139. Nanda SS, Yi DK, Kim K (2016) Study of antibacterial mechanism of graphene oxide using Raman spectroscopy. Sci Rep 6(1):1–12
140. Showalter AR, Duster TA, Szymanowski JES, Na C, Fein JB, Bunker BA (2017) An X-ray absorption fine structure spectroscopy study of metal sorption to graphene oxide. J Colloid Interface Sci 508:75–86
141. Viswanathan K, Ravi T, Boddula R (2019) Synthesis graphene based sensor for strain data and its characterization. Mater Sci Energy Technol 2(2):203–207
142. Ferrari AC, Basko DM (2013) Raman spectroscopy as a versatile tool for studying the properties of graphene. Nat Nanotechnol. 8(4):235–246
143. Bokobza L, Bruneel JL, Couzi M (2014) Raman spectroscopy as a tool for the analysis of carbon-based materials (highly oriented pyrolitic graphite, multilayer graphene and multiwall carbon nanotubes) and of some of their elastomeric composites. Vib Spectrosc 74:57–63
144. Hu X, Tian M, Qu L, Zhu S, Han G (2015) Multifunctional cotton fabrics with graphene/polyurethane coatings with far-infrared emission, electrical conductivity, and ultraviolet-blocking properties. Carbon NY 95:625–633
145. Mahendia S, Heena, Kandhol G, Deshpande UP, Kumar S (2016) Determination of glass transition temperature of reduced graphene oxide-poly(vinyl alcohol) composites using temperature dependent Fourier transform infrared spectroscopy. J Mol Struct 1111:46–54
146. Sajith S (2019) Investigation on effect of chemical composition of bio-fillers on filler/matrix interaction and properties of particle reinforced composites using FTIR. Compos Part B Eng 166:21–30
147. Costa P et al (2017) High-performance graphene-based carbon nanofiller/polymer composites for piezoresistive sensor applications. Compos Sci Technol 153:241–252
148. Pu X et al (2013) One-pot microwave-assisted combustion synthesis of graphene oxide-TiO$_2$ hybrids for photodegradation of methyl orange. J Alloys Compd 551:382–388
149. Han Y, Liu Y, Han L, Lin J, Jin P (2017) High-performance hierarchical graphene/metal-mesh film for optically transparent electromagnetic interference shielding. Carbon NY 115:34–42
150. Xu Y et al (2009) A hybrid material of graphene and poly (3,4-ethyldioxythiophene) with high conductivity, flexibility, and transparency. Nano Res 2(4):343–348
151. Wang P, Han L, Zhu C, Zhai Y, Dong S (2011) Aqueous-phase synthesis of Ag–TiO$_2$-reduced graphene oxide and Pt-TiO$_2$-reduced graphene oxide hybrid nanostructures and their catalytic properties. Nano Res 4(11):1153–1162
152. Vaghri E, Khalaj Z, Dorranian D (2020) Investigating the effects of different liquid environments on the characteristics of multilayer graphene and graphene oxide nanosheets synthesized by green laser ablation method. Diam Relat Mater 103:107697
153. Das S et al (2011) Synthesis and characterization of self-organized multilayered graphene-carbon nanotube hybrid films. J Mater Chem 21(20):7289–7295
154. Xu H et al (2018b) Properties of graphene-metal contacts probed by Raman spectroscopy. Carbon NY 127:491–497
155. Dey A et al (2015) Polymer based graphene/titanium dioxide nanocomposite (GTNC): an emerging and efficient thermoelectric material. Dalt Trans 44(44):19248–19255

156. Hasan M, Banerjee AN, Lee M (2015) Enhanced thermo-optical performance and high BET surface area of graphene@PVC nanocomposite fibers prepared by simple facile deposition technique: N_2 adsorption study. J Ind Eng Chem 21:828–834
157. Zhan Y, Zhang J, Wan X, Long Z, He S, He Y (2018) Epoxy composites coating with Fe_3O_4 decorated graphene oxide: modified bio-inspired surface chemistry, synergistic effect and improved anti-corrosion performance. Appl Surf Sci 436:756–767
158. Greczynski G, Hultman L (2020) X-ray photoelectron spectroscopy: towards reliable binding energy referencing. Progr. Mater. Sci 107:100591 (Elsevier Ltd.)
159. Tajik S, Nasernejad B, Rashidi A (2016) Preparation of silica-graphene nanohybrid as a stabilizer of emulsions. J Mol Liq 222:788–795
160. Zheng Q, Cai Z, Ma Z, Gong S (2015) Cellulose nanofibril/reduced graphene oxide/carbon nanotube hybrid aerogels for highly flexible and all-solid-state supercapacitors. ACS Appl Mater Interfaces 7(5):3263–3271
161. Tan QC, Shanks RA, Hui D, Kong I (2016) Functionalised graphene-multiwalled carbon nanotube hybrid poly(styrene-b-butadiene-b-styrene) nanocomposites. Compos Part B Eng 90:315–325
162. Dai W et al (2015) Enhanced thermal conductivity and retained electrical insulation for polyimide composites with SiC nanowires grown on graphene hybrid fillers. Compos Part A Appl Sci Manuf 76:73–81

Graphene and Carbon Nanotube-Based Hybrid Nanocomposites: Preparation to Applications

Manik Chandra Biswas, Mostakima Mafruha Lubna, Zaheeruddin Mohammed, Md Hasan Ul Iqbal, and Md Enamul Hoque

Abstract The gradual demand for low weight, high strength and structural integrity, low-cost materials have been triggering the necessity for finding new materials. In the past decades, carbon-based nanomaterials gained much attention in the frontier of nanotechnology. Graphene (2D) and carbon nanotubes (CNTs) (1D) are exhibited prominent structural properties among all carbon-based nanomaterials, which make them ideal candidates as reinforcing agents for polymer nanocomposites. Graphene possesses unique and excellent structural properties such as mechanical, thermal, electrical, optical etc. due to its inherited 2D atomic structures. Similarly, CNTs also showed high aspect ration with excellent mechanical, electrical and magnetic properties, resulting in potential filler in high strength composites fabrication. However, pure Graphene sheets and poor CNTs dispersion in polymer matrices restrict wide applications and arise inevitable challenges to incorporate unique controlled functionality. Therefore, hybrid nanocomposites are garnering much attention in the composites sector to tackle real-world problems in numerous areas namely, as energy storage devices, sensors & actuators, electromagnetic shielding, longlasting structures and so on. Highly structurally stable, high electrical and thermal conductive composites are in great demand in the aforementioned areas. This chapter mainly focuses on recent hybrid nanocomposites fabrication based on Graphene and CNTs and their potential

M. C. Biswas (✉) · M. M. Lubna
Fiber and Polymer Science, Department of Textile Engineering, Chemistry and Science, North Carolina State University, Raleigh, NC 27606, USA
e-mail: mbiswas2@ncsu.edu

M. C. Biswas · Z. Mohammed
Department of Material Science and Engineering, Tuskegee University, Tuskegee, AL 36088, USA

M. H. Ul Iqbal
Department of Chemistry and Biochemistry, College of Arts and Sciences, The University of Alabama, Tuscaloosa, Al 35401, USA

M. E. Hoque (✉)
Department of Biomedical Engineering, Military Institute of Science and Technology (MIST), Mirpur Cantonment, Dhaka 1216, Bangladesh
e-mail: enamul1973@gmail.com

applications. We start with the basic overview of Graphene and CNTs, their structural similarities and differences followed by fabrication and processing methods underlying the successful development of these materials with superior performance. The central part of the chapter summarizes major improvement and potential state-of-the-art applications. Lastly, prospects and challenges are discussed so that future researchers can continue the progress and development of these fascinating materials for adoption by industry.

1 Introduction

With the growing world population and the demand for a high-quality life, comfortable transportation, and unparalleled industrialization, the demand for high performance and high structurally integral materials has been enhanced significantly in recent years. Specifically, automotive and aerospace fields required materials which can be considered as potential alternatives to traditional or conventional metal or ceramic-based materials [1]. Metal and ceramic-based materials possess high density which opposes the use of lightweight materials in aerospace as well as the automotive industry. In addition, the high cost (ca. $32,000/kg) of materials for heavy aerospace devices in space restricting their applications followed by high fuel cost. The application of hybrid polymer composites garnered much attention due to overcoming those challenges associated with metal-based composites [2, 3]. The unique attributes of hybrid composites such as lightweight, high strength, high aspect ratio (e.g. length to weight ratio), low cost etc. are comparable to metal or alloys.

Polymer matrix composites (aka PMCs), reinforced with graphene and CNTs are extensively applied in numerous areas namely, aerospace, automotive, structural, construction, sensor, electromagnetic interference (EMI) and so on. Thermoplastics and thermosetting polymers act like matrices and graphene/CNTs as filler or reinforcement materials. Thermosetting polymers are used in industry commercially because of the high ratio of strength/weight compared to other counterparts, thermoplastics polymers. But in some cases, for example, electromagnetic interference (EMI) shielding applications, thermoplastics are more attractive due to recyclability and reformability. Among all thermosetting polymers, epoxy resins showed tremendous potential owing to low rate of shrinkage during processing and a low-pressure requirement for fabricating the composite materials. With the merits of the recent developments of materials engineering and polymer science, the remarkable properties of thermosetting polymers and excellent attributes of graphene/CNTs hybrid allow fabricating high-performance hybrid nanocomposites.

Carbon nanomaterials (i.e. CNTs) and graphene are extensively incorporated in advanced nano-hybrids for their compelling mechanical strength, electrical conductivity, chemically stability, flexibility, and lower density as compared to their metal counterparts [4–8]. Most importantly, carbon nanomaterials offer a combined package of extraordinary properties with a wide range of nanomaterial-matrix compatibility allowing for a wide range of resulting materials from flexible thin films [4, 9–11] to ultralow density aerogel foams [12].

CNTs have an all-carbon tubular geometry consisting of sp^2 carbon atoms considered a rolled version of graphene sheets, the most promising carbon allotropy with unique electrical, mechanical, catalytic, and electrocatalytic properties. Since its discovery by Ijima 1991, CNTs are still dominating the entire material science research. An enormous amount of researches has been done on the production, structure-properties, and target applications, using both the single-walled carbon nanotubes (SWCNTs) and multiwalled carbon nanotubes (MWCNTs) [13].

Ideally, CNTs are made of hexagonal-shaped lattice layers of sp^2—hybridized carbon atoms similar to graphene but in nanotubes, the graphene sheets are fused to form a cylindrically-shaped tube on the edges of CNTs. The SWCNTs have only one single graphene wall and are sealed at both ends. Typically, SWCNTs are internally hollow, have diameters of around 0.4–2 nm and can grow up to several micrometers. CNTs can have two or more walls or graphitic cylindrical layers and called double-walled (DWCNTs) or multiwalled (MWCNTs) carbon nanotubes respectively.

The aspect ratio which is the length-to-diameter ratio of CNTs is generally exceeded 10,000; meaning the CNTs are the most anisotropic materials ever produced. Researchers had found that fibers containing CNTs have 100 GPa Young's modulus count and can to withstand high pressures (~25 GPa) without deforming severely. CNTs also show chirality (dissimilarity between Carbon bonds and the significant angle between the hexagonal planes and the axis). The chirality of CNTs determines electrical behavior. The most common patterns of chirality are armchair, chiral patterns and zigzag [14].

The chiral vector (AA′) of CNTs is usually described as Ch = n. a_1 + m. a_2 (a_1 and a_2 are unit vectors of the hexagonal honeycomb lattice and n and m are integers, Fig. 1, this connects crystallographically equivalent two sites (A and A′). The chiral vector Ch also describes a chiral angle θ, between Ch and the zigzag direction of the graphene sheet. The topology of each nanotube is generally expressed by two integer numbers (m, n), according to the definition CNTs' symmetries can be armchair (n, n), zigzag (n, 0) and chiral (n, m) m ≠ 0. The electronic properties of CNTs rely on both graphene sheet width (tube diameter) and its folding pattern (chirality of the tube), both are functions of (m, n).

CNTs can show both metallic and semiconducting electronic properties, which depends on their chirality. A general rule is if (n = m) armchair CNTs, exhibit a metallic behavior meaning electron conductor (finite value of carriers in the density of states at the Fermi energy). However, CNTs can be operated as semiconductors if their diameter decreases below a certain value because the energy gaps in the semiconducting CNTs are scaled with the inverse of the nanotube diameter. When m = 0, Zigzag CNTs, and chiral nanotubes, where m ≠ n and m − n is not a multiple
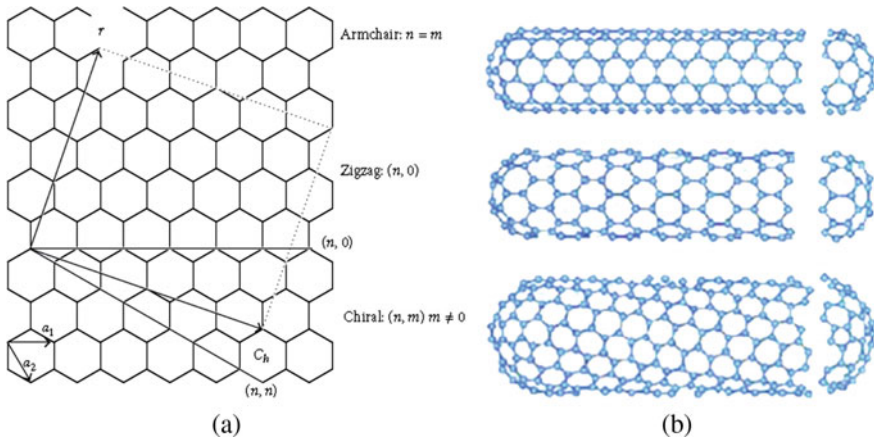
Fig. 1 Schematic representation of **a** formation of CNTs by rolling of a graphene sheet along lattice vectors which leads to the armchair, zigzag, and chiral tubes and **b** the three different types of CNTs [15]

of 3 show semiconducting behavior. Here the energy band structure showcases a very small band gap with a no density of states inside the gap due to the degree of sp^2-to-sp^3 hybridization introduced by the nonflat hexagons of the nanotube walls (no charge carriers at the Fermi energy here) [15, 16] Fig. 2.

In other words, the electron transport characteristics of CNTs are fully controlled by two characteristics of the CNTs, diameter and chirality. Although researchers have found that the theoretical prediction of electronic characteristics is dramatically altered in reality because of the presence of defects and vacancies [18].

Because of their unique combination of extraordinary properties, CNT structures are widely used in combination with other nanomaterials, polymers, metals, and ceramic matrixes to fabricate multifunctional hybrids [19, 20] for applications such as sensors and actuators [21], supercapacitor [22], electromagnetic interference shielding [23], biomedical-tissue engineering [24], targeted drug delivery [25], catalysis [26], oil absorption [27] and water treatment [28].

Besides, the extraordinary characteristics (i.e. Young's modulus = 1 TPa and yield strengths = 100 GPa) shown by the CNTs and graphene, their electrical behavior also make them ideal candidates in NEMS (nano-electro-mechanical systems) like, actuators, nano-springs, and oscillators. There are numerous reports on the inclusion of CNTs and graphene in polymer matrixes, which demonstrated the augmentation in strength and thermal stability of the resulting hybrids or composites [29].
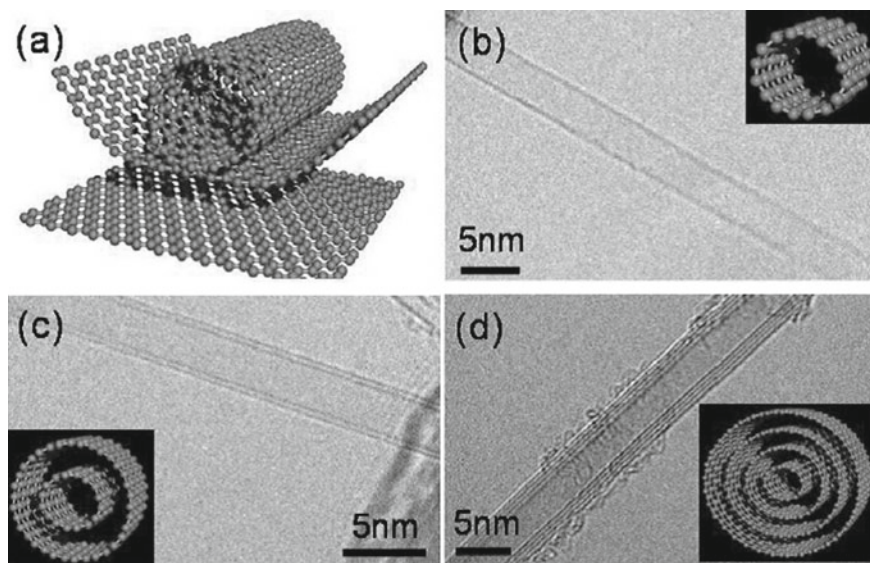
Fig. 2 a Schematic representation of an individual layer of honeycomb-like carbon called graphene, and how this is rolled to form a carbon nanotube; **b–d** HR-TEM images of single-, double- and multi-walled carbon nanotubes (insets are their corresponding images) [17]

2 Advantages of Graphene-CNT Hybridization and Challenges

The field of hybridizing CNTs with graphene is of growing interest and motivated both by the fundamental considerations in electronics application, by advanced lightweight-robust composites fabrication, and also by the active biomedical material applications. The two key aspects of fabricating all-carbon conductive multi-functional material systems are the compatibilization of materials and the functional design architecture. Studies had already proven that graphene-CNT hybrids exhibit higher mechanical resilience, better electrical conductivities and catalytic characteristics in comparison to either CNTs or GO/graphene. Therefore, the hybrids have exceptional properties with the highest edge density per unit area than the other individual carbon nanostructures (SWCNT, MWCNT, graphene sheets, graphite, activated carbon) [30].

Different types of strategies have been investigated by the research community to hybridize CNTs with graphene through dispersion by ultrasonication, surface modification, and in-situ chemical reaction-entrapment. Myriad intelligent 3D designs of nano-hybrids offer ways of integrating more specific performance parameters and tailor the ability of properties like density, directional stability, capacitance, etc.

Stoner et al. demonstrated elaborate studies on the classification of C-nanostructures based on the spatial organization of their edges. Their finding showed

that the 3D hierarchical orientation of graphene-CNT hybrid possesses very high charge density and it provided higher mechanical strength with a large surface area [31]. The application areas are mostly classified as two groups: (1) microscopic electronic devices (e.g. chemical sensors, nano-tweezers and field-effect transistors), and (2) macroscopic applications (e.g. structural components, conductors, and composites) [32–36].

Defects on graphene can compromise the superior properties and graphene research has majorly been focused on producing high-quality graphene with a minimal level of defects. Moreover, the integration process with other matrixes for real-life applications was very challenging. Another major concern in the synthesis is the aggregation of graphene sheets. To eradicate these problems to some extent, 3D structures were fabricated using monolayer or multilayered graphene as synthesizing units and hybridize with CNTs. The macro form (3D interconnected networks) had produced using template-based growth and/or solution/freeze-drying based assemblies. Graphene and CNTs are combined in the hybrid structures not only to get synergistic effect of higher electrical conductivity, and mechanical strength but also CNTs enhance the capability of fabricating macroscopic architecture of 3D graphenes with conductive interconnection among themselves [37].

For the fabrication of the miniaturize structures in microelectronics circuits /micromechanics devices, the bridging of nano-dimensional CNT-graphene is essential and this integration of building blocks for the bottom-up strategies both materials research and molecular dynamic simulation researches are ongoing to find out the best possible performance outcome. The thermo-mechanical performance of pillared graphene-CNTs hybrid (by combining CNTs and graphene sheets to construct a 3D nanonetwork) was investigated through molecular dynamics (MD) simulations by Xu et al. [29] Fig. 3.

In the study Xu, Lanqing, et al. revealed a molecular-level understanding of the behavior of overall structure configuration as well as the graphene-CNT junctions [29]. The anisotropic nature of the 3D hybrid can serve as thermal rectifiers,this can be utilized in multi-directional thermal transport design. The junctions provide the vehicle for plastic deformation which was confirmed by the spatial distributions of stresses. Bonding analysis indicated that the sp^2–sp^3 bond conversion at the cleavages caused the degenerated elastic moduli and the thermal conductivity to the pillared-graphene system. The tensile strength for this system was calculated about 65–72 GPa, with 0.09 calculated to be the associated fracture strain. The stress–strain relations were nearly linear, which provided the opportunity to a new understanding of numerous nanomechanics applications where the key are linear responses, such as pressure sensing or position detecting [29]. In another study, a 3D conductive system of graphene and CNTs were jointly constructed,where the graphene providing a large specific surface area and CNTs offering the conductive pathway. Moreover, CNTs were believed to be served as spacers to the stack of graphene flakes and thus enhancing the surface area as well as providing reinforcement [38–40].

The practical applications, however, the greatest challenge of nanotechnology is the nanoscale size. The most feasible approach of bridging the microscopic structures to macroscale applications is to use the bottom-up synthesis method. CNTs and
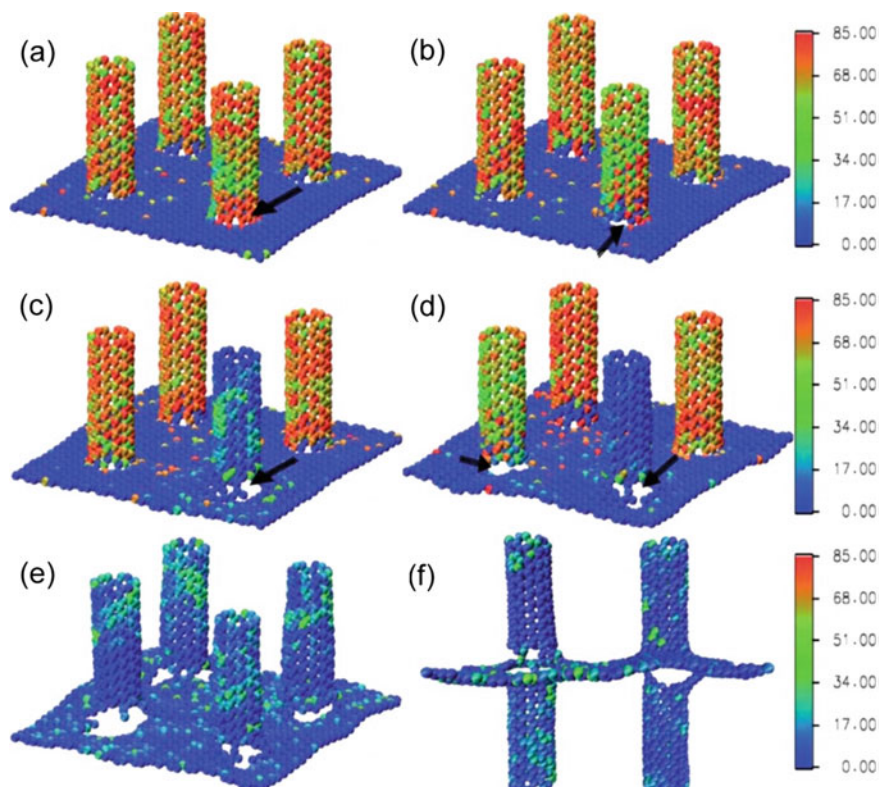
Fig. 3 A typical pillared-graphene nano network showing atomic stress distribution of **a** before bond breaking, during **b** crack nucleation, **c** crack growth, **d** fracture of two pillars, and **e** tearing with the strain applied along the carbon nanotube direction, as illustrated in Fig. 3c. As indicated by the arrows, the first break of the C–C bond occurs at the junction of the pillar and the graphene plane and is then triggered by the easily rotated sp^3 bonds. The stress degrades at the broken region and enlarges at the crack propagation tip, as indicated by the black arrows (**f**, **e**) [29]

graphene are the proper building blocks for promising high-performance advanced applications. In the CNT-graphene hybrid materials, CNTs can offer additional property enhancing and tunability benefits, which largely expand the field of applications and may also have the potential to lower the production cost for next-gen devices.

There are two core challenges in achieving high-performance functionality with graphene-CNT hybrid nano-system; the first one is the dispersion or distribution homogeneity of the conducting nano components–that is the formation of successful uniform distributed networks of contacts. And the second is the limited direct control over key variables like final confirmation and configuration of the arrangement of the nano components other than the overall loading fraction of the graphene or CNTs. Researchers in this field are using numerous fusion methods and modified those methods frequently to satisfy the particular demand of a required set of properties of

the graphene/CNT nano-hybrids. Moreover, researches also ongoing on achieving control over the scalability.

3 Fabrication of Graphene-CNT Hybrid System

The graphene-CNT hybrids were prepared by several approaches including the solution sonication followed by drying or freeze-drying (lyophilization) method [31], Sun et al. [41], CVD method [42], electrostatic spray technique [43], and self-assembly on substrates [37]. The strong pi–pi interaction between CNT and graphene produces 3D network for the material and provides stability of the hybrid product [44].

For better understanding, depending on the nano-material growth and processing techniques we divided the graphene-CNTs hybrid production methods into the following three groups

1. Solution-based methods: sonication and reduction
2. Fabrication using direct growth by the CVD method
3. Combined solution-sonication and CVD method.

3.1 Solution-Sonication Hybridization Method

In this processing category, the fabrication of the hybrid started from pre-grown/pre-produces graphene and CNTs. Where the graphene was usually prepared standard Hummers method and CNTs were grown using the CVD process. The carbon nano-materials were functionalized using various acid treatment processes to activate the surface interaction between them and for the functional design of the nano-hybrids.

Chang, Li-Hsueh, et al. developed a two-step graphene–MWCNT composite fabrication method workable at room temperature [30] Fig. 4.

In another research, Lv, Peng, et al. fabricated graphene/carbon nanotubes (Gr/CNTs) aerogels by a subsequent freeze-drying process [45]. An aqueous dispersion of graphene oxide (GO, pre-produced by modified Hummers method) and acid functionalized CNTs were made with a mass ratio of GO/CNTs = 3:1, then a hydrothermal reaction in an autoclave produce Gr/CNT followed by the freeze-drying process to finally get the Gr/CNT aerogels. The 3D framework of the aerogels was constructed with graphene sheets and entangled CNTs were coating on top of them. Where the CNTs bond the graphene sheets together in a way to avoid the sliding of graphenes under compression; thus improve the stiffness of cell walls, which made the aerogels super-elastic. Resulting Gr/CNT aerogels afforded high compression stability while maintaining the thermal transport paths. The maximum recorded thermal conductivity of Gr/CNT aerogel TIMs was up to 88.5 Wm^{-1} K^{-1} and the thermal interface resistance was as low as 13.6 mm^2 KW^{-1} [45] Fig. 5.
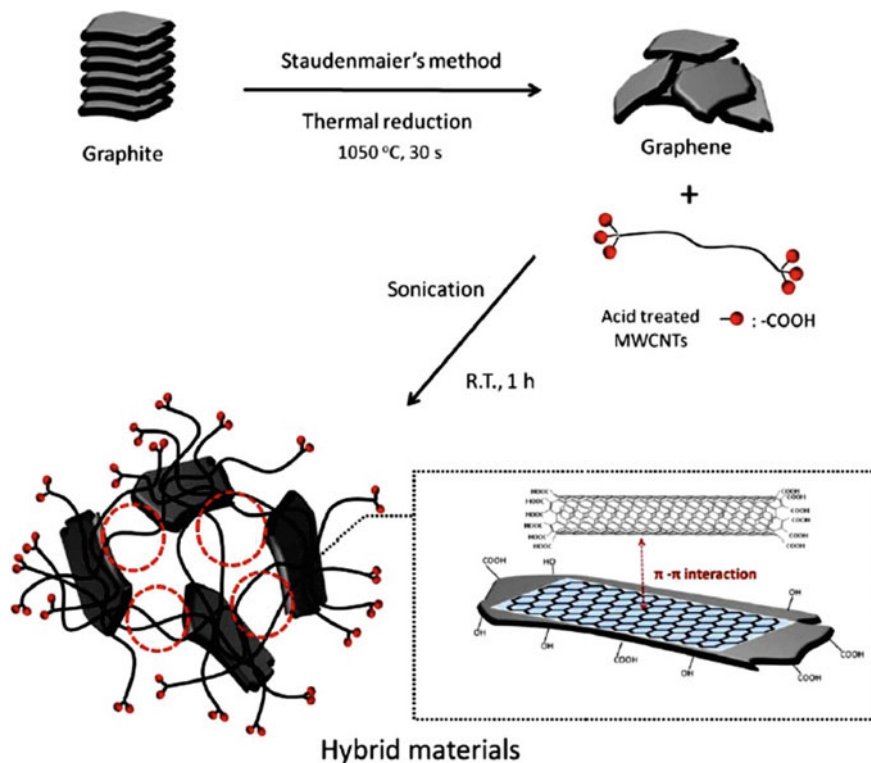
Fig. 4 The schematic mechanism for the preparation of graphene-CNT hybrid material [30]
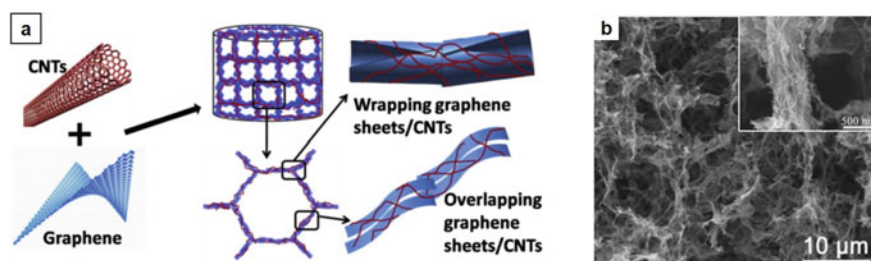
Fig. 5 Schematic representation for the micro-structure of Gr/CNT aerogels preparation, and **b** SEM images of Gr/CNT aerogel [45]

3.2 Fabrication Using Direct Growth by the CVD Growth

In this category, CNTs are grown directly on top of graphene or vice versa using inside CVD furnace using selective growth catalysts and different carbon precursors.
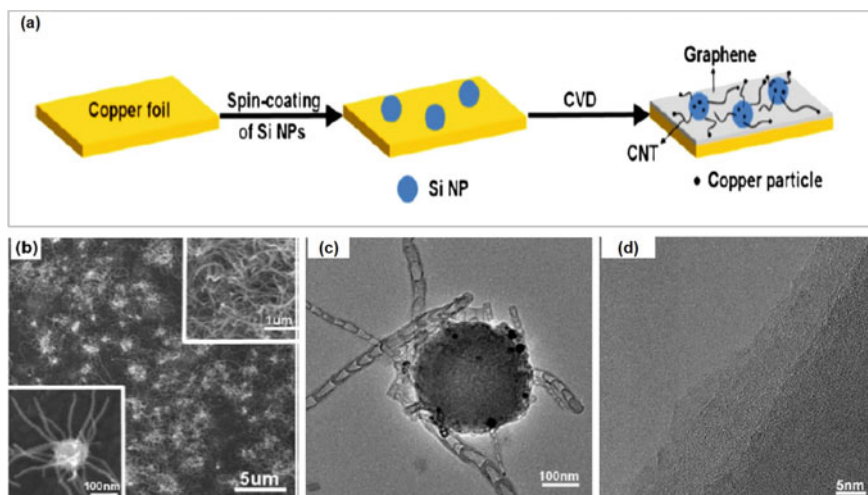
Fig. 6 **a** Schematic of one-step growth of graphene–CNT hybrid materials by CVD on Si NPs pre-coated copper foil, **b** SEM images of graphene–CNT hybrids grown on copper foil at 800 °C. Inset: (top) magnified SEM image of (**b**) and SEM image of CNTs grown from single Si NP (bottom), **c** TEM image of CNTs grown on a Si NP surface, and **d** TEM image of the edge of the grown graphene film [42]

Dong, Xiaochen, et al. showed a simple one-step synthesis process for producing highly conductive graphene–CNT hybrid materials by chemical vapor deposition (CVD), while using solvent ethanol. They decorated a copper foil with silicon nanoparticles (Si NPs) and graphene films were grown on the substrate uniformly while CNTs branched out from Si NPs to form a network on top. CNT density was controlled by the CVD growth temperature [42] Fig. 6.

Dong, Xiaochen, et al. developed a two-step CVD process to formulate graphene–CNT foam. First, the graphene was grown on nickel (Ni) foam, the graphene–Ni substrate was then immersed into the precursor of Ni particle followed by CNTs grown on top using ethanol, which was used as the carbon precursor [46]. Finally, Ni template foam was removed using HCl-etching. The resulting graphene–CNT hybrid foam showed a bulk density of 6.92 mg cm^{-3} and bending resiliency with a large angle. They showed that the hybrid foam can be used for selective removal of oils from the surface of the water with high capacity, proving to its super-oleophilicity and the microporous 3D structure can hold the absorbates [46] Fig. 7.

CNT–graphene hybrid films were fabricated by Nguyen, Duc Dung, et al. by the direct CVD growth method. At first, graphene was grown on Ni substrate in CVD then Fe sputter-coated on top followed by CNT growth inside CVD; acetylene was used as a precursor for both of their growth. The resulting CNT–graphene film behaved like an effective electron field emitter with low turn-on and threshold electric fields of 2.9 and 3.3 V mm^{-1}, respectively that can have numerous flexible electronics applications such as electron field emitters and conductors [47].
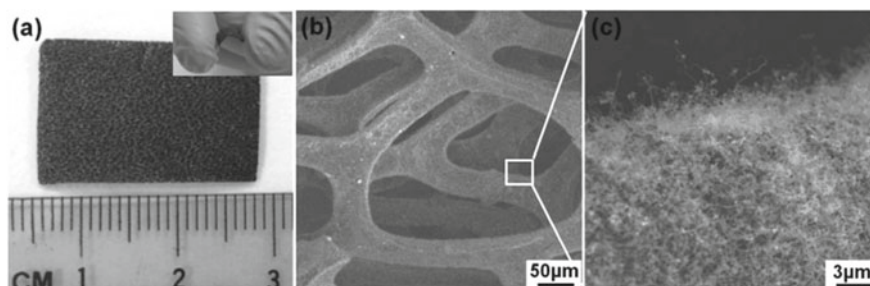
Fig. 7 a Optical image of graphene–CNT hybrid foam. Inset shows the bending of the hybrid, **b**, **c** SEM images of graphene–CNT hybrid foam with different magnifications [46]

Wang, Wei, et al. fabricated graphene-multiwalled CNTs 3D hybrid on Ni foam using an ambient pressure CVD process [48]. The foams possess a very large surface area of 743 m^2 g^{-1}, a high specific capacitance of 286 F g^{-1} which confirms an energy density of 39.72 Wh kg^{-1} and a high power density of 154.67 kW kg^{-1}. These advantages enable the innovative 3D multilayered graphene/CNTs foam to be used as high-performance EDLC electrodes, which are used in energy storage devices [48].

Song, Qiang, et al. demonstrated the fabrication of a lightweight conductive and flexible CNT–multilayered graphene edge plane (MLGEP) [49]. Here, a macroscopic CNT foam is first produced using a SiO$_2$ nanowire foam template-directed CVD method, and then MLGEPs are in situ grown on the CNT cores with seamless junctions by plasma-enhanced CVD (PECVD) resulting in a nanoporous shell without the use of metal catalysts followed by HF etching of the template SiO$_2$ nanowire. The CNT–MLGEP hybrid foam demonstrates high quality EMI shielding effectiveness that exceeds 38.4 or 47.5 dB in X-band frequencies [49].

3.3 Combined Solution-Sonication and CVD Method

Many researchers followed a combined approach to prepare graphene/CNT hybrids. They prepared a specific graphene template films or 3D porous structure using freeze-drying of pre-sonicated stabilized aqueous graphene dispersion followed by CNT growth on top of the graphene in the CVD method.

Kong, Luo, et al. had reported the development of reduced graphene oxide (RGO)/CNTs hybrid in several successive steps [50]. First, GO aerogels were made by sonication dispersion followed by freeze-drying then reduced and CNTs were grown on the RGO surface in a tube furnace at 600 °C. Lastly, the as-prepared (RGO)/CNTs hybrid foam was purified by HCl treatment. This low density (57 mg/cm^3) RGO/CNTs hybrid foams were proven good as electromagnetic interference shielding material and intended to be used in the field of aircraft and spacecraft [50] Fig. 8.
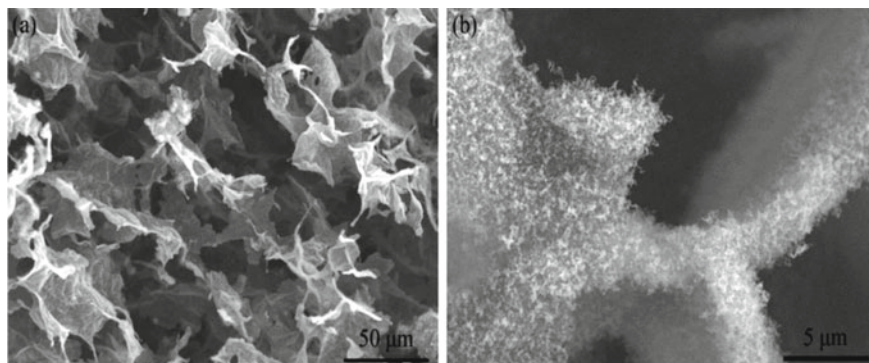
Fig. 8 **a**, **b** SEM images of RGO/CNTs hybrid composite [50]

The almost similar solution-based lyophilization method was used by Vinod, Soumya, et al. to fabricate a 3D graphene-CNTs hybrid and demonstrated how this solution synthesized the technique of making G-CNT hybrids can be adopted to produce large scale composites with an ordered arrangement of CNTs in the structure to enhance the structural stability [37] Fig. 9.

Another combined fabrication method was described by Fan, Zhuangjun, et al. where 3D CNT/graphene sandwich structures with CNT pillars were grown in between graphene layers using the CVD method [51]. This 3D structure showed high-rate transportation of electrolyte ions and electrons throughout the electrode matrix as well as the comprehensive utilization of pseudo and double-layer capacitance meaning proven to possess excellent electrochemical performances.

The supercapacitor based on the CNT-graphene sandwich (CGS) showed a specific capacitance of 385 F g^{-1} at 10 mV s $^{-1}$ in 6 M KOH solution. The new CGS hybrid was intended to be used as media for hydrogen storage, catalysts for fuel cells, electrode material in Li-ion secondary batteries and as components for other clean energy devices [51].
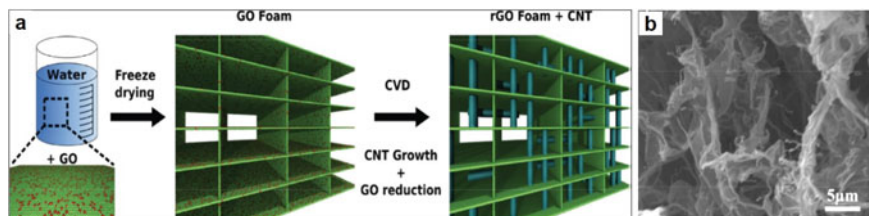
Fig. 9 **a** Schematic of the two-step synthesis process: 3D GO foam synthesized by lyophilization followed by CNT growth by CVD, which results in horizontal and vertical growth of CNTs in a 3D rGO scaffold and **b** the SEM image showing high magnification SEM image of rGO–CNT showing CNT grown along with the horizontal and vertical directions [37]

4 Graphene/CNTs Hybrid Properties

A favorable approach that is being increasingly explored by researchers for the preparation of graphene-based composites is the use of graphene as a hybrid filler in a second material. One of those materials, which is often explored, is CNT. Because of the all-carbon structural similarities of graphene and CNTs, the combination of these two nanomaterials has proven advantageous in getting superior final properties due to the resultant synergistic effect. Moreover, the hybridization counterbalanced some of the drawbacks of a specific nano-filler, and also improved the surface activity with the matrix as per the functionalization route.

4.1 Mechanical Properties

There are two approaches to describe the reinforcement ability of nanoparticles. One is the classical micromechanics approach and the other focuses on the reinforcement at the controlled molecular-level interactions between the nanoparticles themselves or nanofiller and matrix.

The relationships developed to describe the reinforcement relationship between a high-modulus filler in a low modulus matrix by the "rule of mixture" is the overall modulus of the composite (E_c), can be explained as follows [52]:

$$E_c = E_f V_f + E_m (1 - V_f)$$

Here E_m and E_f represent the moduli of the matrix and the filler, respectively whereas, V_m and V_f and are the volume fractions of the matrix and filler, respectively.

This calculation assumes the uniform distribution of the nanofillers within the matrix, perfect bonding between them, a void-free matrix, and does not account for Poisson's ratio. Although this rule of mixture simplifies the system, it has been proven to well define the modulus of composites with low nanofiller loading and has been helpful for the researchers to predict an approximation of the tensile properties of the final composites. In the case of higher nanofiller content, there is a higher nanofiller aggregation, therefore this equation is not applicable.

To overcome this problem and also consider the effect of filler orientation and filler size new semi-empirical formulas were developed. One such equation was developed by Halpin–Tsai [53]. Additionally, the Halpin–Tsai equations consider the orientation of the filler towards either transverse (T) or the longitudinal (L) direction. The equation of modulus that captures these aspects is given by.

$$\frac{E_L}{E_m} = \frac{1 + \xi \eta_L V_f}{1 - \eta_L V_f}$$

$$\frac{E_T}{E_m} = \frac{1 + 2 \eta_T V_f}{1 - \eta_T V_f}$$

where the parameter η is given by:

$$\eta_L = \frac{\left(E_f/E_m\right) - 1}{\left(E_f/E_m\right) + \xi}$$

$$\eta_T = \frac{\left(E_f/E_m\right) - 1}{\left(E_f/E_m\right) + 2}$$

E_f = tensile modulus of the filler and ξ = a shape fitting parameter that describes the orientation geometry of the reinforcing fibers along with the packing arrangement. Many studies have used ξ for the particular characteristics of their filler and especially on their aspect ratio(s). Generally, in the case of nanoplatelets, $\xi = 2/3$ s [54], while in the case of fibers $\xi = 2$ s [55].

Yang et al. in [56] reported a study in which they fabricated hybrid epoxy composites reinforced with multi-graphene platelets (MGPs) (0.9 wt%) and multi-walled carbon nanotubes (MWCNTs) (0.1 wt%), Fig. 10 [56]. There they form a hybrid structure with a combination of amine-functionalized MWCNTs and MGPs. In another set of composites, they combined un-functionalized MWCNTs and MGPs.

Results showed that the ultimate mechanical properties had improved at a higher number in the case of the functionalization of MWCNTs due to the interfacial bonding between fillers. Researchers claimed the formation of the 3D structure using the combination of a 2D-filler (MGPs) and 1D-filler (MWCTNs) had inhibited the
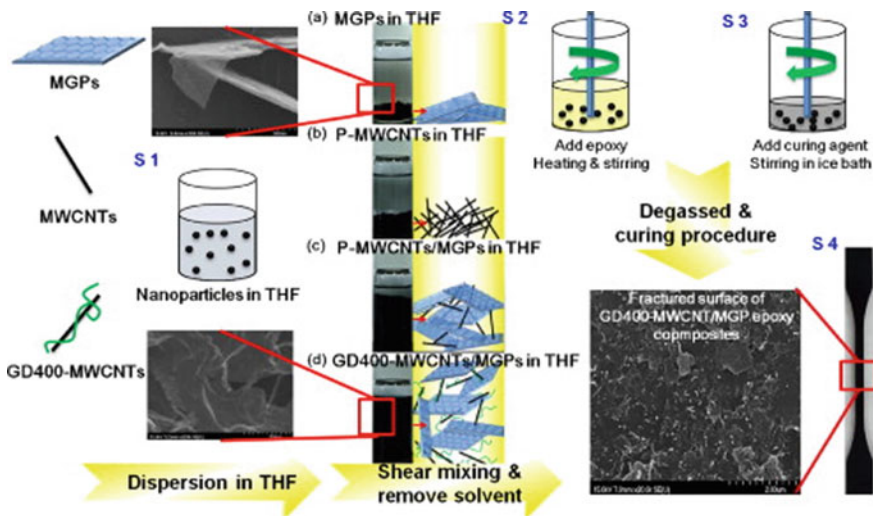
Fig. 10 The fabrication method of the hybrid epoxy composites with Graphene and CNT using solution mixing process [56]

nanofiller surface interaction thus reduce aggregation and increase surface area. Additionally, the presence of the amine groups in the functionalized nanofiller formed a highly cross-linked structure which not only enhanced the tensile strength and the tensile modulus but also increased the elongation properties. The tensile modulus and tensile strength of 0.9 wt% MGP and 0.1 wt% MWCNT reinforced epoxy composites were improved by 22.6% and 14.5% respectively, compared to neat epoxy.

Chatterjee et.al. investigated the effect of the size of graphene nanoplatelets (GNPs) on the mechanical and thermal properties of epoxy/GnP composites [57]. They used two different flake sizes of GnPs (5 and 25 μm). Results showed higher mechanical properties of the composites prepared with the bigger sized GNP flakes at all concentrations as they actively control the failure mechanisms in the composite. They have also used hybrid nanofillers,carbon nanotubes (CNTs) with GnPs in different mixture ratios. Among those composites, the one with the highest CNT content (9:1) provided substantial enhancement in fracture toughness of 76%. An interesting finding was the influence of CNT:GnP ratio on the nanocomposites, as in the combined state the high aspect ratio intrinsic properties of CNTs and the large surface area of GNPs provided a synergistic effect in improving the mechanical strength. An enhancement in flexural modulus was measured with CNT:GnP ratio of 9:1 that demonstrated the highest increase of 17% in comparison to the pure CNT and GNP which were measured to be an increase of 9% and 5%, respectively. Also in the case of the nanocomposite made from 5:1 ratio of CNT:GnP, the flexural modulus was higher than that of the composites prepared with GNP and pure CNT. This dictates an efficient load transfer mechanism from the matrix to the hybrid system of nanofillers.

Moosa et al. also reported similar synergistic effects on the mechanical properties of nanocomposites prepared from functionalized multiwalled CNTs (F-MWCNTs) and GNPs with epoxy matrix [58]. In this study, they showed that the tensile strength of the hybrid nanocomposites significantly varies with the change of the ratio of GNPs and F-MWCNTs in the nanocomposites even though the total filler content was kept constant 0.5 wt%. The maximum increase of mechanical properties was achieved in 5:5 ratio of GNPs and F-MWCNTs; a 54% increase in Young's modulus and a 49% increase in tensile strength compared to that noticed for neat epoxy. Excellent mechanical properties were demonstrated by hybrid nanocomposite having GNPs and FMWCNTs in ratios 9:1, which was because of the better distribution of nanofillers in the composites.

In another work Zhang et. al dispersed functionalized CNTs and functionalized Graphene to achieve a synergistic effect of reinforcement in polyethersulfone (PES) matrix [59]. It was found that the carboxylic functional groups on CNTs were primarily responsible for enhanced interface interaction between the filler materials and effective modulus and strength improvement. For f-G-f-CNTs (Wf-G/Wf-CNTs = 1:1)/PES composite tensile modulus and strength increased to 98 and 12% respectively.

To further explore the effects of hybrid fillers on the mechanical properties of thermoplastics Gang-Ren et al. investigated the effects of GNP, CNT, and hybrid fillers on ultrahigh-molecular-weight polyethylene (UHMWPE) [60]. UHMWPE/MWCNT and UHMWPE/graphene sheet (GNS) composites with a segregated network were

studied. Both the tensile strength and tensile modulus of the resultant nanocomposite were significantly increased at lower nanofiller content and then decreased with increasing nanofiller loading after a certain point. For both the nanofillers, MWCNT, and GNS at 0.25 wt% filler loading the tensile strength of composites increased by 12.8 and 38.0%, from 30.5 to 34.4 and 42.1 MPa, respectively, and the tensile modulus also improved by 23.9 and 73.6% from 401 to 497 and 696 MPa, respectively. The MWCNT exhibited a significant enhancement of the mechanical properties compared to GNS, which was due to the thick segregated network formation in the UHMWPE/MWCNT composites. At lower filler loading, <0.5 wt%, the segregated structure cannot form the macroscopic networks. They explained the mechanical behavior as with higher nanofiller loading large segregated structure formed which gradually touch each other and under stress, the micro-cracks eventually converted into macro-cracks. Therefore, the degradation effect of the segregated structure is larger than the improvement of filler leading to lower mechanical properties.

With the mixture of nanofillers, a hybrid composite was prepared and similar improvement was observed in the mechanical strength. At the ratio of 1:1 (GNS: MWCNT) with 0.5 wt% filler loading, the tensile strength increases by 30.8% from 30.5 to 39.9 MPa, and the tensile modulus also increases by 37.1% from 401 to 638 MPa. While the tensile strength decreased to 27.5, and tensile modulus decreased to 467 MPa when the hybrid nanofiller loading was 2.0 wt%. Another interesting finding of this study is that the critical content of hybrid fillers is 0.5 wt%, which is slightly larger than that of single filler (0.25 wt%). This indicated a synergistic effect of using GNS and MWCNT together, which can lower agglomeration and enhance network hybrid nanofiller distribution within the composite matrix Table 1.

4.2 Electrical Properties

Zhang et. al. in their work reported dispersed functionalized CNTs and functionalized Graphene to achieve a synergistic effect of reinforcement in polyethersulfone (PES) matrix [59]. Those composites with individual 5 wt% loaded nanofillers of f-G/PES, f-CNTs/PES and p-CNTs/PES had an electrical conductivity of 5.82×10^{-4}, 1.43×10^{-4} and 2.65×10^{-4} S/m respectively. For hybrid nanofillers, the conductivity of 1:1 = Wf-G: Wp-CNTs in the f-G-p-CNTs sample was 6.1 times greater than f-G, and 1.34×10^4 times greater than p-CNTs. On the other hand, 1:1 = Wf-G: Wf-CNTs in the f-G-f-CNTs sample showed conductivity 2.2 times greater than f-G and 8.9 times greater than f-CNTs. Therefore, results indicated that a combination of functionalized graphene and non-functionalized CNTs gave the best electrical conductivity in the PES matrix.

Gang-Ren et al. studied the electrical properties of composites made of ultrahigh-molecular-weight polyethylene (UHMWPE) matrix with nanofillers, multi-walled carbon nanotube (MWCNT) graphene sheet (GNS). The preparation procedure involved a segregated network formation of nanofillers by hydrazine reduction, ethanol-assisted dispersion and hot-pressing process [60]. The improvement in

Table 1 Comparative table showing the reinforcing ability of hybrid Graphene and CNT nanoparticles with different matrix

Graphene type	Content (wt%)	CNT type	Content (wt%)	Hybrid content (wt%)	Matrix	Preparation method	Modulus increase (%)	Tensile strength increase (%)	References
GNP	0.26	MWNT	0.24	–	Epoxy	Three roll mill	14	20	[4]
GNP	0.26	MWNT	0.24	–		Three roll mill + CVD	40	36	[4]
GNP	–	MWNT	–	0.1	Epoxy	Solution blending	18	12	[61]
GNP	0.25	fMWNT	0.25	–	Epoxy	Solution blending	54	49	[33]
GNP	0.9	fMWNT	0.1	–	Epoxy	Solution blending	27	35	[62]
GNP	0.5	MWNT	0.5		UHMWPE	Solution blending	37	31	[63]
GNP	–	MWNT	–	0.75	VMQ	Solution blending	137	110	[5]
fGr		fMWNT	5	–	PES	Solution blending	98	12	[25]
GO	0.2	MWNT	0.06	–	Epoxy	Solution blending	11	12	[64]
GO	10	MWNT	5	–	PVA	Solution blending	106	80	[9]
rGO	2.15	MWNT	2.15	–	NR	Sol-blending /melt	100	80	[10]

conductivity and the hybrid effects of nanofillers were examined. Results showed the percolation threshold is about 0.20 wt% for the UHMWPE/MWCNT composites which was considerably lower than the random distribution of CNTs, while the UHMWPE/GNS composites, showed a slightly higher percolation threshold. The low percolation threshold for MWCNT is due to the evenly segregated structure that was efficiently forming the conductive network within the UHMWPE matrix. Although theoretically, GNS is considered more effective in increasing conductivity and is expected to be easily attachable to each other to form a network as it has very high surface energy and high specific surface area. Still, experimental findings demonstrated MWCNT has a lower percolation threshold than that of GNS. These contrary results were explained by the researchers as a consequence of the specific geometry of GNS, although GNS has a large surface area the contact between them had happened to be overlapped but not end-to-end joints within the matrix as a result the GNS had more readily aggregated than MWCNT. This aggregation of GNS caused a higher percolation threshold to form a conductive network within UHMWPE/GNS composites. To get higher conductivity and a lower percolation threshold, a different weight ratio of MWCNT and GNS was introduced as a hybrid nanofiller system within the UHMWPE matrix. Results showed that the hybrid composite has higher conductivity and a lower percolation threshold. With a hybrid ratio of 3:1 = GNS: MWCNT, 0.2 wt% is the percolation threshold of the hybrid composite. which was lower than that of UHMWPE/GNS composites. Additionally, the conductivity of the 0.1 wt% nanofiller loaded hybrid composite was 8.7×10^{-5} S $\times$ cm^{-1}, almost twice that of UHMWPE/GNS composite (1.7×10^{-6} S x cm^{-1}). The 50 wt% increase of MWCNT in the hybrid, as GNS: MWCNT = 1:1 lower the percolation threshold of the hybrid composite to about 0.10 wt% nanofiller, this was lower than that of composite filled with MWCNT or GNS alone Fig. 11.

At 1.0 wt% fillers loading, the conductivity of hybrid composites was found to be almost four times higher than that of the composites reinforced with GNS alone but slightly lower than that of the composites filled with MWCNT alone. This suggested the synergistic efficacy of the hybrid filler of GNS and MWCNT in improving the conductivity of composites. By increasing the MWCNT in the hybrid fillers to 75 wt% (GNS: MWCNT = 1:3), the conductivity and the percolation threshold barely changed. This was explained as in the case of a hybrid nanofiller network, the 2D GNS attachment with stretched 1D MWCNT and formed the hybrid structure Fig. 2. The presence of MWCNT was helpful to prevent the GNS from aggregate. Simultaneously, the fluid viscosity of the matrix was increased through the inclusion of GNS, and the movement of GNS within the molten matrix stretches MWCNT that provided its directional alignment. Consequently, the formation of many junction points among MWCNT/GNS hybrid fillers substantially increased the interface area of junctions. This led to an increase in the electron flow path formation probability of hybrid fillers. They concluded that the GNS only played an important role in the junctions and within the conductive pathways, and thus the composite conductivity still mainly relies on the MWCNT.
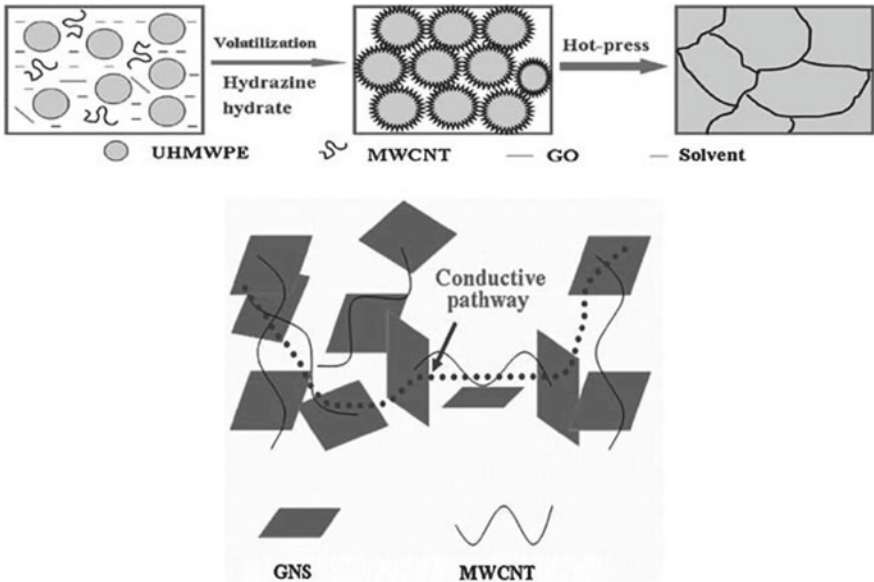
Fig. 11 Formation of conductive pathways in graphene/CNT reinforced composite polymer [60]

4.3 Thermal Properties

The incorporation of nanofillers introduces thermal conductivity, another vital characteristic of the poor thermal conductor matrix polymers, ex: epoxy. The major influencing factors of thermal conductivity of the composites are nanofiller dispersion, nanofiller content, and the crucial one is the polymer-nanofiller interface thermal resistance [63, 65].

According to the Cowan method, thermal diffusivity (α) values are calculated and expressed by the following equation,

$$\alpha = \frac{\eta d^2}{t_{5_0}}$$

Here η, d, and t_{50} are the

Here d, η and t_{50} are the thickness of the specimen, a dimensionless constant, and the time taken for the temperature at the point on the opposite surface to reach 50% of the plateau value, respectively. With the calculated α, next, it is compared with the thermal diffusivity of the standard specimen to obtain the heat capacity (Cp). The thermal conductivity (K) can be determined using the following equation.

$$K = \alpha \rho C_p$$

where, ρ is the density of the specimen.

Yang et al. demonstrated the thermal conductivity of a prepared hybrid epoxy composites reinforced with 0.1 wt% multi-walled carbon nanotubes (MWCNTs) and 0.9 wt% multi-graphene platelets (MGPs) [56]. The thermal conductivity of the carbon nanofillers reinforced epoxy composites was determined at room temperature by a hot disk thermal conductivity analyzer. Even though MGPs were more crystalline their nanocomposite thermal property was least improved when compared to hybrid composites. The reason for the result was because of the lower aspect ratio of MGP aggregation that contributed to the reduced contact area between the epoxy matrix and MGPs. In this case, the thicker polymer layer on the surface of MGPs leads to severe scattering for phonon transport [66]. With 1% hybrid nanofiller loading in P-MWCNT/ MGP/epoxy composites, the thermal conductivity increased 93% as compared with epoxy composites with MGPs or MWCNTs alone. They explained that the improvement was mainly because of two factors. An increase in contact area increases phonon diffusion within hybrid nanofillers and decreases thermal interfacial resistance. Firstly, the contact geometry is altered from 0-D point contact to 1-D linear contact that remarkably increases the contact area within hybrid nanofillers. The larger contact area increases the path for phonon diffusion within hybrid nanofillers that contributes to decreased thermal interfacial resistance. Secondly, the CNT attached to GNPs reduced the aggregation of nanoparticles within the matrix. Furthermore, the highest increase in thermal conductivity was reported for the GD400-MWCNT/MGP/epoxy composites compared to other epoxy composites. The increase in thermal conductivity was more than 146% by the addition of a 1 wt% nanofiller of GD400-MWCNTs/MGPs. This indicates that GD400-MWCNTs are capable of increasing the interaction between hybrid fillers and epoxy matrix [65, 67].

Yu et al. attempted to increase the thermal conductivity of epoxy by introducing nanofiller GNPs and single-walled carbon nanotubes, SWCNTs into the epoxy matrix [68]. They used varied content of nanofiller from 5 to 40 (wt%) and reported positive synergistic effects on thermal conductivity. The improvement in thermal conductivity was mainly ascribed from the bridging of planar nanoplatelets by the flexible SWNTs, this leads to a decrease in thermal interface resistance along with the (2D-1D) hybrid filler network due to the extended area of the SWNT-GNP junctions. Lee et al. remarked an interesting finding that the incorporation of XGNPs and CNTs into the epoxy matrix simultaneously enhances the thermal, electrical, flexural, and electromagnetic interference shielding effectiveness (EMI SE) properties [69]. At a ratio of 5:5 = XGNPs: CNTs and a total of 10 wt% nanofiller content, the flexural modulus of XGNPs/CNT/epoxy hybrid nanocomposite was increased by 1.54 GPa, as compared to that noticed for neat epoxy resin. The Electromagnetic Shielding efficiency, EMI SE of the CNT-XGNP hybrid composite was higher than 25 dB at 100 MHz, where the EMI SE of the XGNP based composite was almost zero.

5 Applications

5.1 Structural Applications

The elastic modulus of the C–C bond of the graphene plane of graphitic carbon is one of the highest of any known material. The reason for such an increase is mainly due to the formation of planar honeycomb lattice in which each every carbon atom is attached to three neighboring carbon atoms by covalent bonds in the plane. Due to the strength derived from these strong covalent bonds, CNTs are expected to be the ultimate high-strength fibers. SWCNTs are resistant to various physical forces. CNTs have highly advantageous properties because of the hexagonal lattice and sp^2-hybridizations between the carbon bonds, thus resulting in a Young modulus around 1 TPa [69] and a tensile strength of 50–100 GPa. MWCNTs are less stronger than SWCNTs in that case. However, advantages such as being cheaper and easier synthesis can be used in strengthening other materials [70]. High aspect ratio and surface are the features that are incorporated into structural nanocomposites.

On the other hand, graphene shows more toughening effects than CNTs. When g-modified epoxy fibers are infiltered with glass fibers, they show improved fatigue life and toughness [71, 72]. Graphene-based polymer composite also exhibits high electrical conductivity, Young's modulus and thermal conductivity [73].

So, taking the advantage of high strength and stiffness from CNTs and high fracture resistance from Graphene a synergistic effect can be implemented for structural applications with these hybrid composites. Particularly in areas where high mechanical and electrical properties are desired. Structural Health Monitoring (SHM) is one such area. These structures are often exposed to a variety of conditions namely, impact, shock loading etc. SHM systems consist of putting a sensor to the outside area or embedding them inside. These sensors sense changes in order to detect damages [74]. However, better sensing can be achieved by embedding high-value multifunctional materials within the bulk material. The primary advantage of self-monitoring materials is non-localized detection in a region, which makes the detection of bulk material possible [75]. Some examples of those particles are carbon-based materials such as short carbon fibers [62], carbon nanotubes [76], graphite particles and graphene nanoplatelets [64, 77]. Combining with the electric network, graphene incorporating polymers make good self-sensing devices [78, 79].

Structural health monitoring (SHM) systems are used vastly in many industries, such as construction, aerospace, wind energy etc. [80]. The system integrity can be vulnerable while the materials or geometry is damaged and hence, self-sensing materials are used [81]. These self-sensing materials could be useful in detecting any structural damage which may lead to huge catastrophic failure if not detected in time.

5.2 Energy Harvesting and Storage

5.2.1 Batteries

In recent years, lithium-ion batteries (LIBs) have garnered much attention because of their tailorable properties. Technological development allows the successful development of new electrode materials for LIBs. However, a higher density and power capability longer shelf-life electrode material is in great demand. Graphene/CNTs hybrid composites exhibited great potential as novel electrode materials for LIBs reported in the literature [78].

Yoo et al. fabricated the first graphene/CNTs hybrid-based electrode materials for LIBs which showed a higher specific capacity of 730 mAh/g in 2008 [82]. But they observed a faster energy fading rate resulting in short life cycles. They ascribed this phenomenon due to poor interface mixing (e.g. physical mixing) of graphene and CNTs with matrix polymers as well as each other. Therefore, effective mixing and network formation for better conductivity is the prime need to achieve high specific capacity and longer life-cycle of the energy storage devices. Chen et al. and Li et al. both demonstrated a chemical vapor deposition (CVD) approach for graphene/CNTs based on composites fabrication and used for LIBs which showed improved capacity, cyclability and higher rate capability. This can be ascribed due to strong bonding and effective network formation which eventually allows for higher charge transportation. Researchers also tried various methods such as π- π stacking, microwave-assisted assembly, electrostatic interaction, unzipping methods etc. for graphene/CNTs hybrid composites fabrication. Recently, Xu et al. fabricated homogeneously grown iron nanoparticles on graphene via the hydrothermal approach for the catalytic growth of CNTs Fig. 12a. This simple and cost-effective method allowed to grow vertically aligned CNTs on graphene Fig. 12b, and the fabricated LIBs based on these composites displayed excellent performance due to the synergetic effect between graphene and CNTs Fig. 12c.

5.2.2 Solar Cells

Due to the synergistic effect of graphene and CNTs in hybrid systems, they got much attention and were studied rigorously in solar cell (SC) or sensitized solar cell (SSC) as a counter electrode, photoanode, electrolytes etc. A continuous flow path is established for electron mobility via forming a bridge between graphene flakes using CNTs, and thus the hybrid system shows high electrical conductivity and excellent cell performance. Zhibin et al. fabricated a graphene nanoribbons/CNTs hybrid electrode and observed high cell performance compared to the Pt electrode. They ascribed due to the formation of bridged CNT structure through unzipping MWCNTs. Chang et al. reported the first time a solution-based method to develop an electrode material based on graphene/MWCNTs on fluorinated tin oxide (FTO) shown in Fig. 13. This electrode they used in dye-sensitized solar cells (DSSCs), for
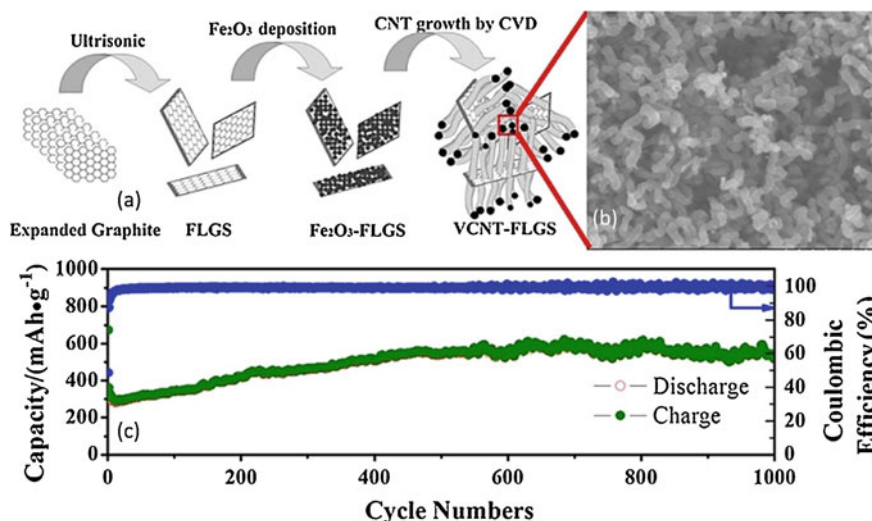
Fig. 12 **a** CVD processing procedure for graphene/CNTs composites, **b** the microscopic image of the composites, **c** the LIBs performance based on the composite anode [83]

promoting green energy. They observed that the electrode showed a higher electron transfer rate of 91.6% and exhibited higher cell performance [84].

5.2.3 Supercapacitors

In recent years, supercapacitors were applauded globally due to their excellent performance such as longer life-cycles, high conductivity, high power density, eco-friendly features etc. The characteristics of the electrode materials and electrolytes govern the performance of the capacitors. Graphene and CNTs showed excellent potential as electrode materials of supercapacitors among all carbonaceous materials. Their inherent characteristics such as high electrical conductivity, thermal stability etc. as well as the synergistic improvement of their inferior properties allow the fabrication of high-performance electrode materials. For example, incorporation of CNTs offer bridge formation between graphene sheets, improve charge transfer capacity, reduce electrical resistance and thereby increase the overall performance of the device. As we mentioned earlier, CNTs might reduce the interlayer stacking between graphene sheets, improve accessibility and mobility of the electrolyte ions. Therefore, researchers have been invested lots of time in high-performance electrode fabrication based on graphene/CNTs hybrid systems.

Yu et al. fabricated graphene/CNTs hybrid composites films using the self-assembly method [85]. They observed the performance of the hybrid as supercapacitors and found an average specific capacitance of 120 F/g. But Fan et al. showed
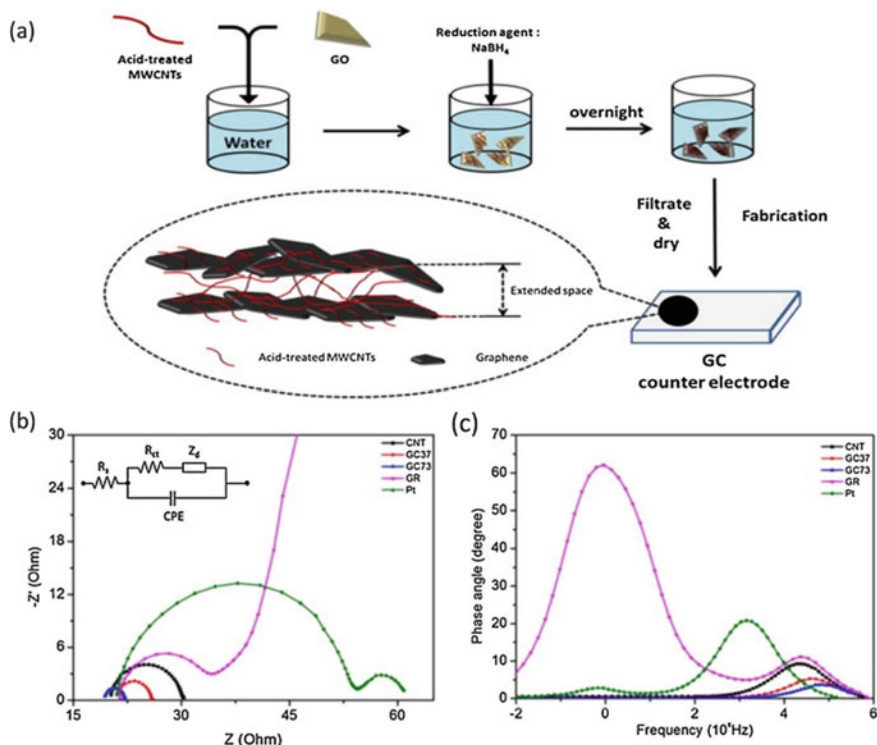
Fig. 13 **a** Preparation of CNT/graphene composite counter electrode and **b**, **c** the performance of the cells based on CNT, graphene/CNT, graphene, Pt counter electrodes. GC37 refers to 30 wt% graphene and 70 wt% MWCNTs, and GC73 refers to 70 wt% graphene and 30 wt% MWCNTs [83, 84]

excellent improvement in specific capacitance 385 F/g using graphene/CNTs sandwich structures. They used the CVD method to fabricated the hybrid layered structure where CNTs reside spaces in between the graphene layers. They attributed that the bridging effect of graphene layers via CNTs enhanced the mobility of the charge carriers, results in high specific capacitance Fig. 14.

5.2.4 Fuel Cells

A fuel cell is a kind of electrochemical cell that converts chemical energy into electrical energy. These cells work as energy storage devices with high conversion efficiency and low discharge. Graphene/CNTs hybrid showed excellent effectiveness for the fabrication of high-performance fuel cells Fig. 15.
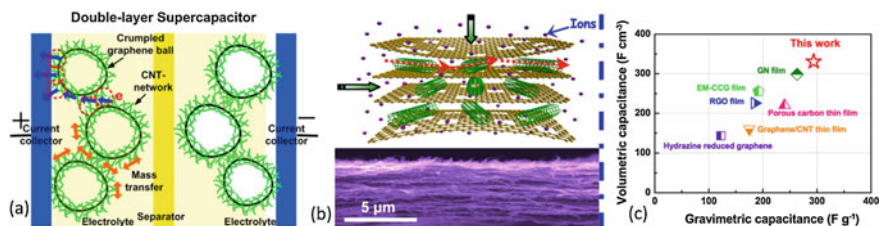
Fig. 14 a Representation of the EDLC based on crumpled graphene ball/ porous CNT composites [86]. **b** Illustration of the ion diffusion behavior for the graphene nanomesh/CNT composites and **c** the capacitance properties of the electrode based on graphene nanomesh/CNT composites [83]
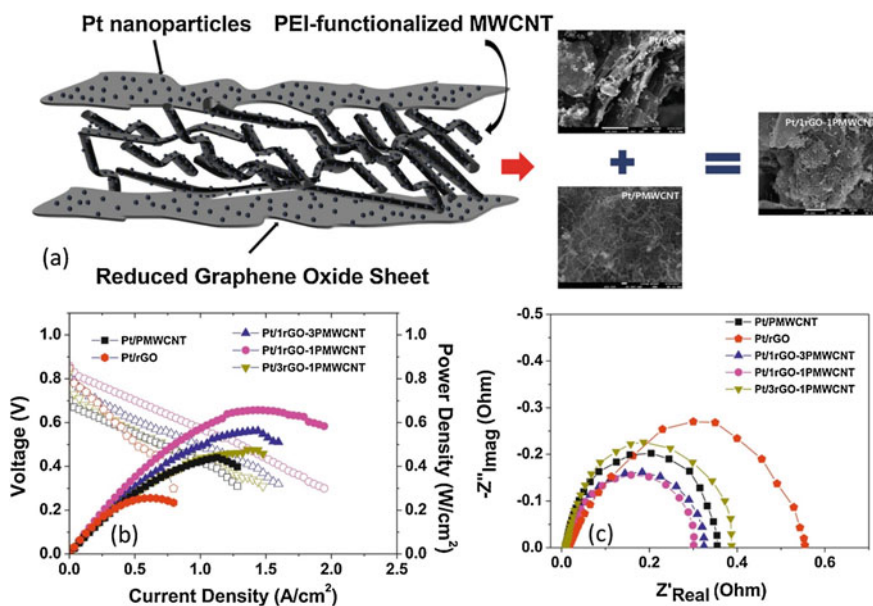
Fig. 15 a Pt/rGO-CNTs composites and **b**, **c** the corresponding cell performance for PEMFCs [83, 87]

5.3 Sensors and Actuators

The first focus here is to define sensors and actuators and discuss the usages of sensors and actuators made by using a graphene-CNT hybrid system.

Firstly, a sensor is an electrical device which receives signals and convert them into a readable data, then responses to the offset of the signal [88]. Sensors are used for monitoring fluid levels, voltage changes etc. in various industrial processes. They correspond to the change in the parameters and can trackback the problem to the central monitoring unit or adjust a function by itself to maintain the balance in the system ("https://www.onupkeep.com/answers/predictive-maintenance/sensors-
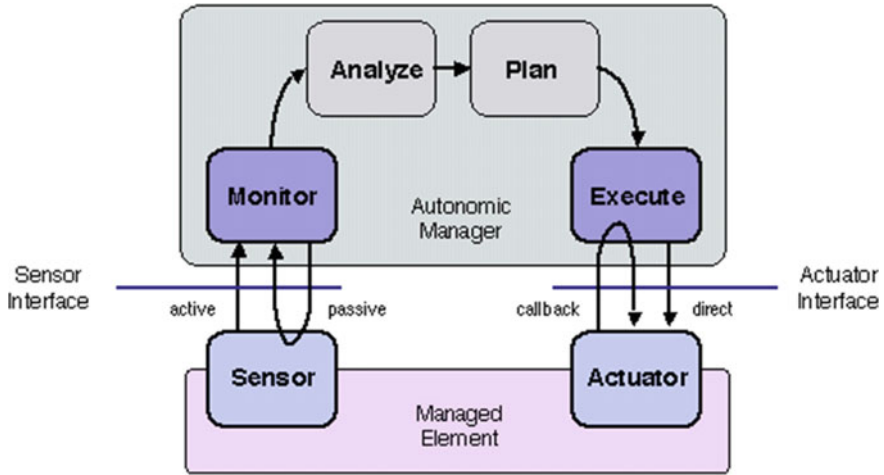
Fig. 16 Schematic diagram of a complete operating process including the functions of actuators and sensors [89]

and-actuators-2/—Google Search"). Whereas, actuators are basically dedicated to converting energy into mechanical energy and cause motion ("Introduction to Transducers, Sensors and Actuators—Google Search"). Actuators can be operated using different means of instrumental methods, such as pneumatic, electric, magnetic etc. ("https://www.onupkeep.com/answers/predictive-maintenance/sensors-and-act uators-2/—Google Search"). So, the basic difference between sensors and actuators is, sensors convert parametric changes into a readable electrical signal to control the process,actuators simply do the exact opposite by converting energy into motion. For executing a task fully, both actuators and sensors are needed, as their functions are complementary to each other Fig. 16.

CNT-infused materials have taken over all the related fields in recent years, which the nanoactuators and sensors synthesis. The applications of different graphene and CNT-based sensors are so vast that, it is predicted to be one of the most influential production systems soon. The main usages of graphene and CNT-based nanoactuators and sensors are:

I. Graphene hybrids in SSCs [90]:

Sensitized solar cells (SSC) are widely known for their low production cost and comparative high efficiency. Dosing graphene in photoanodes and counter electrodes gives extreme mobility to the conductive film of the charge career layer. It also cuts off the need for metal oxide glasses (i.e. FTO, ITO etc.), which helps to reduce the production cost, attain mechanical and chemical sustainability amid unconventional weather and high transmittance. Graphene quantum dots are also used as sensitizers for these SSCs. Graphene hybrids are used mainly to elevate the electron transfer rate and redox rate Table 2.

Table 2 SSC performance after using different graphene hybrids [90]

Electrode with graphene/SNM hybrid	J_{sc}(mA/cm^2)	V_{oc} (V)	FF (%)	n (%)	References
PA: N719/TiO$_2$-Graphene oxide/FTO	13.1	0.77	71	7.26	He et al. [91]
PA: N3/TiO$_2$-rGO/	16.29	0.69	NA	6.97	Yang et al. [65]
PA: N719/TiO$_2$-Graphene nanofibers/FTO	16.2	0.71	66	7.6	Madhavan et al. [92]
PA: Graphene QD/TiO$_2$/FTO	0.2	0.48	58	NA	Yan et al. [93]
PA: ZnO-graphene QD/Cs$_2$CO$_3$/Al	0.196	0.99	24	2.33	Son et al. [94]
PA: (TNS-rGO-CdS QD)$_{10}$/FTO	0.92	1	41	0.38	Wang et al. [48]
CE: CuInS$_2$-rGO/FTO	16.63	0.74	51	6.18	Liu et al. [95]
CE: Cu$_2$S-rGO-PVA binder/FTO	18.4	0.52	46	4.40	Radich et al. [96]
CE: SWCNT-rGO/FTO	12.81	0.9	76	8.37	Zheng et al. [97]
CE: MWCNT-rGO/FTO	16.05	0.75	62.7	7.55	Velten et al. [98]
CE: TiN-rGO-CNT/FTO	14.0	0.642	46	4.13	Youn et al. [99]
PA: MWCNT-rGO-TiO$_2$/FTO	11.27	0.78	70	6.11	Ming-Yu et al. (2011)
CE: rGO-CNT/FTO	11.42	0.77	53	4.66	Li-Hsueh et al. [100]
CE: rGO-CNT/FTO	15.25	0.68	51.05	5.29	Ma et al. [101]
CE: CNT-rGO/graphite paper	12.86	0.78	61.3	6.17	Guang et al. [102]
CE: rGOnanoribbons-CNT/FTO	16.73	0.73	67	8.23	Zhibin et al. [103]
CE: VACNT-graphene paper	14.24	0.68	62.4	6.05	Li et al. [104]
CE: Pt NPs/graphene nanosheets/FTO	18.26	0.72	65	8.54	Tsai et al. [105]
CE: Graphene nanoplateletes-Pt NPs/FTO	14.31	0.735	61.9	6.51	Hoshi et al. [106]

According to the list, it can be clearly stated that graphene improves the Power Conversion Efficiency (PCE%) and Open Circuit Voltage (V_{OC}) of the sensitized solar cells.

II. Gas sensor development [107]

Gas monitors are being widely used in leakage and concentration controls in many production plants. Recent studies have shown that CNT and graphene infused gas sensors are highly performing than the usual gas sensors in the global market (based on semiconductor oxides). Their performance is further enhanced by coupling nanocarbon particles with semiconductor oxides and noble gases. Using CNT in between two conducting posts (MWCNT, SWCNT etc.) results in high electric contact and mechanically sound detectors. It requires only the post-processing steps to fabricate these types of detectors, as they have the self-welding ability. Therefore, these instruments can easily be industrialized. The sensors are also sensitive to the specific gases and their concentrations. The main usability of these sensors is their strong mechanical stability, alongside their small volume consumption, which is useful in environments where corrosive vapors are high in concentration. Graphene gas sensors are even more usable, because of their thermal and optical properties. Graphene oxide (GO) works as an excellent sensor because of its flexibility, reducibility and high electron mobility Table 3.

   The reason of coupling GO with another metal or semiconductor material is attaining more sensitivity, although the overall cost increases a lot. But on the other hand, energy consumption reduces for the semiconductor-incorporated sensors.

III. Biosensing applications:

Due to the rise in the number of diabetic patients worldwide, glucose biosensors are demanded highly. About 90% of the total biosensor market is occupied by glucose biosensors. Both enzymatic and non-enzymatic biosensors are reported to be useful for detecting blood glucose [90]. The next generation GSs use glucose oxidase (GOx) to detect blood-glucose and work by direct electron transfer (DET) from the redox base to the sensor electrode. Graphene CNT-hybrid enables a larger active area for enzyme interaction and creates a 3-dimensional network for efficient electron transfer. G-CNT hybrid modified with ZnO nanoparticles increases the surface coverage Fig. 17.

   Also, modified graphene structures and semiconductor nanomaterials are extremely necessary for DET, that is the reason why these sensors for GQx are easy to prepare, show improved mechanical stability, increase active DET sites on the surface and more compatible with the biological environment.

   However, using CNT-based sensors also enables us to have a flexible surface for the detectors. MWCNTs are more susceptible to glucose detection than SWCNT, as the next-gen biosensors have adapted a layer-by-layer immobilization technique for GOx [86, 108–110], Fig. 18.

   DNA electrochemical sensors and immunosensors are a very small, yet very important part of the biosensor industry. Due to its simplicity and speedy operating process, CNT-based DNA biosensors are vastly used for detecting genetic diseases and genome mutations. Immunosensors are used to record the specific phenomena of antibodies reacting with specific antigens and also detecting different types of proteins. CNT-based immunosensors allow them to detect very low protein signals,

Table 3 Different GO films used to detect different industrially produced gases [107]

Materials	Devices	Detected items	Sensitivity	Response time	Recover time
Graphene (mechanical exfoliation)	Resistor	CO_2	25% (100 ppm)	10 s (RT)	10 s (RT)
Graphene (mechanical exfoliation)	Resistor	NH_3	6% (200 ml/min)	13 s (RT)	20 s (RT)
Graphene (rGO)	Resistor	NO_2	1.5% (100 ppm)	5 min (RT)	20 min (RT)
Graphene (rGO)	Resistor	H2	4.5% (160 ppm)	20 s (RT)	10 s (RT)
Graphene (chemical exfoliation)	Resistor	Toluene	13% (3 ml vaccum filtration)	10 s (RT)	15 s (RT)
Graphene (rGO) film	Resistor	NO_2	20% (20 ppm)	5 min (RT)	15 min (RT)
Graphene (rGO) film	Resistor	NO_2	1.2% (25 ppm)	50 s (RT)	90 s (RT)
Graphene (rGO) film	Resistor	NO_2	10% (1.25 ppm)	25 min (RT)	40 min (RT)
Graphene oxide (GO) film	Resistor	NH_3	/	/	/
Graphene oxide (GO) paper	Electrochemical effect	Ethanol	Detection limit 25 ppm	20 s (RT)	75 s (RT)
Graphene oxide (GO) film	Resistor	SO_2	47% (50 ppm)	50 s (RT)	90 s (RT)
Graphene film (CVD)	Resistor	NO_2	25% (200 ppm)	20 min (RT)	Recovered at 200 °C
Graphene film (CVD)	Resistor	NH_3	90% (1000 ppm)	180 min (RT)	Recovered at 200 °C
Graphene film (CVD, ozone treated)	Resistor	NO_2	80% (200 ppm)	15 min (RT)	30 min (RT)

as the inclusion of carbon nanoparticle, alongside other surface activating metal nanoparticles forms a highly sensitive protein detector. The usability and compatibility of the CNT-based detectors are greater than those of the usual sensors as the carbon-bed of the working electrodes offers an interactive and large surface area of protein suction.

IV. Photochemical and Optical Sensors [90]:

As stated before, sensors and actuators are different types of transducers which deal with the electrical phenomena and movement of the equipment. Chemical and
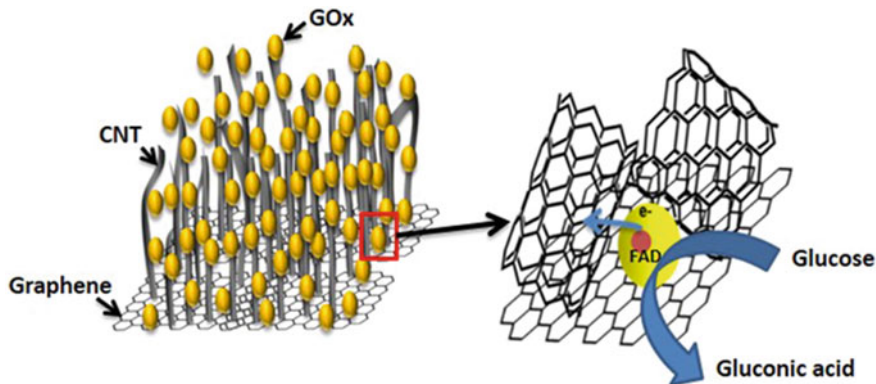
Fig. 17 Diagram of DET process from redox center to G-CNT hybrid sensor surface [90]
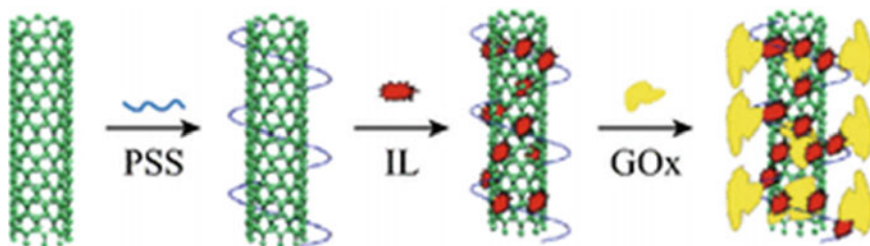
Fig. 18 Immobilization process of GOx using layer-by-layer enzyme absorption method [110]

solar energies can also be converted to an electrical or optical signal by using the optical sensors. The huge surface area and absorptivity of g-SNM hybrid sensors respond more to the low concentration fluid flow and improve the signal-to-noise ratio. Graphene/quantum dot (QD) hybrids allow detection of environmental pollutants, air quality index (AQI) etc. by enabling fluorescent biosensors. Because of the high quantum yield, tunable absorption, stable fluorescence of QD, high quenching ability of graphene; these biosensors are widely being used as optical sensors Fig. 19.

As the graphene and CNT-based nanomaterials are used widely as charge careers, glucose and protein detectors, photoactive sensors etc., the usage of these nanomaterials is increasing exponentially. The primary drawback of these NMs is that they are not reproducible and large-scale production is difficult. However, it can be assured that the multidimensional usage of carbon-based materials is leading towards making this a profitable industrial option in the future and certain technologies will be involved to ease the problematic synthesis processes of CNT and graphene.
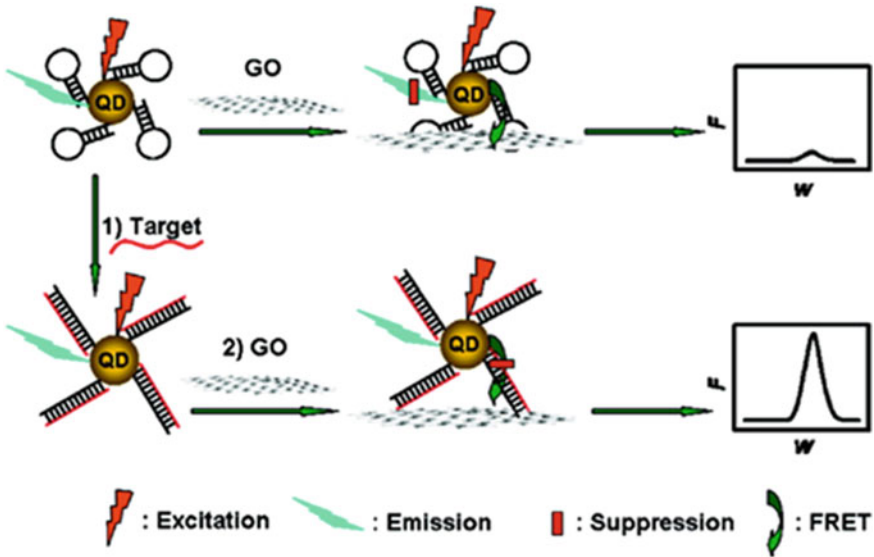
Fig. 19 Mechanism of fluorescent quenching by graphene/QD optical sensors [90]

5.4 EMI Shielding Effect (EMI SE)

The enormous growth of the telecommunication sector in addition to the growing density of electromagnetic interference (EMI) emitters in the environment has triggered the necessity of EMI compatible electronic devices for reliable service. Without EMI shielding, electronic devices might perform poorly and cause health issues resulting in a real threat to economic and social life. Conductive polymer composites (CPCs) having good shielding effects and conductivity are in great demand in telecommunication sectors. Metallic (e.g. SS, Cu, A, Ni, etc.) or carbonaceous (e.g. graphene, CNTs, carbon fibers, etc.) fillers play the key role to make conductive of the insulating polymer matrix. Homogeneous dispersion and attributes of filler materials (e.g. type, functionalization, etc.) are the key parameters to tailor the mechanical and electrical properties of CPCs. Carbonaceous filler materials exhibited excellent performance in EMI shielding compared to metallic fillers. These are the mostly used filler materials in CPCs for EMI shielding.

Layered structured polymer composites showed effective performance in EMI shielding than bulk composites. Hot staking, one of the multilayer structures, showed as an effective method of multilayer structure design of polymer composites. Both graphene and CNTs have been employed, individually, as filler in polymer/graphene or polymer/CNTs composites. But limited research has been carried out as hybrid nanocomposites with graphene/CNTs. Recent findings of synergistic effects of hybrid infusion of graphene and CNTs got much attention from researchers and industries [111–113]. This might be happening because of the effective interface

bonding and network formation between matrix polymer and filler materials. Lin et al. observed that graphene/CNTs have a synergistic effect to enhance the mechanical, electrical and thermal stability as well as EMI SE of PVA/graphene/CNTs composites [112]. A similar finding was observed by Prolongo et al. in Epoxy/graphene/CNT hybrid composites [113]. They found that the synergistic effect of graphene/CNTs enhance the storage modulus of the composites but the thermal and EMI SE did not show any improvement. This can be ascribed due to the poor conducting network in the hybrid composites. Therefore, an effective conducting network is the prerequisite to excel in the EMI SE properties of the polymer composites. Because of the formation of an effective conducting network, Zhou et al. observed an enhanced electrical and EMI SE effect of graphene/CNTs macro assembled carbon-based films.

5.5 Biomedical/tissue Scaffold and Drug Delivery

Biomedical applications of electrically conductive polymers are reasonably gaining continuous interest from researchers all over the world. Drug delivery, implants and tissue engineering are the main attractions of the biomedical engineering era, but the mechanical stability and biocompatibility are the issues which were to be improved. The insurgence of graphene and CNT-infused polymeric composites are hence happening due to the improved properties and compatibility. Conducting polymers are doped with CNT or graphene and different processes are applied to make these hybrid CPs [114] such as:

1. Solution mixing: Nanotubes and graphene are dissolved in the polymer matrix, then the solvent is evaporated to fabricate the polymer.
2. In situ method: Filler tubes are first swollen in the matrix, then the liquid monomer is dispersed with a suitable initiator. Then polymerization of the monomers is initiated using heat or radiation.
3. Melt processing: Nanofillers are diffused in the polymer matrix using injection molding, then the thermoplastic polymer is heated at a high temperature so that the polymeric linkages interchange bonds with filler.
4. Latex technology: This is the most intriguing technology of recent times as this process allows the polymers to be dispersed homogeneously, providing with advantages of high conductivity, sustainability and easy processing. This process includes the preparation of colloidal dispersion of the fillers incorporating them into the polymer matrix to form a bicomponent mixture and step-by-step controlled drying of the colloidal mixture Table 4.

The main applications of the aforementioned CPs are:

1. Electromagnetic pulse protections.
2. EMI shielding device.
3. Artificial muscles.
4. Waterborne coatings.

Table 4 Several conductive composites of different polymeric materials are given below

Composite	Fabrication method	Conductivity (S cm^{-1})
Polystyrene/graphene	Solution mixing	1
Polystryrene terephthalate/CNT	Melt compounding	10^{-3}
Cellulose/graphene NC	Solution mixing	0.72
Polystyrene/graphene NC	Solution mixing	0.252
PU/graphene	In situ polymerization	1.67×10^{-3}
PU/rGO	Solution mixing	10^{-3}
PU/CNT	In situ polymerization	2.30×10^{-4}

5. Stretchable devices for artificial limbs.

One of the most important applications of CPs in biomedical sectors is recreating 3D tissues for damaged organs. The recent advancement in the field of scaffold design for Near-infrared Photothermal therapy (NIR-PTT). Graphene is mainly used in scaffold synthesis because of its growth factor loading and high capacity for NIR absorption [115, 116].

GO (Graphene oxide) is also very important to construct a tissue scaffold and is used regularly in smart therapies [117]. GO embedded scaffolds are susceptible to a certain wavenumber of IR light and it also affects all the tissues which are not IR active. Apart from that application, light-responsive GO-scaffolds are very compatible with the body muscles and tissues (i.e. bones, scull connecting tissues etc.). The main function of the graphene introduced scaffolds is that they can kill bone-decaying osteosarcoma cells, and they can also perform tissue differentiation for damaged cells. Graphene can also prevent the growth of cancer cells while used in cancer infected cell-implant Fig. 20.

As shown in the figure, under NIR irradiation, these scaffolds can kill osteosarcoma cells at 48 °C and paves a pathway for osteogenesis at 42 °C to the bone marrow cells.

In the past decades, nanomaterials of different sizes, shapes and various chemical compositions were used as drug careers. Among the most of them, graphene and GO were the most effective ones, as they set a large surface area, exposing all the atoms while performed as a monolayer, to provide with many active sites to bind [118] Fig. 21.

As it is tough for hydrophobic graphene to get dispersed in aqueous solutions, covalent and non-covalent modifications are implied to bind graphene NMs in the polymer matrix. GO is more soluble in water, but it may aggregate in physiological buffers, thus loosening its stability. Therefore, proper methods are used to keep their biostability and compatibility intact. Recent studies have shown that graphene or GO may show some issues with interaction or biocompatibility. Although they have a unique 2D structure, the results of toxicity tests in the human body are still conflicting.

One of the most important vital facts about using graphene to interact with human cells is the interaction between this and tissues or cells. It is already found that using
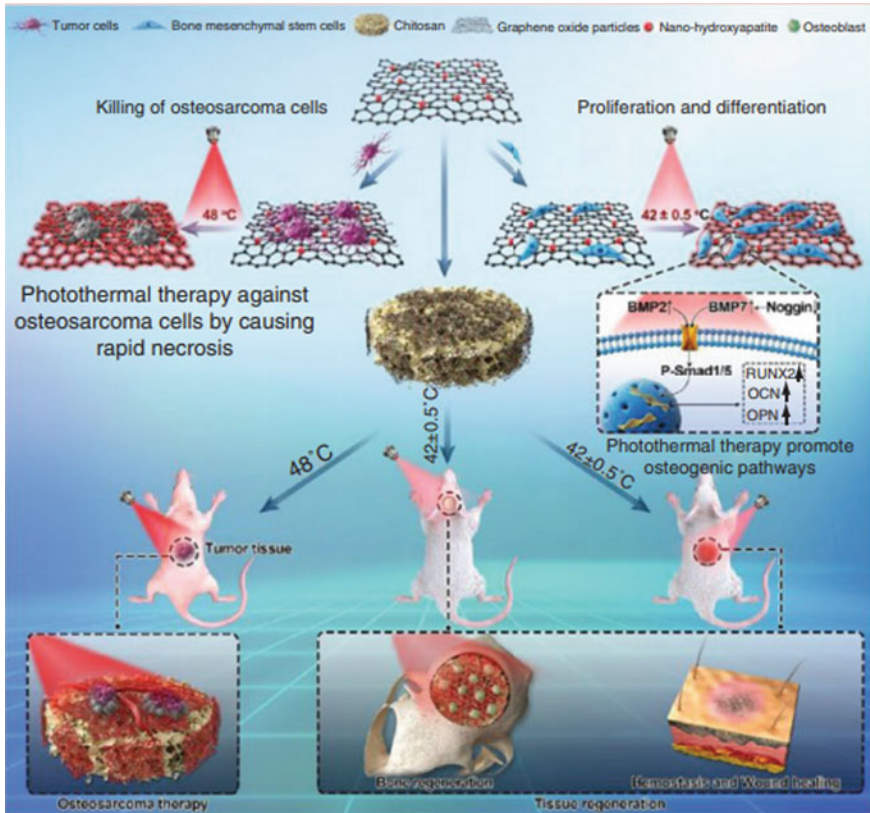
Fig. 20 Fabrication and mechanism of hydroxyapatite/GO and hydroxyapatite/GO/chitosan scaffold [116]

graphene, GO and CNT in biological career, drug delivery and uptake agent, or in the scaffolds; these nanomaterials are biocompatible, structurally sound, hold many active sites, and easier to synthesize. The industrial ability to overcome hurdles like unknown toxicity and dispersing process plays an important role in the future global market of the carbon nanocomposites. Nonetheless, the utility of graphene and CNT-based biomedical equipment is augmenting every year and will be of great demand in the near future, because of the advancement in nanomedical science.

6   Conclusions and Future Outlook

Graphene and CNTs have shown great potential in a variety of fields such as energy, structural, sensors, and so on due to their excellent inherent characteristics like high
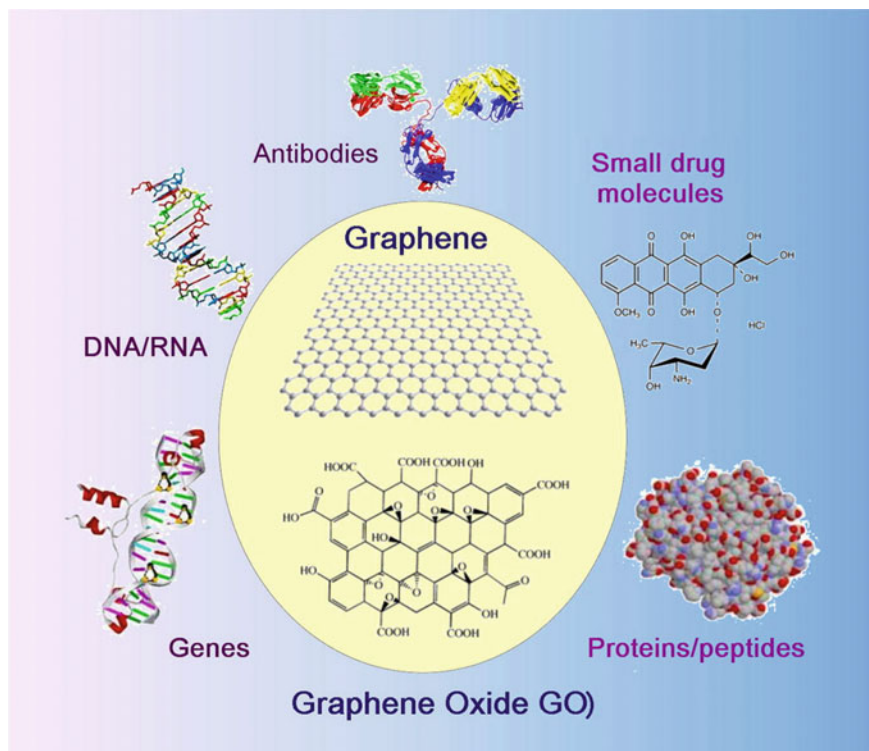
Fig. 21 Application of graphene and GO in various kinds of drug delivery [118]

surface area, high structural integrity, high electrical, thermal and mechanical properties. Applications of graphene, owing to the synergistic effect of their hybrid system, graphene/CNTs not only enhanced their inherent properties but also overcome the drawbacks of the individual component. For instance, graphene sheets are highly reactive and attract each other to form aggregates which can be overcome using CNTs embedded into graphene sheets. The fabrication processes such as CVD, microwave, vacuum filtration, in situ reduction etc. showed promising results but the challenges of their transferring process limit wide application, commercialization and/or adoption by industry. Due to the lack of reproducibility and scaling up limitation, much attention needs on functionalizing graphene or CNTs to replace silicon or tin oxide films. During hybridization, care must take towards properties optimization of individual components, understanding interface structures and fabrication techniques.

Even though there are so many challenges comprised of graphene/CNTs hybrid systems, they showed tremendous opportunities in various applications and played a vital role in the synthesis of novel electrode materials. This chapter allows researchers and scientists in realizing their extraordinary properties which can be used for synthesizing high quality graphene/CNTs hybrid-induced polymer nanocomposites

and high-performance energy-related devices in the future in the field of flexible electronics, sensing, clinical diagnostics, solar cells etc.

References

1. Joshi M, Chatterjee U (2016) Polymer nanocomposite: an advanced material for aerospace applications. In: Advanced composite materials for aerospace engineering. Elsevier, pp 241–264
2. Chakraborty S, Biswas MC (2019) Fused deposition modeling 3D printing technology in textile and fashion industry: materials and innovation. In: Modern concepts in material science. Iris Publishers
3. Chakraborty S, Biswas MC (2020) 3D printing technology of polymer-fiber composites in textile and fashion industry: a potential roadmap of concept to consumer. Compos Struct 112562
4. Biswas MC, Jeelani S, Rangari V (2017a) Composites communications. Composites 4:43–53
5. Biswas MC, Tiimob BJ, Abdela W, Jeelani S, Rangari VK (2019) Nano silica-carbon-silver ternary hybrid induced antimicrobial composite films for food packaging application. Food Pack Shelf Life 19:104–113
6. Volder De, Michael FL, Tawfick SH, Baughman RH, John Hart A (2013) Carbon nanotubes: present and future commercial applications. Science 339(6119):535–539
7. Rangari VK, Apalangya V, Biswas M, Jeelani S (2017) Preparation and microscopic characterization of biobased nanoparticles from natural waste materials. Microsc Microanal 23(S1):1938–1939
8. Rangari VK., Biswas MC, Tiimob BJ, Umerah C (2019) Biodegradable polymer blends for food packaging applications. In: Food packaging: innovations and shelf-life, pp 151
9. Biswas MC (2017) Thesis approved by
10. Biswas MC (2019) Investigation of the influence of film thickness on phase behavior of an immiscible binary polymer mixture. Glob J Eng Sci
11. da Cruz RMS (2019) Food packaging: innovations and shelf-life. CRC Press
12. Wang H, Weibang Lu, Di J, Li Da, Zhang X, Li M, Zhang Z, Zheng L, Li Q (2017) Ultra-lightweight and highly adaptive all-carbon elastic conductors with stable electrical resistance. Adv Func Mater 27(13):1606220
13. Martel R, Schmidt T, Shea HR, Hertel T, Avouris Ph (1998) Single-and multi-wall carbon nanotube field-effect transistors. Appl Phys Lett 73(17):2447–2449
14. Du R, Zhao Q, Zhang Na, Zhang J (2015) Macroscopic carbon nanotube-based 3D monoliths. Small 11(27):3263–3289
15. Dresselhaus G, Dresselhaus MS, Saito R (1998) Physical properties of carbon nanotubes. World Scientific
16. Charlier J-C (2002) Defects in carbon nanotubes. Acc Chem Res 35(12):1063–1069
17. Endo M, Hayashi T, Kim Y-A (2006) Large-scale production of carbon nanotubes and their applications. Pure Appl Chem 78(9):1703–1713
18. Georgakilas V, Perman JA, Tucek J, Zboril R (2015) Broad family of carbon nanoallotropes: classification, chemistry, and applications of fullerenes, carbon dots, nanotubes, graphene, nanodiamonds, and combined superstructures. Chem Rev 115(11):4744–4822
19. Aly K, Lubna M, Bradford P (2020) Low density, three-dimensionally interconnected carbon nanotube/silicon carbide nanocomposites for thermal protection applications. J Eur Ceram Soc
20. Ferreira ADBL, Novoa PRO, Marques AT (2016) Multifunctional material systems: a state-of-the-art review. Compos Struct 151:3–35

21. Huang W, Dai K, Yue Zhai Hu, Liu PZ, Gao J, Zheng G, Liu C, Shen C (2017) Flexible and lightweight pressure sensor based on carbon nanotube/thermoplastic polyurethane-aligned conductive foam with superior compressibility and stability. ACS Appl Mater Interfaces 9(48):42266–42277

22. Ummethala R, Fritzsche M, Jaumann T, Balach J, Oswald S, Nowak R, Sobczak N, Kaban I, Rümmeli MH, Giebeler L (2018) Lightweight, free-standing 3D interconnected carbon nanotube foam as a flexible sulfur host for high performance lithium-sulfur battery cathodes. Energy Storage Mater 10:206–215

23. Zeng Z, Jin H, Chen M, Li W, Zhou L, Zhang Z (2016) Lightweight and anisotropic porous MWCNT/WPU composites for ultrahigh performance electromagnetic interference shielding. Adv Func Mater 26(2):303–310

24. Abarrategi A, Gutierrez MC, Moreno-Vicente C, Hortigüela MJ, Ramos V, Lopez-Lacomba JL, Ferrer ML, del Monte F (2008) Multiwall carbon nanotube scaffolds for tissue engineering purposes. Biomaterials 29(1):94–102

25. Bhirde AA, Patel V, Gavard J, Zhang G, Sousa AA, Masedunskas A, Leapman RD, Roberto Weigert J, Gutkind S, Rusling JF (2009) Targeted killing of cancer cells in vivo and in vitro with EGF-Directed carbon nanotube-based drug delivery. ACS Nano 3(2):307–316

26. Kruusenberg I, Alexeyeva N, Tammeveski K, Kozlova J, Matisen L, Sammelselg V, Solla-Gullón J, Feliu JM (2011) Effect of purification of carbon nanotubes on their electrocatalytic properties for oxygen reduction in acid solution. Carbon 49(12):4031–4039

27. Ong CC, Murthe SS, Mohamed NM, Perumal V, Saheed MSM (2018) Nanoscaled surface modification of poly (Dimethylsiloxane) using carbon nanotubes for enhanced oil and organic solvent absorption. ACS Omega 3(11):15907–15915

28. Camilli L, Pisani C, Gautron E, Scarselli M, Castrucci P, D'Orazio F, Passacantando M, Moscone D, De Crescenzi M (2014) A three-dimensional carbon nanotube network for water treatment. Nanotechnology 25(6):065701

29. Xu L, Wei N, Zheng Y, Fan Z, Wang H-Q, Zheng J-C (2012) Graphene-nanotube 3D networks: intriguing thermal and mechanical properties. J Mater Chem 22(4):1435–1444

30. Yen M-Y, Hsiao M-C, Liao S-H, Liu P-I, Tsai H-M, Ma C-CM, Pu N-W, Ger M-D (2011) Preparation of graphene/multi-walled carbon nanotube hybrid and its use as photoanodes of dye-sensitized solar cells. Carbon 49(11):3597–3606

31. Mani V, Chen S-M, Lou B-S (2013) Three dimensional graphene oxide-carbon nanotubes and graphene-carbon nanotubes hybrids. Int J Electrochem Sci 8(11641):e60

32. Bailey MM, Heddleston JM, Davis J, Staymates JL, Hight Walker AR (2014) Functionalized, carbon nanotube material for the catalytic degradation of organophosphate nerve agents. Nano Res 7(3):390–398

33. Baughman RH, Zakhidov AA, De Heer WA (2002) Carbon nanotubes–the route toward applications. Science 297(5582):787–792

34. Chen Y, Zhang J (2014) Chemical vapor deposition growth of single-walled carbon nanotubes with controlled structures for nanodevice applications. Acc Chem Res 47(8):2273–2281

35. Kong J, Franklin NR, Zhou C, Chapline MG, Peng S, Cho K, Dai H (2000) Nanotube molecular wires as chemical sensors. Science 287(5453):622–625

36. Peng Y, Chen Z, Wen J, Xiao Q, Weng D, He S, Geng H, Lu Y (2011) Hierarchical manganese oxide/carbon nanocomposites for supercapacitor electrodes. Nano Res 4(2):216–225

37. Vinod S, Tiwary CS, Machado LD, Ozden S, Vajtai R, Galvao DS, Ajayan PM (2016) Synthesis of ultralow density 3D graphene–CNT foams using a two-step method. Nanoscale 8(35):15857–15863

38. Kim KH, Tsui MN, Islam MF (2017) Graphene-coated carbon nanotube aerogels remain superelastic while resisting fatigue and creep over -100 to +500 °C. Chem Mater 29(7):2748–2755

39. Sui Z, Meng Q, Zhang X, Ma R, Cao B (2012) Green synthesis of carbon nanotube-graphene hybrid aerogels and their use as versatile agents for water purification. J Mater Chem 22(18):8767–8771

40. You Bo, Wang L, Yao Li, Yang J (2013) Three dimensional N-doped graphene–CNT networks for supercapacitor. Chem Commun 49(44):5016–5018. https://doi.org/10.1039/C3CC41949E

41. Sun H, Xu Z, Gao C (2013) Multifunctional, ultra-flyweight, synergistically assembled carbon aerogels. Adv Mater 25(18):2554–2560

42. Dong X, Li B, Wei A, Xiehong Cao MB, Chan-Park HZ, Li L-J, Huang W, Chen P (2011) One-step growth of graphene-carbon nanotube hybrid materials by chemical vapor deposition. Carbon 49(9):2944–2949. https://doi.org/10.1016/j.carbon.2011.03.009

43. Han P, Yue Y, Liu Z, Wei Xu, Zhang L, Hongxia Xu, Dong S, Cui G (2011) Graphene oxide nanosheets / multi-walled carbon nanotubes hybrid as an excellent electrocatalytic material towards VO 2+ /VO 2 + redox couples for vanadium redox flow batteries. Energy Environ Sci 4(11):4710–4717. https://doi.org/10.1039/C1EE01776D

44. Zhang C, Ren L, Wang X, Liu T (2010) Graphene oxide-assisted dispersion of pristine multi-walled carbon nanotubes in aqueous media. J Phys Chem C 114(26):11435–11440. https://doi.org/10.1021/jp103745g

45. Lv P, Tan X-W, Ke-Han Yu, Zheng R-L, Zheng J-J, Wei W (2016) Super-elastic graphene/carbon nanotube aerogel: a novel thermal interface material with highly thermal transport properties. Carbon 99:222–228. https://doi.org/10.1016/j.carbon.2015.12.026

46. Dong X, Chen J, Ma Y, Wang J, Chan-Park MB, Liu X, Wang L, Huang W, Chen P (2012) Superhydrophobic and superoleophilic hybrid foam of graphene and carbon nanotube for selective removal of oils or organic solvents from the surface of water. Chem Commun 48(86):10660–10662. https://doi.org/10.1039/C2CC35844A

47. Nguyen D, Duc N-H, Chen S-Y, Chueh Y-L (2012) Controlled growth of carbon nanotube—graphene hybrid materials for flexible and transparent conductors and electron field emitters. Nanoscale 4(2):632–638. https://doi.org/10.1039/C1NR11328C

48. Wang W, Guo S, Penchev M, Ruiz I, Bozhilov KN, Yan D, Ozkan M, Ozkan CS (2013) Three dimensional few layer graphene and carbon nanotube foam architectures for high fidelity supercapacitors. Nano Energy 2(2):294–303. https://doi.org/10.1016/j.nanoen.2012.10.001

49. Song Q, Ye F, Yin X, Li W, Li H, Liu Y, Li K et al (2017) Carbon nanotube-multilayered graphene edge plane core-shell hybrid foams for ultrahigh-performance electromagnetic-interference shielding. Adv Mater 29(31):1701583. https://doi.org/10.1002/adma.201701583

50. Kong L, Yin X, Hailong Xu, Yuan X, Wang T, Zhanwei Xu, Huang J, Yang R, Fan H (2019) Powerful absorbing and lightweight electromagnetic shielding CNTs/RGO composite. Carbon 145(April):61–66. https://doi.org/10.1016/j.carbon.2019.01.009

51. Fan Z, Yan J, Zhi L, Zhang Q, Wei T, Feng J, Zhang M, Qian W, Wei F (2010) A three-dimensional carbon nanotube/graphene sandwich and its application as electrode in supercapacitors. Adv Mater 22(33):3723–3728. https://doi.org/10.1002/adma.201001029

52. Young RJ, Lovell PA (2011) Introduction to polymers. CRC Press

53. Affdl JCH, Kardos JL (1976) The Halpin-Tsai equations: a review. Polym Eng Sci 16(5):344–352. https://doi.org/10.1002/pen.760160512

54. Yang Y, Rigdon W, Huang X, Li X (2013) Enhancing graphene reinforcing potential in composites by hydrogen passivation induced dispersion. Sci Rep 3(1):2086. https://doi.org/10.1038/srep02086

55. Halpin JC (1969) Effects of environmental factors on composite materials. DTIC Document. Google Search. n.d. Accessed 26 July 2020. https://www.google.com/search?q=Halpin+JC.+Effects+of+environmental+factors+on+composite+materials.+DTIC+document%3B+1969.&oq=Halpin+JC.+Effects+of+environmental+factors+on+composite+materials.+DTIC+document%3B+1969.&aqs=chrome..69i57j69i60.551j0j4&sourceid=chrome&ie=UTF-8

56. Yang S-Y, Lin W-N, Huang Y-L, Tien H-W, Wang J-Y, Ma C-C, Li S-M, Wang Y-S (2011) Synergetic effects of graphene platelets and carbon nanotubes on the mechanical and thermal properties of epoxy composites. Carbon 49(3):793–803. https://doi.org/10.1016/j.carbon.2010.10.014

57. Chatterjee S, Nafezarefi F, Tai NH, Schlagenhauf L, Nüesch FA, Chu BTT (2012) Size and synergy effects of nanofiller hybrids including graphene nanoplatelets and carbon nanotubes

in mechanical properties of epoxy composites. Carbon 50(15):5380–5386. https://doi.org/10.1016/j.carbon.2012.07.021

58. Moosa AA, Kubba F, Raad M, Ramazani A (2016) Mechanical and thermal properties of graphene nanoplates and functionalized carbon-nanotubes hybrid epoxy nanocomposites. Am J Mater Sci 6(5):125–134

59. Zhang S, Yin S, Rong C, Huo P, Jiang Z, Wang G (2013) Synergistic effects of functionalized graphene and functionalized multi-walled carbon nanotubes on the electrical and mechanical properties of poly(ether sulfone) composites. Eur Polymer J 49(10):3125–3134. https://doi.org/10.1016/j.eurpolymj.2013.07.011

60. Ren P-G, Di Y-Y, Zhang Q, Li L, Pang H, Li Z-M (2012) Composites of ultrahigh-molecular-weight polyethylene with graphene sheets and/or MWCNTs with segregated network structure: preparation and properties. Macromol Mater Eng 297(5):437–443. https://doi.org/10.1002/mame.201100229

61. Biswas MC, Jeelani S, Rangari V (2017b) Influence of biobased silica/carbon hybrid nanoparticles on thermal and mechanical properties of biodegradable polymer films. Compos Commun 4:43–53

62. Baeza F, Javier OG, Zornoza E, Garcés P (2013) Effect of aspect ratio on strain sensing capacity of carbon fiber reinforced cement composites. Mater Des 51:1085–1094

63. Biercuk MJ, Llaguno MC, Radosavljevic M, Hyun JK, Johnson AT, Fischer JE (2002) Carbon nanotube composites for thermal management. Appl Phys Lett 80(15):2767–2769. https://doi.org/10.1063/1.1469696

64. Biswas MC, Tiimob BJ, Abdela W, Jeelani S, Rangari VK (n.d.) Food packaging and shelf life

65. Yang S-Y, Ma C-C, Teng C-C, Huang Y-W, Liao S-H, Huang Y-L, Tien H-W, Lee T-M, Chiou K-C (2010) Effect of functionalized carbon nanotubes on the thermal conductivity of epoxy composites. Carbon 48(3):592–603. https://doi.org/10.1016/j.carbon.2009.08.047

66. Shenogin S, Xue L, Ozisik R, Keblinski P, Cahill DG (2004) Role of thermal boundary resistance on the heat flow in carbon-nanotube composites. J Appl Phys 95(12):8136–8144. https://doi.org/10.1063/1.1736328

67. Liao S-H, Yen C-Y, Hung C-H, Weng C-C, Tsai M-C, Lin Y-F, Ma C-C, Pan C, Ay Su (2008) One-step functionalization of carbon nanotubes by free-radical modification for the preparation of nanocomposite bipolar plates in polymer electrolyte membrane fuel cells. J Mater Chem 18(33):3993–4002. https://doi.org/10.1039/B806054A

68. Yu A, Ramesh P, Sun X, Bekyarova E, Itkis ME, Haddon RC (2008) Enhanced thermal conductivity in a hybrid graphite nanoplatelet—carbon nanotube filler for epoxy composites. Adv Mater 20(24):4740–4744. https://doi.org/10.1002/adma.200800401

69. Lee YS, Park YH, Yoon KH (2017) Flexural, electrical, thermal and electromagnetic interference shielding properties of xGnP and carbon nanotube filled epoxy hybrid nanocomposites. Carbon Lett 24:41–46

70. Soliman EM, Kandil UF, Reda MM, Taha. (2012) The significance of carbon nanotubes on styrene butadiene rubber (SBR) and SBR modified mortar. Mater Struct 45(6):803–816

71. Mannov E, Schmutzler H, Chandrasekaran S, Christian Viets S, Buschhorn F, Tölle RM, Schulte K (2013) Improvement of compressive strength after impact in fibre reinforced polymer composites by matrix modification with thermally reduced graphene oxide. Compos Sci Technol 87:36–41

72. Yavari F, Rafiee MA, Rafiee J, Yu Z-Z, Koratkar N (2010) Dramatic increase in fatigue life in hierarchical graphene composites. ACS Appl Mater Interfaces 2(10):2738–2743

73. Potts JR, Dreyer DR, Bielawski CW, Ruoff RS (2011) Graphene-based polymer nanocomposites. Polymer 52(1):5–25

74. Sebastian J, Schehl N, Bouchard M, Boehle M, Li L, Lagounov A, Lafdi K (2014) Health monitoring of structural composites with embedded carbon nanotube coated glass fiber sensors. Carbon 66:191–200

75. Hu N, Fukunaga H, Atobe S, Liu Y, Li J (2011) Piezoresistive strain sensors made from carbon nanotubes based polymer nanocomposites. Sensors 11(11):10691–10723

76. Heeder N, Shukla A, Chalivendra V, Yang S (2012) Sensitivity and dynamic electrical response of CNT-reinforced nanocomposites. J Mater Sci 47(8):3808–3816

77. Kim Y-J, Cha JY, Ham H, Huh H, So D-S, Kang I (2011) Preparation of piezoresistive nano smart hybrid material based on graphene. Curr Appl Phys 11(1):S350–S352

78. Jeon J-W, Biswas MC, Patton CL, Wujcik EK (2020) Water-processable, sprayable LiFePO4/graphene hybrid cathodes for high-power lithium ion batteries. J Ind Eng Chem 84:72–81

79. Zhao J, He C, Yang R, Shi Z, Cheng M, Yang W, Xie G, Wang D, Shi D, Zhang G (2012) Ultra-sensitive strain sensors based on piezoresistive nanographene films. Appl Phys Lett 101(6):063112

80. Chung DDL (1998) Self-monitoring structural materials. Mater Sci Eng R: Rep 22(2):57–78

81. Farrar CR, Worden K (2007) An introduction to structural health monitoring. Philos Trans Roy Soc A Math Phys Eng Sci 365(1851):303–315

82. Yoo EJ, Kim J, Hosono E, Zhou H-S, Kudo T, Honma I (2008) Large reversible Li storage of graphene nanosheet families for use in rechargeable lithium ion batteries. Nano Lett 8(8):2277–2282. https://doi.org/10.1021/nl800957b

83. Wu X, Mu F, Zhao H (2019) Recent progress in the synthesis of graphene/CNT composites and the energy-related applications. J Mater Sci Technol

84. Chang L-H, Hsieh C-K, Hsiao M-C, Chiang J-C, Liu P-I, Ho K-K, Ma C-CM, Yen M-Y, Tsai M-C, Tsai C-H (2013) A graphene-multi-walled carbon nanotube hybrid supported on fluorinated tin oxide as a counter electrode of dye-sensitized solar cells. J Power Sources 222: 518–525. https://doi.org/10.1016/j.jpowsour.2012.08.058

85. Yu D, Dai L (2010) Self-assembled graphene/carbon nanotube hybrid films for supercapacitors. J Phys Chem Lett 1(2):467–470. https://doi.org/10.1021/jz9003137

86. Mahbub T, Hoque ME (2020) Introduction to nanomaterials and nanomanufacturing for nanosensors. In: Nanofabrication for smart nanosensor applications. Elsevier, pp 1–20

87. Yang HN, Ko YD, Kim WJ (2018) 3-D structured Pt/RGO-polyethyleneimine-functionalized MWCNTs prepared with different mass ratio of RGO and MWCNT for proton exchange membrane fuel cell. Int J Hydro Energy 43(9):4439–4447. https://doi.org/10.1016/j.ijhydene.2017.12.135

88. Introduction to Transducers, Sensors and Actuators—Google Search (n.d.) Accessed 28 July 2020. https://www.google.com/search?q=Introduction+to+Transducers%2C+Sensors+and+Actuators&oq=Introduction+to+Transducers%2C+Sensors+and+Actuators&aqs=chrome..69i57j0l2j69i60.526j0j4&sourceid=chrome&ie=UTF-8

89. Difference Between Actuator and Sensor (2019) Microcontrollers Lab (blog). 16 Feb 2019. https://microcontrollerslab.com/difference-between-actuator-and-sensor/

90. Badhulika S, Terse-Thakoor T, Villarreal CMC, Mulchandani A (2015) Graphene hybrids: synthesis strategies and applications in sensors and sensitized solar cells. Front Chem 3:38

91. He Z, Phan H, Liu J, Nguyen TQ, Tan TTY (2013) Understanding TiO2 size-dependent electron transport properties of a graphene-TiO2 photoanode in dye-sensitized solar cells using conducting atomic force microscopy. Adv Mater 25(47):6900–6904

92. Madhavan AA, Kalluri S, Chacko DK, Arun TA, Nagarajan S, Subramanian KR, Nair AS, Nair SV, Balakrishnan A (2012) Electrical and optical properties of electrospun TiO 2-graphene composite nanofibers and its application as DSSC photo-anodes. Rsc Adv 2(33):13032–13037

93. Yan X, Cui X, Li B, Li LS (2010) Large, solution-processable graphene quantum dots as light absorbers for photovoltaics. Nano Lett 10(5):1869–1873

94. Son DI, Kwon BW, Do Yang J, Park DH, Seo WS, Lee H, Yi Y, Lee CL, Choi WK (2012) Charge separation and ultraviolet photovoltaic conversion of ZnO quantum dots conjugated with graphene nanoshells. Nano Res 5(11):747–761

95. Liu M, Li G, Chen X (2014) One-pot controlled synthesis of spongelike CuInS2 microspheres for efficient counter electrode with graphene assistance in dye-sensitized solar cells. ACS Appl Mater Interfaces 6(4):2604–2610

96. Radich JG, Dwyer R, Kamat PV (2011) Cu2S reduced graphene oxide composite for high-efficiency quantum dot solar cells. Overcoming the redox limitations of S2–/S n 2–at the counter electrode. J Phys Chem Lett 2(19):2453–2460

97. Zheng H, Neo CY, Ouyang J (2013) Highly efficient iodide/triiodide dye-sensitized solar cells with gel-coated reduce graphene oxide/single-walled carbon nanotube composites as the counter electrode exhibiting an open-circuit voltage of 0.90 V.ACS Appl Mater Interfaces 5(14):6657–6664

98. Velten J, Mozer AJ, Li D, Officer D, Wallace G, Baughman R, Zakhidov A (2012) Carbon nanotube/graphene nanocomposite as efficient counter electrodes in dye-sensitized solar cells. Nanotechnol 23(8):085201

99. Youn DH, Seol M, Kim JY, Jang JW, Choi Y, Yong K, Lee JS (2013) TiN nanoparticles on CNT–Graphene hybrid support as noble-metal-free counter electrode for quantum-dot-sensitized solar cells. ChemSusChem 6(2):261–267

100. Li-Hsueh C, Chien-Kuo H, Min-Chien H, Jen-Chi C, Po IL, Kuan-Ku H et al. (2013) A graphene-multi-walled carbon nanotube hybrid supported on fluorinated tin oxide as a counter electrode of dye-sensitized solar cells. J Power Sources 222:518–525

101. Ma J, Zhou L, Li C, Yang J, Meng T, Zhou H et al. (2014) Surfactant-free synthesis of graphene-functionalized carbon nanotube film as a catalytic counter electrode in dye-sensitized solar cells. J Power Sources 247:999–1004

102. Guang Z, Likun P, Ting L, Tao X, Zhuo S (2011) Electrophoretic deposition of reduced graphene-carbon nanotubes composite films as counter electrodes of dye-sensitized solar cells. J Mater Chem 21:14869–14875

103. Zhibin Y, Mingkai L, Chao Z, Weng Weei T, Tianxi L, Huisheng P (2013) Carbon nanotubes bridged with graphene nanoribbons and their use in high-efficiency dye-sensitized solar cells. Angew Chem Int Ed 52:3996–3999

104. Li S, Luo Y, Lv W, Yu W, Wu S, Hou P et al (2011) Vertically aligned carbon nanotubes grown on graphene paper as electrodes in lithium-ion batteries and dye-sensitized solar cells. Adv Energy Mater 1:486–490

105. Tsai CH, Chen CH, Hsiao YC, Chuang PY (2015) Investigation of graphene nanosheets as counter electrodes for efficient dye-sensitized solar cells. Org Electron 17:57–65

106. Hoshi H, Tanaka S, Miyoshi T (2014) Pt-graphene electrodes for dye-sensitized solar cells. Mater Sci Eng B Adv Funct Solid State Mater 190:47–51

107. Xiao Z, Kong LB, Ruan S, Li X, Shijin Yu, Li X, Jiang Yi, Yao Z, Ye S, Wang C (2018) Recent development in nanocarbon materials for gas sensor applications. Sens Actuat B: Chem 274:235–267

108. Lu Y, Biswas MC, Guo Z, Jeon J-W, Wujcik EK (2019) Recent developments in bio-monitoring via advanced polymer nanocomposite-based wearable strain sensors. Biosens Bioelectron 123:167–177

109. Rabbani M, Hoque ME, Mahbub ZB (2020) Chapter 7—nanosensors in biomedical and environmental applications: perspectives and prospects. In: Pal K, Gomes F (eds) Nanofabrication for smart nanosensor applications. Micro and nano technologies. Elsevier, pp 163–186. https://doi.org/10.1016/B978-0-12-820702-4.00007-6

110. Zhu Z (2017) An overview of carbon nanotubes and graphene for biosensing applications. Nano-Micro Lett 9(3):1–24

111. Li Y, Gao F, Xue Z, Luan Y, Yan X, Guo Z, Wang Z (2018) Synergistic effect of different graphene-CNT heterostructures on mechanical and self-healing properties of thermoplastic polyurethane composites. Mater Des 137(January):438–445. https://doi.org/10.1016/j.matdes.2017.10.018

112. Lin J-H, Lin Z-I, Pan Y-J, Chen C-K, Huang C-L, Huang C-H, Lou C-W (2016) Improvement in mechanical properties and electromagnetic interference shielding effectiveness of PVA-based composites: synergistic effect between graphene nano-sheets and multi-walled carbon nanotubes. Macromol Mater Eng 301(2):199–211. https://doi.org/10.1002/mame.201500314

113. Prolongo SG, Moriche R, Ureña A, Flórez S, Gaztelumendi I, Arribas C, Prolongo MG (2018) Carbon nanotubes and graphene into thermosetting composites: synergy and combined effect. J Appl Polym Sci 135(28):46475. https://doi.org/10.1002/app.46475

114. Kaur G, Adhikari R, Cass P, Bown M, Gunatillake P (2015) Electrically conductive polymers and composites for biomedical applications. Rsc Adv 5(47):37553–37567

115. Michael FM, Khalid M, Hoque ME, Ratnam CT (n.d.) PLA/GNP/NHA: Application of poly-lactic acid reinforced with graphene nano-platelets and nanohydroxy apatite hybrids in load bearing bone implants. J Nanomed Nanotech. Accessed 31 July 2019. https://doi.org/10.4172/2157-7439.C1.025

116. Palmieri V, De Spirito M, Papi M (2020) Graphene-based scaffolds for tissue engineering and photothermal therapy. Nanomedicine (0)

117. Sagadevan S, Chowdhury ZZ, Hoque ME, Podder J (2017) Chemically stabilized reduced graphene oxide/zirconia nanocomposite: synthesis and characterization. Mater Res Exp 4(11):115031. https://doi.org/10.1088/2053-1591/aa9a8c

118. Liu J, Cui L, Losic D (2013) Graphene and graphene oxide as new nanocarriers for drug delivery applications. Acta Biomater 9(12):9243–9257

119. https://www.onupkeep.com/answers/predictive-maintenance/sensors-and-actuators-2/. Google Search. n.d. Accessed 28 July 2020. https://www.google.com/search?ei=sbM gX8ShEpCrytMP96OU0AM&q=https%3A%2F%2Fwww.onupkeep.com%2Fanswers% 2Fpredictive-maintenance%2Fsensors-and-actuators-2%2F&oq=https%3A%2F%2Fwww. onupkeep.com%2Fanswers%2Fpredictive-maintenance%2Fsensors-and-actuators-2%2F& gs_lcp=CgZwc3ktYWIQA1CtpwJYracCYI2rAmgAcAB4AIABXYgBXZIBATGYAQCgA QKgAQGqAQdnd3Mtd2l6wAEB&sclient=psy-ab&ved=0ahUKEwiEvpDvi_HqAhWQlXI EHfcRBToQ4dUDCAw&uact=5

120. Wang K, Wan S, Liu Q, Yang N, Zhai J (2013) CdS quantum dot-decorated titania/graphene nanosheets stacking structures for enhanced photoelectrochemical solar cells. RSC Adv 3(45):23755–23761

121. Yen MY, Hsiao MC, Liao SH, Liu PI, Tsai HM, Ma CCM, Pu NW, Ger MD (2011) Preparation of graphene/multi-walled carbon nanotube hybrid and its use as photoanodes of dye-sensitized solar cells. Carbon 49(11):3597–3606

Hybrid Nanocomposites Based on Graphene with Cellulose Nanocrystals/Nanofibrils: From Preparation to Applications

Mohamed Hamid Salim, Zineb Kassab, Ihsane Kassem, Houssine Sehaqui, Rachid Bouhfid, Johan Jacquemin, Abou El Kacem Qaiss, Jones Alami, and Mounir El Achaby

Abstract Hybrid nanocomposites are multicomponent systems inducing unique interconnected 3D network microstructure materials. With the purpose of exploitation of rich natural and under valorised resources, graphene (G) and nanocellulose (NC) have become interesting organic hybrid fillers used for enhancement of the properties of composites. In fact, they combine the unique properties of G with those of the cellulose nanocrystals (CNC) or cellulose nanofibrils (CNF) leading to an exciting area of current interest in the fields of hybrid nanocomposites. These hybrid nanocomposites exhibit unique properties thanks to the synergetic effect of fillers and compatible polymers allowing their potential utilization in various important applications including food packaging, water treatment and energy storage to cite few. Their judicious combination can, therefore, provide environmentally friendly hybrids of low cost, ease processing with specific mechanical, thermal, optical and electrical properties. With respect to the recent advances in material sciences, this chapter pioneers to summarize the recent progress towards the synthesis of hybrid nanocomposites containing G-NC as fillers, and their potential utilizations as advanced materials particularly in food packing, water treatment, energy storages and sensor technology. This chapter has covered main achievements and significant examples of each subject area to demonstrate how this unique class of materials has stimulated research activities. To help the readers, this chapter is subdivided into six topics. The first topic provides an introduction to the G and NC as advanced materials. The

M. H. Salim · Z. Kassab · I. Kassem · H. Sehaqui · J. Jacquemin · J. Alami · M. El Achaby (✉)
Materials Science and Nano-engineering (MSN) Department, Mohammed VI Polytechnic University (UM6P), Lot 660–Hay Moulay Rachid, 43150 Benguerir, Morocco
e-mail: mounir.elachaby@um6p.ma

R. Bouhfid · A. E. K. Qaiss
Composites and Nanocomposites Center (CNC), Moroccan Foundation for Advanced Science, Innovation and Research (MAScIR), Rabat Design Center, Rue Mohamed El Jazouli, Madinat El Irfane, 10100 Rabat, Morocco

J. Jacquemin
Laboratoire PCM2E, Faculté des Sciences, Université de Tours, Parc Grandmont, 37200 Tours, France

second topic focuses on different preparation procedures of G-NC hybrids while the third illustrates their properties. Then, the preparation of hybrid polymer nanocomposites based on G and NC is detailed in the fourth section. Consecutively, the fifth section reports on their properties while the last one identifies current and potential applications of hybrid polymer nanocomposites based on G and NC. This chapter is finally ended with a global conclusion on these promising materials.

1 Introduction

Since the last decade, the design of novel hybrid nanocomposite materials with enhanced properties has gained attention in material science and nanotechnologies [1–3]. On the grounds of hybrid materials, there has been immense interest to carry out investigations on the development and conception of hybrid fillers based on graphene (G) [or modified graphene in particular graphene oxide (GO), graphene oxide nanosheets (GON), reduced graphene oxide (rGO)] and nanocellulose (NC) [which includes cellulose nanocrystals (CNC) and cellulose nanofibrils (CNF)].

On one hand, G has an essential role in the development of original advanced functional nanohybrids because of its high surface area along with unique mechanical properties in combination with its electrical-thermal properties [4–7]. Furthermore, G has an impressive fracture toughness and high elasticity modulus enabling it to be used as a filler in hybrid poly composites materials in a large number of engineering areas [8–11]. On the other hand, NC are natural nanomaterials that follow the biomimetic model and can be found in hybrid materials [12–15]. Both CNC and CNF have different methods of preparations influencing their structural, morphological, and mechanical properties [16–20]. Based on its excellent biocompatibility and biodegradability property, NC-based hybrid is an ideal material for biomedicine, packaging, drug release, or related applications [21–25].

This chapter reviews numerous research works devoted on the possibility to combine G with nanostructured cellulose. This possibility was also stimulated by the observation of a synergistic effect by mixing these materials, allowing the feasibility to formulate nanocomposites with enhanced properties and thus open the door to promising applications in various fields [26–29]. In fact, numerous studies have been conducted to find out the suitable approaches to synthesize hybrid nanocomposites from G and NC as well as to depict their potential impacts and applications [30–32]. Briefly, G-NC hybrids are mostly prepared by combining inorganic compounds with organic species by covalent bonding (chemical) bonding or noncovalent (physical) interactions with unique thermal, chemical, morphological, optoelectronic and mechanical properties [36–38]. Accordingly, this chapter reports recent studies on the elaboration of G-NC based structured hybrid materials as prominent advanced materials driven by their good mechanical properties, thermal capabilities, electrical performances, and physical characteristics [31, 38, 39]. However, as reported in many studies, to increase the performance of the polymer nanohybrid composite, an appropriate dispersion without any aggregation of both G-NC hybrid fillers through a

polymeric matrix is crucial [40]. This could be achieved through physical combining and chemical grafting on the hybrid polymeric nanocomposites inducing a synergistic influence on the behaviour of the G-NC hybrids [37, 41].

2 Preparation of Graphene and Nanocelluloses Hybrids

Many researchers have employed various ways to prepare G-NC reinforced hybrids, including the (i) layer-by-layer assembly, (ii) ultra-sonication, and (iii) ambient pressure drying, (iv) ball milling, (v) liquid phase exfoliation [32, 42, 43]. In addition to these common preparation methods, many other techniques have been adapted for G and NC hybrids processing. All of these preparation methods are described in detail in this section.

2.1 Layer-By-Layer Assembly Technique

Nanohybrids could be fabricated by using a spin assisted layer-by-layer assembly technique (spin-LBL) by alternately depositing a layer of 1D cellulose nanocrystals/nanofibrils and 2D GON. Such a unique combination of 1D and 2D layers induces strong interfacial interactions between nanofillers reinforcing the nanostructure of the layered nanomaterials, and thus their properties [14]. This fabrication process is facile, fast, cheap, and based on a versatile technique allowing the preparation of highly ordered multilayer films with unique structure from various 1D and/or 2D materials [44]. For example, Song et al. have prepared layer-by-layer (LbL) assembled hybrids containing sequentially GO and CNF layers as displayed in Fig. 1 [45]. Their preparation method was done in two steps, during the first step the layers were assembled starting from the flexible CNF substrate; while the second step involved the reduction of GO (Fig. 1) [45].

Thanks to this layer-by-layer assembly, appropriate size, thickness, microstructure and surface roughness of the nanomaterials can be tailored by changing the
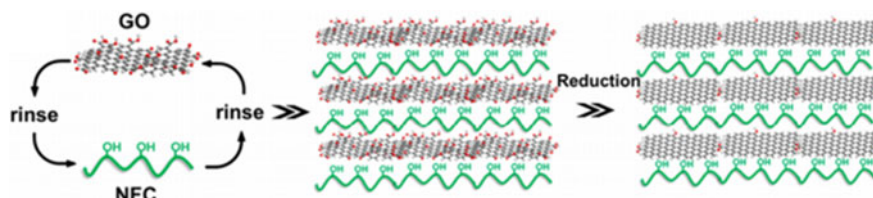
Fig. 1 Schematic representation of the preparation of spin-LBL-assembled hybrids based on GO and CNF (presented in the figure as *NFC*) [45]

centrifugal force to gain effective stress transfer. Substantially, this assembly technique could be used to prepare laminated nanohybrids with high ultimate stress, high Young's modulus and toughness [46].

2.2 Ultrasonication Method

The one-step ultrasonication method was appropriately used to prepare a wide variety of G-NC hybrids by various research groups [14, 26, 41]. In a typical process, ultrasonication involves the dispersion of the nanocellulose and G into water [26, 27]. This allows to reach a G-NC hybrid with a specific 3D interconnected network microstructure, in which hydrogen bonds play a crucial role to organize and stabilize the 2D structure of GO in the presence of the nanocellulose, as illustrated in Fig. 2 [27]. For example, Yao et al. elaborated that CNF could be used to disperse GO by using a sonication treatment, leading thus to a uniform GO-CNF distribution in solution [27]. During such a treatment, the ultrasound energy is transferred through a cavitation effect to both CNF chains and GO. This energy transfer, of approx. 10–100 kJ/mol, corresponds to the energy scale of hydrogen bonds. In other words, thanks to this energy transfer, hydrogen bonds network could be formed through the interaction of abundant oxygen-based moieties in GO with the cellulosic hydroxyl
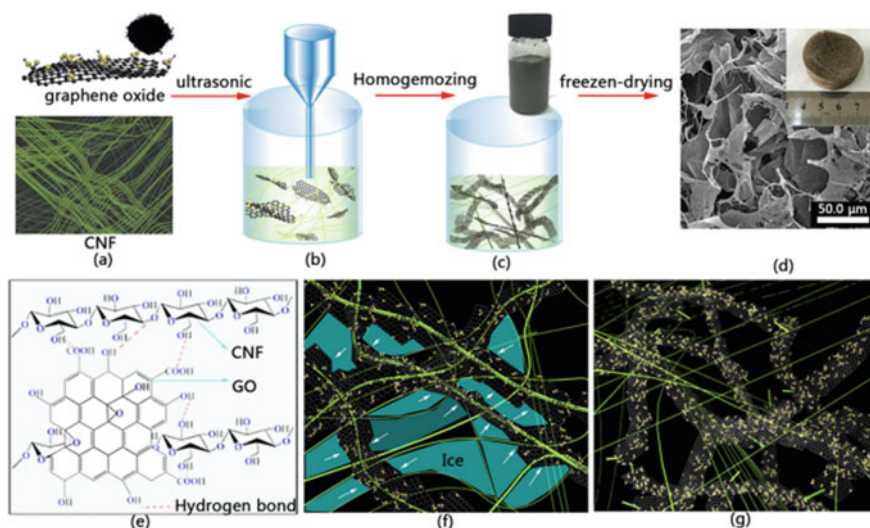
Fig. 2 **a–d** Schematic showing the synthetic steps of the GO-CNF hybrids; **e** CNF combined with GO through hydrogen bonds; **f** schematic formation of the 3D structure; **g** 3D structure of CNF-GO [27]

groups [27]. Afterward, the GO-CNF dispersion is freeze-dried to obtain the so-called GO-CNF hybrid. Consequently, the ultrasonic method allows the preparation of hybrid materials with a 3D interconnected network microstructure [27].

2.3 Ambient Pressure Drying Technique

The ambient pressure drying technique is a safe, cost-effective, and environmentally friendly preparation process, as no complicated equipment is requested to produce low-density organic hybrids [38, 47, 48]. In this context, ultralight G-CNC hybrids were prepared by using an integrated approach based on a two-step reduction process combined with an ambient drying technology [47]. This preparation method seems to avoid the problem of structural collapse induced by shrinking in a conventional method of ambient drying in the case of the G-CNC hybrids. By following this approach, the synthetic process starts with the formation of a stable suspension by following a simple liquid-mixing method, containing rod-like CNC and flake-like GO. Then, the sample is consecutively frozen and thawed out by heating the solution until a reduced hybrid G is obtained. During the final step, the G-CNC hybrid is dried in an oven to produce ultralight G-CNC hybrid [47].

2.4 Ball Milling Process

Ball milling is a grinding technique, which crushes microparticles into extremely fine powders and reduced size [49–51]. In this process, a ball mill is used as a tool for grinding and blending and sometimes for mixing of nanomaterials applicability to essentially all classes of materials [49]. It was found that using this method allowed the formation of graphene nanoparticles in a smaller size range than other synthesis methods [50]. For this reason, researchers have used this process to produce G-NC hybrid nanoparticles for various applications [49, 51]. As exemplified in Fig. 3a, a ball milling technique was used by Wang et al. to exfoliate the graphite under the presence of TEMPO-oxidized CNF suspensions to produce G-CNF hybrid [51]. Furthermore, it was reported that this process succeeded in stabilizing exfoliated G, even in an aqueous solution, due to the tight adsorption of CNF onto the G surface [51]. Accordingly, Fig. 3b illustrates the proposed ball milling graphite exfoliation process in the presence of CNF leading to the formation of the G-CNF hybrid material [51].
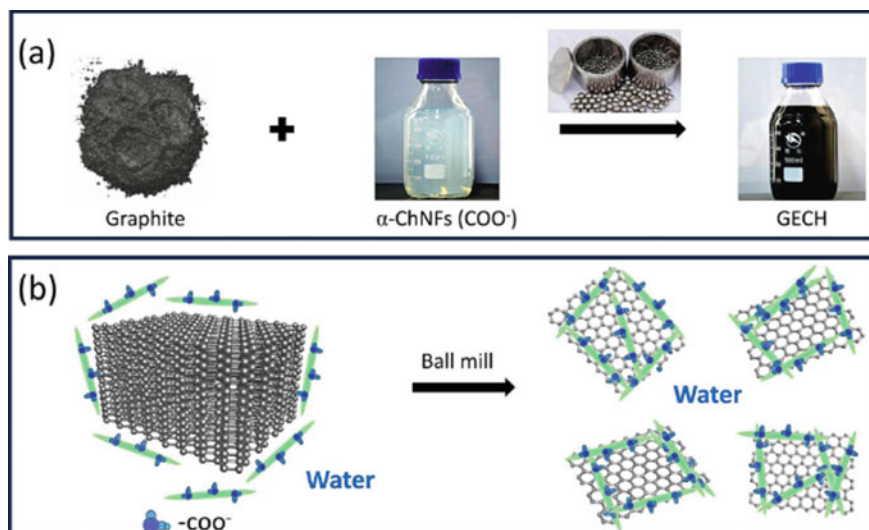
Fig. 3 **a** Ball milling fabrication process of G-CNF hybrids. **b** Schematic representation of the ball milling graphite exfoliation process in the presence of CNF [51]

2.5 Liquid Phase Exfoliation

The liquid-phase exfoliation process requires, generally, three steps including a graphite dispersion in a solution, exfoliation, and purification to remove individual layers [41, 52–54]. The G-CNC hybrid was developed by using a preparation method consisting of a liquid phase graphite exfoliation supported by CNC. This recently documented process allows the stabilization of aqueous dispersions of G flakes [41]. Furthermore, the relative content of CNC in generated G-CNC flakes varied according to the initial G: CNC ratio [41]. Interestingly, as shown with the G, stable and high concentration aqueous dispersions of rGO sheets (>10 mg mL^{-1}) could be also prepared thanks to the GO exfoliation in the presence of CNC [54]. A sandwich-like structure was observed in which rGO is between CNC layers forming the hydrophilic outer surfaces rGO-CNC, enhancing thus its dispersion in water and its thermal stability to reach similar value (>320 °C) to that observed for the pristine CNC or to other specific stabilizers [54].

2.6 Vacuum Filtration Technique

The vacuum filtration technique, also known as vacuum-assisted self-assembly (VASA) method, involves the production of uniformly dispersed G within the nanocellulose films [39, 55, 56]. Generally, the G precursor and a small amount

of water-soluble GO is used to combine with nanocellulose. By changing the dispersibility of GO in an aqueous solution of nanocellulose, GO-NC hybrid films with the different internal structures were obtained through vacuum-assisted self-assembly technique [39, 45, 57]. For example, Chen et al. have prepared GO-CNC hybrids using this preparation method and they have shown that after reduction hybrids exhibit high conductivity and iridescent properties [39]. Similarly, Xiong et al. prepared hairy G-CNF sheets by vacuum-assisted filtration process into strong and porous laminated membranes [42]. According to the literature, G-NC hybrids prepared thanks to this technique display enhanced mechanical properties and wet stability even under intense stirring due to a strong H-bond network enabled by the cellulosic network reinforced by graphene nanolayers achieved thanks to vacuum filtration [39, 42, 55].

3 Properties of Graphene and Nanocelluloses Hybrids

3.1 Surface and Sub-surface-Based Properties

In many cases, collected images of rGO-CNC hybrid from scanning electron microscopy (SEM) show the anisotropic of its structure and its very loosely stacked surface structure containing mainly CNC as shown in Fig. 4 [41, 54, 58]. For example, Ye et al. have reported the preparation of an integrated hybrid material with a sandwich-like structure constituted of uniform coverage of exfoliated rGO sheets onto the CNC surface (Fig. 4) [54]. The presence of strong hydrogen bonds between the GO sheets and the CNC result in their physical adsorption. Furthermore, these interactions are strong enough to prevent rGO's stacking interactions during their reduction. This conclusion is consistent with observations made by Montes et al.
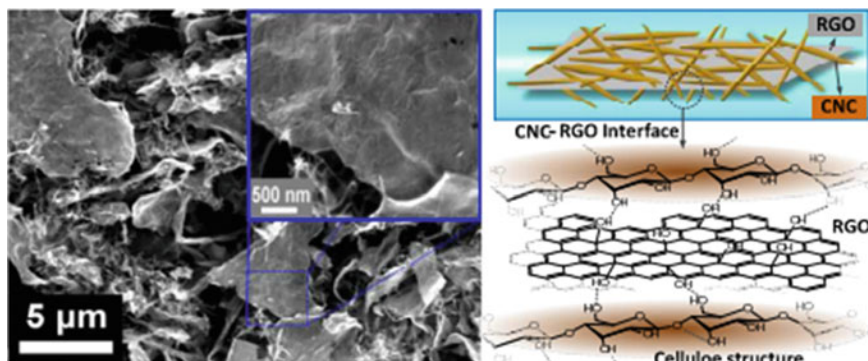

Fig. 4 Schematic illustrations and SEM image of rGO-CNC hybrid [54]
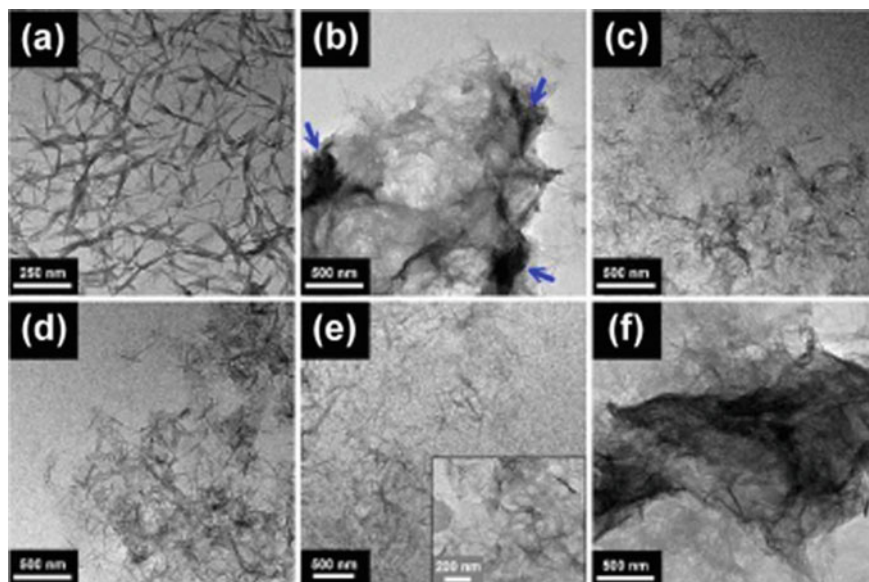
Fig. 5 TEM images of **a** pristine CNC, **b–f** CNC-rGO hybrids at different weight ratios of 1, 3, 6, 10, and 15, respectively [54]

[41]. During this work, the authors have demonstrated thanks to a typical field emission SEM image of a G-CNC hybrid sample with a ratio of 5:95 (G: CNC), that a single G flake is fully surrounded by CNC [41].

However, in their work, Ye et al. compared transmission electron microscopy (TEM) images of very dilute suspensions of pure CNC, rGO-CNC hybrids deposited on carbon- grids with various rGO-CNC ratios [54]. As shown in Fig. 5a, the pristine CNC was a crystalline needle-structure, 5–15 nm in width and 50–250 nm in length, close to the size of CNC formed by sulphuric acid hydrolysis [16, 17, 54, 59, 60]. Some of the sheets were agglomerated for the low start CNC-rGO ratio leading to a folded morphology (marked by the blue arrows in Fig. 5b) due to inadequate CNC adsorption onto the surface of the rGO. Such an issue is less visible by increasing the CNC-rGO ratio (Fig. 5c–e), indicating that the rGO sheets are decorated uniformly by lightweight CNC networks, and most of them are scattered over carbon-coated grids. Finally, as exemplified in Fig. 5f, rGO exfoliation does not seem to be possible by using a sonicated rGO-CNC mixed sample. However, agglomerated rGO sheets are observed highlighting in fact the consequence of the in situ CNC-GO reduction [54]. Similarly, Cao et al. used TEM images to demonstrate the preparation of pure CNC microstructures, rGO nanosheets, and CNC-rGO nanohybrids [61]. During this work, it was also demonstrated that the CNC is self-assembled on single layers of rGO, forming a veined structure of CNC-rGO [61]. These results show that the CNC is capable of (i) mediating the rGO nanosheets dispersion, (ii) preventing

the self-aggregation of graphene layers and (iii) obtaining well distributed CNC-rGO suspensions which are advantageous for the development of 3D interconnected conductive networks [61].

Besides, the atomic force microscopy (AFM) is typically used for the analysis of relatively flat surfaces with topographic features [62–64]. AFM measurements were used in the literature to provide quantitative information on the surface roughness, measurements, and topography of hybrids based on G and NC [14, 37, 39, 44].

For example, AFM was used to depict the 3D structure of G, CNC and their combination leading to hybrid CNC-G nanofillers [14]. During this work, authors report on the dimensions of tested materials, showing that lateral dimensions of hybrid nanosheets are range from ~100 nm to ~2 µm while their thickness was close to ~0.9 nm. Furthermore, it appears that the dimension of the hybrids could be tailored and controlled from that of the former GON and CNC materials. However, as schematized in Fig. 6, the nanofiller thickness could not be determined as CNC layers are directly attached onto the surfaces and edges of GON, forming the targeted 3D interconnected network microstructure [14]. AFM images published by Xiong et al. also illustrated a similar 3D microstructure constituted of building blocks and hairy nanosheets from the hybrids of wrapped GO-CNF [42].
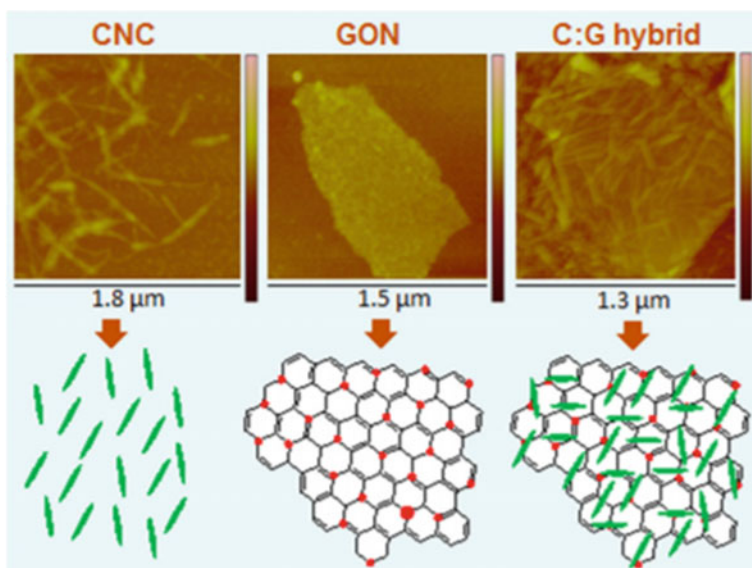
Fig. 6 Tapping mode AFM images and schematic illustrations of CNC, GON, and GO-CNC hybrid (presented in the figure as C:G hybrid and the red dots are the oxygen-containing groups in GON) [14]

3.2   *Chemical Composition, Composition Variation, and Crystal Structure*

Fourier Transform Infrared Spectroscopy (FTIR) is a non-destructive analysis method for investigating chemical functions in materials by detecting the vibrations that define chemical bonds [65–70]. As shown in Fig. 7, bands associated with hydroxyl groups are localized at 3345 cm^{-1} for CNC and 3365 and 3211 cm^{-1} for the GON. However, in the case of the hybrid nanofiller, hydroxyl groups band is shifted, according to its FTIR spectrum, to 3330 cm^{-1} indicating slightly different "hybrid" environments of the formers [14]. Also, the 1715 cm^{-1} band, attributed to the carboxyl moieties observed in the GON spectrum, overlaps with that observed in the hybrid spectrum at 1645 cm^{-1}, which is aligned with the CNC intramolecular hydrogen bonds (Fig. 7). Furthermore, Valentini et al. have also notified that the characteristic absorption peaks in the hybrid spectra are close to the pure CNC curve, which seems to indicate a homogeneous dispersion of stacked GON layers in CNC [71]. These findings also indicate that the cellulose-graphene hybrid nanofillers exhibit good hydrogen interactions and interfacial compatibility [14, 37, 39, 71].

Raman spectroscopy is also a commonly used technique in materials chemistry, providing a structural fingerprint to identify molecules [72–74]. This technique is thus becoming extremely important during the characterization of graphene oxide-coated nanocellulose (G-NC) based hybrid nanomaterials [27, 30, 38, 45, 75, 76]. For example, Burrs et al. used Raman spectroscopy to prove that G-NC hybrids could be partially reduced by using thermal treatments. In contrast, a similar material is further reduced by following a chemical treatment [30].

As shown in Fig. 8a, Song et al. used the Raman spectroscopy to analyze GO, rGO, and hybrids based on rGO-CNF at different ratios. The Raman spectrum of CNF substrate highlights two weak characteristic peaks at around 1096 and 1380 cm^{-1}, whereas hybrid films have stronger Raman peaks close to 1335 (D band) and 1598 (G band) cm^{-1}, highlighting that the rGO nanosheets were successfully assembled onto the CNF substrate. Furthermore, an increase in the number of deposition cycles

Fig. 7 FTIR spectra of CNC, GON, and CNC-GON hybrid (presented as C:G hybrid) [14]
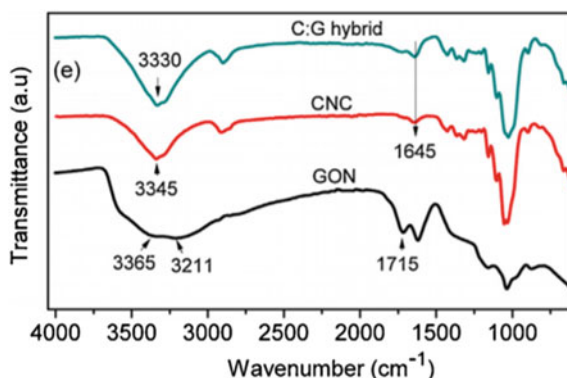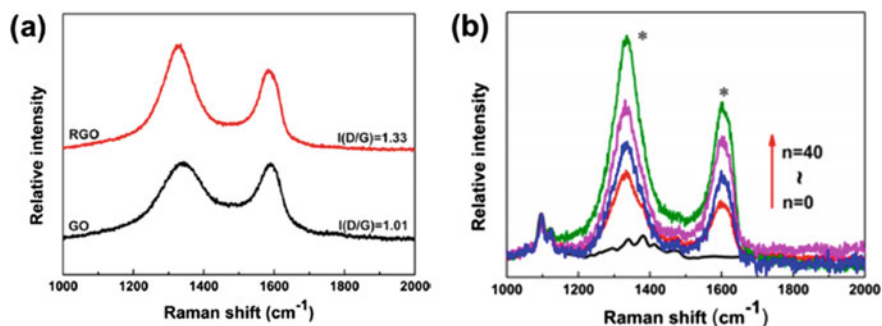
Fig. 8 Raman spectra of **a** GO and rGO. **b** (rGO-CNF)$_n$ hybrid films on a flexible CNF substrate as a function of the number of deposition cycles, n [45]

denoted n in Fig. 8b, induces an increase of the intensity of both D and G bonds of (rGO-CNF)$_n$, attesting the gradual growth of repeating assemblies within the structure of this material [45]. These examples clearly illustrate the possibility of monitoring the synthesis of hybrids using simple spectroscopic techniques like FTIR and Raman.

Material surface changes through any treatment could be followed by X-ray photo-electron spectroscopy (XPS) – another quantitative tool for measuring the elemental composition, chemical state, electronic state of the surface of a material – which also allows the determination of the binding states of the elements [67, 77, 78]. Thus, XPS analysis was mainly used to evaluate the chemical composition of principal elements and the nature of carbon-based bonds on the surface of G-NC hybrids [52, 76, 79]. Figure 9 shows an example of the surface state of the rGO-CNC hybrid published by Ye et al. [54]. During the preparation and characterization of rGO-CNC hybrid, these authors remarked, thanks to XPS analysis, a significant intensity increase for the four mains peaks observed at 285.3, 286.8, 288.0 and 288.3 eV corresponding to bending energies of C–C, C–O, O–C–O, and O–C=O bonds, respectively. In other words, this

Fig. 9 Carbon 1s XPS profile of rGO-CNC hybrid [54]
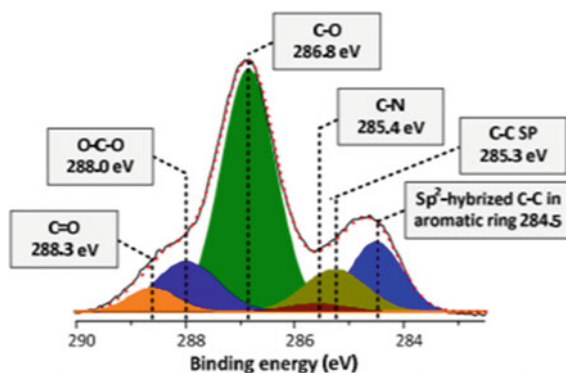
XPS analysis provides thus clear evidence that the CNC structure is covered onto the rGO surface [54].

3.3 Thermal Properties and Density

Among the macroscopic properties of hybrid nanocomposites, the prior knowledge of their thermal stability and their density is crucial for evaluating their real potentials. Generally, the thermal stability of a given material is determined by Thermogravimetric Analysis (TGA), which is a thermal analysis technique based on the measurement of the change in mass of a given sample as a function of the temperature and heating time [80–82]. The bulk density (ρ) of hybrid nanocomposites is generally determined from mass to volume ratio using a pycnometer or by using buoyancy method based on the Archimedes principle.

On the one hand, it was demonstrated in the literature that G-NC materials exhibited improved thermal stability compared to pure cellulose [32, 34, 35]. Furthermore, owing to the powerful nano-effect of graphene on cellulose, a substantial improvement of this thermal stability is observed even at a low graphene loading [35]. To further highlight this enhanced behavior, Ye et al. demonstrated that rGO-CNC hybrids have a thermal stability higher than that of the pristine CNC, which is thermally stable until ~320 °C when mass loss starts to occur [54]. As displayed in Fig. 10a, TGA traces of rGO-CNC hybrids tend to move towards a low-temperature direction by increasing its CNC content as rGO is thermally more stable than CNC. This is further documented thanks to DTG curves, displayed in Fig. 10b, showing that rGO-CNC hybrids have only one main decomposition peak, inducing thus a one-step degradation process, which shifts toward lower temperatures by increasing the CNC content in this hybrid material series, as expected [54].
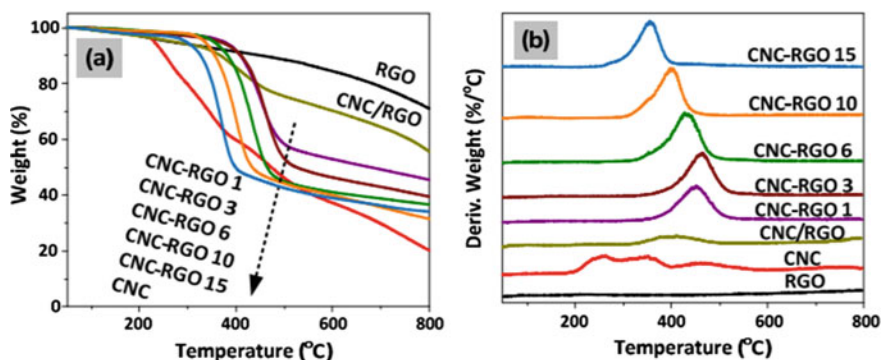
Fig. 10 TGA (**a**) and DTG (**b**) traces of CNC, rGO-CNC blend (presented as CNC/RGO in the figure), and rGO-CNC hybrids (presented as CNC-RGO) [54]

On the other hand, it is also important to note that the knowledge of the density of hybrid materials is essential before their utilization in various fields like energy storage, production of aerogels, water treatment, tissue engineering, etc. [26, 27, 36]. Base on their low-density, both nanocrystals and nanofibrils are widely used as fillers to further enhance the volumetric properties of targeted nanocomposites [19]. Furthermore, as the density of G is also quite low, the combination of CNC or CNF with G could thus induce the formation of low-density hybrid nanocomposites [83]. This unique feature attracts many research groups to use these starting materials to produce light hybrid nanofillers able to be used in various fields [26, 27, 38]. Zhang et al. reported, for exemple, that even if the addition of CNC on G-based hybrids induces an increase of the density of obtained hybrid material, it is still relatively ultra-light to stand on a pistil [47]. Javadi et al. also reported a similar behavior with polyvinyl alcohol (PVA) hybrid-based materials containing G-CNF using a simple, scalable, cost-effective and environmentally friendly freeze-drying method [38]. During this work, these authors reported that these materials present an ultralow density (<35 kg/m^3) along with other excellent properties allowing them to be tested in various applications [38].

4 Preparation of Hybrid Polymer Nanocomposites Based on Graphene and Nanocelluloses

In the light of the two previous sections, devoted to the preparation and main properties of hybrid fillers/charges based on G and NC, in this part, we focus on giving an overview of the preparation of polymer nanocomposites containing these hybrid fillers. Originally, cellulose nanocrystals/cellulose nanofibrils were widely used to reinforce various kinds of polymer matrices in the absence of G [17, 19, 84, 85]. More recently, many researchers focused on the formulation of hybrid polymer nanocomposites by using various types of reinforcement materials and matrices to reach a material combining their main advantages and key properties [14, 36, 41, 86, 87]. In fact, the development of hybrid G-NC composites materials was of interest for various research fields attracting scientists from different communities, inducing thus a wide range of synthesis processes available into the literature [38, 88]. Among those, the commonly applied methods are the solution blending, solvent casting and in situ polymerization, which were used to prepare hybrid nanocomposites with unique properties.

4.1 Solution Blending and Vacuum Filtration

The solution blending approach involves simply mixing or combining two parts in a solution, followed by electrospinning, in which only one portion of the solution
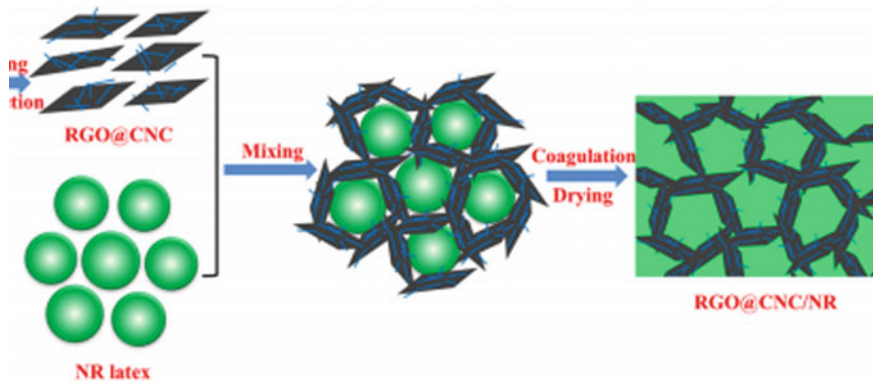
Fig. 11 Schematic diagram of the preparation of NR/rGO-CNC nanocomposites with a 3D conductive network [61]

must be electrospinable [89–91]. In this case, the two parts of the solution include a hybrids material used as a filler and a polymer as a matrix. Afterward, the as-prepared hybrid polymer nanocomposite material is isolated from the solvent using a classical vacuum filtration technique. However, alternative mixing approaches are reported in the literature. For example, as illustrated in Fig. 11, the suspensions of the reduced rGO-CNC nanohybrids and natural rubber (NR) latex could lead to a promising 3D conductive network [61]. During this work, authors used a beaker and vigorous stirring to obtained thus a homogeneous blend [61]. After this mixing step, the co-coagulation was induced by the fast addition of a low concentration sulphuric acid solution.

The solid formed following the coagulation could then be easily isolated and dried through vacuum filtration. Interestingly, this preparation method proved that even the presence of CNC, rGO is located in the interstitial spaces between latex microspheres of the NR during the subsequent coagulation process. According to the authors, the solid NR microspheres provided an excluded volume after a vacuum filtration, washing, and drying treatment, allowing the rGO-CNC nanohybrids to be hosted into their interstitial spaces. This specific organization of the nanohybrids induces a 3D conductive network within the NR matrix [61]. Similarly, PEO/rGO-CNC films could be easily prepared by stirring a rGO-CNC and polyethylene oxide (PEO) blend at 60 °C for 6 h (600 rpm) and by drying the mixed ingredients in a Teflon mold [54]. These two preparation examples provide some interesting insights; however, the high dispersibility in water or organic solvents of the rGO-CNC hybrids, along with their high thermal stability, opens up a wide variety of possible applications.

4.2 Solvent Casting

Solvent casting is a procedure for shaping polymer composite samples by dipping a mold into a polymer solution and drawing off the solvent to leave a polymer composite film adhering to the mold [19, 59, 84, 92, 93]. For example, by using a solvent casting method, El Miri et al. prepared hybrid nanocomposite films based on CNC and GON as fillers, where the loading level of the charges was 5 wt% [14]. As shown in Fig. 12, these authors demonstrated that by casting all mixtures on plastic dishes and thus evaporating off the water, films with high quality and good flexibility could be produced. Similarly, Montes et al. also used this relatively simple and environmentally friendly method to successfully incorporate G-CNC hybrid into poly(vinyl alcohol) (PVA) [41]. Authors reported then that all the resulting films were of outstanding quality, clear (though slightly grayish for those containing graphene), and almost uniform to the naked eye [41]. The solvent casting method was also effectively applied to optimize the formulation of the polylactic acid (PLA) composites through the dispersion of CNC and GO into a PLA matrix to reach enhanced
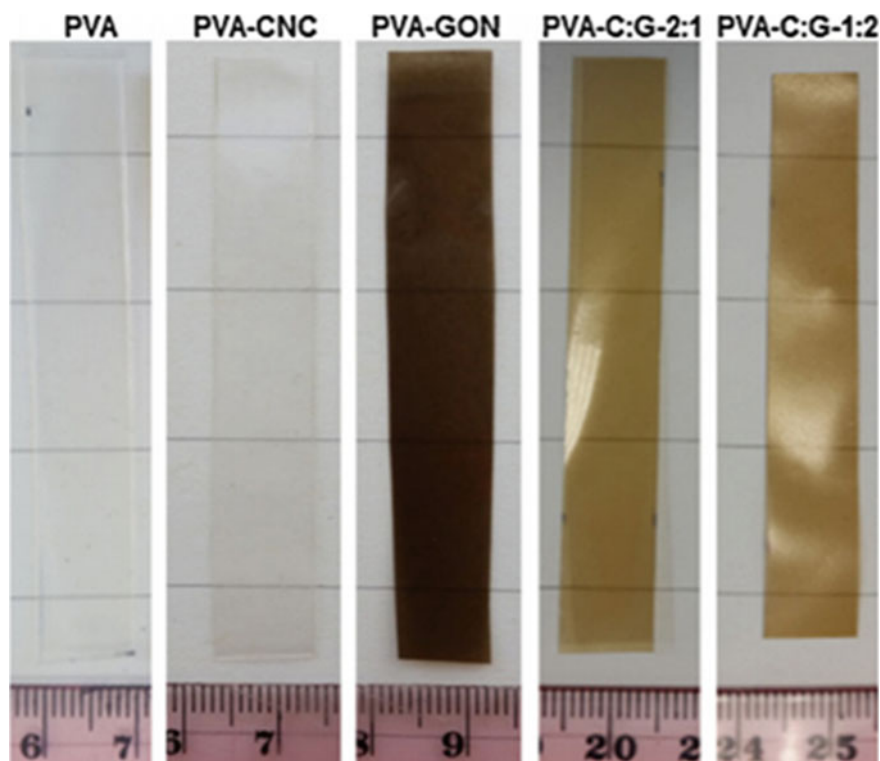
Fig. 12 Digital of prepared neat PVA and its nanocomposite films with CNC, GO and G-CNC hybrid (GO-CNC 2:1 and GO-CNC 1:2) [14]

mechanical and thermal properties as well as improved antimicrobial response of the biodegradable polymer by keeping its inherent transparent optical characteristics [94].

4.3   In Situ Polymerization

In the case of the preparation of G-NC hybrid polymer nanocomposites, an in situ polymerization, generally, starts by dispersing the graphene (or modified graphene) in the selected monomer. After this step, the polymerization could start by adding a suitable initiator [95–97]. Generally, a large range of graphene-based polymer films could be easily prepared thanks to this in situ approach, leading to unique materials with enhanced properties including superior electrical conductivity and mechanical properties [98]. For example, an in situ radical polymerization process was used to prepare polyacrylamide-sodium carboxymethylcellulose (PMC) reinforced with GO and CNC [36]. The addition of both GO and CNC induces, thanks a synergistic effect, a reinforcement of the composite structure leading to exceptional and unique 3D structure, morphology and properties of hybrid polymer nanocomposites [36]. This example provides a clear vision of the main advantages to use this technique during the preparation of hybrid nanocomposites.

5   Properties of Hybrid Polymer Nanocomposites Based on Graphene and Nanocellulose

Several well-known characterization techniques are currently used to analyze and evaluate G-NC hybrid polymer nanocomposites to depict their morphology, structure, and properties [14, 36, 41]. In this regard, characteristic features and properties of hybrid polymer nanocomposites based on G and NC, are most commonly divided into (i) surface and sub-surface-based properties, (ii) chemical composition, composition variation, and crystal structure, (iii) thermal properties and (iv) mechanical properties. The following subsections provide some detailed examples of each class of characteristics of the G-NC based hybrid polymer nanocomposites reported in the literature.

5.1   Surface and Sub-surface-Based Properties

The surface and sub-surface-based properties of hybrid polymer nanocomposites are generally depicted thanks to the Scanning Electron Microscopy (SEM) and Transmission Electron Microscopy (TEM) techniques. The main difference between SEM

and TEM is based on the creation of the image. Indeed, SEM image is created by detecting reflected or knocked-off electrons, whereas TEM image is done thanks to transmitted electrons. In fact, SEM gives information only on the surface of the material (*e.g.* defaults, composition, etc.) while TEM technique could provide information on its inner structure (*e.g.* crystal structure, morphology, and stress state information).

Briefly, the SEM instruments are used to examine and analyse the microstructure morphology of a given material by scanning its surface with a focused beam of electrons. Many researchers have mostly used SEM technique to analyze the morphological structure of hybrid polymer nanocomposites [41, 47, 86]. For example, some authors reported that the morphology characteristics of some hybrid polymer nanocomposites could be observed at an operating accelerating voltage of 20 kV [14]. As shown in Fig. 13, in the case of the GO-CNC reinforced PVA samples, SEM observations are undoubtedly improved by coating a thin conductive carbon layer [14]. As also shown in Fig. 13, the SEM micrographs clearly show the well-dispersed GO-CNC nanofillers within the PVA matrix (the well-white lines are GO and CNC [14]. Furthermore, the authors highlighted thorough their work that no visible agglomerate of nanofillers was observed in the nanocomposites [14]. Interestingly, using SEM Zhang et al. observed that when hybrid composite sheets are broken, some rod-like CNCs could be observed at the breaking edge, indicating thus that some CNC were sandwiched between graphene flakes [47].

TEM is used to image a material thanks to an electron beam [99–101]. Compared to other microscope techniques, TEM provides much higher resolution than is possible with light-based imaging techniques [102–104]. With respect to this technology, researchers preferred TEM analysis to get a measurement of nanoparticle
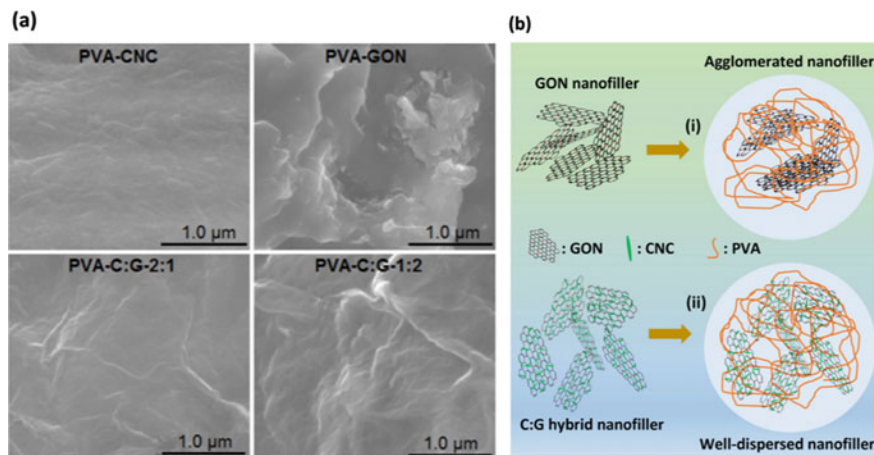
Fig. 13 **a** SEM micrographs of PVA nanocomposites with CNC, GON, and GO-CNC hybrid (GO-CNC 2:1 and GO-CNC 1:2). **b** schematic representations of the dispersion state of (i) GO (ii) GO-CNC hybrid nanofillers within the PVA polymer matrix [14]
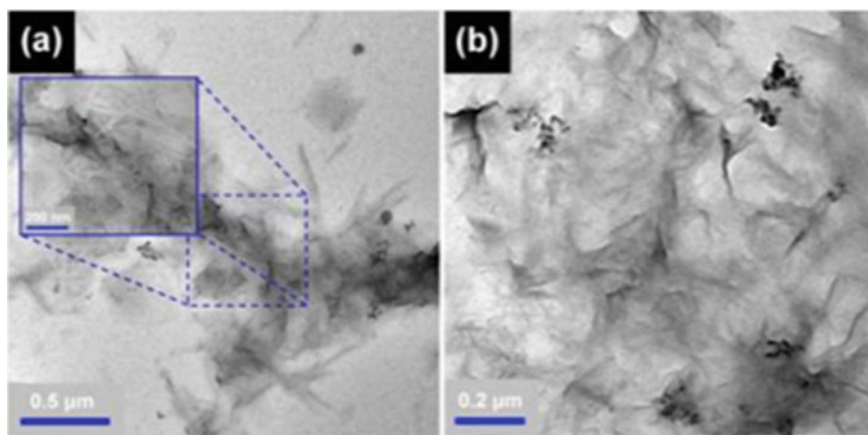
Fig. 14 TEM images of polyethylene oxide/rGO-CNC hybrid composites [54]

size, grain size, size distribution, and morphological information in G-NC based hybrid polymer nanocomposites [28, 36, 37, 44, 54]. For example, as shown in Fig. 14, Ye et al. observed thanks to TEM images the presence of randomly dispersed rGO sheets even at a high rGO-CNC loading (*i.e.* 15 wt%) in polyethylene oxide (PEO)/rGO-CNC composites [54]. Furthermore, Ye et al. also highlighted that rGO sheets were well covered by CNC whiskers (see the dotted blue color frame in Fig. 14), which highlights the compatibility of rGO with the PEO matrix enhanced through the hydrogen bonds network between CNC and PEO [54].

5.2 Chemical Composition, Composition Variation, and Crystal Structures

Chemical composition, composition variation, and crystal structures of hybrid composites are generally analyzed through spectroscopic techniques (FTIR, UV-Visible (UV-Vis), and XPS) and X-Ray Diffraction (XRD) analysis, respectively.

As stated in Sect. 3, FTIR is a kind analytical technique widely used to identify organic, polymeric, and, in some cases, inorganic materials [65, 105, 106]. In practical terms, several research groups use FTIR technique routinely to confirm the chemical structure of G-NC hybrid polymer nanocomposites and interactions among them [52, 71, 107]. For example, FTIR analysis was used to confirm the presence of strong hydrogen interactions occurring in GO-CNC hybrid nanofillers and the PVA matrix [14]. As shown in Fig. 15, during this work, it was observed that by adding the GO-CNC hybrid nanofiller to the PVA neat film, its characteristic hydroxyl band being shifted in the range of 3500–3000 cm^{-1}, suggesting the presence of strong H-bonds in the hybrid polymer nanocomposite material linking the oxygen functional groups

Fig. 15 FTIR spectra of
PVA hybrid nanocomposite
films based on the GO-CNC
hybrid nanofillers [14]
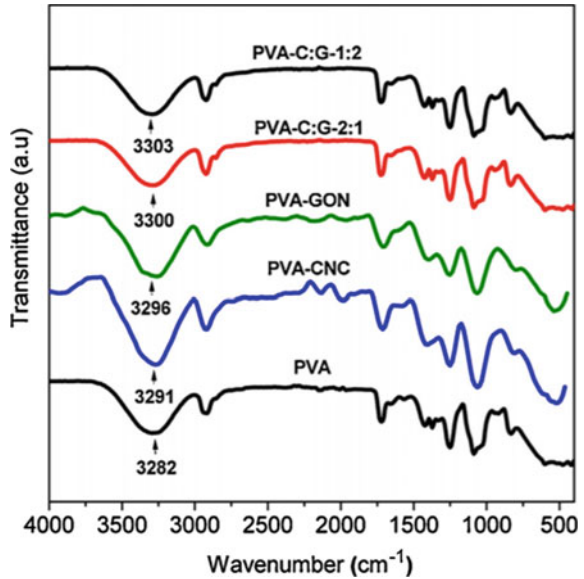
on the GO-CNC surface and the hydroxyl moieties on the macromolecular PVA
matrix [14].

For the last two decades, UV-Visible spectrometers (UV-Vis) have been the most
critical analytical instruments in the modern-day laboratory [17, 19, 66]. Several
research groups have mainly used UV-Vis to depict the optical properties, like the
transparency, of the hybrid polymer nanocomposite materials [37, 41, 55]. Gener-
ally, when the fillers start to agglomerate in the polymer matrix as their concentra-
tion increases, the transmittance will effectively vary with concentration [41]. For
example, as illustrated in Fig. 16 and thanks to UV-Vis measurements, Montes et al.

Fig. 16 UV-Vis absorption
spectra of the PVA neat films
and hybrid nanocomposite
[41]
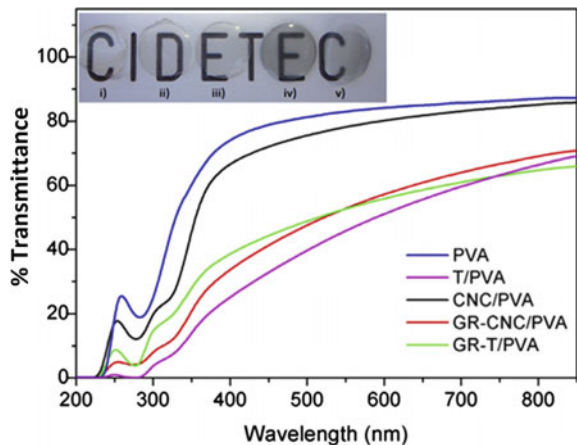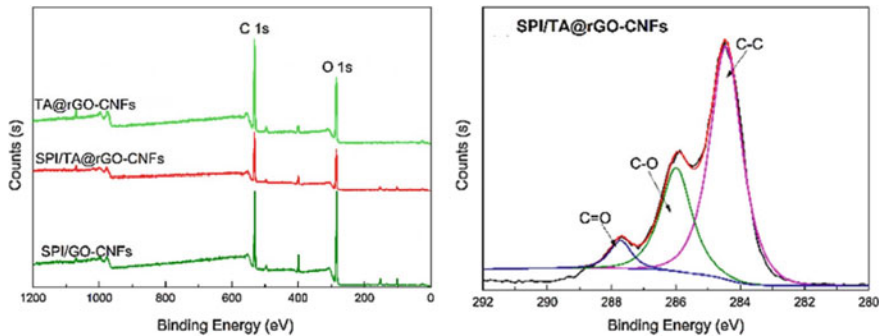
Fig. 17 XPS survey spectra and C 1s core-level spectra of SPI/rGO-CNF films [107]

have clearly demonstrated that the addition of 1 wt% of CNC results in a slight decrease of material transparency compared to the former PVA [41]. Interestingly, these authors also clearly highlighted by UV-VIS that the addition of graphene, with CNC (1 wt% total loading) caused a higher transparency loss even at a very low graphene content (0.05 wt%) [41].

Change on the surface chemical composition of the polymer composites have also been widely investigated through XPS measurements [67, 78, 96, 107, 108]. For example, as shown in Fig. 17 (left) Wang et al. used high-resolution XPS survey spectra to highlight strong interactions in hybrid composites between rGO-CNF hybrid and soy protein isolate (SPI) chains [107]. These authors also analyze the SPI/rGO-CNF film spectra C1 s XPS spectra, shown in Fig. 17 (right), to suggest a potential reaction pathway of rGO-CNF with SPI matrix, which was fingerprinted by the increase of C-OH groups peak with rGO-CNF fillers integration [107]. The findings related to XPS measurements highlighted that the polymer matrix has a crucial role in creating desirable interfacial adhesion in the manufacture of composite films, revealing both covalent and hydrogen bonds thorough the whole material structure [107].

XRD is a characterization tool to study the crystal structure, to detect the presence of crystalline phases in a material, and thus provide crucial information on its chemical composition. Several research groups have used at most frequently used XRD analysis to understand the crystallography structure of the hybrid polymeric materials based on G and NC [27, 47, 86]. For example, Akindoyo et al. notified in the case of the poly (vinyl alcohol) nanocomposites that an increase in the wt% of graphene causes a shift downwards of the XRD pattern of PVA-CNF to the lower angle. The authors attributed this observation to an increase of d-spacing which could be related to a possible bonding interruption between PVA and CNF due to the integration of the graphene [109]. Similarly, Kumar et al. used the X-ray diffraction to analyze pure components and hybrid hydrogels to depict the effect of material composition on the material structure and crystallinity [36]. As shown in Fig. 18, the synthesized GO showed a broad peak around 10.8°, corresponding to the interlayer spacing between each GO sheet, while the CNC characteristic XRD peaks appeared
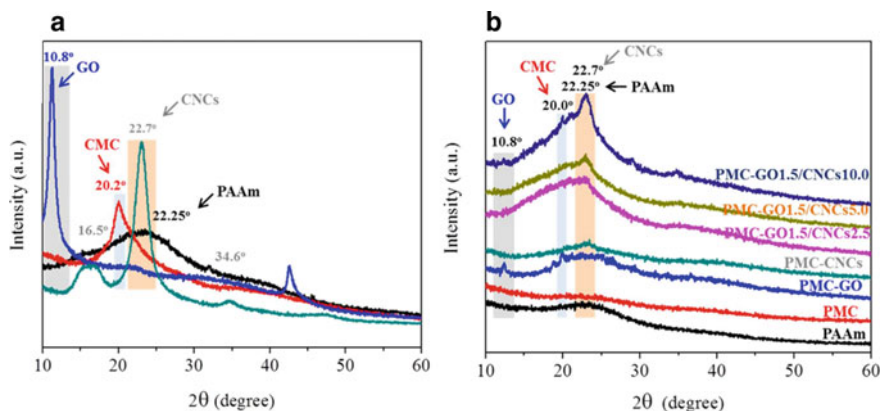
Fig. 18 XRD analysis of **a** pure components and **b** their nanoreinforced hybrids composite [36]

at around 16.5°, 22.7°, and 34.6°. Furthermore, the authors depicted that an increase in cellulose nanocrystals CNC content in polyacrylamide (PMC/GO-CNC) hybrid hydrogels induces a significant increase in the characteristic peaks of CNC (Fig. 18). In contrast, the intensity of the characteristic peak of GO is lower than that observed with PMC-GO hybrid hydrogel [36].

5.3 Thermal Properties

The thermal properties of hybrid composites are generally analyzed through the utilization of both Differential Scanning Calorimetry (DSC) and, as already discussed in Sect. 3, TGA analysis. Essentially, each collected information (weight loss as a function of the temperature, presence of glass transition, melting temperature, etc.) could be used to characterize and/or identify complex materials, such as polymers [38, 54]. For this reason, the TGA equipment was widely used to characterize G-NC based hybrid to depict their composition (*i.e.* their organic and inorganic (filler) content), thermal stability and behaviors over the time or over the temperature, hydration degree, and the residual level of solvent including their moisture content [45, 86, 107]. As shown in Fig. 19, TGA analysis could be used to probe the existence of the synergistic effect between fillers and the matrix. In this specific case, this was observed thanks to the differences between the degradation temperature (T_{onset}) of GO-CNC hybrid, Poly (vinyl alcohol) PVA, and hybrid nanocomposites. Indeed, a synergetic effect was suspected as the T_{onset} for the nanocomposites films containing only CNC or GO was always lower than that of all nanocomposites containing CNC-GO hybrid nanofillers [14].

Briefly, DSC is a thermoanalytical technique in which the change of heat flow into or out of a material is measured as a function of the time or temperature, while the material sample is exposed to a controlled temperature program with the respect

Fig. 19 TGA curves of PVA and its nanocomposites films with CNC and GO as hybrid nanofillers at different ratios [14]
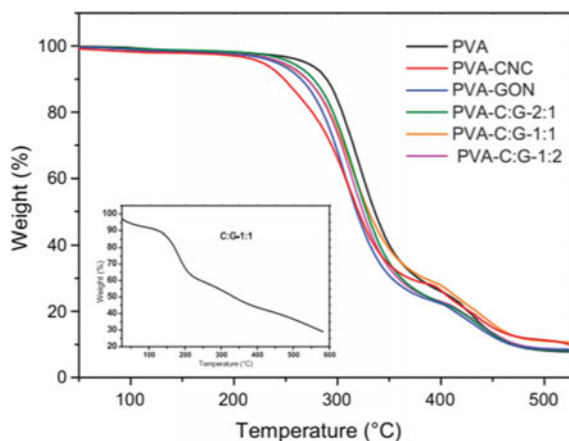
of a reference [110–113]. Practically, several research groups employed DSC analysis to study the effect of hybrid fillers on glass transition (T_g) and melting (T_m) temperatures of hybrid polymer nanocomposite materials [14, 28, 41]. DSC analysis of hybrid polymeric nanocomposite are, generally determined under nitrogen gas with a heating rate lower than 10 °C min^{-1} in a wide temperature range depending on the stability of the matrix used. For example, as shown in Fig. 20, DSC traces could also provide some insight on the structural changes thanks to the knowledge of
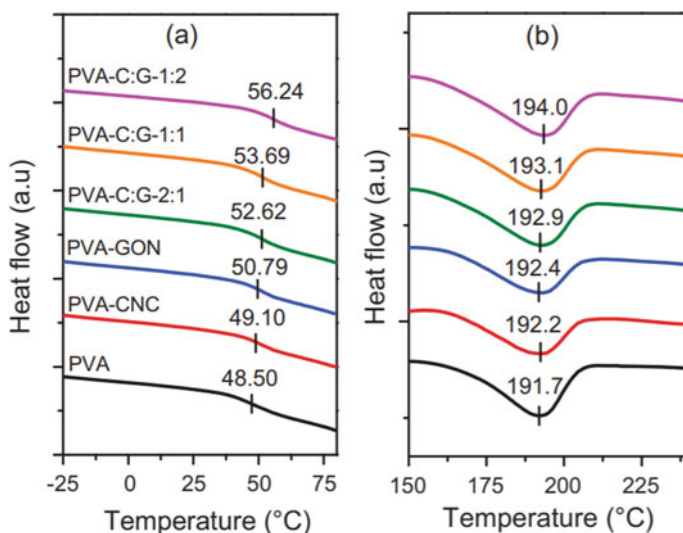
Fig. 20 **a** Glass transition temperature, Tg, and **b** melting temperature, Tm, obtained from DSC traces of PVA and its nanocomposites films with CNC and GO as hybrid nanofillers at different ratios [14]

T_g and T_m. In this particular example, the authors suggested that the increase in T_g and T_m could be related to the inhibition of the mobility of Polyvinyl alcohol (PVA) macromolecular chains resulting from the cross-linking network formed between the PVA and GO-CNC hybrid nanofillers [14]. In other words, useful information could be revealed by combining surface, structural and thermal properties of hybrids nanocomposites.

5.4 Mechanical Properties

The mechanical properties of G-NC hybrid polymeric nanocomposite with different ratios of nanofillers were analyzed by tensile testing [14, 44]. Most of the hybrid nanocomposites present enhanced mechanical properties than those reported for nanocomposites containing G or CNC nanofillers [14, 41, 43, 44]. For example, Montes et al. demonstrated that at 1wt% G-CNC nanofiller loading, leading to PVA/G-CNC hybrid composite, exhibits superior mechanical properties than the neat PVA (*i.e.* an increase of 20 and 50% in the tensile strength and Young's modulus, respectively) or even the PVA-CNC (*i.e.* an increase of 4% and 19% in the tensile strength and Young's modulus, respectively) [41]. Table 1 compares the mechanical properties of various hybrid polymeric nanocomposites reported in the literature. From this table, one can clearly see that in the case of the PVA matrix, GO-CNC filler provides the best mechanical properties enhancement for the formed nanocomposite. This performance improvement with the respect of the former polymer is close to that observed in the case of the SPI/rGO-CNF.

As above-mentioned, G and NC possess unique and very interesting mechanical properties such as high elastic modulus, tensile strength, and fracture toughness. These exciting properties of both the G and NC could explain their use in the development of novel, sustainable and high-quality hybrid nanocomposites [32, 36, 38]. Essentially, dynamic mechanical analysis (DMA) is one of the techniques which was widely applied to study and characterize the viscoelasticity and mechanical

Table 1 Percentage increase in polymer hybrid nanocomposite tensile properties in comparison to neat polymer

Polymer	Filler	Strength (%)	Modulus (%)	References
PVA	G-CNF	39	53	[109]
PVA	GO-CNC	320	124	[14]
PVA	G-CNC	20	50	[41]
PVA	rGO-CNF	87	122	[43]
PLA	rGO-CNC	23	29	[94]
PEO	rGO-CNC	87	170	[54]
SPI	rGO-CNF	281	157	[107]

properties of polymer nanocomposites [36, 38, 47]. For example, mechanical characteristics under compression mode of the GO-CNC based polyacrylamide-sodium carboxymethylcellulose (PMC) hybrid hydrogels in the wet state were analyzed by dynamic mechanical analysis with a preload force of 0.05 N at a rate of 3.0 N min^{-1} [36]. The authors reported that the polyacrylamide-sodium carboxymethylcellulose (PMC) hybrid composite has excellent mechanical stability able to resist even under high compression preventing their deformations, and/or having excellent and quick shape-recovery behavior limiting apparent damage of their structure [36]. Furthermore, during this work, the authors also demonstrated that an increase in CNCs content (from 2.5 to 10.0 wt%) in the PMC/CNC-GO hybrid composite exhibited significant improvement in the compressive strength (from 91.39 to 110.5 kPa) and stiffness [36]. This study highlights the importance of the formulation to reach optimum properties with respect to the former fillers and matrix. Likewise, Javadi et al. carried out compression testing by a dynamic mechanical analyzer of polyvinyl alcohol (PVA) hybrid nanocomposite reinforced by GO and CNF [38]. During their work, the specific compressive strength of the PVA/GO-CNF hybrid aerogels was shown to be considerably higher than that of PVA-based aerogels (more than 6-fold) [38]. However, it is important to notify herein, that an increase of fillers content does not necessarily induce an improvement of the properties automatically with respect to those of the polymeric matrix. For example, Akindoyo et al. clearly demonstrated, as shown in Table 2, that PVA/G-CNF nanocomposites reach a higher storage modulus E' with solely 1 wt% of graphene instead of 3 wt% or 5 wt% [109]. This result could be attributed to a potential increase of the agglomeration of graphene particles within the nanocomposite structure as its wt% content increases driven by an overall increase of van der Waals forces. This hypothesis seems to be also validated by looking at the Tg values of the nanocomposites, which are all higher than pure PVA, and strongly increase with the G content. Indeed, higher Tg is an indicator of decreased polymer chain mobility, which is most likely due to heavy interfacial adhesion, as supported by adhesion factor values reported in Table 2 taken from [109].

Table 2 Dynamic mechanical properties of the PVA and PVA nanocomposites comprising 3 wt% G and CNF at different ratios [109]

Sample code	E'(MPa)	Max Tan δ peak	Tg (°C)	Adhesion factor (A)
PVA	1283	0.31	33.70	0
PVA/CNF	1819	0.19	48.03	−0.37
PVA/CNF—1% G	1477	0.56	47.14	0.88
PVA/CNF—3% G	820	2.28	77.11	6.82
PVA/CNF—5% G	633	2.30	89.83	7.07

6 Applications of Hybrid Polymer Nanocomposites Based on Graphene and Nanocellulose

In this section, we focus on giving an overview of the potential applications of hybrid polymer nanocomposites, which are considered as potential technological materials due to their lightweight, high mechanical strength, thermal properties, chemical resistance, and extended durability [114–117]. Progress made on G-NC hybrid-reinforced polymer nanocomposites open the door for their applications in nanoelectronics, food packaging, energy storage, water treatment, and sensing, as demonstrated in Fig. 21 [14, 27, 43, 118]. According to the literature, G-NC hybrid polymer nanocomposites attract several application fields, while this section is mainly focused on their more significant applications.

Fig. 21 Main application of hybrid nanocomposites based on graphene and cellulose nanocrystals/cellulose nanofibrils

6.1 Food Packaging

The development of nanocomposite based on cellulose nanocrystals/nanofibrils has greatly advanced in the field of food packaging due to the actual growing concern about severe environmental pollution problems. For this reason, research has been devoted to the production of sustainable and environmentally friendly materials [119–122]. In this regard, Kassab et al. prepared different cellulose nanocrystals (CNC) mass fractions (1, 3, 5, and 8 wt%), which were dispersed into polyvinyl alcohol (PVA) matrix to produce PVA-CNC nanocomposite films, using solvent casting method [59]. By adding 8 wt% CNC into a PVA matrix, an increase close to 215, 150, and 45% of Young's modulus, tensile strength, and toughness was observed with the respect to the neat PVA, respectively [59]. In comparison with the previously mentioned work, El Miri et al. prepared PVA hybrid nanocomposites based on GON and CNC at different ratios [14]. In this work, due to the synergistic reinforcement of the filler with the presence of GON, the addition 5 wt% hybrid nanofiller (1:2) was enough to reach superior properties of PVA hybrid nanocomposites with an increase observed in Young's modulus (+320%), tensile strength (+124%), and its toughness (159%) in comparison with the PVA matrix. However, as illustrated in Fig. 22, the addition of the hybrid nanofiller does not seem to have a strong impact on the elongation break of the hybrid material, as similar values to that of the neat PVA matrix were observed [14]. The comparison between PVA/CNC and PVA/GON-CNC nanocomposite films clearly highlights the net benefits of designing hybrid polymer nanocomposites since the synergistic effect enhanced the homogeneity of dispersion by preventing the agglomeration of nanofillers within the polymer matrix [14, 59]. Nevertheless, prior to be potentially used in the food packaging, its negligible ecotoxicity and antibacterial properties must be confirmed.

However, the cytocompatibility test showed that in the case of the poly-lactic acid (PLA), the PLA/rGO-CNC nanocomposite is not toxic to NIH-3T3 cells and as also confirmed by the morphological analysis of the treated cells [94]. Furthermore, in addition to being biocompatible, this later nanocomposite film seems to have antibacterial properties against Gram-positive Staphylococcus aureus (S.aureus) and Gram-negative Escherichia coli bacteria (The E.coli) [94]. Consequently, these results indicate that some nanocomposite films based on cellulose nanocrystals and graphene could be selected as a viable alternative for packaging applications [94].

6.2 Water Treatment

The high growth of human population combined with the exploitation of water resources has resulted in a shortage of freshwater supply in the world because a growing number of contaminants including organic dyestuffs, heavy metal ions, light metal salts, and other impurities are entering water supplies due to human activity
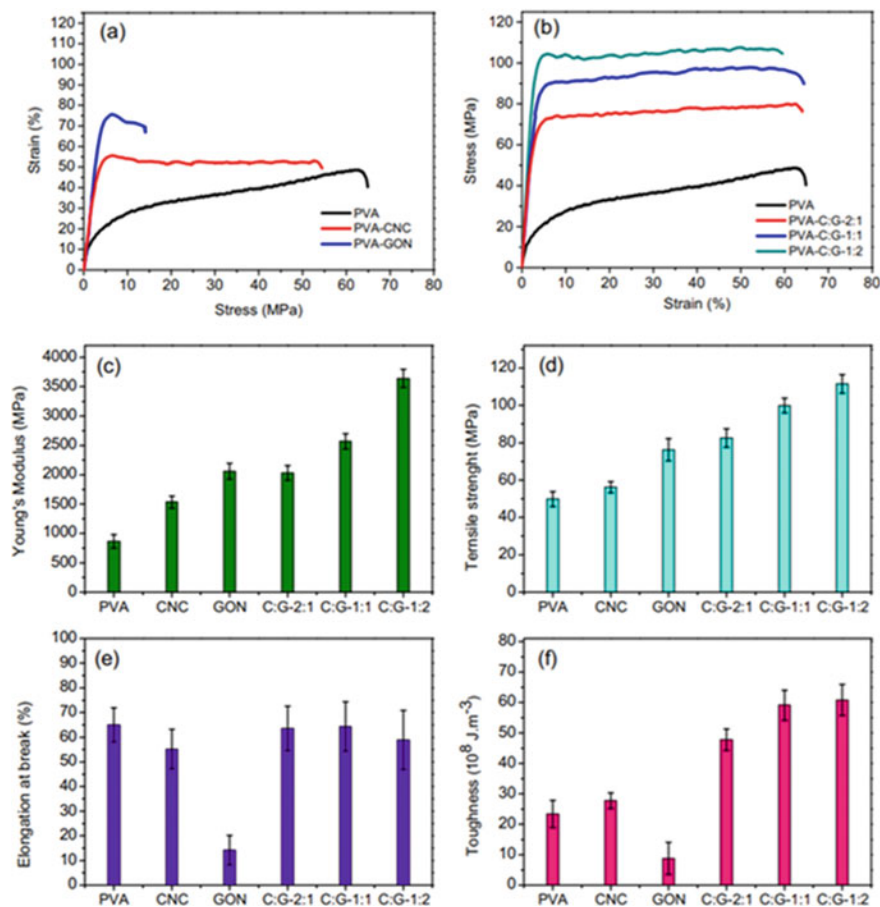
Fig. 22 Typical stress-strain curves (**a**, **b**), Young's modulus (**c**), tensile strength, elongation at break (**e**), and toughness (**f**) of PVA and its nanocomposites with CNC and GO as hybrid nanofiller [14]

[123–126]. To solve such an issue, scientists start to use the graphene in water treatment processes mainly because its unique properties including: high surface area, high thermal conductivity, superior mobility as a charge carrier, good mechanical properties, fracture and breaking strength, specific magnetism and good chemical stability [127–131]. Moreover, the application of nanotechnology in environmental remediation paved the way for the development of nanostructured hybrid composite materials based on G and NC [47, 132, 133]. In this regard, Zhang et al. prepared G-CNC, with the help of the excellent hydrophilicity of cellulose nanocrystals, CNC-G containing 20 wt% CNCs can adsorb water up to 100 times its weight despite the graphene aerogel component. This unique behavior demonstrates the strong hydrophobicity of hybrid polymer nanocomposites [47]. This pioneering work
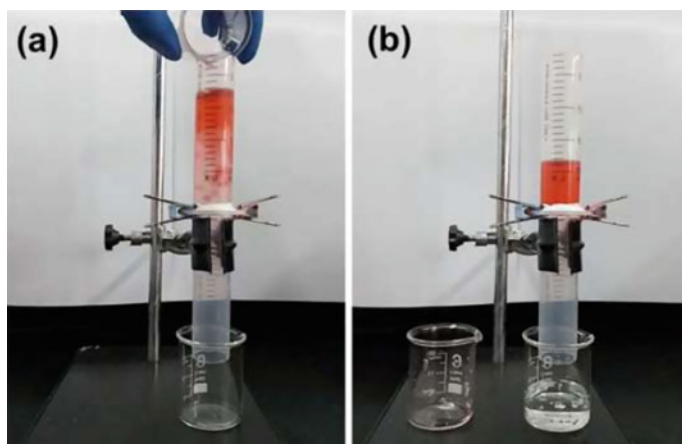
Fig. 23 **a** The pre-wetted GO-CNF membrane was fixed between two plastic tubes; the mixture of hexane and water was put into the upper plastic tube. **b** Water selectively permeated through the GO-CNF membrane, while the oil was repelled and kept in the upper plastic tube [134]

provides thus a promising amphiphilic graphene-based aerogel material with tunable mechanical strength by a simple, economical, and environmental-friendly approach, making it highly potential in wastewater treatment and pressure-sensitive materials [47].

Similarly, Ao et al. successfully fabricated a nanoscale hierarchically structured membrane consisting of GO and electrospun CNF [134]. As a result of its super hydrophilicity and unique structures, the resultant hybrid membrane demonstrated high water flux and superior antifouling performance in separating oil/water mixtures, as shown herein in Fig. 23. Furthermore, this work clearly highlights that the prepared membrane is capable of separating oil/water mixtures in a complex environment, such as highly acidic, alkaline, and salty environments [134].

6.3 Energy Storage

The development of novel technologies intended for the production and storage of electrical energies are significant due to the increase in energy demand [135–137]. Consequently, graphene has aroused interest in this energy field because of its structure based on a monolayer of sp^2 hybridized carbon atoms arranged in a 2D matrix [53, 138]. G-NC based hybrid polymer nanocomposites materials are one of the most promising applications, in which the combination of graphene and polymer chains seems to be a viable technological solution to design future energy devices. Graphene makes possible the insulator to conductor transition at significantly lower loading by providing percolated pathways for electron transfer and making the polymers composite electrically conductive [139]. Recent works report on hybrids

Fig. 24 A novel type of highly flexible and all-solid-state supercapacitor that uses rGO-CNF-CNT hybrid (presented as CNF/RGO/CNT in the figure) [26]
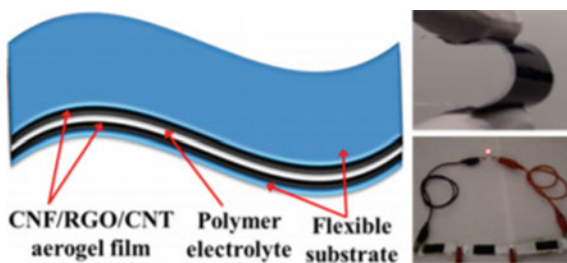
based on G and NC, which may be applied for prospective applications, including supercapacitors and transparent conducting electrode [55, 71, 140, 141]. For example, as shown in Fig. 24, Zheng et al. developed a novel type of highly flexible and all-solid-state supercapacitor that uses rGO-CNF-CNT hybrid aerogels as electrodes and poly(vinyl alcohol) (PVA) gel as the electrolyte [26]. Owing to G-NC hybrid nanocomposites superior electrochemical performance, excellent process scalability, low cost, and environmentally friendliness, the aerogel films may be a promising electrode material for assembling lightweight, flexible, low-cost, and rechargeable energy-storage devices [26, 32, 76].

6.4 Sensor Technology

G-NC based hybrid composite material properties made it highly desirable for its use in chemical sensors and "electronic noses" capable of detecting, quantifying and distinguishing different solvents or vapors in the chemical industry, environmental monitoring, and food industry, etc. [13, 31, 40, 93]. The 3D conductive network of G-CNC hybrid endowed the natural rubber (NR) composites with remarkably improved electrical conductivity (the percolation threshold is twofold lower than that of traditional NR/graphene composites), mechanical properties and, more significantly, organic liquid resistivity response [61]. The G-CNC hybrid composite materials could provide an innovative, quick and environmentally friendly route for the manufacture of liquid sensors capable of detecting and distinguishing specific solvent leakage in the chemical industry as well as monitoring the environment [61, 93].

Owing to their good properties, PVA composite films reinforced with rGO-CNF hybrid can serve to absorb and then desorb moisture even present in an atmospheric air [43]. As shown in Fig. 25, the presence of a water film on the rGO-CNF surface could induce local changes into the structure and thus in resistance of composite films [43]. This is in fact due to a disruption of the strong hydrogen bond interactions between rGO-CNF hybrid with the PVA matrix caused by the presence of water molecules. Consequently, the decrease in the structure and the resistance of nanocomposites could be directly related to the relative humidity leading to their utilization as effective humidity sensors [17, 19, 43, 109]. Such findings demonstrate that G-NC hybrid composite materials have tremendous potential in the preparation of high-precision
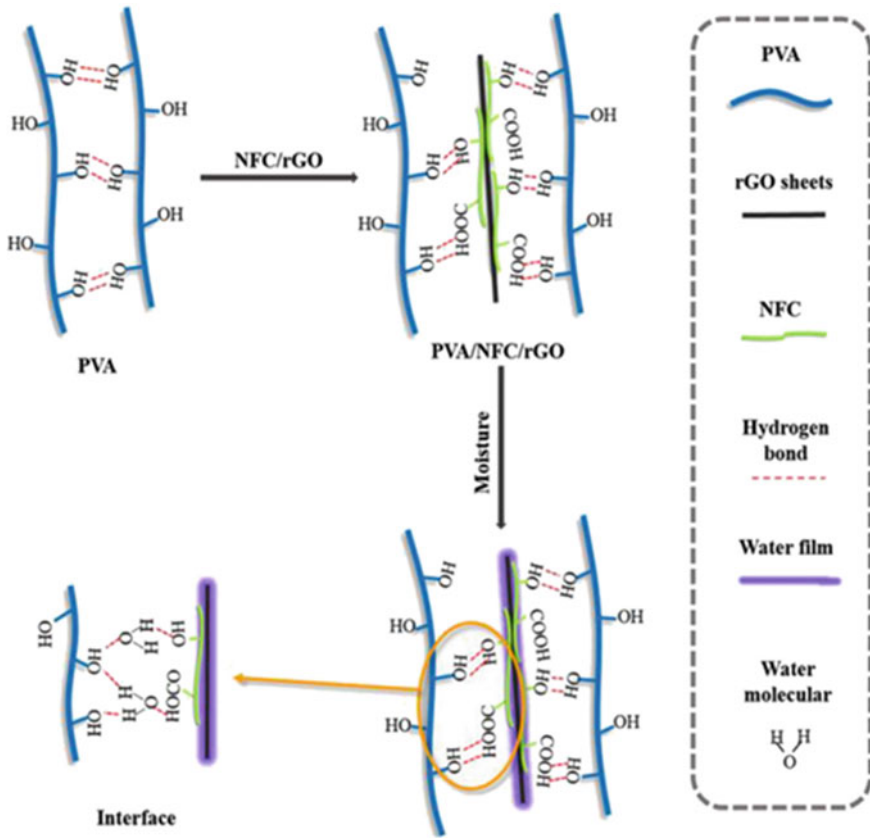
Fig. 25 Schematic description of the process for improved sensitivity performance of PVA films aided by rGO and CNF [43]

sensors, which could be transferred relatively easily to detect selectively other species like light gases or other chemical vapors.

7 Conclusion

In summary, the preparation of G-NC hybrid materials and composites is an attractive research field that is moving very fast. To date, these hybrid nanocomposite materials are mainly prepared thanks to a layer-by-layer assembly, ultrasonication, or in situ polymerization method. However, whatever the preparation method selected, by using G-NC fillers a number of the nanocomposite's properties are superior to

those observed for "classical" materials, such as their mechanical, thermal, crystallinity, surface-based characteristics, to cite few. Based on these enhanced properties, G-NC hybrid materials are now recognized as promising materials for food packaging, water treatment, and energy storage applications.

However, despite the recent progress, highlighted thorough this chapter, G-NC hybrid materials and composites face considerable research challenges that must be solved prior to (i) reaching better synergistic effects, improved properties, and (ii) sketching a proper industrial road map over traditional composite materials. Among these challenges, a major one is linked to the large-scale production of graphene with a high (maximum) purity as the presence of impurities impacts on the overall quality and properties of the composite materials. For the development of hybrid composite materials, the homogenous dispersion of G-NC in the polymer matrix must be ensured and well-controlled to minimize their agglomeration, nonhomogeneous distribution, and interfacial interactions during the testing procedures. However, in the light of the current advances in material sciences, one can clearly see all the potential and future opportunities to design hybrid composites containing both the G-NC. Furthermore, new research outcomes are expected to be reported in the near future, allowing these hybrids to move quickly from the rank of fundamental materials to novel technological materials offering industrial solutions to the production companies and their users.

References

1. Pal S, Patra AS, Ghorai S, Sarkar AK, Das R, Sarkar S (2015) Modified guar gum/SiO$_2$: Development and application of a novel hybrid nanocomposite as a flocculant for the treatment of wastewater. Environ Sci Water Res Technol 1:84–95. https://doi.org/10.1039/c4ew00023d
2. Chen J, Jia C, Wan Z (2014) Novel hybrid nanocomposite based on poly(3,4-ethylenedioxythiophene)/ multiwalled carbon nanotubes/graphene as electrode material for supercapacitor. Synth Met 189:69–76. https://doi.org/10.1016/j.synthmet.2014.01.001
3. Fan W, Xia YY, Tjiu WW, Pallathadka PK, He C, Liu T (2013) Nitrogen-doped graphene hollow nanospheres as novel electrode materials for supercapacitor applications. J Power Sources 243:973–981. https://doi.org/10.1016/j.jpowsour.2013.05.184
4. Artiles MS, Rout CS, Fisher TS (2011) Graphene-based hybrid materials and devices for biosensing. Adv Drug Deliv Rev 63:1352–1360. https://doi.org/10.1016/j.addr.2011.07.005
5. Rashidi Nodeh H, Wan Ibrahim WA, Kamboh MA, Sanagi MM (2017) New magnetic graphene-based inorganic–organic sol-gel hybrid nanocomposite for simultaneous analysis of polar and non-polar organophosphorus pesticides from water samples using solid-phase extraction. Chemosphere 166:21–30. https://doi.org/10.1016/j.chemosphere.2016.09.054
6. Rashidi Nodeh H, Sereshti H, Gaikani H, Kamboh MA, Afsharsaveh Z (2017) Magnetic graphene coated inorganic-organic hybrid nanocomposite for enhanced preconcentration of selected pesticides in tomato and grape. J Chromatogr A 1509:26–34. https://doi.org/10.1016/j.chroma.2017.06.032
7. Leung KCF, Xuan S, Zhu X, Wang D, Chak CP, Lee SF, Ho WKW, Chung BCT (2012) Gold and iron oxide hybrid nanocomposite materials. Chem Soc Rev 41:1911–1928. https://doi.org/10.1039/c1cs15213k

8. Chen YF, Bi JQ, Yin CL, You GL (2014) Microstructure and fracture toughness of graphene nanosheets/alumina composites. Ceram Int 40:13883–13889. https://doi.org/10.1016/j.ceramint.2014.05.107

9. Dimov D, Amit I, Gorrie O, Barnes MD, Townsend NJ, Neves AIS, Withers F, Russo S, Craciun MF (2018) Ultrahigh performance nanoengineered graphene-concrete composites for multifunctional applications. Adv Funct Mater 28:1–12. https://doi.org/10.1002/adfm.201705183

10. Lahiri D, Dua R, Zhang C, De Socarraz-Novoa I, Bhat A, Ramaswamy S, Agarwal A (2012) Graphene nanoplatelet-induced strengthening of ultrahigh molecular weight polyethylene and biocompatibility in vitro. ACS Appl Mater Interfaces 4:2234–2241. https://doi.org/10.1021/am300244s

11. Graphene L, Rafiee M, Rafiee J, Wang Z, Song H, Yu Z, Koratkar N (2009) Enhanced mechanical properties of nanocomposites at low graphene content. ACS Nano 3:3884–3890. https://doi.org/10.1021/nn9010472

12. Gebauer D, Oliynyk V, Salajkova M, Sort J, Zhou Q, Bergström L, Salazar-Alvarez G (2011) A transparent hybrid of nanocrystalline cellulose and amorphous calcium carbonate nanoparticles. Nanoscale 3:3563–3566. https://doi.org/10.1039/c1nr10681c

13. Nypelö T, Rodriguez-Abreu C, Rivas J, Dickey MD, Rojas OJ (2014) Magneto-responsive hybrid materials based on cellulose nanocrystals. Cellulose 21:2557–2566. https://doi.org/10.1007/s10570-014-0307-2

14. El Miri N, El Achaby M, Fihri A, Larzek M, Zahouily M, Abdelouahdi K, Barakat A, Solhy A (2016) Synergistic effect of cellulose nanocrystals/graphene oxide nanosheets as functional hybrid nanofiller for enhancing properties of PVA nanocomposites. Carbohydr Polym 137:239–248. https://doi.org/10.1016/j.carbpol.2015.10.072

15. Kassab Z, Abdellaoui Y, Salim MH, El Achaby M (2020) Cellulosic materials from pea (Pisum Sativum) and broad beans (Vicia Faba) pods agro-industrial residues. Mater Lett 280:128539. https://doi.org/10.1016/j.matlet.2020.128539

16. El Achaby M, Kassab Z, Barakat A, Aboulkas A (2018) Alfa fibers as viable sustainable source for cellulose nanocrystals extraction: application for improving the tensile properties of biopolymer nanocomposite films. Ind Crops Prod 112:499–510. https://doi.org/10.1016/j.indcrop.2017.12.049

17. Kassab Z, Boujemaoui A, Ben Youcef H, Hajlane A, Hannache H, El Achaby M (2019) Production of cellulose nanofibrils from alfa fibers and its nanoreinforcement potential in polymer nanocomposites. Cellulose 26:9567–9581. https://doi.org/10.1007/s10570-019-02767-5

18. Kassab Z, Syafri E, Tamraoui Y, Hannache H, Qaiss AEK, El Achaby M (2019) Characteristics of sulfated and carboxylated cellulose nanocrystals extracted from Juncus plant stems. Int J Biol Macromol. https://doi.org/10.1016/j.ijbiomac.2019.11.023

19. Kassab Z, Mansouri S, Tamraoui Y, Sehaqui H, Hannache H, Qaiss AEK, El Achaby M (2020) Identifying Juncus plant as viable source for the production of micro- and nano-cellulose fibers: application for PVA composite materials development. Ind Crops Prod 144:112035. https://doi.org/10.1016/j.indcrop.2019.112035

20. Kassab Z, Abdellaoui Y, Salim MH, Bouhfid R, Qaiss AEK, El Achaby M (2020) Micro- and nano-celluloses derived from hemp stalks and their effect as polymer reinforcing materials. Carbohydr Polym 245:116506. https://doi.org/10.1016/j.carbpol.2020.116506

21. Zhang N, Zang GL, Shi C, Yu HQ, Sheng GP (2016) A novel adsorbent TEMPO-mediated oxidized cellulose nanofibrils modified with PEI: preparation, characterization, and application for Cu(II) removal. J Hazard Mater 316:11–18. https://doi.org/10.1016/j.jhazmat.2016.05.018

22. Dong S, Roman M (2007) Fluorescently labeled cellulose nanocrystals for bioimaging applications. J Am Chem Soc 129:13810–13811. https://doi.org/10.1021/ja076196l

23. Xu X, Liu F, Jiang L, Zhu JY, Haagenson D, Wiesenborn DP (2013) Cellulose nanocrystals vs. cellulose nanofibrils: a comparative study on their microstructures and effects as polymer reinforcing agents. ACS Appl Mater Interf 5:2999–3009. https://doi.org/10.1021/am302624t

24. Du H, Liu W, Zhang M, Si C, Zhang X, Li B (2019) Cellulose nanocrystals and cellulose nanofibrils based hydrogels for biomedical applications. Carbohydr Polym 209:130–144. https://doi.org/10.1016/j.carbpol.2019.01.020

25. Hamad W (2006) On the development and applications of cellulosic nanofibrillar and can. J Chem Eng 84:513–519

26. Zheng Q, Cai Z, Ma Z, Gong S (2015) Cellulose nanofibril/reduced graphene oxide/carbon nanotube hybrid aerogels for highly flexible and all-solid-state supercapacitors. ACS Appl Mater Interf 7:3263–3271. https://doi.org/10.1021/am507999s

27. Yao Q, Fan B, Xiong Y, Jin C, Sun Q, Sheng C (2017) 3D assembly based on 2D structure of cellulose nanofibril/graphene oxide hybrid aerogel for adsorptive removal of antibiotics in water. Sci Rep 7:1–13. https://doi.org/10.1038/srep45914

28. Wang F, Drzal LT, Qin Y, Huang Z (2015) Multifunctional graphene nanoplatelets/cellulose nanocrystals composite paper. Elsevier Ltd. https://doi.org/10.1016/j.compositesb.2015.04.031

29. Gao K, Shao Z, Li J, Wang X, Peng X, Wang W, Wang F (2013) Cellulose nanofiber-graphene all solid-state flexible supercapacitors. J Mater Chem A 1:63–67. https://doi.org/10.1039/c2ta00386d

30. Burrs SL, Bhargava M, Sidhu R, Kiernan-Lewis J, Gomes C, Claussen JC, McLamore ES (2016) A paper based graphene-nanocauliflower hybrid composite for point of care biosensing. Biosens Bioelectr 85:479–487. https://doi.org/10.1016/j.bios.2016.05.037

31. Yan C, Wang J, Kang W, Cui M, Wang X, Foo CY, Chee KJ, Lee PS (2014) Highly stretchable piezoresistive graphene-nanocellulose nanopaper for strain sensors. Adv Mater 26:2022–2027. https://doi.org/10.1002/adma.201304742

32. Xing J, Tao P, Wu Z, Xing C, Liao X, Nie S (2019) Nanocellulose-graphene composites: a promising nanomaterial for flexible supercapacitors. Carbohydr Polym 207:447–459. https://doi.org/10.1016/j.carbpol.2018.12.010

33. Yang W, Zhao Z, Wu K, Huang R, Liu T, Jiang H, Chen F, Fu Q (2017) Ultrathin flexible reduced graphene oxide/cellulose nanofiber composite films with strongly anisotropic thermal conductivity and efficient electromagnetic interference shielding. J Mater Chem C 5:3748–3756. https://doi.org/10.1039/C7TC00400A

34. Zhang X, Liu X, Zheng W, Zhu J (2012) Regenerated cellulose/graphene nanocomposite films prepared in DMAC/LiCl solution. Carbohydr Polym 88:26–30. https://doi.org/10.1016/j.carbpol.2011.11.054

35. Ouyang W, Sun J, Memon J, Wang C, Geng J, Huang Y (2013) Scalable preparation of three-dimensional porous structures of reduced graphene oxide/cellulose composites and their application in supercapacitors. Carbon N Y 62:501–509. https://doi.org/10.1016/j.carbon.2013.06.049

36. Kumar A, Rao KM, Han SS (2018) Mechanically viscoelastic nanoreinforced hybrid hydrogels composed of polyacrylamide, sodium carboxymethylcellulose, graphene oxide, and cellulose nanocrystals. Carbohydr Polym 193:228–238. https://doi.org/10.1016/j.carbpol.2018.04.004

37. Sadasivuni KK, Kafy A, Zhai L, Ko HU, Mun S, Kim J (2015) Transparent and flexible cellulose nanocrystal/reduced graphene oxide film for proximity sensing. Small 11:994–1002. https://doi.org/10.1002/smll.201402109

38. Javadi A, Zheng Q, Payen F, Javadi A, Altin Y, Cai Z, Sabo R, Gong S (2013) Polyvinyl alcohol-cellulose nanofibrils-graphene oxide hybrid organic aerogels. ACS Appl Mater Interf 5:5969–5975. https://doi.org/10.1021/am400171y

39. Chen Q, Liu P, Sheng C, Zhou L, Duan Y, Zhang J (2014) Tunable self-assembly structure of graphene oxide/cellulose nanocrystal hybrid films fabricated by vacuum filtration technique. RSC Adv 4:39301–39304. https://doi.org/10.1039/c4ra05921b

40. Shao C, Li X, Lin S, Zhuo B, Yang S, Yuan Q (2020) Characterization of nanocellulose–graphene electric heating membranes prepared via ultrasonic dispersion. J Mater Sci 55:421–437. https://doi.org/10.1007/s10853-019-04006-5

41. Montes S, Carrasco PM, Ruiz V, Cabañero G, Grande HJ, Labidi J, Odriozola I (2015) Synergistic reinforcement of poly(vinyl alcohol) nanocomposites with cellulose nanocrystal-stabilized graphene. Compos Sci Technol 117:26–31. https://doi.org/10.1016/j.compscitech.2015.05.018

42. Xiong R, Kim HS, Zhang L, Korolovych VF, Zhang S, Yingling YG, Tsukruk VV (2018) Wrapping nanocellulose nets around graphene oxide sheets. Angew Chemie Int Ed 57:8508–8513. https://doi.org/10.1002/anie.201803076

43. Xu S, Yu W, Yao X, Zhang Q, Fu Q (2016) Nanocellulose-assisted dispersion of graphene to fabricate poly(vinyl alcohol)/graphene nanocomposite for humidity sensing. Compos Sci Technol 131:67–76. https://doi.org/10.1016/j.compscitech.2016.05.014

44. Xiong R, Hu K, Grant AM, Ma R, Xu W, Lu C, Zhang X, Tsukruk VV (2016) Ultrarobust transparent cellulose nanocrystal-graphene membranes with high electrical conductivity. Adv Mater 28:1501–1509. https://doi.org/10.1002/adma.201504438

45. Song N, Jiao D, Cui S, Hou X, Ding P, Shi L (2017) Highly anisotropic thermal conductivity of layer-by-layer assembled nanofibrillated cellulose/graphene nanosheets hybrid films for thermal management. ACS Appl Mater Interf 9:2924–2932. https://doi.org/10.1021/acsami.6b11979

46. Markutsya S, Jiang C, Pikus Y, Tsukruk VV (2005) Freely suspended layer-by-layer nanomembranes: testing micromechanical properties. Adv Funct Mater 15:771–780. https://doi.org/10.1002/adfm.200400149

47. Zhang X, Liu P, Duan Y, Jiang M, Zhang J (2017) Graphene/cellulose nanocrystals hybrid aerogel with tunable mechanical strength and hydrophilicity fabricated by ambient pressure drying technique. RSC Adv 7:16467–16473. https://doi.org/10.1039/c6ra28178h

48. Li M, Jiang H, Xu D, Yang Y (2017) A facile method to prepare cellulose whiskers—silica aerogel composites. J Sol-Gel Sci Technol 1–8. https://doi.org/10.1007/s10971-017-4384-1

49. Cui S, Wei P, Li L (2018) Preparation of poly (propylene carbonate)/graphite nanoplates-spherical nanocrystal cellulose composite with improved glass transition temperature and electrical conductivity. Compos Sci Technol 168:63–73. https://doi.org/10.1016/j.compscitech.2018.09.012

50. Lin L, Ecke N, Kamerling S, Sun C, Wang H, Song X, Wang K, Zhao S, Zhang J, Schlarb AK (2018) Study on the impact of graphene and cellulose nanocrystal on the friction and wear properties of SBR/NR composites under dry sliding conditions. Wear 414–415:43–49. https://doi.org/10.1016/j.wear.2018.07.027

51. Wang K, Ma Q, Pang K, Ding B, Zhang J, Duan Y (2018) One-pot synthesis of graphene/chitin nanofibers hybrids and their remarkable reinforcement on Poly(vinyl alcohol). Carbohydr Polym 194:146–153. https://doi.org/10.1016/j.carbpol.2018.04.036

52. Wei X, Huang T, Yang J, Zhang N, Wang Y, Zhou Z (2017) Green synthesis of hybrid graphene oxide/microcrystalline cellulose aerogels and their use as superabsorbents. J Hazard Mater 335:28–38. https://doi.org/10.1016/j.jhazmat.2017.04.030

53. Tang L, Wang Y, Li Y, Feng H, Lu J, Li J (2009) Preparation, structure, and electrochemical properties of reduced graphene sheet films. Adv Funct Mater 19:2782–2789. https://doi.org/10.1002/adfm.200900377

54. Ye YS, Zeng HX, Wu J, Dong LY, Zhu JT, Xue ZG, Zhou XP, Xie XL, Mai YW (2016) Biocompatible reduced graphene oxide sheets with superior water dispersibility stabilized by cellulose nanocrystals and their polyethylene oxide composites. Green Chem 18:1674–1683. https://doi.org/10.1039/c5gc01979f

55. Nan F, Chen Q, Liu P, Nagarajan S, Duan Y, Zhang J (2016) Iridescent graphene/cellulose nanocrystal film with water response and highly electrical conductivity. RSC Adv 6:93673–93679. https://doi.org/10.1039/c6ra20133d

56. Putz KW, Compton OC, Palmeri MJ, Nguyen SBT, Brinson LC (2010) High-nanofiller-content graphene oxide-polymer nanocomposites via vacuum-assisted self-assembly. Adv Funct Mater 20:3322–3329. https://doi.org/10.1002/adfm.201000723

57. Patole AS, Patole SP, Jung SY, Yoo JB, An JH, Kim TH (2012) Self assembled graphene/carbon nanotube/polystyrene hybrid nanocomposite by in situ microemulsion polymerization. Eur Polym J 48:252–259. https://doi.org/10.1016/j.eurpolymj.2011.11.005

58. Xian-qing X, Yu-liang B, Hui L, Qingqing Z, Rong L, Tetsuo M (2018) Study on mechanical and electrical properties of cellulose nanofibrils/graphene-modified natural rubber. Mater Chem Phys. https://doi.org/10.1016/j.matchemphys.2018.11.041

59. El Achaby M, Kassab Z, Aboulkas A, Gaillard C, Barakat A (2018) Reuse of red algae waste for the production of cellulose nanocrystals and its application in polymer nanocomposites. Int J Biol Macromol 106:681–691. https://doi.org/10.1016/j.ijbiomac.2017.08.067

60. Kassab Z, Kassem I, Hannache H, Bouhfid R, Qaiss AEK, El Achaby M (2020) Tomato plant residue as new renewable source for cellulose production: extraction of cellulose nanocrystals with different surface functionalities. Cellulose 7:1–17. https://doi.org/10.1007/s10570-020-03097-7

61. Cao J, Zhang X, Wu X, Wang S, Lu C (2016) Cellulose nanocrystals mediated assembly of graphene in rubber composites for chemical sensing applications. Carbohydr Polym 140:88–95. https://doi.org/10.1016/j.carbpol.2015.12.042

62. Wagner R, Moon RJ, Raman A (2016) Mechanical properties of cellulose nanomaterials studied by contact resonance atomic force microscopy. Cellulose 23:1031–1041. https://doi.org/10.1007/s10570-016-0883-4

63. Lahiji RR, Xu X, Reifenberger R, Raman A, Rudie A, Moon RJ (2010) Atomic force microscopy characterization of cellulose nanocrystals. Langmuir 26:4480–4488. https://doi.org/10.1021/la903111j

64. Nemes-Incze P, Osváth Z, Kamarás K, Biró LP (2008) Anomalies in thickness measurements of graphene and few layer graphite crystals by tapping mode atomic force microscopy. Carbon N Y 46:1435–1442. https://doi.org/10.1016/j.carbon.2008.06.022

65. Mansur HS, Oréfice RL, Mansur AAP (2004) Characterization of poly(vinyl alcohol)/poly(ethylene glycol) hydrogels and PVA-derived hybrids by small-angle X-ray scattering and FTIR spectroscopy. Polym (Guildf) 45:7193–7202. https://doi.org/10.1016/j.polymer.2004.08.036

66. Kassab Z, Aziz F, Hannache H, Ben Youcef H, El Achaby M (2019) Improved mechanical properties of k-carrageenan-based nanocomposite films reinforced with cellulose nanocrystals. Int J Biol Macromol 123:1248–1256. https://doi.org/10.1016/j.ijbiomac.2018.12.030

67. Luan P, Oehrlein GS (2019) Characterization of ultrathin polymer films using p-polarized ATR-FTIR and its comparison with XPS. Langmuir 35:4270–4277. https://doi.org/10.1021/acs.langmuir.9b00316

68. Watkins D, Hosur M, Tcherbi-narteh A, Jeelani S (2014) Extraction and characterization of lignin from different biomass resources. Integr Med Res 4:26–32. https://doi.org/10.1016/j.jmrt.2014.10.009

69. Silvério HA, Flauzino Neto WP, Dantas NO, Pasquini D (2013) Extraction and characterization of cellulose nanocrystals from corncob for application as reinforcing agent in nanocomposites. Ind Crops Prod 44:427–436. https://doi.org/10.1016/j.indcrop.2012.10.014

70. Renouard S, Hano C, Doussot J (2014) Characterization of ultrasonic impact on coir, fl ax and hemp fi bers. Mater Lett 1–5. https://doi.org/10.1016/j.matlet.2014.05.018

71. Valentini L, Cardinali M, Fortunati E, Torre L, Kenny JM (2013) A novel method to prepare conductive nanocrystalline cellulose/graphene oxide composite films. Mater Lett 105:4–7. https://doi.org/10.1016/j.matlet.2013.04.034

72. Wang X, Huang SC, Huang TX, Su HS, Zhong JH, Zeng ZC, Li MH, Ren B (2017) Tip-enhanced Raman spectroscopy for surfaces and interfaces. Chem Soc Rev 46:4020–4041. https://doi.org/10.1039/c7cs00206h

73. Zhang X, Tan QH, Bin Wu J, Shi W, Tan PH (2016) Review on the Raman spectroscopy of different types of layered materials. Nanoscale 8:6435–6450. https://doi.org/10.1039/c5nr07205k

74. Ding SY, Yi J, Li JF, Ren B, Wu DY, Panneerselvam R, Tian ZQ (2016) Nanostructure-based plasmon-enhanced Raman spectroscopy for surface analysis of materials. Nat Rev Mater 1. https://doi.org/10.1038/natrevmats.2016.21

75. Wicklein B, Kocjan A, Salazar-Alvarez G, Carosio F, Camino G, Antonietti M, Bergström L (2015) Thermally insulating and fire-retardant lightweight anisotropic foams based on

nanocellulose and graphene oxide. Nat Nanotechnol 10:277–283. https://doi.org/10.1038/nnano.2014.248

76. Song N, Cui S, Jiao D, Hou X, Ding P, Shi L (2017) Layered nanofibrillated cellulose hybrid films as flexible lateral heat spreaders: the effect of graphene defect. Carbon N Y 115:338–346. https://doi.org/10.1016/j.carbon.2017.01.017

77. Al-Gaashani R, Najjar A, Zakaria Y, Mansour S, Atieh MA (2019) XPS and structural studies of high quality graphene oxide and reduced graphene oxide prepared by different chemical oxidation methods. Ceram Int 45:14439–14448. https://doi.org/10.1016/j.ceramint.2019.04.165

78. Navratil R, Kotzianova A, Halouzka V, Opletal T, Triskova I, Trnkova L, Hrbac J (2016) Polymer lead pencil graphite as electrode material: voltammetric, XPS and Raman study. J Electroanal Chem 783:152–160. https://doi.org/10.1016/j.jelechem.2016.11.030

79. Ryu J, Lim JS, Ahn S, Jo SM, Ko FK, Lee JH, Hwang JY (2018) Structure and properties of graphene oxide/cellulose hybrid fibers via divalent metal ions treatment. Cellulose 25:517–525. https://doi.org/10.1007/s10570-017-1535-z

80. Wang N, Ding E, Cheng R (2007) Thermal degradation behaviors of spherical cellulose nanocrystals with sulfate groups. Polymer (Guildf) 48:3486–3493. https://doi.org/10.1016/j.polymer.2007.03.062

81. Ridzuan MJM, Majid MSA, Afendi M, Mazlee MN, Gibson AG (2016) Thermal behaviour and dynamic mechanical analysis of Pennisetum purpureum/glass-reinforced epoxy hybrid composites. Compos Struct 152:850–859. https://doi.org/10.1016/j.compstruct.2016.06.026

82. Fitaroni LB, De Lima JA, Cruz SA, Waldman WR (2015) Thermal stability of polypropylene-montmorillonite clay nanocomposites: Limitation of the thermogravimetric analysis. Polym Degrad Stab 111:102–108. https://doi.org/10.1016/j.polymdegradstab.2014.10.016

83. Kuila T, Bose S, Kumar A, Khanra P, Hoon N, Hee J (2012) Effect of functionalized graphene on the physical properties of linear low density polyethylene nanocomposites. Polym Test 31:31–38. https://doi.org/10.1016/j.polymertesting.2011.09.007

84. Kassab Z, El Achaby M, Tamraoui Y, Sehaqui H, Bouhfid R, Qaiss AEK (2019) Sunflower oil cake-derived cellulose nanocrystals: extraction, physico-chemical characteristics and potential application. Int J Biol Macromol 136:241–252. https://doi.org/10.1016/j.ijbiomac.2019.06.049

85. Kassab Z, Ben Youcef H, Hannache H, El Achaby M (2019) Isolation of cellulose nanocrystals from various lignocellulosic materials: physico-chemical characterization and application in polymer composites development. Mater Today Proc 13:964–973. https://doi.org/10.1016/j.matpr.2019.04.061

86. Duan J, Gong S, Gao Y, Xie X, Jiang L, Cheng Q (2016) Bioinspired ternary artificial nacre nanocomposites based on reduced graphene oxide and nanofibrillar cellulose. ACS Appl Mater Interf 8:10545–10550. https://doi.org/10.1021/acsami.6b02156

87. Burrs SL, Vanegas DC, Bhargava M, Mechulan N, Hendershot P, Yamaguchi H, Gomes C, McLamore ES (2015) A comparative study of graphene-hydrogel hybrid bionanocomposites for biosensing. The Analyst 140:1466–1476. https://doi.org/10.1039/c4an01788a

88. Kulandaivalu S, Abdul Shukur R, Sulaiman Y (2018) Improved electrochemical performance of electrochemically designed layered poly(3,4-ethylenedioxythiophene)/graphene oxide with poly(3,4-ethylenedioxythiophene)/nanocrystalline cellulose nanocomposite. Synth Met 245:24–31. https://doi.org/10.1016/j.synthmet.2018.08.002

89. Ma HL, Zhang L, Zhang Y, Wang S, Sun C, Yu H, Zeng X, Zhai M (2014) Radiation preparation of graphene/carbon nanotubes hybrid fillers for mechanical reinforcement of poly(vinyl alcohol) films. Radiat Phys Chem 118:21–26. https://doi.org/10.1016/j.radphyschem.2015.03.028

90. Nan X, Ma J, Liu J, Zhao J, Zhu W (2016) Effect of surfactant functionalization of multi-walled carbon nanotubes on mechanical, electrical and thermal properties of epoxy nanocomposites. Fibers Polym 17:1866–1874. https://doi.org/10.1007/s12221-016-6388-9

91. Verma M, Chauhan SS, Dhawan SK, Choudhary V (2017) Graphene nanoplatelets/carbon nanotubes/polyurethane composites as efficient shield against electromagnetic polluting

radiations. Compos Part B Eng 120:118–127. https://doi.org/10.1016/j.compositesb.2017. 03.068

92. Sanchez-Garcia MD, Gimenez E, Lagaron JM (2008) Morphology and barrier properties of solvent cast composites of thermoplastic biopolymers and purified cellulose fibers. Carbohydr Polym 71:235–244. https://doi.org/10.1016/j.carbpol.2007.05.041

93. Dong B, Zhang L, Wu Y (2016) Highly conductive natural rubber–graphene hybrid films prepared by solution casting and in situ reduction for solvent-sensing application. J Mater Sci 51:10561–10573. https://doi.org/10.1007/s10853-016-0276-y

94. Pal N, Dubey P, Gopinath P, Pal K (2017) Combined effect of cellulose nanocrystal and reduced graphene oxide into poly-lactic acid matrix nanocomposite as a scaffold and its anti-bacterial activity. Int J Biol Macromol 95:94–105. https://doi.org/10.1016/j.ijbiomac.2016. 11.041

95. Wang JY, Yang SY, Huang YL, Tien HW, Chin WK, Ma CCM (2011) Preparation and prop-erties of graphene oxide/polyimide composite films with low dielectric constant and ultrahigh strength via in situ polymerization. J Mater Chem 21:13569–13575. https://doi.org/10.1039/ c1jm11766a

96. Bose S, Kuila T, Uddin ME, Kim NH, Lau AKT, Lee JH (2010) In-situ synthesis and charac-terization of electrically conductive polypyrrole/graphene nanocomposites. Polymer (Guildf) 51:5921–5928. https://doi.org/10.1016/j.polymer.2010.10.014

97. Tripathi SN, Saini P, Gupta D, Choudhary V (2013) Electrical and mechanical properties of PMMA/reduced graphene oxide nanocomposites prepared via in situ polymerization. J Mater Sci 48:6223–6232. https://doi.org/10.1007/s10853-013-7420-8

98. Ray D, Sain S (2016) In situ processing of cellulose nanocomposites. Compos Part A Appl Sci Manuf 83:19–37. https://doi.org/10.1016/j.compositesa.2015.09.007

99. Kaushik M, Basu K, Benoit C, Cirtiu CM, Vali H, Moores A (2015) Cellulose nanocrys-tals as chiral inducers: enantioselective catalysis and transmission electron microscopy 3D characterization. J Am Chem Soc 137:6124–6127. https://doi.org/10.1021/jacs.5b02034

100. Robertson AW, Warner JH (2013) Atomic resolution imaging of graphene by transmission electron microscopy. Nanoscale 5:4079–4093. https://doi.org/10.1039/c3nr00934c

101. Ping J, Fuhrer MS (2012) Layer number and stacking sequence imaging of few-layer graphene by transmission electron microscopy. Nano Lett 12:4635–4641. https://doi.org/10.1021/nl3 01932v

102. Zheng Q, Kvit A, Cai Z, Ma Z, Gong S (2017) A freestanding cellulose nanofibril-reduced graphene oxide-molybdenum oxynitride aerogel film electrode for all-solid-state supercapac-itors with ultrahigh energy density. J Mater Chem A 5:12528–12541. https://doi.org/10.1039/ c7ta03093b

103. Ling S, Li C, Adamcik J, Wang S, Shao Z, Chen X, Mezzenga R (2014) Directed growth of silk nanofibrils on graphene and their hybrid nanocomposites. ACS Macro Lett 3:146–152. https://doi.org/10.1021/mz400639y

104. Wei D, Haque S, Andrew P, Kivioja J, Ryhänen T, Pesquera A, Centeno A, Alonso B, Chuvilin A, Zurutuza A (2013) Ultrathin rechargeable all-solid-state batteries based on monolayer graphene. J Mater Chem A 1:3177–3181. https://doi.org/10.1039/c3ta01183f

105. Yang Z, Peng H, Wang W, Liu T (2010) Crystallization behavior of poly(ε-caprolactone)/layered double hydroxide nanocomposites. J Appl Polym Sci 116:2658–2667. https://doi.org/10.1002/app

106. Ramesh S, Ang GP (2010) Impedance and FTIR studies on plasticized PMMA-LiN(CF3SO2)2 nanocomposite polymer electrolytes. Ionics (Kiel) 16:465–473. https://doi. org/10.1007/s11581-009-0417-2

107. Wang Z, Kang H, Zhao S, Zhang W, Zhang S, Li J (2018) Polyphenol-induced cellu-lose nanofibrils anchored graphene oxide as nanohybrids for strong yet tough soy protein nanocomposites. Carbohydr Polym 180:354–364. https://doi.org/10.1016/j.carbpol.2017. 09.102

108. Wang Z, Wei P, Qian Y, Liu J (2014) The synthesis of a novel graphene-based inorganic-organic hybrid flame retardant and its application in epoxy resin. Compos Part B Eng 60:341–349. https://doi.org/10.1016/j.compositesb.2013.12.033

109. Akindoyo JO, Ismail NH, Mariatti M (2019) Performance of poly(vinyl alcohol) nanocomposite reinforced with hybrid TEMPO mediated cellulose-graphene filler. Polym Test 80:106140. https://doi.org/10.1016/j.polymertesting.2019.106140

110. Xu JZ, Liang YY, Huang HD, Zhong GJ, Lei J, Chen C, Li ZM (2012) Isothermal and nonisothermal crystallization of isotactic polypropylene/graphene oxide nanosheet nanocomposites. J Polym Res 19. https://doi.org/10.1007/s10965-012-9975-5

111. Ryu SH, Sin JH, Shanmugharaj AM (2014) Study on the effect of hexamethylene diamine functionalized graphene oxide on the curing kinetics of epoxy nanocomposites. Eur Polym J 52:88–97. https://doi.org/10.1016/j.eurpolymj.2013.12.014

112. Zhang F, Peng X, Yan W, Peng Z, Shen Y (2011) Nonisothermal crystallization kinetics of in situ nylon 6/graphene composites by differential scanning calorimetry. J Polym Sci Part B Polym Phys 49:1381–1388. https://doi.org/10.1002/polb.22321

113. Bak JM, Lee T, Seo E, Lee Y, Jeong HM, Kim BS, Il Lee H (2012) Thermoresponsive graphene nanosheets by functionalization with polymer brushes. Polymer (Guildf) 53:316–323. https://doi.org/10.1016/j.polymer.2011.11.057

114. Notake K, Gunji T, Kokubun H, Kosemura S, Mochizuki Y, Tanabe T, Kaneko S, Ugawa S, Lee H, Matsumoto F (2016) The application of a water-based hybrid polymer binder to a high-voltage and high-capacity Li-rich solid-solution cathode and its performance in Li-ion batteries. J Appl Electrochem 46:267–278. https://doi.org/10.1007/s10800-016-0930-8

115. Liu J, Ma Y, Xu T, Shao G (2010) Preparation of zwitterionic hybrid polymer and its application for the removal of heavy metal ions from water. J Hazard Mater 178:1021–1029. https://doi.org/10.1016/j.jhazmat.2010.02.041

116. Gu A (2006) High performance bismaleimide/cyanate ester hybrid polymer networks with excellent dielectric properties. Compos Sci Technol 66:1749–1755. https://doi.org/10.1016/j.compscitech.2005.11.001

117. Houbertz R, Domann G, Cronauer C, Schmitt A, Martin H, Park JU, Fröhlich L, Buestrich R, Popall M, Streppel U, Dannberg P, Wächter C, Bräuer A (2003) Inorganic-organic hybrid materials for application in optical devices. Thin Solid Films 442:194–200. https://doi.org/10.1016/S0040-6090(03)00982-9

118. Wong D, Yim C, Park SS (2020) Hybrid manufacturing of oxidation resistant cellulose nanocrystals-copper-graphene nanoplatelets based electrodes. Int J Precis Eng Manuf Green Technol 7:375–389. https://doi.org/10.1007/s40684-019-00093-6

119. Noorbakhsh-Soltani SM, Zerafat MM, Sabbaghi S (2018) A comparative study of gelatin and starch-based nano-composite films modified by nano-cellulose and chitosan for food packaging applications. Carbohydr Polym 189:48–55. https://doi.org/10.1016/j.carbpol.2018.02.012

120. Ferrer A, Pal L, Hubbe M (2017) Nanocellulose in packaging: advances in barrier layer technologies. Ind Crops Prod 95:574–582. https://doi.org/10.1016/j.indcrop.2016.11.012

121. Orasugh JT, Saha NR, Rana D, Sarkar G, Mollick MMR, Chattoapadhyay A, Mitra BC, Mondal D, Ghosh SK, Chattopadhyay D (2018) Jute cellulose nano-fibrils/hydroxypropylmethylcellulose nanocomposite: a novel material with potential for application in packaging and transdermal drug delivery system. Ind Crops Prod 112:633–643. https://doi.org/10.1016/j.indcrop.2017.12.069

122. Lavoine N, Givord C, Tabary N, Desloges I, Martel B, Bras J (2014) Elaboration of a new antibacterial bio-nano-material for food-packaging by synergistic action of cyclodextrin and microfibrillated cellulose. Innov Food Sci Emerg Technol 26:330–340. https://doi.org/10.1016/j.ifset.2014.06.006

123. Westerhoff P, Alvarez P, Li Q, Gardea-Torresdey J, Zimmerman J (2016) Overcoming implementation barriers for nanotechnology in drinking water treatment. Environ Sci Nano 3:1241–1253. https://doi.org/10.1039/c6en00183a

124. Alvarez PJJ, Chan CK, Elimelech M, Halas NJ, Villagrán D (2018) Emerging opportunities for nanotechnology to enhance water security. Nat Nanotechnol 13:634–641. https://doi.org/10.1038/s41565-018-0203-2

125. Baruah S, Najam Khan M, Dutta J (2016) Perspectives and applications of nanotechnology in water treatment. Environ Chem Lett 14:1–14. https://doi.org/10.1007/s10311-015-0542-2
126. Jassby D, Cath TY, Buisson H (2018) The role of nanotechnology in industrial water treatment. Nat Nanotechnol 13:670–672. https://doi.org/10.1038/s41565-018-0234-8
127. Sreeprasad TS, Maliyekkal SM, Lisha KP, Pradeep T (2011) Reduced graphene oxide-metal/metal oxide composites: facile synthesis and application in water purification. J Hazard Mater 186:921–931. https://doi.org/10.1016/j.jhazmat.2010.11.100
128. Han Y, Xu Z, Gao C (2013) Ultrathin graphene nanofiltration membrane for water purification. Adv Funct Mater 23:3693–3700. https://doi.org/10.1002/adfm.201202601
129. Gao H, Sun Y, Zhou J, Xu R, Duan H (2013) Mussel-inspired synthesis of polydopamine-functionalized graphene hydrogel as reusable adsorbents for water purification. ACS Appl Mater Interf 5:425–432. https://doi.org/10.1021/am302500v
130. Chen Y, Chen L, Bai H, Li L (2013) Graphene oxide-chitosan composite hydrogels as broad-spectrum adsorbents for water purification. J Mater Chem A. 1:1992–2001. https://doi.org/10.1039/c2ta00406b
131. Chem JM (2012) Versatile agents for water purification 8767–8771. https://doi.org/10.1039/c2jm0005e
132. Xiaolin D, Zi W, Jinjing P, Wenli G, Qiao L, Lin L, Juming Y (2019) High photocatalytic activity of Cu@Cu$_2$ O/RGO/cellulose hybrid aerogels as reusable catalysts with enhanced mass and electron transfer. React Funct Polym 138:79–87. https://doi.org/10.1016/j.reactfunctpolym.2019.02.016
133. Das L, Das P, Bhowal A, Bhattachariee C (2020) Synthesis of hybrid hydrogel nano-polymer composite using Graphene oxide, Chitosan and PVA and its application in waste water treatment. Environ Technol Innov 18:100664. https://doi.org/10.1016/j.eti.2020.100664
134. Ao C, Yuan W, Zhao J, He X, Zhang X, Li Q, Xia T, Zhang W, Lu C (2017) Super-hydrophilic graphene oxide@electrospun cellulose nanofiber hybrid membrane for high-efficiency oil/water separation. Carbohydr Polym 175:216–222. https://doi.org/10.1016/j.carbpol.2017.07.085
135. Serrano E, Rus G, García-Martínez J (2009) Nanotechnology for sustainable energy. Renew Sustain Energy Rev 13:2373–2384. https://doi.org/10.1016/j.rser.2009.06.003
136. Wang ZL, Wu W (2012) Nanotechnology-enabled energy harvesting for self-powered micro-/nanosystems. Angew Chemie Int Ed 51:11700–11721. https://doi.org/10.1002/anie.201201656
137. Gómez H, Ram MK, Alvi F, Villalba P, Stefanakos E, Kumar A (2011) Graphene-conducting polymer nanocomposite as novel electrode for supercapacitors. J Power Sources 196:4102–4108. https://doi.org/10.1016/j.jpowsour.2010.11.002
138. Zhu Y, Murali S, Cai W, Li X, Suk JW, Potts JR, Ruoff RS (2010) Graphene and graphene oxide: synthesis, properties, and applications. Adv Mater 22:3906–3924. https://doi.org/10.1002/adma.201001068
139. Xia X, Wang Y, Zhong Z, Weng GJ (2017) A frequency-dependent theory of electrical conductivity and dielectric permittivity for graphene-polymer nanocomposites. Carbon N Y 111:221–230. https://doi.org/10.1016/j.carbon.2016.09.078
140. Valentini L, Bittolo Bon S, Fortunati E, Kenny JM (2014) Preparation of transparent and conductive cellulose nanocrystals/graphene nanoplatelets films. J Mater Sci 49:1009–1013. https://doi.org/10.1007/s10853-013-7776-9
141. Weng Z, Su Y, Wang DW, Li F, Du J, Cheng HM (2011) Graphene-cellulose paper flexible supercapacitors. Adv Energy Mater 1:917–922. https://doi.org/10.1002/aenm.201100312

Hybrid Nanocomposites Based on Graphene and Nano-clay: Preparation, Characterization, and Synergistic Effect

Hamid Essabir, Marya Raji, Rachid Bouhfid, and Abou El kacem Qaiss

Abstract In the past two decades, polymer nanocomposite materials have tired great interest from both scientists and engineers due to their enhanced properties caused by the addition of nanoscale fillers. New functional nanocomposites have been continually emerging in industry applications. The potential incorporation of the profits of inorganic materials together with those of polymers can allow a wide choice of utilization for these nanocomposites. Hybrid polymer-based nanofillers are generally used as safe and ecofriendly tools to advance crop production in various industrial produce. This chapter summarizes the preparation, characterization, and applications of hybrid polymer nanocomposites based on graphene and clay. Remarkable high elastic modulus and fracture toughness enables the Montmorionite clay and graphene to be used in an enormous number of promising industrial applications also as a reinforcing agent in polymer nanocomposites. Though, irreversible agglomeration of Montmorionite and graphene sheets and the weak compatibility with most polymer matrix limit its potential as a reinforcing agent to fabricate polymer nanocomposites. Synergistic effects by the nanofillers on the nanocomposite's properties are presented, attempting a rationalization on the basis of the available data.

Keywords Hybrid nanocomposite · Clay · Graphene · Mechanical properties · Rheology

H. Essabir · M. Raji · R. Bouhfid · A. E. Qaiss (✉)
Institute of Nanomaterials and Nanotechnology (NANOTECH), Laboratory of Polymer Processing, Moroccan Foundation for Advanced Science, Innovation and Research (MAScIR), Rabat, Morocco
e-mail: a.qaiss@mascir.com

H. Essabir
Mechanic Materials and Composites (MMC), Laboratory of Energy Engineering, Materials and Systems, National School of Applied Sciences of Agadir, Ibn Zohr University, Agadir, Morocco

1 Introduction

Polymer nanocomposites (PNCs) are new-emerging polymer composites consisting of a polymer with nanofillers dispersed in the polymer matrix. The nanocomposites technology includes the study of multi-phase material where at least one of the constituent phases has a dimension less than 100 nm. The importance of nanocomposites lies in their multifunctionality and the possibility of achieving unique combinations of properties that are impossible with traditional materials [1, 2]. The incorporation of nano-fillers in polymer structures makes it possible to profoundly modify their mechanical, thermal, electrical or barrier properties; which allows them to broaden their fields of application [3–5]. Nanofillers such as carbon nanotubes, carbon nanofibers, graphene and clay nanoparticles have been widely used as reinforcements for the manufacture of high-performance nanocomposites [6–8]. The use of inorganic nanomaterials as fillers in the preparation of polymer/inorganic nanocomposites has attracted increasing interest due to their unique properties and many potential applications in the industrial sectors [9, 10]. Until now, the majority of research has focused on polymer nanocomposites based on lamellar materials of natural origin, such as montmorillonite clay or synthetic clay of double lamellar hydroxide type. Clay and clay minerals, either as they are or after modification, are known as materials of the twenty first century because they are abundant, inexpensive and environmentally friendly [11–13]. Clay minerals have been widely used to develop functional nanomaterials, due to the versatility of silicates to assemble different types of active species at the nanometer scale [14]. For example, metal oxide nanoparticles, polymers or biological components can be assembled with clays which have given rise to a wide variety of nano architectures of interest as catalysts, absorbents, and nanocomposites of polymer clay among other applications [15].

Recently, graphene, which consists of a single layer of graphite, has gained considerable attention in the field of nanocomposite materials based on polymers because of its great potential to improve the mechanical, electrical, thermal and barrier characteristics. Gas from polymer matrices [16–19]. However, the use of this type of filler for the development of new, more efficient materials can be limited by the tendency of graphite sheets to agglomerate, preventing their good dispersion in polymer matrices in the molten state. Consequently, several academic studies have been carried out to increase its compatibility with polymer matrices because the properties of the resulting nanocomposites strongly depend on the state of dispersion and the interfacial adhesion between the charge and the macromolecular chains of the matrix [20, 21]. Obtaining a good level of dispersion of graphitic nanofillers in polymer matrices is achieved by modification of the polymer, synthesis of coupling agents and/or functionalization of graphene nano-sheets [7]. Currently, GON, Black phosphorous, Fe_3O_4, nano-clay have been extensively used as a single nanofiller for improving the properties of polymer [22–25]. In this background, it was concluded that using of low nanofillers content (<3 wt%) improved the nanocomposites properties compared to neat polymer. However, beyond 3 wt%, the nanofillers agglomeration phenomena occur limiting the nanofillers reinforcing efficiency. Otherwise, the combination of

graphene with other nanomaterials can link adjacent nanosheets and inhibit their agglomeration, allowing the material to reach its highest potential to improve the performance of nanocomposites [22–25]. The use of mixtures of fillers in the preparation of hybrid materials has revealed great potential for the latter in comparison with pure matrices and with mixtures obtained with fillers taken separately [26–29]. Indeed, nano-reinforcement classical composites by montmorillonites have given them exceptional improvements in terms of elastic modulus, mechanical resistance, barrier properties, fire properties and thermal behavior [30–33].

It is in this perspective that this chapter is written, which presents a new way of obtaining hybrid nanocomposite materials with polymer matrices which are very attractive from the point of view of properties, mainly caused by the good dispersion of the reinforcements in the matrix. The approach we propose is based on the combination of graphene (GNs) with MMT clay to improve the dispersion of the first in the polymer matrices studied. The manufacturing of these kind of nanocomposites based on hybridization of nanofillers, and their incorporation into the polymer matrix, constitute a promising avenue for the development of innovative materials, primarily by improving the mechanical properties of nanocomposite films in applications where good strength and flexibility are required, such as in applications of 'packaging.

2 Nanocomposite Technology

The growing interest in polymer nanocomposites stems from the perfection of fundamental properties and, also, the development of new materials to meet different applications. Significant changes in the properties of polymer nanocomposites have occurred through the incorporation of nanofillers such as nanoclay, graphene, carbon nanotubes, metal oxides and double layered hydroxide [34–36]. Nanocomposites materials can take many forms, but they can be divided into several categories based on the nature of the matrix, the morphology of the reinforcement and the architecture of the reinforcement. In a nanocomposite material, the matrix ensures the cohesion and orientation of the reinforcement. It also makes it possible to transmit to the load the stresses to which the nanocomposite is subjected [35, 36].

Polymer-based nanocomposites are usually considered by lower mechanical properties and thermal stability [37, 38], but particular performances of the polymer matrix may match to confer specific characteristics, in terms of transparency, fluid permeability, biodegradation and optical properties, which are attractive in different fields of application (biomedical, environmental, etc.) [39–41]. Generally, heterogeneity of nanocomposites is attributed to the desirability of including finely dispersed fillers, in turn, based on metallic, ceramic or polymeric nanomaterials, capable of imparting a wide range of catalytic, magnetic, electrical, optical and biological nanocomposite [42, 43]. The reduced size of the nanoscale fillers allows the selected properties to be improved, while minimizing the loss of other properties of the nanocomposite. This

simultaneously improves several desirable properties, namely conductivity, permeability, bioactivity, UV protection, flame retardancy by properly dispersing different types of modified nanofillers [42].

The classification of nanomaterials is based on dimensions, which lie in the nanorange (100 nm). They include the following: (a) 0D materials with all dimensions at the nanoscale, i.e. no dimension greater than 100 nm. The most common example of 0D nanomaterials is the nanoparticle. These nanoparticles can be amorphous or crystalline, ceramic, metallic, or polymeric. (b) 1D materials have at least one dimension in the nanometric range. They include needle-shaped materials having a nanoscale dimension such as nanoplatelets, nanorods, nanoclays and nanosheets. (c) 2D two-dimensional materials in the nanorange. They are nanofibers, nanotubes, nanorods and whiskers. (d) 3D materials characterized by the three dimensions in the nanorange. Some examples of them are nanogranules, nanoclays and equiaxed nanoparticles. Nanomaterials can be crystalline or amorphous or polycrystalline [44]. They can be composed of single-phase or multiphase chemical elements. They can come in various shapes and forms and composed of different constituents, including metals, ceramics or polymeric materials.

The fabrication of hybrid nanofillers nanocmposites is beneficial to improve the uniform dispersion of the elementary nanofillers among hybrid nanofillers in the polymer matrix. Hybrid nanofillers and nanocomposites are composed of two or more materials. As the nanofillerss have small size, large surface area, high surface energy, high chemical activity and instability; surface atoms on nanofillers have many unsaturated electrons or empty orbits, and will cause surface defects affecting the nanoparticles' nature [45–47]. Hybrid nanofillers can cover surface defects, and offer higher stability [48]. Therefore, hybridization of nanofillers have great potential in applications. These various components can be molecules, oligomers or polymers, aggregates, or even particles. These materials are therefore nanocomposites, or even composites on a molecular scale. The hybrid nanocomposites can be classified according to several criteria: thus, depending on the chemical, physical composition, dispersion/distribution of fillers, affinity between fillers and matrix [49, 50].

3 Challenges in Processing and Manufacturing of Polymer Nanocomposites

Nanocomposite materials have the potential to redefine the field of conventional composite materials that in terms of manufacturing process, performances, and industrial applications. Due to their exceptional outstanding properties polymer nanocomposites have tremendous market potential specially as a replacement for current composites and for creating new markets, while the advance of processing-manufacturing technologies in terms of quantity and value for marketing will be one

of the major challenges. The major problems encountered in polymeric nanocomposite materials are the dispersion of nanofillers in the polymer matrix, the compatibility between nanofillers and polymeric matrices or chemical adhesion and the degree of dispersion and distribution of nanofillers. Homogeneous dispersion of nanofillers in the polymer matrix using existing mixing techniques is very difficult due to the strong tendency of fine fillers to agglomerate [51].

Degassing is another serious issue when processing a nanocomposite. The air trapped during the driving of the material at molten state into the mold, with a highly viscosity character, (5–10% by weight clay in the matrix), inductees damage (cracking) and rupture of the material which can occur under low stresses. To maximize anisotropic (unidirectional) properties such as modulus, strength, and toughness, it is indispensable to align the nanofillers in the nanocomposite matrix. To advance distribution/dispersion and compatibility in polymer matrix, nanofillers are being treated and functionalized.

Even more, there is still an absence of real-time characterization instrumentation, methods, tools, as well as a deficiency of affordable infrastructure (equipment, facilities, qualified personnel, design tools). In general, they exist two major problems and have not yet been resolved: (1) The existence of a chemical bond (chemical compatibility) between the nanofillers and the matrix (2) The conservation of the intrinsic properties of nanofillers (mechanical, electrical and thermal properties) if there is a chemical bond between the nanofillers and the matrix. To increase the mechanical properties of advanced nanocomposite materials, many works have to be profoundly examined and this is certainly a challenging area for all scientist working in the composite's community [51]. Clay and Graphene are a multifunctional reinforcing material that can improve the chemical and physical properties of polymer matrix (structural, mechanical, thermal, electrical) with low content.

3.1 Reinforcing Effect of Nanofillers in Polymer

This paragraph investigates the "nano effect" on the mechanical properties of the polymer matrix, especially a summary of the mechanical mechanism and behavior regarding nanocomposites, as example nanocomposites based on epoxy resin and filled with different nanofillers will be reported. In a previous review article [23, 51, 52], it was demonstrated that depending on the type of nanofillers, the integration of nanofillers has a substantial effect on the rigidity and strength of nanocomposites. Critical factors such as preserving a homogeneous distribution/dispersion, good affinity and chemical compatibility between nanofillers and matrix and also a good adhesion between them are highlighted. The effect of surface functionalization, its relevance and its hardening mechanism were also examined and discussed.

3.1.1 Clay in Polymer Nanocomposite

Clay is a mineral from the silicate family, more precisely phyllosilicates (silicates in layers). Their structure can be identified by X-ray study; it is characterized by the superposition of sheets composed of tetrahedral or octahedral layers. In the space between the layers, or interfoliar space, are placed various cations such as K, Na, Ca. The clay is generally obtained from the alteration by water of other silicates (except quartz). It is for this reason that it is found systematically in soils and surface formations. An ultra-fine detrital mineral, it is also found very frequently in sedimentary rocks. Mixed with another mineral such as calcite it will form marl. Roughly speaking, clay minerals are essentially microcrystalline secondary minerals based on hydrous magnesium or aluminum silicates and carry negative charges that have sheet-like structures with very fine particle size and a general chemical formula (Ca, Na, H)(Al, Mg, Fe, Zn)$_2$(Si, Al)$_4$O$_{10}$(OH)$_2$–xH$_2$O, where x represents the variable amount of water.

Polymer/clay nanocomposites are two-phase systems, made up of a polymer matrix and nanofillers distributed and dispersed in the matrix. The most regularly used inorganic nanofillers in polymer nanocomposites belong to a family of 2:1 phyllosilicate, which have a sheet silicate structure. Montmorillonite, vermiculite and hectorite are among the most usually used nanofillers in polymer clay nanocomposites [11, 32, 53]. The manufacturing of a nanocomposite needs a homogeneous distribution/dispersion of the fillers in the polymer matrix at the nanometric scale [24, 54]. The exceptional performance of montmorillonite clay as a matrix reinforcement is resolute by its large specific surface area and high aspect ratio. The coating with a surfactant, such as quaternary ammonium salts, helps to expand the chemical compatibility and consequently to offer a strong interfacial adhesion between the clay and the polymer macromolecular chains, thus contributing to good reinforcement effect and hence good barrier properties [2, 37–43].

Based on the degree of the clay dispersion and structure, there is existence of three kinds of nanocomposites morphologies as: intercalated, exfoliated and aggregated structure. In the intercalated structure, clay is delaminated to some extent: thus, polymer chains can diffuse into the galleries between them. However, in the exfoliated structure, clay is completely broken apart into single layered platelets, which are homogeneously distributed/ dispersed in the matrix. The exfoliated structure is the most desirable state as it can provide excellent thermal and mechanical properties at very low clay contents [33]. Finally, in the aggregated structure, clay is well distributed in the polymer matrix, but the single clay layers are not delaminated.

In general, most polymer nanocomposites are in a state between intercalated and exfoliated [55]. Due to the enhanced properties of the resulted nanocomposites which have advantages compared with the neat polymer matrix, in terms of improved mechanical, thermal and barrier properties. Based on this results the polymer nanocomposites has become one of great interest in food packaging applications [56].

Clay nanoplatelets Montmorionite (MMT) is a layered alumina silicate. The chemical structure of MMT contains two fused silica tetrahedral sheets sandwiching

an edge shared octahedral sheet of either aluminum or magnesium hydroxide and an interlayer region containing Na_1 or Ca_{21} [55]. Each layer is about 1 nm thick with a lateral dimension of 100–1000 nm [55]. Montmorillonite is widely used as filters, adsorbents, catalysts, encapsulation of functional substances molecules, reinforcement agent in polymer nanocomposites, and organisms [57–59]. Also, being hydrophilic, MMT has swelling, intercalation, and ion exchange properties [59]. Nonetheless, this clay (MMT) has exceptional mechanical strengths and optical transparency, as well as being relatively cheap. It can also be dispersed and pre-treated in common solvents and even in an aqueous environment [55, 60, 61]. Addition of clay as fillers into the polymer matrix has been widely demonstrated to improve thermal, mechanical and rheological properties [8, 62]. In a recent research Raji el al. [63] investigated the effect of organically modification of three kind of clay as montmorillonite, halloysite and sepiolite. These clays were used as nanofillers for PP at different concentration (1–5 wt%). According to the experimental data, all the used clays were successfully intercalated using the silane molecules by decreasing the size of the clay nanoparticles, by changing their chemical composition and increasing their spacing d. The efficiency of the silylation process as a good means of improving the matrix-nanofillers interaction was demonstrated by comparing the mechanical characteristics of clay nanocomposites before and after grafting with organosilanes, and the results showed that the Young's modulus of PP increases from 1034 MPa to an optimum 2657.9, 2716.8 and 2956.5 MPa at 5 wt% for MMT, Hallo and SEP corresponding to a percentage gain of 157, 162, 186%, respectively. Though, in the case of functionalized-clays nanocomposites, the Young's modulus of PP was higher than of the neat clay's nanocomposites at the same clay concentration. Authors conclude that that the addition of the nanoorganoclay allows improving the proprieties of silane grafted clays nanocomposites, which can endorse better interfacial adhesion between the organoclay and the polypropylene and their great spatial dispersion-distribution. Many research efforts have explored improving the performance of thermoplastic nanocomposites by adding clay as nanofillers [53, 57, 64]. Clay nanoplatelets have shown good performance, which allows remarkable improvements in the properties of polymer matrices. There are many types of clay which depend on their structure. Although all clay minerals contain two types of leaves (leaves), the tetrahedron (T) and the octahedron (O). In general, the structure of the clay and the size of the clay had a clear effect on the mechanical and thermal properties of the nanocomposite [63]. The montmorillonite powder was subjected to scanning electron microscopy (SEM) to study the morphology of their granules. A small amount of montmorillonite powder was poured over the carbon tape, then the excess was blown off with an air gun to ensure that small pieces of powder remained on the tape. An overall view using the micrographs of the clay powder can be observed in Fig. 4. However, the stronger nanoplatelets intermolecular forces, that is a cohesive tension which makes an attempt to the clay nanoplatelets to aggregate and to form the agglomerates [65]. Figure 1 show that the montomorillonite possess a plate-like morphology with nanometric size. The used clay as nanofillers is a local variety (density of 1.63 g/cm^3) with diameter average of 12 μm (Fig. 1). This type of clay was more effective than
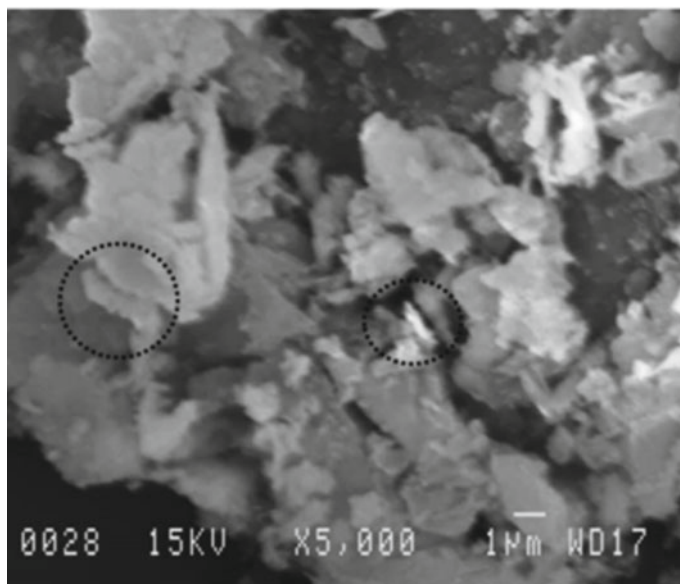
Fig. 1 SEM image of Montomorillonite

talc to enhance the mechanical and thermal properties of the polymer matrix [63, 66].

To investigate the structural properties of the chemical nature of the used MMT the FTIR study was done and presented in Fig. 2. The FTIR spectra shows intensive vibrations in the bands of 3620, 1645,1416, 1134, 1007, 881, 874, and 778 cm^{-1}. The bands near 3620 and 3400 cm^{-1} are the indicative of montmorillonite which corresponds to Al O–H stretch vibrations, for bound water and Al$_2$OH on MMT [67]. The band in the region of 1645 cm^{-1} is attributed to the –OH bending mode of adsorbed water [68]. The peak at 1416 cm^{-1} belongs to the C–O stretching vibration in calcite [69]; whilst the absorbance at 1134 cm^{-1} is assigned to Si–O stretching, out-of-plane Si–O stretching mode of montmorillonite [70]. The band at 1004 cm^{-1} is typical of Si–O–Si and Si–O–Al lattice vibrations stretching (in plane) vibration for layered silicates [71]. The IR bands at 945, 814 and 719 cm^{-1} are attributed to Al–Al–OH, Al–Fe–OH and Al–Mg–OH bending vibrations [68].

The recognition of chemical components and crystallographic structure of MMT clay was performed by X-ray diffraction analysis (XRD). Diffraction patterns were analyzed using X'Pert High Score software. The X-ray diffraction pattern of MMT (Fig. 3) shows the characteristic peaks of quartz (SiO$_2$) and other associated clay minerals such as dolomite (MgCa(CO$_3$)$_2$), Illite ((K, H$_3$O)(Al,Mg,Fe)$_2$(Si,Al)$_4$O$_{10}$[(OH)$_2$, (H$_2$O)]), and Calcite (CaCO$_3$).

Figure 4 investigates the thermal degradation behavior of Montomorillonite by using a Thermogravemetric analysis test. It is observed from this figure that the thermal decomposition occurs in two major steps: the first one around 82 °C (14%
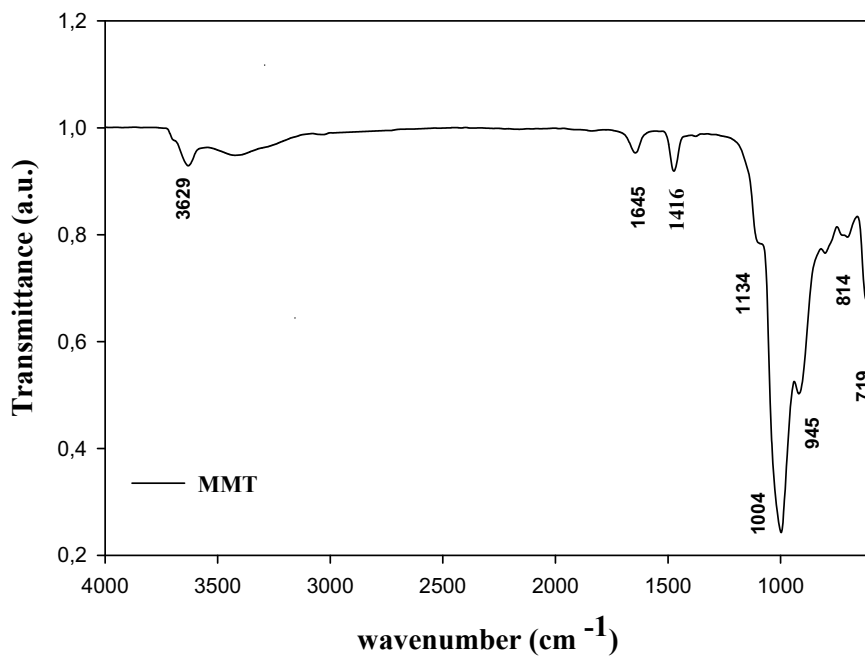
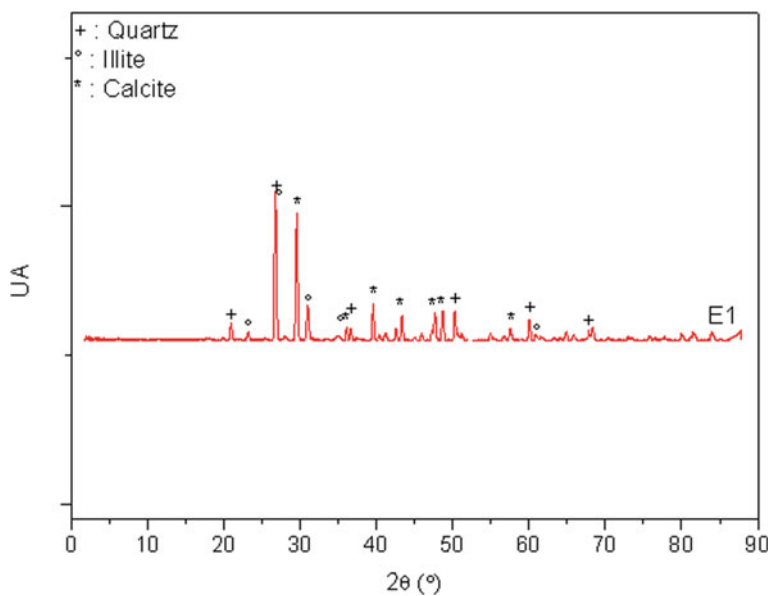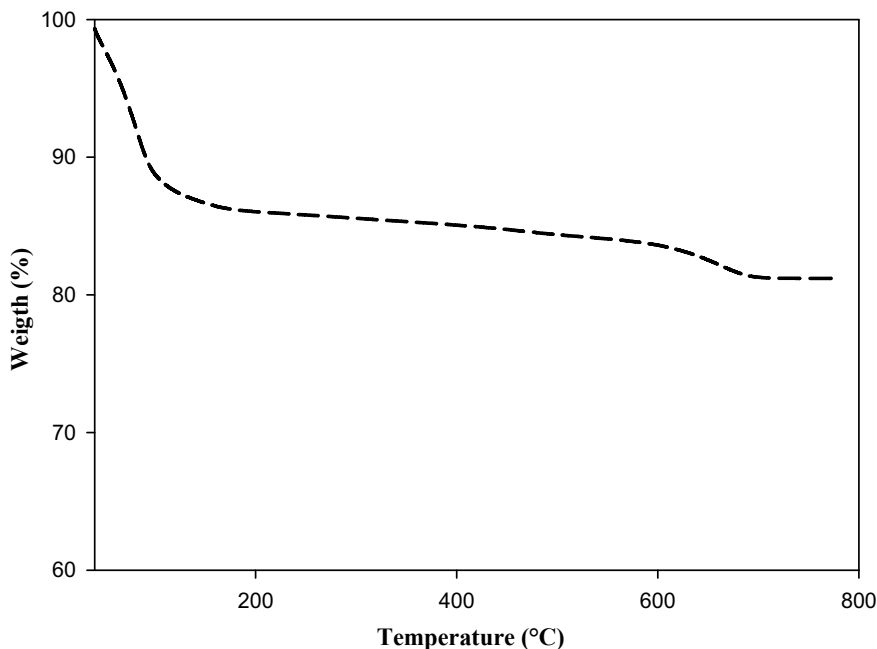**Fig. 2** FT-IR spectra of Montomorillonite

Fig. 3 X-ray diffraction 'd' values of Montomorillonite

Fig. 4 Thermogravemetric analysis of Montomorillonite

weight loss) is due to free water and interlayer water residing between the alumi-
nosilicate layers and related to the hydration spheres of the cations [72], while the
second weight loss between 500 and 700 °C (2% weight loss) is due to dehydrox-
ylation of the aluminosilicate lattice [71]. One can, therefore, conclude that MMT
exhibits excellent thermal stability, with a maximum weight loss of around 20% at a
temperature of 800 °C.

3.1.2 Graphene Nanoplatelets

Graphene is a monolayer of sp^2-hybridized carbon atoms arranged in a two-
dimensional lattice. It can be produced by the exfoliation of graphite nanosheets
[51, 73]. Graphene can also be stretched at an elongation of approximately 20%
of its initial length and has exceptional thermal and mechanical properties with a
Young's modulus of 1 TPa [23, 73] and tensile strength of 130 GPa, and it is the most
mechanically resistant material. It has a thermal conductivity of about 5000 W/(m K)
and a high electrical conductivity up to 6000 S/cm [74]. In addition, graphene has
a high specific surface (theoretically the measured value is 2600 m^2/g) and high
impermeability to gas. The most important properties of a graphene nanoplate are
summarized in Table 1.

Table 1 Properties of graphene nanoplate [51, 74]

Properties	Values
Dimensionality	2D
Young's modulus	~1 (TPa)
Strength	~130 (MPa)
Thermal conductivity	5.103 W/(m K)
Electrical conductivity	6.103 (S/cm)
Gas permeability	Impermeable

Due to its two-dimensional structure, Graphene has rapidly become one of the most popular materials for technological application due to it excellent thermal, mechanical and electrical properties [20, 22]. Graphene has become a preferred and significantly better nanofiller for polymers than other nanocarbon and inorganic nanofiller materials. But, this application of graphene is hampered by the poor solubility of graphene in most common solvents. Also, the large surface area of graphene results in significant aggregation and agglomeration of the nanosheets in a polymer matrix due to large van der Waals interactions. A challenge is to achieve good dispersion and distribution of the atomically thin sheets of graphene within the polymer matrix, to remedy this problem an appropriate surface modification has been applied to produce graphene oxide (GO) nanosheets [75–77]. These are quasi-two-dimensional honeycomb lattice materials with oxygen containing functional groups (such as hydroxyl, epoxide, carbonyl and carboxyl) on their basal planes and edges. These functional groups are effective in improving interfacial bonding between the GO nanosheets and the polymer matrix. Hence, exfoliation and a uniformly dispersed structure can be achieved [78, 79]. Due to excellent barrier properties, graphene-based nanocomposites have significant potential not only in packaging applications but also in sensitive electronic devices, such as organic light emitting diodes (OLEDSs) [80, 81]. The effect of graphene on the thermal, mechanical and rheological behavior of polymer nanocomposites has also been recently studied by several research groups: it has been verified that the incorporation of graphene nanoplatelets increases the performances of neat polymer, confirming graphene as an effective reinforcing agent for polymers matrix, while a study on particle size effect and fracture behavior of polymer graphene nanocomposites has shown that fracture toughness increases with decreasing particle size of graphene nano-platelets [20, 24]. In other studies, it has been confirmed that better dispersion of graphene in matrix gives higher fracture toughness and fracture energy.

Essabir et al. [51] have investigated the effect of graphene as nanofillers into polypropylene (PP), high-density polyethylene (HDPE), polyvinylidene fluoride (PVDF), and polyamide-6 (PA6)/acrylonitrile–butadiene–styrene (ABS) blend polymer matrix. The study focused on the graphene nanocomposites manufactured by extrusion and a solution blending method, followed by the casting–evaporation approach. Authors conclude by a close investigation of all properties of the manufactured nanocomposites. The structural, thermal, mechanical, and electrical properties of the manufactured nanocomposites were greatly improved by the addition of small

mass fractions of graphene nanosheets (<3%). And as conclusion the authors illustrates that the effectiveness of graphene nanofiller as reinforcement to achieve specific properties in polymer nanocomposites produced by the extrusion process.

The most promising methods for producing large quantities of graphene nanosheets are based on exfoliation and reduction of graphite oxide (OG). Graphite oxide is made up of a stack of graphene oxide sheets, whose space between these is between 6 and 10 Å [74, 75]. It has also been produced by alternative methods] in which graphite is oxidized using strong oxidants such as $KMnO_4$, $KClO_3$ and $NaNO_2$ in the presence of sulfuric acid (H_2SO_4) or its mixture with nitric acid (HNO_3). Since its discovery in 2004, several processes for the synthesis of graphene have been developed. Indeed, the production of this material can be carried out using one of the methods listed below [75]:

- Chemical vapor deposition (DCV);
- Chemical conversion;
- Reduction of carbon monoxide (CO);
- Decompression of carbon nanotubes;
- Separation/exfoliation of graphite or graphite derivatives (graphite oxide (OG) or graphite fluoride.

The production of graphene nanosheets (NFG) from natural graphite through the chemical oxidation path of graphite has been confirmed by X-ray diffraction. The intermediate product of OG was taken from the reaction flask after the oxidation step. After washing and drying, the graphite oxide powder was examined by XRD and the result obtained was compared with that of natural graphite in terms of interplanar space. Figure 5 shows the DRX spectra of the products studied. The X-ray spectrum of the graphite powder shows the hexagonal structure according to the orientation
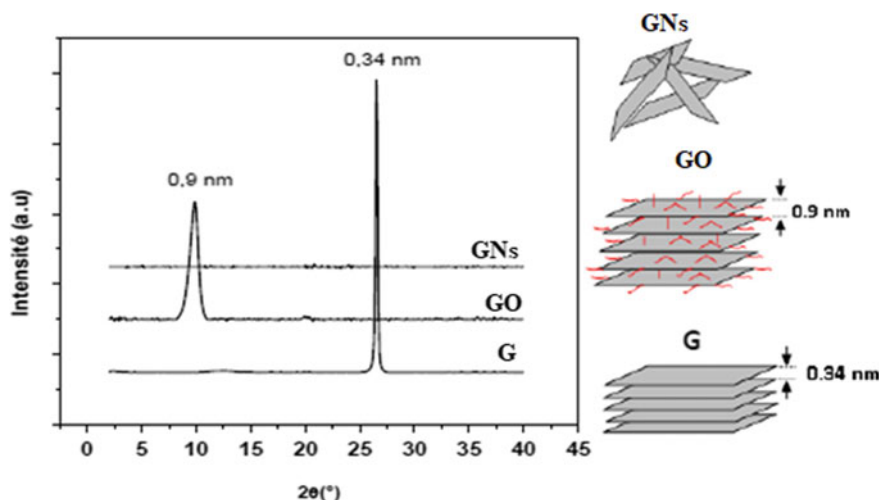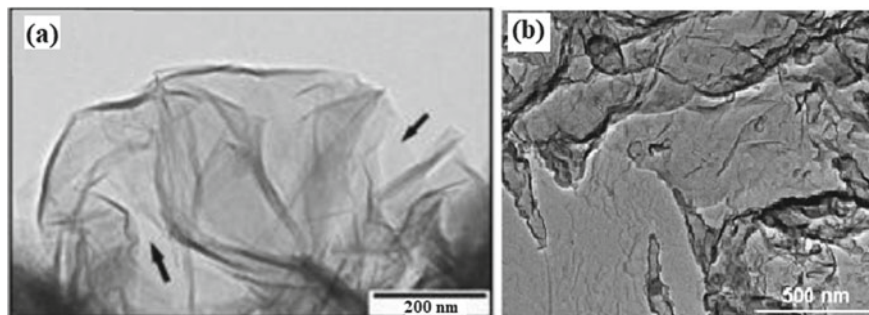

Fig. 5 X-ray spectrum of graphite, graphene oxide, graphene nanosheet

Fig. 6 Images of GNs: **a** SEM and **b** TEM

(200), as was revealed by the single peak at $2\theta = 26.23°$ which corresponds to a spacing of ~0.34 nm between graphite planes [74, 75]. During the oxidation of graphite to graphite oxide, an increase in the interplanar space is observed due to the formation of groups containing oxygen and water molecules interposed within the layered structure, with a displacement from the 2θ peak from 26.23° to ≈10°. This corresponds to a new interplanar distance of 0.9 nm in the graphite oxide structure. Furthermore, the absence of any secondary peaks indicates that the graphite has been completely oxidized [74, 75].

The morphology and structure of graphene nanosheets (NFG) obtained by the chemical reduction of graphene oxide was observed by the transmission electron microscope (TEM) showing the existence of planar structures individual nanosheets (Fig. 6), and it is clear that the nanosheets are gathered together with crumpled structures due to their planar geometries, with a thickness less than 1 nm [74, 75]. As mentioned above, the reduction of graphene oxide nanosheets (GNs) often results in a gradual decrease in their hydrophilicity; which makes the graphene nanosheets thus obtained very hydrophobic, resulting in significant agglomerations of the individual nanosheets.

The structure and properties of graphite depend on the particular synthesis method and the degree of chemical oxidation. It generally retains the layered structure of graphite, but the surface of the layers is oxygenated and the spacing is approximately two to three times greater (0.65–0.9 nm) than that of graphite. This increase in the spacing comes from the intercalation of the oxygen-containing groups between the layers of graphite thus weakening the van der Waals forces between the layers which allows easy exfoliation via sonication in an aqueous or organic medium. As previously mentioned, graphite oxide is the intermediate material for the preparation of graphene nanosheets and graphene oxide. However, the graphite oxide product, in dried powder form, was characterized by the FT-IR technique to determine the nature of the groups formed during the oxidation (Fig. 7).

The IRTF spectrum obtained for graphene oxide is shown in Fig. 8. The existence of several transmission bands confirms the presence of a variety of oxygen groups on the surfaces and edges of each graphene oxide plane [82]. The bands
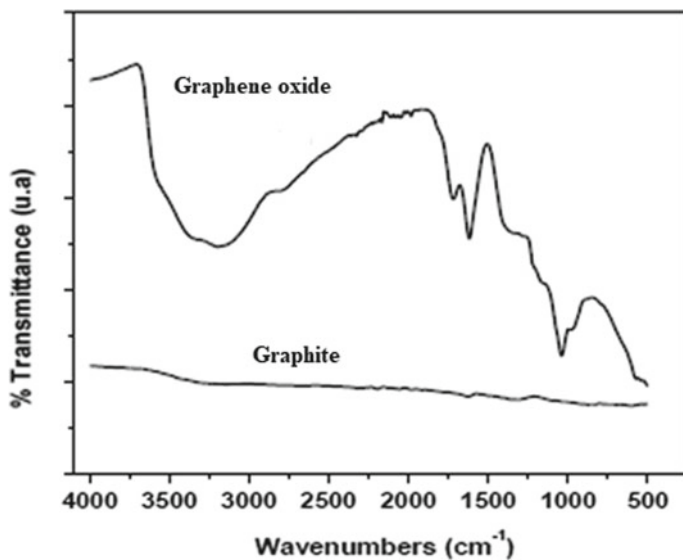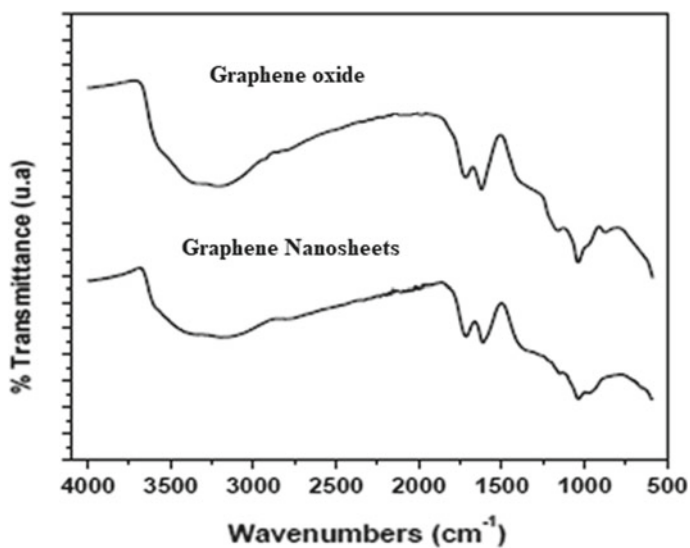
Fig. 7 FTIR spectrum of graphite and graphene oxide


Fig. 8 FTIR spectrum of graphene oxide and graphene nanosheets

at 3680 cm^{-1} and 1410–1280 cm^{-1} are attributed to the O–H hydroxyl group [74, 75]. The intense band at 1713 cm^{-1} is attributed to the elongation vibration of the carbonyl group (=O), the band at 1612 cm^{-1} is attributed to the bond C=C, and the vibrations at 981 and 1036 cm^{-1} are assigned to the epoxy group [74, 75]. In addition, several vibration bands of the C–H bond can be observed around 2000–3340 cm^{-1} [51]. Finally, the band at 3650 cm^{-1} is allocated to the water molecules [51]. It is clear that the two spectra have the same transmission bands, because there is no difference between them in terms of chemical composition; which confirms that the same oxygen groups are still present in the structure of exfoliated graphene oxide. Consequently, the coupling between the DRX technique and that of IRTF for graphite oxide and graphene oxide exfoliated in DMF shows that there is only one difference between the two products, it is the elimination of stacking in layers after the exfoliation of graphite oxide into graphene oxide nanoplans.

Thermogravimetric analysis (ATG) was used to examine the thermal stability of the carbonic derivatives studied in this part (graphite, graphite oxide, exfoliated graphene oxide and graphene).

Figure 8 shows the ATG curves obtained in air for graphite, graphite oxide, and graphene. The thermal stability of graphite oxide and graphene was compared with that of graphite. From Fig. 3, for graphite we observe an onset of mass loss at a temperature around 650 °C by the carbon combustion mechanism leading to the formation of carbon dioxide (CO_2). Graphite oxide is thermally unstable, it breaks down in three stages [7, 21]. The first degradation is attributed to the decomposition of the water molecules, presented in the graphite oxide structure, at a temperature around 100 °C; which corresponds to a loss of ~5%. The second stage of degradation begins around 200 °C where a considerable loss of mass (~30%) has occurred, corresponding to the decomposition of the functional oxygen groups. The final mass loss around 550° is attributed to the oxidation of carbon. Finally, graphene shows high thermal stability, with a low mass loss (5%) observed around 300 °C revealing the oxidation of amorphous carbon in the graphene sample [74, 75]. It should be noted that graphene shows a lower thermal stability than that of natural graphite, this is probably due to the size effect (Fig. 9).

4 Hybrid Nanocomposites Properties

The final properties of nanofillers-based polymer nanocomposites depend strongly on the processing technique in the course of nanocomposite manufacturing. The functionality of nanofillers components is critical to lower filler loading rate, making them highly dispersed and organized sheets within polymer matrix to enhance overall properties of nanocomposites. In particular, the mechanical properties such as Young's modulus, tensile strength, strain at yield, and flexural strength depend on the specific aspect ratio, surface area, organization, and loading content of graphene materials. Dispersion, distribution, component affinity, and morphological properties are all
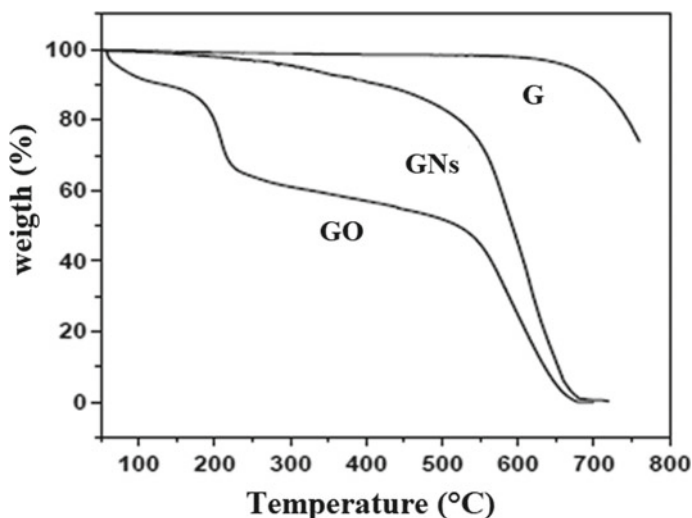
Fig. 9 TGA curves of graphite, graphene oxide and graphene nanosheets

of great importance in determining the ultimate stiffness, strength, ductility, and toughness of polymer nanocomposites under various nanofillers content.

Many Recent literature studies on development and characterization of a new hybrid nanofillers nanocomposites formulation have mainly focused on thermoplastics and thermosets [7, 83–85]. To have a successful hybrid nanocomposite in terms of performances the major key the synergistic effect of various nanofillers to improving the physico-chemical properties.

The dependence between intrinsic properties of each nanofiller, in term shape, size, surface characteristics, and the way they are combined have a direct impact on a change in morphology and microstructure of the resulted material. In general, an interconnected 3-D microstructural lattice can be formed when two kinds of nanofillers are combined in a hybrid nanofiller, which radically affects the properties of the final nanocomposites [83–85]. Presently, numerous hybrid nanofillers have been used as reinforcements for high performance nanocomposites. Generally, the use of such hybrid nanofillers as a dispersed phase was achieved in order to increase the final properties of the formulated nanocomposites, to introduce some new properties, or to resolve some specifics difficulties lie to the agglomeration phenomenon and/or interfacial adhesion [86, 87].

Hybrid nanocomposites were prepared using numerous quantities of Graphene nanosheet and MMT. In this instance, different clay (MMT) and GNs ratios (see Table 2) were mixed with PP using a heated internal mixer (Thermo Haake Rheomix, Germany). The blending conditions were set at 200 °C and 60 rpm for 50 g of compound in each case. Under these conditions, a homogeneous dispersion and distribution of both clay (MMT) and GNs can be achieved in PP. The matrix was

Table 2 Composition of the studied formulation (wt%)

| Ratio	PP	MMT	GN
3:0	97	3	0
2.25:0.75	97	2.25	0.75
1.5:1.5	97	1.5	1.5
0.75:2.25	97	0.75	2.25
0:3	97	0	3

introduced first in the mixing cavity. After 30 s, clay (MMT) and/or GNs were carefully introduced and blended for 5 min. At that point, the measured torque was constant. The rolls are then stopped and the nanocomposite was removed from the heated chamber before being cut into small pieces for hot press molding. Compression molding was done in an automatic CARVER press under the following operating conditions: steel mold with dimensions of 100 mm × 100 mm × 1.5 mm. Both upper and lower plates were heated to 200 °C, after which a force of 2000 lbs was applied. Finally, the nanocomposites were cooled to room temperature by air followed by water cooling.

4.1 Morphological and Structural Properties

For polymer nanocomposites, the degree of improvements (structural, thermal, mechanical, and electrical properties) is strongly related to the dispersion/distribution of graphene and the nanocomposite microstructure. The morphological characterization is important to establish structure–property relationships for the manufactured materials. Scanning electron microscopy was used to examine the dispersion/distribution of used nanofillers (clay and GNs) in the polypropylene matrix. Figure 2 illustrates distinctive SEM images (different magnifications) of the cryofractured surface of the nanocomposites. Thus, the SEM can provide information on the degree of adhesion between graphene and polymer. It can be realized that the surfaces are relatively rather rougher and tortuous, in the other hand it is clear the homogeneous dispersion of MMT and GNs inside PP was achieved and no clear filler aggregates can be observed, which might indicate that the melt compounding conditions were optimum to manufacture these hybrid nanocomposites and should lead to good nanocomposite properties.

In comparison with microscopic techniques (SEM), the FT-IR can provide a faster insight into degree of interfacial adhesion by creation of a novel's bands between nanofillers and matrix. The FTIR spectrum of the MMT, GNs, PP, and hybrid nanocompositesare shown in Fig. 10. The bands at 3364 and 1326 cm^{-1} be attributed respectively to the stretching and the in-plane deformation of the O–H bonds in hydroxyl groups [4]. The peaks around 1623 cm^{-1} can be assigned to the stretching vibration of C=O in carboxyl groups, while the band at 1104 cm^{-1} correspond to C=O in epoxide [4]. The PP spectrum presents typical bands at 2950–2838,
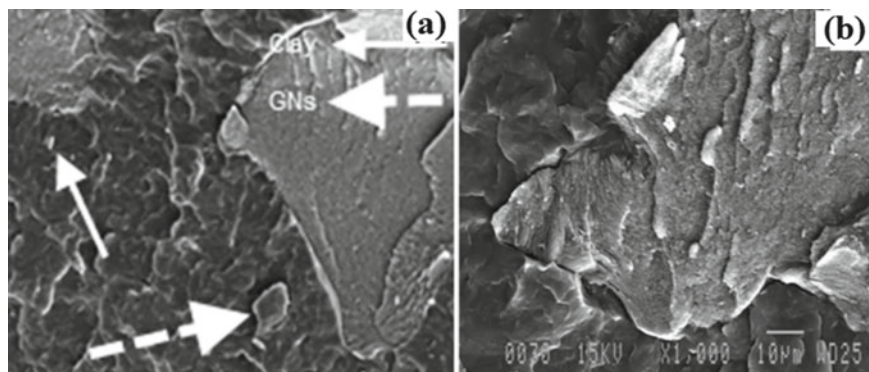
Fig. 10 SEM images of hybrid nanocomposites based on MMT and GNs (1.5:1.5)

1455–1453, and 1376 cm^{-1} which are assigned to C–H stretching, –CH$_3$ bending, and C–H bending, respectively [4]. Furthermore, the FTIR spectra of all hybrid nanocomposites show the presence of a new band at 1118 cm^{-1} compared to neat PP. This new band is attributed to the stretching vibration of Si–O, Si–O–Si, and the deformation of hydroxyl groups due to the introduction of montmorillonite in PP.

4.2 Mechanical Performances

The mechanical strength of a material is a function of many aspects: the most significant of them are the intrinsic strength of the atom–atom bonds and the absence of structural defects in the lattice. Defects play a considerably vital role in tensile failure progressions, since in order to break a defect-free specimen, it would be critical to overawed any cohesive forces present in the surface perpendicular to the tensile load. In fact, the presence of faults greatly reduces the resistance required to break the sample. Therefore, to allow nanofillers to fail under tensile load, it is necessary to break all carbon–carbon covalent bonds which are recognized as the strongest in nature [20, 30, 51, 61, 74, 88].

Tensile tests were used to show the effect of the hybridization of Graphene and MMT on the Young's modulus, tensile strength, and strain at yield a function of MMT/GNs content. From Fig. 11a, it is clear that the Young's modulus of all hybrid nanocomposites (1590–1840 MPa) are much higher (53–78%) than neat PP (1034 MPa). The hybrid nanocomposites have intermediate values between those extremes which increase with GNs addition, thus confirming that a unique synergistic effect of the GNs:MMT hybrid nanofillers on the reinforcing of the PP was clearly observed. Logically, the increase of the Young's modulus with the low MMT or GNs content (3 wt%) is attributed to their respectively high intrinsic properties in terms of rigidity. The obtained gains are closely related to the good dispersion/distribution and high aspect ratios of both nanofillers into the polymer matrix [20, 30, 61]. So,
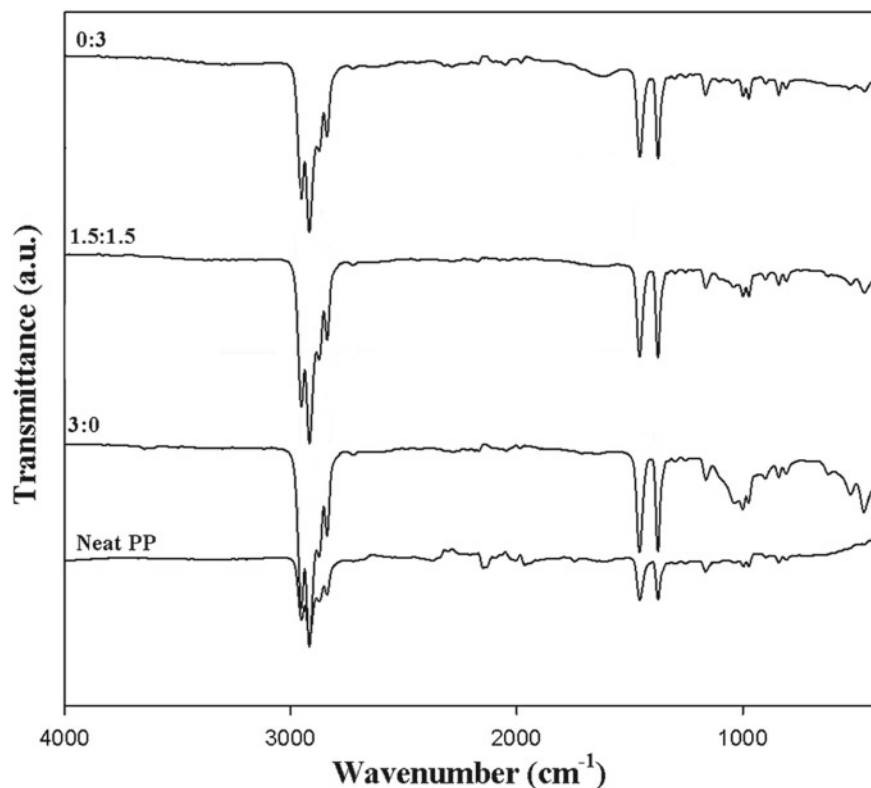
Fig. 11 FTIR spectrum of neat PP and hybrid nanocomposites (MMT: GNs)

compared to GNs or MMT, the hybrid nanofiller showed a positive properties in strengthening the PP nanocomposite, at the same level of filler (3% by weight). This is due to the synergistic effect induced by the combination of NG and MMT. Such synergistic interactions led to the formation of an interconnected network structure, which explains the very strong increase in tensile properties of the PP matrix. In the MMT-reinforced nanocomposite, the relatively inferior mechanical properties were due to agglomeration. These agglomerates can prevent efficient transfer of charge to the nanosheet and can cause a decrease in the aspect ratio. In addition, the interfacial adhesion between the hybrid nanofiller and the polymer matrix could be improved [20, 30, 51, 74]. As a result, the network of hybrid nanofillers acts as an effective reinforcement in the parent system, which provides superior tensile properties than hybrid nanocomposites. In this case, efficient stress transfer occurred from the polymer chains to the hybrid dispersed nanofiller, which provided additional resistance to the nanocomposites [20, 30, 51, 74]. In consequence, the hybrid nanofiller network acts as an efficient reinforcement in the parent system, which provides superior tensile properties to the hybrid nanocomposites. In this case, effective stress

transfer occurred from the polymer chains to the dispersed hybrid nanofiller, which provided additional strength to the nanocomposites.

From Fig. 11b, the studied tensile properties were affected by the variation of mass ratio of GNs and MMT in the hybrid nanofillers. Notably, the reinforcing efficiency of hybrid nanofillers is higher than that of GNs and MMT, because the hybrid nanocomposite shows the superior improvement of the tensile properties, while the relatively inferior improvement is observed for the GNs nanocomposite, thus confirming that the synergetic effect was more pronounced in the hybrid nanofiller containing an equal amount of GNs and MMT (1.5:1.5). This result is due to the extremely small thickness of flat GNs (two-dimensional geometry) leading to a wrinkled topography at the nanoscale, resulting in an improved mechanical interlocking/adhesion at the nanosheet-matrix interface [30, 61, 74, 88]. In addition, GNs has higher specific surface area compared to MMT resulting in a substantial interphase zone around each nanosheet in PP/GNs nanocomposites for which the mobility of the matrix polymer chains was reduced.

Interestingly, the strain at yield of PP was also affected by the addition of different hybrid nanofillers. the value decreases (from 4 to 1.5%) with increasing GNs content in the hybrid nanocomposites. This trend (Fig. 11b) can be related to several factors, but graphene nanosheets have very high intrinsic mechanical properties with exceptionally high surface area making them good nanofiller for the enhancement of the mechanical properties of a polymer matrix. However, increasing stiffness generally lead to lower ductility/deformability of the resulted nanocomposites. Finally, it can be stated that the combination of stiff nanofillers like GNs with clay conferring more ductility is a good compromise between the mechanical properties the nanocomposites using GNs or MMT alone.

Dynamic rheological measurements can be an effective tool to quantify the dispersion of graphene into polymer systems. In linear viscoelastic behavior, elastic modulus (G′) at low frequency can give very important information about the quality of graphene nanosheets dispersed within the polymer matrix; however, the development of a linear plateau level of G′ at low frequency is an indication of the rheological percolation threshold that is connected with the formation of an interconnected network of graphene nanosheets [61, 88]. The percolation threshold determined from the G′ measurements can be used to roughly quantify the dispersion and the level of interaction between graphene nanosheets and the polymer chains. The same observations can be provided by measuring the complex viscosity of the nanocomposite polymer systems.

Figure 12a, shows the effects of the nanofillers on the torsion modulus (G^*) of the nanocomposites. As for the tensile modulus, a significant increase in the torsion modulus is obtained with clay/GNs addition. Thus, large-scale polymer relaxations in the nanocomposites were effectively restrained by the presence of the nanofillers. It can be seen that the complex moduli (at 1 Hz) of the hybrid nanocomposites show intermediate values between that of MMT (2.7×10^5 Pa) and GNs nanocomposites (3.8×10^5 Pa). However, GNs is more effective in restraining the PP polymer relaxations than MMT. This is due to their higher surface area and higher aspect ratio compared to clay. Together with its high surface area and nanoscale flat surface,
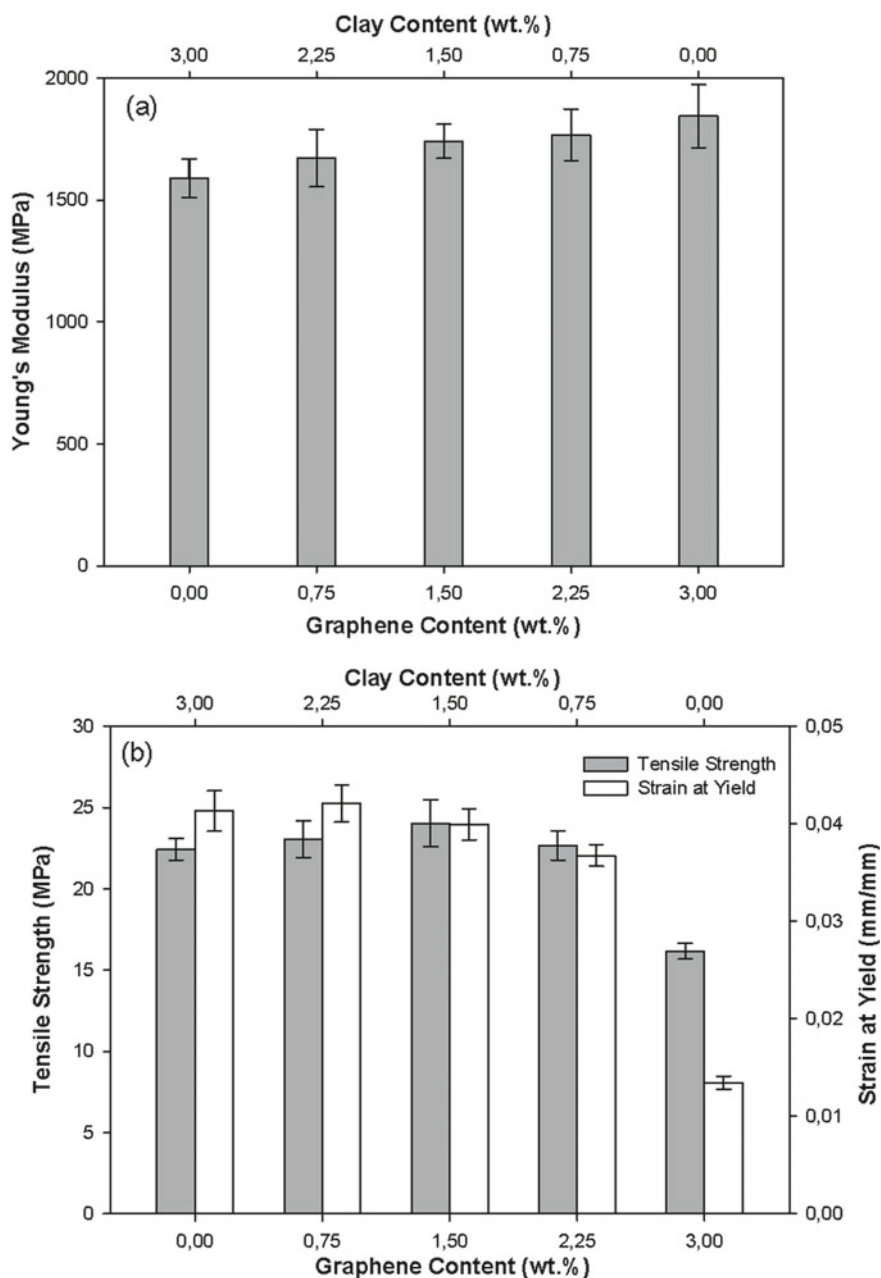
Fig. 12 Tensile properties of MMt and GNs hybrid nanocomposites

GNs led to stronger interfacial interactions with the PP and thus substantially larger influence on the chain motion of the host polymer [4, 20]. The shear stress from the torsion torque is applied at the nanofiller/matrix interface which is stronger for GNs leading to higher torsion moduli compared to clay nanocomposites.

Moreover, the frequency also plays an important role in the nanocomposite's response. It is clear from Fig. 12b, that G* increases with increasing frequency. This can be explained by the viscoelastic behavior of polymer nanocomposites; i.e. the behavior is more solid-like at higher frequencies for which the polymer molecules do have not have enough time to relax and follow the deformation imposed [4, 20]. This can be better detected in Fig. 4b via tan δ curves. It can be seen that tan δ is not much affected by the composition (almost constant tan δ at any MMT/GNs ratio). On the other hand, tan δ decreases with increasing frequency indicating that the materials have a more elastic character over a viscous behavior (Fig. 13).

5   Conclusion

This chapter highlights the reinforcing efficiency of graphene nanosheets and Montmorionite clay in polymer nanocomposites, especially a method of addressing the dispersion problem, since these water-dispersible nanofillers, at high loading content, tends to agglomerate within the polymer matrix. In this chapter we demonstrated that the combination of Montmorionite (MMT) and GNs in a novel hybrid nanocomposite was highly operative to overcome the agglomeration and poor dispersion and distribution phenomenon. An extensive discussion has been provided on the mechanical and rheological behavior of polymer matrix containing those hybrid nanofillers. Reasonably, the results obtained for the hybrid nanofiller reinforced nanocomposite were largely greater compared to those found for nanocomposites containing either MMT or GNs nanofillers, at the same loading level. This result was attributed to the synergistic effect between nanofillers which progresses the distribution/dispersion homogeneity by avoiding the agglomeration ot the nanofillers within the polymer, resulting in nanocomposites with heightened properties. If this can be realized, more applications can benefit from using these hybrid particles.

The preparation of these hybrid nanofillers and their integration into a polymer provided an original method for the development of novel multifunctional nanocomposites based on the combination of existing nanomaterials, mainly by improving the mechanical properties of nanocomposite films in applications where good strength, ductility and reduced moisture absorption are required.
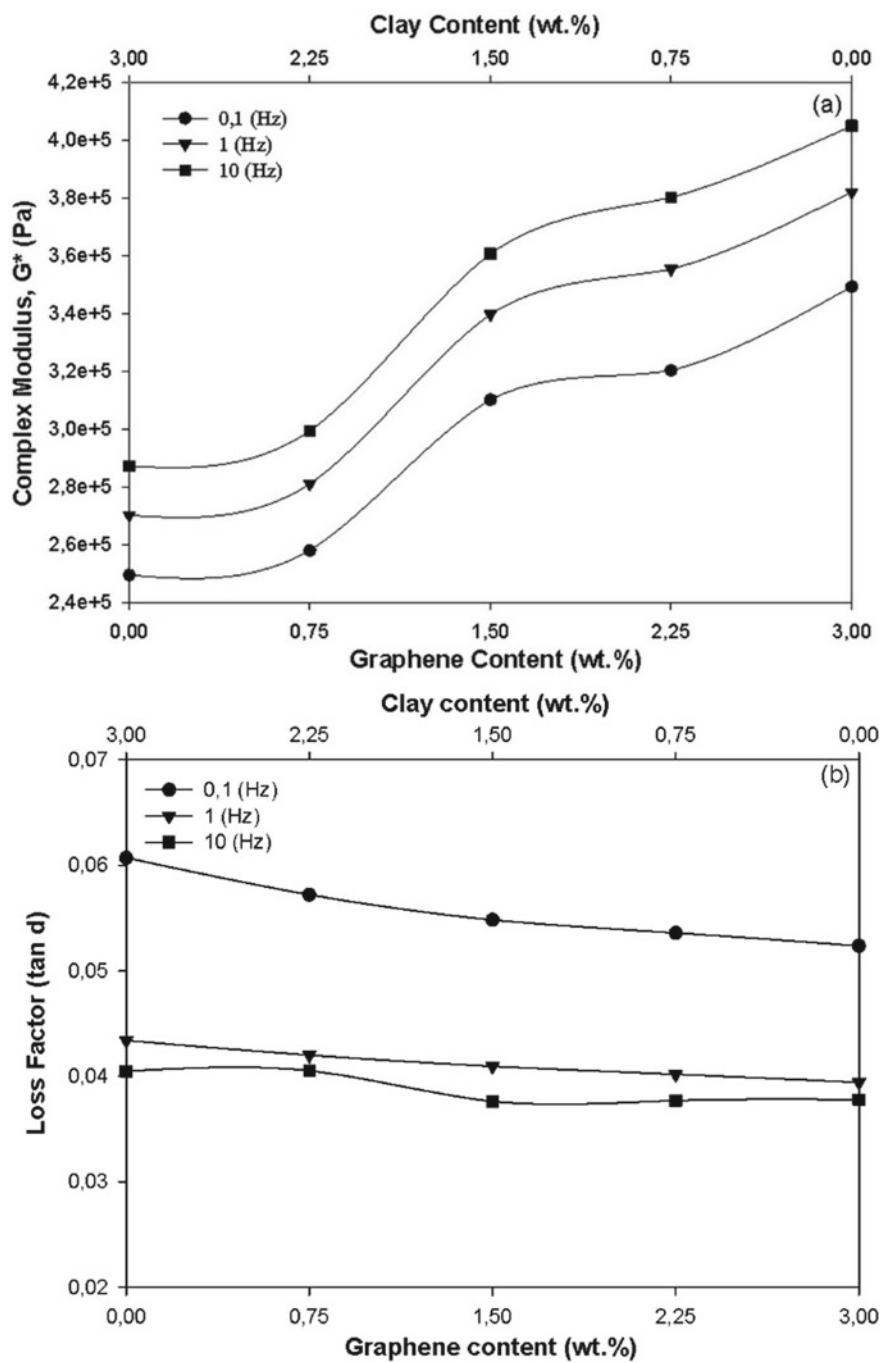
Fig. 13 Rheological properties on torsional mode of hybrid nanocomposites

References

1. Khalaj MJ, Ahmadi H, Lesankhosh R, Khalaj G (2016) Study of physical and mechanical properties of polypropylene nanocomposites for food packaging application: nano-clay modified with iron nanoparticles. Trends Food Sci Technol 51:41–48. https://doi.org/10.1016/j.tifs.2016.03.007

2. Shrivastava S, Jadon N, Jain R (2016) Next-generation polymer nanocomposite-based electrochemical sensors and biosensors: a review. TrAC Trends Anal Chem 82:55–67. https://doi.org/10.1016/j.trac.2016.04.005

3. Chen L, Zhou CH, Fiore S, Tong DS, Zhang H, Li CS, Ji SF, Yu WH (2016) Functional magnetic nanoparticle/clay mineral nanocomposites: Preparation, magnetism and versatile applications. Appl Clay Sci 127–128:143–163. https://doi.org/10.1016/j.clay.2016.04.009

4. Mekhzoum MEM, Essabir H, Rodrigue D, Qaiss AK, Bouhfid R (2016) Graphene/montmorillonite hybrid nanocomposites based on polypropylene: morphological, mechanical, and rheological properties. Polym Compos (2016). https://doi.org/10.1002/pc.24166

5. Raji M, Nekhlaoui S, El Hassani IEEA, Essassi EM, Essabir H, Rodrigue D, Bouhfid R, el kacem Qaiss A (2019) Utilization of volcanic amorphous aluminosilicate rocks (perlite) as alternative materials in lightweight composites. Compos Part B Eng 165:47–54. https://doi.org/10.1016/j.compositesb.2018.11.098

6. Sanusi OM, Benelfellah A, Aït Hocine N (2020) Clays and carbon nanotubes as hybrid nanofillers in thermoplastic-based nanocomposites—a review. Appl Clay Sci 185:105408. https://doi.org/10.1016/j.clay.2019.105408

7. Bensalah H, Gueraoui K, Essabir H, Rodrigue D, Bouhfid R, el kacem Qaiss A (2017) Mechanical, thermal, and rheological properties of polypropylene hybrid composites based clay and graphite. J Compos Mater 51:3563–3576. https://doi.org/10.1177/0021998317690597

8. Nekhlaoui S, Essabir H, Bensalah MO, Fassi-Fehri O, Qaiss A, Bouhfid R (2014) Fracture study of the composite using essential work of fracture method: PP-SEBS-g-MA/E1 clay. Mater Des 53. https://doi.org/10.1016/j.matdes.2013.07.089

9. Qaiss AEK, Bouhfid R, Essabir H (2014) Natural fibers reinforced polymeric matrix: thermal, mechanical and interfacial properties. https://doi.org/10.1007/978-3-319-07641-6_14

10. Essabir H, Bouhfid R, Qaiss A (2017) Alfa and doum fiber-based composite materials for different applications. In: Lignocellul. Fibre Biomass-Based Compos. Mater Process Prop Appl 147–164. https://doi.org/10.1016/B978-0-08-100959-8.00008-1

11. Nekhlaoui S, Essabir H, Kunal D, Sonakshi M, Bensalah MO, Bouhfid R, Qaiss A (2015) Comparative study for the talc and two kinds of moroccan clay as reinforcements in polypropylene-SEBS-g-MA matrix. Polym Compos 36:675–684. https://doi.org/10.1002/pc.22986

12. Raji M, Essabir H, Essassi EM, Rodrigue D, Bouhfid R, Qaiss AK (2016) Morphological, thermal, mechanical, and rheological properties of high density polyethylene reinforced with Illite clay. Polym. Compos (2016). https://doi.org/10.1002/pc.24096

13. Essabir H, Bouhfid R, El kacem Qaiss A (2018) Fracture surface morphologies in understanding of composite structural behavior. In: Structural health monitoring of biocomposites, fibre-reinforced composites and hybrid composites. Elsevier, pp 277–293. https://doi.org/10.1016/B978-0-08-102291-7.00014-9

14. Zabihi O, Ahmadi M, Nikafshar S, Chandrakumar Preyeswary K, Naebe M (2018) A technical review on epoxy-clay nanocomposites: Structure, properties, and their applications in fiber reinforced composites. Compos Part B Eng 135:1–24. https://doi.org/10.1016/j.compositesb.2017.09.066

15. Handbook of clay science, vol 5, 2nd edn. (n.d.). https://www.elsevier.com/books/handbook-of-clay-science/bergaya/978-0-08-099364-5. Accessed 30 May 2020

16. Salzano de Luna M, Wang Y, Zhai T, Verdolotti L, Buonocore GG, Lavorgna M, Xia H (2019) Nanocomposite polymeric materials with 3D graphene-based architectures: from design strategies to tailored properties and potential applications. Prog Polym Sci 89:213–249. https://doi.org/10.1016/j.progpolymsci.2018.11.002

17. Zhang H, Xing W, Li H, Xie Z, Huang G, Wu J (2019) Fundamental researches on graphene/rubber nanocomposites. Adv Ind Eng Polym Res 2:32–41. https://doi.org/10.1016/j.aiepr.2019.01.001

18. Singh P, Shandilya P, Raizada P, Sudhaik A, Rahmani-Sani A, Hosseini-Bandegharaei A (2020) Review on various strategies for enhancing photocatalytic activity of graphene based nanocomposites for water purification. Arab J Chem 13:3498–3520. https://doi.org/10.1016/j.arabjc.2018.12.001

19. Tabandeh-Khorshid M, Kumar A, Omrani E, Kim C, Rohatgi P (2020) Synthesis, characterization, and properties of graphene reinforced metal-matrix nanocomposites. Compos Part B Eng 183:107664. https://doi.org/10.1016/j.compositesb.2019.107664

20. Raji M, Essabir H, Rodrigue D, Bouhfid R, Qaiss A (2017) Influence of graphene oxide and graphene nanosheet on the properties of polyvinylidene fluoride nanocomposites, Polym Compos. https://doi.org/10.1002/pc.24292

21. Alam SN, Sharma N, Kumar L (2017) Synthesis of graphene oxide (GO) by modified hummers method and its thermal reduction to obtain reduced graphene oxide (rGO)*. Graphene 06:1–18. https://doi.org/10.4236/graphene.2017.61001

22. Bouhfid N, Raji M, Bensalah M, el kacem Qaiss A (2019) Functionalized graphene and thermoset matrices-based nanocomposites: mechanical and thermal properties. Funct Graph Nanocompos Their Deriv 47–64. https://doi.org/10.1016/B978-0-12-814548-7.00003-9

23. Tiouitchi G, Raji M, Mounkachi O, Ali MA, Mahmoud A, Boschini F, Essabir H, Bouhfid R, el kacem Qaiss A (2019) Black phosphorus-based polyvinylidene fluoride nanocomposites: synthesis, processing and characterization. Compos Part B Eng 175. https://doi.org/10.1016/j.compositesb.2019.107165

24. Essabir H, Raji M, Essassi EM, Rodrigue D, Bouhfid R, Qaiss A (2017) Morphological, thermal, mechanical, electrical and magnetic properties of ABS/PA6/SBR blends with Fe$_3$O$_4$ nano-particles. J Mater Sci Mater Electron 28. https://doi.org/10.1007/s10854-017-7639-2

25. Raji M, El M, Mekhzoum M, Rodrigue D, Bouh R (2018) Effect of silane functionalization on properties of polypropylene / clay nanocomposites. Compos Part B 146:106–115. https://doi.org/10.1016/j.compositesb.2018.04.013

26. Haddar M, Elloumi A, Koubaa A, Bradai C, Migneault S, Elhalouani F (2018) Synergetic effect of Posidonia oceanica fibres and deinking paper sludge on the thermo-mechanical properties of high density polyethylene composites. Ind Crops Prod. https://doi.org/10.1016/j.indcrop.2018.04.075

27. Essabir H, Boujmal R, Bensalah MO, Rodrigue D, Bouhfid R, Qaiss AEK (2019) Mechanical and thermal properties of hybrid composites: Oil-palm fiber/clay reinforced high density polyethylene. Mech Mater 98. https://doi.org/10.1016/j.mechmat.2016.04.008

28. Essabir H, Raji M, Bouh R (2016) Nanoclay and natural fibers based hybrid composites: mechanical, morphological, thermal and rheological properties. In: Nanoclay reinforced polymer composites, pp 29–49. https://doi.org/10.1007/978-981-10-0950-1

29. Kakou CA, Essabir H, Bensalah M-O, Bouhfid R, Rodrigue D, Qaiss A (2015) Hybrid composites based on polyethylene and coir/oil palm fibers. J Reinf Plast Compos 34 (2015). https://doi.org/10.1177/0731684415596235

30. Essabir H, Raji M, Bouhfid R, Qaiss AK (2016) Nanoclay And Natural Fibers Based Hybrid Composites: Mechanical, Morphological, Thermal And Rheological Properties. In: Nanoclay Reinforced Polymer Composites, pp 29–49. https://doi.org/10.1007/978-981-10-0950-1

31. Leszczyńska A, Njuguna J, Pielichowski K, Banerjee JR (2007) Polymer/montmorillonite nanocomposites with improved thermal properties. Part I. Factors influencing thermal stability and mechanisms of thermal stability improvement. Thermochim Acta 453:75–96. https://doi.org/10.1016/j.tca.2006.11.002

32. Bee SL, Abdullah MAA, Bee ST, Sin LT, Rahmat AR (2018) Polymer nanocomposites based on silylated-montmorillonite: a review. Prog Polym Sci 85:57–82. https://doi.org/10.1016/j.progpolymsci.2018.07.003

33. Zhu TT, Zhou CH, Kabwe FB, Wu QQ, Li CS, Zhang JR (2019) Exfoliation of montmorillonite and related properties of clay/polymer nanocomposites. Appl Clay Sci 169:48–66. https://doi.org/10.1016/j.clay.2018.12.006

34. Mutiso RM, Winey KI (2015) Electrical properties of polymer nanocomposites containing rod-like nanofillers. Prog Polym Sci 40:63–84. https://doi.org/10.1016/j.progpolymsci.2014.06.002

35. Bharadwaz A, Jayasuriya AC (2020) Recent trends in the application of widely used natural and synthetic polymer nanocomposites in bone tissue regeneration. Mater Sci Eng C 110:110698. https://doi.org/10.1016/j.msec.2020.110698

36. Pourhashem S, Saba F, Duan J, Rashidi A, Guan F, Nezhad EG, Hou B (2020) Polymer/Inorganic nanocomposite coatings with superior corrosion protection performance: a review. J Ind Eng Chem. https://doi.org/10.1016/j.jiec.2020.04.029

37. Llorens A, Lloret E, Picouet PA, Trbojevich R, Fernandez A (2012) Metallic-based micro and nanocomposites in food contact materials and active food packaging. Trends Food Sci Technol 24:19–29. https://doi.org/10.1016/j.tifs.2011.10.001

38. Zahran M, Marei AH (2019) Innovative natural polymer metal nanocomposites and their antimicrobial activity. Int J Biol Macromol 136:586–596. https://doi.org/10.1016/j.ijbiomac.2019.06.114

39. Malha M, Nekhlaoui S, Essabir H, Benmoussa K, M.-O. Bensalah, F.-E. Arrakhiz, R. Bouhfid, A. Qaiss, Mechanical and thermal properties of compatibilized polypropylene reinforced by woven doum, J. Appl. Polym. Sci. 130 (2013). https://doi.org/https://doi.org/10.1002/app.39619.

40. Essabir H, Raji M, Laaziz SA, Rodrigue D, Bouhfid R (2018) Thermo-mechanical performances of polypropylene biocomposites based on untreated, treated and compatibilized spent coffee grounds. Compos Part B. https://doi.org/10.1016/j.compositesb.2018.05.020

41. Essabir H, Hilali E, El Minor H, Bensalah MO, Bouhfid R, Qaiss A (2015) Mechanical and thermal properties of polymer composite based on natural fibers: moroccan luffa sponge/high density polyethylene. J Biobased Mater Bioenergy 9. https://doi.org/10.1166/jbmb.2015.1524

42. Zari N, Raji M, El Mghari H, Bouhfid R, Qaiss AEK (2018) Nanoclay and polymer-based nanocomposites: Materials for energy efficiency. In: Polymer-clay nanocomposites for environmental applications A. Woodhead Publishing Series in Composites Science and Engineering. University of Ottawa Press, pp 76–103. https://doi.org/10.1016/B978-0-08-102262-7.00003-9

43. Raji M, Essabir H, Essassi EM, Rodrigue D, Bouhfid R, Qaiss AK (2016) Morphological, thermal, mechanical, and rheological properties of high density polyethylene reinforced with illite clay. Polym Polym Compos 16:101–113. https://doi.org/10.1002/pc.24096

44. Abdellaoui H, Raji M, Essabir H, Bouhfid R, el kacem Qaiss A (2019) Nanofibrillated cellulose-based nanocomposites. In: Bio-based polymers and nanocomposites. Springer International Publishing, Cham, pp 67–86. https://doi.org/10.1007/978-3-030-05825-8_4

45. Hashim AF, Youssef K, Roberto SR, Abd-Elsalam KA (2020) Hybrid inorganic-polymer nanocomposites: Synthesis, characterization, and plant-protection applications. In: Multifunct Hybrid Nanomater Sustain Agri-Food Ecosyst pp 33–49. https://doi.org/10.1016/b978-0-12-821354-4.00003-0

46. Mallakpour S, Khadem E (2020) Polymer layered double hydroxide hybrid nanocomposites. In: Layered double hydroxide polymer Nanocomposites. Elsevier, pp 531–564. https://doi.org/10.1016/b978-0-08-101903-0.00013-1

47. George K, Biswal M, Mohanty S, Nayak SK, Panda BP (2020) Nanosilica filled EPDM/Kevlar fiber hybrid nanocomposites: mechanical and thermal properties. Mater Today Proc. https://doi.org/10.1016/j.matpr.2020.02.817

48. Bouhfid N, Raji M, Boujmal R, Essabir H, Bensalah M-O, Bouhfid R, el kacem Qaiss A (2019) Numerical modeling of hybrid composite materials. Model Damage Process Biocomposites Fibre-Reinforced Compos Hybrid Compos 57–101. https://doi.org/10.1016/B978-0-08-102289-4.00005-9

49. Darabdhara G, Das MR, Singh SP, Rengan AK, Szunerits S, Boukherroub R (2019) Ag and Au nanoparticles/reduced graphene oxide composite materials: synthesis and application in diagnostics and therapeutics. Adv Colloid Interface Sci 271:101991. https://doi.org/10.1016/j.cis.2019.101991

50. Bagotia N, Choudhary V, Sharma DK (2019) Synergistic effect of graphene/multiwalled carbon nanotube hybrid fillers on mechanical, electrical and EMI shielding properties of polycarbonate/ethylene methyl acrylate nanocomposites. Compos Part B Eng 159:378–388. https://doi.org/10.1016/j.compositesb.2018.10.009

51. Bouhfid R, Essabir H, El Kacem Qaiss A (2016) Graphene-based nanocomposites: mechanical, thermal, electrical, and rheological properties. In: Rheology and processing of polymer nanocomposites. Wiley, pp 405–430. https://doi.org/10.1002/9781118969809.ch12

52. Lim J, Kim M-C, Goh M, Yeo H, Shin DG, Ku B-C, You N-H (2013) Synthesis and characterization of polybenzoxazole/graphene oxide composites via in situ polymerization. Carbon Lett. https://doi.org/10.5714/CL.2013.14.4.251

53. Coppola B, Cappetti N, Di Maio L, Scarfato P, Incarnato L (2017) Layered silicate reinforced polylactic acid filaments for 3D printing of polymer nanocomposites. In: RTSI 2017—EEE 3rd International forum on research and technologies for society and industry proceedings, pp 3–6. https://doi.org/10.1109/RTSI.2017.8065892

54. Qaiss A, Bouhfid R, Essabir H (2015) Effect of processing conditions on the mechanical and morphological properties of composites reinforced by natural fibres. In: Manufacturing of natural fibre reinforced polymer composites. Springer International Publishing, pp 177–197. https://doi.org/10.1007/978-3-319-07944-8_9

55. Mekhzoum MEM, Raji M, Rodrigue D, el kacem Qaiss A, Bouhfid R (2020) The effect of benzothiazolium surfactant modified montmorillonite content on the properties of polyamide 6 nanocomposites. Appl Clay Sci 185:105417. https://doi.org/10.1016/j.clay.2019.105417

56. Raji M, Qaiss AEK, Bouhfid R (2020) Effects of bleaching and functionalization of kaolinite on the mechanical and thermal properties of polyamide 6 nanocomposites. RSC Adv 10:4916–4926. https://doi.org/10.1039/c9ra10579d

57. Xu W, Peng J, Ni D, Zhang W, Wu H, Mu W (2020) Preparation, characterization and application of levan/montmorillonite biocomposite and levan/BSA nanoparticle. Carbohydr Polym 234:115921. https://doi.org/10.1016/j.carbpol.2020.115921

58. Mohammadi M, Rezaei Mokarram R, Shahvalizadeh R, Sarabandi K, Lim LT, Hamishehkar H (2020) Immobilization and stabilization of pectinase on an activated montmorillonite support and its application in pineapple juice clarification. Food Biosci 36. 100625. https://doi.org/10.1016/j.fbio.2020.100625

59. Du X, Guang W, Cheng Y, Hou Z, Liu Z, Yin H, Huo L, Lei R, Shu C (2020) Thermodynamics analysis of the adsorption of CH4 and CO2 on montmorillonite. Appl Clay Sci 192:105631. https://doi.org/10.1016/j.clay.2020.105631

60. Raji M, El M, Mekhzoum M, Qaiss K (2016) Nanoclay modification and functionalization for nanocomposites development : effect on the structural, morphological, mechanical and rheological properties. Mater Sci. https://doi.org/10.1007/978-981-10-1953-1

61. Raji M, El M, Mekhzoum M, Qaiss AK, Bouhfid R (2016) Nanoclay modification and functionalization for nanocomposites development: effect on the structural, morphological, mechanical and rheological properties. In: Nanoclay reinforced polymer composites, pp 1–34. https://doi.org/10.1007/978-981-10-0950-1

62. Nekhlaoui S., Essabir H, Kunal D, Sonakshi M, Bensalah MO, Bouhfid R, Qaiss A (2014) Comparative study for the talc and two kinds of moroccan clay as reinforcements in polypropylene-SEBS-g-MA matrix. Polymer Composites 10. https://doi.org/10.1002/pc.22986

63. Raji M, Essassi E, Essabir H, Rodrigue D, El kacem Qaiss A, Bouhfid R (2019) Properties of nano-composites based on different clays and polyamide 6/acrylonitrile butadiene styrene blends. In: Bio-based polymers and nanocomposites: preparation, processing, properties & performance. Springer International Publishing, pp 107–128. https://doi.org/10.1007/978-3-030-05825-8_6

64. Rodrigues C, de Mello JMM, Dalcanton F, Macuvele DLP, Padoin N, Fiori MA, Soares C, Riella HG (2020) Mechanical, thermal and antimicrobial properties of chitosan-based-nanocomposite with potential applications for food packaging. J Polym Environ 28:1216–1236. https://doi.org/10.1007/s10924-020-01678-y

65. Akin O, Tihminlioglu F (2012) Effect of organo-modified clay addition on properties of polyhydroxy butyrate homo and copolymers nanocomposite

66. Essabir H, Nekhlaoui S, Bensalah MO, Rodrigue D, Bouhfid R, Qaiss A (2017) Phosphogypsum waste used as reinforcing fillers in polypropylene based composites: structural, mechanical and thermal properties. J Polym Environ 25. https://doi.org/10.1007/s10924-016-0853-9

67. Kumar R, Yakabu MK, Anandjiwala RD (2010) Effect of montmorillonite clay on flax fabric reinforced poly lactic acid composites with amphiphilic additives. Compos Part A Appl Sci Manuf 41:1620–1627. https://doi.org/10.1016/j.compositesa.2010.07.012

68. Yu-shan XIE, Shao-zao TAN, Ma-hua L, Ren-fu LIU (2010) Structure and Antibacterial Activity of Modified Montmorillonite. Mol Catal 26:509–513

69. Yürüdü C, Işçi S, Ünlü C, Atici O, Ece ÖI, Güngör N (2005) Synthesis and characterization of HDA/NaMMT organoclay. Bull Mater Sci 28:623–628

70. Atici O (2005) Synthesis and characterization of HDA/NaMMT Organoclay. Bull Mater Sci 28:623–628

71. Xie A, Yan W, Zeng X, Dai G, Tan S, Cai X, Wu T (2011) Microstructure and antibacterial activity of phosphonium montmorillonites. Bull Korean Chem Soc 32:1936–1938. https://doi.org/10.5012/bkcs.2011.32.6.1936

72. Carastan DJ, Amurin LG, Craievich AF, Gonçalves C, Demarquette NR (2013) Morphological evolution of oriented clay-containing block co- polymer nanocomposites under elongational flow. Eur Polym J 49:1391–1405. https://doi.org/10.1016/j.eurpolymj.2013.02.036

73. Mekhzoum MEM, Essabir H, Rodrigue D, Qaiss AK, Bouhfid R (2018) Graphene/montmorillonite hybrid nanocomposites based on polypropylene: morphological, mechanical, and rheological properties. Polym Compos 39:2046–2053. https://doi.org/10.1002/pc.24166

74. Essabir H, Raji M, Bouhfid R, el kacem Qaiss A (2019) Rheological properties of functionalized graphene and polymeric matrices–based nanocomposites. In: Functionalized graphene nanocomposites and their derivatives. Elsevier, pp 109–120. https://doi.org/10.1016/b978-0-12-814548-7.00006-4

75. Raji M, Zari N, el Kacem Qaiss A, Bouhfid R (2018) Chemical preparation and functionalization techniques of graphene and graphene oxide. In: Functionalized graphene nanocomposites and their derivatives. Synthesis, processing and application. Elsevier, pp 1–20. https://doi.org/10.1016/B978-0-12-814548-7.00001-5

76. Guo Y, Yang X, Ruan K, Kong J, Dong M, Zhang J, Gu J, Guo Z (2019) Reduced graphene oxide heterostructured silver nanoparticles significantly enhanced thermal conductivities in hot-pressed electrospun polyimide nanocomposites. ACS Appl Mater Interfaces 11:25465–25473. https://doi.org/10.1021/acsami.9b10161

77. Arif MF, Alhashmi H, Varadarajan KM, Koo JH, Hart AJ, Kumar S (2020) Multifunctional performance of carbon nanotubes and graphene nanoplatelets reinforced PEEK composites enabled via FFF additive manufacturing. Compos Part B Eng 184:107625. https://doi.org/10.1016/j.compositesb.2019.107625

78. Alam MF, Khan MS, Uddin I, Khan SN, Ahmad I (2020) Exfoliation synthesis of graphene and optimization with alkali halides salts. Surf and Interfaces 20:100548. https://doi.org/10.1016/j.surfin.2020.100548

79. Tian R, Jia X, Yang J, Li Y, Song H (2020) Large-scale, green, and high-efficiency exfoliation and noncovalent functionalization of fluorinated graphene by ionic liquid crystal. Chem Eng J 395:125104. https://doi.org/10.1016/j.cej.2020.125104

80. Zhang Q, Lu Y, Liu Z, Yu H, Duan Y, Liu L, Chen S, Huang W (2019) Highly efficient organic-inorganic hybrid perovskite quantum dot/nanocrystal light-emitting diodes using graphene electrode and modified PEDOT:PSS. Org Electron 72:30–38. https://doi.org/10.1016/j.orgel.2019.05.046

81. Chuang MK, Lin CH, Chen FC (2020) Accumulated plasmonic effects of gold nanoparticle−decorated PEGylated graphene oxides in organic light-emitting diodes. Dye Pigment 180:108412. https://doi.org/10.1016/j.dyepig.2020.108412

82. Pfaffeneder-Kmen M, Casas IF, Naghilou A, Trettenhahn G, Kautek W (2017) A multivariate curve resolution evaluation of an in-situ ATR-FTIR spectroscopy investigation of the electrochemical reduction of graphene oxide. Electrochim Acta 255:160–167. https://doi.org/10.1016/j.electacta.2017.09.124

83. Rostami A, Vahdati M, Alimoradi Y, Karimi M, Nazockdast H (2018) Rheology provides insight into flow induced nano-structural breakdown and its recovery effect on crystallization of single and hybrid carbon nanofiller filled poly(lactic acid). Polymer (Guildf) 134:143–154. https://doi.org/10.1016/j.polymer.2017.11.062

84. Li L, Xu L, Ding W, Lu H, Zhang C, Liu T (2019) Molecular-engineered hybrid carbon nanofillers for thermoplastic polyurethane nanocomposites with high mechanical strength and toughness. Compos Part B Eng 177:107381. https://doi.org/10.1016/j.compositesb.2019.107381

85. Mondal S, Ravindren R, Bhawal P, Shin B, Ganguly S, Nah C, Das NC (2020) Combination effect of carbon nanofiber and ketjen carbon black hybrid nanofillers on mechanical, electrical, and electromagnetic interference shielding properties of chlorinated polyethylene nanocomposites. Compos Part B Eng (2020) 108071. https://doi.org/10.1016/j.compositesb.2020.108071

86. Boujmal R, Kakou CA, Nekhlaoui S, Essabir H, Bensalah M-O, Rodrigue D, Bouhfid R, el kacem Qaiss A (2017) Alfa fibers/clay hybrid composites based on polypropylene. J Thermoplast Compos Mater (2017). https://doi.org/10.1177/0892705717729197

87. Raji M, Essabir H, Bouhfid R, El Kacem Qaiss A (2017) Impact of chemical treatment and the manufacturing process on mechanical, thermal, and rheological properties of natural fibers-based composites. In: Handbook of Composites from Renewable Materials. Wiley, Hoboken, pp 225–252. https://doi.org/10.1002/9781119441632.ch71

88. Boujmal R, Kakou CA, Nekhlaoui S, Essabir H, Bensalah M-O, Rodrigue D, Bouhfid R, el kacem Qaiss A (2018) Alfa fibers/clay hybrid composites based on polypropylene. J Thermoplast Compos Mater 31 (2018) 974–991. https://doi.org/10.1177/0892705717729197

Graphene and Silver Nanoparticle Based Hybrid Nanocomposites for Anti-bacterial Applications

Chandrasekar Muthukumar, Senthilkumar Krishnasamy, Theivasanthi Thirugnanasambandan, Senthil Muthu Kumar Thiagamani, Naveen Jesuarockiam, and Suchart Siengchin

Abstract Microbial infection and colonization due to the bacteria are considered as a serious issue in the biomedical equipment's and food packaging industry which causes threat to the human health and affects the food quality. In the recent years, bacterial microorganisms having strong resistance against the antibiotics have also been identified. Silver nanoparticles are the most promising materials to resolve this issue due to their inherent anti-microbial characteristic. Current advancements in nanotechnology paved the way for the innovation of functional nanomaterials with the unique physical and chemical properties. Recently, graphene and their derivatives have gained significant attention due to the functionalization of metallic nanoparticles and metal oxide on its surface. This chapter explores the bactericidal activity of the

C. Muthukumar (✉)
School of Aeronautical Sciences, Hindustan Institute of Technology and Science, Padur, Kelambakkam, Chennai, Tamilnadu 603103, India
e-mail: chandrasekar.25j@gmail.com

S. Krishnasamy
Center of Innovation in Design and Engineering for Manufacturing (CoI-DEM), King Mongkut's University of Technology North Bangkok, 1518 Wongsawang Road, Bangsue, Bangkok 10800, Thailand

T. Thirugnanasambandan
International Research Centre, Kalasalingam Academy of Research and Education, Anand Nagar, Krishnankoil 626126, Srivilliputhur, Tamilnadu, India

S. M. K. Thiagamani
Department of Mechanical Engineering, Kalasalingam Academy of Research and Education, Anand Nagar, Krishnankoil, Tamilnadu 626126, India

N. Jesuarockiam
School of Mechanical Engineering, Vellore Institute of Technology, Vellore, Tamilnadu 632014, India

S. Siengchin
Department of Mechanical and Process Engineering, The Sirindhorn International Thai-German Graduate School of Engineering (TGGS), King Mongkut's University of Technology North Bangkok, 1518 Wongsawang Road, Bangsue, Bangkok 10800, Thailand

nanocomposites infused with the silver nanoparticle (AgNP) and graphene derivatives such as the graphene oxide and the reduced graphene oxide. Various methods employed in the fabrication of the nanocomposites, antibacterial test methods and the inhibition mechanisms against the gram $+$ and gram$-$ bacteria are discussed in detail.

Keywords Nanocomposites · Silver nanoparticles · Graphene oxide · Antibacterial activity

1   Introduction

Microbial infection caused by the pathogenic bacteria leads to food poisoning and chronic diseases in mankind. Pathogenic bacteria are generally classified into the gram$^+$ and gram$^-$ as shown in Table 1. Nanoparticles (NPs) usually in size less than 100 nm in at least one dimension can be synthesized by using the top-down and bottom-up approaches. Flexibility and gas barrier properties of polymeric matrix composites can be enhanced using the nanometals and metal oxides of silver, magnesium, zinc [1–6].

The nanocomposites are well suited in biomedical applications like (i) tissue engineering (ii) anticancer (iii) antibacterial, and (iv) drug delivery [7, 8]. For instance, Li et al. [9] and Sadhukhan et al. [10] developed the nanocomposites using graphene oxide, AgNPs and metal oxides such as the cuprous oxide (CuO) and zinc oxide (ZnO). They reported that these combinations could be an efficient alternative to antibiotics. Moreover, these nanocomposites have excellent physico-chemical properties, high stability and they could also prevent the formation of bacteria on solid surfaces. Recently, Indira Devi et al. analyzed the antibacterial characteristics of silver nanoparticles (AgNPs) in the polypropylene based hybrid composites. Hybrid composites reinforced with Ag content were effective against both the gram$^+$ and gram$^-$ bacteria [11]. In another study [12], adding AgNPs on antimicrobial properties of banana peel powder and cellulose matrix hybrid composites were examined. After the addition of AgNPs in the cellulose matrix as well as the composite, inhibition zone was formed. Tien et al. [13] incorporated various nanoparticles of both inorganic and organic particles as coating material into the matrix for producing the antibacterial properties. They highlighted that the coating of nanoparticles provides some more benefits such as (i) protection against the bacteria (ii) increasing the service life of the nanocomposite (iii) to avoid the disinfections in air and water and (iv) cost-effective material.

Table 1 Common gram$^+$ and gram$^-$ bacterial microorganisms

Gram$^+$	Gram$^-$
Staphylococcus epidermidis	Psuedomonas aeruginosa
Staphylococcus aureus	Escherchia coli
Bacillus cereus	Listonella anguillarum

1.1 Need for the Hybrid Nanocomposites with Ag-GO Nanoparticles

AgNP has been approved for use in the clothing used for wound dressing and I-flow catheter by the Food and Drug Administration in the USA. This is due to the ability of the AgNP to prevent the bacterial growth. Despite of their commercial success as a constituent in the wound dressing material, toxic nature of the AgNP which kills the active cells around the wound is of major concern [14]. Recently, graphene and their byproducts such as the graphene oxide (GO) and reduced graphene oxide (rGO) was found to improve the bacterial resistance in the composites. GO possesses good mechanical strength, large surface area and high adsorption capacity which allow deposition of the metallic nanoparticles and metal oxide on its surface [15]. Also, GO has relatively more oxygen containing functional group on its surface than the rGO and produces higher percentage of ROS [16]. Many researchers have proposed the use of graphene, GO and rGO functionalized with the AgNP to obtain a synergistic effect against the pathogenic bacteria in the polymers such as poly-lactic acid (PLA) [17], poly-vinyl alcohol (PVA) [18], etc. intended for packaging in the processed food, meat, food products, etc.

The basis of the hybridization is to blend two or more individual nanoparticles together and as well use them along with the polymers to develop a better functional material. The hybrid functional material displays multiple functionalities while retaining specific properties like the individual constituents. For instance, (a) AgNP-Graphene Quantum Dots (Ag-GQD) mixture prepared by Habiba et al. Ag-GQD which has quantum dots aims at reducing the cytotoxic effects of both the graphene and AgNP [14] and (b) (a) rGO-Fe-Ag bi-metallic nanocomposite prepared by the Ahmad et al. [19]. Iron (FeNP) which possesses the electrical conductivity and magnetic properties can be used along with the rGO-Ag combination.

Factors such as the (a) relationship between the structure & properties of the individual constituents and (b) compatibility between the constituents is the deciding factor on the success of the hybrid functional materials intended for a specific application [20]. In the next section, various methods used by the researchers to synthesize rGO-AG and other nanopariceels in hybrid combination are discussed. Fabrication methods to develop the rGO-Ag polymer based nanocomposites are also highlighted.

2 Fabrication Methods of the Graphene-AgNP Based Composites

2.1 Chemical Process

AgNPs-GO nanohybrids are prepared by chemical method by mixing 5 ml GO solution and 0.0034 g $AgNO_3$ for 30 min followed by the addition of 15 ml distilled

water. Then an aqueous solution of $NaBH_4$ (5 ml, 3.35×10^{-3} M) is added dropwise as a reducing agent at a speed of 1 ml/minute and stirred for 4 h at room temperature. The color change confirms the formation of AgNPs. The AgNPs-GO nanocomposite is washed and centrifuged at 18000 rpm for 30 min to obtain the final product [21].

2.2　Sonochemical Process

Chitosan can be reinforced with graphene oxide nanosheets (GOns) synthesized by the modified Hummer's method to improve the mechanical strength and stability while with the AgNP to improve the antimicrobial properties of the nanocomposite. 1 g of the graphite powder and 0.5 g $NaNO_3$ are continuously stirred in 23 ml of conc. H_2SO_4 for 1 h. After that 3 g of $KMnO_4$ is added and stirred for about 2-3 h for complete oxidation followed by the addition of 46 ml of distilled water and stirred for 30 min. Finally, dilution of the product is then done with distilled water and 10 ml of 30% H2O2 solution is added to stop the reaction. The product is then finally washed with 10% conc. HCl to remove metal ions. To prepare AgNP, starch is used as reducing as well as capping agent using silver nitrate ($AgNO_3$) as precursor. For this 1% (w/v) of aqueous soluble starch at 70 °C is stirred with $AgNO_3$ solution and NaOH is added to the reaction mixture. The color change indicates the formation of AgNPs. Nanocomposite with a 1:1 ratio of the GO:Chitosan and 0.01% of AgNP is prepared by magnetic stirring and sonication of the constituents [15].

20 mM of aqueous solution of $AgNO_3$ and 5 mL of an aqueous solution of GO (0.5 mg/mL) is vigorously stirred at room temperature for 48 h. The resulting mixture is centrifuged at 14,000 rpm for 10 min and washed in ultrapure water. The dry GO/AgNPs after the lyophilization is dissolved in ultrapure water and sonicated for 6 h. The exfoliated GO curl into scroll and mainly AgNPs are wrapped into carbon nanoscrolls which are confirmed from the TEM images [22].

Smaller sized AgNP (4 nm) can be prepared with a lower concentration of the silver precursor and at lower temperatures. Chemical method is applied to reduce silver nitrate with ascorbic acid as reducing agent without any stabilizing agent. Silver atoms are formed which agglomerate into oligomeric clusters leading to the formation of colloidal AgNPs. GO is then used to rectify the agglomeration since it possesses abundant oxygenated functional groups which can act as anchoring sites for attaching AgNPs. Modified Hummers method is usually employed to obtain high quality rGO by chemical means. Even though initially mechanical exfoliation method was identified to prepare graphene, this method is used globally to get high quality graphene for various applications. Graphite is oxidized to graphite oxide which is then reduced to get rGO. 6 g of $KMnO_4$ is slowly added to a mixture containing graphite (2 g), H_2SO_4 (50 mL), and $NaNO_3$ (1 g) at 0 °C. After 1 h at 35 °C in a water bath, 100 mL de-ionized water is added slowly and 10 mL of 30% H2O2 is mixed into the solution. The final product is centrifuged, washed repeatedly with water, HCl and deionized water to reach neutral pH. This material is re-dispersed in water which is then subjected to ultrasonication to get single layer graphene. The

rGO-AgNP nanocomposite is synthesized via the in-situ method using L-ascorbic acid (AA) as reducing agent. 0.5 mg/mL of rGO powder in deionized water is added with ammonium hydroxide to attain a pH of 10. Then, 1.5 mM of aqueous $AgNO_3$ solution is added to the dispersion under continuous stirring and heated at 60 °C in an oil bath. An aqueous solution of AA was added at a weight ratio between the AA and $AgNO_3$ of 2.07. GO-AgNP nanocomposite is obtained by the freeze-drying [23].

The GO-Ag nanohybrid composite is prepared by dispersing GO in a solvent dimethyl formamide (DMF). The solution is subjected to sonication for 30 min to which the precursor for silver i.e. $AgNO_3$ is added. DMF is able to serve as a reducing agent as well as a solvent to carry out the reaction. A further sonication for 30 min results in a stable brown colloid solution which is magnetic stirred for 10 h at 60 °C for the complete reduction of $AgNO_3$ [24].

2.3 Green Synthesis

AgNPs prepared by the conventional chemical methods using strong reducing agents like hydrazine and sodium borohydride are poisonous and not environment friendly. A green and low-cost method can be used to synthesis the AgNP/GO nanocomposite using glucose as a reducing and stabilizing agent. This process is versatile and environmentally friendly because it occurs only in the aqueous solution. The final product can be obtained by dispersing the resultant in water or in common organic solvents without the need of any stabilizers such as polymers or surfactants. 15 mg of GO powder in 15 mL of water is subjected to sonication for 1 h. After that 0.75 g glucose is added to this solution under stirring. The precursor for AgNPs is made ready by adding 0.55 mol/L of ammonia and 0.06 mol/L of $AgNO_3$ in the aqueous solution. The final product is mixed with the GO and glucose-containing solution and stirred for 0.5 h. The AgNP/GO nanocomposite is obtained by centrifugation, washed repeatedly and dried [25].

GO prepared using the Hummer and Offeman method is then modified to rGO by the thermal expansion of GO under argon at 1050°C for 30 s followed by hydrogen reduction at 400 °C for 2 h.

50 mg rGO and 50 mg Ag (hexafluoro acetyl acetonato) are pressurized with the $scCO_2$ to 27.6 MPa at 40°C in a 10 ml stainless steel high-pressure reactor for 24 h. Then CO_2 is released and hydrogen is introduced into the reactor. Silver ions are reduced to silver nanoparticles and deposited over the graphene sheets. The $scCO_2$ is an environmentally benign solvent and nontoxic. Also, it possesses low viscosity and surface tension which can increase the production rates of materials [26].

2.4 Two-Step Synthesis

The impregnation of GO in cellulose membrane makes the membrane more porous and also improves the attachment of AgNPs while preventing the leaching of Ag + ions. A slow release of Ag + ions is achieved to get superior antibacterial activity out of this membrane. The synthesis process of hybrid nanocomposite cellulose membrane with GO-Ag NPs involves two steps. In the first step, cellulose membranes containing graphene oxide (GO) is produced in an acid coagulating bath. In the second step, silver nanoparticles (Ag NPs) are in situ synthesized onto the membranes. A transparent cellulose solution is prepared by stirring cotton linter fiber and precooled ($-12\ °C$) aqueous solution of NaOH/urea at room temperature. GO-cellulose solution mixture is then produced and regenerated in acetic acid coagulation bath and the membranes are made. The membrane is then immersed in silver ammonia complex, $Ag(NH_3)^{2+}$ and glucose to get AgNPs under the microwave irradiation. The electrostatic interaction between the positively charged silver ammonia complex and negatively charged oxygenated functional groups of GO enhances the deposition of AgNPs. The amount of Ag NPs with GO is much greater when compared to that of the neat cellulose membrane [27].

3 Antibacterial Tests

Resistance or inhibition against the bacteria could be assessed both qualitatively and quantitatively. Some of the important studies on the antibacterial analysis of Ag and graphene-based nanocomposites were tabulated in Table 2.

Some of the methods mentioned above used for the investigation of bacterial resistance of the GO-Ag based nanocomposites are explained in detail [24].

3.1 Bauer-Kirby Disk Diffusion Method

In general, bacteria exist as colonies which are represented as colony forming units (CFU). The presence of antibiotic hinders the bacterial growth and its colonies. Bauer-Kirby disk diffusion method is also termed as "disc diffusion antibiotic Sensitivity test". In this method, 1×10^5 CFU/ml of a bacterial suspension containing E.coli and S.aureus is spread evenly into the agar culture medium enclosed in a glass container. A disk shaped composite specimen of 10 mm diameter is then placed into the agar medium with bacterial suspension and incubated for 18 h at a temperature of 37 °C. Resistance against the microorganism in inferred through the formation of inhibition zone around the composite specimen. In quantitative terms, diameter of the inhibition zone can be measured.

Table 2 Reported work on the antibacterial studies of graphene and silver nanoparticle-based hybrid composites

Nanocomposite	Type of method	References
Decoration of graphene oxide using silver nanoparticles and copper oxide nanoparticles	Disc-diffusion	[28]
Graphene oxide, silver nanoparticles, graphene oxide/silver nanoparticles	Optical density and plate colony-counting	[29]
Oxalis corniculata leaf extract/silver nanoparticles and Oxalis corniculata leaf extract/silver nanoparticles/graphene oxides	Disc-diffusion	[30]
PLA/graphene oxide- silver nanoparticle;	Disc-diffusion	[17]
Organically modified silicate coatings with reduced graphene oxide/silver nanoparticles	Shaking flask	[31]
Copper oxide/graphene oxide, copper oxide/graphene oxide/silver nanoparticles	Disc-diffusion	[32]
Silver nanoparticle- decorated reduced graphene oxide	Disc-diffusion	[33]
Silver nanoparticles/graphene oxide	Broth micro-dilution	[34]
Graphene oxide, carbon fibre, silver nanoparticles/graphene oxide/carbon fibre	Disc-diffusion	[35]
PVA/graphene oxide/silver nanoparticles	EUCAST dilution method	[18]
Reduced graphene oxide/silver nanoparticles	Resazurin-based Microtitre Dilution Assay	[36]
Silver nanoparticles/graphene oxide	Shaking method	[37]
Reduced graphene oxide/silver nanoparticles	Disc-diffusion	[38]

3.2 Fluorescent-Based Cell Wall/Membrane Integrity Assay

In this method, a disk shaped composite specimen is incubated at 37 °C for 12 h in the agar culture medium with a bacterial suspension containing 1×10^6 CFU/ml of the E.coli and S.aureus. A phosphate-buffered saline was used to rinse the exposed specimen at least thrice. Then, a fluorescent dye kit containing SYTO 9 (green stain) and propidium iodide (red stain) is applied to the incubated composite specimen. When viewed under a fluorescent microscope, live bacterial cells are represented by a green fluorescent stain while the dead bacterial cells with broken cell wall membrane are represented by the red fluorescent stain.

3.3 Reactive Oxygen Species Generation (ROS)

The bacterial cells are cleaned before their exposure to the composite specimen using the method as follows. A bacterial suspension of 1×10^6 CFU/mL is incubated for 30 min at 37 °C in the phosphate-buffered saline containing 20 μm of the 2,7-dichlorofluorescein diacetate. After washing the bacterial cells, it is spread over the composite specimen for 18 h. Presence of ROS is detected by the micro-plate reader.

3.4 Turbidity Test

It is a quantitative method in which the bacterial resistance is represented as inhibition %. A disk shaped composite specimen of 10 mm diameter is immersed in the test tube filled with the broth containing a bacterial suspension of 1×106 CFU/ml and incubated at 37 °C in a rotary shaker between 2 and 6 h. Bacterial inhibition is calculated by the change in the optical density measured using a spectrophotometer at a wavelength of 600 nm with and without the composite in the broth inside the test tube.

Bacterial inhibition $\% = \frac{X_o - X_1}{X_o} \times 100$.

where X_1 is the optical density of the setup with the composite inside the broth after inoculation and X_o is the optical density of the broth medium without the composite before the inoculation.

This method is based on the amount of light absorbed through a suspension of bacteria. The amount of absorbed light is proportional to the turbidity of the medium. It is a rapid and very simple method to measure the bacterial growth. Spectrophotometer or calorimeter can be used to for turbidimetric measurement. If the suspension contains more bacteria very less amount of light can be passed through the suspension. On the other hand, more amount of light passing through the suspension is an indication of less bacterial growth.

4 Bacterial Inhibition of the GO-Ag Based Nanocomposites

As discussed above, researchers have used both the qualitative and quantitative methods to assess the bacterial resistance of the Ag-GO based nanocomposites films. Jang et al. demonstrated that GO-Ag solution prepared by sonication and centrifugation process showed resistance to bacterial growth at 4 mg/mL against the gram$^+$ bacteria (S. epidermidis) while it was 63 mg/mL concentration against the gram$^-$ bacteria (P. aeruginosa) [34]. Nguyen et al. examined the effect of rGO-Ag concentration on the bacterial resistance against the B.cereus, S.aureus, E.coli and L.anguillarum. As the concentration of rGO-Ag was increased from 2 to10 μg/mL

in the interval of 2, CFU dropped significantly such that almost no CFU was visible at a concentration of the 10 µg/mL [39].

Bacterial inhibition rate assessed from the turbidity test for the PLA-polyglycolic acid/Ag-GO scaffold against E.coli is shown in Fig. 1. Clearly, GO and AgNP used as standalone reinforcement can promote bacterial resistance in the composite compared to the pure polymer. However, hybrid nanocomposites with Ag-GO showed even better performance and the inhibition rate increased from 70% to nearly 100% by increasing the AgNP concentration from 0.5 to 1 and 1.5 wt.%. larger inhibition zones obtained from the Agar disk diffusion test further confirmed the superior antibacterial activity due to the increasing AgNP in the nanocomposites [26].

Increase in the bactericidal activity for the PLA/Ag-GO nanocomposites up to 7 wt.% Ag against the gram- E.coli and gram + S.aureus was reported by Liu et al. However, the resistance was comparatively lower against the gram + bacteria for
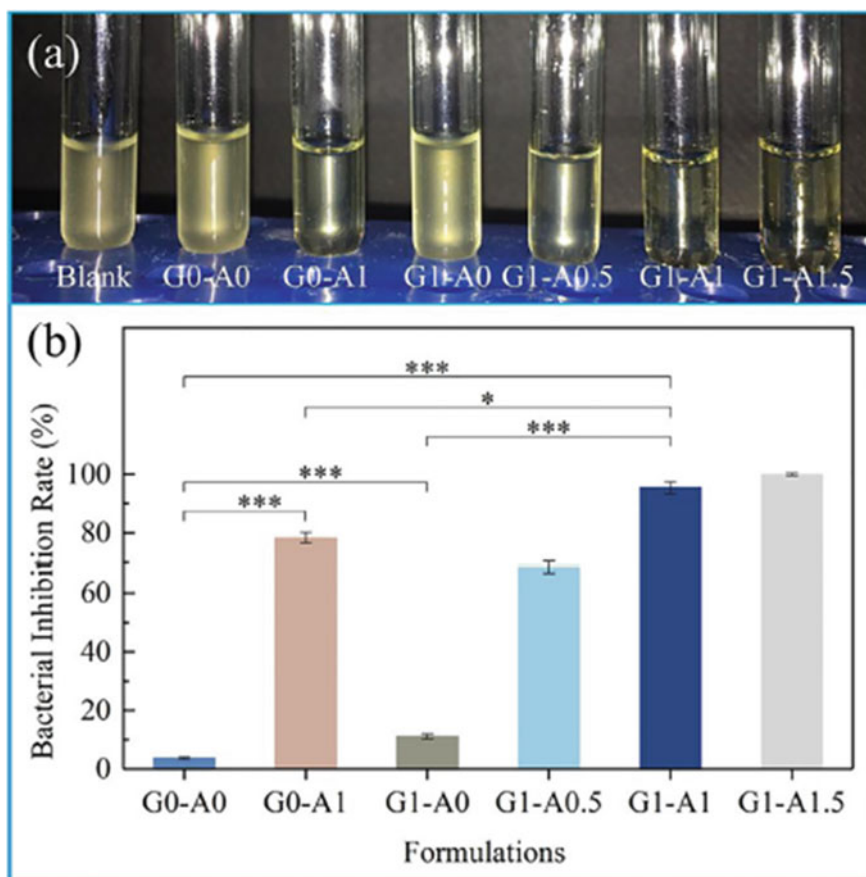
Fig. 1 Bacterial resistance of the PLA-polyglycolic acid/Ag-GO nanocomposites obtained from the turbidity test [26]
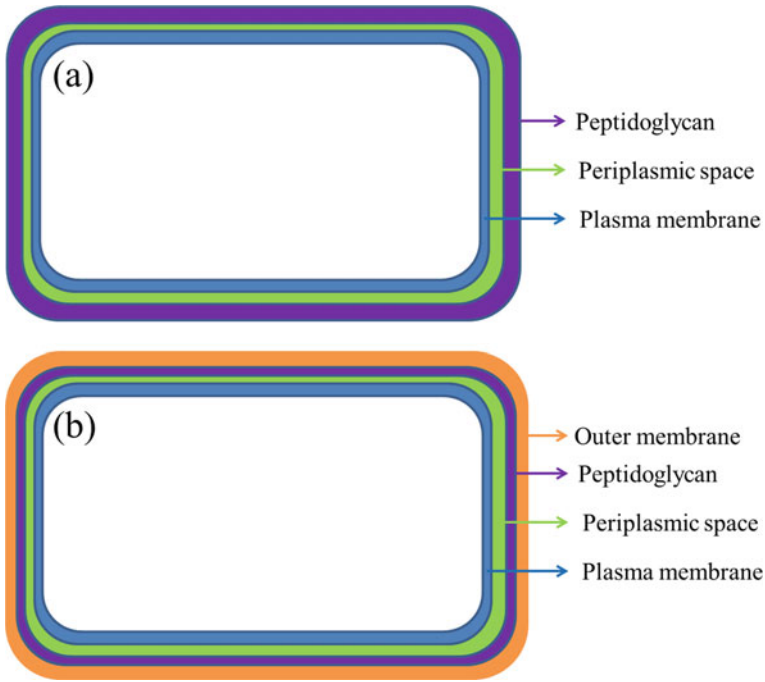
Fig. 2 Morphological difference in the bacterial cell **a** Gram$^+$ bacteria and **b** Gram$^-$ bacteria

similar configuration than against the gram- bacteria [24]. The dissimilarity in bactericidal activity against gram + and gram- bacteria is attributed to the morphological difference in their bacterial cell wall as shown in Fig. 2.

5   Bacterial Inhibition Mechanism

5.1   AgNP

AGNP undergoes oxidation in the presence of oxygen and water thereby releases Ag + ions. Once the Ag + ions comes into contact with the thiol group of the bacterial cell wall, oxidative decomposition occurs which leads to the formation of the reactive oxygen species (ROS) like the hydroxyl group, superoxide ions and hydrogen peroxide [14].

5.2 Graphene and Their Byproducts

According to Cai et al. [40], GO and rGO inhibits bacterial growth due to the inherent sharp edges in their structure which induces physical damage to the bacterial cell wall by piercing them or through their cutting action. In addition to this, other mechanisms identified by various researchers have been compiled by Han et al.: (a) oxidative stress which produces ROS. ROS can cause lipid peroxidation, fragmentation of DNA and decrease in the enzymatic activity within the bacterial cell, (b) Flow of electrons from the bacterial cell to the graphene which has positive charge on its surface can lead to destruction of the cell wall membrane, (c) Encasing and confinement of the bacterial cell with graphene or GO can damage the cell wall membrane and disrupt their functioning, (d) Photo-thermal ablation characteristic of GO in presence of the polythiophenes, goldNP and glycol chitosan which causes thermal decomposition of the bacteria and (e) Graphene interrupts the inter-protein interaction and causes reduction in the metabolism of the bacterial cell [16].

5.3 Synergistic Effect of Graphene and Their By-Products Along with AgNP

The mechanism of the GO-AgNP that provides superior bacterial resistance to the polymer is described in the Fig. 3.

6 Conclusion

In general, silver nanoparticles (AgNP) and graphene and their byproducts such as graphene oxide (GO) and reduced graphene oxide (rGO) were found to have anti-bacterial characteristic and can be used as standalone bactericidal agents. The large surface area of graphene and their by-products allows the functionalization of metallic nanoparticle and metal oxide on its surface. This feature provides an option to obtain a functional hybrid bactericide with enhanced functionalities and physic-chemical properties. Among the various metallic nanoparticles, AgNP being a natural anti-septic has applications in the wound dressing material to prevent infections from the bacterial growth. Studies have shown that AgNP-GO and AgNP-rGO based hybrid nanocomposites have better bacterial inhibition activity than the individual materials. This is mainly due to the synergistic effect of the hybrid Ag-graphene combination. The Ag-GO based hybrid nanocomposites have resistance to both the gram$^+$ and gram$^-$ bacteria. However, hybrid nanocomposites are more effective in curbing the gram$^+$ bacteria. This is specifically due to the morphological difference in the cell wall membrane and composition of the bacteria. Recent studies have
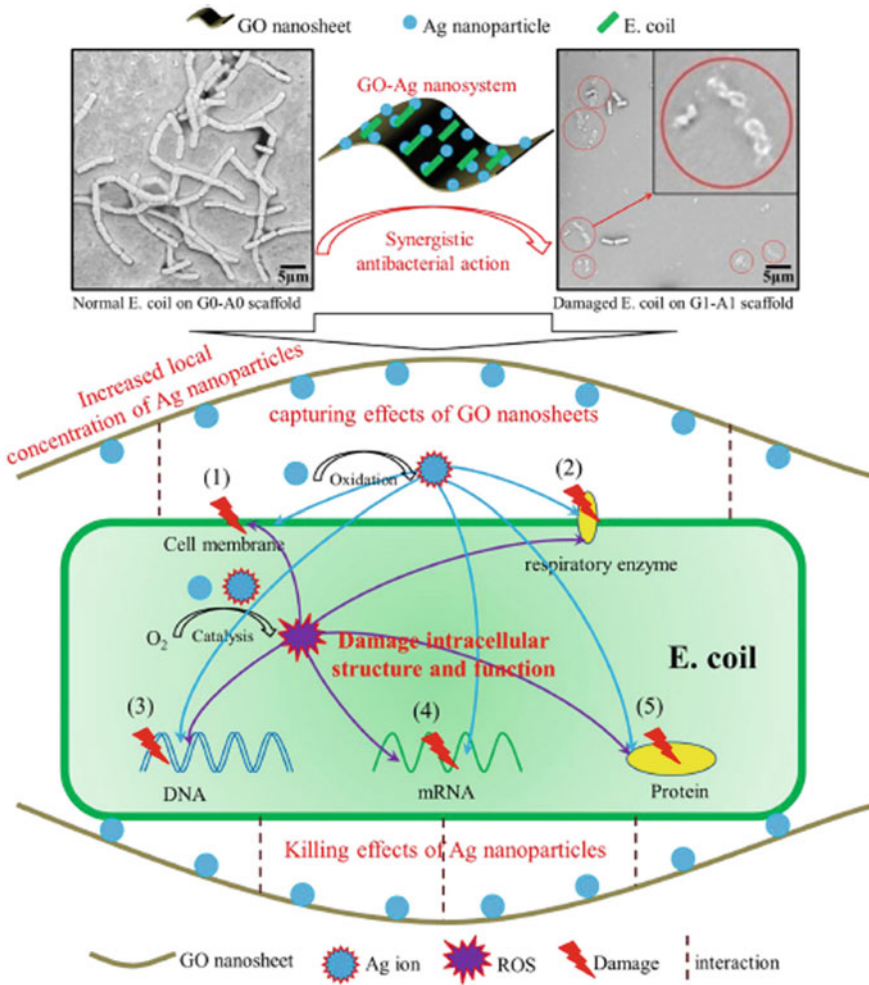
Fig. 3 Synergistic mechanism of GO-AgNP responsible for the bacterial inhibition in the polymer [26]

also shown that addition of quantum dots and iron nanoparticles (FeNP) to the Ag-Graphene combination help to reduce the cytotoxic effects as well imparts electrical conductivity and magnetic properties to the nanocomposites.

References

1. Saraswathi MSSA, Rana D, Alwarappan S, Gowrishankar S, Vijayakumar P, Nagendran A (2019) Polydopamine layered poly (ether imide) ultrafiltration membranes tailored with silver

nanoparticles designed for better permeability, selectivity and antifouling. J Ind Eng Chem 76:141–149

2. Karimi-Maleh H, Fakude CT, Mabuba N, Peleyeju GM, Arotiba OA (2019) The determination of 2-phenylphenol in the presence of 4-chlorophenol using nano-Fe$_3$O$_4$/ionic liquid paste electrode as an electrochemical sensor. J Colloid Interface Sci 554:603–610

3. Bijad M, Karimi-Maleh H, Farsi M, Shahidi S-A (2018) An electrochemical-amplified-platform based on the nanostructure voltammetric sensor for the determination of carmoisine in the presence of tartrazine in dried fruit and soft drink samples. J Food Meas Charact 12(1):634–640

4. Cheraghi S, Taher MA, Karimi-Maleh H (2017) Highly sensitive square wave voltammetric sensor employing CdO/SWCNTs and room temperature ionic liquid for analysis of vanillin and folic acid in food samples. J Food Compos Anal 62:254–259

5. Umasankareswari T, Singh G, Prabha SS, Al-Hashem A, Kumaran SS, Rajendran S (2020) Toxicity of silver and other metallic nanoparticles. In: Nanotoxicity, Elsevier, pp 125–141

6. Stensberg MC, Wei Q, McLamore ES, Porterfield DM, Wei A, Sepúlveda MS (2011) Toxico-logical studies on silver nanoparticles: challenges and opportunities in assessment, monitoring and imaging. Nanomedicine 6(5):879–898

7. Šlouf M et al (2011) Preparation of stable Pd nanoparticles with tunable size for multiple immunolabeling in biomedicine. Mater Lett 65(8):1197–1200

8. Adlim M, Bakar MA, Liew KY, Ismail J (2004) Synthesis of chitosan-stabilized platinum and palladium nanoparticles and their hydrogenation activity. J Mol Catal A Chem 212(1–2):141–149

9. Li J et al (2014) High-sensitivity paracetamol sensor based on Pd/graphene oxide nanocom-posite as an enhanced electrochemical sensing platform. Biosens Bioelectron 54:468–475

10. Sadhukhan S et al (2019) Green synthesis of cadmium oxide decorated reduced graphene oxide nanocomposites and its electrical and antibacterial properties. Mater Sci Eng C 99:696–709

11. ID MP, et al (2019) Antimicrobial properties of poly(propylene) carbonate/Ag nanoparticle-modified tamarind seed polysaccharide with composite films. Ionics (Kiel), pp 3461–3471

12. Thiagamani SMK, Rajini N, Siengchin S, Rajulu AV, Hariram N, Ayrilmis N (2019) Influence of silver nanoparticles on the mechanical, thermal and antimicrobial properties of cellulose-based hybrid nanocomposites. Compos Part B Eng 165:516–525

13. Vu TV, Nguyen-Tri P, Nguyen TH, Nguyen TV, Nguyen TA (2020) Antibacterial nanocom-posite coatings. In: Nanotoxicity, Elsevier, pp 355–364

14. Habiba K et al (2015) Synergistic antibacterial activity of PEGylated silver–graphene quantum dots nanocomposites. Appl Mater Today 1(2):80–87

15. Pounraj S, Somu P, Paul S (2018) Chitosan and graphene oxide hybrid nanocomposite film doped with silver nanoparticles efficiently prevents biofouling. Appl Surf Sci 452:487–497

16. Han W, Wu Z, Li Y, Wang Y (2019) Graphene family nanomaterials (GFNs)—promising materials for antimicrobial coating and film: a review. Chem Eng J 358:1022–1037

17. Bakhsheshi-Rad HR, et al (2020) Co-incorporation of graphene oxide/silver nanoparticle into poly-L-lactic acid fibrous: a route toward the development of cytocompatible and antibacterial coating layer on magnesium implants. Mater Sci Eng C 111: 110812

18. Cobos M, De-La-Pinta I, Quindós G, Fernández MJ, Fernández MD (2020) Synthesis, physical, mechanical and antibacterial properties of nanocomposites based on poly(vinyl alcohol)/graphene oxide-silver nanoparticles. Polymers (Basel) 12:3

19. Ahmad A, Li L, Bao J, Jia X, Xu Y, Guo X (2016) Antibacterial activity of graphene supported FeAg bimetallic nanocomposites. Colloids Surf B Biointerf 143:490–498

20. Mohapatra S, Nguyen TA, Nguyen-Tri P (2018) Noble metal-metal oxide hybrid nanoparticles: Fundamentals and applications, Elsevier

21. Marta B et al (2015) Designing chitosan–silver nanoparticles–graphene oxide nanohybrids with enhanced antibacterial activity against Staphylococcus aureus. Colloids Surfaces a Physicochem Eng Asp 487:113–120

22. Li C et al (2013a) The antifungal activity of graphene oxide–silver nanocomposites. Biomaterials 34(15):3882–3890

23. Cobos M, De-La-Pinta I, Quindós G, Fernández MJ, Fernández MD (2020) Graphene oxide–silver nanoparticle nanohybrids: synthesis, characterization, and antimicrobial properties. Nanomaterials 10(2):376

24. Liu C, Shen J, Yeung KWK, Tjong SC (2017) Development and antibacterial performance of novel polylactic acid-graphene oxide-silver nanoparticle hybrid nanocomposite mats prepared by electrospinning. ACS Biomater Sci Eng 3(3):471–486

25. Li J et al (2013b) Green synthesis of silver nanoparticles–graphene oxide nanocomposite and its application in electrochemical sensing oftryptophan. Biosens Bioelectron 42:198–206

26. Shuai C et al (2018) A graphene oxide-Ag co-dispersing nanosystem: dual synergistic effects on antibacterial activities and mechanical properties of polymer scaffolds. Chem Eng J 347:322–333

27. Chook SW et al (2015) Antibacterial hybrid cellulose–graphene oxide nanocomposite immobilized with silver nanoparticles. RSC Adv 5(33):26263–26268

28. Menazea AA, Ahmed MK (2020) Synthesis and antibacterial activity of graphene oxide decorated by silver and copper oxide nanoparticles. J Mol Struct 1218:128536

29. Huong et al (2020) Optimization of the antibacterial activity of silver nanoparticles-decorated graphene oxide nanocomposites. Synth Met 268:116492

30. Jakhar V, Sharma DK (2020) A sustainable approach for graphene–oxide surface decoration using Oxalis corniculata leaf extract–derived silver nanoparticles: their antibacterial activities and electrochemical sensing. Dalt Trans

31. Liu Z et al (2020) Integrated dual-functional ORMOSIL coatings with AgNPs@ rGO Nanocomposite for Corrosion resistance and Antifouling applications. ACS Sustain. Chem. Eng. 8(17):6786–6797

32. Hajipour P, Bahrami A, Eslami A, Hosseini-Abari A (2020) Chemical bath synthesis of CuO-GO-Ag nanocomposites with enhanced antibacterial properties. J Alloys Compd 821:153456

33. Wu J et al (2020) One-step eco-friendly synthesis of Ag-reduced Graphene Oxide Nanocomposites for Antibiofilm application. J Mater Eng Perform 29(4):2551–2559

34. Jang J, Choi Y, Tanaka M, Choi J (2020) Development of silver/graphene oxide nanocomposites for antibacterial and antibiofilm applications. J Ind Eng Chem 83:46–52

35. Tian H et al (2020) Graphene-based antibacterial films with enhanced mechanical properties. Integr Ferroelectr 206(1):79–86

36. Jose PPA, Kala MS, Joseph AV, Kalarikkal N, Thomas S (2020) Reduced graphene oxide/silver nanohybrid as a multifunctional material for antibacterial, anticancer, and SERS applications. Appl Phys A Mater Sci Process 126(1):1–16

37. Liao J, He S, Guo S, Luan P, Mo L, Li J (2019) Antibacterial Performance of a mussel-inspired Polydopamine-Treated Ag/Graphene Nanocomposite Material. Materials (Basel) 12(20):3360

38. Pratheesya T, Harish S, Navaneethan M, Sohila S, Ramesh R (2019) Enhanced antibacterial and photocatalytic activities of silver nanoparticles anchored reduced graphene oxide nanostructure. Mater. Res Express 6(7):74003

39. Kim B-K, Jo Y-L, Shim J-J (2012) Preparation and antibacterial activity of silver nanoparticles-decorated graphene composites. J. Supercrit. Fluids 72:28–35

40. Cai X et al (2012) The use of polyethyleneimine-modified reduced graphene oxide as a substrate for silver nanoparticles to produce a material with lower cytotoxicity and long-term antibacterial activity. Carbon N. Y. 50(10):3407–3415

Hybrid Nanocomposites Based on Graphene and Gold Nanoparticles: From Preparation to Applications

Aneeya K. Samantara, Rajat K. Tripathy, and J. N. Behera

Abstract Excellent electronic conductivity, large specific surface area, robust chemical as well as thermal stability and interesting physicochemical properties make graphene as a novel material for multimodal applications. On the other hand, the noble metal nanostructures dominant over their bulk counterpart and employed in many of the applications ranging from biomedical to energy for sustainability. Among others, the gold nanoparticles (Au NPs) are well known for their application in sensing, electrocatalysis and etc. However, the hybrid nanocomposite of graphene and Au NP shows better specificity and efficiency which depends on the synthesis methods. This chapter constitutes a brief discussion on the recent reports emphasizing the existed synthesis protocols for graphene, Au NPs, graphene/Au NP composites and their application. This will be an informative chapter for the current researchers and scholars working in the field of nanoscience and nanotechnology.

Keywords Graphene hybrids · Au NPs · Sensors · ORR

1 Introduction

Discovery of graphene is the landmark achievement for the nanoscience and materials sciences representing the stable two dimensional carbon material. It is a thin carbon sheet (~0.35 nm) composed of sp2 hybridized carbon atoms arranged in a honeycomb like structure. It is otherwise known as an important allotropic form of carbon and building blocks for other carbon nanostructures i.e. fullerenes, carbon nanotubes and etc. Individual graphene sheets can be stacked (by means of Van der Waals force of attraction) and form the three dimensional graphite. The pristine graphene possesses excellent properties like high surface area (~2630 m^2/g; nearly six times more than carbon nanotubes), highest electronic conductivity (2×10^5 cm^2 V^{-1} s^{-1}; originated

A. K. Samantara · R. K. Tripathy · J. N. Behera (✉)
National Institute of Science Education and Research (NISER), Khordha, Odisha 752050, India
e-mail: jnbehera@niser.ac.in

Homi Bhabha National Institute, (HBNI), Mumbai, India

from the delocalization of π-electrons), higher Young's modulus (0.1 TPa), better thermal conductivity (~5000 W m^{-1} K^{-1}), extraordinary charge/carrier mobility and chemical inertness. Therefore the scientific community has been motivated to employ graphene in many of the advanced applications ranging from sensing/biomedical application to energy conversion and storage systems demanding its scalable production. In this regard, various synthetic methodologies like chemical vapour deposition, electrochemical/chemical exfoliation, mechanical cleavage, reduction of graphene oxide and etc. have been investigated. Although each of these methods have many advantages and associated with certain limitations. Among them, the oxidation of graphite to form graphene oxide and its reduction to reduced graphene oxide (rGO) presumed to be an efficient method for the salable synthesis of qualitative graphene. This process involves the oxidative cleavage of graphite followed by their reduction (either by chemical of thermal) to reduced graphene oxide. However due to the van der Waals interactions, the reduced graphene sheets inclines to form irreversible agglomerates and even restack to graphitic crystals. Therefore different organic molecules and inorganic particles have been selected to functionalize the surface of graphene sheets. In comparison to the organic entities, the inorganic particles not only prevent the restacking/agglomeration of individual sheets but also lead to the formation of graphene based hybrids showing improved physicochemical properties.

The noble metal nanoparticles received special interest due to their fascinating extraordinary physicochemical properties. But the self-aggregation tendency (due to higher surface charge) of these nanoparticles reduces its surface to volume ratio thereby showing poor performances. To overcome this obstacle, the plausible solution is to anchor the nanoparticles to a suitable substrate. Owing to its extraordinary physicochemical properties, graphene has been selected as a conductive substrate and growth platform for these nanoparticles forming hybrids thereby availing their high surface to volume ratio. Moreover, the oxygenated functionalities of chemically modified graphene (i.e. graphene oxide or reduced graphene oxide) avails abundant number of nucleating sites for the growth of metal nanoparticles. Therefore various methodologies have been formulated for the synthesis of hybrids of graphene with noble metals like Au, Ag, Pd and Pt etc. and explored their application in designing of electrochemical sensors, surface enhanced Raman scattering, catalysis, fuel cell, magnetism, optoelectronics and etc. [19, 21, 23, 30, 35, 41, 52, 58, 74]. In these hybrids, the 2D nano sheets of graphene not only provides an ideal platform to anchor the metal nanostructures but also improves the electrical conductivity as well as the interfacial heat/electron transfer liberated by these adhered nanomaterials restricting the nanoparticle aggregation. Moreover the integration of metal nanoparticles on graphene surface may also bring about new characteristics and properties of the hybrid extending its application in various fields. Specifically, the graphene (RG) hybrids of gold nanoparticles (Au NPs) attracts tremendous attention in fields of electrocatalysis, electro analysis, surface enhance Raman scattering and etc. Therefore various research groups have designed facile synthetic protocols for the scalable preparation of Au NPs/RG hybrids and explored their multidirectional application. In this chapter we are presenting a brief discussion on the synthesis of graphene, Au NPs and Au NPs/RG hybrids. Also a detailed physicochemical property along

with application of the Au NPs/RG hybrids with updated literature is incorporated followed by summary and perspectives in this particular field with updated literature support.

2 Synthesis

2.1 Synthesis of Graphene

Novoselov et al. in 2004 successfully demonstrated the separation of graphene layers (both the single and few layered graphene) from graphite rod using micromechanical cleavage method [45]. This method generates high quality graphene but lacks in scalability. Therefore various research groups throughout the globe have developed different synthetic routes for the preparation of graphene without compromising the quality [44, 48]. Some important methods are mechanical exfoliation, synthesis on SiC surface, bottom-up synthesis from structurally defined organic molecules, chemical vapour deposition (CVD) of molecular precursor, electrochemical exfoliation, liquid exfoliation, ball milling, chemical or thermal reduction of oxidized graphite, unzipping of carbon nanotubes, arc-discharge of graphite and etc. [12, 45, 46, 65, 72]. Owing to poor scalability and higher production costs, the methods like unzipping of nanotubes, mechanical exfoliation, synthesis on SiC and different bottom-up synthesis processes are necessarily restricts the commercial production of graphene. However the CVD technique is widely used for the synthesis of graphene that involves the deposition of hydrocarbons on a suitable metal/semiconducting substrate at higher temperature and inert atmosphere. But the limitations like requirement of high reaction temperature, sophisticated instrumentation added more cost per unit production of graphene. In addition to this, the lower scalability and moderate graphene purity limits the CVD method for industrial graphene synthesis [39]. On the other hand, the liquid exfoliation method is more focused that proceed via two steps as (i) dispersion of pristine/expanded graphite in a suitable solvent to weaken the existing van der Waals forces among individual layers followed by (ii) exfoliation of individual sheets by applying an external driving force like shearing force, electric field and ultra-sonication to make exfoliation [3, 47, 64]. But this method is associated with very low yield leaving behind unexfoliated graphite particles which needs an additional step for separation [47]. However, scalability and cost effectiveness attracts the liquid phase exfoliation method for bulk production of graphene [3].

In addition to this method, the reduction of graphene oxide (GO) is widely employed for the bulk production of graphene. Graphene oxide is the highly oxidized form of graphene that formed by extensive oxidation of graphite powder using strong oxidizing agents. In this regard, various oxidation procedures are been developed and categorized on the basis of oxidizing agent, reaction medium and source of graphite taken [9, 25, 49, 56]. Among them the modified Hummer method is widely followed. In a typical procedure, the graphite powder mixed with concentrated H_2SO_4 followed

by addition of $KMnO_4$ crystals under stirring condition and left to stir for next two hours. Thereafter the reaction mixture is diluted with deionized water and added H_2O_2 till effervescence ceased. The suspension is filtered and washed repeatedly using dilute HCl and deionized water to remove the unreacted $KMnO_4$ and sulphates. The brown colored residues thus collected, lyophilized and stored in dry and cool place for further use. During this oxidation process, the π-π conjugation of graphene gets partially disrupted and developed oxygenated functional groups. From the spectroscopic analysis, it has been well documented that, epoxy and hydroxyl groups are developed on the basal plane whereas the aldehyde, ketone and carboxylic functional groups are developed at the edge sites. Because of the extensive oxidation, the metallic properties of graphite changed and developed semiconducting behavior in GO. Therefore the removal of these functional groups became indispensable to meet the criteria to employ in electronic and other important applications. Out of others, the thermal annealing, hydrothermal, solvothermal methods and chemical reduction processes are employed for the effective reduction of GO [7, 49]. However, in most of the cases, complete removal of these functional groups are not possible thereby the graphene thus obtained is termed as reduced graphene oxide (rGO). The existed residual oxygen moieties improves the hydrophilicity of graphene and avails active centers for the nucleation and growth of metal nanoparticles. Therefore this method of graphene preparation is widely used for preparation of graphene hybrids for targeted applications [8, 50, 55].

2.2 Synthesis of Gold Nanoparticles

Due to the interesting physicochemical properties, gold nanoparticles occupy dominant position among other noble metal nanostructures. However, its broad application demands the exploration of simple, facile and eco-friendly synthesis processes. Therefore various synthetic chemists have designed different methodologies for the preparation of Au NPs of different shapes/sizes with better yield and monodispersity. Spherical gold nanoparticles are synthesized over 2000 years in different media including air, glass, salt matrices, polymers and etc. Thereafter different chemical reducing agents (sodium citrate, plant extracts, ascorbic acid, $NaBH_4$ and etc.) are employed for the synthesis of spherical Au NPs, but the citrate mediated reduction process has a significant importance. This method has been introduced by Turkevitch in 1951 that involves the synthesis of monodisperse spherical Au NPs in aqueous medium. In a standardized method, 95% of chloroauric acid ($HAuCl_4$) solution taken in a round bottom flask and heated to its boiling point. Thereafter 5 ml of sodium citrate solution (1%) added in a drop wise manner under stirring condition and a change in the solution colour from light yellow to greyish-pink is visualized and turned wine red after 5 min. According to the electron microscopic analysis, the Au NPs thus formed are spherical in shape with diameter around 20 nm. Also by changing the reaction time and concentration of sodium citrate solution, variable sized Au NPs are synthesized.

However the shape controlled synthesis of gold nanoparticles with non-spherical surface morphology has been demonstrated successfully from last two decades. This anisotropic growth of Au NPs mainly proceeds through the seed mediated growth mechanism. It is a two-step synthesis process; (i) in the first step, very small, spherical Au NPs (seeds) are synthesized under conditions of high chemical super saturation and (ii) then these seeds are added to a medium containing more gold ions, mild reducing agent and morphology directing agents. The second step proceeds in a mild reducing condition and slower step compared to that of first step (seed preparation). This seed mediated growth is an efficient and popular approach for the synthesis of gold nanorods. In this case, the cationic surfactant micelle (Cetyl trimethylammonium bromide; CTAB) acts as a soft template and plays an important role in directing the nanoparticle growth and colloidal stability. For instance, Murphy's group have synthesized the Au nanorods following a multistep seeding process [26]. At first the selective reduction of Au(III) to Au(I) has been performed by adding ascorbic acid (a mild reducing agent) to an aqueous CTAB solution of HAuCl$_4$. Thereafter the Au seed solution is added to the growth medium that catalyses the reduction of Au(I) on their surfaces. By tuning the reaction conditions and seeding process, Au nanorods with aspect ratio 4.6 to 18 have been prepared. On increasing the pH, concentration of surfactant and addition of extra halide ions directed the formation of planar nanostructures [2, 20]. For instance, following a three step growth of citrated capped Au seeds in a solution of HAuCl$_4$, CTAB and NaOH, Mirkin et al. have prepared trigonal Au nano prisms with 65% yield [40]. The edge length of nano prisms are about 144 and 8 nm thickness. Thereafter different synthesis approaches have been explored for the preparation of branched Au NPs, nano needles, nano sheets, platonic like morphology (cubes, octahedra, peanuts, faceted spheres etc.) and etc. [26, 27, 32, 51].

2.3 Synthesis of Graphene/Gold Nanoparticle Hybrids

Several methods have been formulated for the synthesis of Au NPs/graphene hybrid. Among them the chemical reduction, electrochemical deposition, photochemical reduction, pulsed laser ablation, thermal reduction, sonochemical reduction, microwave irradiation methods are well documented [1, 16, 24, 28]. The UV–visible spectroscopy is employed to identify the formation of Au NPs as well as the effective reduction of graphene oxide to reduced graphene oxide in the hybrid. Generally graphene oxide shows two absorption bands at 231 and 300 nm assigned to the π-π* and n-π* electronic transitions. However, a red shift in the absorption maxima from 231 to 267 nm has been realized in case of rGO, which may be due to the removal of oxygen functionalities and restoration of conjugated system. Further the formation of Au NPs on the graphene sheet in the hybrid can be identified from the surface plasmon resonance band at 530 nm and shows a red or blue shift depending upon the particle size [6]. The chemical reduction process is a facile and

less time consuming method that proceeds via three different steps as (i) adsorption/reduction, (ii) nucleation and (iii) growth. Here, a stable dispersion of graphene oxide are prepared either in water or in a polar organic solvent (generally ethanol) and allowed to mix with the metal precursor (i.e. $HAuCl_4$) in presence of a suitable reducing agent. Generally, hydrazine hydrate, oleylamine, sodium borohydride, sodium citrate, ascorbic acid and glucose are used as reducing agents for the hybrid preparation [38, 42, 69]. The positively charged metal ions adsorbed onto the oxygen functionalities present on the surface of graphene oxide or reduced graphene oxide by means of electrostatic interactions followed by the reduction with aid of reducing agent and subsequent growth of nanoparticles. During the course of reaction, both the metal precursor and graphene oxide get reduced simultaneously forming the Au NPs/rGO hybrid [15]. Interestingly, the density of Au NPs on the rGO surface in the hybrid can be easily tuned by manipulating the amount of oxygen functionalities present on the graphene oxide surface. The Au NPs/rGO hybrid synthesis through chemical reduction method is an easy process; however in this method it is not possible to control the shape/size and morphology of the nanoparticles. Therefore in many instances, larger sized nanoparticles get developed onto the reduced graphene surface [75]. In order to tackle this, various chelating ligands and molecules are added to the reaction medium that control the growth of the nanoparticle and form stabilize it on the rGO surface. For instance, Wang et al. have synthesized Au NPs/rGO hybrid by using $NaBH_4$ as reducing agent in presence of poly (diallyldimethylammonium chloride) (PDDA) cation in aqueous medium [62]. Here the PDDA acts as a linker that stabilizes and controls the growth of the Au NPs on the surface of rGO preventing their accumulation. In another work, Dong et al. have developed an in situ chemical reduction method for the preparation of Au NPs/rGO hybrid using hydrazine hydrate and sodium dodecyl sulphate (SDS) [10]. The use of SDS not only improved the hydrophilicity of the hybrid but also restricted the rGO sheets from restacking. Therefore a stable suspension of Au NPs/rGO hybrid has been obtained. Similarly a uniform distribution of Au nanoparticles (20 nm size) on a rippled graphene is obtained using sodium citrate as reducing agent in aqueous medium [17]. Numerous reports are available on the synthesis of Au NPs/rGO hybrid by using hydrazine hydrate and $NaBH_4$ as reducing agent; however the toxic nature of these reducing agents restricts the application of hybrids in biomedical applications. Thereafter much more effort have been devoted and various green reducing agents (glucose, plant extracts, ethanol, ethylene glycol, dopamine and etc.) are explored (Fu et al. 2010; [14, 29, 37]. The Au NPs/graphene hybrid are also been prepared by simple mixing the gold precursor ($HAuCl_4^-$) with aqueous suspension of graphene oxide in ambient reaction conditions without using any chemical reducing agents [22]. Here the oxygen functionalities played a vital role as redox centers for the reduction and growth of Au nanoparticles.

Seed mediated growth is another effective approach for the synthesis of larger sized nanoparticles (up to 300 nm) for targeted applications. Initially, smaller sized nanoparticles are prepared using chemical reduction method and employed as seeds for subsequent growth. By using 2-mercaptosuccinic acid as the reducing agent, Niu et al. for the first time synthesized Au NPs up to size 30–150 nm [43]. Following this

innovative approach, Sidorov et al. in 2012 have synthesized graphene hybrids of Au nanoparticles and nanorods [54]. At first, highly oriented graphene is deposited onto Si/SiO$_2$ surface; functionalized with (aminopropyl) trimethoxysilane (APTS) followed by growing Au nanoparticles by seed mediated method. In this process the authors were able to grow both the Au nanoparticles (605 ± 298 nm) and nanorods (30–40 nm) on graphene surface.

The electrochemical reduction method is also widely adopted for the synthesis of Au NPs/graphene hybrids [59, 63, 76]. In this method, on application of an optimized potential, the Au NPs/rGO hybrid with higher purity can be synthesized. It is a less time consuming and facile method with excellent reproducibility. Furthermore, the surface morphology as well as size of the Au nanoparticles can be easily controlled by tuning the reaction time and precursor concentrations. The electrochemical reduction method proceeds through three different steps as (i) assembling of graphene/rGO on the conductive electrode surface, (ii) immersion of the electrode into the electrolyte containing the metal precursor and (iii) application of potential. At first, the working electrode is prepared either by drop casting the graphene/rGO onto the electrode surface (glassy carbon, indium tin oxide coated glass electrode etc.) or by electrodepositing graphene onto it [57]. After that the electrode gets immersed into the electrolyte (either aqueous or ionic liquid) containing metal salt (generally HAuCl$_4$). On application of an optimized potential, the Au^{3+} ions get reduced and deposited onto the rGO/graphene that already on the working electrode surface forming the Au NPs/rGO hybrid [13].

However, the photoreduction method is one of the greener process (excludes the use of chemical reducing agents) for the synthesis of small sized, stable and homogeneous Au NPs on graphene surface. It's a very simple method involving the exposure of the dispersion containing graphene oxide or photo reduced graphene oxide and metal precursor. For example, Huang et al. have synthesized octadecanethiol capped Au NPs/rGO hybrid following the photoreduction method [24]. At first, a uniform dispersion of rGO (photo reduced GO) in ethanol containing HAuCl$_4$ and 1-octadecanethiol is prepared using sonication. On exposing the dispersed solution to xenon lamp (for 2 min), Au NPs of an average size 1.2 ± 0.3 nm are prepared and deposited onto the rGO surface. The uniform and fast heating characteristics enables the microwave irradiation technique for the synthesis of uniform, stable and small sized gold nanoparticle compared to other conventional methods. Here the rapid transformation of microwave energy to heat energy facilitate the simultaneous reduction of graphene oxide and gold precursor forming Au NPs/rGO hybrid [21]. Berry and co-worker have synthesized dispersible Au NPs on the rGO surface without using the capping agent. A uniformly dispersed Au NPs/rGO hybrids has been obtained by exposing the aqueous dispersion of graphene oxide and HAuCl$_4$ to microwave irradiation for only two minute (Fig. 1). In this case, the oxygen functionalities of graphene oxide act as stabilizer, which stabilizes the metal nuclei during the course of reduction process [28]. In absence of graphene oxide, agglomeration of Au NPs takes place in the aqueous reaction medium forming larger particles.
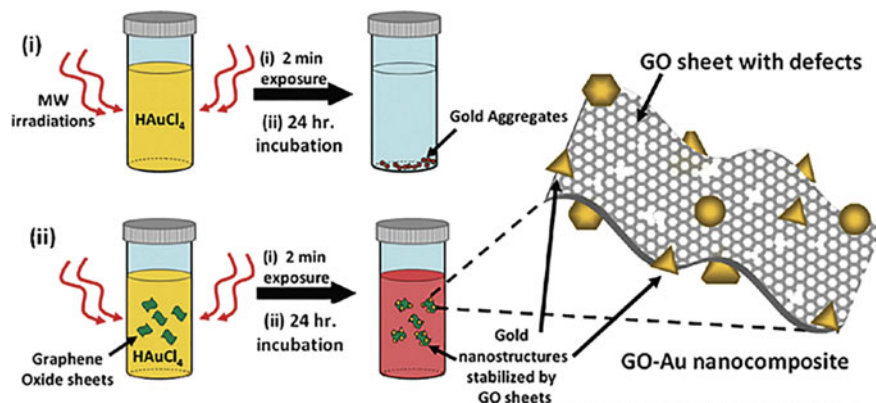
Fig. 1 (i) Aggregation of Au particles when Au salt solution is subjected to microwave irradiation in absence of GO, (ii) Formation of Au NPs on GO sheets under microwave irradiation. Reprinted with permission from [28]

3 Electrochemical Applications

Sensing

Gold nanoparticles are having strong adsorption ability, better electrical conductivity, excellent compatibility and are capable to avail appropriate microenvironment for the immobilization of various molecules and entities. On the other hand, the two dimensional structure, excellent electrical/thermal conductivity, higher surface area and chemical inertness of graphene/reduced graphene oxide make it a suitable support material to adhere or to nucleate various metal nanoparticles especially Au NPs. Interestingly the combined benefits of both the components (Au NPs and rGO) are achieved in the Au NP/rGO hybrid nanostructure thereby motivating to employ in many applications ranging from sensing to energy conversion/storage systems. Moreover, the higher selectivity, better specificity and biocompatibility facilitate the Au NPs to develop electrochemical sensors for the detection of wide range of analytes (i.e. biomolecules, metal ions, inorganic compounds and etc.). For example, Zhang et al. have synthesized Au/rGO hybrid through in situ redox reaction between $AuCl_4^-$ and graphene oxide and explored its sensing performance towards the detection of H_2O_2 in food [70]. The sensing efficiency of the hybrid was monitored by the reduction of H_2O_2 in a buffer solution (pH 5.8) with better reproducibility and storage stability. The Au NP/rGO casted glassy carbon surface was integrated with thionine catalase conjugates and used as active working electrode for the detection process. Under optimal conditions, the hybrid electrode shows a dynamic response in a range of 0.1 μM to 2.3 mM (towards H_2O_2) with a limit of detection of 0.01 μM at 3 s. The accessibility to the analytes and stability in biological environment has also been improved by immobilizing hydrophilic Au NPs onto the graphene surface. Therefore the surface of pristine Au NPs are subjected to functionalized and grown in situ onto

the graphene surface. In a particular work, using sodium citrate as reducing agent, the carboxylate functionalized Au NPs are in situ immobilized onto the graphene surface thereby generating Au NPs/graphene hybrid (Chen et al. 2011). Further the selectivity and sensitivity for the detection of glucose has been improvised attaching glucose oxidase (GOD) to it. The GOD has been covalently bound through condensation reaction among the terminal amine group of lysine residues of GOD and carboxylic group of Au NPs/graphene hybrid. The final Au NPs/graphene/GOD shows excellent performance for the detection of glucose in human blood with 80% initial signal retention after four month storage (at 4 °C). Not only the carbohydrates, but also various amino acids, DNA and specific sequences of DNA are detected using Au NPs/graphene hybrid electrode [5, 11, 34]. In another work, a multilayer film electrode was made by layer by layer deposition of polymer functionalized graphene and polyamidoamine dendrimer functionalized Au NPs [67]. The electrode shows excellent sensing activity of dopamine between 1 and 60 mM with a detection limit of 0.02 mM. The oxygenated functionalities at the edge sites of rGO and synergistic effect of Au NPs with rGO in the Au NPs/rGO hybrid are acting as active reaction sites enhancing the electron transfer between enzymes and electrode surface. Therefore the Au NPs/rGO hybrids are employed for the electrochemical detection of various enzymes and co-enzymes. For instance, the Au NPs/rGO hybrid electrodes are used for the detection of β-nicotinamide adenine dinucleotide (β-NADH; a coenzyme involved in the redox reactions of the cellular respiration) by means of catalytic oxidation at an appropriate potential [4]. The electrochemical detection of analytes is also well documented by using Au NPs/graphene hybrids modified electrodes with self-assembled monolayers. This technique provides better electronic conductivity and excellent adhesion of the hybrid onto the electrode surface thereby improving the repeatability as well as sensitivity of the sensing process. Shi et al. have prepared a three dimensional Au NP/graphene hybrid on self-assembled monolayer (of 4-aminothiophenol) modified gold film following a hydrothermal method (at 10 °C for 6 h) [53]. The 3D electrode possess significantly large accessible surface area, higher stability, better electrical conductivity and excellent substrate binding strength. It shows an impressive sensing performance for the detection of Hg^{2+} with an ultralow detection limit of 50 aM with a wide linear range of 0.1 fM to 0.1 μM even in real water sample. These results suggested that, the Au NPs/graphene hybrid have potential in analytical and bioanalytical application. But there is much more work to do prior to the commercial development of the hybrid based materials and their property improvement including detection sensitivity, specificity, selectivity, storage stability and so on. Furthermore, more work on the determination of biocompatibility of the hybrid material is need to explore for in vivo implementation.

Electrocatalysis

Fuel cell is assumed as the one and only efficient technology to substitute the traditional fossil fuel and its efficiency strongly depends on the catalyst material. Generally platinum is considered as the most suitable material to be employ as electrocatalyst for fuel cells that catalyze the cathodic half cell (oxygen reduction reaction; ORR) at lower overpotential with maximum efficiency. However the high cost and limited

reserve demand an exploration of a substitute. Compared to other noble metals, Au gathers more attention due to its higher electrocatalytic activity in both the oxidation and reduction reactions and excellent methanol/carbon monoxide tolerance. Further Au is one of the inert metal in its bulk and catalyze efficiently on reducing their size to nano scale. Many reports portrays the excellent ORR catalytic behavior of Au NPs when their size reduced to 2 nm. Unfortunately the self-aggregation, dissolution and destruction during the catalytic process strictly reduce the catalytic efficiency and lifetime of the device [61]. After many trials, using graphene as the support material Au NPs hybrids have been developed and successfully demonstrated the electrocatalytic performances along with better durability. In these cases, graphene not only acts as a conducting support but also tightly immobilize the Au NPs on its surface prohibiting the aggregation thereby improving the electrocatalytic efficiency [31, 36]. Chen et al. have prepared Au NPs/rGO hybrid by simultaneous reduction of Au^{3+} and graphene oxide on a glassy carbon electrode and observed an excellent ORR activity [18]. The hybrid electrode shows pronounced electrocatalytic ORR activity with onset potential at 0.12 V (vs. Ag/AgCl) and reduction potential at -0.06 V in 0.1 M H2SO$_4$ medium. However the catalytic performance observed to be improved by tuning the shape and morphology of the Au NPs. Therefore by manipulating the reaction conditions and varying the precursors various Au NPs/graphene hybrids were designed and explored their electrocatalytic performances. As discussed in the above section, GO/rGO acts as a reducing agent and avails active sites for the nucleation and growth of metallic nanoparticles. Therefore by simply adding the metal precursor ($HAuCl_4$) to the rGO suspension followed by ultrasonication and stirring, the hybrids of Au NPs/rGO are prepared [68]. The hybrid showed an impressive electrocatalytic ORR activity comparable to that of Pt based catalysts. In another work, following similar methodology, Xu's group have synthesized Au nanodendrite/GO hybrid avoiding the use of any additional surfactants and reducing agents [33]. The as prepared hybrid catalyze the ORR by following a four electron path with superior stability and methanol tolerance compared to the commercial Pt/C. Not only the Au NPs but also the graphene hybrids of Au nanoclusters are well documented towards ORR catalytic activity. For example, uniformly distributed Au nanocluster/rGO hybrid prepared by using citric acid reducing agent shows excellent electrocatalytic behavior for ORR [66]. Moreover the hybrid shows better durability and methanol tolerance compared to the commercial Pt/C. Additionally the Au NPs/graphene hybrids shows better catalytic activities for the reduction of many more inorganic molecules like NO_2, CO_2, 4-nitro phenol and etc. [60, 71, 73].

4 Conclusion

This chapter presents insights into various methods used for homogeneous decoration of Au NPs on graphene/rGO surface forming Au NPs/rGO hybrids. The strong adhesion of the Au NPs onto graphene surface facilitate the charge transfer process, make the Au NPs to avail more exposed metallic sites for catalysis and restricts

from self-degradation during the electrochemical processes. Moreover, the these hybrids have attracted considerable attention due to their excellent physicochemical properties and thereby employed in many of the advanced applications like detection of biomolecules, hazardous metallic ions and as active electrocatalysts in fuel cells. Additionally, the selectivity and specificity of the Au NPs and conductive of 2D graphene surface synergistically improves the sensing performance of the hybrid material. Although numerous synthetic methods for the preparation of these graphene based hybrids are reported to the date, but still more economic and facile methodologies are need to explore to address their commercial application.

References

1. Adhikari B, Biswas A, Banerjee A (2012) Graphene Oxide-Based Supramolecular Hydrogels for Making Nanohybrid Systems with Au Nanoparticles. Langmuir 28:1460–1469. https://doi.org/10.1021/la203498j
2. Busbee BD, Obare SO, Murphy CJ (2003) An Improved Synthesis of High-Aspect-Ratio Gold Nanorods. Adv. Mater. 15:414–416. https://doi.org/10.1002/adma.200390095
3. Cai M, Thorpe D, Adamson DH, Schniepp HC (2012) Methods of graphite exfoliation. J. Mater. Chem. 22:24992–25002. https://doi.org/10.1039/C2JM34517J
4. Chang H, Wu X, Wu C, Chen Y, Jiang H, Wang X (2011) Catalytic oxidation and determination of β-NADH using self-assembly hybrid of gold nanoparticles and graphene. Analyst 136:2735–2740. https://doi.org/10.1039/C1AN15197E
5. Chen Y, Jiang B, Xiang Y, Chai Y, Yuan R (2011) Target recycling amplification for sensitive and label-free impedimetric genosensing based on hairpin DNA and graphene/Au nanocomposites. Chem. Commun. 47:12798–12800. https://doi.org/10.1039/C1CC14902D
6. Chen Y, Li Y, Sun D, Tian D, Zhang J, Zhu J-J (2011) Fabrication of gold nanoparticles on bilayer graphene for glucose electrochemical biosensing. J. Mater. Chem. 21:7604–7611. https://doi.org/10.1039/C1JM10293A
7. Choucair M, Thordarson P, Stride JA (2009) Gram-scale production of graphene based on solvothermal synthesis and sonication. Nat. Nanotechnol. 4:30–33. https://doi.org/10.1038/nnano.2008.365
8. Das JK, Samantara AK, Sree Raj KA, Rout CS, Behera JN (2019) Synthesis of Ge4Se9 nano plates and a reduced graphene oxide composite of Ge4Se9 for electrochemical energy storage application. Dalt Trans 48:15955–15961. https://doi.org/10.1039/c9dt03351c
9. Dikin DA, Stankovich S, Zimney EJ, Piner RD, Dommett GHB, Evmenenko G, Nguyen ST, Ruoff RS (2007) Preparation and characterization of graphene oxide paper. Nature 448:457–460. https://doi.org/10.1038/nature06016
10. Dong X, Huang W, Chen P (2010) In Situ Synthesis of Reduced Graphene Oxide and Gold Nanocomposites for Nanoelectronics and Biosensing. Nanoscale Res Lett 6:60. https://doi.org/10.1007/s11671-010-9806-8
11. Du Y, Guo S, Dong S, Wang E (2011) An integrated sensing system for detection of DNA using new parallel-motif DNA triplex system and graphene–mesoporous silica–gold nanoparticle hybrids. Biomaterials 32:8584–8592. https://doi.org/10.1016/j.biomaterials.2011.07.091

12. Forbeaux I, Themlin J-M, Debever J-M (1998) Heteroepitaxial graphite on $6H\ensuremath{-}\mathrm{SiC}(0001):$ Interface formation through conduction-band electronic structure. Phys. Rev. B 58:16396–16406. https://doi.org/10.1103/PhysRevB.58.16396

13. Fu C, Kuang Y, Huang Z, Wang X, Du N, Chen J, Zhou H (2010) Electrochemical co-reduction synthesis of graphene/Au nanocomposites in ionic liquid and their electrochemical activity. Chem. Phys. Lett. 499:250–253. https://doi.org/10.1016/j.cplett.2010.09.055

14. Fu X, Bei F, Wang X, O'Brien S, Lombardi JR (2010) Excitation profile of surface-enhanced Raman scattering in graphene–metal nanoparticle based derivatives. Nanoscale 2:1461–1466. https://doi.org/10.1039/C0NR00135J

15. Gao W, Alemany LB, Ci L, Ajayan PM (2009) New insights into the structure and reduction of graphite oxide. Nat. Chem. 1:403–408. https://doi.org/10.1038/nchem.281

16. Gattass RR, Mazur E (2008) Femtosecond laser micromachining in transparent materials. Nat. Photonics 2:219–225. https://doi.org/10.1038/nphoton.2008.47

17. Goncalves G, Marques PAAP, Granadeiro CM, Nogueira HIS, Singh MK, Grácio J (2009) Surface Modification of Graphene Nanosheets with Gold Nanoparticles: The Role of Oxygen Moieties at Graphene Surface on Gold Nucleation and Growth. Chem. Mater. 21:4796–4802. https://doi.org/10.1021/cm901052s

18. Govindhan M, Chen A (2015) Simultaneous synthesis of gold nanoparticle/graphene nanocomposite for enhanced oxygen reduction reaction. J. Power Sources 274:928–936. https://doi.org/10.1016/j.jpowsour.2014.10.115

19. Guo S, Dong S, Wang E (2010) Three-Dimensional Pt-on-Pd Bimetallic Nanodendrites Supported on Graphene Nanosheet: Facile Synthesis and Used as an Advanced Nano-electrocatalyst for Methanol Oxidation. ACS Nano 4:547–555. https://doi.org/10.1021/nn9014483

20. Ha TH, Koo H-J, Chung BH (2007) Shape-Controlled Syntheses of Gold Nanoprisms and Nanorods Influenced by Specific Adsorption of Halide Ions. J. Phys. Chem. C 111:1123–1130. https://doi.org/10.1021/jp066454l

21. Hassan HMA, Abdelsayed V, Khder AERS, AbouZeid KM, Terner J, El-Shall MS, Al-Resayes SI, El-Azhary AA (2009) Microwave synthesis of graphene sheets supporting metal nanocrystals in aqueous and organic media. J. Mater. Chem. 19:3832–3837. https://doi.org/10.1039/B906253J

22. He YQ, Zhang NN, Liu Y, Gao JP, Yi MC, Gong QJ, Qiu HX (2012) Facile synthesis and excellent catalytic activity of gold nanoparticles on graphene oxide. Chinese Chem. Lett. 23:41–44. https://doi.org/10.1016/j.cclet.2011.10.005

23. Huang X, Li S, Huang Y, Wu S, Zhou X, Li S, Gan CL, Boey F, Mirkin CA, Zhang H (2011) Synthesis of hexagonal close-packed gold nanostructures. Nat. Commun. 2:292. https://doi.org/10.1038/ncomms1291

24. Huang X, Zhou X, Wu S, Wei Y, Qi X, Zhang J, Boey F, Zhang H (2010) Reduced Graphene Oxide-Templated Photochemical Synthesis and in situ Assembly of Au Nanodots to Orderly Patterned Au Nanodot Chains. Small 6:513–516. https://doi.org/10.1002/smll.200902001

25. Hummers WS, Offeman RE (1958) Preparation of Graphitic Oxide. J. Am. Chem. Soc. 80:1339. https://doi.org/10.1021/ja01539a017

26. Jana NR, Gearheart L, Murphy CJ (2001a) Wet Chemical Synthesis of High Aspect Ratio Cylindrical Gold Nanorods. J. Phys. Chem. B 105:4065–4067. https://doi.org/10.1021/jp0107964

27. Jana NR, Gearheart L, Murphy CJ (2001b) Seed-Mediated Growth Approach for Shape-Controlled Synthesis of Spheroidal and Rod-like Gold Nanoparticles Using a Surfactant Template. Adv. Mater. 13:1389–1393. https://doi.org/10.1002/1521-4095(200109)13:18%3c1389::AID-ADMA1389%3e3.0.CO;2-F

28. Jasuja K, Linn J, Melton S, Berry V (2010) Microwave-Reduced Uncapped Metal Nanoparticles on Graphene: Tuning Catalytic, Electrical, and Raman Properties. J. Phys. Chem. Lett. 1:1853–1860. https://doi.org/10.1021/jz100580x

29. Jeon EK, Seo E, Lee E, Lee W, Um M-K, Kim B-S (2013) Mussel-inspired green synthesis of silver nanoparticles on graphene oxide nanosheets for enhanced catalytic applications. Chem. Commun. 49:3392–3394. https://doi.org/10.1039/C3CC00115F

30. Kamat PV (2002) Photophysical, Photochemical and Photocatalytic Aspects of Metal Nanoparticles. J. Phys. Chem. B 106:7729–7744. https://doi.org/10.1021/jp0209289

31. Kim S-S, Kim Y-R, Chung TD, Sohn B-H (2014) Tunable Decoration of Reduced Graphene Oxide with Au Nanoparticles for the Oxygen Reduction Reaction. Adv. Funct. Mater. 24:2764–2771. https://doi.org/10.1002/adfm.201303968

32. Kou X, Zhang S, Yang Z, Tsung C-K, Stucky GD, Sun L, Wang J, Yan C (2007) Glutathione- and Cysteine-Induced Transverse Overgrowth on Gold Nanorods. J. Am. Chem. Soc. 129:6402–6404. https://doi.org/10.1021/ja0710508

33. Li X-R, Li X-L, Xu M-C, Xu J-J, Chen H-Y (2014) Gold nanodendrities on graphene oxide nanosheets for oxygen reduction reaction. J. Mater. Chem. A 2:1697–1703. https://doi.org/10.1039/C3TA14276K

34. Liang J, Chen Z, Guo L, Li L (2011) Electrochemical sensing of l-histidine based on structure-switching DNAzymes and gold nanoparticle–graphene nanosheet composites. Chem. Commun. 47:5476–5478. https://doi.org/10.1039/C1CC10965K

35. Lightcap IV, Kosel TH, Kamat PV (2010) Anchoring Semiconductor and Metal Nanoparticles on a Two-Dimensional Catalyst Mat. Storing and Shuttling Electrons with Reduced Graphene Oxide. Nano Lett. 10:577–583. https://doi.org/10.1021/nl9035109

36. Lim D-H, Wilcox J (2012) Mechanisms of the Oxygen Reduction Reaction on Defective Graphene-Supported Pt Nanoparticles from First-Principles. J. Phys. Chem. C 116:3653–3660. https://doi.org/10.1021/jp210796e

37. Liu J, Hu C, Xu J, Jiang F, Chen F (2014) Enhanced photocatalytic performance of partially reduced graphene oxide under simulated solar light through loading gold nanoparticles. Mater. Lett. 134:134–137. https://doi.org/10.1016/j.matlet.2014.07.097

38. Majumder S, Satpati B, Kumar S, Banerjee S (2018) Multifunctional Reduced Graphene Oxide Wrapped Circular Au Nanoplatelets: Enhanced Photoluminescence, Excellent Surface-Enhanced Raman Scattering, Photocatalytic Water Splitting, and Non-Enzymatic Biosensor. ACS Appl. Nano Mater. 1:3945–3955. https://doi.org/10.1021/acsanm.8b00730

39. Miller, J.R., Outlaw, R.A., Holloway, B.C., 2010. Graphene Double-Layer Capacitor with ac Line-Filtering Performance. Science (80-.). 329, 1637 LP – 1639. doi:https://doi.org/10.1126/science.1194372

40. Millstone JE, Park S, Shuford KL, Qin L, Schatz GC, Mirkin CA (2005) Observation of a Quadrupole Plasmon Mode for a Colloidal Solution of Gold Nanoprisms. J. Am. Chem. Soc. 127:5312–5313. https://doi.org/10.1021/ja043245a

41. Murphy CJ, Sau TK, Gole AM, Orendorff CJ, Gao J, Gou L, Hunyadi SE, Li T (2005) Anisotropic Metal Nanoparticles: Synthesis, Assembly, and Optical Applications. J. Phys. Chem. B 109:13857–13870. https://doi.org/10.1021/jp0516846

42. Muszynski R, Seger B, Kamat PV (2008) Decorating Graphene Sheets with Gold Nanoparticles. J. Phys. Chem. C 112:5263–5266. https://doi.org/10.1021/jp800977b

43. Niu J, Zhu T, Liu Z (2007) One-step seed-mediated growth of 30–150 nm quasispherical gold nanoparticles with 2-mercaptosuccinic acid as a new reducing agent. Nanotechnology 18:325607. https://doi.org/10.1088/0957-4484/18/32/325607

44. Novoselov KS, Fal′ko VI, Colombo L, Gellert PR, Schwab MG, Kim K (2012) A roadmap for graphene. Nature 490:192–200. https://doi.org/10.1038/nature11458

45. Novoselov, K.S., Geim, A.K., Morozov, S. V, Jiang, D., Zhang, Y., Dubonos, S. V, Grigorieva, I. V, Firsov, A.A., 2004. Electric field in atomically thin carbon films. Science (80-.). 306, 666–669. doi:https://doi.org/10.1126/science.1102896

46. Obraztsov AN (2009) Making graphene on a large scale. Nat. Nanotechnol. 4:212–213. https://doi.org/10.1038/nnano.2009.67

47. Paton KR, Varrla E, Backes C, Smith RJ, Khan U, O'Neill A, Boland C, Lotya M, Istrate OM, King P, Higgins T, Barwich S, May P, Puczkarski P, Ahmed I, Moebius M, Pettersson H, Long E, Coelho J, O'Brien SE, McGuire EK, Sanchez BM, Duesberg GS, McEvoy N, Pennycook TJ, Downing C, Crossley A, Nicolosi V, Coleman JN (2014) Scalable production of large quantities of defect-free few-layer graphene by shear exfoliation in liquids. Nat. Mater. 13:624–630. https://doi.org/10.1038/nmat3944

48. Raccichini R, Varzi A, Passerini S, Scrosati B (2015) The role of graphene for electrochemical energy storage. Nat. Mater. 14:271–279. https://doi.org/10.1038/nmat4170
49. Samantara AK, Chandra Sahu S, Ghosh A, Jena BK (2015) Sandwiched graphene with nitrogen, sulphur co-doped CQDs: an efficient metal-free material for energy storage and conversion applications. J. Mater. Chem. A 3:16961–16970. https://doi.org/10.1039/c5ta03376d
50. Samantara AK, Kamila S, Ghosh A, Jena BK (2018) Highly ordered 1D NiCo2O4 nanorods on graphene: An efficient dual-functional hybrid materials for electrochemical energy conversion and storage applications. Electrochim. Acta 263:147–157. https://doi.org/10.1016/j.electacta.2018.01.025
51. Sau TK, Murphy CJ (2004) Room Temperature, High-Yield Synthesis of Multiple Shapes of Gold Nanoparticles in Aqueous Solution. J. Am. Chem. Soc. 126:8648–8649. https://doi.org/10.1021/ja047846d
52. Scheuermann GM, Rumi L, Steurer P, Bannwarth W, Mülhaupt R (2009) Palladium Nanoparticles on Graphite Oxide and Its Functionalized Graphene Derivatives as Highly Active Catalysts for the Suzuki−Miyaura Coupling Reaction. J. Am. Chem. Soc. 131:8262–8270. https://doi.org/10.1021/ja901105a
53. Shi L, Wang Y, Ding S, Chu Z, Yin Y, Jiang D, Luo J, Jin W (2017) A facile and green strategy for preparing newly-designed 3D graphene/gold film and its application in highly efficient electrochemical mercury assay. Biosens. Bioelectron. 89:871–879. https://doi.org/10.1016/j.bios.2016.09.104
54. Sidorov AN, Sławiński GW, Jayatissa AH, Zamborini FP, Sumanasekera GU (2012) A surface-enhanced Raman spectroscopy study of thin graphene sheets functionalized with gold and silver nanostructures by seed-mediated growth. Carbon N. Y. 50:699–705. https://doi.org/10.1016/j.carbon.2011.09.030
55. Stankovich S, Dikin DA, Dommett GHB, Kohlhaas KM, Zimney EJ, Stach EA, Piner RD, Nguyen ST, Ruoff RS (2006) Graphene-based composite materials. Nature 442:282–286. https://doi.org/10.1038/nature04969
56. Stankovich S, Dikin DA, Piner RD, Kohlhaas KA, Kleinhammes A, Jia Y, Wu Y, Nguyen ST, Ruoff RS (2007) Synthesis of graphene-based nanosheets via chemical reduction of exfoliated graphite oxide. Carbon N. Y. 45:1558–1565. https://doi.org/10.1016/j.carbon.2007.02.034
57. Ting SL, Guo CX, Leong KC, Kim D-H, Li CM, Chen P (2013) Gold nanoparticles decorated reduced graphene oxide for detecting the presence and cellular release of nitric oxide. Electrochim. Acta 111:441–446. https://doi.org/10.1016/j.electacta.2013.08.036
58. Tiwari JN, Tiwari RN, Kim KS (2012) Zero-dimensional, one-dimensional, two-dimensional and three-dimensional nanostructured materials for advanced electrochemical energy devices. Prog. Mater. Sci. 57:724–803. https://doi.org/10.1016/j.pmatsci.2011.08.003
59. Vedala H, Sorescu DC, Kotchey GP, Star A (2011) Chemical Sensitivity of Graphene Edges Decorated with Metal Nanoparticles. Nano Lett. 11:2342–2347. https://doi.org/10.1021/nl2006438
60. Wang Qi, Wang Q, Li M, Szunerits S, Boukherroub R (2016) One-step synthesis of Au nanoparticle–graphene composites using tyrosine: electrocatalytic and catalytic properties. New J. Chem. 40:5473–5482. https://doi.org/10.1039/C5NJ03532E
61. Wang Y-J, Wilkinson DP, Zhang J (2011) Noncarbon Support Materials for Polymer Electrolyte Membrane Fuel Cell Electrocatalysts. Chem. Rev. 111:7625–7651. https://doi.org/10.1021/cr100060r
62. Wang Y, Zhang S, Du D, Shao Y, Li Z, Wang J, Engelhard MH, Li J, Lin Y (2011) Self assembly of acetylcholinesterase on a gold nanoparticles–graphene nanosheet hybrid for organophosphate pesticide detection using polyelectrolyte as a linker. J. Mater. Chem. 21:5319–5325. https://doi.org/10.1039/C0JM03441J
63. Wang Z, Zhang J, Yin Z, Wu S, Mandler D, Zhang H (2012) Fabrication of nanoelectrode ensembles by electrodepositon of Au nanoparticles on single-layer graphene oxide sheets. Nanoscale 4:2728–2733. https://doi.org/10.1039/C2NR30142C
64. Wei D, Grande L, Chundi V, White R, Bower C, Andrew P, Ryhänen T (2012) Graphene from electrochemical exfoliation and its direct applications in enhanced energy storage devices. Chem. Commun. 48:1239–1241. https://doi.org/10.1039/C2CC16859F

65. Wu Y, Wang B, Ma Y, Huang Y, Li N, Zhang F, Chen Y (2010) Efficient and large-scale synthesis of few-layered graphene using an arc-discharge method and conductivity studies of the resulting films. Nano Res. 3:661–669. https://doi.org/10.1007/s12274-010-0027-3

66. Xu S, Wu P (2014) Facile and green synthesis of a surfactant-free Au clusters/reduced graphene oxide composite as an efficient electrocatalyst for the oxygen reduction reaction. J. Mater. Chem. A 2:13682–13690. https://doi.org/10.1039/C4TA01417K

67. Yang Y, Asiri AM, Du D, Lin Y (2014) Acetylcholinesterase biosensor based on a gold nanoparticle–polypyrrole–reduced graphene oxide nanocomposite modified electrode for the amperometric detection of organophosphorus pesticides. Analyst 139:3055–3060. https://doi.org/10.1039/C4AN00068D

68. Yin H, Tang H, Wang D, Gao Y, Tang Z (2012) Facile Synthesis of Surfactant-Free Au Cluster/Graphene Hybrids for High-Performance Oxygen Reduction Reaction. ACS Nano 6:8288–8297. https://doi.org/10.1021/nn302984x

69. Yu H, Xu P, Lee D-W, Li X (2013) Porous-layered stack of functionalized AuNP–rGO (gold nanoparticles–reduced graphene oxide) nanosheets as a sensing material for the microgravimetric detection of chemical vapor. J. Mater. Chem. A 1:4444–4450. https://doi.org/10.1039/C3TA01401K

70. Zhang B, Cui Y, Chen H, Liu B, Chen G, Tang D (2011) A New Electrochemical Biosensor for Determination of Hydrogen Peroxide in Food Based on Well-Dispersive Gold Nanoparticles on Graphene Oxide. Electroanalysis 23:1821–1829. https://doi.org/10.1002/elan.201100171

71. Zhang M, Lu X, Wang H-Y, Liu X, Qin Y, Zhang P, Guo Z-X (2016) Porous gold nanoparticle/graphene oxide composite as efficient catalysts for reduction of 4-nitrophenol. RSC Adv. 6:35945–35951. https://doi.org/10.1039/C6RA01772J

72. Zhao W, Fang M, Wu F, Wu H, Wang L, Chen G (2010) Preparation of graphene by exfoliation of graphite using wet ball milling. J. Mater. Chem. 20:5817–5819. https://doi.org/10.1039/C0JM01354D

73. Zhao Y, Wang C, Liu Y, MacFarlane DR, Wallace GG (2018) Engineering Surface Amine Modifiers of Ultrasmall Gold Nanoparticles Supported on Reduced Graphene Oxide for Improved Electrochemical CO2 Reduction. Adv. Energy Mater. 8:1801400. https://doi.org/10.1002/aenm.201801400

74. Zhou X, Huang X, Qi X, Wu S, Xue C, Boey FYC, Yan Q, Chen P, Zhang H (2009) In Situ Synthesis of Metal Nanoparticles on Single-Layer Graphene Oxide and Reduced Graphene Oxide Surfaces. J. Phys. Chem. C 113:10842–10846. https://doi.org/10.1021/jp903821n

75. Zhuo Q, Ma Y, Gao J, Zhang P, Xia Y, Tian Y, Sun X, Zhong J, Sun X (2013) Facile Synthesis of Graphene/Metal Nanoparticle Composites via Self-Catalysis Reduction at Room Temperature. Inorg. Chem. 52:3141–3147. https://doi.org/10.1021/ic302608g

76. Zou C, Yang B, Bin D, Wang J, Li S, Yang P, Wang C, Shiraishi Y, Du Y (2017) Electrochemical synthesis of gold nanoparticles decorated flower-like graphene for high sensitivity detection of nitrite. J. Colloid Interface Sci. 488:135–141. https://doi.org/10.1016/j.jcis.2016.10.088

Hybrid Nanocomposites Based on Graphene and Titanium Dioxide for Wastewater Treatment

Hanane Chakhtouna, Nadia Zari, Hanane Benzeid, Abou el kacem Qaiss, and Rachid Bouhfid

Abstract Since its discovery by Fujishima and Honda, titanium dioxide photocatalyst have been extensively used for environmental management and wastewater purification. TiO_2 photocatalyst showed higher photocatalytic performances toward different organic pollutants, pharmaceutical compounds, and bacteria. However, it exhibited large band gap and can only be excited under UV-light irradiation, which presents only 5% of solar terrestrial radiation. In addition, to the fast electron–hole (e^-/h^+) pair recombination that limits its photocatalytic activity. Therefore, the incorporation of graphene and its derivatives, known by their exceptional mix of chemical, physical, mechanical and electronic properties, is found advantageous to enhance electron mobility, suppress the recombination of e^-/h^+ pairs and shift its visible light photocatalytic ability. This chapter aims to introduce TiO_2/graphene hybrid nanocomposites from the fundamental component, synthesis methods, physico-chemical and electronic properties to their application as powerful materials in the wastewater treatment field.

Keywords Hybrid nanocomposites · Graphene · Graphene oxide · TiO_2 · Recombination · Wastewater treatment

1 Introduction

The use of nanomaterials with sizes smaller than 100 nm in at least one dimension in wastewater treatment has attracted great interest of scientists and more attention of researchers for the advantages of their unique physical and chemical properties. Besides that, it is well known that at this nanoscale, these nanomaterials

H. Chakhtouna · N. Zari · A. Qaiss · R. Bouhfid (✉)
MAScIR Foundation, Composites and Nanocomposites Center, Rabat Center Design, Av Mohamed Jazzouli Madinat Al Irfane, Rabat, Morocco
e-mail: r.bouhfid@mascir.com

H. Chakhtouna · H. Benzeid
Laboratoire de Chimie Analytique et de Bromatologie, Faculté de Médecine et de Pharmacie, Université Mohamed V, Rabat, Morocco

possess some novel properties, which is different from their normal size equivalents, including porous structure, enriched surface functional groups, large specific area, and low-cost [1]. Indeed, various nanomaterials, with unique functionalities have been used to solve major environmental problems and have shown their efficiency in other environmental applications especially in wastewater treatment. Carbonaceous nanomaterials [2], clays [3], zeolites [4], metal oxides [5], polymer and biopolymer nanocomposites [6] are the most common nanomaterials used for the elimination of a wide range of contaminants in water purification field. Thus, graphene and its derivatives have gained immense attention due to its abundant availability, chemical and thermal stabilities excellent adsorption capacity and eco-friendly nature [7]. Yet, adsorbent materials are unable to degrade pollutants, they only allow their transformation from liquid phase to solid one, generating another type of pollution. From the literature, adsorption capability of graphene can be improved by its combination with semiconductor photocatalysts. TiO_2 is one of the most photocatalyst explored for wastewater treatment, thanks to its great photoactivity, nontoxicity, chemical inertness and cheapness [8]. However, in its turn, its photocatalytic performances were limited by numerous factors, namely, (i) poor affinity toward organic pollutants, (ii) quick recombination of the photogenerated electron/hole pairs and (iii) larger band gap that limits its absorption of solar radiation. Nevertheless, the absorption in the visible domain is the most important object of heterogeneous photocatalysis. Studies have showed that the combination of graphene or its derivatives with TiO_2 photocatalyst, not only solve the problem related to the adsorption process, but also allows to improve the TiO_2 photocatalytic performances via the minimization of its band gap, and the suppression of the recombination of photogenerated electron/hole pairs. This chapter book will be divided into two main parts, the first one aims to introduce graphene and TiO_2 nanomaterials via the presentation of their properties and their higher power to removal different contaminants from wastewater, whether by adsorption or photocatalysis process. The second part will be focused on TiO_2/graphene hybrid nanocomposites as new type of efficient photocatalyst. It addresses the synthetic strategies for their preparation, different characterization techniques used to more understand what is really going on and finally to present their recent research progress on the wastewater treatment field.
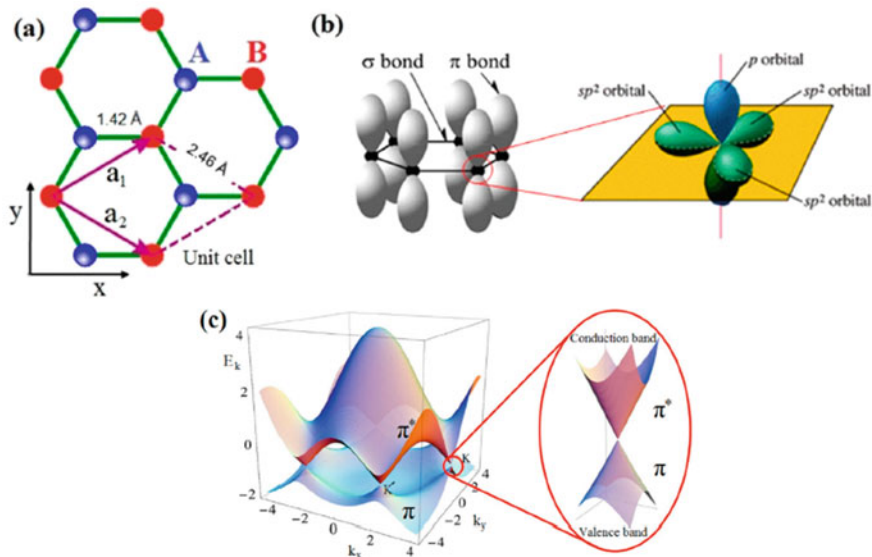
2 Graphene

Graphene is one of the most auspicious and bright material nanofillers applied in the last ten years for the preparation of novel hybrid nanocomposites with extraordinary properties and high performances for application in various areas. Graphene is a crystalline allotropic form of carbon consisting of a single layer of carbon atoms arranged in a hexagonal lattice that constitutes the basis structural element of other allotropes, namely, graphite, carbon nanotubes and fullerenes. Its unique structure provides several appealing peculiarities, which makes it an attractive and cost-effective adsorbent in the wastewater treatment field. The following section

concisely presents the graphene material, its structure and morphology, introduces its physic-chemical properties as well as the mechanism involved during adsorption process.

2.1 Structure and Morphology

To better understand graphene, it is helpful to start first with its crystalline structure. According to the literature, graphene is known as a two-dimensional (2D) arrangement of carbon atoms (A and B) of monoatomic thickness arranged in a hexagonal network, similar in the shape to that of a honeycomb (Fig. 1a). The distance between two carbon atoms is 1.42 Å [9], while the lattice constant is around of 2.46 Å [7]. Each carbon atom is covalently linked to three other atoms through strong σ bonds of sp^2 hybrid orbitals, while the p_z orbitals perpendicular to the graphene plane (Fig. 1b), form π bonds that hybridize together to form the π and π* bonds (Fig. 1c) [10].

Graphene can be found in various forms, namely, monolayer, bilayer, and multilayers. In the case of multilayers (between 3 and 10 layers), carbon atoms can be stacked in different stacking configurations, namely, AA, AB, ABC and AAB, which exhibit different structural and electronic properties as shown in Fig. 2. Among them, the AB and ABC stackings are the commonly found in natural graphite [12]. Based on the literature, synthesis of graphene under different forms, can be achieved via

Fig. 1 **a** Bravais lattice and **b**, **c** structure bonds of graphene [11]
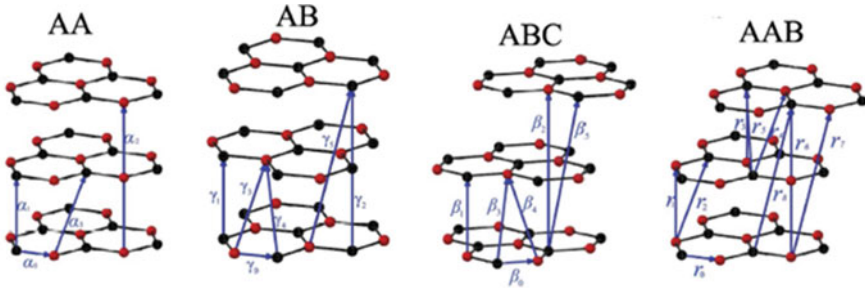
Fig. 2 Geometric structures of AA, AB, ABC and AAB-stacked graphene [12]

numerous techniques that has been reviewed in previous works. However, mechanical exfoliation, chemical reduction, and epitaxial growth remain the most synthesis methods commonly used for producing graphene with highest quality [13, 14].

2.2 Physico Chemical Properties

Despite its short history, graphene has attracted considerable attention as one of the promising materials for a range of applications, including nano-biotechnology, electronic and photonic systems, energy storage, and environmental applications. Harder than diamond yet more elastic than rubber, tougher than steel yet lighter than aluminum, graphene offer unique physico-chemical properties including high theoretical specific surface area (~2630 m^2/g), abundant functional groups such as, hydroxyl, carboxyl in graphene oxide and reduced graphene oxide forms, that play an essential role for its adsorption behaviors. In addition, graphene is known as a super light material with a planar density of 0.77 mg/m^2 and a thickness of 0.334 nm, promoting its use in industrial scale. It also possesses high electron mobility, superior mechanical properties, exceptional thermal conductivity and high potential adsorption capacity (Fig. 3) [15].

However, graphene suffers from some drawbacks. It is exhibited no porosity and no functional groups [16], is easy to agglomerate and difficult to disperse due to strong π-π stacking, hydrophobic interaction between the layers, which makes it unable to perform well for decontamination purposes in its pure form [17]. Besides that, the two graphene derivatives, namely, graphene oxide (GO) and reduced graphene oxide (RGO) are the largest explored in the wastewater treatment field. Compared to the neat graphene, GO and RGO, are porous, contain abundant functional groups on their surface such as –COOH, –C=O and –OH, as displayed in the Fig. 4. The presence of such functional groups on their surface makes them more hydrophilic and therefore greater affinity for contaminants. Another interesting property of GO and RGO are their opened-up layer structure, that plays important role for adsorption application.
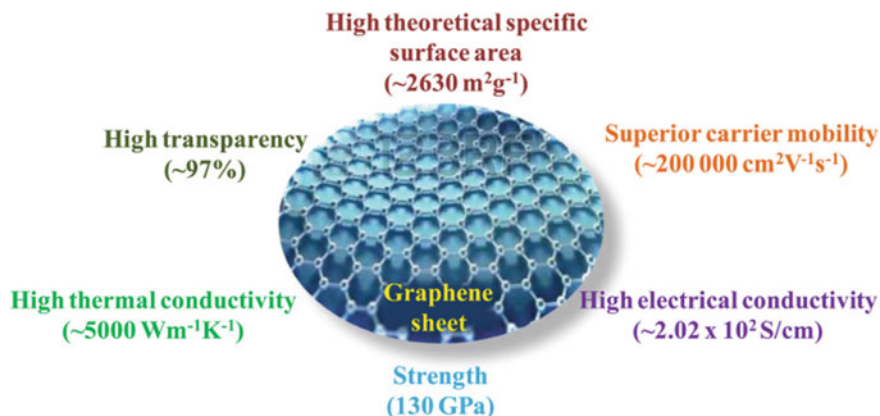
Fig. 3 Fundamental properties of graphene sheet [15]
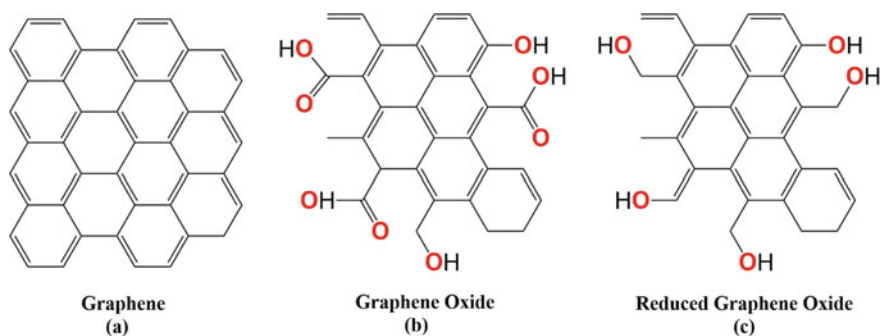
Fig. 4 Structures of **a** graphene and its derivatives, **b** graphene oxide (GO) and **c** reduced graphene oxide (RGO)

2.3 Adsorption Capacity and Mechanisms

Adsorption is one of the commonly method employed to remove organic and inorganic contaminants in water and wastewater thanks to its simplicity, convenience and low-cost [18]. Several recent studies have been provided and confirmed evidence of carbonaceous materials, in general, and graphene-based materials for the removal of organic and inorganic contaminants from effluents. A higher surface area, chemical stability, open-up layer morphology (in the case of GO and RGO) and high adsorption affinity, as shown previously, make graphene a potential candidate for the adsorption of different contaminants from sewage including organic and pharmaceutical compounds and heavy metals [16, 19]. According to the structure of graphene, it could form physical interactions, such as Vander Waals forces, π bonds or electrostatic forces with organic compounds without any change in its chemical or physical properties. Chia et al. [20] have developed graphene oxide (GO) via simple Hummer's

method for the methylene blue dye adsorption. The GO prepared exhibits maximum adsorption capacity 700 mg/g at 300 mg/L, due to its larger specific surface area and its unique two-dimensional structure. The adsorption capacity of GO increased with increasing pH, initial MB concentration, and temperature. The Langmuir and interparticle diffusion models were found to best describe MB adsorption on GO, suggesting that the adsorption process is dominated by the external mass transfer of MB molecules to the surface of GO. Moreover, the thermodynamic study showed that the adsorption process is endothermic and non-spontaneous, which is totally normal since the MB removal percentage increased with temperature, indicating that the adsorption of methylene blue dye involves anion-cation interactions and $\pi-\pi$ stacking. Al-Khateeb et al. [19] have explored the graphene nanoplatelets (GNPs) ability towards dangerous pharmaceutical pollutants, specifically acetaminophen (APAP), aspirin (ASA) and caffeine (CAF). The resulting material exhibited higher specific surface area of 635.2 m^2/g. The effect of different environmental parameters was studied, and the results revealed that all targeted pollutants were successfully removed at 296 K, in pH of 8, after 10 min using 10 mg GNPs. Moreover, their adsorption were found to be best described by both pseudo-second-order and intraparticle diffusion models, indicating that intraparticle diffusion is a part of the adsorption mechanism beside hydrogen bonding and $\pi-\pi$ interactions [21].

3 TiO$_2$ Photocatalyst

Although adsorption eliminate pollutants from wastewater, it cannot completely remove pollutants. This technique transforms only pollutants from the liquid phase to the solid one, generating another type of pollutant, which requires additional treatment. Therefore, coupling graphene with photocatalyst materials such as TiO$_2$ is an efficient strategy to enhance the pollutant removal process via the combination effect of adsorption sites on the graphene and the reactivity of a photocatalyst toward contaminant degradation, and limit the fast electron–hole pair recombination. The following section aims to briefly introduce titanium dioxide photocatalyst, its textural and chemical properties as well as its efficiency in wastewater treatment as one of the powerful photocatalyst used to eliminate organic pollutants and bacteria from sewage.

3.1 Structure and Properties

After Fujishima and Honda's discovery in 1972 [22] for splitting water into oxygen and hydrogen using a TiO$_2$ photoelectrode, titanium dioxide have been proving to be an efficient photocatalyst for the removal of organic contaminants and bacteria from sewage. It is due to its chemical stability, inertly, long durability, super hydrophilicity, strong oxidizing ability, nontoxicity, environmentally friendly nature and low cost

[8]. In nature, titanium dioxide exists in four fundamental crystalline phases, namely, rutile, anatase, brookite and $TiO_2(B)$ (bronze). In all forms, each Ti^{4+} ion is coordinated to an octahedron of six oxygen ions (O^{2-}), forming TiO_6 octahedra. The structural difference of these phases is attributed to the different stacking arrangements of their octahedra. Anatase and rutile have tetragonal structures, with space groups $I_{41/amd}$ and $P_{42/mnm}$ for anatase and rutile, respectively. Both crystalline phases are made up of an octahedron of oxygen atoms around a titanium atom (TiO_6 octahedron) linked by different corners and edges. In anatase, each TiO_6 octahedron relates to eight neighbors: four share edges and four share corners, with respect to rutile, each octahedron relates to ten neighbors: two edge-sharing pairs and eight corner-sharing oxygen atoms. Brookite, on the other hand, crystallizes in an orthorhombic crystalline structure with space group P_{bca}, in which both edges and corners are shared. Wherein, TiO_2 (B) has monoclinic crystal system, with space group $C_{2/m}$, in which both edges and corners are shared by the TiO_6 octahedra having a perovskite-like layered structure. Their spatial representation as well as their key properties are shown in Fig. 5 and Table 1, respectively.

Thermodynamically, rutile is the stable form of bulk titania, while anatase is metastable, and transferring to rutile under higher temperature, typically higher or equal to 400 °C, depending upon the methods and conditions of synthesis, as shown in the Fig. 6. However, many studies have suggested that anatase is thermodynamically
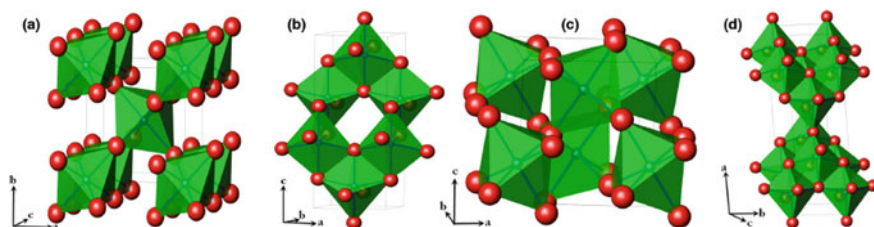
Fig. 5 Different TiO_2 crystallographic structures **a** Rutile, **b** Anatase, **c** Bronze, and **d** Brookite [23]

Table 1 TiO_2 crystallographic crystalline properties [23]

Structure	Space group	Lattice parameter values (nm)	Density (g cm^{-1})	Band gap (eV)
Anatase	Tetragonal $I_{41/amd}$	a = 0.378 and c = 0.951	3.79	3.22
Rutile	Tetragonal $P_{42/mnm}$	a = 0.459 and c = 0.296	4.13	3.02
Brookite	Orthorhombic P_{bca}	a = 0.917, b = 0.546, c = 0.514	3.99	3.10
TiO_2(B) (bronze)	Monoclinic $C_{2/m}$	a = 1.217, b = 0.374 and c = 0.651 β = 107, 30°	3.64	3.05
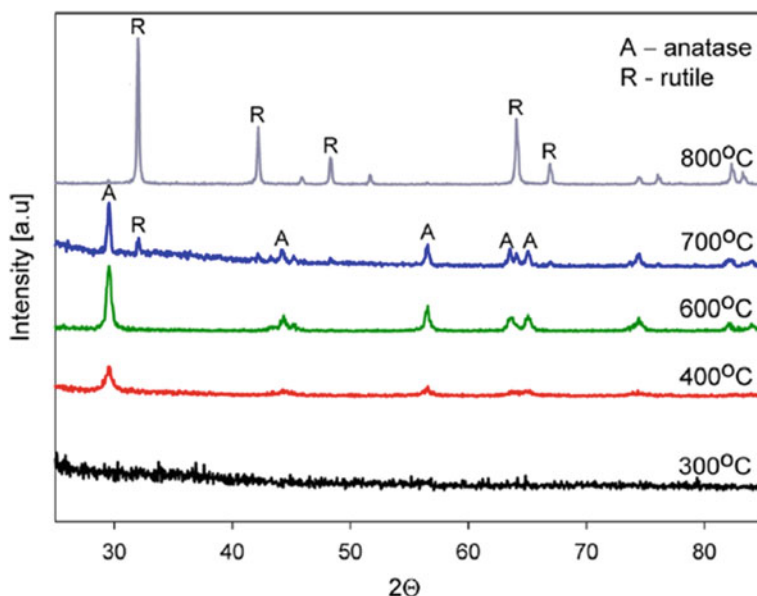
Fig. 6 XRD patterns of TiO$_2$ powders annealed at different temperatures [25]

more stable when the size is in nanoscale, in particular for nanoparticles below 11 nm [24].

Anatase and rutile are the most widely phases applied in photocatalysis studies but offer different activities. The anatase phase has a higher photocatalytic activity, compared to rutile one, thanks to its larger band gap, smaller grain size and higher surface energy, while it has been demonstrated that mixed phases of anatase and rutile with well-defined proportions show greater photocatalytic performances than the pure single anatase or rutile. The Degussa TiO$_2$ (P25), used today as a benchmark photocatalyst for photocatalytic studies, is composed of a mixture of 80% anatase and 20% rutile, with specific BET surface area of 50 m^2/g. It exhibits high photocatalytic performances, which is related to the high separation efficiency of the hetero-phase interface junction formed between anatase and rutile phases that facilitates the transformation of the photogenerated electrons and therefore suppress the electron-holes recombination, as shown in Fig. 7 [26].

Up to now, several methods have been proposed to synthesize titanium dioxide photocatalyst, either through chemical or physical routes. These techniques including sol–gel, hydrothermal, solvothermal, micelle and inverse micelle, direct oxidation and many others [27, 28]. Moreover, it was found that different techniques often produce different results. Indeed, synthesis method and the operating conditions (pH, duration, and temperature) affects strongly TiO$_2$ morphology as well as its structural, chemical and electronic properties. According to the literature [29], TiO$_2$
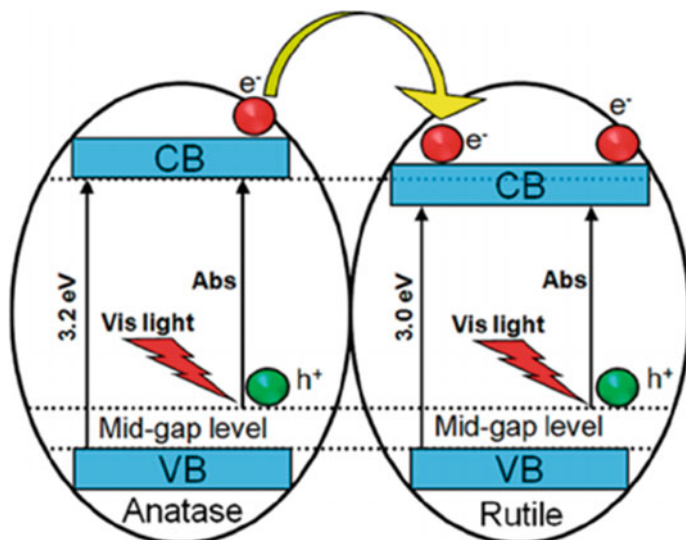
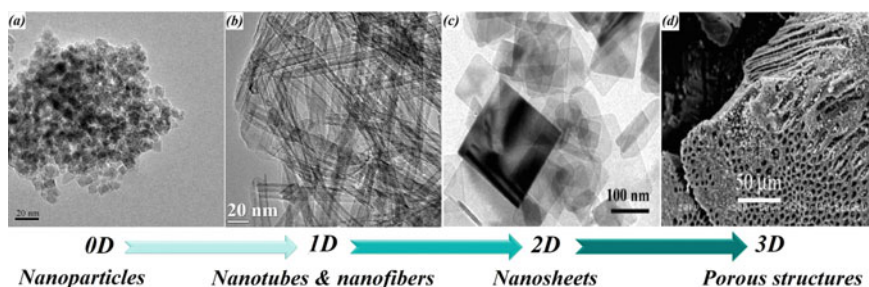**Fig. 7** Schematic of the heterophase interface junction between anatase and rutile phases

Fig. 8 TiO$_2$ photocatalysts classification [27]

can be existed in many forms and morphologies, namely, microspheres, nanoparticles, nanofibers, nanotubes, nanosheets, and hierarchically porous, which can be divided into four main categories as illustrated in Fig. 8.

3.2 Basic Principles and Mechanism for Photocatalytic Pollutants Removal

The electronic structure of TiO$_2$ as a semiconductor plays an important role in photocatalysis. When TiO$_2$ semiconductor is irradiated with a photon of sufficient energy is equal to or higher than its band gap energy (h$\nu \geq$ E$_g$), electrons (e$^-$) and holes
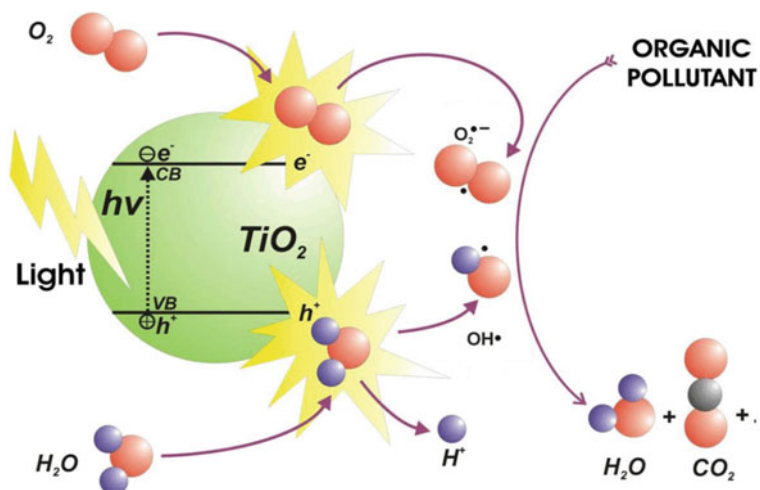
Fig. 9 Principle of TiO$_2$ semiconductor photocatalysis

(h$^+$) are generated in conduction and valence band respectively (Fig. 9). The holes interact with water (H$_2$O) on the surface to generate highly reactive hydroxyl radical (OH•), while the electrons interact with the oxygen adsorbed on the TiO$_2$ surface to form superoxide anion (O$_2$•$^-$) radicals as shown in the Fig. 9. These species attack easily different pollutants namely, organic dyes, phenolic compounds, pesticides, and bacteria, leading to their damage.

Due to its promising photocatalytic activity, TiO$_2$ photocatalyst has shown higher photodegradation ability toward a large range of pollutants in aqueous solutions under UV light. That include anionic and cationic dyes, organic and pharmaceutical compounds, metal ions and bacteria. In this context, Sohrabi and Ghavami [30] studied the photocatalytic decolorization of an azo-reactive textile dye, Direct Red 23, in aqueous suspension using TiO$_2$ powder under UV light. They found that after 140 min of irradiation under UV light in a TiO$_2$ aqueous solution, 83.58% of dye was decomposed. They also studied the degradation rate for the decomposition of dye as function of different parameters. At low pH (pH = 2), 99.83% of Red 23 was decomposed after only 90 min. In view of the advantages of TiO$_2$ photocatalyst, they also tested the photocatalytic activity of different photocatalyst, namely, ZnO, SnO$_2$ and Fe$_2$O$_3$ for the degradation of Red 23. Compared to other photocatalyst, TiO$_2$ photocatalyst was found to be more efficient at low pH for the degradation of Red23 dye. Successful degradation of anionic and cationic dyes with TiO$_2$ photocatalyst under UV irradiation was reported by Lachheb and his co-authors [31]. The five dyes were totally degraded and mineralized. The organic part was converted into CO$_2$, heteroatoms were released to innocuous diluted inorganic final products, Sulfur is released to sulfate, while nitrogen is converted first into ammonium before its slow oxidation into nitrate. TiO$_2$ photocatalyst exhibits excellent photocatalytic bacterial activity against various bacteria and viruses. Matsunga

et al. [32] were first reported the antibacterial activity of TiO_2 powder photocatalyst for killing *Escherichia coli* bacteria. The cells were completely sterilized after 60 min, when 10^2–10^3 cells per ml were utilized. The authors mentioned that the cell death was caused by a decrease in the concentration of Coenzyme A (Co A) and an increase in the dimeric CoA concentration. Doping TiO_2 with silver, platinum or other metals improved the photocatalytic bactericidal activity of TiO_2 nanomaterials, especially for higher cells concentration. Recently, Zeng and his collaborators [33] have been prepared Ag/TiO_2 nanoparticles with a long-term antibacterial efficiency via sample and facile dopamine-assisted method. The prepared photocatalyst showed high activity in the elimination of both the Gram-positive *Bacillus subtilis* and the Gram-negative *Escherichia coli* bacteria under visible light. This higher antibacterial activity is attributed to both silver ions and reactive oxygen species generated during the TiO_2 activation that adhere to cell membrane, leading to their damage.

Despite all merits, quick recombination of electron (e^-) and hole (h^+) pairs remains the major problem that limits the TiO_2 practical application. In this regard, graphene with its unique structure and interesting properties appears as a very promising material for solve the recombination process. The combination of the photocatalyst with graphene or with one of its derivatives not only enhancing the adsorptive capacity of TiO_2 via the increase of the surface area but also prevent the e^-/h^+ recombination. Therefore, the next section aims to present TiO_2/graphene hybrid nanocomposites and their application on water purification field. Most of studies shown that the activity of those hybrid nanocomposite is higher than that of pure TiO_2 or graphene, owing to the presence of heterogeneous junctions between TiO_2 and graphene that delays or even suppresses the recombination of photogenerated electron–hole pairs phenomena.

4 TiO₂/graphene Hybrid Nanocomposites Based on Graphene and Titanium Dioxide and Their Application on Water Purification Field

The unique structure of graphene as well as its fabulous properties recently presented provide ideal supportive behavior for photocatalyst materials. The development of new binary nanocomposites combining graphene with TiO_2 photocatalyst aims to alleviate the inadequacies of each single material and produce nanocomposite materials with higher efficiency for pollutants removal via synergistic effect. This part of this chapter highlights the synthesis techniques, characteristics and the application of hybrid nanocomposites based on graphene and titanium dioxide on water purification field.

4.1 Synthesis Methods

Based on the literature, the first TiO₂/graphene hybrid nanocomposite synthesized for the degradation of organic pollutants by photocatalysis, was prepared by Li and his coworkers in 2009 using hydrothermal method [34]. From then on, various methods and deposition technologies have been proposed to synthesize TiO₂/graphene hybrid nanocomposites with different morphologies including sol–gel, hydrothermal, solvothermal, mechanical mixing, chemical vapor (CVD), etc. [35, 36]. Each synthesis method has its own pros and cons in terms of the complexity of preparation and the quality of the final product. Therefore, the synthesis technique must be simple, efficient on a large scale and cost effective. In addition, the concentration of both materials (TiO₂ and graphene) should be optimized to avoid their agglomeration, which results in the reduction in their efficiency. Here, we will be focused only on the methods and techniques commonly used for the TiO₂/graphene hybrid composites preparation.

4.1.1 Hydrothermal Method

As mentioned before, hydrothermal method was the first technique used to synthesize TiO₂/graphene hybrid nanocomposite and stills the main preparation method. Hydrothermal technique is an environmentally friendly, simple, and efficient strategy for the TiO₂/graphene hybrid nanocomposites preparation. It involves reactions under controlled temperature and high pressure. The main steps in the hydrothermal technique are illustrated in Fig. 10. Li and its coauthors [34] have successfully synthesized a TiO₂/graphene hybrid composite via hydrothermal method. Graphene oxide obtained from graphite by Hummer's method was dissolved with P25, in the presence of water and ethanol, under homogenous stirring and then placed in a Teflon-sealed autoclave at 120 °C for 3 h. The resulting P25/graphene composite show higher photocatalytic efficiency toward methylene blue dye compared with both bare P25 and P25-CNTs with same carbon content. Recently, Nguyen and Juang [37] have prepared RGO/TNT hybrid composites with different amounts of RGO via a facile hydrothermal method using GO and P25 as precursors. SEM micrographs showed that the RGO sheets were totally recovered with titanate. In addition, the 3% RGO/TNT composite exhibited higher BET specific surface compared to P25, titanate nanotube and other materials. In addition, it was observed that the composite response under visible light increased with increasing the RGO content, 95% decolorization and 78.8% mineralization were achieved after 3 h of visible light irradiation.
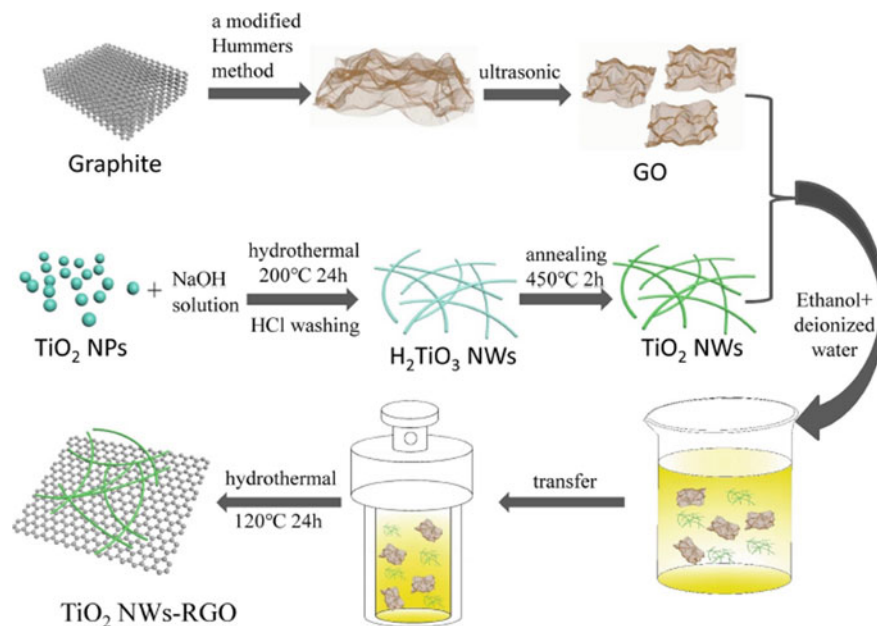
Fig. 10 Schematic representation of hydrothermal process to synthesize TiO_2/RGO nanocomposite [38]

4.1.2 Solvothermal Method

Solvothermal method is among the efficient techniques used to synthesize TiO_2/graphene hybrid nanocomposite (Fig. 11). It is simple and like hydrothermal technique, the difference between them lies in the solvent used. Solvothermal requires an organic solvent, whereas hydrothermal requires only water. Thus, the properties of final product are not the same; the hydrothermal provides better control in terms of crystallinity, size and ban gap. In this context, Awang and Talalah [39] have compared two TiO_2/graphene oxide composites synthesized though both solvothermal and hydrothermal techniques. It was found that the composite prepared via solvothermal method shows the highest crystallite size and the largest band gap compared to that prepared via hydrothermal technique, and therefore lower photodegradation capacity. In the other hand, Yadav and Kim [40] have prepared anatase TiO_2-graphene oxide nanocomposites with different GO loadings by a solvothermal method for the degradation of gaseous benzene under UV light irradiation. The SEM micrograph of nanocomposites reveals the non-spherical morphology of TiO2 nanoparticles existing on GO sheets. The anatase nanoparticles were well dispersed on graphene oxide sheets. The TEM reveals also that the TiO2 NPs are well connected to GO surface. UV–Vis DRS measurements were made to study the optical properties of the anatase TiO2-GO nanocomposites. The nanocomposite showed a red shift in the absorption edge attributed to the formation of chemical bonds of Ti–O–C
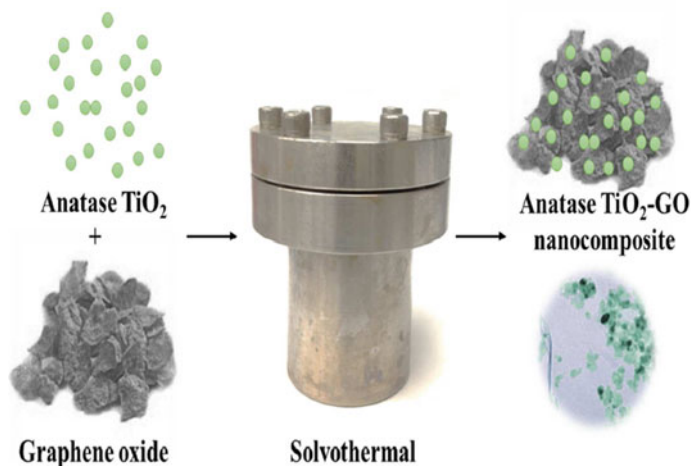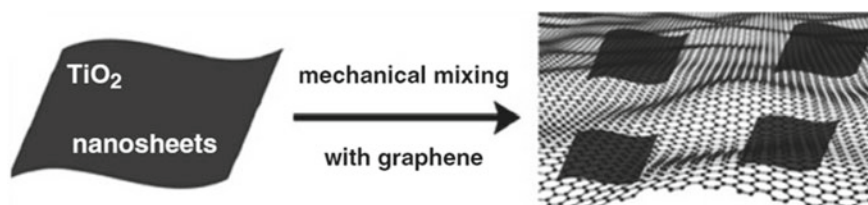
Fig. 11 Schematic representation of solvothermal process to synthesize TiO$_2$-GO nanocomposite [40]

between TiO2 and graphene. The nanocomposites prepared shows better photocatalytic activity to degrade benzene gas than pure TiO2 due to the synergistic effect of graphene and TiO2.

4.1.3 Mechanical Mixing Method

Mechanical mixing method is one of the most technique used to synthesize TiO$_2$/graphene hybrid nanocomposites, owing to its simplicity, facile control of the reaction conditions and the possibility to produce TiO$_2$/graphene composite with homogenous distribution [35]. This method involves two steps, namely, mixing and sonication. The first step consists the mixing of TiO$_2$ and graphene/graphene oxide under stirring, while sonication aims to ensure good contact between the different compounds and provide the exfoliation of graphene. Zhang et al. [41] have prepared ternary P25/GO/Pt hybrid nanocomposite via mechanical mixing method. The (Pt/GO)/P25 nanocomposite showed the highest hydrogen production, with an increase of about 3 times than that of Pt/P25 due to the introduction of GO that improves light adsorption in the visible light region and enhance the photocatalytic performance. Li et al. [42] have prepared 3D TiO$_2$-reduced graphene oxide hydrogel by simple mechanical mixing method followed by sonication for the removal of Cr(VI) from aqueous solutions. The method consists of mixing P25 photocatalyst with graphene oxide in the presence of sodium ascorbate as reducing agent. TEM images shows the lamellar structure of RGO with some chiffon-like ripples and wrinkles with TiO$_2$ nanospheres in the size of 20 nm uniformly dispersed on the RGO sheets. The composite exhibits highly connected pores and large specific surface

Fig. 12 Schematic representation of TiO$_2$/graphene hybrid composite via mechanical mixing technique [43]

area, which provide abundant active sites and facilitate the diffusion of chrome ions (Fig. 12).

4.1.4 Sol–Gel Method

Sol–gel is one of the advanced techniques, which usually employs the compounds with high activity as the precursors. Is applied to obtain an intimate mixing and strong chemical bonding between graphene and TiO$_2$, involving hydrolysis and condensation reactions. The method is simple and allows the preparation of homogenous TiO$_2$/graphene hybrid composites with excellent compositional control. Another interesting advantage of sol–gel method is that elevated pressure and temperature are not required. In addition, strong chemical interaction between TiO$_2$ and GO are obtained via sol–gel technique, contrary to mechanical mixing method, which the interaction are very weak [44]. The challenge of the sol-method is how to control the particle size and uniform dispersion of the TiO$_2$ on graphene sheets. Atout et al. [45] have prepared TiO$_2$/reduced graphene oxide nanocomposites via two preparation methods, namely, sol–gel and hydrothermal techniques. The purpose of this study was to show that other parameters than the composition can be influenced the photocatalytic activity of the elaborated materials. It was observed that the TiO$_2$/RGO nanocomposite prepared via sol–gel route presented improved textural properties and excellent photodegradation efficiency than those prepared by hydrothermal one. TEM micrographs revealed that the TiO$_2$ were more homogenously distributed on RGO in the case of the composite prepared with sol–gel method compared with its analogous obtained by hydrothermal route. Its efficiency for methylene blue dye removal was very highest, 93% of methylene blue was degraded against only 82% in the case of the composite prepared by hydrothermal method (Fig. 13).

4.2 TiO$_2$/graphene Hybrid Nanocomposites Characterization

Physical, chemical, and mechanical properties of hybrid nanocomposites based on graphene and titanium dioxide can vary with synthesis methods previously described.
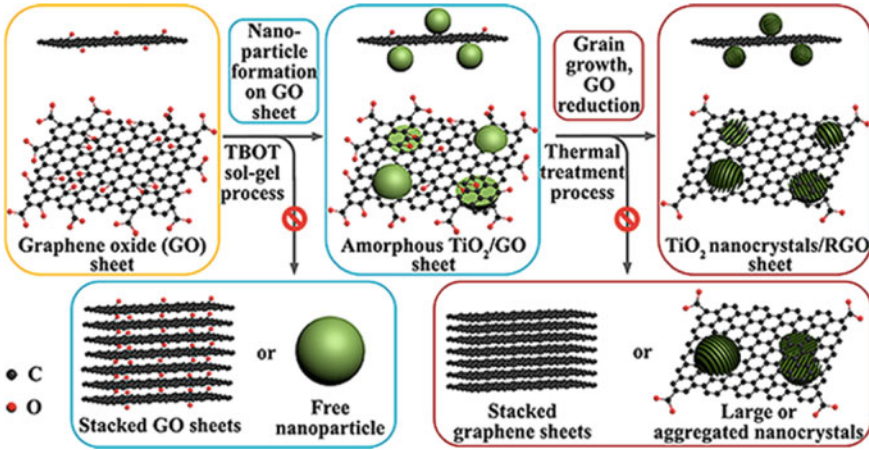
Fig. 13 Schematic illustration for TiO$_2$/graphene composite preparation though sol–gel technique [46]

Their characterization plays a vital role in determining the mechanisms involved during the degradation of different pollutants. Especially that their photocatalytic activity is strongly depending on the structure, the morphology as well as their surface properties.

4.2.1 X-Ray Diffraction

One of the most important challenges during the preparation of TiO$_2$/graphene hybrid nanocomposites is the difficulty of reducing graphene oxide into graphene single layer, which is an important step to obtain hybrid nanocomposites with higher photocatalytic efficiency. X-Ray diffraction is widely used for the determination for the structure of hybrid nanocomposites as well as to confirm the presence of TiO$_2$ without disruption of its crystal structure. XRD analysis (Fig. 14) confirmed the successful reduction of GO into RGO via hydrothermal technique [38]. In addition, it was observed that the main diffraction peaks of TiO$_2$ before and after RGO addition are similar, indicating that the incorporation of RGO does not result any disruption of the crystal structure of TiO$_2$.

4.2.2 Scanning and Transmission Electron Microscopies

SEM and TEM are considered as the most popular characterization techniques for following the TiO$_2$/graphene hybrid nanocomposites morphologies. They provide better information about the degree of dispersion of TiO$_2$ nanoparticles on the graphene surface. The morphology and compositions of G-TiO$_2$ composite prepared

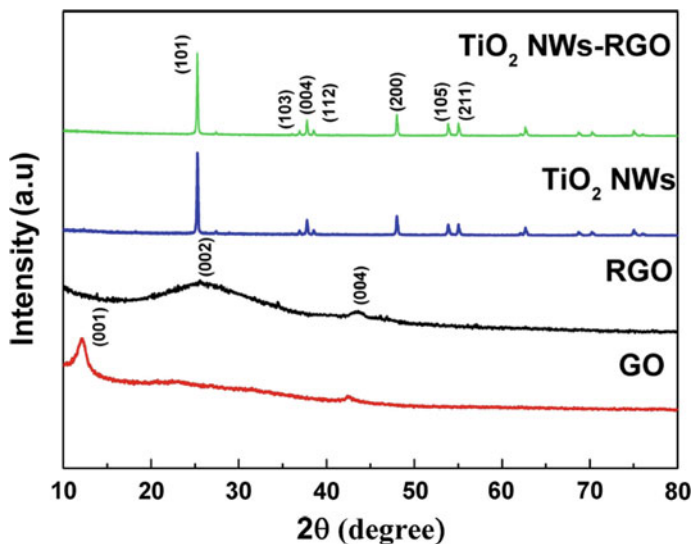**Fig. 14** XRD patterns of the GO, RGO, TiO$_2$ and TiO$_2$/RGO [38]

by Zhou et al. [47] are illustrated in the Fig. 15. SEM micrographs and TEM images showed that the graphene sheets are totally covered with TiO$_2$ particles with an average crystallite size of 15 nm, while the high-resolution TEM image indicates a well-defined crystallinity of TiO$_2$ with lattice spacing of 0.352 nm, corresponding to the (101) planes of anatase.

4.2.3 Infrared Spectroscopy

Infrared spectroscopy is often used to identify functional groups and to confirm the interactions between TiO$_2$ and graphene. Figure 16 illustrated FTIR spectra of P25g, graphene oxide and P25-GO-1% composite prepared by Liu and his collaborators via solvothermal method [48]. The FTIR spectrum of graphene oxide reveals the presence of three major peaks located at 3428, 1730, 1626, 1386 and 1056 cm^{-1}, which are attributed to O–H stretching and bending vibrations, C=O, C=C, tertiary C–OH and C–O groups, respectively. moreover, it was detected that both 1730 and 1065 cm^{-1} peaks were disappeared after the addition of P25. The absence of such peaks on the P25-GR composite indicates the successful reduction of GO to graphene via solvothermal method. Furthermore, the P25-GR composite showed a much plumper absorption at around 654 cm^{-1}, which was attributed to the combination of Ti–O–Ti vibration and Ti–O–C vibration, confirming the strong chemical interactions between GO and TiO$_2$.
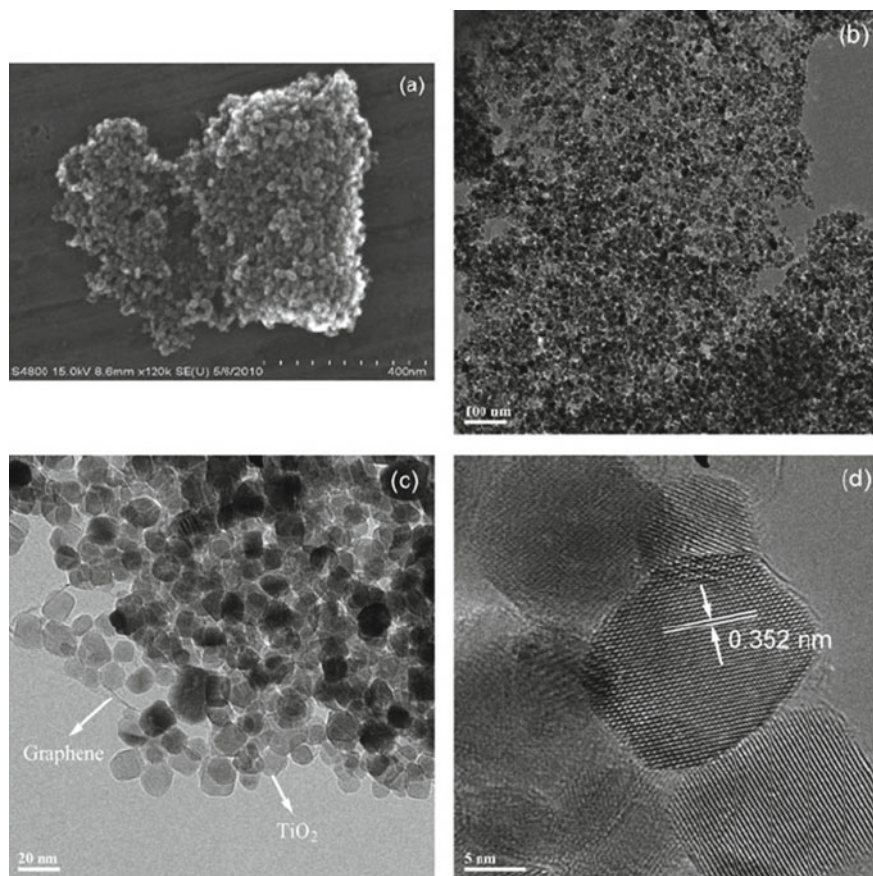
Fig. 15 SEM and TEM images of G/TiO$_2$ composites [47]

4.2.4 Raman Spectroscopy

Raman spectroscopy is a complementary technique to infrared spectroscopy that provide more information about composition and characteristics of the resulting material such as the number and quality of the graphene layers as well as the crystal phase structure of TiO$_2$. Figure 17 shows the Raman spectra of GO, RGO, TiO$_2$ NWs and TiO$_2$ NWs-RGO nanocomposite prepared by Yue et al. [38]. The Raman spectrums of GO and RGO reveal the presence of two peaks at 1352 and 1594 cm^{-1} were ascribed to D and G bands hybridized carbon atoms, respectively. Thus, it was detected that the intensity ratio of the D and G bands of RGO was lower compared to that of GO, which confirms that GO was successfully reduced to RGO after hydrothermal synthesis [42]. Moreover, TiO$_2$ NWs-RGO nanocomposite contains the main peaks of TiO$_2$ and both D-band and G-band of RGO, indicating the success of the combination of that TiO$_2$ and RGO and the strong interaction between them.
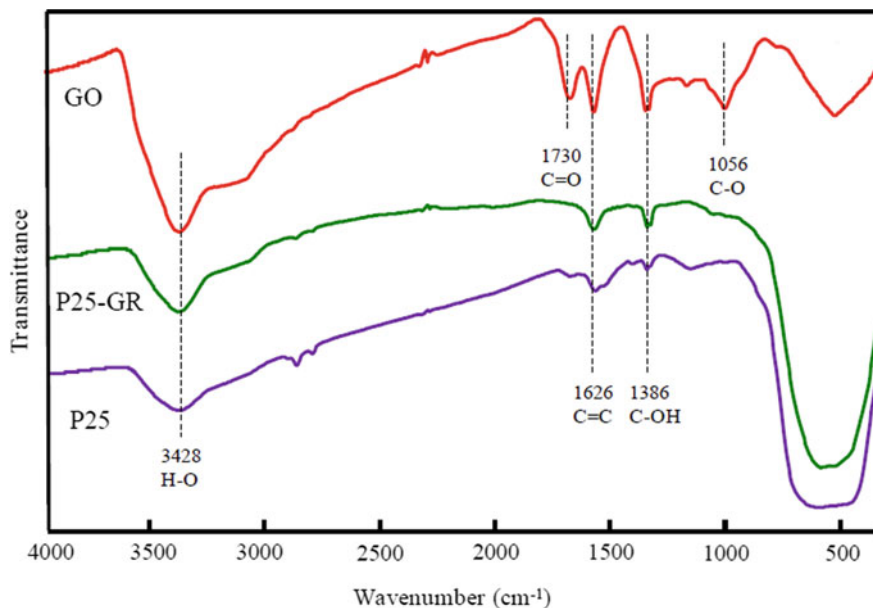
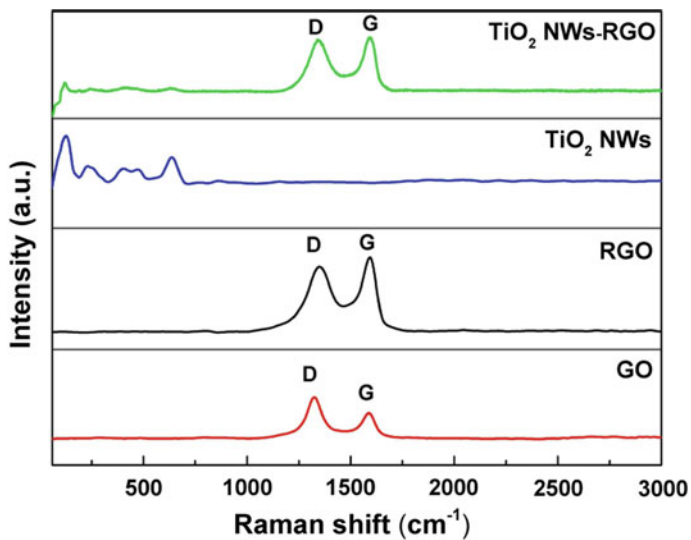**Fig. 16** The FTIR spectrums of GO, P25 and P25-GO-1% composite [48]

Fig. 17 Raman spectra of TiO$_2$/RGO nanocomposite compared to starting products [38]

4.2.5 Textural Properties (S_{BET}, Pore Size Distribution and the Total Pore Volume)

The surface and pore size distribution as well as the total pore volume of TiO_2/graphene hybrid nanocomposites were usually characterized via the nitrogen adsorption/desorption measurements. These parameters are very interesting because they have a largely powerful effect on the final application. Indeed, composites with higher specific surface area and important porosity present higher adsorption and photocatalytic activities. Shah et al. [49] have demonstrated that all composites prepared during their work via hydrothermal technique exhibited high surface areas, as RGO content increased. It reaches a value of $2600 m^2$/g. This specific surface area enhancement positively influenced its photocatalytic activity compared to P25 and TiO_2 photocatalysts (Fig. 18).
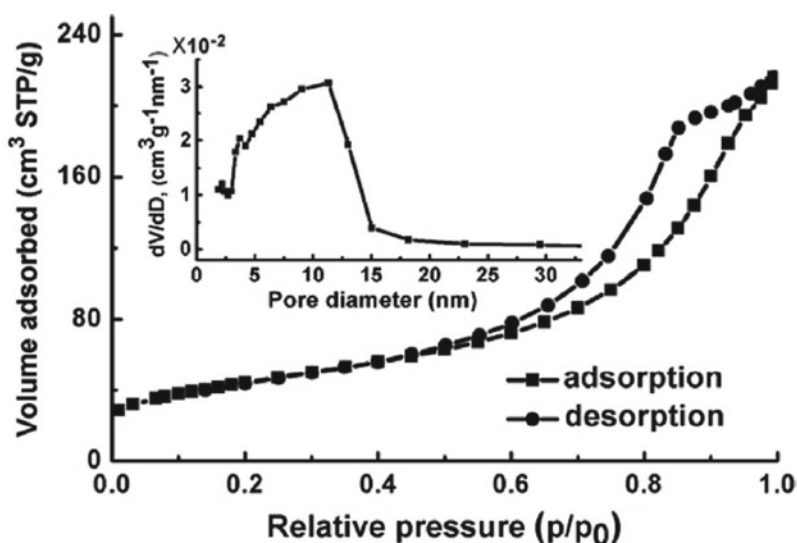
samples	^{a}surface area ($m^2\ g^{-1}$)	^{b}pore volume ($cm^3\ g^{-1}$)	^{c}average pore size (nm)
P25	39.0	0.13	27.9
TiO_2	81.8	0.43	15.8
TiO_2−1 wt % RGO	99.2	0.26	11.5
TiO_2−2 wt % RGO	115.0	0.28	9.3
TiO_2−5 wt % RGO	158.7	0.34	7.6
TiO_2−8 wt % RGO	169.1	0.20	4.0

Fig. 18 BET surface area and pore size distribution of TiO_2/RGO nanocomposites [49]
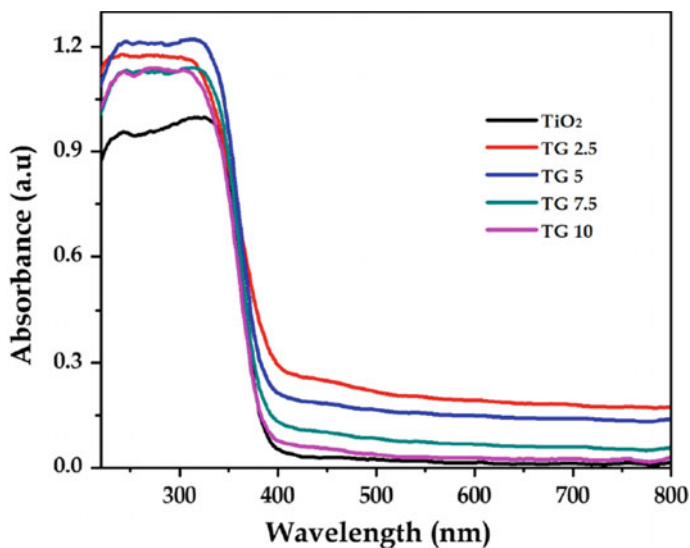
Fig. 19 UV–Vis spectra of TiO$_2$/graphene nanocomposites with different G loadings [50]

4.2.6 UV–Visible Absorption Spectroscopy

As already mentioned, the combination of TiO$_2$ and graphene materials allows to shift the TiO$_2$ response to visible light regions, which constitutes the major purpose of heterogeneous photocatalysis application. Therefore, UV–Visible spectroscopy was used to confirm the major changes that may occur during the preparation of TiO$_2$/graphene hybrid composites. As shown in the Fig. 19 all TiO$_2$/graphene composites prepared via microwave-assisted method, with different graphene amount, showed a red shift in the absorption edge and a strong absorption in the whole visible light range from 400 to 800 nm, in contrast to pure TiO$_2$ [50]. This highly visible light response is attributed to the narrow of their band gap energy after the addition of graphene, as well as to the electronic interactions between graphene and TiO$_2$ nanoparticles that delays the e$^-$/h$^+$ recombination.

4.3 Application on Wastewater Treatment Field

The photodegradation of different pollutants in sewage using TiO$_2$/graphene hybrid nanocomposites is one of the important and efficient strategy for environmental management and wastewater purification. Owing to its promising physical and chemical properties with the ease of processability, graphene and its derivatives provide ideal supportive behavior for TiO$_2$ photocatalyst. According to the literature, it was found that TiO$_2$/graphene hybrid nanocomposites present better photocatalytic

performances toward organic pollutants, heavy metals and other inorganic contaminants, compared to the bare TiO_2 or graphene [51]. This enhancement is attributed to both lower band gap and recombination rate of the e^-/h^+ pairs. Indeed, thanks to its electronic properties, graphene can easily collect the electron and suppress charge recombination.

Nguyen and his collaborator Juang [37] have realized a series of photocatalytic tests using different simples, namely, P25, and TiO_2/graphene oxide nanocomposites with different GO loadings, to evaluate the role of incorporating graphene oxide on the photocatalytic ability. The photocatalytic activity of different samples was assessed via the oxidation of Methylene blue and Orange G dyes under both UV and visible lights. The composite with 3wt%RGO displayed the highest photocatalytic capacity, thereabouts 100% decolorization and 77.4% mineralization were attained after 1 h of UV irradiation, against 95% decolorization and 78.8% mineralization after 3 h of visible light irradiation. The authors attributed the significant enhancement to the reduction in the band gap energy of TiO_2 after the addition of RGO that allows efficient electron transfer and therefore higher photocatalytic activity. Furthermore, it was found that all composites exhibited lower affinity toward towards anionic dyes compared to the P25, due to their negatively charged surface that creates more repulsions interactions. To confirm that what is happening is attributed to ROS species, the authors added different amounts of isopropanol (IPA), p-benzoquinone (p-BQ), and iodide anions to methylene blue solutions. These elements serve as hydroxyl radical, superoxide anion and hole scavengers, respectively. It was found that the MB degradation was slightly lower in the presence of such elements, indicating the important role of both hydroxyl and superoxide radicals in MB degradation under visible light irradiation. Efficient removal of Cr(VI) by 3D TiO2-reduced graphene oxide hydrogel was reported by Li et al. [42]. After 60 min of UV irradiation, all of Cr(VI) were removed by the TiO_2/RGO composite against only 73.6% using the pure TiO_2, while the reduced graphene oxide was found incapable of photocatalysis, confirming the synergetic effect of both graphene and titanium dioxide on the adsorption of Cr(VI) ions. In addition, the authors were studied the mechanisms involved during the removal of Cr(VI) using the TiO_2/rGO composite. It was found that the Cr(VI) elimination can be realized through two pathways, Cr(VI) ions were firstly adsorbed on the 3D network structure of the composite via graphene that owns higher surface area and abundant functional groups and then reduced to Cr(III) ions thanks to the reactive super-oxidant species generated by TiO_2 photocatalyst.

TiO_2/Graphene hybrid nanocomposites can be also used for the inactivation of pathogenic microorganisms present in water. Recently Noreen et al. [52] found that the TiO_2/graphene nanocomposites doped by silver and synthesized via hydrothermal route could be effectively utilized against *Campylobacter jejuni* bacteria under visible light. The bare TiO_2 showed activity against all tested bacteria, which is in accordance with the Sect. (3.2). Moreover, it was observed a large increase of the composite antibacterial activity after the addition of silver, confirming the dominant role of incorporating silver in the composite. Indeed, silver ions have the ability either interact with thiol groups of vital bacterial enzymes, or penetrate to cytoplasmic membrane for interacting with DNA, inducing photocatalytic antibacterial activity
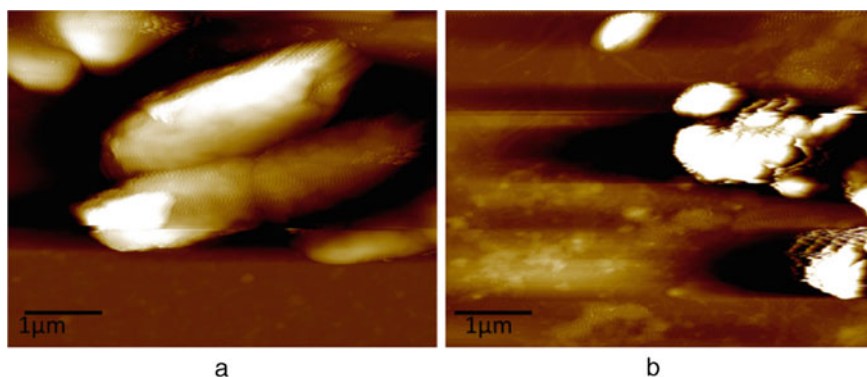
Fig. 20 Effect of Ag/TiO$_2$/GR hybrid nanocomposite on cellular morphology of *C. jejuni* [52]

in both cases. These hypotheses were confirmed by the cytoplasmic leak test, which showed the release of a large quantity of DNA and RNA from *Campylobacter jejuni* cells after the Ag-TiO$_2$/graphene exposition (Fig. 20).

5 Conclusion and Future Perspectives

This work presents an extensive bibliographic study on recent investigations of TiO$_2$/graphene hybrid nanocomposite from their synthesis methods, characterization to their applications in environmental applications, specifically in the wastewater treatment. Based on different research studies carried out in this area, it was found that TiO$_2$/graphene hybrid nanocomposite present higher affinity towards a wide range of pollutants and bacteria due to their important textural, chemical, and physical properties. Indeed, graphene and its derivatives, with high porosity, large specific surface area and abundant functional groups enhance the adsorption of different pollutants on the surface of the hybrid nanocomposite and improve the adsorption of different contaminants due to several mechanisms that can be involved such as electrostatic interactions, hydrogen bonding, π-π interactions and many others. Moreover, due to their important electronic properties, they can act as electrons attractor, preventing the charge recombination phenomena. Finally, the incorporation of graphene leads to narrowing of the band gap and red shift the adsorption in the visible region of the spectrum. Despite the numerous advantages described above, the applications of TiO$_2$/graphene hybrid nanocomposite still confined only on the laboratory scale. The weak dispersion and poor bonding between TiO$_2$ and graphene are the two major challenges hinder their industrial applications. In addition, some fundamental questions remain open. Is the enhancement of the photocatalytic activity of TiO$_2$/graphene hybrid nanocomposites is attributed only to its huge surface area and electronic conductivity extending the life of electron–hole pairs?

Can 3D TiO$_2$/graphene hybrid nanocomposites be useful and more efficient than 2D TiO$_2$/graphene hybrid nanocomposites for the removal of pollutants from sewage?

References

1. Qu X, Alvarez PJJ, Li Q (2013) Applications of nanotechnology in water and wastewater treatment. Water Res 47(12):3931–3946
2. Gusain R, Kumar N, Sinha S (2020) Recent advances in carbon nanomaterial-based adsorbents for water purification. Coord Chem Rev 405:213111
3. Kausar A et al (2018) Dyes adsorption using clay and modi fi ed clay : a review. J Molec Liquids 256:395–407
4. Mahmoodi NM, Saffar-Dastgerdi MH (2019) Zeolite nanoparticle as a superior adsorbent with high capacity: synthesis, surface modification and pollutant adsorption ability from wastewater. Microchem J 145:74–83
5. Hu LJWJS, Zhong LS, Song WG (2008) Synthesis of hierarchically structured metal oxides and their application in heavy metal ion removal. Adv Mater, 2977–2982
6. Abdeen Z, Mohammad SG (2014) Study of the adsorption efficiency of an eco-friendly carbohydrate polymer for contaminated aqueous solution by organophosphorus pesticide, vol 2014, pp 16–28
7. Mukhopadhyay G, Behera H (2010) Emerging two-dimensional materials : graphene and its other structural analogues, pp 1–12
8. Charles G, Roques-carmes T, Becheikh N, Falk L, Commenge J, Corbel S (2011) Determination of kinetic constants of a photocatalytic reaction in micro-channel reactors in the presence of mass-transfer limitation and axial dispersion. J Photochem Photobiol Chem 223(2–3):202–211
9. Lee S, Park S (2012) Comprehensive review on synthesis and adsorption behaviors of graphene-based materials 13(2):73–87
10. Systems N (2011) The sp2 nanocarbons : prototypes for nanoscience and nanotechnology, pp 3–16
11. Yazdi GR, Iakimov T, Yakimova R (2016) Epitaxial graphene on SiC : a review of growth, no. 0001
12. Properties E, View BS, Do TN (2017) Optical properties of graphene in magnetic and electric field, March 2016
13. Shams SS (2015) Graphene synthesis : a review, May 2018
14. Choi W et al (2010) Synthesis of graphene and its applications : a review 8436
15. Khan ME, Khan MM, Cho MH (2018) Recent progress of metal–graphene nanostructures in photocatalysis
16. Cao Y, Li X (2014) Adsorption of graphene for the removal of inorganic pollutants in water purification : a review, pp 713–727
17. Morales-torres S, Pastrana-martínez LM (2012) Design of graphene-based TiO2 photocatalysts—a review, pp 3676–3687
18. Wu X, Hu J, Qi J, Hou Y, Wei X (2020) Graphene-supported ordered mesoporous composites used for environmental remediation : a review. Separation and Purification Technology, p 116511
19. Al-khateeb LA, Almotiry S, Abdel M (2014) Adsorption of pharmaceutical pollutants onto graphene nanoplatelets. Chem Eng J 248:191–199
20. Chia C, Nur FR, Mohd SS, Sarani Z, Huang N, Lim H (2013) Methylene blue adsorption on graphene oxide. Sains Malaysiana 42:819–826
21. Jiang X, Liu L, Zeng Y, Xiao G, Hu F, Hu X, Wang X, Li H, Zhou T, Tan L (2016) Removal of 17β-estradiol by few-layered graphene oxide nanosheets from aqueous solutions: external influence and adsorption mechanism. Chem Eng J 284:93–102

22. Fujishima A, Honda K (1972) Electrochemical photolysis of water at a semiconductor electrode. Nature 238:37–38
23. Aravindan V, Lee Y, Yazami R (2015) TiO$_2$ polymorphs in ' rocking-chair ' Li-ion batteries. Biochem Pharmacol
24. Bet-Moushoul E, Mansourpanah Y, Farhadi K, Tabatabaei M (2016) TiO$_2$ nanocomposite based polymeric membranes: a review on performance improvement for various applications in chemical engineering processes, vol 283. Elsevier B.V
25. Miszczak S, Pietrzyk B (2015) Anatase-rutile transformation of TiO$_2$ sol-gel coatings deposited on different substrates. Ceram Int 41(6):7461–7465
26. Wang C, Wang H, Chen Q, Ren B, Duan R, Guan R (2019) Synchronous regulation of morphology and crystal phase of TiO$_2$ via a facile green hydrothermal approach and their photocatalytic activity. Mater Res Bull 109:90–97
27. Mamaghani AH, Haghighat F, Lee C (2018) Hydrothermal/Solvothermal synthesis and treatment of TiO$_2$ for photocatalytic degradation of air pollutants: Preparation, characterization, properties, and performance. Chemosphere
28. Behzadnia A, Montazer M, Rashidi A, Rad MM (2014) Sonosynthesis of nano TiO 2 on wool using titanium isopropoxide or butoxide in acidic media producing multifunctional fabric. Ultrasonics Sonochemistry
29. Nakata K, Fujishima A (2012) TiO2 photocatalysis: design and applications. J Photochem Photobiol, C 13:169–189
30. Sohrabi MR, Ghavami M (2008) Photocatalytic degradation of direct red 23 dye using UV/TiO$_2$: effect of operational parameters 153:1235–1239
31. Lachheb H et al (2002) Photocatalytic degradation of various types of dyes (Alizarin S , Crocein Orange G , Methyl Red , Congo Red , Methylene Blue) in water by UV-irradiated titania, vol 39, pp 75–90
32. Photosemiconductor TU (1988) Continuous-sterilization system that uses photosemiconductor powders, 54(6):1330–1333
33. Zeng Lu XEW, Fang Zhou H, Liao JJ, Yang YY, Wang K, Ming Che L, He N, Dong Chen X, Song R, Fang Cai W, Liu H (2019) A facile dopamine-assisted method for the preparation of antibacterial surfaces based on Ag/TiO$_2$ nanopartilces. Appl Surf Sci 481:1270–1276
34. Zhang H, Lv X, Li Y, Wang Y, Li J (2009) P25-graphene composite as a high performance photocatalyst. Am Chem Soc 4(1)
35. Decontamination W (2018) Dioxide/graphene oxide nanocomposites: synthesis, water decontamination
36. Tang B, Chen H, Peng H, Wang Z, Huang W (2018) Graphene modified TiO$_2$ composite photocatalysts: mechanism, progress and perspective, pp 27–30
37. Nguyen CH, Juang R (2019) Efficient removal of methylene blue dye by a hybrid adsorption–photocatalysis process using reduced graphene oxide/titanate nanotube composites for water reuse. J Indus Eng Chem
38. Yue HY, Guan H, Gao X, Yao F, Wang Q, Zhang T (2018) Hydrothermal synthesis of TiO$_2$ nanowires-reduced graphene oxide nanocomposite to enhance electrochemical performance in supercapacitor, pp 12455–12460
39. Awang H, Talalah NI (2019) Synthesis of reduced graphene oxide-titanium (rGO-TiO2) composite using a solvothermal and hydrothermal methods and characterized via XRD and UV-Vis, pp 17–28
40. Yadav HM, Kim J (2016) Solvothermal synthesis of anatase TiO$_2$-graphene oxide nanocomposites and their photocatalytic performance. J Alloys Compounds
41. Zhang L, Xi Z, Xing M, Zhang J (2013) Effects of the preparation order of the ternary P25/GO/Pt hybrid photocatalysts on hydrogen production. Int J Hydrogen Energy pp 1–9
42. Li Y et al (2016) Removal of Cr(VI) by 3D TiO$_2$-graphene hydrogel via adsorption enriched with photocatalytic reduction. Appl Catal B 199:412–423
43. Zhen M, Liu L, Yuan Z (2016) Facile preparation and lithium storage properties of TiO$_2$@graphene composite electrodes with low carbon content. Chem Eur J 22:11943–11948
44. Giovannetti R (2017) Recent advances in graphene based TIO$_2$

45. Hicham Atouta FM, Álvarezb MG, Cheblia D, Bouguettouchaa A, Tichitc D, Llorcad J (2017) Enhanced photocatalytic degradation of methylene blue: preparation of TiO_2/reduced graphene oxide nanocomposites by direct sol-gel and hydrothermal methods. Mater Res Bull 95:578–587
46. Li W et al (2013) Sol−gel design strategy for ultradispersed TiO_2 nanoparticles on graphene for high-performance lithium ion batteries. J Am Chem Soc, pp 0–3
47. Zhou K, Zhu Y, Yang X, Jiang X, Li C (2011) Preparation of graphene—TiO_2 composites with enhanced photocatalytic activity. New J Chem, pp 353–359
48. Liu J, Wang L, Tang J, Ma J (2016) Photocatalytic degradation of commercially sourced naphthenic acids by TiO_2-graphene composite nanomaterial. Chemosphere 149:328–335
49. Kan Z, Park JH (2012) Green synthesis of biphasic TiO_2-reduced graphene oxide nanocomposites with highly enhanced photocatalytic activity
50. Gayathri S, Kottaisamy M, Ramakrishnan V (2018) Facile microwave-assisted synthesis of titanium dioxide decorated graphene nanocomposite for photodegradation of organic dyes, vol 127219, no. 2015
51. Bhanvase BA, Shende TP, Sonawane SH (2017) A review on graphene—TiO_2 and doped graphene—TiO_2 nanocomposite photocatalyst for water and wastewater treatment, 2515, no. December 2016
52. Noreen Z, Khalid NR, Abbasi R, Javed S, Ahmad I, Bokhari H (2019) Materials science & engineering C visible light sensitive Ag/TiO_2/graphene composite as a potential coating material for control of Campylobacter jejuni. Mater Sci Eng C 98:125–133

Hybrid Nanocomposites Based on Graphene and Zinc Oxide Biosensor Applications

R. D. A. A. Rajapaksha

Abstract Graphene is ideal reinforcing material today, has a unique 2D nanostructure with few nanometer gaps between particle layers. 130 GPa strength gain high thermal conductivity and electric conductivity. Apart from mechanical strength, high surface to volume ratio, ease of functionalization, and other physicochemical properties gain remarkable properties in sensing and biosensing applications. Graphene-based inorganic composite is gained new attention to various applications because of the synergic effect of the composite. Graphene-based ZnO gains new properties such as mechanical, thermal, electrical, and binding to the composite material. Graphene/ZnO reinforced composite gain high stability, sensitivity, rapidity, and selectivity and low LOD to the biosensors.

Keywords Nanoparticle · Potentiometry · Voltammetry · Impedimentary · Conductometry · Biomaterial · Self-assembly · Protein · DNA

1 Introduction

Graphene is a two-dimensional (2D) flat monolayer of carbon atoms attached as a honeycomb lattice [1]. Zero bandgap, high conductivity, and high transparency are outstanding properties of graphene. The charge carrier mobility of Graphene is 250,000 cm^2 V^{-1} s^{-1} at room temperature, and thermal conductivity is 5000 W m^{-1} K^{-1} with the electrical conductivity of 6000 S cm^{-1} [2]. Another important unique property of graphene is the ability to combine with inorganic nanoparticles. Graphene has in-plane elastic modulus (0.5–1 TPa) and tensile strength (130 GPa) due to the sp^2 hybrid bonding of carbon atoms [3]. High electrical conductivity, fast carrier mobility, large surface area, and high capacity to immobilize molecules are desired properties of graphene to be used in biosensors [4]. Conjugated system of graphene is known to facilitate the electron transfer between the bioreceptor and transducer of

R. D. A. A. Rajapaksha (✉)
Department of Nano-Science Technology, Faculty of Technology, Wayamba University of Sri Lanka, Kuliyapitiya, Sri Lanka
e-mail: asanka@wyb.ac.lk

the biosensor. Moreover, some of the graphene-based nanomaterials with conjugated system are known to special abilities to quench the fluorescent signal of biosensors producing 'on-off' molecular switches [5].

Biosensors consist of three main components, namely a bio receptor, transducer and signal processor. The bio-receptor moiety of biosensors has greater affinity to recognize the desired complementary target analyte than that of the other molecules with similar structure of noncomplementary targets. The high selectivity and specificity of a biosensor is greatly hinged on its ability to make perfect complementarity in host-guest chemistry. The receptors which have been immobilized a priori onto transducer surface via spacer group permits to have harnessed the effect of preorganization affording the augmented selectivity toward a desired analyte [6]. The biological reactions taking place in living milieu of cells leverage its cell-signaling cascades to magnify its faint signals in situ generated. Such concatenation of interlined cell-signaling cascades are managed to produce a macroscopically observable changes to external beholders.

The analytical characteristics of the system depend on the inter-component correlation and the intra-component properties of each unit. These biological receptors such as ssDNA, antibodies, hormones, cells, etc., have been immobilized on the transducer surface. Biological signal transforms to electrical signals by using transducer [6, 7]. Typically the sensors sense physical changes in the surroundings and translate them to a readable quantity. In here, the transducer transforms this readable signal (energy) into another type. For example, in electrochemical analytical devices, the sensor senses changes from light, temperature, pH, ion concentration, etc. and transforms them into electrical signals. Response time (rapidity) and sensitivity of the system depend on the transducer. Biological receptor and nanotechnology-based transducers help to create a miniaturized device and bioelement-nanoparticle functionalized transducer interface which is useful to enhance signal amplification capabilities. There are different types of miniaturized transducers that can be used in the sensors and biosensors such as interdigitated electrode (IDE) and various types of nano-gap based systems, ion selective field effect transducer (ISFET), cantilever systems etc. [8–10]. As the third part of the biosensor system, the key tasks of the processing circuit are to amplify the signal, process the signal and allow to view in a display by user-friendly manner [11–13]. Various electrochemical methods (voltammetric, potentiometric, conductometric and impedimetric) can commonly be used in sensitive detections. Different types of nanomaterials have an enormous potential to be used in improving the efficiency of these types of miniaturized transducer-based analytical systems [13–16]. Nanoparticle functionalized label-free biosensors, nanoparticle tags in bioassay dependent biosensors and nanoparticle bioassay sandwich dependent electrochemical systems can be used in analytical systems. The role of usage of NPs in analytical systems improve the sensitivity and selectivity of the device, contributing to early detection of disease in a medical diagnosis. Figure 1 shows the schematic of biosensor architecture.

Graphene oxide (GO) and reduced graphene oxide (rGO) are widely utilized in graphene composites-based biosensor applications. A graphene sheet with its basal plane decorated by oxygen-containing groups such as hydroxyl, epoxy, carboxyl, and
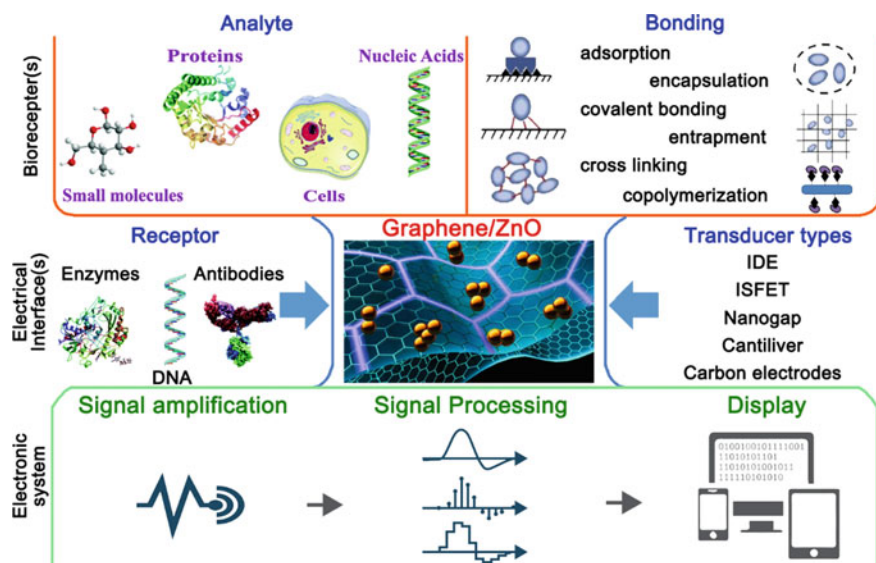
Fig. 1 Biosensor architecture of Graphene/ZnO based biosensor

carbonyl groups are called graphene oxide [17, 18]. Excellent biological response and materials safety are the remarkable properties of GO for sensor applications [19, 20]. There are several synthetic routes available in literatures to prepared GO and rGO, namely Modified Hummer's method, top-down approach, sticky tape method, solvent interface trapping film formation method, David Boyd method and just to name a few [19]. Reduced GO (rGO) sheets are chemically derived graphene specially used in the biosensor field [21]. Chemical, electrochemical, thermal, and photothermal microwave reduction are nifty techniques used to synthesize reduced graphene oxide from graphene oxide (Karthila). According to Ghanbari and Moludi, rGO facilitates large active sites for molecule immobilizing [22, 23].

Nowadays, researchers have focused on nanocomposites to take synergetic advantage and enhance the properties of available materials. Many scholars have chosen graphene as a filling agent for composites due to its exceptional electronic, thermal, and mechanical properties [24]. Lawal had reported about graphene-polymer nanocomposite, graphene/activated carbon nanocomposite, graphene/metal oxide nanocomposite, graphene/metal nanocomposite, and graphene/fibres nanocomposite. Among them, graphene/metal oxide nanocomposite are promising nanocomposites in the biosensor applications. George and coworkers had stated that metal oxide is the appropriate material to enhance the sensing ability of graphene [25]. According to Saleh and Fadillah, metal oxides can induce the structural changes, and which lead to change in lattice symmetry and other concomitant other parameters facilitating to build the 3D conductive porous network having enhanced the charge transferring and other electrical properties [name few desired electrical properties). Finally, this makes the changes the surface properties which lead to increase
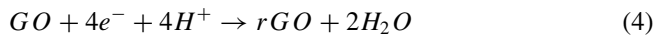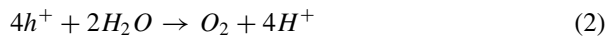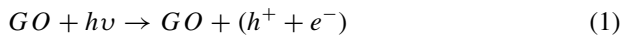
the chemical activity and conductivity [26]. For few examples, TiO_2, ZnO, MnO_2, Cu_2O, SnO_2, and NiO are the leading metal oxide nanoparticles used in biosensor applications [27, 28].

ZnO has received significant consideration due to its outstanding properties such as wide bandgap, high abundance, low cost, and hexagonal wurtzite crystal structure [29]. According to Yue and coworkers, excellent catalytic properties, rapid electron transferring, large surface area, and high chemical stability are the other properties of ZnO nanoparticles [30]. The synergetic effect of graphene and ZnO nanocomposite could have been the cause to enhance the electron transferring rate and conductivity [31]. In addition to that, photocatalytic activities, energy storage capability, sensing activity, nonlinear optical switching capability, and optoelectronic characteristics will have a promise to be improved by this combination. Joshi et al. reported that this composite has shown enhanced photocatalytic performance by reducing the recombination rate of charge-carriers [32]. Further, they reported that graphene could have been the cause to enhance the roughness and surface area of the nanocomposite, which may lead to improve the photoelectrochemical reaction.

This chapter covers the synthesis of graphene/ZnO nanocomposites, interaction of graphene with ZnO, and graphene/ZnO based biosensor applications. Graphene-ZnO composite based biosensors such as enzymatic, nucleic acid and immune-based two-electrode and three-electrode electrochemical biosensors are discussed in this chapter. Their performance and electrical characterization have been done by contemporary electrical characterization techniques, such as voltammetry, amperometry, potentiometry, and impedometry.

2   Interaction between Graphene/GO/rGO and ZnO

In here, functionalized GO sheets with carboxyl, hydroxyl, and epoxy groups can attract positively charge metal ions. These metal ions attach to the surface and edges of GO sheets through oxidation and reduction reactions. These attachment sites create nucleation sites to grow nanostructures on the graphene sheets. In the meantime, the reduction of GO and metal ions form metal-graphene nanocomposites. GO create photogenerated electrons, which can reduce the metal ions. The following reactions will explain the above phenomenon.

$$GO + h\upsilon \rightarrow GO + (h^+ + e^-) \tag{1}$$

$$4h^+ + 2H_2O \rightarrow O_2 + 4H^+ \tag{2}$$

$$M^+ + GO(e^-) \rightarrow GO + M \tag{3}$$

$$GO + 4e^- + 4H^+ \rightarrow rGO + 2H_2O \tag{4}$$

Chemisorption, physisorption, covalent bonding, van der waals, and electrostatic interaction are other mechanisms where nanostructures are attached to the graphene sheets. Because of these attachments, restacking, and aggregation of the graphene sheets will be reduced.

3 Synthesis of Graphene and ZnO Composites

There are many reported methods based on the ZnO nanostructures synthesized on the graphene/GO/rGO nanosheets.

3.1 Hydrothermal/Solvothermal Synthesis

The hydrothermal method is a promising method for the synthesis of a variety of inorganic nanoparticles under controlled temperature and pressure. If the solution medium is non-aqueous, the process can be called as solvothermal. This method can be used to produce homogeneous crystalline powders with high purity and ultrafine size distribution. Low processing temperature and less reaction time are the main advantages of this method. The closed stainless steel autoclave Teflon-lined framework is used in the hydrothermal synthesis. When the Vessel's temperature rises, the pressure within the vessel often rises, and the disintegration of the thermodynamically unstable compounds intensifies if the critical pressure of the water exceeds the pressure. Hence, the macromolecules are broken down into nano-size particles in the aqueous solution. Absolute ethanol was used as a solvent for the production of ZnO. The benefit of ethanol is to boost gel-like GO dispersion [33]. This method is used to decorate ZnO nanoparticles on the graphene, GO, and rGO nanosheets (Fig. 2).

Junwei et al. have synthesized different ZnO nanostructures on rGO by an in-situ hydrothermal reaction for nonenzymatic electrochemical N_2H_4 sensors. The size and shape of ZnO on RGO surface can be effective controlled by adjusting the mass ratio of Zn^{2+} to RGO. After the combination of ZnO with RGO, the conductivity of ZnO-RGO composites can be improved, leading to higher sensitivity for N_2H_4 determination [34]. Chang et al. have developed ZnO nanoroad/Graphene heterostructure by a facile in situ hydrothermal growth method [35]. Balasubramaniam et al. have used low temperature hydrothermal method without any reducing agent [36].
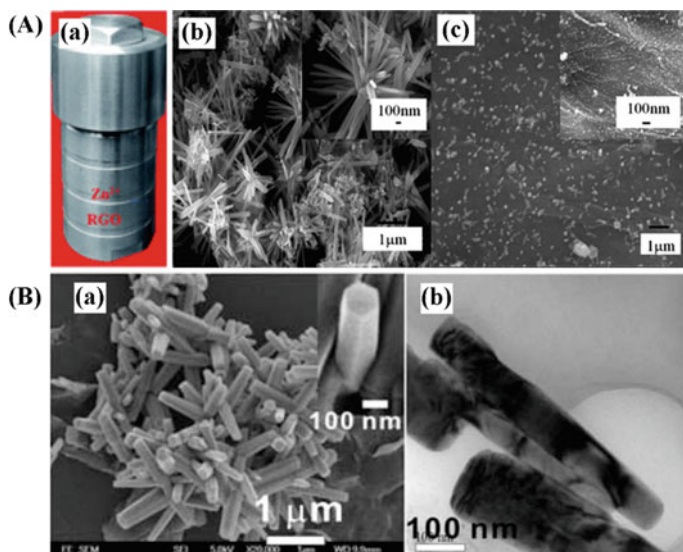
Fig. 2 Hydrothermal synthesis of ZnO QD/graphene composite films. (A-**a**) Schemes for hydrothermal synthesis of ZnO nanorods/graphene heterostructures, (A-**b**) SEM image of ZnO nanorods (A-**c**) SEM image of ZnO nanorods/graphene film [34], (B-**a**) SEM micrographs of ZnO QD/graphene hybrid film, (B-**b**) TEM micrographs of ZnO QD/graphene hybrid film [35]

3.2 Graphene-Based ZnO Using Microwave-Assisted Hydrothermal Synthesis

This approach can be used to synthesize the complex binary or ternary metal oxides, including zeolites. Because of minimal synthesis times and high localized heat, nanoparticle prepared by this method had made uniform particle size distribution. Microwave heating is based on the reaction conditions and molecular properties of the materials and usually takes place with the 2.45 GHz microwave frequency. The size of the ZnO nanoparticles varied between 10 and 100 nm. The synthesis of ZnO nanocomposites with microwave-assisted graphene has also been reported [37]. The growth of ZnO nanostructures is constrained by graph sheets. T. Lu et al. have performed important work on the synthesis of ZnO decorated graphene nanocomposites using the microwave with a high specific capacity. In here GO, NaOH and zinc sulphate were used as reactants [35]. Kajbafvala et al. has been carried out the synthesis of the ZnO wires (sword form) by microwave energy. The raw materials included methanol, tri-ethanol amine, dehydrated zinc acetate, and sodium hydroxides. The length of the ZnO nanowire was in the range of ~1 to 4 inches, and the width was 80–250 nm. S. Meti et al. has prepared nanocomposite of rGO/ZnO by using microwave-assisted hydrothermal method. Here, they synthesized GO by following the Tang Lau method and used the GO for the preparation of rGO/ZnO.

3.3 Sol–Gel Synthesis

Synthesis of ZnO nanocomposites by the sol–gel method has now become ubiquitous, are used in various applications. Zinc precursors, additives, and solvent are used for the synthesis process, which is based on hydrolysis and co-condensation of the hydrolyzed precursors into ZnO nanocomposites. Pourshahan et al. developed ZnO nanocomposites using zinc acetate as zinc precursor in alcoholic solvents such as methanol and ethanol. The ZnO nanorods were synthesized at 500 °C for 60 min by using the calcination technique. Para et al. used zinc acetate, glacial acetate, and ammonium acetate as reacting materials to synthesize ZnO-nanoparticles. H. Li et al. developed a Nanocomposite ZnO/graphene film as an anode for lithium-ion batteries using the aqueous solution of zinc acetate, ethanol, graphene, and lithium hydroxide. Demes et al. studied the effects on the morphology of ZnO nanowires of various amine agents such as mono and diethanolamine [38]. Zimmermann et al. also studied the impact of ZnO film development on various substrates [39]. They have synthesized ZnO quantum dots and studied their development by reacting with ethylene glycol, Zinc acetate, NaOH, 2-Propanol, and ethylene glycol.

3.4 Electrochemical Growth

The electrochemical method, through the deposition of ZnO, is effective because of the effective dimensions controlling manner. In this method, applied potential and solution concentration are the tunable measurement factors. Oxygen saturated aqueous salt solution is used to deposition of ZnO at a lower temperature (<100 °C). The growth of ZnO from planer film to nanosized islands depends on the variation of growth parameters such as substrate lattice parameters, electrolyte (chloride, nitrate, perchlorate, etc.), pre-activation surface treatment, amount of the oxygen content and applied potential.

Wong et al. have used a cathodic electrodeposition method to grow ZnO nanorods. Polycrystalline Zn foil was used to grow ZnO in the aqueous zinc chloride/calcium chloride at 80 °C. Electrochemical synthesis of ZnO on the GaAs substrate was carried out under aqueous zinc nitrate electrolyte solution by the Zeng et al. ZnO nanopillars was deposited on the single crystal of gold in the aqueous electrolyte solution of the $ZnCl_2$/KCl using electrochemical deposition (ECD) method by the Liu et al. ECD deposition of transparent ZnO under zinc nitrate aqueous solution by M. Izaki.

3.5   Biological Synthesis of the ZnO Nanoparticles

Compared to other methods, the biological synthesis process for ZnO nanoparticles is economical, effective, and environmentally friendly. For the production of nanoparticles, this process uses plant extracts, microorganisms, and enzymes and. The nanoparticles synthesized by this process were used in applications of biosensors, water purification applications, catalysts, antibacterial, and antivirals. ZnO nanoparticles were produced from extracts of plants, food sources, and microbes.

Al-Dhabi and coworkers used an aqueous extract of Scadoxus Multiflorus (S. multiflorus) leave powder to synthesize the ZnO nanoparticles. Khalil el al. have used Sageretia thea (Osbeck) mediated synthesis of the ZnO nanoparticles. Venkalesan and coworkers used the extract of Ipomoea pes-caprae leaves for the synthesis of ZnO nanoparticles [40].

4   Enzyme-Immobilized Graphene/ZnO Based Biosensors

Graphene-based Enzymatic biosensors can be seen in various applications in numerous areas such as biomedical, environmental, agriculture, food and beverage industries, pharmaceutical, etc. According to the detection principle, these biosensors can be categorized as electrochemical, optical, piezoelectric, etc. different electrochemical biosensors are various bio receptors that can be seen, such as enzymatic, nucleic acids, antibody, etc.

4.1   Glucose Oxidase

Glucose biosensors are attracting an increasing interest due to the drastic improvement in the number of diabetic patients. The availability of affordable and reliable techniques to measure blood glucose levels is very important in diabetes treatments. Hyperglycemia is a critical situation where blood glucose level is higher than 7 mmol/L (126 mg/dL) when fasting and higher than 11.1 mmol/L (200 mg/dL) 2 h after a meal [41]. If the blood glucose level is less than 2 mmol/L, it leads to unconsciousness situations. In enzymatic glucose biosensors, the following reaction will occur with the presence of Glucose Oxidase [42].

$$\beta - D - glucose + O_2 + H_2O \xrightarrow{GOx} C_6H_{12}O_7 + H_2O_2 \tag{5}$$

$$H_2O_2 \xrightarrow{GOx} O_2 + 2H^+ + 2e^- \tag{6}$$
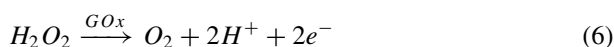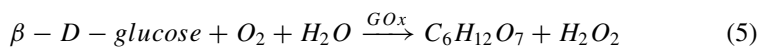
Graphene/ZnO nanocomposite is a promising hybrid composite used in enzymatic glucose biosensors. These composites provide catalytic and other essential benefits through their synergetic effects.

Kavitha, Lee, and Park had developed glucose biosensors using graphene/ZnO nanocomposite as shown in Fig. 3 [43]. They used graphene because of super electrical and thermal conductivity, good mechanical properties, lateral quantum confinement, high carrier mobility at room temperature, high chemical stability, and large specific surface area. ZnO NPs also important nanomaterial, which facilitates excellent contribution sensor applications. The research team had a focused wide bandgap (3.37 eV) and a wide bandgap (60 meV) of ZnO NPs at room temperature. Besides, the high surface-to-volume ratio and quantum confinement effect also highlighted the properties of ZnO NPs. The combination of ZnO and graphene-enhanced the immobilization in native configuration and feasibility of direct electron transfer. The nanocomposite was developed by using situ thermal decompositions of zinc benzoate dihydrazinate on the graphene surface. This technique has many merits, such as uniform size, high yield, no impurities, simple preparation, low cost, and decomposition temperature. They used Ag/AgCl as a reference electrode and ZnO/graphene/GOx as the working electrode. The sensor has shown high sensitivity for glucose detection.

Hwa and Subramani had fabricated a voltammetric glucose biosensor by using GR–CNT–ZnO composite [44]. According to their report, conductivity, chemical stability, economics, and flexibility are the common characteristics of graphene. Besides, graphene sheets have hydrophobic, low polar, and high π-electron density,
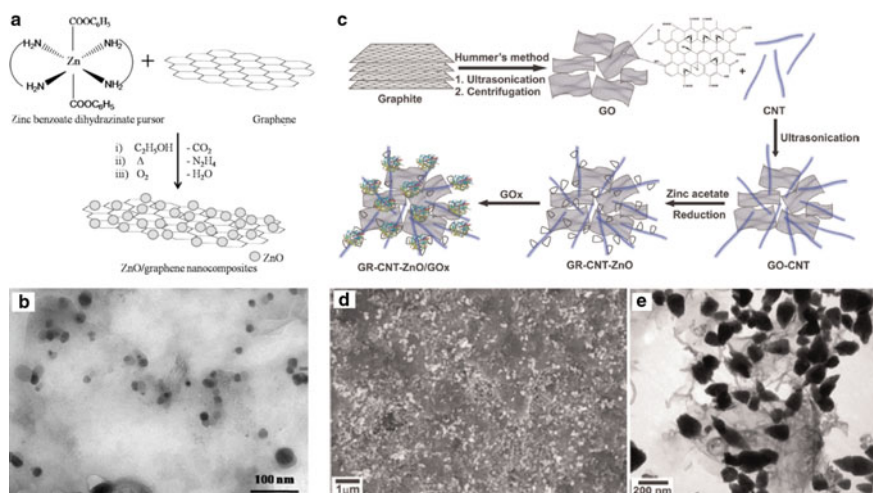

Fig. 3 **a** Schematic showing the decomposition pathway of the precursor and the deposition of ZnO nanoparticles on graphene, **b** TEM image of the ZnO-coated graphene, **c** Schematic representation of the preparation of GR–CNT–ZnO composite, **d** SEM image of GR–CNT–ZnO, and **e** TEM image of GR–CNT–ZnO [43]

which facilitates easy immobilization of molecules via covalent or non-covalent bonding. Non-toxic, high electron transferring rate, and electrochemical activity are the key characteristics of ZnO utilized in this research. High electrocatalytic activity and electron-transfer rate are the most essential properties of CNT widely use in sensor applications. With the combined effect of the GR and CNT, ZnO nanostructures facilitate high absorption of enzymes because of their specific surface area, chemical stability, and excellent biocompatibility. First, they synthesized GO–CNT composite through a simple solution-based approach. GR–CNT–ZnO composite was prepared through the simultaneous reduction of GO and zinc acetate by using sodium borodihydride (NaBH4). The research team had highlighted high selectivity, sensitivity, rapidity, fidelity, low cost, and portability as the merits of electrochemical techniques. The GR–CNT–ZnO/GOx modified GCE sensor had shown 5.362 $\mu A\ mM^{-1}\ cm^{-2}$ with a limit of detection as 4.5 μM. The repeatability, stability, and reproducibility of the sensor were very high.

Another Graphene/ZnO@Pd composite based dual-enzyme biosensor was developed by Gu et al. [45]. For in vivo simultaneous detections of glucose. They highlighted specific surface area and outstanding properties of electrical, mechanical, and thermal as the key performance of graphene utilized in this research. The use of Pd and ZnO had facilitated large active surface area and fast electron transfer. Finally, Graphene/ZnO@Pd acted as an excellent electrocatalyst H_2O_2 reduction. There were two major steps in the preparation of Graphene/ZnO@Pd composite. First graphene oxide support to disperse ZnO nanorods via hydrothermal path while reducing the graphene oxide to reduced graphene sheet. In the second step, the Graphene/ZnO composite was supported to reduce and disperse Pd NPs with exposition to UV light. The sensor has shown excellent linearity as 20 μM for glucose detection with 2.39 μM. The research team tested this biosensor for L-lactate detection also.

4.2 Cholesterol Oxidase

Cholesterol detection has received much interest in the biomedical field due to the increase in the number of patients. The blood cholesterol level is a key parameter for diagnosing many disorders such as coronary heart disease, hypertension, anemia, brain thrombosis, and many more deceases [46]. Generally, the level of cholesterol in human blood serum is less than 5.17 mM, and 70% of them are in ester form. The other 30% exists as sterols [47]. In the past few decades, scholars have focused on finding convenience methods to detect blood cholesterol levels. Electrochemical enzymatic biosensors offer many merits, such as high sensitivity, intrinsic selectivity, and fast response [48]. Cholesterol oxidize in enzymatic biosensors can represent as follows [46].

$$Cholesterol + O_2 \xrightarrow{ChOx} Cholest - 4 - en - 3 - one + H_2O_2 \qquad (7)$$

$$H_2O_2 \xrightarrow{E} O_2 + 2H^+ + 2e^- \tag{8}$$
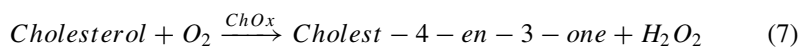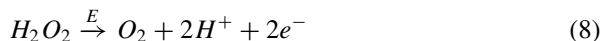
Watanabe and coworkers had developed graphene decorated zinc oxide NPs based biosensor for cholesterol detection as shown in Fig. 4 [49]. They have reported many reasons for the use of graphene such as high signal to volume ratio, high loading of bio-analyte, and specific surface area. Large surface area, superior biocompatibility, and non-toxicity are the highlighted properties of zinc oxide NPs. They followed the electrochemical technique because of simplicity, low cost, and rapidity. ZnO/graphene nanocomposite was fabricated through Microwave irradiation. ZnO was dispersed on the surface of graphene, especially in edges of graphene. The sensor showed 1.3 $\mu A/\mu M\ cm^2$ of sensitivity ($R^2 = 0.980$) with a 5.0 $\mu mol\ L^{-1}$ limit of detection. Excellent stability, repeatability, and reproducibility are the other highlighted benefits this sensor.

Wu et al. had developed enzymatic cholesterol biosensor using zinc oxide, graphene oxide, chitosan, and silver nanowires [50]. 1D nanostructures of ZnO have unique properties such as non-toxicity, excellent biocompatibility, large surface area excellent chemical stability, super electrochemical activities, and low cost. A wide bandgap and high electron mobility may lead to efficient electron transport. High isoelectric point (9.5) of ZnO may help to immobilized low biomaterials as protein and enzymes. Because of extraordinary electronic properties and specific surface area, the research team used graphene oxide for enhancing the sensitivity. AgNWs are support to maintain the surface area, and chitosan acts as a conductive bridge between ZnO and AgNWs. The composite may enhance the catalytic activity of the biosensor. ZnO nanostructures were spin-coated on the AgNWs and GO-CS membrane. The biosensor (ChOx/ZnO/AgNWs/GO-CS/ITO) was shown 9.2 $\mu A\ \mu M^{-1}\ cm^{-2}$. Sensitivity and 0.287 μM limit of detection with high stability.
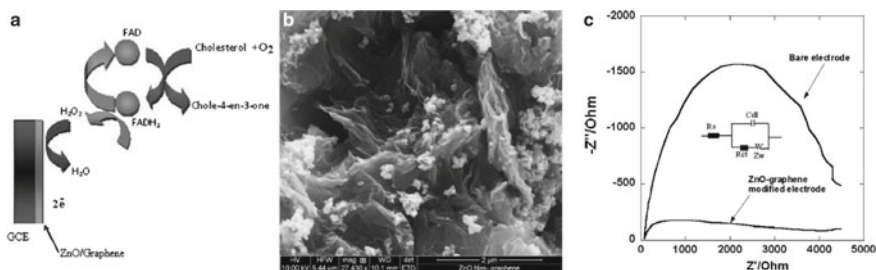
Fig. 4 **a** Cholestarrol detection mechanism of ChOx/ZnO/Graphene biosensor, **b** SEM image of ZnO- graphene nanocomposite, and **c** electrochemical impedance spectroscopy [49]

4.3   Urease

Urea detection is very important for fields of clinical diagnostics, pharmaceutical industry, food industry, environmental protection, fertilizer industry. Urea is a waste product of protein metabolism, and nitrogen is the major component of it [51]. The normal urea concentration in blood serum is 1.33–3.33 mM, and any deviation of this level may cause renal failure, nephritic syndrome, hepatic failure, dehydration, cachexia, urinary tract obstruction, shock, burns and gastrointestinal issues [52]. In the commercial milk industry, urea use as an adulterant, and cut off urea level is 11.7 mM [53]. Electrochemical enzymatic biosensors provide remarkable benefits in the sense of urea detection. According to Lakard et al., urease hydrolysis to ammonium and bicarbonate ions as follows [54].
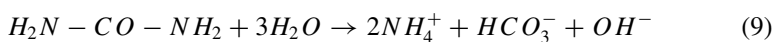
$$H_2N - CO - NH_2 + 3H_2O \rightarrow 2NH_4^+ + HCO_3^- + OH^- \tag{9}$$

Excellent selectivity, simplicity, ease of miniaturization, and low cost are the major advantages of urease enzyme electrode base biosensors [55].

A novel ZnO–graphene composite based impedimetric urea biosensor was developed by Karimi and coworkers [56]. They used ZnO due to its unique features such as non-toxicity, well stability, good biocompatibility, large surface area, and high isoelectric point. Super thermal conductivity, larger surface area, electrical conductivity, and excellent mechanical strength are the remarkable properties of graphene. The synthesized composite has facilitated high surface area and better loading of enzymes. The spin coating technique was used to synthesize the ZnO–Gr thin films. The sensor has shown high sensitivity, wide dynamic range (5–125 mg dL^{-1}), low limit of detection (3.36 mg dL^{-1}), and fast response time (5 s).

5   Nucleic Acid-Immobilized Graphene/ZnO Based Biosensors

Nucleic acid-based biosensors have received increasing interest due to their outstanding features of high specificity, sensitivity, and easy manipulation. The use of DNA is important for selective biological recognition [57]. DNA and RNA are the most commonly used nucleic acids in many sensor applications. Three dimensional single-stranded DNA and RNA structures bind with specific targets with high affinity and specificity. According to Hong et al., RNA aptamers have a higher binding affinity than DNA aptamer [58]. But RNA is more prone to nuclease degradation than DNA. The nucleic acid structure consists of stem-loop, bulges, and hairpin, which can identify binding pockets for target via noncovalent bindings. Because of high specificity, this technique is widely used in biosensor applications. In electrochemical DNA biosensors measured generated electrochemical signal due to hybridization of prob

ssDNA and target ssDNA [59]. Graphene and ZnO nanostructures are promising materials with having outstanding properties used in biosensors.

Low et al. had fabricated graphene and ZnO nanocomposite based amperometric DNA biosensor for Avian Influenza H5 detection [31]. According to their report, electrical conductivity, super thermal and electrochemical characteristics, rapid electron mobility, and specific surface area as extraordinary properties of graphene. Further, they reported wide bandgap, high isoelectric point, large exciton binding energy, biocompatibility, and biodegradability as unique properties of ZnO. The synergetic effect of graphene/ZnO composite may enhance the sensor performance as enhancing electron transferring rate and conductivity, improving photocatalytic performance, enhance storage capabilities, and sensing properties. Low-temperature solvothermal synthesis technique used to synthesis graphene/ZnO composite. This method is economical, safe, and enhance the quality of graphene. The sensor had shown 3.2580 μA mM^{-1} sensitivity and a 7.4357 μM detection limit.

Another graphene/ZnO composite based DNA biosensor was developed by Low and coworkers for Coconut Cadang-Cadang Viroid (CCCVd) RNA detection as shown in Fig. 5 [60]. Because of chemical inertness, excellent electron transferring, and specific surface area graphene had selected as one of the materials for sensor fabrication. Wide bandgap, large exciton binding energy, high catalytic activity, non-toxicity, biocompatibility, chemical stability, and excellent conductivity are outstanding properties of ZnO utilized in the sensor. The synergetic effect of graphene/ZnO donated high surface area, superior conductivity, high electrocatalytic, and optimum immobilization matrix of ZnO. Low-temperature solvothermal processing treatment was used for the synthesis of graphene/ZnO. This method reduced the defects and conserved the pristine structure of graphene. The target
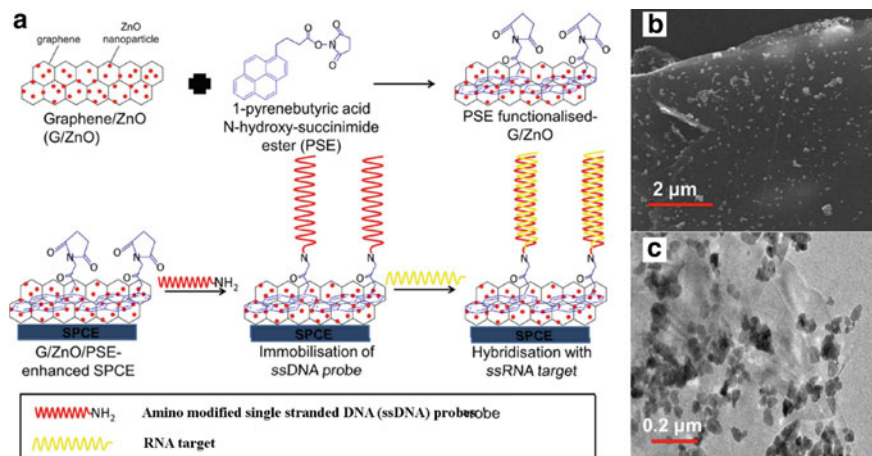
Fig. 5 **a** Schematic diagram for the development of graphene/ZnO nanocomposite-modified electrochemical impedance genosensor for ssRNA detection. **b**, and **c** SEM and TEM analyses of graphene/ZnO nanocomposite [60]

was covalently immobilized on to the graphene/ZnO composite surface through a bio-linker (1-pyrenebutyric acid N-hydroxysuccinimide ester). The linear range of the sensor was 1.0×10^{-11} to 1.0×10^{-6} M with the limit of detection as 4.3×10^{-12} M.

Zhang et al. had developed ZnO nanowire and graphite microfiber based biosensor for DNA hybridization [61]. High isoelectric point (IEP 9.5), high adsorption, wide bandgap, excellent stability, good biocompatibility, large specific surface area, and high electron communication properties are highlighted characteristics of ZnO. One dimensional (1D) structure and excellent conductivity are outstanding properties of graphite used in the sensor development. In-situ synthesized ZnO NWs were fabricated on graphite microfiber using the hydrothermal method. The diameter of graphite microfibers was 6 μm, and ZnO nanowires were in a 100–150 nm range. DNA probe was immobilized onto the ZnO nanowires through strong electrostatic interaction. The sensor detection range was 1.0×10^{-14} to 1.0×10^{-7} M. Finally; biosensor had shown excellent selectivity and high stability with 3.3×10^{-15} M limit of detection.

6 Antibody-Immobilized Graphene/ZnO Based Biosensors

Immunosensors are promising biosensor types widely used in agriculture, food and pharmaceutical industries, clinical analysis, and diagnostics epidemic disease control and prevention programs [62]. Mostly, antibodies are taken as bio receptors, and antigens are used as targets [63]. In the molecular recognition process, antibody and antigen formed stable immunocomplex, and the generated electrical signal was identified by the transducer. High sensitivity, low cost, and miniaturization are some major benefits of immunosensors. Nowadays nanostructures, play a major role in the sensing field by improving electrochemical activities of transducers, conjugating with biomolecules, and electrochemical labeling. Among them, the graphene/ZnO composite has received increasing interest due to their unique properties.

Cheng and coworkers had developed ZnO, graphene, glucose oxidase, and Au NPs based immunosensors for cancer biomarker detection as shown in Fig. 6 [64]. They used ZnO NPs because of fast electron transferring, excellent chemical stability, good biocompatibility, and high electrochemical activity. GOD decorated graphene had exhibited excellent sensitivity and high stability. ZnONPs decorated graphene (ZnONPs@Gra) were synthesized by using linking reagent as glutaraldehyde (GA). Antibody (Ab2) was linked to ZnONPs@Gra composite to form ZnONPs and GOD labeled Ab$_2$. Finally, it was immobilized on to the electrode surface through sandwich immunoreactions. The sensor detection range was 10 pg mL^{-1} to 80 ng mL^{-1}, and the limit of detection was 3.3 pg mL^{-1}.

Sun et al. had fabricated ZnO, reduced graphene oxide (rGO), and silver nanoparticles based microfluidic paper-based analytical device (μ-PAD) for clinical applications [65]. Low consumption of the analyte, portability, low cost, easy to handle, and disposability are the prominent advantages of μ-PAD. According to their article,
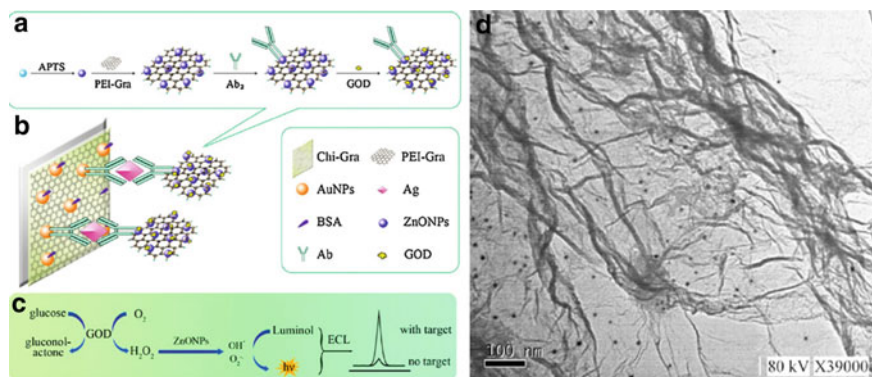
Fig. 6 **a** The schematic of the preparation procedure of ZnONPs at graphene-GOD-Ab$_2$, **b** the fabrication of proposed ECL immunosensor, **c** the mechanism of the multiple signal amplification strategy, **d** the TEM image of ZnONPs at graphene nanocomposites [64]

high chemical stability, excellent electrical conductivity, and unique surface area are the distinctive properties of rGO. On the other hand, ZnO facilitates accelerate electron transfer between immobilized biomolecule and electrode. Also, high surface to volume ratio, low tendency to agglomerate, and specific electron transferring are the other merits of ZnO. A low-temperature hydrothermal technique was used to grow ZNRs on rGO-PWE. It has facilitated a better platform to capture antibodies (Ab$_1$). The sensor was used to detect human chorionic gonadotropin (HCG), prostate-specific antigen (PSA), and carcinoembryonic antigen (CEA). The biosensor had shown excellent specificity, high sensitivity, high stability, and good reproducibility. The linear range of sensors for HCG, PSA, and CEA were 0.002–120 mIU mL^{-1}, 0.001–110 ng mL^{-1}, and 0.001–100 ng mL^{-1}, respectively.

Another tumor biomarker detection sensor was developed by Fang and colleagues using Au/ZnO/RGO composite for Alpha-fetoprotein detection [66]. Because of high catalytic efficiency, high surface-to-volume ratio, biological compatibility, and non-toxicity, the team selected ZnO for their sensor fabrication. RGO had played a major role due to specific surface area, fast electron transferring, and biocompatibility. Au/ZnO/RGO composite was synthesized via a simple one-step hydrothermal route with a C$_{12}$N$_3$ surfactant. Because of the synergetic effect, nanocomposite was enhanced the loading capacities of Ab$_1$. The sensor detection limit was 0.01 pg mL^{-1} with high selectivity, good reproducibility, and well stability.

7 Other Types of Biosensor

7.1 *Uric Acid, Ascorbic Acid and Dopamine Detection*

Uric acid is an output of purine derivatives in human metabolism, and it is an indicator of gout, hyperuricemia, Lesch–Nyhan syndrome, and renal diseases [67]. The level of uric acid is related to alcohol consumption, high cholesterol, diabetes, obesity, heart diseases, and kidney disease [68]. According to the literature, serum uric acid level is a risk for cardiovascular disease [69]. Electrochemical enzymatic biosensors provide remarkable facilities in the sense of uric acid detection. Excellent selectivity, simplicity, ease of miniaturization, and low cost are the major advantages of the electrode surface modification approach [70]. PH and temperature are important factors that affect sensor performance. Many researchers focused on nanomaterials to enhance sensor performance. Among them, graphene-zinc oxide composite is a leading hybrid composite used in many studies due to their unique properties and synergetic effect.

Zhang and coworkers had developed an electrochemical biosensor for uric acid, ascorbic acid and dopamine detection by using RGO–ZnO composite as shown in Fig. 7 [71]. Good biocompatibility, conductivity, and high abundancy of graphite sources at a low price are the unique features of graphene. RGO–zinc oxide composite was synthesized by spontaneous reduction of GO through Zn slice in a one-pot approach. By using the modified Hummers technique, GO was produced from graphite powder. The RGO–zinc oxide composite was able to increase the electroactive surface area and sensitivity of the sensor. The biosensor has shown excellent reproducibility and high stability with a 3.71 µM limit of detection. Same time the sensor has been used to detect dopamine and ascorbic acid simultaneously.

Ghanbari and Moludi also developed uric acid detection biosensor using flower-like ZnO, polyaniline nanofiber, and reduced graphene oxide [22]. Excellent electrical conductivity, specific surface area, and high chemical stability are highlighted
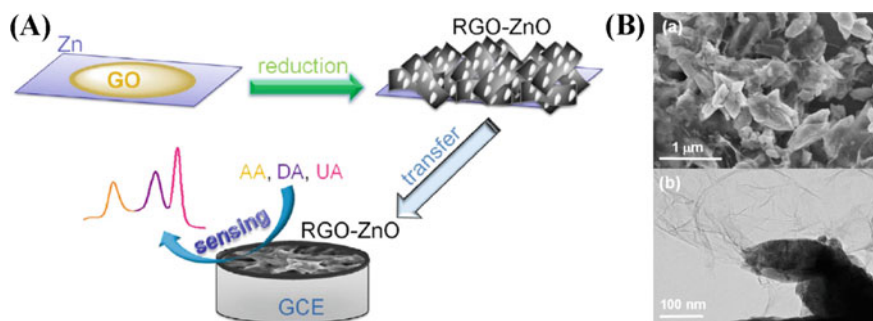
Fig. 7 (A)Schematic illustration of fabrication process of the RGO-ZnO/GCE electrochemical biosensor, (B-**a**) SEM image of RGO-ZnO and (B-**b**) TEM image of RGO-ZnO [71]

features of graphene. Wide bandgap energy, non-toxicity, high electron transferring rate, large surface area, excellent electrochemical activity, crystalline structure, super mechanical properties, good biocompatibility, and good environmental acceptability are the remarkable properties of ZnO. Reduced graphene oxide (RGO) was synthesized from graphene oxide through electrochemical reduction by applying a constant cathodic potential. Through situ electrochemical syntheses, PANI/RGO composite was prepared. ZnO/PANI/RGO composite was prepared by electrochemical deposition of ZnO nanoparticles. Good selectivity, high sensitivity, wide linear detection range (0.1–100 and 100–1000 μM), and low limit of detection (0.042 μM) are the remarkable performance of the sensor.

Another uric acid detection biosensor was developed by Fu and colleagues [72]. They used reduced graphene oxide and ZnO nanorods for electrode modification. High surface area, easy to process, high electron transferring rate, and safety are the key characteristics of graphene. ZnO/RGO could enhance the electrocatalytic activity. ZnO/RGO composite was synthesized through the simple one-pot hydrothermal method. The sensor liner detection range was 1–800 μM, and the limit of detection was 0.312 μM. And also sensor had shown well stability with excellent anti-interference property.

8   Concluding Remarks

Graphene is ideal reinforcing material today, has a unique 2D nanostructure with few nanometer gaps between particle layers. 130 Gpa strength gain high thermal conductivity and electric conductivity. Apart from mechanical strength, high surface to volume ratio, ease of functionalization, and other physicochemical properties gain remarkable properties in sensing and biosensing applications. Graphene-based inorganic composite is gained new attention to various applications because of the synergic effect of the composite. Graphene/ZnO nanocomposite gains new properties such as mechanical, thermal, electrical, and binding to the composite material. Those properties gain high stability, sensitivity, rapidity, selectivity and low LOD for biosensors applications.

References

1. Anand K, Singh O, Singh RC (2014) Different strategies for the synthesis of graphene/ZnO composite and its photocatalytic properties. Appl Phys A Mater Sci Process 116(3):1141–1148. https://doi.org/10.1007/s00339-013-8198-x
2. Khan M et al (2015) Graphene based metal and metal oxide nanocomposites: synthesis, properties and their applications. J Mater Chem A 3(37):18753–18808. https://doi.org/10.1039/c5ta02240a
3. Nieto A, Bisht A, Lahiri D, Zhang C, Agarwal A (2017) Graphene reinforced metal and ceramic matrix composites: a review. Int Mater Rev 62(5):241–302. https://doi.org/10.1080/09506608.

2016.1219481

4. Peña-Bahamonde J, Nguyen HN, Fanourakis SK, Rodrigues DF (2018) Recent advances in graphene-based biosensor technology with applications in life sciences. J Nanobiotechnol 16(1):1–17. https://doi.org/10.1186/s12951-018-0400-z

5. Kou J, Nguyen EP, Merkoçi A, Guo Z (2020) 2-dimensional materials-based electrical/optical platforms for smart on-off diagnostics applications. 2D Mater 7(3). doi: https://doi.org/10.1088/2053-1583/ab896a

6. Rajapaksha RDAA, Hashim U, Afnan Uda MN, Fernando CAN, De Silva SNT (2017) Target ssDNA detection of E.coli O157:H7 through electrical based DNA biosensor. Microsyst Technol 23(12):5771–5780. doi: https://doi.org/10.1007/s00542-017-3498-2

7. Parmin NA et al (2019) Voltammetric determination of human papillomavirus 16 DNA by using interdigitated electrodes modified with titanium dioxide nanoparticles. Microchim Acta 2:2–10

8. Rajapaksha RDAA, Hashim U, Fernando CAN (2017) Design, fabrication and characterization of 1.0 μm Gap Al based interdigitated electrode for biosensors. Microsyst Technol 23(10):4501–4507. https://doi.org/10.1007/s00542-017-3373-1

9. Fernando CAN, Liyanaarachchi US, Rajapaksha RDAA (2013) Explanation of the photocurrent quantum efficiency (Φ) enhancements through the CAN's model equation for the p-CuI sensitized methylviolet-C 18 LB films in the photoelectrochemical cells (PECs) and Cu/n-Cu 2 O/M-C 18 /p-CuI solid-state photovoltaic cells. Semicond Sci Technol 28(4):045017. https://doi.org/10.1088/0268-1242/28/4/045017

10. Rajapaksha RDAA, Hashim U, Gopinath SCB, Fernando CAN (2018) Sensitive pH detection on gold interdigitated electrodes as an electrochemical sensor. Microsyst Technol 24(4):1965–1974. https://doi.org/10.1007/s00542-017-3592-5

11. Rajapaksha RDAA, Hashim U, Natasha NZ, Uda MNA, Thivina V, Fernando CAN (2017) Gold nano-particle based Al interdigitated electrode electrical biosensor for specific ssDNA target detection. IEEE Reg Symp Micro Nanoelectron 191–194

12. Rajapaksha RDAA, Hashim U, Uda MNA, Fernando CAN (2018) High-performance electrical variable resistor sensor for E. coli. J Telecommun Electron Comput Eng 10(1):61–64

13. Yahaya NAN, Rajapaksha RDAA, Uda MNA, Hashim U (2017) Ultra-low current biosensor output detection using portable electronic reader. AIP Conf Proc 1885. doi: https://doi.org/10.1063/1.5002430

14. Rajapaksha RDAA (2020) Self-assembling smart materials for biomaterials applications. In: Polymer nanocomposite-based smart materials. Elsevier Ltd, pp 121–147

15. Rajapaksha RDAA, Hashim U, Gopinath SCB, Parmin NA, Fernando CAN (2021) Nanoparticles in electrochemical bioanalytical analysis. In: Nanoparticles in analytical and medical devices. Elsevier Ltd, pp 83–112

16. Letchumanan I, Md Arshad MK, Gopinath SCB, Rajapaksha RDAA, Balakrishnan SR (2020) Comparative analysis on dielectric gold and aluminium triangular junctions: impact of ionic strength and background electrolyte by pH variations. Sci Rep 10(1):1–10. doi: https://doi.org/10.1038/s41598-020-63831-w

17. Marcano DC et al (2010) Improved synthesis of graphene oxide. ACS Nano 4(8):4806–4814. https://doi.org/10.1021/nn1006368

18. Dékány I et al (2006) Evolution of surface functional groups in a series of progressively oxidized graphite oxides. Chem Mater 18(11):2740–2749. https://doi.org/10.1021/cm060258

19. Ghorai TK (2019) Graphene oxide-based nanocomposites and biomedical applications. Elsevier Ltd

20. Sun X et al (2008) Nano-graphene oxide for cellular imaging and drug delivery. Nano Res 1(3):203–212. https://doi.org/10.1007/s12274-008-8021-8

21. Ray SC (2015) Application and uses of graphene oxide and reduced graphene oxide, no. ii. Elsevier Inc.

22. Ghanbari K, Moloudi M (2016) Flower-like ZnO decorated polyaniline/reduced graphene oxide nanocomposites for simultaneous determination of dopamine and uric acid. Anal Biochem 512:91–102. https://doi.org/10.1016/j.ab.2016.08.014

23. Prasad K et al (2017) Synergic bactericidal effects of reduced graphene oxide and silver nanoparticles against Gram-positive and Gram-negative bacteria. Sci Rep 7(1):1–11. https://doi.org/10.1038/s41598-017-01669-5

24. Lawal AT (2019) Graphene-based nano composites and their applications. A review. Biosens Bioelectron 141:111384. doi: https://doi.org/10.1016/j.bios.2019.111384

25. George JM, Antony A, Mathew B (2018) Metal oxide nanoparticles in electrochemical sensing and biosensing: a review. Microchim Acta 185(7). doi: https://doi.org/10.1007/s00604-018-2894-3

26. Saleh TA, Fadillah G (2019) Recent trends in the design of chemical sensors based on graphene–metal oxide nanocomposites for the analysis of toxic species and biomolecules. TrAC—Trends Anal Chem 120:115660. https://doi.org/10.1016/j.trac.2019.115660

27. Li P, Zhang B, Cui T (2015) TiO2 and shrink induced tunable nano self-assembled graphene composites for label free biosensors. Sens Actuators B Chem 216:337–342. https://doi.org/10.1016/j.snb.2015.03.111

28. Jang HD, Kim SK, Chang H, Roh KM, Choi JW, Huang J (2012) A glucose biosensor based on TiO_2-Graphene composite. Biosens Bioelectron 38(1):184–188. https://doi.org/10.1016/j.bios.2012.05.033

29. Shetti NP, Bukkitgar SD, Reddy KR, Reddy CV, Aminabhavi TM (2019) ZnO-based nanostructured electrodes for electrochemical sensors and biosensors in biomedical applications. Biosens Bioelectron 141:111417. doi: https://doi.org/10.1016/j.bios.2019.111417

30. Yue HY et al (2020) Highly sensitive and selective dopamine biosensor using Au nanoparticles-ZnO nanocone arrays/graphene foam electrode. Mater Sci Eng C 108:110490. https://doi.org/10.1016/j.msec.2019.110490

31. Low SS, Tan MTT, Loh HS, Khiew PS, Chiu WS (2016) Facile hydrothermal growth graphene/ZnO nanocomposite for development of enhanced biosensor. Anal Chim Acta 903:131–141. https://doi.org/10.1016/j.aca.2015.11.006

32. Joshi BN, Yoon H, Na SH, Choi JY, Yoon SS (2014) Enhanced photocatalytic performance of graphene-ZnO nanoplatelet composite thin films prepared by electrostatic spray deposition. Ceram Int 40(2):3647–3654. https://doi.org/10.1016/j.ceramint.2013.09.060

33. Rajeswari V, Jayavel R, Clara Dhanemozhi A (2017) Synthesis and characterization of graphene-zinc oxide nanocomposite electrode material for supercapacitor applications. Mater Today Proc 4(2):645–652. doi: https://doi.org/10.1016/j.matpr.2017.01.068

34. Ding J, Zhu S, Zhu T, Sun W, Li Q (2015) RSC Advances Hydrothermal synthesis of zinc oxide-reduced graphene oxide nanocomposites for an electrochemical hydrazine sensor. RSC Adv 5:22935–22942. https://doi.org/10.1039/C5RA00884K

35. Chang H et al (2011) A highly sensitive ultraviolet sensor based on a facile in situ solution-grown ZnO nanorod/graphene heterostructure. Nanoscale 3(1):258–264. https://doi.org/10.1039/c0nr00588f

36. Saravanakumar B, Mohan R, Kim S (2013) Facile synthesis of graphene/ZnO nanocomposites by low temperature hydrothermal method. Mater Res Bull 48(2):878–883. https://doi.org/10.1016/j.materresbull.2012.11.048

37. Ke Q, Wang J (2016) Graphene-based materials for supercapacitor electrodes—a review. J Mater 2(1):37–54. https://doi.org/10.1016/j.jmat.2016.01.001

38. Demes T et al (2016) New insights in the structural and morphological properties of sol-gel deposited ZnO multilayer films. J Phys Chem Solids 95:43–55. https://doi.org/10.1016/j.jpcs.2016.03.017

39. Zimmermann LM, Baldissera PV, Bechtold IH (2016) Stability of ZnO quantum dots tuned by controlled addition of ethylene glycol during their growth. Mater Res Express 3(7):1–9. https://doi.org/10.1088/2053-1591/3/7/075018

40. Khalil AT et al (2017) Sageretia thea (Osbeck.) mediated synthesis of zinc oxide nanoparticles and its biological applications. Nanomedicine 12(15):1767–1789. https://doi.org/10.2217/nnm-2017-0124

41. Fitzpatrick D (2015) Glucose biosensors. Implant Electron Med Devices, pp 37–51. doi: https://doi.org/10.1016/b978-0-12-416556-4.00004-8

42. McIlwaine F, Gerogiorgis DI (2018) Dynamic modelling and simulation of reactive transport phenomena in an amperometric blood glucose biosensor, vol 43. Elsevier Masson SAS

43. Kavitha T, Gopalan AI, Lee KP, Park SY (2012) Glucose sensing, photocatalytic and antibacterial properties of graphene-ZnO nanoparticle hybrids. Carbon N. Y. 50(8):2994–3000. https://doi.org/10.1016/j.carbon.2012.02.082

44. Hwa KY, Subramani B (2014) Synthesis of zinc oxide nanoparticles on graphene-carbon nanotube hybrid for glucose biosensor applications. Biosens Bioelectron 62:127–133. https://doi.org/10.1016/j.bios.2014.06.023

45. Gu H, Yang Y, Zhou X, Zhou T, Shi G (2014) Online electrochemical method for continuous and simultaneous monitoring of glucose and l-lactate in vivo with graphene hybrids as the electrocatalyst. J Electroanal Chem 730:41–47. https://doi.org/10.1016/j.jelechem.2014.06.002

46. Viswanathan P, Ramaraj R (2018) Functionalized graphene nanocomposites for electrochemical sensors. Elsevier Inc.

47. Vidal JC, Garcia-Ruiz E, Espuelas J, Aramendia T, Castillo JR (2003) Comparison of biosensors based on entrapment of cholesterol oxidase and cholesterol esterase in electropolymerized films of polypyrrole and diaminonaphthalene derivatives for amperometric determination of cholesterol. Anal Bioanal Chem 377(2):273–280. https://doi.org/10.1007/s00216-003-2120-x

48. Lin X, Ni Y, Kokot S (2016) Electrochemical cholesterol sensor based on cholesterol oxidase and MoS2-AuNPs modified glassy carbon electrode. Sens Actuators B Chem 233:100–106. https://doi.org/10.1016/j.snb.2016.04.019

49. Watanabe E, Spidle R, Caudle S, Manani G, Wanekaya AK, Mugweru A (2014) Electrochemical method for analysis of cholesterol based on in situ synthesized graphene decorated with zinc oxide nanoparticles. ECS Solid State Lett 3(1):5–9. https://doi.org/10.1149/2.001401ssl

50. Wu Q et al (2016) Amperometric cholesterol biosensor based on zinc oxide films on a silver nanowire-graphene oxide modified electrode. Anal Methods 8(8):1806–1812. https://doi.org/10.1039/c6ay00158k

51. Chirizzi D, Malitesta C (2011) Lecture notes in electrical engineering: foreword. Lect Notes Electr Eng LNEE 91:335–338. doi: https://doi.org/10.1007/978-94-007-1324-6

52. Pundir CS, Jakhar S, Narwal V (2019) Determination of urea with special emphasis on biosensors: a review. Biosens Bioelectron 123:36–50. https://doi.org/10.1016/j.bios.2018.09.067

53. Sarkara P, Dasa J (2013) Enzymatic electrochemical biosensor for urea with polyaniline grafted conducting hydrogel composite modified electrode. RSC Adv 6:7. https://doi.org/10.1039/C6RA12159D.This

54. Lakard B et al (2011) Urea potentiometric enzymatic biosensor based on charged biopolymers and electrodeposited polyaniline. Biosens Bioelectron 26(10):4139–4145. https://doi.org/10.1016/j.bios.2011.04.009

55. Dindar B, Karakuş E, Abasıyanık F (2011) New urea biosensor based on urease enzyme obtained from helycobacter pylori. Appl Biochem Biotechnol 165(5–6):1308–1321. https://doi.org/10.1007/s12010-011-9348-2

56. Ghayedi Karimi K, Mozaffari SA, Ebrahimi M (2018) Spin-coated ZnO–graphene nanostructure thin film as a promising matrix for urease immobilization of impedimetric urea biosensor. J Chinese Chem Soc 65(11):1379–1388. doi: https://doi.org/10.1002/jccs.201800031

57. Sun J et al (2019) Signal enhancement of electrochemical DNA biosensors for the detection of trace heavy metals. Curr Opin Electrochem 17:23–29. https://doi.org/10.1016/j.coelec.2019.04.007

58. Hong KL (2019) An overview of DNA/RNA-based monitoring tools and biosensors: benefits and applications in the environmental toxicology. Elsevier Inc

59. Drummond TG, Hill MG, Barton JK (2003) Electrochemical DNA sensors. Nat Biotechnol 21(10):1192–1199. https://doi.org/10.1038/nbt873

60. Low SS, Loh HS, Boey JS, Khiew PS, Chiu WS, Tan MTT (2016) Sensitivity enhancement of graphene/zinc oxide nanocomposite-based electrochemical impedance genosensor for single stranded RNA detection. Biosens Bioelectron 94:365–373. doi: https://doi.org/10.1016/j.bios.2017.02.038

61. Zhang J, Han D, Yang R, Ji Y, Liu J, Yu X (2019) Electrochemical detection of DNA hybridization based on three-dimensional ZnO nanowires/graphite hybrid microfiber structure. Bioelectrochemistry 128:126–132. https://doi.org/10.1016/j.bioelechem.2019.04.003
62. Ahmed MU, Zourob M, Tamiya E (2019) Detection science series editor-immunosensors. R Soc Chem
63. Patra S, Roy E, Madhuri R, Sharma PK (2017) A technique comes to life for security of life: the food contaminant sensors. Elsevier Inc.
64. Cheng Y et al (2012) Highly sensitive luminol electrochemiluminescence immunosensor based on ZnO nanoparticles and glucose oxidase decorated graphene for cancer biomarker detection. Anal Chim Acta 745:137–142. https://doi.org/10.1016/j.aca.2012.08.010
65. Sun G et al (2015) Multiplexed enzyme-free electrochemical immunosensor based on ZnO nanorods modified reduced graphene oxide-paper electrode and silver deposition-induced signal amplification strategy. Biosens Bioelectron 71:30–36. https://doi.org/10.1016/j.bios.2015.04.007
66. Fang X, Liu J, Wang J, Zhao H, Ren H, Li Z (2017) Dual signal amplification strategy of Au nanopaticles/ZnO nanorods hybridized reduced graphene nanosheet and multienzyme functionalized Au@ZnO composites for ultrasensitive electrochemical detection of tumor biomarker. Biosens Bioelectron 97:218–225. https://doi.org/10.1016/j.bios.2017.05.055
67. Numnuam A, Thavarungkul P, Kanatharana P (2014) An amperometric uric acid biosensor based on chitosan-carbon nanotubes electrospun nanofiber on silver nanoparticles. Anal Bioanal Chem 406(15):3763–3772. https://doi.org/10.1007/s00216-014-7770-3
68. Arslan F (2008) An amperometric biosensor for uric acid determination prepared from uricase immobilized in polyaniline-polypyrrole film. Sensors 8(9):5492–5500. https://doi.org/10.3390/s8095492
69. Dussossoy D, Py ML, Pastor G, Boulenc X (1996) Development of a two-site immunoassay of recombinant urate oxidase (SR 29142) and its use for determination of pharmacokinetic parameters in rats and baboons. J Pharm Sci 85(9):955–959. https://doi.org/10.1021/js960009s
70. Özcan A, Şahin Y (2010) Preparation of selective and sensitive electrochemically treated pencil graphite electrodes for the determination of uric acid in urine and blood serum. Biosens Bioelectron 25(11):2497–2502. https://doi.org/10.1016/j.bios.2010.04.020
71. Zhang X, Zhang YC, Ma LX (2016) One-pot facile fabrication of graphene-zinc oxide composite and its enhanced sensitivity for simultaneous electrochemical detection of ascorbic acid, dopamine and uric acid. Sens Actuators B Chem 227:488–496. https://doi.org/10.1016/j.snb.2015.12.073
72. Fu L, Zheng Y, Wang A, Cai W, Deng B, Zhang Z (2016) An electrochemical sensor based on reduced graphene oxide and Zno nanorods-modified glassy carbon electrode for uric acid detection. Arab J Sci Eng 41(1):135–141. https://doi.org/10.1007/s13369-015-1621-1

Hybrid Nanocomposites Based on Graphene and Its Derivatives: From Preparation to Applications

Ansa Kanwal, Asim Ali Yaqoob, Affia Siddique, Showkat Ahmad Bhawani, Mohamad Nasir Mohamad Ibrahim, and Khalid Umar

Abstract Graphene has obtained an excessive amount of interest and popularity from worldwide owing to its atypical physiochemical, chemical, thermal and mechanical stability-based properties. Graphene, a one atom thick plain sheet with sp^2 bonding and the carbon atoms are compactly packed in structure to form crystal lattice. Many approaches are known to synthesize the graphene derivatives and therefore, it is essential to discuss a list of distinguished approaches like exfoliation and cleavage, thermal chemical vapor deposition etc. The most commonly used hybrid graphene nanocomposite synthesis approaches and their significant applications are also summarized in this chapter.

Keywords Graphene · Graphene derivatives · Graphene synthesis · Hybrid nanocomposites · Applications

1 Introduction of Graphene and Its Derivatives

In current years, a planer sheet having one atom thickness and sp^2-bonded carbon atoms, called graphene, with its densely packed honeycomb crystal lattice, has received significant consideration for its use in next generation electronic devices. This is based on some of its incomparable properties such as chemical inertness, optical transmittance, increased thermal conductivity, ballistic transport, super hydrophobicity and high current density at nanometer (nm) scale [1, 2]. Reportedly,

A. Kanwal · A. Siddique · M. N. M. Ibrahim
Department of Chemistry, Mirpur University of Science and Technology, AJK, Mirpur 102650, Pakistan
e-mail: mnm@usm.my

A. A. Yaqoob · K. Umar
School of Chemical Sciences, Universiti Sains Malaysia, 11800 Penang, Malaysia

S. A. Bhawani (✉)
Faculty of Resource Science and Technology, Universiti Malaysia Sarawak, 94300 Kota Samarahan, Malaysia
e-mail: sabhawani@gmail.com

first sample of graphene was obtained through micromechanical cleavage of graphite with sticky tape. The reported method is still widely used in academic research and industrial work [3]. This technique permitted simple production of high-quality graphene crystals and provided a foundation for massive research work in this field. Extraordinary electrical properties have fascinated the use of graphene in future electronics such as elements of integrated circuits, ballistic transistors, transparent conducting electrodes, sensors, and field emitter. Graphene shows high mobility of electron (or hole) and low Johnson noise (sound caused by thermal agitation of electrons, regardless of applied voltage, in a conductor at equilibrium), making it suitable for its possible use in field effect transistors (FET) [4]. Considering electrical and low noise making properties of graphene, it can be used as an excellent sensor. It is very proficient to detect adsorbed molecules due to its 2D structure. Due to optical transparency and high electrical conductivity, graphene seems to have the potential to be used as transparent conducting electrodes in liquid crystal displays, touch-screens, organic light-emitting diodes (OLEDs) and organic photovoltaic cells [5]. Majority of these remarkable applications necessitated the development of mono-layer graphene on an appropriate substrate but that is tricky to control and yet to be accomplished. Most of the synthesis of graphene is centered on mechanical exfoliation of graphite and thermal graphitization of a silicon carbonaceous substrate and lately, by chemical vapor deposition [6]. Similar other organic compounds such as polyaromatic hydrocarbons, graphene can go through several chemical reactions which give modified product forming covalent bonds with different functional groups. In general, basic principles of organic synthesis can be applied for these reactions. However, during these reactions, several limitations must be considered owing to the graphene skeleton scale and reactivity difference of graphene with hydrocarbons [7]. A variety of methods for modification of graphene using functional groups like pnictogens (N, P, As, Sb, Bi), halogens (F, Cl, Br, I), chalcogens (O, S, Se), atomic boron, silicon as well as some other, compound functional groups, such as aryl and alkyl hydrocarbons were reported during the past few years. Even though lots of functionalization methods have been reported, only two of them (covalent functionalization with hydrogen and fluorine) produced stoichiometric graphene counterpart [8]. The synthesis of fluorographene, a fully fluorinated graphene, has been accomplished by using "top-down" and "bottom-up" techniques working on mechanical exfoliation of fluorographene and direct fluorination of graphene, correspondingly. Similarly, different methods for synthesis of fully hydrogenated graphene are also documented [9]. Beside these two stoichiometric derivatives, there is also a huge amount of partially derivatized graphene with different degree of functionalization. However, graphene has different forms which are shown in Fig. 1 [10]. This chapter includes the brief introduction of graphene-based hybrid nanocomposites along with their potential application in several fields. The most important synthesis route of graphene and potential approaches for its hybrid nanocomposites are also considered.
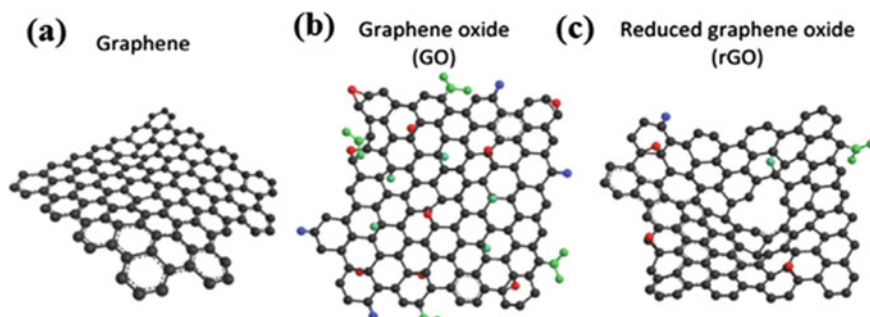
Fig. 1 Basic form of graphene derivatives of graphene

2 Graphene Based Hybrid Nanocomposites

Nanocomposite is a solid multi-phase material that has at least one phase having one, two or three dimensions measuring lower than 100 nm or structures with nano-scale repeating intervals in various phases to grow the material [12, 13]. Nanocomposites based on graphene are at present the only application of graphene already commercialized across-the-board. A continuous increase in the number of products containing these nanocomposites is observed, from tennis rackets, to bicycles, to skis [14]. Yet, the performance of such products is not as good as to that of pristine graphene sheets, which simply outshine well-established materials such as copper, silicon or steel. The most plausible explanation for this distinction in their properties is that it is not completely known how two-dimensional (2D)-based composites function at the nanoscale level and, more importantly, what is the final output (mechanical, electrical, etc.) that can be achieved when they are integrated into a bulk material [15]. Therefore the major purpose of 'Nanocomposites' research package is to translate some exceptional characteristics of materials, like graphene, from the single-sheet level to the macro scale, producing new composite materials that combine the exceptional structural, thermal, electronic, optical and electrochemical properties of graphene with those of more conventional, bulk materials. As stated by Odegard et al. [16], the introduction of nanoparticles is a promising choice to upgrade the mechanical properties of composites and the carbon-based nanoparticles are potentially the most favorable choice among the wide range of nanoparticles available. As explained by Saito and co-workers [17], nanostructures based on carbon like graphene nanosheets (GN) and carbon nanotubes (CNT) provide extraordinary electrical, mechanical, and thermal properties. Characteristics of CNTs have been tested experimentally and confirmed by numerical simulations. As, according to Yasmin et al. [18], nanocomposites based on graphene may act as an alternative choice for engineering uses owing to their exceptional rigidity and specific strength. Fine cost/benefit relationship is another reason for the increased attention on use of graphene nanosheets. Polymer composites also offer one of the most potential

applications in this field. The activity of polymer matrix can be enhanced by the integration of nanoscale filler such as GO, Al, Zn, Si, etc. Polymeric composite, having silicate fillers as exfoliated layers, have been studied in start of 1950s. This study is used in current biotechnological and biomedical applications [19].

3 Synthesis Method for Graphene and Its Derivatives

The attempt to synthesize monolayer graphite was made as early as in 1975, when Lang et al. [20] demonstrated the development of single- and multi-layered graphite via thermal decomposition of carbon at single crystal Pt substrates. Though, at that time, owing to the absence of uniformity among characteristics of these sheets, created on various Pt crystal planes and inability in recognizing the valuable uses of these sheets, this method was left without thoroughly analysis. In 1999, following a long silence, scattered experiments for the fabrication of graphene were announced [21]. However, the credit goes to Novoselov et al. in 2004, for graphene discovery [22]. They publicized the reproducible production of graphene by exfoliation for the first time. Until then, this approach is and always has been pursued, together with attempts to establish new methods for effective synthesis of graphene at industrial scale. The important point is that the synthesis of different materials based on graphene is managed properly so the properties can be imparted for precise applications. It is well-known that the fabrication of graphene may be achieved by two major routes, the top-down and the bottom-up [23, 24]. Bottom-up approaches include production of graphene using alternate carbon resources whereas top-down methods include isolation of stacked graphite layers in order to obtain single graphene sheets as shown in Fig. 2 [25]. One of the main problems in commercialization of graphene is fabrication of top-quality material in a repeatable way, at a broader level and minimal expenses [26]. While this remains a significant challenge, a variety of different techniques have been established to synthesize graphene over the last few years as described below.

3.1 Exfoliation and Cleavage

Graphite, a layered structure of several graphene sheets held together by weak van der Waals force. As a matter of fact, it is feasible to obtain graphene using a high purity graphite sheet when those weak forces are broken. In exfoliation method, chemical or mechanical energy is used for splitting the weak forces to isolate individual graphene sheets. Viculis et al. [6] made first effort in this field using potassium metal to insert into layered structure of a pure graphite sheet, expanding the van der waals gap among the layers and then exfoliated it by dispersion of the carbon sheets in ethanol. The exfoliated sheets produced nanoscrolls during sonication. The presence of 40 ± 15 layers in each sheet was reported by TEM analysis. Even though the
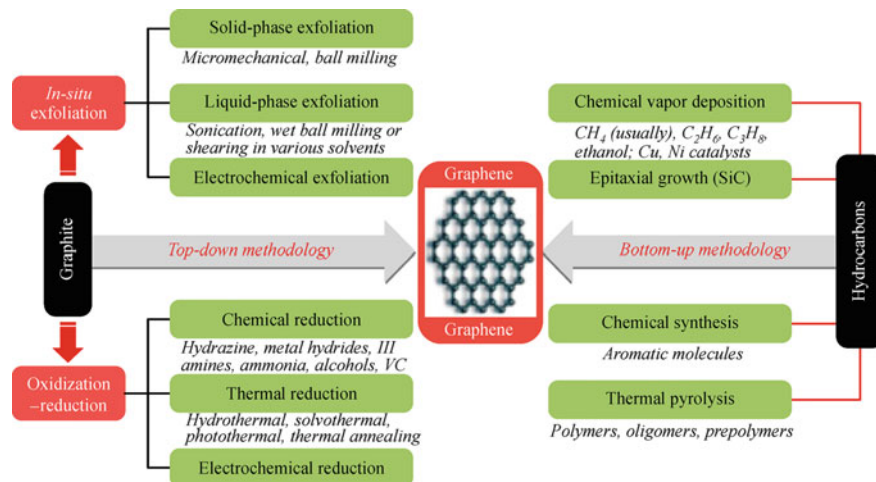
Fig. 2 Schematic illustration for graphene synthesis (adapted from Ref. [25] with Elsevier permission)

thickness of carbon nanoscrolls was higher than some graphene layers, the process revealed that it is feasible to rip sheets of graphene from graphite practically. The method had to be modified to eventually obtain few layers of graphene. The struggle ended up taking about 20 more months, when Novoselov et al. [27] reported the formation of few-layers graphene by exfoliation. It is a repetitive peeling process. In this research work, dry etching of a widely accessible highly oriented pyrolytic graphite (HOPG) sheet, with 1 mm thickness, in oxygen plasma resulted in several 5 μm deep mesas with an area of 0.4–4 mm^2. Then it was placed on a photoresist and baked to glue the mesas to the photoresist. Using a scotch tape then, layers were stripped from graphite sheet. Slim flakes separated from photoresist showed single to few layers' graphene sheet, when moved to a Si substrate. Later, this method was applied to generate 2D atomic crystals of several other materials [23]. This method of graphene sheet production was considered as very efficient and simple. Therefore, it drew the significant consideration from the scientific community. It was also demonstrated that a slight changes in the original process can lead to the production of large (~10 μm) and plane graphene flakes through adjusting the substrate bond of HOPG to Si and controlling the process of exfoliation [28]. In another experiment, the scientists were able to generate single to few layers of graphene on borosilicate glass surface using bulk graphite and exfoliation method. But each of these developments addressed the need to modify the bonding to the substrate to produce graphene sheets having large-area [29]. These approaches demonstrate a strong potential to be used at industrialized level to produce large size electronic devices based on graphene. Another experiment was carried out by Stankovich et al. [30], with a little different approach, applying liquid phase exfoliation and using the hydrophobic properties of exfoliated graphite nanosheets and graphite oxide by the

process of ultrasonification in aqueous suspension, attempted to reduce the films at 100 °C for 24 h in hydrazine hydrate. However, the material was not fully reduced as some amount of oxygen was still there in the structure. So, the obtained sheets can be referred as partly reduced exfoliated nano graphite oxide sheets. Hernandez et al. established a fresh approach of generating mono- to few-layers graphene sheets, focusing on the advantages and disadvantages of exfoliation in liquid phase, by dispersing and exfoliating high-quality graphite in N-methyl-pyrrolidone [31]. The product obtained for monolayer was 1 wt%, That can be increased to 12 wt%, with more refining. The efficiency of this procedure is determined by the assumption that, energy needed for exfoliation of graphite into mono layer graphene was counteracted by the interaction between solvent and graphene, using the solvent that has a comparable surface energy as that of graphene. This liquid phase exfoliation method, using organic solvent, holds a potential of graphene production at large scale. A similar process was applied by Lotya et al. [32] to develop mono- to few-layer graphene using sodium dodecylbenzene sulfonate (SDBS) for dispersion of graphite powder, followed by sonication, resulting in exfoliation of graphite into graphene. There have been several such efforts to fabricate graphene using graphite oxide powder or graphite and various solvents [33–37]. The exfoliation method shows great potential to manufacture graphene at large scale. Many of the latest modifications, by liquid phase exfoliation, also rendered it promising for the manufacture of large-size product. However, the products obtained through liquid phase exfoliation bear the limitation, because of oxidation and reduction processes, the structure show many defects resulting in reduced electrical characteristics of graphene. Future innovations require focusing on managing the layers count and reducing the levels of impurity so that this method can be applied to a level of industrial scale production.

3.2 Thermal Chemical Vapor Deposition Techniques

Thermal chemical vapor deposition (CVD) is quite a new practice used to synthesize graphene. The first report published in 2006 about the planar few layer graphene (PFLG) produced using chemical vapor deposition [38]. The report was about the production of graphene on Ni foils using a natural, minimal cost and environmentally friendly precursor, camphor. Starting with evaporation at 1800 °C, camphor was then pyrolyzed at 700–850 °C in the other chamber of the CVD furnace, using argon gas as the carrier. The sample was then left on room temperature for cooling, leading to the formation of few-layer graphene sheets on Ni foils. In HRTEM analysis, the resulting graphene showed multiple folds and was anticipated to have around 35 layers of graphene sheets. The research work brought up a novel synthesis method for graphene, however many problems were still to be solved, such as reducing the folds and managing the number of layers etc. Thermal chemical vapor deposition was used in another experiment to grow 1–2 nm thick graphene sheet on Ni substrate, but same approach failed to synthesize graphene using Si as substrate [39]. In this process a mixture of Hydrogen and Methane (92:8 ratios) was used as

precursor with 80 Torr pressure and initiated by DC discharge. Graphitic films having nanometer thickness (verified by Auger Electron Spectroscopy) showed atomically smooth micrometer-sized areas, isolated through ridges. The creation of ridge was attributed to thermal expansion coefficient difference among graphite and Ni, while the process of nucleation was credited to heteroepitaxial growth of graphene on Ni. Afterward, the formation of three to four-layer graphene on 500 μm thick polycrystalline Ni foils was reported by Yu et al. [40] using thermal CVD method. In this study, a mixture of Methane, Hydrogen and Argon (0.15:1:2) was applied as a precursor at 315 cm flow rate and 1000 °C temperature for 20 min to complete the synthesis process. Moderate cooling rates were confirmed for the synthesis of graphene on Ni by HRTEM and Raman spectroscopic analyses, whereas high and low cooling conditions were observed to have adverse effects on graphene synthesis. Carbon solubility in Ni and kinetics of carbon segregation were considered as base for this difference. Ni shows good solubility for carbon atoms. If the process is carried out at slow cooling rate, Carbon atoms find enough time to disperse into Ni, hence segregation is not observed on the surface. Carbon atoms segregate and generate graphene at moderate cooling conditions while at higher cooling rate, although Carbon atoms show segregation on Ni surface but produced a defective, less crystalline structure of graphene. This research work provided the crucial information about the mechanism of growth of graphene by thermal CVD process. In order to understand this mechanism better, the next objective was to grow graphene on larger scale so numerous research groups were focusing their attentions on this subject. A novel method for growth of substrate-free, few-layered graphene was proposed by Wang et al. [41]. They used an envelope of Argon and Methane gas (volume ratio 4:1 and flow rate of 375 mL/min) and MgO-supported Co catalysts for the growth of graphene in a ceramic boat. The system was kept at 1000 °C for 30 min. Catalyst (MgO and Co) was removed by washing the product with concentrated HCl, followed by several washings using distilled water and the product was then dried at 70 °C. In this study, 500 mg of catalyst powder mixture was believed to synthesize 50 mg of graphene. The existence of rippled graphene sheets with minimum five layers was confirmed by HRTEM, SEM and Raman spectroscopic study of the product. Even though this method of graphene formation is still under examination, an innovative opportunity for larger scale production of graphene was created by this approach. Thermal CVD was applied to synthesize single to few layers' graphene on 1–2 cm^2 polycrystalline Ni film in a recent study. The 500 nm thick Ni film was evaporated on a SiO$_2$/Si substrate followed by annealing in Argon and Hydrogen atmosphere keeping the temperature at 900–1000 °C for 10-20 min. Ni grains (5–20 μm in size) were produced by the annealing process. The CVD process was carried out using 5–25 cm CH$_4$ and 1500 cm H$_2$ at 900–1000 °C for 5–10 min. The graphene was formed on Ni while the size of each graphene was determined by the size of Ni grains. Later, the graphene was transferred to other substrates, retaining its electrical properties, making it feasible for different electronic applications. Graphene, which was synthesized by this method and then shifted onto a glass surface, displayed an optical transmittance of about 90%. The graphene synthesized in this method might be considered for fascinating applications in next generation solar cells due to its

electrical properties and high transmittance together with the ability to be fabricated on large scale using pre-patterned substrate. Similar synthesis approach applied by de Arco et al. in an independent study has also shown comparable properties of graphene [39]. Kim et al. displayed the graphene growth on 300 nm thick Ni film, mounted on SiO_2/Si substrate using same approach. They claimed to optimize Ni thickness in order to obtain best quality of graphene. The graphene was synthesized by thermal CVD carried out in a mixture of Argon, Methane and Hydrogen gas (200:50:65 sccm) at 1000 °C preceded by quick cooling (10 °C s − 1) in Argon envelope. Reportedly, the high cooling rate was observed to be critical for minimizing the layers count and successful transition of graphene on certain substrates. Later, this graphene was effectively transferred on a flexible and transparent substrate formed of polydimethylsiloxane (PDMS). The transferred caused no effect on its properties and visible spectrum showed 80% transparency for these structures. The author also observed that the etching of nickel layers in a mild pH value can also be achieved using aqueous $FeCl_3$ solution, without causing any precipitation and formation of gaseous products. While, etching with HNO_3 produces gaseous products damage the graphene structure [38]. The growth of highly crystalline few-layer graphene on polycrystalline Ni substrates (1 cm^2) was reported in a very recent study. The product was obtained by precisely controlling the temperature, growth time and gas ratios. With further improvement of the process, graphene was synthesized by thermal CVD on a 1 cm^2 Cu foil [40]. Graphene obtained by this process showed high quality and uniformity. Two different and simple procedures were followed to transfer graphene on other substrates making it applicable in different fields. However, the growth of graphene on Cu substrate was found to be self-limiting. This fact was credited to limited Carbon solubility in Cu. As compared to Ni, where the reported process was precipitation, this process was reported as surface-catalyzed process [42].

Recent developments in growth of graphene by thermal CVD process have verified the reproducibility of high-quality graphene on 1 cm sized substrate and efficient transport on several new substrates along with Si, glass and PDMS. Such improvements develop latest opportunities for introduction of graphene in photovoltaic and flexible electronics. Yet, challenges such as graphene growth on wafer size substrates and efficient control of the layers count have to be addressed in coming years in order to stimulate more interest in actual applications. CVD, being a complex process needs accurate control of synthesis conditions (type of precursors, pressure, temperature, deposition time). Nevertheless, CVD is an appealing technique for synthesis of high-quality graphene. Table 1 shows summary of some recent work on graphene synthesis by various CVD techniques.

3.3 Epitaxial Method

A common method to grow graphene is through thermal decomposition of Si on single crystal surface plane (0001) of 6H-SiC. The formation of graphene was observed on H_2-etched surface of 6H-SiC when it was kept at around 1250–1450 °C,

Table 1 Summery of graphene preparation by using CVD with different conditions

Synthesis method	Precursor	Operating Temperature (°C)	Nature of product	Reference
CVD	Cu (H$_2$/CH$_4$)	1070	Single crystal graphene	[43]
	N$_2$	1000	High quality graphene powder	[44]
	Cu/CH$_4$	1060	Polycrystal single layer graphene powder	[45]
	Metal/CH$_4$	1000	Metal decorated graphene	[46]
	Cu	1050	High quality graphene powder	[47]
	NiCu/CH$_4$	1100	Single layer graphene	[48]
	PET and glass material	150	Defect free graphene powder	[49]
	Cu/CH$_4$	1000	Monolayer graphene	[50]
	Cu/CH$_4$	1030	High quality graphene	[51]
	Cu/CH$_4$	1000	High quality graphene	[52]
	1,2-dichlorobenzene/CH$_4$	No heating	Graphene nanostrips	[53]

for 1–20 min. Graphene, which was developed epitaxially on the above said surface, usually showed 1 to 3 layers and the layer count was depending on temperature used during this decomposition process. Rollings et al. [54] developed graphene sheets using similar method and managed to synthesize one atom thick graphene films. The persistent success of this method drew the interest of the semiconductor industry owing to the possibility that this technique can be a promising method in the post-CMOS era. A detailed analysis on this subject has been presented by Hass et al. [55] where they addressed the problems related to the graphene growth on various faces of SiC and the electronic properties of graphene obtained by this method. In a major improvement towards this process, consistent graphene films in mm scale were fabricated on SiC substrate covered with a thin film of Ni, at a comparatively lower temperature of around 750 °C. The additional benefit of this process is the continuity of film formed along the entire surface of SiC substrate. This method

is quite suitable for the industrial applications because of its broad range production of graphene. Emtsev et al. [56] showed large-scale production of monolayer graphene films using same method, at standard pressure. This process was expected to generate wafer-size sheets of graphene. Although, semiconductor industries are particularly interested in this technique of graphene growth on SiC, but problems such as limiting the thickness of film and continuous generation of larger area graphene need to be addressed before this technique could be carried out on industrial scale. A variety of other important issues have been identified through the detailed review of research work available with reference to epitaxial growth of graphene layers on SiC substrates. Different structure has been observed for the graphene developed on SiC (0001) and SiC (000⁻1). Unexpected rotational stacking was observed in graphene films with a thickness of up to 60 layers when it was developed on SiC (0001) surface and this stacking was a possible explanation of the behavior of these sheets as discrete graphene sheets. However, this peculiar behavior was not found in graphene grown on SiC (000⁻1). The future scientific work needs to be geared towards understanding the process involved in both the growths and application of this experience in the development of practical tools. Another significant concern is the composition and electronic features of the interface layer formed between substrate surface and graphene layer as it is recognized to influence the characteristics of graphene formed [57]. The influence of the interface is not clearly explained yet and the future work ought to be focused on addressing this problem. This process is intended to be applied on industrial scale to produce wafer sized graphene, once the issues regarding growth mechanism and influence of interface are addressed and the process is able to control the layer count efficiently.

3.4 Chemical Reduction of Graphene Oxide

Another effective route for graphene synthesis, in terms of larger scale production and expense, is chemical reduction of graphene oxide (GO). However, a shortcoming of this method is the agglomeration of reduced graphene films [58]. In fact, this method generally requires hazardous reducing agents like sodium borohydride or hydrazine, which shows harmful effect on the environment. The utilization of green reducing agents in place of hazardous ones has now become a most interesting topic in field of graphene synthesis. Most of the reducing agents are found environment friendly and the materials produced are biocompatible and easily dispersible, thus beneficial in many aspects [59]. The systematic mechanism of exfoliation, oxidation and reduction processes are given in Fig. 3.
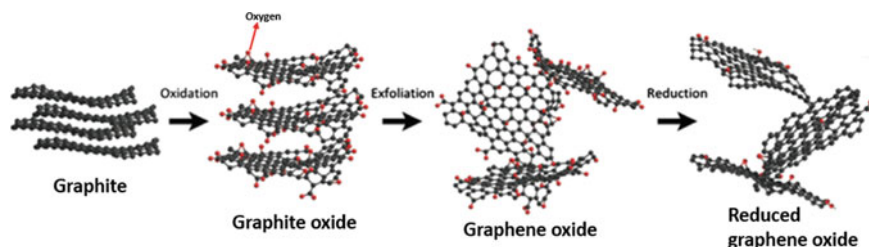
Fig. 3 Systematic illustration of oxidation, exfoliation and reduction method

4 Synthesis of Hybrid Graphene Nanocomposites

The graphene has fascinated substantial study consideration. The revolutionary opto-electronic, magnetic and catalytic properties of graphene-based nanocomposites rely on hybridization between semiconductor nanoparticles (NPs). NPs are measured as a stabilizer in contradiction of accumulation of single graphene sheets through durable van der Waals forces among layers of graphene. This enhances surface area to remove the pollutants from target solution. For this cause, additional energies and novel methods were necessary to prepare the nanocomposites based on graphene. In contaminant elimination, semiconductors commonly revised the graphene structure morphology and make them very active in several water treatment applications. Some most used methods are mentioned here.

4.1 Solvothermal/Hydrothermal Method

The solvothermal and hydrothermal process is playing a very significant role in several scientific fields regarding either elementary or determined research. During the last years, such approaches were strongly developed, particularly with the extension of nano crystallites. A chemical reaction is carried out between several types of precursors in aqueous medium at higher temperature than boiling temperature. The solvent concerning sulphides and oxide are used in solvothermal synthesis, which is an emerging topic of further research. The solvent depends on its physical properties such as density, polarity, dielectric constant etc. The chemical properties also depend on interaction between additives and reactants. Marlinda et al. [60] studied the hydrothermal process to prepare reduced graphene oxide/zinc oxide (rGO/ZnO) nanocomposites. This superficial process detained hydrothermal behavior of an interruption comprising graphene oxide (GO), zinc acetate-1-hydrates, NaOH and $NH_3 \cdot H_2O$. In a distinctive process, GO was accomplished by using Hummers' method and ZnO was prepared by using zinc acetate-1-hydrates in presence of chemical method. Each product was slowly mixed for 60 min until to obtained misty dark brown liquid. Later, the solution was treatment at 180 °C for 24 h. The production
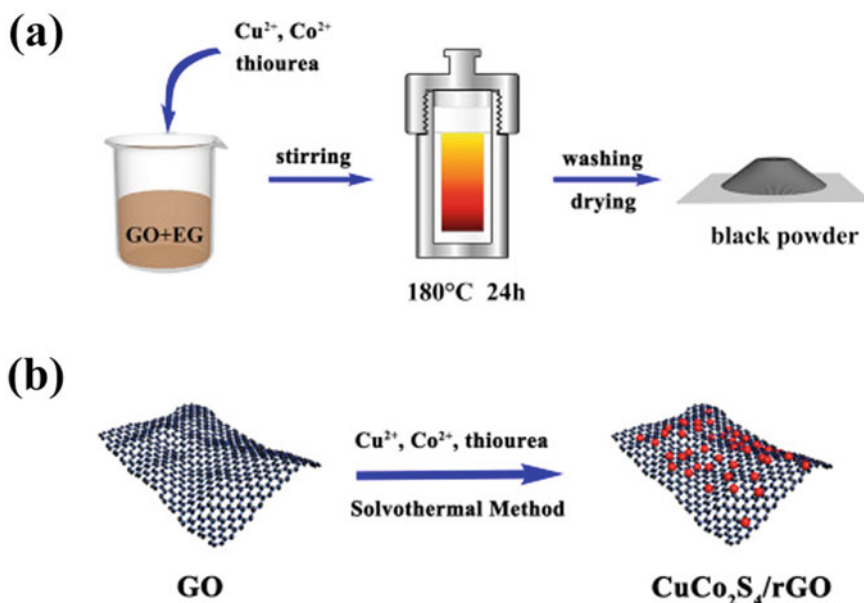
Fig. 4 **a** Synthesis by using hydrothermal method. **b** Synthesis by using solvothermal method (adapted from Ref. [62] with Elsevier permission)

of product was prospered through washing with ethanol or distilled water and then dried for 24 h at 60 °C. Ahmad et al. [61] synthesized graphene–silver-zinc oxide nanocomposites through using a solvothermal method for wastewater treatment. In typical procedure, decontaminated GO was mixed with ethylene glycol (EG) through ultrasonication (3 or 4 h) and more followed through centrifugation to get a yellow brown solution. Similarly, zinc acetate and silver acetate were mixed into EG to get brown solution and after that mixed both solutions simultaneously into NaOH solution and stirred 6 h and autoclaved for 24 h. Final product was nanocomposite which recovered after proper washing with ethanol. Yanmei et al. [62] studied the difference between solvothermal and hydrothermal techniques and systematic illustration are shown in Fig. 4. They studied the CuCo2S4/rGO oxide nanocomposite which are synthesized by using hydro and solvothermal method.

4.2 Sol–Gel Method

Azarang et al. [63] doped ZnO nanoparticle on Graphene oxide sheets with several concentration of Graphene oxide through a modest sol–gel method using a matrix of gelatin by taking gelatin, $Zn (NO_3)_2 \cdot 6H_2O$ and distilled water as initial substances. A gelatin matrix was synthesized first, through addition of gelatin into distilled water at 55–60 °C. Zinc nitrate separately liquefied in minor amount of GO solution, and water
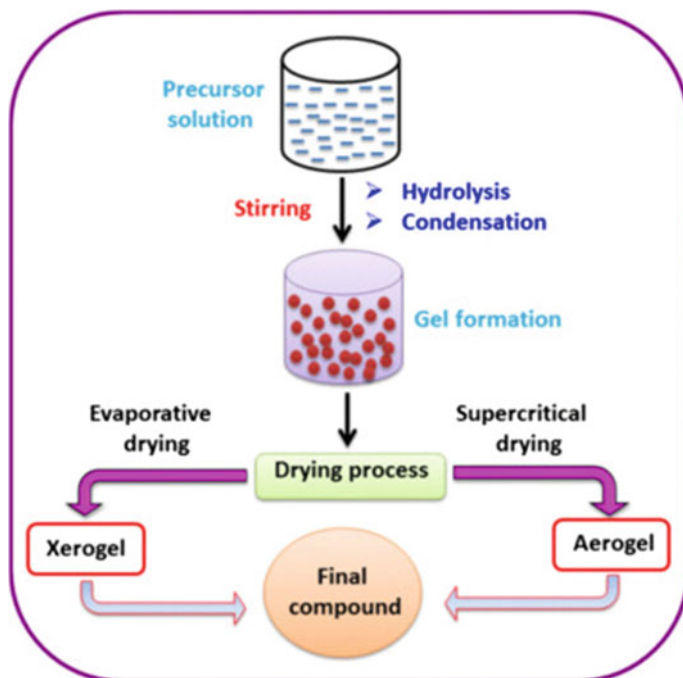
Fig. 5 Sol-gel synthesis mechanism (adapted from Ref. [64] with Elsevier permission)

was then added to gelatin solution. The reaction combination was kept on heating and stirring until dark brown gel is formed. Finally, in order to prepared nanocomposite, the gel was calcinated at 300 °C and continued through post-annealing method for 2 h at 400 °C in presence of argon gas to remove gelatin. The general route of sol-gel method is described in Fig. 5.

4.3 In Situ Growth

Similarly, in situ growth method is one of effective method used to prepare the hybrid nanocomposite. For example, graphene/ZnO nanocomposite in which Zn^{2+} ion was coated on GO sheet with the addition of NaOH and $NaBH_4$ at 150 °C and prepared product was graphene/ZnO nanocomposite subsequently reduction of GO. The ZnO NPs developed on graphene showed a size range in between 10 and 20 nm. Chang et al. [65] studied the ZnO nanorod/graphene composite formation through in situ growth. In a definitive process, graphene and ZnO quantum dots mixed together in self-assured ratio to get a mixture that cast on surface of substrates collectively with glass, polyethylene terephthalate, SiO_2/n-Si and quartz to make ZnO/graphene thin films. To produce an enhanced adhesion on surface of substrates, thin films

were galvanized by using the 100 °C heat to disperse water content and absorbed zinc nitrate for in situ growth to achieve ZnO nanorods/graphene nanocomposites. Finally, the reaction mixture was eroded with condensed water for elimination of loosely involved ZnO nanorods. A superficial, single-step system for in situ growth of mono graphene coated zinc oxide nanocomposites was reported by Sahatiya and Badhulika [66] through electrospinning towards the electrodes and its subsequent use for ultraviolet (UV).

5 Applications of Hybrid Graphene Nanocomposites

The application of graphene and its derivatives are attracting great interest due to the excellent properties and economic stability of material. Some of the most used applications are briefly summarized in this chapter which depends on graphene and its hybrid composite material.

1. Functionalized hybrid nanocomposites are thoroughly examined for their use in the energy-related technologies like electrochemical energy devices and solar energy conversion. Graphene and graphene nanocomposites are believed to enclose a significant prospective in photoelectrochemical and photovoltaic devices owing to their exceptional optical and electronic properties. Though pure graphene was initially investigated as transparent electrodes in solar cells and its nanocomposites have also been proven to be efficient transparent electrodes in photoelectrochemical and photovoltaic device [67]. In addition, graphene may either be a conductive substrate or functional component like electron acceptor in photoelectrochemical and photovoltaic devices. These nanocomposites showed several uses in photovoltaic and photoelectrochemical (PEC) systems. The photo-electrodes of graphene nanocomposites sensitized with CdS quantum dots (QDs) were used in photoelectrochemical solar cells where they exhibited 3-folds increase in photocurrent generation than the pure QDs PEC cells [68].

2. Graphene films have been extensively studied their applications in supercapacitor. Supercapacitors based on pure graphene sheets have exceptionally long phase stability but have low capacitance due to electronic double-layer structure. As a result, several attempts have been carried out to combine graphene with pseudo capacitance materials so that the capacitance can be improved. Also, the exceptional electronic character of graphene can improve the electrochemical stability of the supercapacitor electrodes [69].

3. Graphene nanocomposites showed a number of applications in the electrocatalysts of fuel cells. Though atomically doped graphene sheets are used as electrocatalysts, graphene nanocomposites are found to be potential substitute for noble metal as electrocatalysts. Graphene nanocomposites are commonly applied as electrocatalysts in methanol oxidation fuel cells, oxygen evolution reaction, oxygen reduction reaction and hydrogen evolution reaction. These nanocomposites showed a significant impact on electrocatalytic oxidation of methanol.

Nanocomposites with Pt cluster size of less than 0.5 nm were synthesized by Yoo et al. [70]. These nanocomposites displayed an exceptionally high methanol oxidation rate in comparison to Pt/carbon black catalysts.

4. Due to special characteristics of graphene as charge transporter and electron acceptor, graphene nanocomposites displayed the capacity of their use in artificial photosynthesis like photoelectrochemical and photochemical water splitting. Graphene can act as an effective co-catalyst in order to offset noble metal co-catalysts like Pt which are commonly used in inorganic semiconductors-based photochemical splitting of water. In photoelectrochemical water splitting, the role of graphene is found as both cocatalysts and conductive channels when used in nanocomposite photoelectrodes. TiO_2-graphene nanocomposites have been used in photochemical solar water splitting systems, with graphene acting as cocatalysts for improvement of charge separation in radiation [71].

5. Applications of functionalized graphene nanocomposites in environment such as sensing and tracking to remediation have shown quite a potential in recent years. Graphene and graphene nanocomposites are common systems for the identification of inorganic ions, biomolecules, and microorganism as well as for elimination of harmful species in atmosphere. These nanocomposites offer multiple uses in heavy metal ions detection. The graphene oxide/aptamer hybrids are prepared via self-assembly of the graphene-based planes and DNA. The graphene oxide/aptamer hybrids showed ultra-low fluorescence record due to the incredibly improved quenching performance of GO for dyes fluorescence, increasing the sensitivity of the hybrids. Hybrid aptamer sensors for Hg^{2+} ions exhibited sensitivity of 30 nM and exceptional specificity for other heavy metal ions [72]. In a different study, graphene nanohybrids prepared with silver specific cytosine-rich oligonucleotide (SSO) were found to be highly sensitive for silver ions (Ag^+) having a detection restrict of 5 nM and quantification restrict of 20 nM. These sensors were also efficient in the in actual environmental specimens like river water, where fluorescence expressions were 2 times stronger in 100 nM Ag^+ in river as compared to the river water without Ag^+.

6. Many organic compounds are considered as serious pollutants in environment. This problem is addressed by using graphene nanocomposites for photodegradation or direct removal of organic matter. TiO_2/graphene nanocomposites were introduced by Zhang et al. [73] as photocatalyst in the photo degradation of methyl blue (MB), an organic dye. TiO_2/graphene nanocomposites are considered as an excellent photocatalyst for dye degradation due to its high adsorption for dyes, impactful charge separation and enhanced spectrum of light absorption at both UV and visible light as seen in Fig. 6. TiO_2/graphene nanocomposites display much improved photocatalytic activity as compared to pure TiO_2 and TiO_2/CNTs photocatalysts.

7. Another major problem in industrial and daily environment is vapor pollution. Graphene has displayed outstanding activity for the detection of vapors particularly Cl_2, SO_2, CO_2, NO, H_2, NH_3, CO, NO_2 and few organic vapors like toluene, acetone and benzene [74]. At the initial stages of the development of graphene
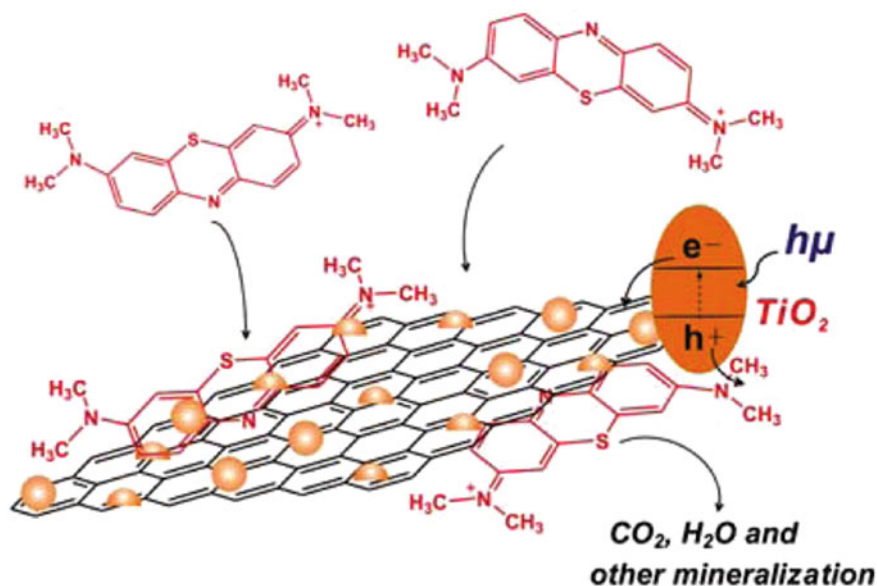
Fig. 6 Graphic presentation of TiO_2/graphene nanocomposite used as photocatalysts for degradation of organic pollutants (adapted from Ref. [73], with ACS permission)

based environmental vapor sensors, pure graphene was employed in the sensors with remarkable sensitivity even detecting the NO_2 at single molecule level.

8. Graphene and graphene composites have also been studied for detection and removal of bacteria because the interaction among graphene and bacteria is quite interesting when put together in specific application. Graphene act as an impenetrable cage for bacteria that enables direct and real time observation retaining the topological and dimensional properties of bacteria under pressure of 150 torr and beam current of 150 A/cm^2. [75] Graphene nanocomposites are used for detection of bacteria. Graphene oxide sheets functionalized with antibodies were developed and used as biocatalyst probes for sulfate-reducing bacteria (SRB) and GO-mediated silver enhancements were used to sense sulfate-reducing bacteria with high sensitivity using potentiometric stripping analysis (PSA). The device showed a detection range of 1.8×10^2 to 1.8×10^8 cfu mL^{-1} and a limit of 50 cfu mL^{-1} as indicated in Fig. 7.

6 Conclusion and Perspective

A lot of developments have been observed in synthesis, functionalization and uses of graphene nanocomposites. Worldwide upsurges of energy pave the way for practical and commercial uses of graphene nanocomposites, progressing to next-generation energy transfer and storage systems. The enormous potential of graphene
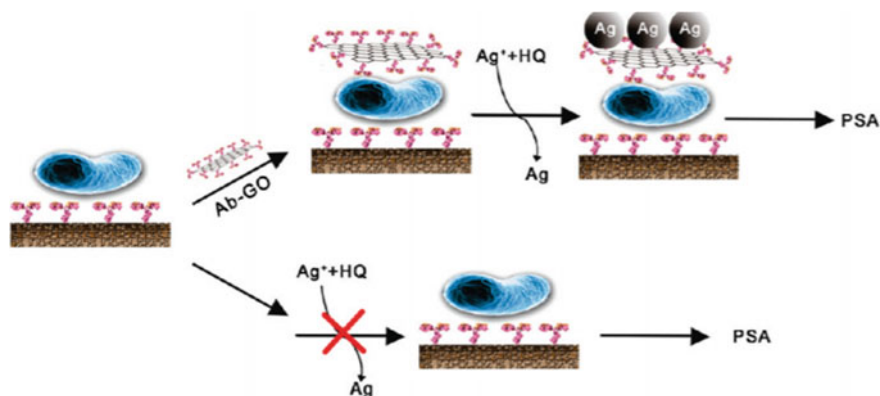
Fig. 7 GO/Silver hybrid developed for sensing sulfate-reducing bacteria (SRB) (adapted from Ref. [76], with ACS permission)

nanocomposites in power sector has been proven repeatedly by a vast quantity of promising work in photoelectrochemical and photovoltaic devices, LIB, fuel cells, artificial synthesis, and supercapacitors. Specifically, supercapacitors and LIB based on graphene nanocomposites, show extreme potential in energy storage devices. Even so, many other issues need to be solved before putting these devices into actual industrial applications, starting with the large-scale processing of top-quality graphene which still needs working on it. On lab scale testing, these energy devices perform well. In order to get high performance devices at industrial scale, a significant quantity of high-quality graphene nanocomposites is required and it has to be stable in chemical and electronic properties during this whole process. Next is the poor performance of graphene nanocomposites based photoelectrochemical and photovoltaic devices in most prototype systems. More research work is to be done in order to optimize the material and fabrication process to enhance the efficiency of these devices.

Then in term of environmental applications, nanocomposites based on graphene have significant prospective for the identification of heavy metal ions and microorganisms like bacteria and the removal of organic material like dyes. In developing countries, the applications of graphene nanocomposites in photodegradation of organic pollutants are gaining more attention owing to the rise in the contamination of water resources caused by organic matter. However, it is quite early to anticipate the wide scale uses of nanocomposites for monitoring and restoration of environment as the basic concerns regarding the impact of graphene on ecosystem and human environment mostly remains unresolved. While graphene nanocomposites still face these problems, it remains among the most successful energy and environmental research platform. It is expected that in near future, large scale applications of devices based on graphene, in electrodes in photovoltaics, optoelectronics and electrochemical energy storage systems can be accomplished. Further groundbreaking technologies founded

on graphene and graphene nanocomposites, along with the development in both theoretical physics and chemistry and practical methods, would extend the perspectives and open new doors to human life.

References

1. Chen JH, Jang C, Xiao S, Ishigami M, Fuhrer MS (2008) Intrinsic and extrinsic performance limits of graphene devices on SiO_2. Nat Nanotechnol 3(4):206 (Apr)
2. Geim AK, Kim P (2008) Carbon wonderland. Sci Am 298(4):90–97 (Apr 1)
3. Novoselov KS, Geim AK, Morozov SV, Jiang D, Zhang Y, Dubonos SV, Grigorieva IV, Firsov AA (2004) Electric field effect in atomically thin carbon films. science 0306(5696):666–669 (Oct 22)
4. Katsnelson MI (2007) Graphene: carbon in two dimensions. Mater Today 10(1–2):20–27 (Jan 1)
5. Geim AK, Novoselov KS (2010) The rise of graphene. In: Nanoscience and technology: a collection of reviews from nature journals 2010, pp 11–19
6. Viculis LM, Mack JJ, Kaner RB (2003) A chemical route to carbon nanoscrolls. Science 299(5611):1361 (Feb 28)
7. Wang X, Sun G, Routh P, Kim DH, Huang W, Chen P (2014) Heteroatom-doped graphene materials: syntheses, properties and applications. Chem Soc Rev 43(20):7067–7098
8. Zbořil R, Karlický F, Bourlinos AB, Steriotis TA, Stubos AK, Georgakilas V, Šafářová K, Jančík D, Trapalis C, Otyepka M (2010) Graphene fluoride: a stable stoichiometric graphene derivative and its chemical conversion to graphene. small 6(24):2885–2891 (Dec 20)
9. Schäfer RA, Englert JM, Wehrfritz P, Bauer W, Hauke F, Seyller T, Hirsch A (2013) On the way to graphane—pronounced fluorescence of polyhydrogenated graphene. Angew Chem Int Ed 52(2):754–757 (Jan 7)
10. Raizada P, Sudhaik A, Singh P (2019) Photocatalytic water decontamination using graphene and ZnO coupled photocatalysts: a review. Mater Sci Energy Technol (May 2)
11. Yaqoob AA, Parveen T, Umar K, Ibrahim M, Nasir M (2020) Role of nanomaterials in the treatment of wastewater: a review. Water 12(2):495
12. Yaqoob AA, Khan RM, Saddique A (2019) Review article on applications and classification of gold nanoparticles. Int J Res 6(3):762–768
13. Yaqoob AA, Umar K, Ibrahim MN (2020) Silver nanoparticles: various methods of synthesis, size affecting factors and their potential applications—a review. Appl Nanosci 13:1 (Mar)
14. Shams SS, Zhang R, Zhu J (2015) Graphene synthesis: a review. Mater Sci Poland 33(3):566–578 (Sept 1)
15. Wang Y, Guo L, Qi P, Liu X, Wei G (2019) Synthesis of three-dimensional graphene-based hybrid materials for water purification: a review. Nanomaterials 9(8):1123 (Aug)
16. Odegard GM, Frankland SJ, Gates TS (2005) Effect of nanotube functionalization on the elastic properties of polyethylene nanotube composites. Aiaa J 43(8):1828–1835 (Aug)
17. Saito R, Dresselhaus G, Dresselhaus MS (2005) Physical properties of carbon nanotubes. Imperial
18. Yasmin A, Luo JJ, Daniel IM (2006) Processing of expanded graphite reinforced polymer nanocomposites. Compos Sci Technol 66(9):1182–1189 (Jul 1)
19. Ansari S, Giannelis EP (2009) Functionalized graphene sheet—poly (vinylidene fluoride) conductive nanocomposites. J Polym Sci Part B: Polym Phys 47(9):888–897 (May 1)
20. Lang B (1975) A LEED study of the deposition of carbon on platinum crystal surfaces. Surf Sci 53(1):317–329 (Dec 1)
21. Rokuta E, Hasegawa Y, Itoh A, Yamashita K, Tanaka T, Otani S, Oshima C (1999) Vibrational spectra of the monolayer films of hexagonal boron nitride and graphite on faceted Ni (755). Surf Sci 1(427):97–101 (June 1)

22. Shioyama H (2001) Cleavage of graphite to graphene. J Mater Sci Lett 20(6):499–500
23. Novoselov KS, Jiang D, Schedin F, Booth TJ, Khotkevich VV, Morozov SV, Geim AK (2005) Two-dimensional atomic crystals. Proc Natl Acad Sci 102(30):10451–10453 (Jul 26)
24. Novoselov KS, Geim AK, Morozov SV, Jiang D, Zhang Y, Dubonos SV, Grigorieva IV, Firsov AA (2004) Electric field effect in atomically thin carbon films. Science 306(5696):666–669 (Oct 22)
25. Yang Y, Han C, Jiang B, Iocozzia J, He C, Shi D, Jiang T, Lin Z (2016) Graphene-based materials with tailored nanostructures for energy conversion and storage. Mater Sci Eng: R Rep 1(102):1–72 (Apr)
26. Tour JM (2014) Top-down versus bottom-up fabrication of graphene-based electronics. Chem Mater 26(1):63–71 (Jan 14)
27. Britnell L, Gorbachev RV, Jalil R, Belle BD, Schedin F, Katsnelson MI, Eaves L, Morozov SV, Mayorov AS, Peres NM, Castro Neto AH (2012) Electron tunneling through ultrathin boron nitride crystalline barriers. Nano Lett 12(3):1707–1710 (Mar 14)
28. Huc V, Bendiab N, Rosman N, Ebbesen T, Delacour C, Bouchiat V (2008) Large and flat graphene flakes produced by epoxy bonding and reverse exfoliation of highly oriented pyrolytic graphite. Nanotechnology 19(45):455601 (Oct 9)
29. Shukla A, Kumar R, Mazher J, Balan A (2009) Graphene made easy: high quality, large-area samples. Solid State Commun 149(17–18):718–721 (May 1)
30. Choi W, Lahiri I, Seelaboyina R, Kang YS (2010) Synthesis of graphene and its applications: a review. Crit Rev Solid State Mater Sci 35(1):52–71 (Feb 11)
31. Hernandez Y, Nicolosi V, Lotya M, Blighe FM, Sun Z, De S, McGovern IT, Holland B, Byrne M, Gun'Ko YK, Boland JJ (2008) High-yield production of graphene by liquid-phase exfoliation of graphite. Nat Nanotechnol 3(9):563 (Sept)
32. Lotya M, Hernandez Y, King PJ, Smith RJ, Nicolosi V, Karlsson LS, Blighe FM, De S, Wang Z, McGovern IT, Duesberg GS (2009) Liquid phase production of graphene by exfoliation of graphite in surfactant/water solutions. J Am Chem Soc 131(10):3611–3620 (Mar 18)
33. Nethravathi C, Rajamathi M (2008) Chemically modified graphene sheets produced by the solvothermal reduction of colloidal dispersions of graphite oxide. Carbon 46(14):1994–1998 (Nov 1)
34. Tung VC, Allen MJ, Yang Y, Kaner RB (2009) High-throughput solution processing of large-scale graphene. Nat Nanotechnol 4(1):25 (Jan)
35. Tung VC, Chen LM, Allen MJ, Wassei JK, Nelson K, Kaner RB, Yang Y (2009) Low-temperature solution processing of graphene—carbon nanotube hybrid materials for high-performance transparent conductors. Nano Lett 9(5):1949–1955 (May 13)
36. Elif Ö, Belma Ö, İlkay Ş (2017) Production of biologically safe and mechanically improved reduced graphene oxide/hydroxyapatite composites. Mater Res Express 4(1):015601 (Jan 16)
37. Dasgupta A, Sarkar J, Ghosh M, Bhattacharya A, Mukherjee A, Chattopadhyay D, Acharya K (2017) Green conversion of graphene oxide to graphene nanosheets and its biosafety study. PloS One 12(2)
38. Somani PR, Somani SP, Umeno M (2006) Planer nano-graphenes from camphor by CVD. Chem Phys Lett 430(1–3):56–59 (Oct 19)
39. Obraztsov AN, Obraztsova EA, Tyurnina AV, Zolotukhin AA (2007) Chemical vapor deposition of thin graphite films of nanometer thickness. Carbon 45(10):2017–2021 (Sept 1)
40. Yu Q, Lian J, Siripongpert S, Li H, Chen YP, Pei SS (2008) Graphene segregated on Ni surfaces and transferred to insulators. Appl Phys Lett 93(11):113103 (Sept 15)
41. De Arco LG, Zhang Y, Kumar A, Zhou C (2009) Synthesis, transfer, and devices of single-and few-layer graphene by chemical vapor deposition. IEEE Trans Nanotechnol 8(2):135–138 (Jan 20)
42. Fauzi FB, Ismail E, Ani MH, Bakar SN, Mohamed MA, Majlis BY, Din MF, Abid MA (2018) A critical review of the effects of fluid dynamics on graphene growth in atmospheric pressure chemical vapor deposition. J Mater Res 33(9):1088–1108 (May)
43. Liu B, Xuan N, Ba K, Miao X, Ji M, Sun Z (2017) Towards the standardization of graphene growth through carbon depletion, refilling and nucleation. Carbon 1(119):350–354 (Aug)

44. Moreno-Bárcenas A, Perez-Robles JF, Vorobiev YV, Ornelas-Soto N, Mexicano A, Garcia AG (2018) Graphene synthesis using a CVD reactor and a discontinuous feed of gas precursor at atmospheric pressure. J Nanomater 2018

45. Yin S, Zhang X, Xu C, Wang Y, Wang Y, Li P, Sun H, Wang M, Xia Y, Lin CT, Zhao P (2018) Chemical vapor deposition growth of scalable monolayer polycrystalline graphene films with millimeter-sized domains. Mater Lett 15(215):259–262 (May)

46. Pogacean F, Biris AR, Socaci C, Coros M, Magerusan L, Rosu MC, Lazar MD, Borodi G, Pruneanu S (2016) Graphene–bimetallic nanoparticle composites with enhanced electro-catalytic detection of bisphenol A. Nanotechnology 27(48):484001 (Nov 2)

47. Lavin-Lopez MP, Sanchez-Silva L, Valverde JL, Romero A (2017) CVD-graphene growth on different polycrystalline transition metals. AIMS Mater Sci 19(4):194–208 (Jan)

48. Pekdemir S, Onses MS, Hancer M (2017) Low temperature growth of graphene using inductively-coupled plasma chemical vapor deposition. Surf Coat Technol 15(309):814–819 (Jan)

49. Vlassiouk IV, Stehle Y, Pudasaini PR, Unocic RR, Rack PD, Baddorf AP, Ivanov IN, Lavrik NV, List F, Gupta N, Bets KV (2018) Evolutionary selection growth of two-dimensional materials on polycrystalline substrates. Nat Mater 17(4):318–322 (Apr)

50. Park BJ, Choi JS, Eom JH, Ha H, Kim HY, Lee S, Shin H, Yoon SG (2018) Defect-free graphene synthesized directly at 150 C via chemical vapor deposition with no transfer. ACS Nano 12(2):2008–2016 (Feb 27)

51. Kasikov A, Kahro T, Matisen L, Kodu M, Tarre A, Seemen H, Alles H (2018) The optical properties of transferred graphene and the dielectrics grown on it obtained by ellipsometry. Appl Surf Sci 15(437):410–417 (Apr)

52. Xu X, Zhang Z, Dong J, Yi D, Niu J, Wu M, Lin L, Yin R, Li M, Zhou J, Wang S (2017) Ultrafast epitaxial growth of metre-sized single-crystal graphene on industrial Cu foil. Sci Bull 62(15):1074–1080 (Aug 15)

53. Chin HT, Lee JJ, Hofmann M, Hsieh YP (2018) Impact of growth rate on graphene lattice-defect formation within a single crystalline domain. Sci Rep 8(1):1–6 (Mar 6)

54. Rollings E, Gweon GH, Zhou SY, Mun BS, McChesney JL, Hussain BS, Fedorov AV, First PN, De Heer WA, Lanzara A (2006) Synthesis and characterization of atomically thin graphite films on a silicon carbide substrate. J Phys Chem Solids 67(9–10):2172–2177 (Sept 1)

55. Hass J, De Heer WA, Conrad EH (2008) The growth and morphology of epitaxial multilayer graphene. J Phys: Condens Matter 20(32):323202 (Jul 18)

56. Emtsev KV, Bostwick A, Horn K, Jobst J, Kellogg GL, Ley L, McChesney JL, Ohta T, Reshanov SA, Röhrl J, Rotenberg E (2009) Towards wafer-size graphene layers by atmospheric pressure graphitization of silicon carbide. Nat Mater 8(3):203–207 (Mar)

57. Choucair M, Thordarson P, Stride JA (2009) Gram-scale production of graphene based on solvothermal synthesis and sonication. Nat Nanotechnol 4(1):30 (Jan)

58. De Silva KK, Huang HH, Joshi RK, Yoshimura M (2017) Chemical reduction of graphene oxide using green reductants. Carbon 1(119):190–199 (Aug)

59. Choi YJ, Kim E, Han J, Kim JH, Gurunathan S (2016) A novel biomolecule-mediated reduction of graphene oxide: a multifunctional anti-cancer agent. Molecules 21(3):375 (Mar)

60. Marlinda AR, Huang NM, Muhamad MR, An'Amt MN, Chang BY, Yusoff N, Harrison I, Lim HN, Chia CH, Kumar SV (2012) Highly efficient preparation of ZnO nanorods decorated reduced graphene oxide nanocomposites. Mater Lett 1(80):9–12 (Aug)

61. Ahmad M, Ahmed E, Hong ZL, Khalid NR, Ahmed W, Elhissi A (2013) Graphene–Ag/ZnO nanocomposites as high performance photocatalysts under visible light irradiation. J Alloy Compd 15(577):717–727 (Nov)

62. Gong Y, Zhao J, Wang H, Xu J (2018) CuCo2S4/reduced graphene oxide nanocomposites synthesized by one-step solvothermal method as anode materials for sodium ion batteries. Electrochim Acta 1(292):895–902 (Dec)

63. Azarang M, Shuhaimi A, Yousefi R, Sookhakian M (2014) Effects of graphene oxide concentration on optical properties of ZnO/RGO nanocomposites and their application to photocurrent generation. J Appl Phys 116(8):084307 (Aug 28)

64. Rao BG, Mukherjee D, Reddy BM (2017) Novel approaches for preparation of nanoparticles. In: Nanostructures for novel therapy, pp 1–36. Elsevier (Jan 1)

65. Chang H, Sun Z, Ho KY, Tao X, Yan F, Kwok WM, Zheng Z (2011) A highly sensitive ultraviolet sensor based on a facile in situ solution-grown ZnO nanorod/graphene heterostructure. Nanoscale 3(1):258–264

66. Sahatiya P, Badhulika S (2015) One-step in situ synthesis of single aligned graphene–ZnO nanofiber for UV sensing. RSC Adv 5(100):82481–82487

67. Cui S, Mao S, Lu G, Chen J (2013) Graphene coupled with nanocrystals: opportunities and challenges for energy and sensing applications. J Phys Chem Lett 4(15):2441–2454 (Aug 1)

68. Hong W, Xu Y, Lu G, Li C, Shi G (2008) Transparent graphene/PEDOT–PSS composite films as counter electrodes of dye-sensitized solar cells. Electrochem Commun 10(10):1555–1558 (Oct 1)

69. Yan J, Ye Q, Wang X, Yu B, Zhou F (2012) CdS/CdSe quantum dot co-sensitized graphene nanocomposites via polymer brush templated synthesis for potential photovoltaic applications. Nanoscale 4(6):2109–2116

70. Yoo E, Okata T, Akita T, Kohyama M, Nakamura J, Honma I (2009) Enhanced electrocatalytic activity of Pt subnanoclusters on graphene nanosheet surface. Nano Lett 9(6):2255–2259 (June 10)

71. Zhang XY, Li HP, Cui XL, Lin Y (2010) Graphene/TiO₂ nanocomposites: synthesis, characterization and application in hydrogen evolution from water photocatalytic splitting. J Mater Chem 20(14):2801–2806

72. Wen Y, Xing F, He S, Song S, Wang L, Long Y, Li D, Fan C (2010) A graphene-based fluorescent nanoprobe for silver (I) ions detection by using graphene oxide and a silver-specific oligonucleotide. Chem Commun 46(15):2596–2598

73. Zhang H, Lv X, Li Y, Wang Y, Li J, Li M (2010) P25-graphene composite as a high performance photocatalyst. ACS Nano 4:380–386

74. Mohanty N, Berry V (2008) Graphene-based single-bacterium resolution biodevice and DNA transistor: interfacing graphene derivatives with nanoscale and microscale biocomponents. Nano Lett 8(12):4469–4476 (Dec 10)

75. Wan Y, Wang Y, Wu J, Zhang D (2011) Graphene oxide sheet-mediated silver enhancement for application to electrochemical biosensors. Anal Chem 83(3):648–653 (Feb 1)

76. Wan Y, Lin Z, Zhang D, Wang Y, Hou B (2011) Impedimetric immunosensor doped with reduced graphene sheets fabricated by controllable electrodeposition for the non-labelled detection of bacteria. Biosens Bioelectron 26(5):1959–1964 (Jan 15)

Rheological Properties of Hybrid Nanocomposites Based on Graphene and Other Nanoparticles

Fatima-Zahra Semlali Aouragh Hassani, Rachid Bouhfid, and Abou el Kacem Qaiss

Abstract The development of promising nanomaterials is mainly associated with their use in industrial applications, medicine, biology and ecology. Many of the existing materials may not satisfy all the modern civilization fundamental requirements, leading researchers to develop hybrid materials that may present higher properties than the individual components. Hybrid graphene nanocomposites have attracted much attention recently because of their unique structure and remarkable mechanical, electrical, thermal and rheological properties. The main attention in this chapter is firstly focused on the graphene-based hybrid nanocomposites, their different types, synthesis methods and application fields. Then on the rheological properties of graphene-based hybrid materials, in order to quantify the dispersion of hybrid nanofillers in polymer matrices.

Keywords Nanocomposites · Hybrid materials · Graphene · Carbon allotrope · Rheological properties

1 Introduction

The emergence of nanotechnologies aims to develop new composite materials and miniaturized components. Graphene nanocomposites have generated intense interest among scientists due to their unique properties. The dispersion and the interfacial interactions between the nanofillers and the polymer matrix are essential to obtain improved properties of these nanocomposites. Understanding the physicochemical properties of nanocomposites based on insulating or semiconductor polymers and graphene or carbon derivatives, provides very useful information for their applications in various fields including energy storage and conversion, electrochemistry, optics and composite materials [1, 2]. Indeed, graphene is a carbon nanomaterial with a two-dimensional (2D) sheet structure, composed of sp^2 carbon atoms arranged

F.-Z. Semlali Aouragh Hassani · R. Bouhfid · A. K. Qaiss (✉)
Composites and Nanocomposites Center, Moroccan Foundation for Advanced Science,
Innovation and Research (MAScIR), Rabat, Morocco
e-mail: a.qaiss@mascir.com

283

in a honeycomb structure. It is considered the "thinnest material in the universe" with enormous application potential. Experimental studies show that graphene has excellent mechanical, thermal and electrical properties. These intrinsic properties of graphene have aroused enormous interest in its use in industry. A very important application which can exploit the properties of graphene is its incorporation into polymer matrices to manufacture multifunctional nanocomposites with very low loading rate. The production of such nanocomposites requires that graphene sheets must be produced in large quantities, but they must also be dispersed and distributed homogeneously within the polymer matrices [1, 2].

In order to fully expand the graphene applications and to increase the carbon-based materials performance, graphene can be combined with other types of reinforcement such as nanoparticles, nanofibers and nanosheets; or mixed with another allotropic carbon type (Diamond, Fullerene, Nanofiber, Nanotube, Polyaromatic) [2, 3]. The advantage of this hybridization lies in the combination of the properties provided, on the one hand, by the polymer matrix (ease of processing, etc.), and, on the other hand, by those of the combined reinforcements (hardness, color…), and thus opening up a wide field of applications for these hybrid materials (optoelectronics, catalytic systems, the medical or pharmaceutical field) [2–4]. However, the simple incorporation of these hybrids does not necessarily allow good dispersion in the polymer matrix [5]. To overcome these drawbacks, constant efforts have been made to link covalently hybrid reinforcements based on graphene and polymer chains. The rheological characterization remains an effective tool for quantifying the dispersion of the hybrid in nanocomposite systems [5, 6]. This rheological study of graphene-based hybrid composites will make it possible to study the behavior or response of materials under the effect of the stresses or deformations applied to them. Indeed, the determination of the rheological properties of the material such as the viscosity and the elastic/viscous modules, which are a function of the deformation and the stress applied to the material, will allow the microstructure evaluation and the hybrid nanocharges dispersion in the matrices polymers [5, 6]. However, an increase in the complex viscosity at low shear gradient is related to the good dispersion of the nanofillers in the matrix.

The aim of this chapter is to present, firstly, the graphene and its use as reinforcement for polymer matrices as well as a bibliographic review on its synthesis. Secondly, to explain more precisely the different types of graphene-based hybrid materials, their different methods of synthesis and their fields of application. Finally, the last part of this chapter was devoted to the rheological study of different graphene-based hybrid materials, and thus quantifying the hybrid nanocharges dispersion in the matrices polymers.

2 Graphene Nanocomposite Materials

The concept of nanocomposite refers to any combination of two or more phases, at least one of which is nanometric in one dimension. This very general definition

brings together all the associations between metals, ceramics and polymers. In this study, we will focus on nanocomposites based on polymers charged by nanoparticles, at least one of whose dimensions is of the order of a nanometer or a few tens of nanometers. These are graphene nanoparticles, which once introduced into a matrix, bring particular properties to the material.

2.1 Nanocomposite Materials

In general, various nanocomposites exist and can be classified mainly according to the type of the matrix and the reinforcement.

2.1.1 Matrix Classification

Metals, ceramics, thermosetting or thermoplastic polymers are frequently used as a matrix. The addition of reinforcement is useful to improve the mechanical characteristics [7–9]. The role of the matrix is to transfer mechanical stresses to the reinforcements by protecting the reinforcement against external aggressions. The matrix must therefore be deformable and have good compatibility with the reinforcement. Given these constraints, the matrices used are often polymers, modified by various adjuvants and additives: polar head grafting, molding agents, stabilizers, antioxidants, pigments, etc. [10]. Polymers are molecular materials, that is, each polymer chain is an individual entity and its interaction with other chains is generally weak. The polymer chains can take different conformations and can orient themselves under mechanical stress. The polymers are characterized not by a single molecular weight but by an average molecular weight characteristic of the distribution and of the average of the chains weight.

Indeed, the reinforcements are not always uniformly dispersed. It is possible to define different types of composites according to the dispersion of the reinforcement within the matrix.

Interactions appear at all scales which lead to the definition of different interfaces which influence mechanical and electrical behavior. Let's see in more detail the morphologies associated with the reinforcement in the case of sheet nanocomposites which are specifically the subject of this work [10, 11].

2.1.2 Reinforcement Classification

A nanocomposite is a composite material whose reinforcement has at least one of the three dimensions of the order of a nanometer [12–14]. They can be classified in the same way as composites, according to the morphology of the reinforcement which is dispersed there and more particularly according to the number of their nanometric

dimension. We will also find fiber and particle composites, a new type of composite called lamellar reinforcements.

It is necessary now to define the different forms of reinforcement. Three classes of reinforcement then appear, nanoparticles with three nanometric dimensions, nanofibers and sheets (leaflet) (Fig. 1) [12].

– *Nanoparticles with three nanometric dimensions: nanoparticles*.

The three dimensions of the particle are in the nanometer range. This category includes, for example: Atomic aggregates; Metallic nanoparticles (gold, iron, cobalt, silver, platinum…); Fullerenes.

The gain of specific physical properties (optical, electrical, magnetic, etc.) is sought when adding this type of particle; the mechanical reinforcement is only secondary here.

– *Nanoparticles with two nanometric dimensions: nanofibers*.

Nanofibers are particles of which two dimensions are on the order of a nanometer. The third is much larger. The characteristic size is the form factor. It is defined as the ratio of the length to the diameter of the fiber and is often greater than 100. There are hollow fibers, the best known being carbon nanotubes, and solid fibers (nanowires).

– *Nanoparticles with one nanometric dimension: sheets*.

The sheets have two preferred directions. The particle has a dimension of the order of a nanometer and the two others of the order of a micrometer. The form factor is then defined as the ratio of the length of the sheet to the thickness. The arrangement of the sheets and their orientation will generate the desired properties. This family of particles comes from naturally laminated materials. The main precursors used for the manufacture of nanocomposites with a polymer matrix are, on the one hand, double sheet hydroxides and, on the other hand, swelling clays also called smectites. These nanosheets are characterized respectively by positive and negative charges on the surface.
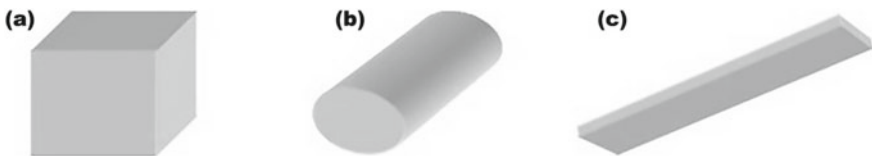
Fig. 1 Schematic representation of the different reinforcements. **a** nanoparticle; **b** nanofiber; **c** nanosheet

## 2.2 History and Presentation of Graphene

For more than 100 years, chemists have endeavored to synthesize carbon-based molecules with different forms and physicochemical properties. Among the best known are amorphous carbon [15], graphite [16], graphene [17], fullerene [18], carbon nanotube [19] and the diamond [20] (Fig. 2). Also, more sophisticated forms such as graphene nanoribbons [21], nano-horns [22], nanocones [23] and carbon nanofibers [24] have been developed more recently. In general, these molecules are known for their electrical properties, their hardness and their high mechanical resistance, as well as for their chemical and thermal stability.

Graphene, an allotropic form of carbon, is a two-dimensional crystal (monoplane) of carbon, the stack of which constitutes graphite. In 1940, researchers theoretically found that graphene is a block in the graphite stack [25]. In 2004, Geim succeeded in identifying a single layer of graphene [17] which was previously considered to be thermodynamically unstable and that it could not exist under ambient conditions [26].

It has been considered to be the building block of all other allotropies of graphitic carbon at different dimensions [27] (Fig. 3). For example, graphite (3D carbon allotropy) consists of graphene sheets stacked on top of each other and separated by a distance of 3.4 Å. Discovered in 1985 by Smalley, Kroto and Curl, fullerenes, which constitute the third allotropic form of carbon, appear as closed molecules, of spherical shape. The most famous is C60, the appearance of which is illustrated by a football, but there are many others, all made up of an even number of carbon atoms. When

Fig. 2 Representation of the carbon atom and its main allotropes
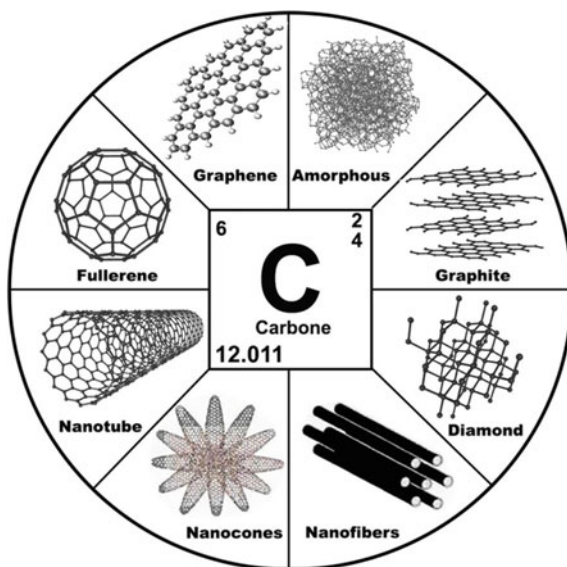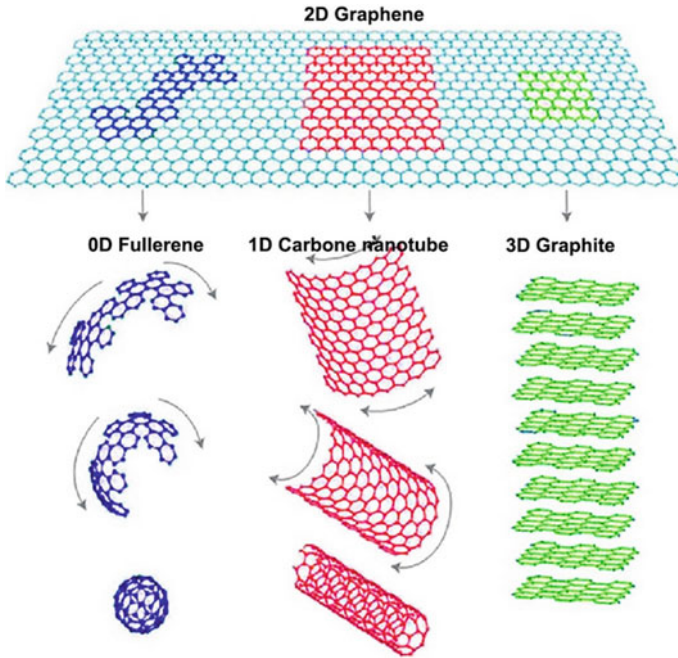
Fig. 3 Graphene sheets as building block of all other allotropies of graphitic carbon at different dimensions

this number becomes very large, the almost spherical shape is no longer mechanically stable and the structure evolves towards that of carbon nanotubes, discovered in 1991 by Iijima [19]. The single-sheet carbon nanotubes, formed by a graphene plane wound on it, are closed at their ends by two half-fullerenes. There are also multi-sheet nanotubes where several graphene planes are wound concentrically; the ends of the tubes having a more complex structure.

2.3 Properties of Graphene

Graphene is a unique layer of carbon atoms wrapped in a dense, honeycomb crystal lattice. The carbon–carbon bond in graphene (sp^2) is about 0.142 nm in length [28]. The thickness of graphene is 0.35–1 nm (Fig. 4).

Due to their exceptional electronic, thermal and mechanical properties such as the electron mobility of 200,000 cm^2/Vs, the thermal conductivity of 5000 W/mK, the Young's modulus of 1.0 TPA, the breaking strength of 130 GPa, and their high specific surface of 2630 m^2/g; nanometric graphene materials have recently attracted considerable attention. In addition, graphene has a very high electrical conductivity,
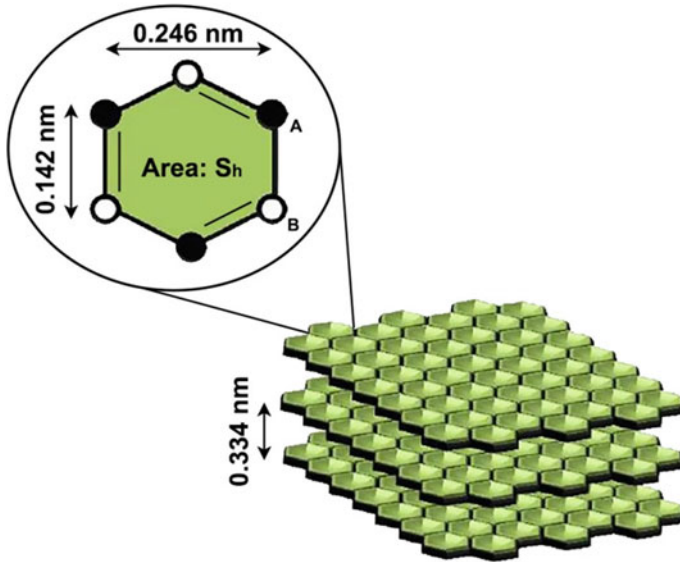
Fig. 4 Distance from carbon to carbon bond of graphene

up to 6000 S/cm, and unlike carbon nanotubes (NTC), chirality is not a factor in its electrical conductivity [29–32].

2.4 Graphene Preparation Techniques

Graphene occurs naturally in graphite crystals, where it occurs as a stack of sheets. Several techniques aimed at making it usable have emerged in recent years.

2.4.1 "Bottom-Up" Techniques

In Bottom-Up processes, graphene can be prepared by a variety of experimental techniques such as: the chemical vapor deposition (CVD) technique, arc discharge, the epitaxial growth on a SiC substrate, chemical conversion, CO reduction, opening of carbon nanotube and self-assembly of surfactants. CVD and epitaxial growth techniques allow the preparation of small quantities of graphene sheets with a large lateral size and without structural defects. They are more attractive than micromechanical cleavage for the production of graphene for basic studies and electronic applications, but they are not desirable sources for the production of graphene nanosheets for polymer nanocomposites which require a large quantity of graphene in the form powder [33, 34] (Fig. 5).
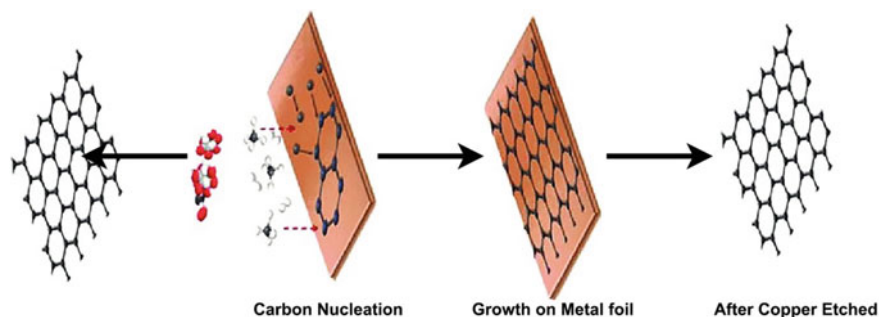
Carbon Nucleation   **Growth on Metal foil**   **After Copper Etched**

Fig. 5 "Bottom-up" technique

2.4.2 "Top-Down" Techniques

In top-down techniques, graphene or modified graphene sheets are produced by the separation or exfoliation of graphite or graphite derivatives (such as graphite oxide and graphite fluoride). Exfoliation consists of removing a very thin layer of graphite using an adhesive tape, then repeating the operation ten times on the samples so that they are as fine as possible. They are then deposited on a silicon dioxide plate where an optical identification will make it possible to select the samples made up of a single layer.

The first experimental method used for the production of graphene is micromechanical cleavage [17]. This method leads to the production of graphene sheets of large lateral size and of high structural quality, but in very limited quantities. However, the graphite was directly exfoliated into graphene nanosheets by a sonication treatment in the presence of surfactants; however, this technique does not lead to total exfoliation of the graphite. Dissolving graphite in acids also presents a direct exfoliation method which makes it possible to obtain graphene nanosheets; on the other hand the nature of the acid used and the cost of its elimination can limit the effectiveness of this technique. Furthermore, electrochemical exfoliation of graphite has been used in the presence of ionic liquids as a good method for producing large quantities of functionalized graphene nanosheets [35]. One of the "Top Down" methods is the chemical reduction of graphene oxide. The principle consists in oxidizing graphite in an acid medium then using hydrazine or another reducing solvent to purify the graphene. This method can produce large quantities of graphene, but of lower quality. Thermal reduction of graphite oxide at a temperature of 1000 °C can produce well reduced and exfoliated graphene. In Fig. 6 we schematize the "Top-Down" processes in which graphite or graphite oxide are used as starting materials for the production of graphene nanosheets in large quantities [33, 34]. In general, these methods are suitable for large-scale production aimed at applications of polymer-based composites. "Top-Down" techniques have significant economic advantages over "Botton-up" methods.
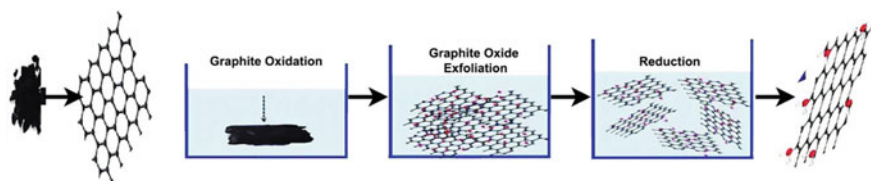
Fig. 6 "Top-Down" technique

2.4.3 Direct Graphite Exfoliation

The micromechanical cleavage of graphite constitutes the first experimental method used for the production of graphene [17]. Thanks to this approach, graphene sheets of large lateral size and of high structural quality can be produced, but in very limited quantities, which is only suitable for fundamental studies or electronic applications [17]. More recently, however, graphite has been directly exfoliated into individual or multiple graphene nanosheets via ultrasound treatment in the presence of surfactants such as polyvinylpyrrolidone (PVP) [36] or *N*-methylpyrrolidone (NMP) [37]. Dissolving graphite in super acids also presents a method of direct exfoliation which makes it possible to obtain graphene nanosheets [38]. Furthermore, electrochemical exfoliation of graphite in the presence of ionic liquids has been developed as an effective technique for producing large quantities of functionalized graphene nanosheets [35] (Fig. 7). The advantage of this latter method is that it makes it possible to produce graphene nanosheets functionalized with imidazolium groups which can assist the dispersion of the nanosheets in aprotic solvents [35]. Direct exfoliation of graphite via sonication has the advantage of producing large quantities of nanosheets which can be used in nanocomposite applications, but the separation of exfoliated nanosheets
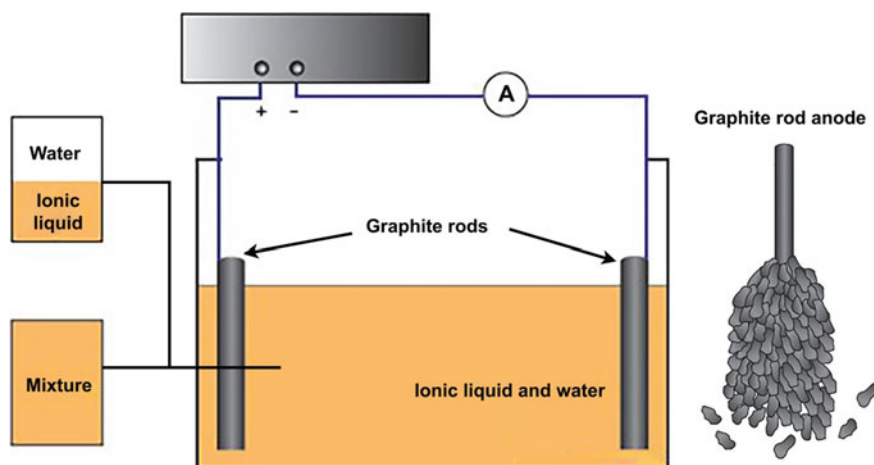

Fig. 7 Schematic representation of direct graphite exfoliation

from the unexfoliated quantity of graphite presents a major problem, because this technique does not allow total exfoliation of graphite [36, 37]. On the other hand, the method of dissolving graphite in chlorosulfonic acid [39] has the potential to produce graphene nanosheets in large quantities, but the dangerous nature of the acid used and the cost of its elimination can limit the effectiveness of this technique (Fig. 7).

3 Graphene Hybrid Nanocomposite Materials

Nowadays, polymers occupy a very important part of our daily life. Other times, with the development of polymer materials in fields with high added values such as optics, electronics or biomaterials, the polymers generally available are not sufficient to meet the requirements of these sectors. It is therefore necessary to develop new materials with exceptional properties and with great ease of implementation (often provided by the polymer component). In order to reconcile all these aspects, it is common to arrive at the desired product to combine the properties of different materials, whether organic or inorganic. This is the framework for the synthesis of organic/inorganic hybrid materials. Indeed, the synergy between the optical, thermal and/or electrical properties of inorganic particles and the physico-chemical properties of polymer materials opens up a wide field of applications for these objects. We can cite for example the use of hybrid materials in fields such as optoelectronics [40], catalytic systems [41], the medical or pharmaceutical field [42]. The concept of (nano) hybrid materials is increasingly used and it is sometimes difficult to identify what these terms represent. This concept brings together a multitude of materials and structures that need to be defined. These materials can take different "forms" as shown in Fig. 8, depending on the intended application. This designation includes both copolymers, one of the blocks of which is obtained from an "inorganic" monomer and the other block of which is a purely organic polymer, as well as porous networks (meso- and nanometric). An important part of hybrid materials is represented by the chemical modification of inorganic particles or surfaces by organic molecules. Sanchez et al. [39] defines a hybrid material as a material consisting of at least an organic phase and an inorganic phase, in which at least one of these phases has a dimension between one tenth and one hundred nanometers. It therefore appears that Sanchez's hybrid is an organic/inorganic Kelly nanocomposite. In addition, Sanchez distinguishes two types of hybrids according to the mode of arrangement between the constituents:

– **Class I hybrids** are materials in which the organic/inorganic interactions are weak (Van der Waals type, or electrostatic)
– **Class II hybrids** are materials in which the organic/inorganic interactions are strong (of the covalent or iono-covalent type).

The use of the term "hybrid" is intrinsically more precise than that of "nanocomposite", and makes it possible to appreciate the mode of interaction between the organic phase and the inorganic phase.
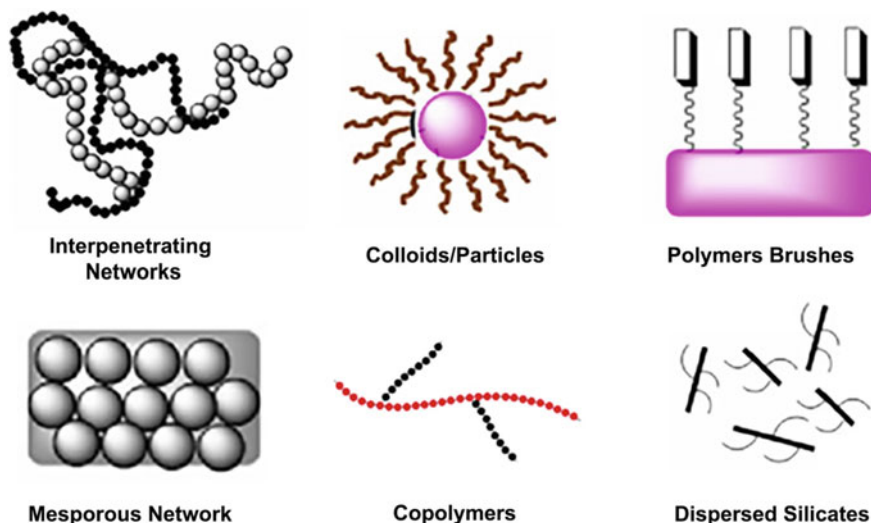
Fig. 8 Examples of organic/inorganic hybrid materials

For hybrids in which the inorganic phase consists of stacks of sheets, we will be able to distinguish, in addition to the mode of cohesion between the phases, three different types of conformation, see Fig. 9:

– The organic phase does not penetrate into the interfoliar space (between the sheets of the stack), and embeds the inorganic phase. As there is no -strictly speaking- physical interaction between the organic and inorganic phases, this material cannot be qualified as a hybrid. It is rather a nanocomposite [4].
– The organic phase enters the interfoliar space, and the consistency between the inorganic sheets is preserved over the entire extent of the stack. As the material seems to be composed of a regular alternation of inorganic sheets and organic sheets: it is an interstratified hybrid [4].
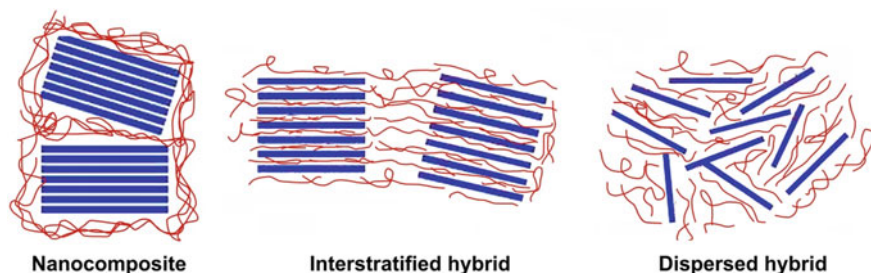
Fig. 9 Hybrid nanocomposites

– The organic phase enters the interfoliar space, but there is no longer any order at the long distance between the inorganic sheets. As the latter seem to be dispersed in the organic matrix: it is a dispersed hybrid [4].

3.1 Methods of Synthesis of Hybrid Materials

Generally speaking, there are two ways of making hybrid materials:

– Either from stacks of existing sheets and makes them interact with the organic phase to form the hybrid material.
– Or to make the organic phase interact at the time of the formation of the sheets themselves.

The strategies which offer the advantage of being able to get rid of the synthesis of the sheets can be qualified as "post creation" methods. While those which consist in making a hybrid directly from a molecular assembly can be qualified as "ab initio" methods.

3.1.1 Syntheses of Class I Hybrids

As has been specified, in class I hybrids the cohesion between the organic and inorganic phases is ensured by weak interactions (of the Van der Waals, or electrostatic type) [39]. This mode of cohesion promotes the use of post creation synthesis methods (such as intercalation, or in situ polymerization [43, 44], in which the inorganic matrix is already formed.

Intercalation Synthesis

This post creation synthesis method consists in the direct intercalation of organic molecules of variable size, but not charged, between the inorganic lamells already formed (Fig. 10a). To achieve this objective, the inorganic matrix is immersed in an organic solvent. The solvent then enters the interfoliar space (causing the appearance of a more or less stable suspension) if the enthalpy of formation of the interstratification is greater than the entropy of dispersion of the two parts in the solvent [45].

However, to promote the intercalation of molecules of large steric hindrance, it is possible to use the method of "host displacement". This two-step method consists in first removing the sheets with a small molecule (called "spacer"), then in replacing the "spacer" with the desired molecule [46]. The interleaf, already discarded, can then more easily accommodate the large molecule, see Fig. 10b.
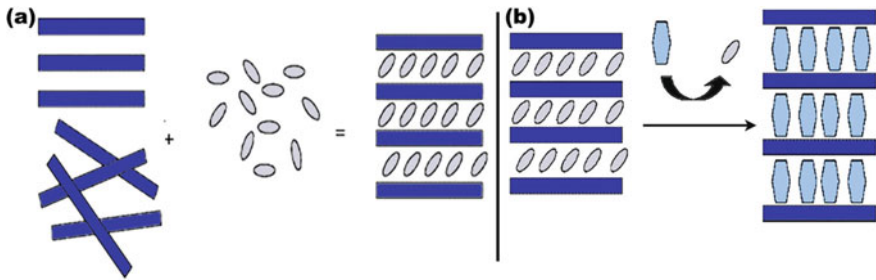
Fig. 10 a Intercalation of small organic molecules between the inorganic lamells. **b** Host substitution intercalation
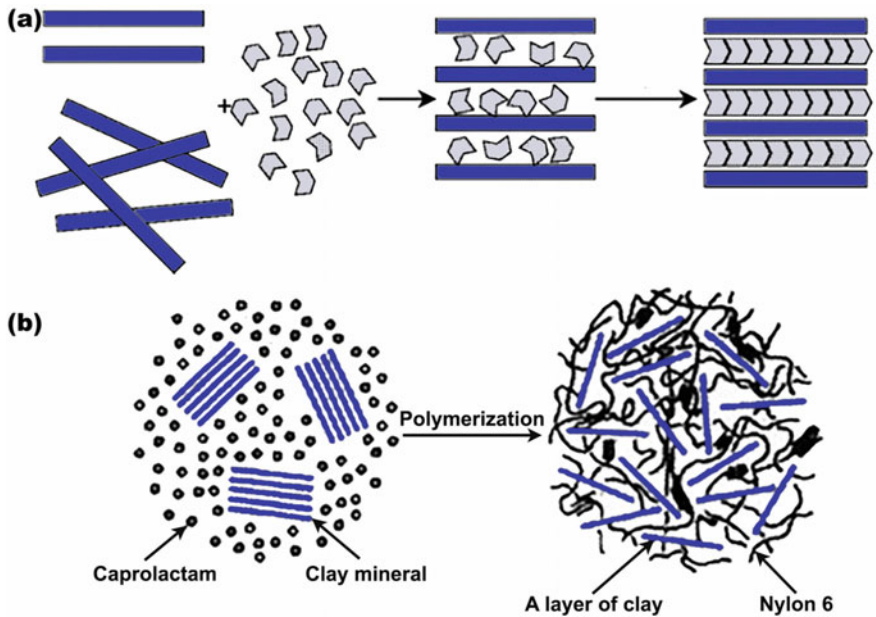
Fig. 11 a In-situ polymerization of monomer in inorganic lamellar material. **b** First synthesis of microcomposites by in-situ polymerization carried out at the Toyota research center

Synthesis by In-Situ Polymerization

In-situ polymerization is a two-step synthesis method, see Fig. 11a:

– The first step consists of interposing the monomer in the interlayer. This step can be carried out using one of the intercalation strategies previously developed (direct intercalation, or host substitution).
– Once the monomers have been inserted into the interfoliar space, their polymerization is activated thermally, chemically, or even by UV treatment [43, 44].

By controlling the initial monomer concentration and the degree of polymerization, it is possible to obtain both inter-layered and dispersed hybrids.

In situ polymerization was originally developed by Toyota's research center to make dispersed micro composite materials; in this case, to strongly disperse montmorillonite in a nylon 6 matrix [29, 30], Fig. 11b.

At present, this method of synthesis is used extensively [43] to make hybrids, or micro composites, highly dispersed in extremely varied organic matrices (epoxy, polypropylene, polyethylene terephthalate, etc.) [47] for advanced applications (mechanical, flame retardant, gas tightness, etc.) [47].

Precipitation Syntheses II

It is also possible to directly form hybrids with low cohesion between the organic and inorganic phases, ie to form class I hybrids using an ab initio strategy.

The strategy consists in precipitating a homogeneous molecular assembly from a solution in the presence of the desired organic phase. The use of water-soluble polymers (for example: polyvinyl alcohol (PVA), hydroxyethylcellulose (HEC), polyacrylonitrile (PACN)) is therefore particularly suitable for producing class I hybrids by this method [48]. By controlling the content of organic phase in the solution, it is as well possible to obtain an interstratified hybrid as a dispersed hybrid [48].

This method also makes it possible to precisely control the purity and the initial contents of the various constituents. This ensures both their good homogeneity in the solution, as well as the quality of the hybrid obtained (both in terms of its composition and its distribution).

3.2   Syntheses of Class II Hybrids

In class II hybrids, the cohesion between the organic and inorganic phases is no longer ensured by weak interactions as before, but by strong interactions (of ionic or covalent type) [39]. In general, the production of materials having this type of cohesion is favored by the use of ab initio methods. However, under certain conditions, such hybrids can also be created using post creation strategies.

3.2.1   Post Creation Syntheses of Class II Hybrids

It is possible to use the strategies developed previously (intercalation, intercalation by host substitution, or even in situ polymerization) to produce class II hybrids, provided that cationic organic molecules are used.

However, the limited number of cationic organic molecules greatly restricts the number of hybrids that can thus be produced. These hybrids are of great interest, however, because they have very anisotropic ion conduction properties [49].

Another type of post-creation synthesis of class II hybrids consists in reacting trialcoxysilanes (RSi(OR′)₃) on the SiOH sites on the surface of the sheets, and consequently covalently linking alkyl groups to the sheets. However, if this strategy gives good results in lamellar silicates rich in SiOH sites as in magaadites [50], or kenyaite [51], it remains marginal in the case of phyllosilicates [52] since the SiOH sites are structural defects in the tetrahedral layers of silicon, and are therefore few.

3.2.2 Ab Initio Synthesis of Class II Hybrids

As we have seen previously, this synthesis strategy consists in making the hybrid directly. For example, in the case of clays, the difficulty of such a method therefore lies in the realization of the clay itself, since it is done in nature at high temperatures and pressures which are not favorable to the realization of a hybrid material [53, 54].

However, one can synthesize clays other than by reproducing in the laboratory the conditions encountered in nature. In general, all of the methods used all fall under the same strategy based on sol–gel chemistry, which consists in condensing a homogeneous molecular assembly from a solution containing the precursors of the hybrid [53, 54].

The solution of precursors being homogeneous, the formation of a hybrid material is obtained, either by catalysis, or by precipitation by increasing the pH by addition of sodium hydroxide. The differences between the methods lie in their maturation (or not) in temperature, even in an autoclave [53, 54].

To accommodate the steric constraints linked to the presence of organic radicals, as well as to create the least structural constraints unfavorable to the organization of the material; the organic groups are oriented by pointing towards the interleaf. These class II hybrids are composed of a regular alternation of inorganic and organic sheets. They are therefore, by synthesis, interstratified [53, 54].

3.3 Type of Hybrid Material

In order to increase the performance of carbon-based materials and to tailor tailor-made applications, hybrid materials have been developed to obtain, for example, composites of the graphene oxide (OG)-allotropic carbon type (Diamond, Fullerene, Nanofiber, Nanotube, Polyaromatic), HQ-organic molecule (Amino acid Nucleic acid, DNA, Antibody, Aptamer, Biomarker, Enzyme, Peptide, Small molecule, Protein), HQ-living organism (Bacterium, Cell, Virus) and OG-nanoparticle (Metal, Metal oxide, Quantum dot). The new trend in the field of carbon chemistry research is to develop new carbon-based structures mixing two allotropes such as carbon nanotube and fullerene (Fig. 12a) [55], graphene and carbon nanotube (Fig. 12b) [56, 57] or graphene and diamonds (Fig. 12c) [58]. Also, it is possible to graft bioactive molecules on the surface of allotropes (Fig. 12d) [59], a drug, a protein, a peptide, or a nucleic acid [60], and also living organisms such as a bacteria, cell or virus [61].
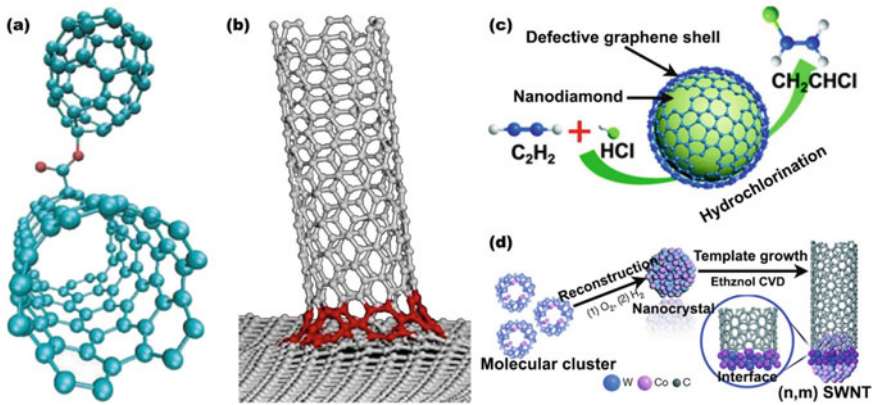
Fig. 12 Hybrid materials. **a** carbon nanotube and fullerene, **b** graphene and carbon nanotube, **c** graphene and diamonds, **d** graft bioactive molecules on the surface of allotropes

Recently, hybrid materials of the graphene-metallic nanoparticle type [2] have been specially developed for the emerging field of nanoelectronics.

4 Rheological Properties of Hybrid Nanocomposites Based on Graphene

4.1 Nanocomposite Rheology

Work on the rheological behavior of nanocomposites i.e. macroscopic viscoelastic behavior has often made it possible to better understand the structures and relationships responsible for the reinforcement of polymers by particles. The rheology therefore places itself here on the border between structural determination and physical properties of nanocomposites; moreover this technique is often the key in understanding and improving the implementation [5].

4.1.1 Linear Dynamic Response

Measurements of dynamic rheometry, in the linear domain, show that it is commonly accepted that the presence of charges in a Newtonian polymer matrix has an influence on the viscoelastic modules G', G'' and therefore on the complex viscosity η^*. For low mass concentrations, many authors have observed a strong increase in viscosity at low frequency, going as far as the loss of the Newtonian plateau. In the absence of particles, one observes for the pure polymer matrices a zone of flow at low frequency resulting in evolutions of the modules according to the frequency such as $G' \propto \omega^2$

and $G'' \propto \omega$, typical of a behavior liquid. The increase in the particle rate leads to an increase in the modules and a gradual disappearance of the flow zone. The modulus G' increasing faster than G'' it is possible that the latter becomes higher. In this case we observe a transition from a behavior of the liquid to solid type. The evolution of G' as a function of frequency can become close to zero, in this case we observe an elastic plateau (Fig. 13). The appearance of this transition depends mainly on the particle rate and/or their degree of individualization [62, 63].

Ren et al. [64] attribute the liquid–solid transition to percolation or jamming. The hydrodynamic interactions that the tactoids and/or the individual sheets have with each other (Fig. 14) limit the relaxations and increase the elasticity of the system, hence the appearance of a G-shaped plateau. The percolation rate is reached here for very low clay rates unlike conventional reinforcements. This is explained by the anisotropy of the tactoids and mainly that of the sheets having large form factors [65], confirming the fact that an exfoliated nanocomposite has a lower percolation point than an interleaved nanocomposite. However, the precise determination of the percolation point is not well established. Jeon et al. [66] use the value of the slope of G' and consider the appearance of percolation when it is close to zero. In another
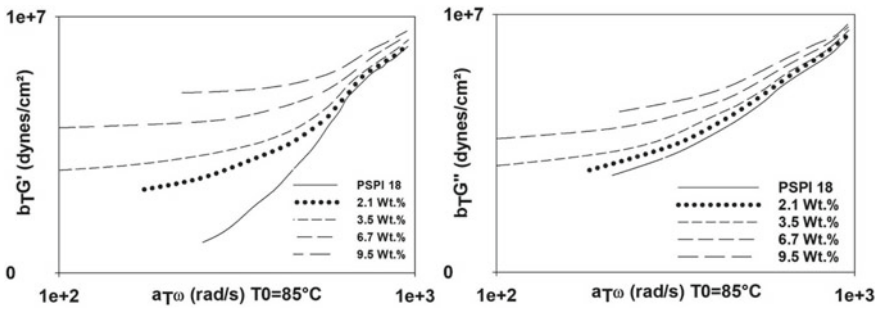

Fig. 13 Time–temperature superposition giving the evolution of modules G' and G'' as a function of the particle rate in a PS-PI matrix
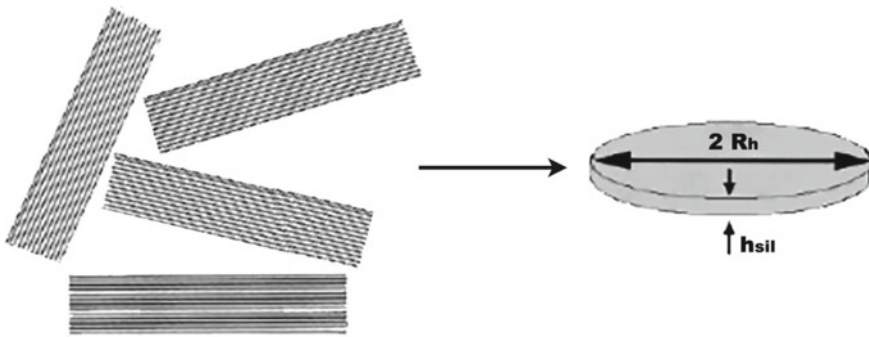

Fig. 14 Hydrodynamic interactions of particles in nanocomposites

publication [67] the same authors look at the evolution of the value of G′ at low frequency as a function of the particle fraction. In this case, the percolation fraction ϕ_p corresponds to the start of the divergence of G′.

The appearance of these changes can also be linked to a slowing down of the dynamics of the matrix chains and to the confinement of the polymer. The increase in viscosity of confined chains has been observed [68] and explained by a decrease in relaxation caused by a decrease in the space allowing movement. This idea is also supported by Lim et al. [69]. However, Galgali et al. [70] by calculating the activation energy of the chain flow in the presence of charges shows that it remains close to that of the matrix alone. Their conclusion is that the rheological behavior of nanocomposites, particularly at low frequency, is not due to the confinement of the chains.

The time–temperature superposition principle (STT) could be applied in some systems. The teams having carried out it explain that only polymer chains have relaxations sensitive to temperature and that the relaxations associated with particles or aggregates are very weak [65]. This does not exclude that there are chains which are blocked on the surface of particles [65]. Wu et al. [71] by drawing a Han diagram [72] also come to the conclusion that the relaxation of the tactoids is independent of the temperature. STT cannot however always be applied. Lee et al. [73] observed a variation of the hydrogen bonds with the temperature, these having a predominant role on the behavior of the sample and in particular on the compatibility between the matrix and the modified particles. Gefler et al. [74] observe a deviation from STT attributed to a decrease in the affinity of surfactants with particles, which has the effect of increasing gelation.

4.1.2 Non-linear Dynamic Response

The linear range is limited to smaller deformations in the presence of particles. Indeed, the appearance of a rheo-fluidizing character under shear appears for weaker deformations than for the pure matrix [65, 72, 73]. This phenomenon is attributed to an alignment of the particles [65, 72, 73]. Following alignment, a liquid type behavior under low shear of small amplitude is observed after the prolonged application of high shear (Fig. 15).

4.1.3 Stationary Flow

The steady state flow experiments made it possible to observe for the samples the presence of a higher Newtonian plateau at low gradient. For faster shearing, a shear thinning behavior appears at lower gradients in the presence of charges [5]. The shear thinning character increases with concentration and is attributed to an orientation of the particles by Hyun et al. [75]. The orientation of particles under flow has been demonstrated by X-ray diffraction measurements at small angles [63]. In some cases, a divergence in viscosity appears at low gradient for the samples above the percolation

**Fig. 15** Observation of the effect of a high amplitude shear on the modules G′ and G″: particle alignment
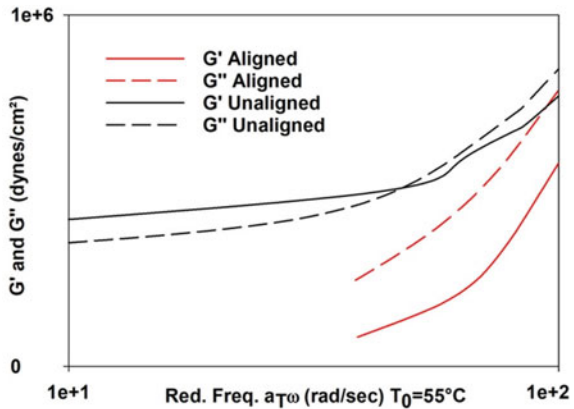
point. This divergence is associated with solid behavior with a flow threshold [6]. Applying too much stress breaks the network and allows the alignment of particles under flow. The authors having tried to apply the semi empirical law of Cox–Merz [76] (allowing to relate the dynamic viscosity to the viscosity in flow $\eta.(\omega) = \eta\,(\dot{\gamma})$ for $\omega = \dot{\gamma}$) note that this one works good for pure matrices but fails for nanocomposites and mainly for the most concentrated (above the percolation point); the decrease in flow viscosity compared to dynamic viscosity is generally explained by the alignment of the clay particles [77]. Ren et al. [77] seem to show that the alignment coming from a dynamic shear leads to a more "regular" parallel structure than that coming from a flow.

4.1.4 Transient Flow

Generally, for nanocomposites, the stress presents an overshoot in transient regime which increases with the rate in particles, the degree of exfoliation, but also the waiting time between two successive tests showing the possibility for the system to evolve with rest and in particular to restructure [73]. The overshoot is thus associated with the response of the particles and not with the viscoelastic response of the polymer. Solomon et al. [6] performed transient flow on nanocomposites based on polypropylene. By plotting the stresses $\tau(t)$ as a function of the deformation, they observed a resetting of the curves and a deformation associated with the maximum of the stress independent of the speed (Fig. 16).

This type of registration is characteristic of a sample that does not have a characteristic time scale. This result is comparable to that observed in the case of liquid crystals and non-Brownian suspensions of discs or sticks. Here, they interpret their results by explaining that it is not Brownian relaxations or orientational relaxations that are at the origin of the response of the sample; which would confirm the presence of a three-dimensional network responsible for the dynamic viscoelastic plateau. Ren et al. [64] as well as Wu et al. [71] confirm this idea. Solomon et al. [6] also studied the
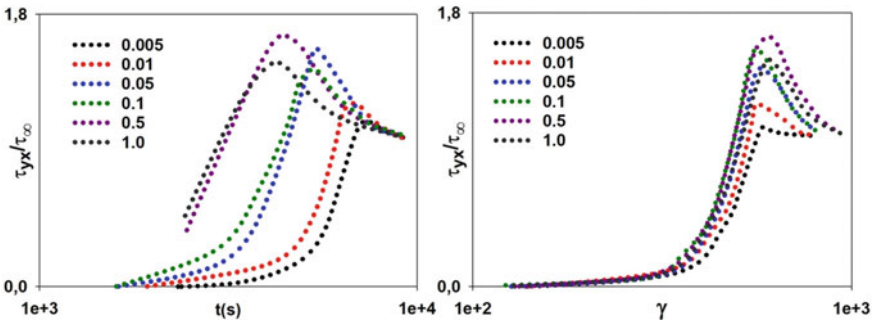
Fig. 16 Transient study of nanocomposites

behavior of samples having undergone two successive shears in opposite directions with a rest period in between. They deduce from their observations that the samples restructure thanks to the attractive interactions and not to Brownian movements which would be slower. The high sensitivity of rheology (and mainly of module G') to the state of dispersion and to structures shows that it is a powerful means of nanocomposite analysis. Zhao et al. [62] show through rheology that samples with comparable results in XRD i.e. even d_{001} measured, lead to different behaviors in rheology. Some authors use rheology to determine precise characteristics of the samples: Wagener et al. [78] relate the value of the slopes of dynamic viscosity to the degree of exfoliation of the particles. Jeon et al. [66] use rheology to calculate form factors. After having determined a volume fraction of percolation and based on the evolution of dynamic viscosities as a function of the fraction in particles, they determine an intrinsic viscosity. Applying the Douglas and Garbochi approximation then allows them to obtain their form factor.

4.2   Rheology of Hybrid Nanocomposites Based on Graphene

To manufacture materials based on graphene nanosheets with specific rheological properties, graphene may be combining with the three classes of reinforcements (nanoparticles, nanofibers and sheets) or with carbon-based materials (the most commonly used are diamond and carbon nanotube).

4.2.1   Graphene/Nanoparticles Hybrid Material

Zhan et al. [79] manufactured a new material based on the hybridization of magnetite nanoparticles and graphene nanosheets as a reinforcement of poly(arylene ether nitrile) (magnetite-GNs/PEN). The implementation was carried out firstly by the covalent deposition of magnetite nanoparticles on the surface of graphene nanosheets
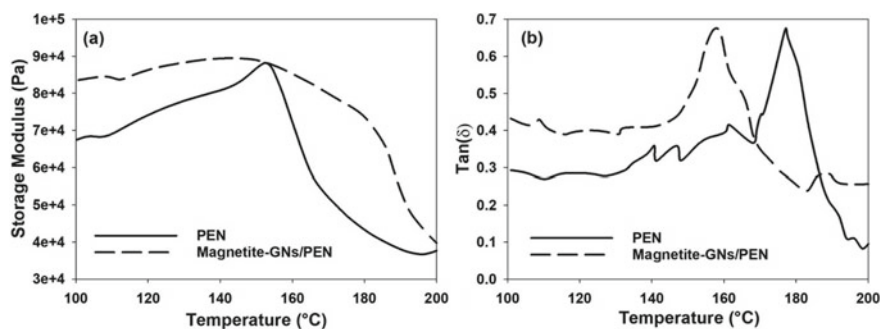
Fig. 17 Rheological properties of PEN and magnetite-GNs/PEN hybrid nanocomposite with 3 wt% of magnetite-GNs: **a** Storage modulus and **b** Tan (δ)

in the presence of iron (III) chlorides through a simple solvothermal method, thus resulting in the manufacture of magnetite-GN hybrids. Then, according to the solution casting method, the hybrid was compounded with PEN to obtain the magnetic composite (magnetite-GNs/PEN). In order to carry out dynamic rheological measurements, the rheometer (TA Instruments Rheometer AR-G2) equipped with a parallel-plate geometry (25 mm in diameter) was used. Then, the dynamic frequency sweep measurements were carried out on the samples (diameter = 25 mm and thickness = 1 mm) in a temperature range from 100 to 200 °C at the frequency of 0.1 rad/s. The results clearly show an improvement in the storage module and the loss module in the glassy state with the addition of the magnetite-GNs hybrid, compared to virgin PEN. In their investigation, Zhan et al. explained that behavior by the higher Tg of magnetite-GNs/PEN hybrid nanocomposite compared to pure PEN. Effectively, the Tg of the all materials was determined from the onset temperature of the tanδ curve in the rheological sweep (Fig. 17b), and a shift to higher temperature for the nanocomposite was observed compared to neat PEN.

4.2.2 Graphene/Nanosheet Hybrid Material

Mekhzoum et al. [80] prepare hybrid nanocomposites based on polypropylene (PP) reinforced with different amounts of clay nanosheet (MMT) and graphene (GN). The different MMT/GN ratios were mixed with PP using an internal mixer heated to 200 °C (Thermo Haake Rheomix, Germany). Then, the nanocomposites are removed from the heated chamber before being cut into small pieces for hot press molding. The viscoelastic properties of the hybrid nanocomposites were evaluated using the MCR 500 rheometer (Physica) equipped with a CTD600 oven with parallel plate geometry (25 mm in diameter). The viscosity tests were carried out at 200 °C according to a deformation of 5% and a frequency sweep between 500 and 0.5 Hz. From the Fig. 18 it was clearly observed that the complex viscosity increase with increasing GNs and MMT content until reaching the maximum (1.5:1.5). In general, the PP alone exhibits

Fig. 18 Melt rheological
properties of the
nanocomposites as a
function of MMT/GNs ratio
in terms of complex viscosity
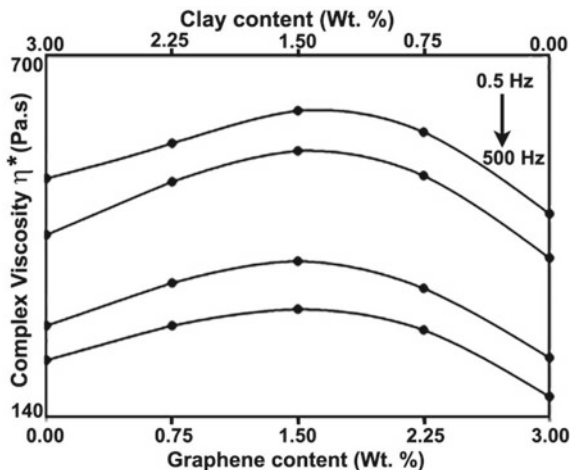
Newtonian behavior at very low frequencies and a shear thinning at high frequency.
However, it has been noted that the addition of the hybrid changes the dynamic
rheological behavior of the nanocomposites. Indeed, the addition of the hybrid to the
PP at different concentration results in the formation of an interconnected network
structure which hinders the movement of the macromolecular chains, and therefore
results in a non-terminal effect and a transition in behavior from liquid to solid at
low frequency. That said, at low frequency the polymer chains have time to relax,
but at a higher frequency, the molecules do not have enough time to relax and follow
the applied deformation.

4.2.3 Graphene/Nanofiber Hybrid Material

Sun et al. [81] investigate the combined effects of Cellulose nanofibers (CNFs) and
graphene nano-platelets on the properties of oil well cement (OWC) matrix. The
hybrid GNP/CNF mixture was prepared by adding GNP to the CNF suspension
produced by the sulfuric hydrolysis method. Then, the OWC suspension was mixed
with a water/OWC ratio of 0.38 with a vacuum mixer, before the addition of different
GNP/CNF ratio. The rheological properties of CNF/GNP-OWC composites were
carried out through a stress controlled rheometer (AR2000ex, TA Instruments Inc.,
New Castle, DE, USA) with the cone and plate geometry (Angle: 2°, Diameter:
60 mm) at three different temperatures (20, 40 and 60 °C). In order to fit the recorded
shear stress-shear rate curves, four different models were used (Bingham-Plastic
model, Herschel-Bulkley model, Vocadlo model and Vom Berg model). From the
Fig. 19 it can be clearly observed that the CNF/GNP-OWC composite present a
typical shear thinning behavior with reduced shear viscosity at higher shear rates.
To conclude, that the use of CNF and GNP lead to an increase in the flow stresses of
the CNF/GNP-OWC suspension and the flow stress values is greatly influenced by
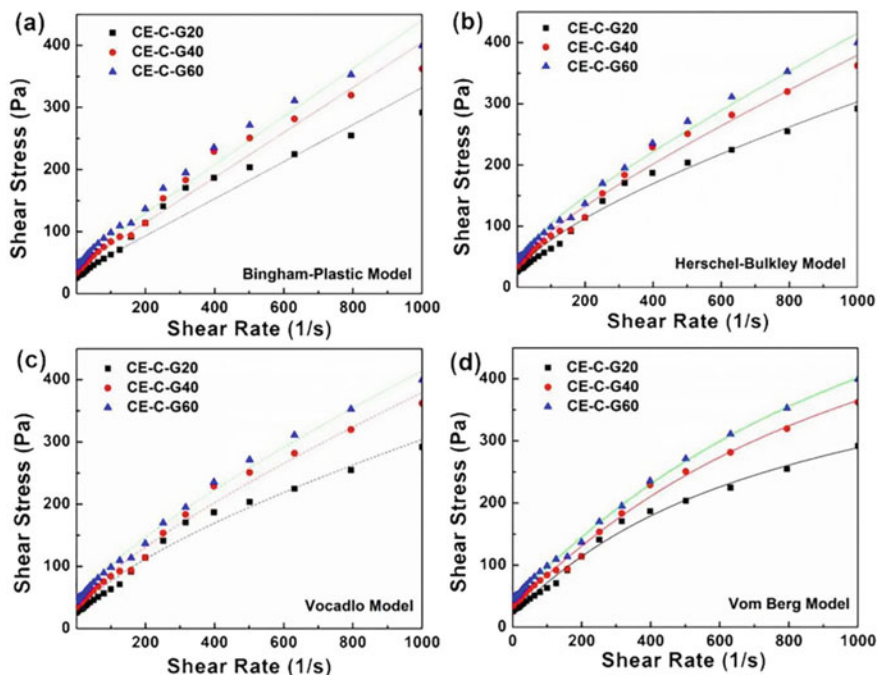
Fig. 19 Experiment data and fitted shear stress-shear rate curves of CNF/GNP-OWC slurries at different temperatures 20, 40 and 60 °C: **a** Bingham-Plastic model, **b** Herschel Bulkey model, **c** Vocadlo model, and **d** Vom Berg model

the temperature. While the comparison of the four rheological models showed that the Vom Berg model provided the best results of the shear speed-shear stress curve of CNF/GNP-OWC suspensions with a correlation factor better than 0.99.

4.2.4 Graphene Nanosheets/Nanoparticles/Nanofiber Hybrid Material

Nanda et al. [82] prepare a trihybrid hydrogel where coexist three distinctly different nanostructures such as nanofibers (based on amino acids "Py-W"), nanosheet (graphene oxide "GO") and nanoparticles (gold "AuNPs"). The trihybrid hydrogel was prepared by the gradual incorporation of graphene oxide in the native hydrogel matrix, and then by synthesizing gold nanoparticles in situ in the hydrogel matrix containing GO. Rheological studies have been performed to address the difference between the native hydrogel and hybrid hydrogels rheological properties (Oscillatory stress sweep experiments have been performed at 25 °C). From the rheological studies (Fig. 20), it can be seen that the storage modulus (G′) exceed the loss modulus (G″) in the linear viscoelastic region (LVR) for all the materials, which is an indication of the formation of a typical soft solid-like gel-phase material. While after the LVR region, the loss modulus (G″) has crossed the storage modulus and thus

Fig. 20 Rheological studies
of native hydrogel and
trihybrid hydrogel in terms
of storage and loss modulus
as a function of oscillatory
stress
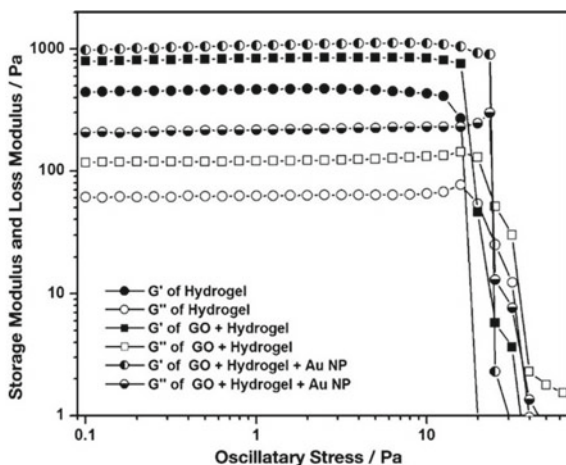
indication the transformation into solution state. To conclude, this rheological study
reveals that the addition of GO to the native gel increases the rigidity of the mixture,
but the addition of the third element (gold nanoparticles) to hybrid hydrogel further
increases the rigidity of this trihybrid system.

4.2.5 Graphene/Allotropic Carbon Hybrid Material

Graphene/Diamond

Zhang et al. [83] design an hybrid nanofiller based on nanodiamond (ND)-decorated
graphene oxide (GO) using 4,4′-methylene diphenyl diisocyanate as the coupling
agent to reinforce a rubber matrix (carboxylated styrene-butadiene rubber (XSBR))
to obtain XSBR/ND@GO nanocomposites. The targeted XSBR/ND@GO nanocom-
posites were fabricated by latex compounding method. First, XSBR latex and a
quantitative amount of pre-sonicated ND@GO aqueous suspension were mixed and
stirred, then the emulsion was immediately co-coagulated using $CaCl_2$ solution to be
dried in an oven at 60 °C for 72 h. The strain dependence of the storage modulus of the
elaborate materials was determined using a rubber processing analyzer (RPA2000)
at a frequency of 1.67 Hz, temperature of 60 °C and strain deformation from 0.7 to
300%. From Fig. 21a it was clearly noticed that all the nanocomposites presented
a dependence of distinct nonlinear rheological amplitude, commonly called Payne
effect, which gives an outline of the interfacial interaction and the nature of the
filler network in a filler-matrix system. Indeed, the XSBR and its hybrid compos-
ites present a progressive reduction in the storage module with increasing strain
deformation; nevertheless the crescent addition of the ND@GO load considerably
improves the storage module, which implies a new formation of a sophisticated
network. However, the filling network can be divided into three types, depending on
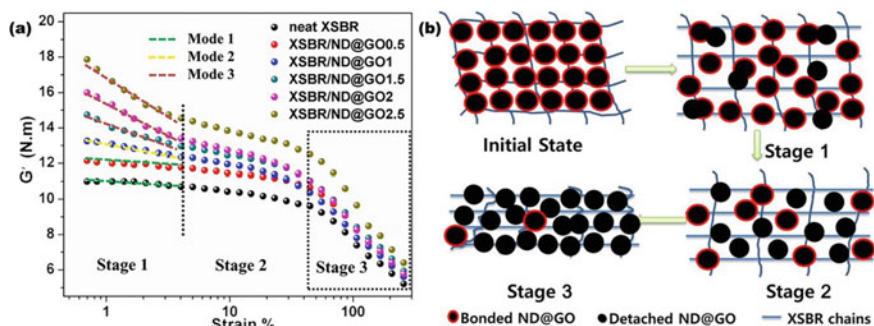
Fig. 21 **a** Rheological properties of XSBR and its hybrid nanocomposites. **b** Schematic representation of filler-rubber network variation during external force application

the filling concentration (Flexible filling networks; rigid load networks; and mixed load networks). Therefore, nanocomposites containing 0.5 phr ND @ GO belong to the flexible network, in which the particles of nanocharges are separated by the polymer chains. In this case, the initial storage module is weak and decreases slowly (Mode 1). In the case of the rigid charge network, the concentration of the charge nanoparticles increases strongly to a specifically high level and the particles come into contact or overlap, leading to a high initial storage module. Once the external forces are applied, the filling network decomposes severely at a small deformation (deformation at ~0.7%), and therefore the module decreases rapidly in stage 1. While, the network of mixed loads, the dependence on the deformation of the storage module is between those of the flexible type and of the rigid type (Fig. 21b).

Graphene/Nanotube

Arjmand et al. [84] manufactured a binary nanocomposite material based on the hybridization of Carbon Nanotube (MWCNT) and Graphene Nanoribbon (GNR) to reinforce Polyvinylidene Fluoride (PVDF) polymer. The MWCNT/GNR/PVDF nanocomposites were prepared via a melt-mixing method using an Alberta Polymer Asymmetric Minimixer (APAM) at 240 °C and 235 rpm. First, the hybrid nanofillers MWCNT/GNR were dry mixed at different concentrations, then added to PVDF matrix previously masticated. Finally, the nanocomposites were molded using the hot Carver compression molder press (Carver Inc., Wabash, IN) at 220 °C under 38 MPa pressure for 10 min to make disk samples with a 2.5 cm diameter suitable for rheological testing. Rheological measurements were performed using an Anton-Paar MCR 302 rheometer at 240 °C using 25 mm cone-plate geometry with a cone angle of 1° and a truncation of 47 μm. Figure 22 depicts the shear-stress growth ($\tau_{12}^+(t)$) normalized with respect to its steady-state value (τ_∞) as a function of time for nanocomposites with 2.7 wt% nanofiller content.
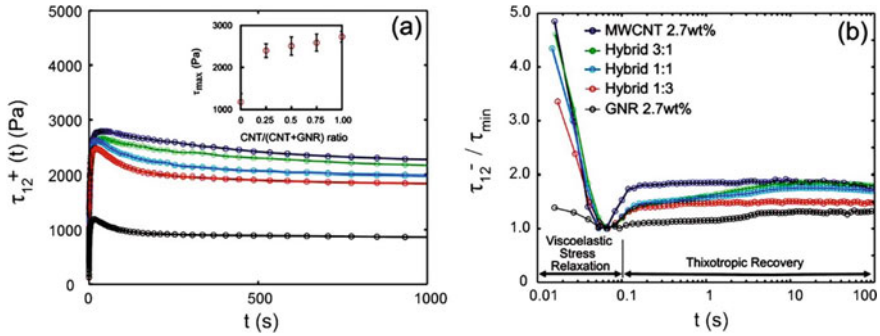
Fig. 22 a Shear-stress growth ($\tau 12 + (t)$) as a function of time for the nanocomposites. **b** Temporal variation of shear stress for the nanocomposites

For molten polymer nanocomposites, the stress overshoot refer to the transition from a solid-like to liquid-like behavior under almost resting. The corresponding breaking stress is noted τ_{max} in the inset of Fig. 22a. Figure 22b shows the temporal variation of the shear stress at the time of a progressive reduction of the shear rate from 0.1 to 10^{-4} s^{-1}. The immediate monotonic decrease corresponds to a relaxation of the viscoelastic stresses reaching a residual stress not zero (τ_{min}) at t ~ 0.06 s. After the initial reduction, at longer times, the stress response increased, reaching a new steady state value. Thus, the GNR nanofillers have a very weak capacity to efficiently recover from flow-induced anisotropy. Therefore, as the MWCNT/GNR ratio decreases, the presence of GNR deteriorates the structural stability of the MWCNT microstructure and the coherence of the movement of the nanotube domains. From Fig. 22 it can be concluded that, the hybrid samples have the ability of the MWCNT network super-structure to recover from the shear-induced anisotropy decreased significantly as the MWCNT-GNR ratio decreased. This could be attributed to a decrease in network interconnectivity and to prevent direct tube-to-tube contact due to the presence of GNR.

5 Conclusion

Hybrid materials are today the subject of immense interest, making it possible to combine the properties of hybrid reinforcement and polymer matrix. This combination can also lead to completely new properties and opens up a wider field of investigation. Due to their exceptional electronic, thermal, mechanical and rheological properties, hybrid graphene nanocomposites graphene materials have recently attracted considerable attention. This chapter presented first, the Graphene history, properties and preparation techniques, then detailed, the hybrid graphene nanocomposites synthesis methods, types and application fields. Indeed, graphene can be mixed with other types of reinforcement such as nanoparticles, nanofibers and nanosheets;

or combined with another allotropic carbon type (Diamond, Fullerene, Nanofiber, Nanotube, Polyaromatic). The main advantage of this hybridization is the materials properties improvement, but the addition of hybrids does not necessarily allow good dispersion in the polymer matrix. For this, the rheological study of graphene based hybrid nanocomposites remains an effective tool for quantifying the dispersion of the hybrid in nanocomposite systems. At the end of this chapter, the rheological properties of the graphene mixed with others nanofiller were studied, such as nanoparticles (magnetite nanoparticles), Nanosheets (clay), Nanofibers (Cellulose nanofibers) and allotropics carbon (Diamond and Nanotube). Overall, it can be said that prospects for the use of hybrid graphene nanocomposites in the future are very interesting and may bring many unexpected results.

References

1. Zhang C, Liu TX (2012) A review on hybridization modification of graphene and its polymer nanocomposites. Chin Sci Bull 57(23):3010–3021
2. Hu C, Lu T, Chen F, Zhang R (2013) A brief review of graphene–metal oxide composites synthesis and applications in photocatalysis. J Chin Adv Mater Soc 1(1):21–39
3. Dmitriev AS (2019) Hybrid graphene nanocomposites: thermal interface materials and functional energy materials. Graph Prod Appl [Working Title], 1–23
4. Jawaid M, el Kacem Qaiss A, Bouhfid R (2016) Nanoclay reinforced polymer composites: natural fibre/nanoclay hybrid composites. Eng Mater (July), 301
5. Ouarhim W, Semlali Aouragh Hassani F-Z, el Kacem Qaiss A, Bouhfid R (2019) Rheology of polymer nanocomposites. In: Rheology of polymer blends and nanocomposites theory, modelling and applications, pp 73–96
6. Solomon MJ, Almusallam AS, Seefeldt KF, Somwangthanaroj A, Varadan P (2001) Rheology of polypropylene/clay hybrid materials. Macromolecules 34(6):1864–1872
7. Semlali Aouragh Hassani F-Z, Ouarhim W, Zari N, Bouhfid R, el Kacem Qaiss A (2019) Natural fiber-based biocomposites. In: Biodegradable composites materials, manufacturing and engineering, pp 49–79
8. Semlali Aouragh Hassani F-Z et al (2019) Injection molding of short coir fiber polypropylene biocomposites: prediction of the mold filling phase. Polym Compos 40(10):4042–4055
9. Semlali Aouragh Hassani F-Z et al (2019) Mechanical properties prediction of polypropylene/short coir fibers composites using a self-consistent approach. Polym Compos 40(5):1919–1929
10. Berthelot J (1999) Matériaux composites, comportement et analyse des structures. Edition TEC & DOC, Cachan
11. Liste des termes, expressions et définitions adoptés et publiés au Journal officiel de la République française, vocabulaire des polymères, J.O., 01 mars 2002. Lexique de la recherche clinique et de la médecine factuelle
12. Coll MW et al (2015) Les nanotechnologies. Edition Dunod, Paris (2003)
13. Semlali Aouragh Hassani F-Z et al (2019) N-silylated benzothiazolium dye as a coupling agent for polylactic acid/date palm fiber bio-composites. J Polym Environ 0123456789
14. Semlali Aouragh Hassani F-Z, El Bourakadi K, Merghoub N, el Kacem Qaiss A, Bouhfid R (2020) Effect of chitosan/modified montmorillonite coating on the antibacterial and mechanical properties of date palm fiber trays. Int J Biol Macromol 148:316–323
15. Jenkins EW (1973) The polymorphism of elements and compounds. Methuen, London
16. Heilig ML (1994) United States patent office. ACM SIGGRAPH Comput Graph 28(2):131–134

17. Grigorieva IV, Firsov AA, Novoselov KS, Geim AK, Morozov SV, Jiang D, Zhang Y, Dubonos SV (2004) Electric field effect in atomically thin carbon films. Science 306(5696):666–669

18. Kroto RE, Heath HW, O'Brien JR, Curl SC, Smalley RF (1985) C_{60} buckminsterfullerene. Nature 318(6042):162–163

19. Iijima S (1991) Helical microtubules of graphitic carbon. Nature 354(6348):56–58

20. Moissan H (1894) Nouvelles expériences sur la reproduction du diamant. C R Acad Sci 118:320–326

21. Wakabayashi M, Fujita K, Ajiki M, Sigrist H (1999) Electronic and magnetic properties of nanographite ribbons. Phys Rev B Condens Matter Mater Phys 59(12):8271–8282

22. Iijima F, Yudasaka S, Yamada M, Bandow R, Suenaga S, Kokai K, Takahashi K (1999) Nano-aggregates of single-walled graphitic carbon nano-horns. Chem Phys Lett 309(3–4):165–170

23. Naess SN, Elgsaeter A, Helgesen G, Knudsen KD (2009) Carbon nanocones: wall structure and morphology. Sci Technol Adv Mater 10(6):1–6

24. Morgan P (2005) Carbon fibers and their composites. Taylor & Francis Group, CRC Press, USA

25. Wallace PR (1947) The band theory of graphite. Phys Rev 71(9):452–457

26. Landau LD, Lifshitz EM (1967) Theory of elasticity, vol 7. Ouvrage, Editions MIR, Moscou

27. Schedin F et al (2007) Detection of individual gas molecules adsorbed on graphene. Nat Mater 6(9):652–655

28. Reddy CD, Rajendran S, Liew KM (2006) Equilibrium configuration and continuum elastic properties of finite sized graphene. Nanotechnology 17(3):864–870

29. Lee C, Wei X, Kysar JW, Hone J (2008) Measurement of the elastic properties and intrinsic strength of monolayer grapheme. Science (80-) 321(5887):385–388

30. Balandin AA et al (2008) Superior thermal conductivity of single-layer graphene. Nano Lett 8(3):902–907

31. Bolotin KI et al (2008) Ultrahigh electron mobility in suspended graphene. Solid State Commun 146(9–10):351–355

32. Chang CW, Liao YC (2016) Accelerated sedimentation velocity assessment for nanowires stabilized in a non-Newtonian fluid. Langmuir 32(51):13620–13626

33. Kulkarni HB, Tambe P, Joshi GM (2018) Influence of covalent and non-covalent modification of graphene on the mechanical, thermal and electrical properties of epoxy/graphene nanocomposites: a review. Compos Interfaces 25(5–7):381–414

34. Patil U et al (2015) Nanostructured pseudocapacitive materials decorated 3D graphene foam electrodes for next generation supercapacitors. Nanoscale 7(16):6999–7021

35. Liu N, Luo F, Wu H, Liu Y, Zhang C, Chen J (2008) One-step ionic-liquid-assisted electrochemical synthesis of ionic-liquid-functionalized graphene sheets directly from graphite. Adv Funct Mater 18(10):1518–1525

36. Bourlinos AB, Georgakilas V, Zboril R, Sterioti TA, Stubos AK (2009) Liquid-phase exfoliation of graphite towards solubilized graphenes. Small 5(16):1841–1845

37. Hernandez Y et al (2008) High-yield production of graphene by liquid-phase exfoliation of graphite. Nat Nanotechnol 3(9):563–568

38. Behabtu N et al (2010) Spontaneous high-concentration dispersions and liquid crystals of graphene. Nat Nanotechnol 5(6):406–411

39. Sanchez C, Ribot F, Rozes L, Alonso B (2000) Design of hybrid organic-inorganic nanocomposites synthesized via sol–gel chemistry. Mol Cryst Liq Cryst Sci Technol Sect A Mol Cryst Liq Cryst 354(Dec 2013):143–158

40. Shipway AN, Katz E, Willner I (2000) Nanoparticle arrays on surfaces for electronic, optical, and sensor applications. Angew Chem (Int Ed Engl) 39(Suppl 15):19–52

41. Daniel MC, Astruc D (2004) Gold nanoparticles: assembly, supramolecular chemistry, quantum-size-related properties, and applications toward biology, catalysis, and nanotechnology. Chem Rev 104(1):293–346

42. Dizhbite T et al (2007) Elaboration and characterization of organic/inorganic hybrid nanoporous material incorporating Keggin-type Mo–Si polyanions. J Phys Conf Ser 93(1):012011

43. Vaia RA, Emmanuel P (2001) Polymer nanocomposites: status and opportunities. MRS Bull 26(5):394–401
44. Schöllhorn R (1996) Intercalation systems as nanostructured functional materials. Chem Mater 8(8):1747–1757
45. Vaia RA, Giannelis EP (1997) Lattice model of polymer melt intercalation in organically-modified layered silicates. Macromolecules 30(25):7990–7999
46. Komori Y, Sugahara Y, Kuroda K (1998) A kaolinite-NMF-methanol intercalation compound as a versatile intermediate for further intercalation reaction of kaolinite. J Mater Res 13(4):930–934
47. Alexandre M, Dubois P (2000) Polymer-layered silicate nanocomposites: preparation, properties and uses of a new class of materials. Mater Sci Eng R Rep 28(1):1–63
48. Carrado KA, Xu L (1998) In situ synthesis of polymer–clay nanocomposites from silicate gels. Chem Mater 10(5):1440–1445
49. Aranda P, Ruiz-Hitzky E (1999) Poly(ethylene oxide)/NH$_4$$^+$-smectite nanocomposites. Appl Clay Sci 15(1–2):119–135
50. Kikuta K, Ohta K, Takagi K (2002) Synthesis of transparent magadiite-silica hybrid monoliths. Chem Mater 14(7):3123–3127
51. Leu CM, Wu ZW, Wei KH (2002) Synthesis and properties of covalently bonded layered silicates/polyimide (BTDA-ODA) nanocomposites. Chem Mater 14(7):3016–3021
52. Mukkanti K, Subba Rao YV, Choudary BM (1989) Selective and sequential reduction of nitroaromatics by montmorillonitesilylaminepalladium(II) complex. Tetrahedron Lett. 30(2):251–252
53. Caillère S, Hénin S, Rautureau M (1982) Minéralogie des argiles, tome 1: structure et propriétés physico-chimiques, 2nd edn. Masson
54. Caillère S, Hénin S, Rautureau M (1982) Minéralogie des argile, tome 2: classification et nomenclature, 2nd edn. Masson
55. Nasibulin AG et al (2007) A novel hybrid carbon material. Nat Nanotechnol 2(3):156–161
56. Parker CB, Raut AS, Brown B, Stoner BR, Glass JT (2012) Three-dimensional arrays of graphenated carbon nanotubes. J Mater Res 27(7):1046–1053
57. JT Group (2012) James' bond: a graphene/nanotube hybrid. Physorg, 27–29
58. Lan G et al (2019) Defective graphene@diamond hybrid nanocarbon material as an effective and stable metal-free catalyst for acetylene hydrochlorination. Chem Commun 55(10):1430–1433
59. Zhang W, Zhu S, Luque R, Han S, Hu L, Xu G (2016) Recent development of carbon electrode materials and their bioanalytical and environmental applications. Chem Soc Rev 45(3):715–752
60. Krueger A (2008) Diamond nanoparticles: jewels for chemistry and physics. Adv Mater 20(12):2445–2449
61. Wang Y, Li Z, Wang J, Li J, Lin Y (2011) Graphene and graphene oxide: Biofunctionalization and applications in biotechnology. Trends Biotechnol 29(5):205–212
62. Zhao J, Morgan AB, Harris JD (2005) Rheological characterization of polystyrene–clay nanocomposites to compare the degree of exfoliation and dispersion. Polym (Guildf) 46(20):8641–8660
63. Koo CM, Kim MJ, Choi MH, Kim SO, Chung IJ (2003) Mechanical and rheologaical properties of the maleated PP-layaerd silicate nanocomposites with different morphology. J Appl Polym Sci 88:1526–1535
64. Ren J, Casanueva BF, Mitchell CA, Krishnamoorti R (2003) Disorientation kinetics of aligned polymer layered silicate nanocomposites. Macromolecules 36(11):4188–4194
65. Ren J, Silva AS, Krishnamoorti R (2000) Linear viscoelasticity of disordered polystyrene-polyisoprene block copolymer based layered-silicate nanocomposites. Macromolecules 33(10):3739–3746
66. Jeon HS, Rameshwaram JK, Kim G, Weinkauf DH (2003) Characterization of polyisoprene—clay nanocomposites prepared by solution blending. Polym (Guildf) 44(19):5749–5758
67. Jeon HS, Rameshwaram JK, Kim G (2004) Structure-property relationships in exfoliated polyisoprene/clay nanocomposites. J Polym Sci Part B Polym Phys 42:1000–1009

68. Luengo G, Schmitt FJ, Hill R, Israelachvili J (1997) Thin film rheology and tribology of confined polymer melts: contrasts with bulk properties. Macromolecules 30(8):2482–2494
69. Lim YT, Park OO (2000) Rheological evidence for the microstructure of intercalated polymer/layered silicate nanocomposites. Macromol Rapid Commun 21(5):231–235
70. Galgali G, Ramesh C, Lele A (2001) A rheological study on the kinetics of hybrid formation in polypropylene nanocomposites. Macromolecules 34(4):852–858
71. Wu D, Zhou C, Hong Z, Mao D, Bian Z (2005) Study on rheological behaviour of poly(butylene terephthalate)/ montmorillonite nanocomposites. Eur Polym J 41(9):2199–2207
72. Dae Han C, Kim JK (1993) On the use of time-temperature superposition in multicomponent/multiphase polymer systems. Polym (Guildf) 34(12):2533–2539
73. Lee KM, Han CD (2003) Rheology of organoclay nanocomposites: effects of polymer matrix/organoclay compatibility and the gallery distance of organoclay. Macromolecules 36(19):7165–7178
74. Gelfer MY et al (2005) Relationships between structure and rheology in model nanocomposites of ethylene-vinyl-based copolymers and organoclays. Macromolecules 38(9):3765–3775
75. Hyun YH, Lim ST, Choi HJ, John MS (2001) Rheology of poly(ethylene oxide)/organoclay nanocomposites. Macromolecules 34(23):8084–8093
76. Cox WP, Merz EH (1958) Correlation of dynamic and steady flow viscosities. J Polym Sci 28(118):619–622
77. Ren J, Krishnamoorti R (2003) Nonlinear viscoelastic properties of layered-silicate-based intercalated nanocomposites. Macromolecules 36(12):4443–4451
78. Wagener R, Reisinger TJG (2003) A rheological method to compare the degree of exfoliation of nanocomposites. Polym (Guildf) 44(24):7513–7518
79. Zhan Y, Meng F, Yang X, Liu X (2011) Magnetite-graphene nanosheets (GNs)/poly(arylene ether nitrile) (PEN): fabrication and characterization of a multifunctional nanocomposite film. Colloid Surf A Physicochem Eng Asp 390(1–3):112–119
80. Mekhzoum MEM, Essabir H, Rodrigue D, el Kacem Qaiss A (2016) Graphene/montmorillonite hybrid nanocomposites based on polypropylene: morphological, mechanical, and rheological properties. Polym Compos 39(6):1–8
81. Sun X, Wu Q, Zhang J, Qing Y, Wu Y, Lee S (2017) Rheology, curing temperature and mechanical performance of oil well cement: combined effect of cellulose nanofibers and graphene nano-platelets. Mater Des 114:92–101
82. Nanda J, Biswas A, Adhikari B, Banerjee A (2013) A gel-based trihybrid system containing nanofibers, nanosheets, and nanoparticles: modulation of the rheological property and catalysis. Angew Chem Int Ed 52(19):5041–5045
83. Zhang Y, Park SJ (2018) Influence of the nanoscaled hybrid based on nanodiamond@graphene oxide architecture on the rheological and thermo-physical performances of carboxylated-polymeric composites. Compos Part A Appl Sci Manuf 112:356–364
84. Arjmand M, Sadeghi S, Khajehpour M, Sundararaj U (2017) Carbon nanotube/graphene nanoribbon/polyvinylidene fluoride hybrid nanocomposites: rheological and dielectric properties. J Phys Chem C 121(1):169–181

Graphene Based Aluminum Matrix Hybrid Nano Composites

Subrata Mondal

Abstract There is a growing demand for the light weight nano composite materials for advanced material applications, such as aerospace, automobile, electrical appliances, biomedical etc. because of their high specific strength/stiffness, improved temperature stability, improved wear and corrosion resistance etc. Properties of aluminum matrix can be significantly improved with well dispersed/distributed low concentration of nano reinforcements. Various types of carbon based nano reinforcements such as carbon nanotube, graphene, carbon nanofibers, fullerenes etc. are widely used for the fabrication of advanced metal matrix nano composites materials. This chapter discusses graphene based aluminum matrix hybrid nano composites for the applications in advanced material fields. Starting with the graphene as a prospective nano reinforcement for the hybrid nano composites, various common methods for the manufacturing of hybrid nano composites, mechanism of reinforcement dispersion/distribution in the hybrid nano composites are discussed. This followed by microstructure and properties of hybrid nano composites are included. The chapter has been concluded with few prospective applications of graphene based aluminum matrix hybrid nano composites in advanced materials fields.

Keywords Nanocomposites · Nano-reinforcements · Aluminum matrix · Hybrid nanocomposites · Graphene · Specific strength · Tribological property · Interfacial interaction

1 Introduction

There is a growing research interest on materials with superior properties and due to this, material scientists are developing novel materials with improved properties [1–5]. For various industrial applications, there is a genuine need for light weight and high performance materials. Now a days, composite materials are used widely

S. Mondal (✉)
Mechanical Engineering Department, National Institute of Technical Teachers' Training and Research (NITTTR) Kolkata, FC Block, Sector III, Salt Lake City, West Bengal 700106, India
e-mail: subratamondal@yahoo.com

in various areas, because of their light weight, high strength to weight ratio, high modulus and other tailorable functional properties. Composites materials can be engineered from at least two different materials with marked differences in physical or chemical properties which remained bonded together, while, retain their microscopic identity. Major phase in composite material is known as matrix phase, while, minor phase is termed as reinforcement phase. In the nature, we have several composite materials which served as a bench mark to the material scientists for the fabrication of advanced engineered composite materials. Two such natural composite materials are wood and bone. Wood is a natural composite composed with cellulosic fibrils as reinforced phase and lignin as the matrix phase, while, bone is composed of hydroxyapatite as reinforcement phase and collagen protein as matrix phase. Depending on the type of matrix phase, artificially manufactured composite materials can be classified as metal matrix composite, ceramic matrix composite, and polymer matrix composite. Reinforcement phase in the composite materials can be of various organic or inorganic particles, fibers, or ultra-high strength whiskers [6–9].

Metal matrix composites (MMC) contain at least two constituent phases with one being a metal which is known as matrix phase [10, 11]. Generally, reinforcement phase in the metal or metallic alloy matrix composites are ceramic or other inorganic compounds or various carbon based reinforcement materials [12–14]. Common reinforcement phase for the fabrication of MMC are silicon carbide, alumina, boron carbide, graphite, carbon nanotube, graphene etc. [15–17]. Metal matrix nano composites has given much importance as compared to the micro particle reinforced metal matrix composites, due to their superior properties with low concentration of reinforcement phase. In metal matrix nano composites, metal or alloy is the matrix phase, while, reinforcement particles has at least one dimension is equal to or less than 100 nm [18]. Properties of metal matrix nano composites depends on type, concentration, shape, size and dispersion/distribution of nano particles in matrix phase.

Aluminum or its alloys are attracted much attention as matrix phase for the manufacturing of metal matrix composites or nanocomposites because of its several advantages viz. light weight, ductility, cost effectiveness etc. [19–21] Aluminum matrix composites or nano composites are potential materials for applications in various fields because of their improved specific strength, modulus and stiffness. Some of the potential applications of aluminum matrix based composites or nano composites are in the fields of aerospace, aircraft, automobile, defense, electrical appliance, biomedical etc. [22–24]. These composites have been manufactured by number of techniques. Some of the common manufacturing methods for the preparation of metal matrix composites or nano composites are powder metallurgy, casting, spray deposition etc. Among these techniques, powder metallurgy method produced consistently better properties of composites or nano composite materials [25].

Hybrid metal matrix composite materials are new advanced composite materials as compared with the conventional MMC [26]. This type of metal matrix nano composites can have more than one reinforcement phases among these at least one as nano reinforcement phase. Two or more reinforcement particles in a single metal

or alloy matrix can produce better mechanical properties than their individual counterpart in the metal matrix composite. Further, secondary reinforcement phase in the metal matrix can improve other functional properties together with enhancement of mechanical properties of the nano composite materials [27]. Different nano reinforcements have different shape, size and properties, therefore, hybridization of nano composites can provide improved mechanical properties and other functional properties with reduced weight and cost. In this chapter, an overview on graphene based hybrid aluminum matrix nano composite are presented. Various common methods for the fabrication of nano composites, mechanism of dispersion or distribution of nano reinforcements in the hybrid nano composites, microstructure and properties of nano composites, and few of the prospective applications of aluminum matrix graphene hybrid nano composites are discussed.

2   Potential Reinforcing Materials in Composites

Dispersed phase in the composite materials is known as reinforcement phase [28]. Reinforcement phase in the resultant composite enhances mechanical and other functional properties which depends on the type and concentration of reinforcement phase [29–32]. Composite material properties can be altered by selecting appropriate type of reinforcement phase and by varying proportion of reinforcement phase. Further, mechanical properties of composites materials depends on size and shape of the reinforcement phases. Size of the reinforcement phase could be macro, micro and nano size, while, shape of reinforcement phase could be cylindrical, tubular, spherical, plate type etc. with regular or irregular geometry [33–37]. Few common shape of reinforcing materials with specific examples which are commonly used for the fabrication of composites or nano composites materials are enlisted in Table 1. Together with type, shape and concentration of reinforcement phase, good dispersion and distribution of reinforcing particles is also very important to improve properties of resultant composites materials [38]. Depending on type of dispersion and distribution of reinforcement materials in the metal matrix, four types of situation can be arises viz. good dispersion and good distribution, good dispersion and poor distribution, poor dispersion and good distribution, and finally, poor dispersion and poor distribution. Figure 1 shows schematically the two situations viz. good dispersion and good distribution, and good distribution and poor dispersion of reinforcement phase in the

Table 1 Few common shapes of reinforcement phases for the manufacturing of composite/nano composite materials

| Shape of reinforcement phase	Typical example
Cylindrical	Carbon fiber
Tubular	Carbon nanotube
Particulate (e.g. spherical)	Alumina particle, fullerenes
Plate like	Clay, graphene
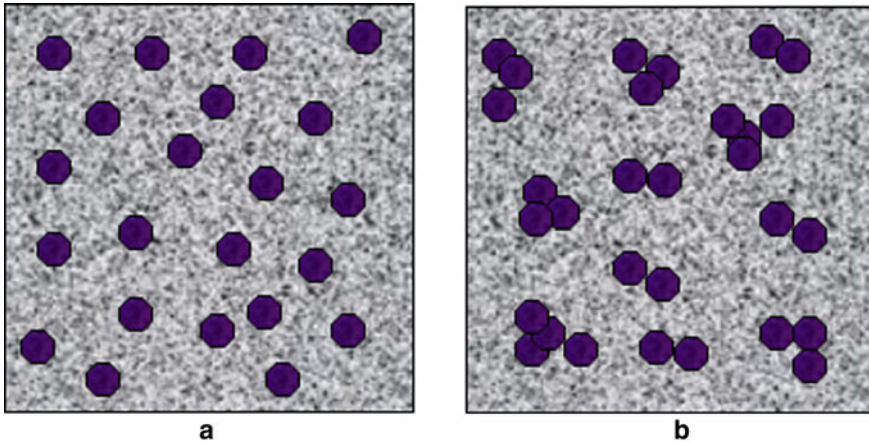
Fig. 1 Schematic showing good dispersion and good distribution **a**, and poor dispersion and good distribution **b** of reinforcement phases in the matrix phase of resultant composite material

matrix phase of resultant composite material. Interfacial bonding between reinforcement phase and matrix phase is another important parameter for the enhancement of mechanical properties of resultant composite materials [39].

3 Metal Matrix Composites and Nano Composites

Composite materials are artificially manufactured by using at least two different materials that are bonded together by physical and/or chemical means while maintaining their microscopic identity, and make the resultant composite material superior to the properties as compared with their individual component materials. Therefore, composites materials are artificially manufactured multiphasic materials [40, 41]. In the composite materials, different phases can be identified microscopically while they are bonded together by physical and/or chemical means. Major phase in the composite material is known as matrix phase while minor phase is termed as reinforcement phase. The major role of matrix phase is to hold the reinforcement phase in the resultant composites, allow the fabrication into desired shape and helps for load transfer from relatively weak matrix phase to reinforcement phase and vice versa during the loading process. Properties of composite material depends on matrix phase and reinforcement phase. As per the selection of matrix type, composite materials can be classified as polymer matrix composite, ceramic matrix composite and metal matrix composite [42–45]. While, depending on size of reinforcement phase composites can be termed as micro composite and nano composites. In case of micro composites, size of the reinforcement phase in the micrometer range, whereas, in case of nano composites, at least one dimension of the reinforcement phase is less than or equal to 100 nm. Few of the common metal used as matrix phase for

the fabrication of metal matrix composites are magnesium, aluminum, titanium, copper and their alloy [11, 20, 46–48]. Whereas, some of the common reinforcement phases used for the manufacturing of metal matrix composites are silicon carbide, aluminum oxide, boron carbide, titanium dioxide, carbon nanotube, graphene, carbon nanofibers etc. [49–54]. Due to the demand of high specific strength and high toughness metal based materials, metal matrix based composites/nano composites are preferred as compared with the monolithic metal. Characteristics of metal matrix composites materials are determined by their microstructure, dispersion/distribution of reinforcement phase and interfacial interaction between dissimilar reinforcement phase and matrix phase. Microstructure includes microstructure of both reinforcement phase and matrix phase. Pure aluminum and alloyed aluminum is one of the most investigated matrix materials for the fabrication of metal matrix composites or nano composites due to their several interesting properties such as low density, very good ductility, low cost etc. Aluminum matrix composites are light weight high performance composite materials which can be reinforced with wide variety of reinforcement materials viz. continuous (Fig. 2)/discontinuous fibers, whiskers or particulates [23, 55, 56]. Properties of aluminum matrix composites can be tailored
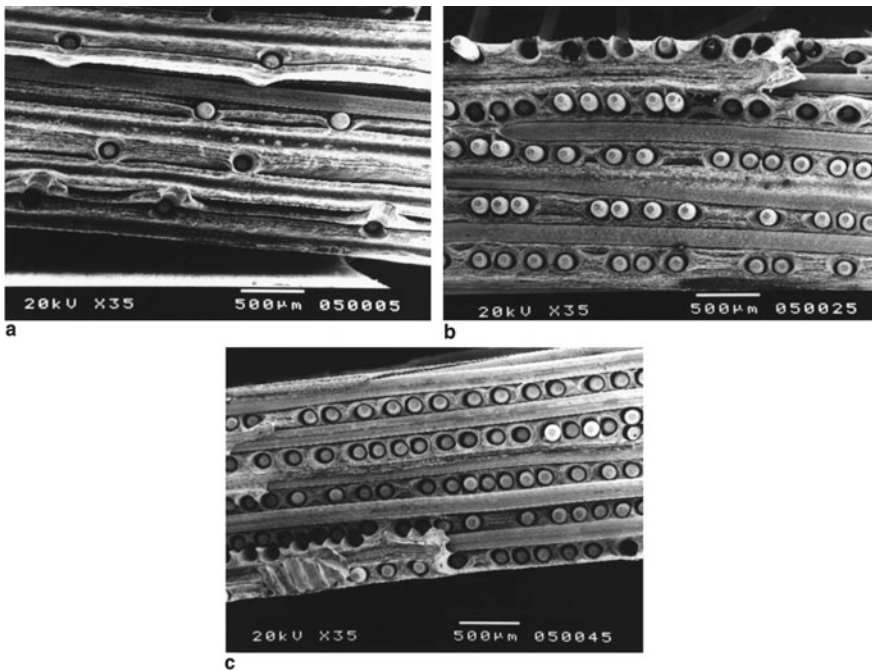
Fig. 2 Scanning electron microscopic fractographies of 0°/90° dual directional molybdenum fiber reinforced aluminum composites with different concentration of molybdenum fibers such as 5 vol% (**a**), 25 vol% (**b**), and 45 vol% (**c**). Reproduced with permission from Ref. [59] © 2005 Elsevier Ltd.

by selecting appropriate proportion of matrix phase, reinforcement type and concentration, and processing routes. Depending on the selection of matrix phase, reinforcement phase and processing routes, the advantages of aluminum matrix composites as compared to the pure aluminum metal are as follows [57, 58]:

- Improved specific strength
- Improved stiffness
- Reduced density depending on the type of reinforcement phase
- Improved wear resistance
- Improved damping capability
- Improved thermal property
- Tailored electrical performance etc.

These advantages offers aluminum matrix composites as an excellent candidate for many structural and functional applications, which include electrical appliances, aerospace, defense, automotive, sports etc. [57].

4 Overview of Graphene

Graphene based nanomaterials are novel nanomaterial which attracted much attention in the last decade due to their interesting physical, chemical, thermal and electrical properties [60–63]. These nanomaterials can be potentially used in various areas such as electronic, sensor, energy, potential nano reinforcement for the fabrication of nano composite, biomedical fields e.g. biomedicine, diseases detection therapy etc. [64–66]. Graphene nanomaterials can be classified based on number of single atomic sheet of hexagonal carbon layer, oxygen content and their chemical composition. Broad family of graphene nanomaterials include graphene, graphene oxide, reduced graphene oxide and functionalized graphene [64]. Graphene is an allotrope of carbon and a single atomic sheet of hexagonal carbon structure [65, 66]. Due to its several excellent properties viz. nano size, extra ordinary mechanical, electrical and thermal properties, graphene has been widely used as potential reinforcement phase for the manufacturing of polymer matrix, metal matrix and ceramic matrix nano composites. Due to its nano dimension and low density, graphene required very low concentration to achieve desirable properties. Graphene nano sheet consists of a single atomic layer of sp^2 hybridized carbon atoms, and it can be manufactured by top down and bottom up approach. Graphene nanomaterial can be prepared by mechanical or chemical exfoliation of graphite, chemical vapor deposition technique etc. Exfoliation from graphite to produce graphene is a promising method because of low cost and potential for high scalability [60]. Graphene has several interesting properties which include high specific surface area, excellent thermal conductivity, high intrinsic mobility, and it is hydrophobic in nature due to the absence of oxygen groups [64]. Heat energy is applied in the carbon source to produce fragments of carbon which recombine to form densely packed honeycomb lattice of one-atom thickness graphene [65, 67].

5 Aluminum Matrix Nano Composites

Aluminum or its alloy has been extensively used as matrix phase for the manufacturing of metal matrix composite or nano composites, due to its several excellent properties such as low density, good ductility, cost effectiveness etc. There is a growing research interest on aluminum matrix nano composites, due to the superior mechanical properties of the resultant composite materials such as specific stiffness, modulus, wear resistance and fatigue properties [68]. In the aluminum matrix nano composite, aluminum is a matrix phase with reinforcement phase could be generally ceramic or other inorganic materials. Some of the most widely used reinforcement phase for the aluminum matrix nano composites are SiC nanoparticles, alumina nanoparticles, TiO_2 nanoparticles, carbon nanotube, carbon nanofiber, graphene etc. Nassar and Nassar reported aluminum matrix nano composites reinforced with nano sized TiO_2 particles manufactured by using powder metallurgy technology. Their experimental results revealed that tensile strength and hardness of nano composite increased while ductility decreases with increasing volume fraction of nanoparticles. However, nano composite shows superior wear property. Changes of these properties with reinforcement concentration is possibly due to the hindered movement of matrix dislocation by nanoparticles in resultant nano composite materials which leads to the increased hardness and strength, while, decreased ductility [68]. Maleki et al. reported aluminum matrix based nano composites with magnetic nickel ferrite ($NiFe_2O_4$) nanoparticles as reinforcement material produced by powder metallurgy method. Experimental results revealed that yield stress and ultimate tensile strength have been increased with increasing concentration of nano reinforcement up to 5 wt%, however, dropped with 10 wt% of nano reinforcement. Relative density and elongation of the nano composites deceased as the weight percentage of nano reinforcement increased [69]. Major challenges for the manufacturing of metal matrix nano composites are agglomeration, inhomogeneous dispersion of nano reinforcement materials, and poor interfacial interaction between dissimilar reinforcement phase and matrix phase. Figure 3 shows surface morphology of Al matrix nano composites with different concentration of nano reinforcements [69].

6 Aluminum/alloy Matrix Graphene Reinforced Hybrid Nano Composites

Recently, there is a significant research interest on hybrid nano composite for advanced material applications. Hybrid nano composite consists of a matrix phase and more than one reinforcement materials among these at least one reinforcement material is nanomaterial. Incorporation of more than one reinforcement materials can offered better enhancement of properties of the matrix phase as compared with single reinforcement phase [70]. Aluminum matrix hybrid nano composites can be
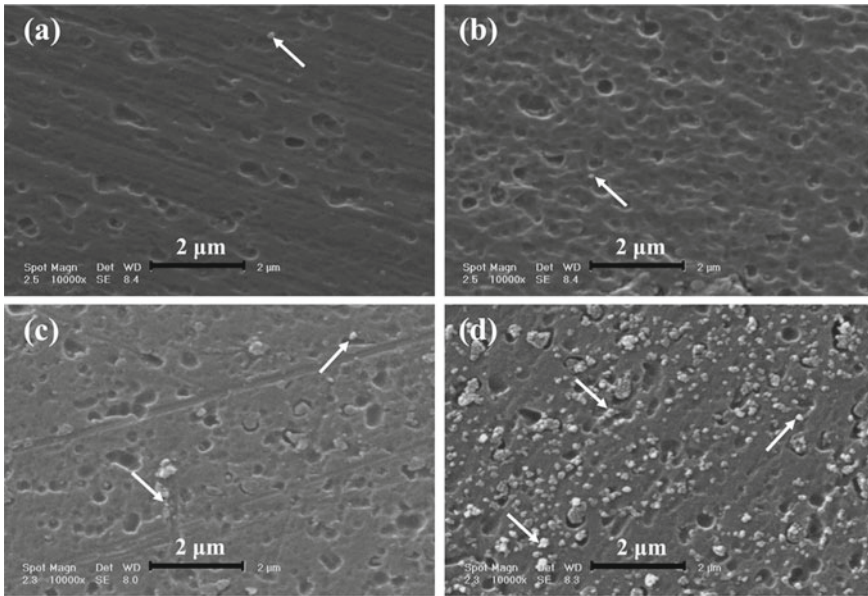
Fig. 3 Scanning electron microscopic (SEM) of extruded Al-NiFe$_2$O$_4$ nano composites with different concentrations of nano reinforcements: **a** 1 wt%, **b** 2.5 wt%, **c** 5 wt%, and **d** 10 wt% reinforcements phase. Arrows indicates the dispersion of NiFe$_2$O$_4$ nanoparticles in the Al matrix. Reproduced with permission from Ref. [69] © 2018 Elsevier Ltd. and and Techna Group S.r.l.

considered as a novel materials due its higher specific strength, light weight, corrosion resistance, and other improved functional properties which depends on the type of selected nano reinforcement phases. Various hybrid combinations of nano reinforcement phases based on graphene can be considered as prospective candidates of nano reinforcement phases for the fabrication of hybrid nano composites. Graphene together with other nanoparticles such metal oxide nanoparticles (viz. TiO$_2$, SiO$_2$, SnO$_2$, Fe$_3$O$_4$) or other type of carbon based nano reinforcements can be used for the manufacturing of graphene based hybrid nano composites [71]. Graphene can be used as prospective reinforcement for the manufacturing of aluminum matrix hybrid nano composite due it's interesting properties. Graphene is a 2D carbon based nanomaterial with interesting electrical properties, light weight, high surface area and impressive mechanical properties [72]. Properties of aluminum matrix based graphene reinforced hybrid nano composites depends on selection of other nano reinforcement phase, concentration of nano reinforcement phase, processing routes, processing parameters and microstructural evolution during the manufacturing of aluminum matrix hybrid nano composites. Powder metallurgy technique can be selected for the preparation of aluminum matrix hybrid nano composites due its simple steps of mixing, compaction and sintering [73].

Jauhari et al. discussed aluminum alloy 6061 matrix graphene and SiC reinforced hybrid nano composite fabricated by using powder metallurgy method. They have

selected aluminum alloy 6061 as matrix phase due its low density, structural rigidity, and its feasibility to incorporate wide range of nano particles and subsequent improvement of mechanical properties. Nano reinforcement phase graphene has flake size of 10 nm and SiC has particle size of 10 μm. Properties like density, hardness have been studied with respect to various proportion of reinforcement phases. Hot pressed compacted samples were sintered by ultrasonic and conventional sintering method. Hardness of graphene reinforced hybrid nano composite is superior as compared with monolithic aluminum alloy. Further, experimental results revealed that microwave sintering process enhanced higher hardness than the conventional sintering process. SiC reinforcement at lower concentration (<1 wt%) encapsulated by graphene nano sheet rendered uniform dispersion of reinforcement phase in the aluminum alloy matrix [74]. Agglomeration of SiC in the aluminum matrix is a challenge for the manufacturing of aluminum matrix nano composites [75]. Encapsulation of SiC by graphene nano sheet can prevent agglomeration of reinforcement in the hybrid nano composite based on aluminum matrix [76].

Agarwal et al. presented aluminum alloy 7075 matrix graphene reinforced hybrid nano composite fabricated by using squeeze cast method. Alloy matrix has been reinforced with 1 wt% of 5–8 nm thickness graphene and 0.5 wt% of hexagonal boron nitrite (h-BN) with particle size of 100–200 nm. Experimental results revealed that there are approximately 30%, 11% and 10% improvement of ultimate tensile strength, Vickers micro hardness and Rockwell hardness, respectively, as compared with pure alloy. In order to improve the dispersion and distribution of nano reinforcement phase, mixture has been ball milled. Microstructure study revealed that grain size decrement of the hybrid nano composite as compared with aluminum 7075 alloy. Reduced grain size in the hybrid nano composite improved the mechanical properties [77]. Du et al. discussed aluminum 7075 matrix based graphene hybrid nano composite. Aluminum alloy matrix has been reinforced with graphene (1 wt%) and SiC (0.25–2 wt%) nanoparticle, and fabricated by using ball milling and vacuum hot pressing. Microstructure study revealed graphene and SiC nanoparticles are homogeneously distributed on the grain boundary of alloy matrix, and SiC nanoparticles are well dispersed between graphene nano sheet which improved wettability between SiC nanoparticle and aluminum matrix. Micro hardness property of hybrid nano composite has been improved with increasing SiC nano particle reinforcement in the alloy matrix material. Wear loss of the hybrid nano composites decreases with increasing SiC nano particle. Further, coefficient of friction of hybrid nano composite material has been decreased with increase of SiC nano particle concentration in the nano composite. Improvement of tribological property for the hybrid nano composite material is possibly due to the formation of dry lubricant layer between mating metal molecules. Coefficient of friction of hybrid nano composite has been decreased due to the formation of graphene solid lubricant layer between wear surfaces, thereby, reduces the contact area. Further, incorporation of graphene reduces the concentration of SiC nanoparticles which subsequently beneficial for the improvement of toughness of hybrid nano composite materials [78].

Girisha et al. discussed hybrid nano composite based on aluminum (Al) matrix. Together with graphene (GR), multi walled carbon nanotube (MWCNT) and nano

diamond (ND) were used for the manufacturing of hybrid nano composites. Properties of Al/MWCNT, and hybrid Al/GR/MWCNT and Al/GR/MWCNT/ND nano composites were compared. Nano composites were prepared by using powder metallurgy and casting methods. Nano composites produced by using powder metallurgy route showed better mechanical properties as compared with nano composites produced by casting method. Young modulus and yield strength have been increased for aluminum/MWCNT nano composite as compared with pure aluminum matrix. Further, increment of mechanical properties were observed with graphene based hybrid nano composites [30]. Ghasali et al. reported carbon nanotube and graphene reinforced hybrid aluminum matrix nano composite fabricated by spark plasma sintering, microwave and conventional technique. As the concentration of carbon nanomaterials in the hybrid nano composite is limited on the surface, therefore, they have used fracture determination method to detect the graphene and carbon nanotube in the hybrid nano composite. Field emission scanning electron micrograph (FESEM) of surface factrography for graphene and CNT reinforced hybrid nano composite revealed uniform distribution of nano reinforcement phase in the matrix material produced by spark plasma sintering method (Fig. 4) [79].

Synergistic strengthening effect in hybrid nano composite material was observed when secondary reinforcement was used together with graphene. Reinforcement of alumina anchored graphene in the aluminum matrix hybrid nano composite revealed around 131% improvement of tensile strength with 1 vol% of hybrid reinforcement concentration as compared with pure aluminum. Hybrid nano composite shows around 11% of elongation with same concentration of hybrid reinforcement, thus exhibiting strength-ductility synergy due to the formation of interlocking network of hybrid nano reinforcement phase, which is a beneficial for the effective load transfer from the weak matrix phase to the strong reinforcement nanoparticles. Microstructure study revealed homogeneous distribution of reinforcement phase in the aluminum matrix [80]. Yaqoob et al. studied synergizing strategy and hybrid ratio of graphene and CeO_2 on mechanical property enhancement of aluminum alloy 6061. Nanomaterials are reinforced in the aluminum alloy matrix by friction stir. Microstructure study revealed that nanomaterials have been influenced the grain refining due to the pinning effect in retarding grain growth. Hardness and tensile strength of hybrid nano composite have been improved due to the grain refinement and obstruction imposed by nanoparticles due to the dislocation movement. 50/50 vol% of reinforcement is an optimum in improving tensile strength and micro-hardness [81]. Li et al. reported synergistic strengthening effect of aluminum based hybrid nano composite reinforced with carbon nanotube and graphene, due to the formation of planner network of reduced graphene and carbon nanotube (Fig. 5), which improves load transfer between components phases. As compared with dual reinforcement phase, without reduced graphene, CNT was separately sandwiched between aluminum matrix, while, with only graphene reinforcement, graphene sheet would irreversibly agglomerated [82].

Copper nanoparticle modified graphene reinforced aluminum matrix nano composite exhibited uniform dispersion of nano reinforcement in the hybrid nano composite and strong interfacial bonding between reinforcement phase and matrix
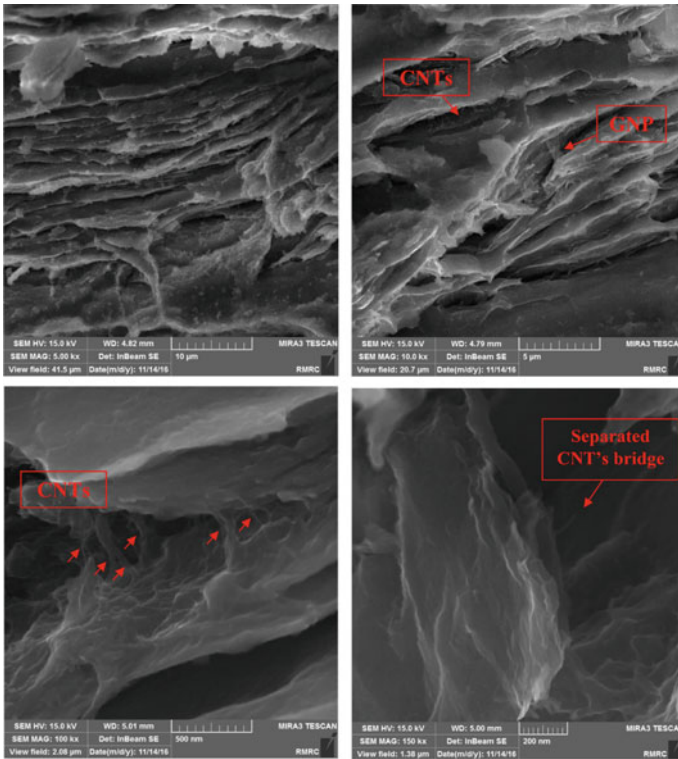
Fig. 4 FESEM of surface fractrography of graphene and CNT reinforced hybrid aluminum matrix nano composite. Reproduced with permission from Ref. [79] © 2018 Politechnika Wrocławska. Published by Elsevier B.V.

phase, thus promote effective load transfer between components phases. 0.75 wt% reinforcement concentration showed 68% increase of tensile strength and total elongation of 17.5% [83].

7 Fabrication of Graphene Based Aluminum Matrix Hybrid Nano Composites

Manufacturing of metal matrix nano composites can be classified into two major groups, viz. ex situ and in situ. In ex situ method reinforcement phases are added to liquid or powdered metal, whereas, in situ method refer to the formation of nano reinforcement phase by reaction during processing [84]. One of the major problem for the bulk production of metal matrix nano composites is low wettability of reinforcement materials in the metal matrix phase, further, high surface energy of nano
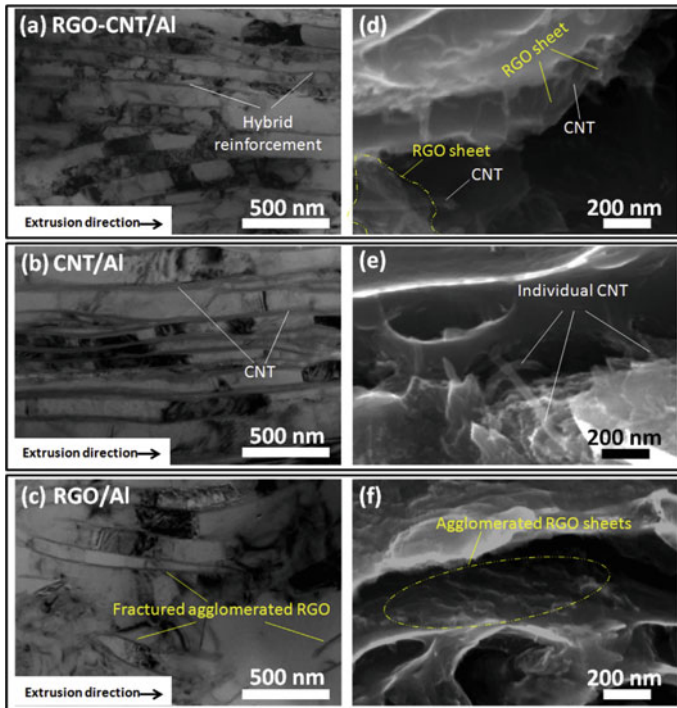
Fig. 5 Transmission electron microscopic cross sectional images (**a–c**) and scanning electron microscopic images of fracture surface (**d–f**). Reproduced with permission from Ref. [82] © 2015 Elsevier Ltd.

reinforcement phase lead to inhomogeneous dispersion and distribution of reinforcement materials in the metal matrix phase. Aluminum matrix graphene and carbon nanotube reinforced hybrid nano composites can be principally produced by using three procedures such as (i) solid phase process, (ii) liquid phase process and (iii) two phase (solid–liquid) processes. Each process has its own advantages and disadvantages, however, there are few challenges for the manufacturing of graphene based hybrid aluminum matrix nano composites as follows:

(a) Homogeneous dispersion and distribution of nanoparticles in the aluminum or its alloy matrix.
(b) Improvement of interfacial interaction between nanoparticles and matrix phase.
(c) Structural stability of nano reinforcement phases during the fabrication of hybrid nano composites.

Among various methods for the manufacturing of metal matrix hybrid nano composites, powder metallurgy method has been widely used because of its several advantages, such as simples steps, high rate of production, ability to incorporate higher concentration of nano reinforcement phases, variation of properties, reduction of machining, production of complex shape, reduction of scraps etc. Therefore

powder metallurgy methods have been employed as solid phase process for the manufacturing of aluminum matrix hybrid nano composites. The process of powder metallurgy consists of several simple steps which include (a) production of metal powder; (b) mixing of powders; (c) compaction of powder to obtain the desired shape and finally, (d) sintering of the compacted sample in order to improve cohesive strength between molecules. Sintering is an essential step in powder metallurgy method. During sintering process, particles are fused together to improve the cohesion between particles. Sintering step is carried out in absence of oxygen, either in vacuum or in presence of inert gas flow, in order to prevent the arial oxidation [58].

One of the major drawback for the manufacturing of hybrid metal matrix nano composites by using the liquid phase process is cluster formation of reinforcement phase in the metal even though mechanical stirring has been employed before casting [84]. Agglomeration of nanoparticles is possibly due to the poor wettability of reinforcement phase, high viscosity of molten metal and high specific surface area of nano sized reinforcement material. Semi solid process can be used for the particle reinforcement nanocomposites. Semi solid process for the fabrication of hybrid nanocomposite can be performed at lower temperature than liquid phase process. Application of lowered temperature reduces the possibility of thermochemical degradation of reinforcement phase during nano composite fabrication [84].

8 Prospective Applications of Graphene Reinforced Hybrid Aluminum Matrix Nano Composites

As on the date, to the best of knowledge of the author, metal matrix hybrid nano composites reinforced with nano particles are not being fully employed in the commercial fields due to the recent development of this kind of novel materials. However, metal matrix hybrid nano composites shows several improved properties as compared with conventional metal matrix composites, therefore, these novel materials can be considered as prospective candidates for the substitution of conventional composite or monolithic metal for application in structural, electrical and other advanced material applications [74]. Aluminum/alloy matrix based graphene hybrid nano composites have potential for application in automobile, aviation, space craft due to their low density [30, 85]. Frequent replacement of parts and assemblies in many engineering applications is a commonly encountered phenomena due to the materials loss by wear. Operating economy also severely affected by wear due to reasons like: (i) material loss, (ii) high fuel usage and (iii) frequent replacement of engineering parts [86]. Tribological property of aluminum matrix based graphene hybrid nano composite has been improved due the excellent lubricant property of graphene. Reinforcement of 1% gamma Al_2O_3 nanoparticle/graphene in the aluminum matrix significantly decreased the coefficient of friction [87]. Zeng et al. reported reduced wear rate for hypoeutectic aluminum–silicon matrix based nano

composite reinforced with silicon carbide and reduced graphene oxide as compared with only silicon carbide reinforced composite, due to the self-lubricating property of reduced graphene oxide [88]. Therefore, aluminum/alloy matrix graphene hybrid nano composite can be excellent candidates for the areas where the materials is exposed to wear and friction [78]. Graphene has excellent electrical and thermal conductivity, therefore, graphene reinforced hybrid aluminum nano composite can improve thermal [89, 90] and electrical properties of matrix material which can find applications where heat dissipation and electrical conductivity are required. Thermal management is critical for miniaturized electronic devices. Effective heat dissipation can reduce operating temperature and improve performance, efficacy and service life [91]. Reinforcement of micro particle alumina and graphene in the aluminum matrix can enhance corrosion resistance up to factor of 2.5–4 as compared with pure aluminum. Improvement of corrosion resistance for hybrid nanocomposite material, could find applications in ship building industry [90].

9 Summary

Graphene due to its unique properties raise a great interest as potential reinforcement for the nanocomposite materials. Metal based hybrid nano composites are novel materials with potential for advanced materials applications. Aluminum or its alloy can be considered as an excellent matrix materials for the manufacturing of light weight hybrid graphene based nano composites. This chapter provide an overview of graphene as potential reinforcement for the manufacturing of aluminum matrix based hybrid nano composite by using various common methods, dispersion mechanism of graphene reinforcement in the aluminum/its' alloy matrix, microstructure and properties of hybrid nano composites, and some of the prospective applications of Al matrix graphene based hybrid nano composites.

References

1. Pisarevskaya EY, Makarychev YB, Dremova NN, Girina GP, Efimov ON (2018) A study of a novel nanocomposite material based on reduced graphene oxide and poly(o-phenylenediamine). Prot Met Phys Chem Surf 54(3):393–401
2. Huang JY, Limqueco J, Chieng YY, Li X, Zhou WB (2017) Performance evaluation of a novel food packaging material based on clay/polyvinyl alcohol nanocomposite. Innov Food Sci Emerg Technol 43:216–222
3. Sagnelli D et al (2019) Starch/poly (glycerol-adipate) nanocomposite film as novel biocompatible materials. Coatings 9(8). Art. no. 482
4. Gamboa RAM, Jaramillo-Quintero OA, Altamirano YAA, Concha-Guzman MO, Rincon ME (2019) A novel nanocomposite based on NiO_x-incorporated P3HT as hole transport material for Sb2S3 solar cells with enhanced device performance. J Colloid Interface Sci 535:400–407
5. Al-Amshany ZM, Hussein MA (2018) Novel $Pd/ZnWO_4$ nanocomposite materials for photocatalytic degradation of atrazine. Appl Nanosci 8(3):527–536

6. Li T, Wang ZX, Yu JR, Wang Y, Zhu J, Hu ZM (2019) Cu (II) coordination modification of aramid fiber and effect on interfacial adhesion of composites. High Perform Polym 31(9–10):1054–1061

7. Wang HX et al (2019) Stress dependence of indentation modulus for carbon fiber in polymer composite. Sci Technol Adv Mater 20(1):412–420

8. Li SP et al (2019) The microstructure and mechanical properties of $Mg_2B_2O_5$ whisker-reinforced ZK60 composites fabricated by powder metallurgy. Mater Res Exp 6(9). Art. no. 0965b9

9. Wang XC et al (2019) High impact strength for polypropylene/titanate whisker composites with dual compatibilizing agents. Polym Compos 40(9):3421–3428

10. Subramaniam B, Natarajan B, Kaliyaperumal B, Chelladurai SJS (2019) Wear behaviour of aluminium 7075-boron carbide-coconut shell fly ash reinforced hybrid metal matrix composites. Mater Res Exp 6(10). Art. no. 1065d3

11. Zhou HB et al (2019) Effects of ZrO_2 crystal structure on the tribological properties of copper metal matrix composites. Tribol Int 138:380–391

12. Singh MK, Gautam RK (2019) Structural, mechanical, and electrical behavior of ceramic-reinforced copper metal matrix hybrid composites. J Mater Eng Perform 28(2):886–899

13. Zhou FM, Zhang HX, Sun CX, Dai J (2019) Microstructure and wear properties of multi ceramics reinforced metal-matrix composite coatings on Ti–6Al–4V alloy fabricated by laser surface alloying. Surf Eng 35(8):683–691

14. Dong SH, Zhou JQ, Hui D, Wang L (2015) Fracture toughness of nanocrystalline metal matrix composites reinforced by aligned carbon nanotubes. J Mater Res 30(21):3267–3276

15. Chandio AD, Ansari MB, Hussain S, Siddiqui MA (2019) Silicon carbide effect as reinforcement on aluminium metal matrix composite. J Chem Soc Pak 41(4):650–654

16. Reddy PS, Kesavan R, Ramnath BV (2018) Investigation of mechanical properties of aluminium 6061-silicon carbide, boron carbide metal matrix composite. Silicon 10(2):495–502

17. Venkatesh R, Rao VS (2018) Thermal, corrosion and wear analysis of copper based metal matrix composites reinforced with alumina and graphite. Def Technol 14(4):346–355

18. Saheb N et al (2012) Spark plasma sintering of metals and metal matrix nanocomposites: a review. J Nanomater. Art. no. 983470

19. Aybarc U, Dispinar D, Seydibeyoglu MO (2018) Aluminum metal matrix composites with SiC, Al_2O_3 and graphene—review. Arch Foundry Eng 18(2):5–10

20. Bhoi NK, Singh H, Pratap S (2020) Developments in the aluminum metal matrix composites reinforced by micro/nano particles—a review. J Compos Mater 54(6):813–833

21. Pasha BAM, Kaleemulla M (2018) Processing and characterization of aluminum metal matrix composites: an overview. Rev Adv Mater Sci 56(1):79–90

22. Schmidt A, Siebeck S, Gotze U, Wagner G, Nestler D (2018) Particle-reinforced aluminum matrix composites (AMCs)-selected results of an integrated technology, user, and market analysis and forecast. Metals 8(2). Art. no. 143

23. Lu ZZ et al (2019) Fabrication and mechanical properties of carbon fiber-reinforced aluminum matrix composites with Cu interphase. Acta Metall Sin 55(3):317–324 (in Chinese)

24. Muley AV, Aravindan S, Singh IP (2015) Nano and hybrid aluminum based metal matrix composites: an overview. Manuf Rev 2. Art. no. 15

25. Harrigan WC (1998) Commercial processing of metal matrix composites. Mater Sci Eng A 244(1):75–79

26. Bose S, Pandey A, Mondal A (2018) Comparative analysis on aluminum-silicon carbide hybrid green metal matrix composite materials using waste egg shells and snail shell ash as reinforcements. Mater Today-Proc Proc Pap 5(14):27757–27766

27. Reddy AP, Krishna PV, Rao RN (2017) Al/SiCNP and Al/SiCNP/X nanocomposites fabrication and properties: a review. Proc Inst Mech Eng Part N J Nanomater Nanoeng Nanosyst 231(4):155–172

28. Yarahmadi A, Rajabi M, Noghani MT, Taghiabadi R (2019) Synthesis of aluminum-CNTs composites using double-pressing double-sintering method (DPDS). J Nanostruct 9(1):94–102

29. Ciomaga CE et al (2019) Functional properties of percolative $CoFe_2O_4$-$PbTiO_3$ composite ceramics. J Alloy Compd 775:90–99
30. Girisha L, Deshpande M, Naik GL, Mahanthesh MR (2019) Mechanical characterization of nanomaterial reinforced aluminum-based hybrid nanocomposites. Adv Nano Res 2(1):32–41
31. Moskalyuk OA, Tsobkallo ES, Yudin VE, Shibanova AV, Malafeev KV, Morganti P (2018) Effect of functional disperse fillers on mechanical properties of fibrous polymeric composite materials. Fibre Chem 50(3):209–214
32. Takagi H (2019) Review of functional properties of natural fiber-reinforced polymer composites: thermal insulation, biodegradation and vibration damping properties. Adv Compos Mater 28(5):525–543
33. Singh R, Singh B, Tarannum H (2019) Mechanical properties of jute fiber-reinforced UP/PU hybrid network composites. Polym Polym Compos 27(9):546–556
34. Alibeigloo A (2018) Coupled thermoelasticity analysis of carbon nano tube reinforced composite rectangular plate subjected to thermal shock. Compos Part B-Eng 153:445–455
35. Kawabata K, Sato E, Kuribayashi K (2002) Creep deformation behavior of spherical Al_2O_3 particle-reinforced Al–Mg matrix composites at high temperatures. Acta Mater 50(13):3465–3474
36. Kondo S, Ohkawa S, Uo M, Sugawara T, Watari F (1996) Fracture toughness of spherical silica reinforced composite resin. J Dent Res 75:2192–2192
37. El-Sabbagh SH, Mahmoud DS, Ahmed NM, Ward AA, Sabaa MW (2017) Composites of styrene butadiene rubber/modified clay: mechanical, dielectric and morphological properties. Pigm Resin Technol 46(3):161–171
38. Lin W, Shi QQ, Chen H, Wang JN (2019) Mechanical properties of carbon nanotube fibers reinforced epoxy resin composite films prepared by wet winding. Carbon 153:308–314
39. Liu et al YX (2019) Effects of micron heterogeneous metal particles on the microstructure and mechanical properties of 7075Al hybrid composites. J Alloy Compd 808. Art. no. 151727
40. Ahmadi M, Ansari R, Hassanzadeh-Aghdam MK (2019) Finite element analysis of thermal conductivities of unidirectional multiphase composites. Compos Interfaces 26(12):1035–1055
41. Liu W, Bian LC (2019) A new energy-based effective strain theory for mechanical properties of multiphase composites. Eur J Mech A-Solids 76:279–289
42. Andrew JJ, Srinivasan SM, Arockiarajan A, Dhakal HN (2019) Parameters influencing the impact response of fiber-reinforced polymer matrix composite materials: a critical review. Compos Struct 224. Art. no. 111007
43. Chen YF et al (2019) Yield and failure theory for unidirectional polymer-matrix composites. Compos Part B-Eng 164:612–619
44. Li LB (2019) Time-dependent damage and fracture of fiber-reinforced ceramic-matrix composites at elevated temperatures. Compos Interfaces 26(11):963–988
45. Jayaseelan P, Christy TV, Vijay SJ, Nelson R (2019) Effect of tool material, profile and D/d ratio in friction stir welding of aluminium metal matrix composites. Mater Res Exp 6(9). Art. no. 096590
46. Satyanarayana T, Rao PS, Krishna MG (2019) Influence of wear parameters on friction performance of A356 aluminum-graphite/granite particles reinforced metal matrix hybrid composites. Heliyon 5(6). Art. no. e01770
47. Chelliah NM, Pambannan P, Surappa MK (2019) Effects of processing conditions on solidification characteristics and mechanical properties of in situ magnesium metal matrix composites derived from polysilazane precursor. J Compos Mater 53(26–27):3741–3755
48. Niknam SA, Saberi M, Kouam J, Hashemi R, Songmene V, Balazinski M (2019) Ultrafine and fine particle emission in turning titanium metal matrix composite (Ti-MMC). J Central South Univ 26(6):1563–1572
49. Sangeethkumar E, Jaikumar M, Sridath KMN, Ramanathan V, Sathyamurthy R (2019) Tribological study on hybrid metal matrix composites for application in automotive sector. Mater Res Exp 6(5). Art. no. 055703
50. Munisamy B, Madhavan VRB, Chinnadurai E, Janardhanan J (2019) Prediction of mechanical properties of Al6061 metal matrix composites reinforced with zircon sand and boron carbide. Mater Test 61(6):537–542

51. Ranganath G, Sharma SC, Krishna M, Muruli MS (2002) A study of mechanical properties and fractography of ZA-27/titanium-dioxide metal matrix composites. J Mater Eng Perform 11(4):408–413

52. Aristizabal K, Katzensteiner A, Leoni M, Mucklich F, Suarez S (2019) Evolution of the lattice defects and crystalline domain size in carbon nanotube metal matrix composites processed by severe plastic deformation. Mater Charact 154:344–352

53. Cao HJ et al (2019) Graphene interlayer for enhanced interface thermal conductance in metal matrix composites: an approach beyond surface metallization and matrix alloying. Carbon 150:60–68

54. Jang JH, Han KS (2007) Fabrication of graphite nanofibers reinforced metal matrix composites by powder metallurgy and their mechanical and physical characteristics. J Compos Mater 41(12):1431–1443

55. da Silva CC, Volpato GM, Fredel MC, Tetzlaff U (2019) Low-pressure processing and microstructural evaluation of unidirectional carbon fiber-reinforced aluminum-nickel matrix composites. J Mater Process Technol 269:10–15

56. Wang FC, Li JJ, Shi CS, Liu EZ, He CN, Zhao NQ (2019) In-situ synthesis of $MgAlB_4$ whiskers as a promising reinforcement for aluminum matrix composites. Mater Sci Eng A-Struct Mater Prop Microstruct Process 764. Art. no. 138229

57. Surappa MK (2003) Aluminium matrix composites: challenges and opportunities. Sadhana-Acad Proc Eng Sci 28:319–334

58. Malaki M et al (2019) Advanced metal matrix nanocomposites. Metals 9(3). Art. no. 330

59. Chen LG, Lin SJ, Chang SY (2006) Tensile properties and thermal expansion behaviors of continuous molybdenum fiber reinforced aluminum matrix composites. Compos Sci Technol 66(11–12):1793–1802

60. Phiri J, Gane P, Maloney TC (2017) General overview of graphene: production, properties and application in polymer composites. Mater Sci Eng B 215:9–28

61. Coroş M, Pogăcean F, Măgeruşan L, Socaci C, Pruneanu S (2019) A brief overview on synthesis and applications of graphene and graphene-based nanomaterials. Front Mater Sci J 13(1):23–32

62. Krishnan SK, Singh E, Singh P, Meyyappan M, Nalwa HS (2019) A review on graphene-based nanocomposites for electrochemical and fluorescent biosensors. RSC Adv 9(16):8778–8881

63. De Marchi L, Pretti C, Gabriel B, Marques PAAP, Freitas R, Neto V (2018) An overview of graphene materials: properties, applications and toxicity on aquatic environments. Sci Total Env 631–632:1440–1456

64. Dasari Shareena TP, McShan D, Dasmahapatra AK, Tchounwou PB (2018) A review on graphene-based nanomaterials in biomedical applications and risks in environment and health. Nano-Micro Lett J 10(3). Art. no. 53

65. Choi W, Lahiri I, Seelaboyina R, Kang YS (2010) Synthesis of graphene and its applications: a review. Crit Rev Solid State Mater Sci 35(1):52–71

66. Saifuddin N, Raziah AZ, Junizah AR (2013) Carbon nanotubes: a review on structure and their interaction with proteins. J Chem. Art. no. 676815

67. Donaldson K et al (2006) Carbon nanotubes: a review of their properties in relation to pulmonary toxicology and workplace safety. Toxicol Sci 92(1):5–22

68. Nassar AE, Nassar EE (2017) Properties of aluminum matrix nano composites prepared by powder metallurgy processing. J King Saud Univ Eng Sci 29(3):295–299

69. Maleki A, Taherizadeh AR, Issa HK, Niroumand B, Allafchian AR, Ghaei A (2018) Development of a new magnetic aluminum matrix nanocomposite. Ceram Int 44(13):15079–15085

70. Mekhzoum MEM, Essabir H, Rodrigue D, el Kacem Qaiss A, Bouhfid R (2018) Graphene/montmorillonite hybrid nanocomposites based on polypropylene: morphological, mechanical, and rheological properties. Polym Compos 39(6):2046–2053

71. Zhao S et al (2018) Synergistic effect of graphene and silicon dioxide hybrids through hydrogen bonding self-assembly in elastomer composites. Rsc Adv 8(32):17813–17825

72. Saba N, Jawaid M (2019) Functionalized graphene reinforced hybrid nanocomposites and their applications. In: Jawaid M, Bouhfid R, el Kacem Qaiss A (eds) Functionalized graphene nanocomposites and their derivatives. Elsevier, pp. 205–218 (Chapter 10)

73. Sharifi EM, Karimzadeh F (2011) Wear behavior of aluminum matrix hybrid nanocomposites fabricated by powder metallurgy. Wear 271(7):1072–1079

74. Jauhari S, Kumar HGP, Xavior MA (2016) Synthesis and characterization of AA 6061-Graphene-SiC hybrid nanocomposites processed through microwave sintering. IOP Conf Ser: Mater Sci Eng 149. Art. no. 012086

75. Zeng X, Liu W, Xu B, Shu GG, Li QL (2018) Microstructure and mechanical properties of Al-SiC nanocomposites synthesized by surface-modified aluminium powder. Metals 8(4). Art. no. 253

76. Fadavi Boostani A et al (2015) Enhanced tensile properties of aluminium matrix composites reinforced with graphene encapsulated SiC nanoparticles. Compos Part A Appl Sci Manufact 68:155–163

77. Agarwal P, Kishore A, Kumar V, Soni SK, Thomas B (2019) Fabrication and machinability analysis of squeeze cast Al 7075/h-BN/graphene hybrid nanocomposite. Eng Res Exp 1(1). Art no. 015004

78. Du XM, Zheng KF, Zhao T, Liu FG (2018) Fabrication and characterization of Al 7075 hybrid composite reinforced with graphene and SiC nanoparticles by powder metallurgy. Dig J Nanomater Biostruct 13(4):1133–1140

79. Ghasali E, Sangpour P, Jam A, Rajaei H, Shirvanimoghaddam K, Ebadzadeh T (2018) Microwave and spark plasma sintering of carbon nanotube and graphene reinforced aluminum matrix composite. Arch Civ Mech Eng 18(4):1042–1054

80. Liu XH et al (2019) Synergistic strengthening effect of alumina anchored graphene nanosheets hybrid structure in aluminum matrix composites. Fullerenes Nanotubes Carbon Nanostruct 27(8):640–649

81. Yaqoob B, Pasha RA, Awang M, Nasir MA, Hussain A, Nazir K (2019) Comparison of mixing strategies and hybrid ratio optimization for mechanical properties enhancement of Al-CeO$_2$-GNP's metal matrix composite fabricated by friction stir processing. Metall Microstruct Anal 8(4):534–544

82. Li Z, Fan GL, Guo Q, Li ZQ, Su YS, Zhang D (2015) Synergistic strengthening effect of graphene-carbon nanotube hybrid structure in aluminum matrix composites. Carbon 95:419–427

83. Wang J, Zhang X, Zhao NQ, He CN (2019) In situ synthesis of copper-modified graphene-reinforced aluminum nanocomposites with balanced strength and ductility. J Mater Sci 54(7):5498–5512

84. Casati R, Vedani M (2014) Metal matrix composites reinforced by nano-particles—a review. Metals 4(1):65–83

85. Xavior MA, Kumar JPA (2017) Machinability of hybrid metal matrix composite—a review. In: Yeh WC, Zhao L (eds) 13th global congress on manufacturing and management, vol 174. Procedia engineering, pp 1110–1118

86. Arif S, Alam T, Ansari AH, Shaikh MBN (2019) Morphological characterization, statistical modelling and tribological behaviour of aluminum hybrid nanocomposites reinforced with micro-nano-silicon carbide. J Asian Ceram Soc, 1–15

87. Vaziri HS, Shokuhfar A (2019) Synthesis of nanoalumina/graphene oxide hybrid for improvement tribological property of aluminum. Trans Indian Inst Metal 72(7):1687–1695

88. Zeng X, Yu JG, Fu DF, Zhang H, Teng J (2018) Wear characteristics of hybrid aluminum-matrix composites reinforced with well-dispersed reduced graphene oxide nanosheets and silicon carbide particulates. Vacuum 155:364–375

89. Saboori A, Pavese M, Badini C, Fino P (2017) Microstructure and thermal conductivity of Al-graphene composites fabricated by powder metallurgy and hot rolling techniques. Acta Metall Sin-Engl Lett 30(7):675–687

90. Elshina LA, Muradymov RV, Kvashnichev AG, Vichuzhanin DI, Molchanova NG, Pankratov AA (2017) Synthesis of new metal-matrix Al-Al$_2$O$_3$-graphene composite materials. Russ Metall 8:631–641

91. Shtein M, Nadiv R, Buzaglo M, Regev O (2015) Graphene-based hybrid composites for efficient thermal management of electronic devices. ACS Appl Mater Interfaces 7(42):23725–23730

Hybrid Nanocomposites Based on Graphene and Ferrite Nanoparticles: From Preparation to Application

R. D. A. A. Rajapaksha and C. A. N. Fernando

Abstract Ferrites are composite materials which are widely used in mature technologies like permanent magnets, circuitry, microwave devices and magnetic recording. Now a days the range of application expanded to different fields like photocatalysis, biosensors, bioimaging, gas sensors and many other fields. At least one metal cation included Fe^{3+} containing large class of oxides is the basic elements of ferrite and applied as powder form and films or ceramic bodies. The remarkable properties of hybrid nanocomposites of ferrite and graphene incorporated devices shows high performance in numerous applications in analytical medical equipment such as sensors, biosensors; electronic devices such as memory devices, semiconductor devices; energy devices such as solar cells, electrocatalytic and photocatalytic based chemical storage devices and many other fields.

Keywords Ferrite · Nanocomposite · Transition metals · Synthesis · Nanostructures · Voltammetry · Synergetic effect · Adsorption

1 Introduction

Graphene and ferrite nanocomposites have become promising material for enormous applications due to their extraordinary characteristics. According to the past studies, these composites are used in different applications such as sensors and biosensors, solar cells, photoelectrochemical cells, batteries, supercapacitors, etc., in biomedical, material science, engineering, agriculture, and many other fields. The synergetic effect of both graphene and ferrite may enhance the surface area, electron transferability, conductivity, and stability of the composite. According to Zahid et al., graphene-ferrite nanocomposite has remarkable properties such as adsorption enhanced photocatalysis, low leaching catalysis, magnetic separation, bandgap in visible spectral range, fast adsorption [1]. Kaur and Kaur had reported excellent

R. D. A. A. Rajapaksha (✉) · C. A. N. Fernando
Department of Nano Science Technology, Faculty of Technology, Wayamba University of Sri Lanka, Kuliyapitiya, Sri Lanka
e-mail: asanka@wyb.ac.lk

adsorption and photocatalytic activity of graphene and ferrite nanocomposite due to synergetic effect [2].

Ferrite is one of the best candidates for many composites because of its small particle size, availability of many surface active sites, high adsorption capability, ease to separate, tunable chemical composition, nonconductive, and high surface area to volume ratio [3]. Ferrites can be categorised according to their crystal structure as spinels, garnets, hexagonal ferrites, and orthoferrites [1]. In another way, ferrite can classify as a soft, hard, square loop, microwave-based on magnetic properties. Different types of ferrites can be synthesised via the ceramic method and chemical route techniques. The techniques which are used to synthesise ferrite nanoparticles include co-precipitation, hydrothermal, sol–gel, thermal decomposition, solvothermal, sonochemical, microwave-assisted, microemulsion, polyol, and electrochemical, mechanical milling, and laser ablation [1]. Dhal et al. stated that spinel magnesium ferrite NPs have outstanding properties such as super thermal stability, smaller bandgap, low cost, non-toxicity, and magnetic properties [4]. These properties of ferrite nanoparticle-based composites are used in many applications. For example, adsorption of heavy metals, alcohol decomposition, oxidative hydrocarbon dehydration, degradation of dyes, decomposition of hydrogen peroxide, and oxidation of carbon monoxide [5].

Nowadays, graphene plays a major role in the scientific world due to its extraordinary features. In graphene, a flat monolayer of carbon atoms is packed tightly into a structure 2D honeycomb lattice [6]. Because of this structure, graphene has high flexibility, excellent electrical conductivity, super thermal stability, and outstanding mechanical properties. The graphene's specific surface area may lead to electromagnetic shields to absorb incident electromagnetic waves [7]. Due to low density and high dielectric loss, graphene can be used as an electromagnetic wave absorber at high frequencies in the gigahertz range [8]. The graphene's high thermal conductivity will enhance the charge carrier rate ($200,000 \, cm^2 \, V^{-1} \, s^{-1}$) at room temperature [9]. Many researchers have used functionalised graphenes such as graphene oxide (GO) and reduced graphene oxide (rGO) for their research work due to their unique features. Bhattacharyya et al. reported various graphene properties such as high surface area, excellent dielectric permittivity, and lightweight [10]. Unique two-dimensional structure, high specific surface area, electron mobility, and excellent chemical and electrochemical stability lead rGO a promising candidate enormously in medical and other fields of applications [11].

The synergetic effect of graphene and ferrite may use in numerous industrial applications. There are many synthesis techniques used to synthesised graphene and ferrite nanocomposites. The following figure (Fig. 1) depicts some synthesis techniques and applications of graphene/ferrite nanocomposites.
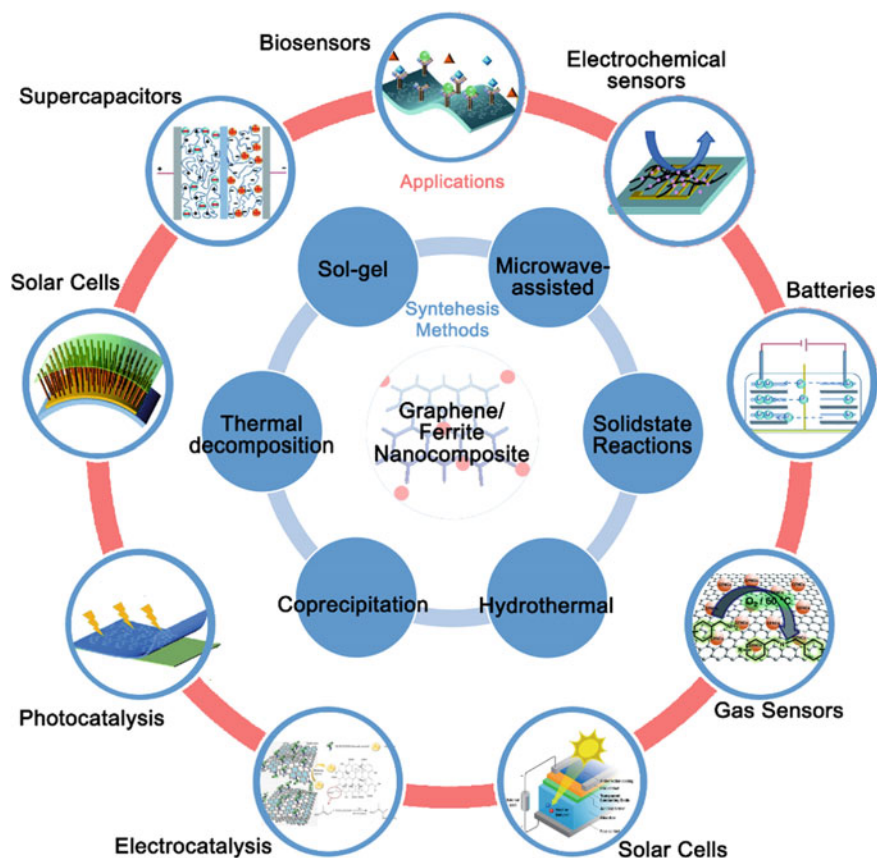
Fig. 1 Synthesis methods and applications of graphene/ferrite nanocomposites

2   Synthesis of Graphene and Ferrite Nanocomposites

Ferrite nanoparticles can be synthesised by bottom-up and top-down approaches, which are based on physical and chemical methods. Coprecipitation, thermal methods, solid-state reactions, and sol–gel methods are clarified here.

2.1   Co-precipitation

In this method, precipitation of insoluble or less soluble products is formed from metal precursor aqueous solutions by facilitating high supersaturating conditions, pH adjustment, or precipitating agents. This process consists of nucleation, growth,

coarsening, agglomeration processes, and thermal treatment. As the thermal treatment, intermediate precipitate decomposes into the form of ferrite or crystallising oxide. This method is used to synthesise orthoferrites or spinel ferrites [1, 12, 13].

2.2 Sol–gel Method

In this technique, metal alkoxide solution undergoes hydrolysis, condensation polymerisation reactions, and heat treatment to crystallise the ferrite and remove the volatile by-products. The temperature of the preparation of the sol–gel will lie 25^-200 °C [14]. Simple, low cost, ability to tune for the preparation of a large range of orthoferrites, and spinel ferrites structures are the main advantages of this technique [15, 16].

2.2.1 Sol–gel Auto-Combustion Process

In this technique, GO is added to the ferrite solution and ultra-sonicated for few minutes (15 min). The solution will be evaporated at 100 °C with continuous stirring to form dark brown viscous GO xerogel. By increasing the temperature up to 220 °C, a dark-brown mass will be obtained. The powder formed is calcined at 600 °C for two hours to obtain graphene/ferrite nanocomposite. Bhattacharyya and coworkers had synthesised $Ni_{0.5}Zn_{0.5}Fe_2O_4$ ferrite (NZF)-GO hybrid by using this technique [10].

2.3 Thermal Method

Thermal decomposition, hydrothermal, solvothermal, and microwave-assisted method are some of the popular thermal methods of ferrite nanoparticle synthesis. In thermal decomposition, precursors, surfactants, and organic solvents are used during the heat treatment to form ferrite. In this method, the temperature will increase up to 500 °C. But in hydrothermal, solvothermal, and microwave-assisted methods, the temperature maintains between 100 and 200 °C. Temperature, pressure, process duration, solvent type, surfactant, and precursors are the main factors that will affect ferrite's properties [17, 18].

2.3.1 Thermal Decomposition

In this technique, organometallic precursors (as metallic acetylacetonates and carbonyls) with the presence of organic solvents and surfactants such as oleic acid and hexadecyl amine thermally decompose to the synthesis of ferrite NPs. The

applied temperature is based on the type of precursor material. The shape and size are controlled by the temperature, concentration of precursors, and the heating rate. Uniform morphology, narrow distribution particle size, and high mono-dispersion are the key benefits of this technique [19, 20].

2.3.2 Hydrothermal

This method is used in the large-scale production of ferrite NPs. During this process, soluble divalent and trivalent transition metal salts are dissolved separately and mixed with the mole ratio of 1:2, respectively. The organic solvent (ethylene glycol or ethanol) is added dropwise with continuous vigorous stirring. Finally, the solution will be heated under high pressure in the autoclave. The nanoparticle size and size distribution depend on the temperature, pressure, reaction time, and the proper mixture of the solvent [21, 22] (Fig. 2).

Keziban Atacan had synthesised $CuFe_2O_4/rGO$ nanocomposite. The GO was obtained from graphite powder by means of the modified Hummers' method. The synthesis method is based on 1.5 g of graphite was preoxidised with 8 ml H_2SO_4, 3 g of $K_2S_2O_4$ and 2.5 g of P_2O_5 at 80 °C for 2 h. Then, 120 mL $H2SO_4$ and 17 g of $KMnO_4$ are added to continue oxidation. Subsequently, the graphite oxide is exfoliated to GO via sonication for 30 min. $CuFe_2O_4/rGO$ nanocomposite is synthesised by a hydrothermal method. 80 mg of GO was dispersed into 40 mL of ethanol under sonication for 30 min. 0.1705 g of $CuCl_2 \cdot 2H_2O$ (0.001 mol) and 0.5406 g of $FeCl_3 \cdot 6H_2O$ (0.002 mol) are dissolved in 30 mL of ethanol with stirring for 30 min at room temperature. The above two solutions are then mixed together. The mixture is adjusted to pH 12 with 6M NaOH solution and stirred for 30 min. The solution is poured into a Teflon-lined autoclave and heated at 180 °C for 24 h. The reaction mixture is cooled to room temperature, and the product was separated with a magnet, washed with DW and ethanol, finally dried at 60 °C for 12 h [23].
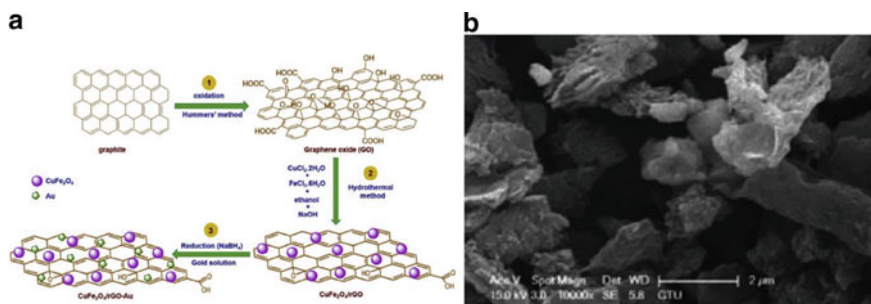
Fig. 2 a The synthesis process of $CuFe_2O_4/rGO$, b the SEM image of $CuFe_2O_4/rGO$ [23]

2.3.3 Solvothermal

Both aqueous and non-aqueous solvents are used to produce nanoparticles. The physical properties are depended on temperature, reaction time, solvent, precursors, and surfactant. This method is useful for the synthesis of physical and chemical properties improved nanoparticles, which can use in the industrial and biomedical field and scalable production [24, 25].

2.3.4 Microwave-Assisted

In this technique, energy is directly applied via molecular interaction with the EMR to the material. In their electromagnetic energy convert to thermal energy, and as a result, heat is generated. The reaction time is very short, and the temperature will lie between 100 and 200 °C. With the use of an exhausting drain connected to the Teflon vessel, the generated vapor is eliminated. Reasonable cost, high-quality, narrow size distribution, and good reproducibility are the advantages of this technique [26, 27].

2.4 Solid-State Reaction

Solid-state reaction methods are a kind of top-down approach, and spinel ferrites such as $CoFe_2O_4$, $CuFe_2O_4$, and $NiFe_2O_4$ are synthesised using this method. In this technique, solid precursors are treated at high temperature. But low specific surface of ferrite is one of the disadvantage of this technique. Low-cost, less time consumption and easy up-scaling are some advantages of solid-state reaction methods [28, 29].

2.5 Ultra-Sonication Route

Bashir and coworkers had used this method to prepare $Ni_{0.9}Cu_{0.1}Fe_2O_4$/rGO nanocomposite [30]. According to their technique, rGO suspension is added into the ferrite nanoparticles suspension and ultra-sonication for 60 min to obtain homogeneous dispersion. Then homogeneous mixture is filtered to dry the rGO to obtain the copper substituted nanocrystalline nickel ferrite particles decorated onto the graphene sheets.

3   Applications of Graphene and Ferrite Nanocomposites

3.1   Biosensor Applications

With the development of nanocomposites based materials, the bulk size of analytical based devices are changed to miniaturised devices. For example, instead of bulk size analytical based equipment in bioanalytical fields replaced by the nanosensors and actuator based miniaturised devices [31–33]. High surface to volume ratio, electron transfer efficiency, and biocompatibility increase the sensitivity and selectivity, which is the pathway to high-efficient biosensors. In electrochemical sensors, nanomaterials increase the electron transfer efficiency between biomolecules and transducer.

The biosensor consists of three major parts, receptor, transducer, and signal processor. The analytical characteristics of the device depend on the inter-component correlations and the intra-component properties of each element. The specificity of the device depends on the receptor, which is a biological recognition element. It specifically reacts with the target analyte of interest. These biological receptors (ssDNA, antibody, enzyme, cells, etc.) are immobilised on the transducer surface [33–35]. The transducer converts the biological reaction to an electrical signal. Response time (rapidity) and the device's sensitivity depend on the surface to volume ratio of the nanomaterials and the transducer [36–39]. Nanomaterials and nanostructured transducers help to develop miniaturised devices and enhance the signal amplification capabilities too. Usually, in the biosensors, biological reactions produce extra small signals. The major tasks of the processing circuit are to amplify the extra small signals and process them towards a readable state in the display in a user-friendly way.

Atacan had developed $CuFe_2O_4$/rGO nanocomposite decorated gold NPs based electrochemical biosensor for L-cysteine detection (Fig. 3a) [23]. They used graphene as its specific surface area, high electrical conductivity, modification easiness, good biocompatibility, and high thermal and chemical stability. High reactivity, moisture
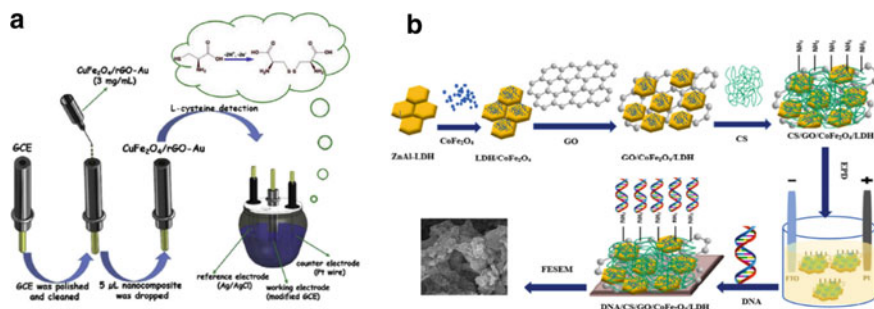
Fig. 3 a Schematic illustration of the electrochemical detection and oxidation reaction of L-Cys using $CuFe_2O_4$/rGO-Au [23]. **b** Schematic illustration the fabrication of DNA/GO/CoFe$_2$O$_4$/LDH/FTO bioelectrode [40].

insensitivity, easy separation, high specific and practical availability, and environmental friendliness are the key characteristics of CuFe2O4. Hummers' method and hydrothermal method were used to synthesise the $CuFe_2O_4$/rGO nanocomposite. The synergetic effect of the $CuFe_2O_4$/rGO-Au composite has shown high efficient electrocatalytic activity. The sensor has shown 100.01 mAmM^{-1} cm^{-2} sensitivity and 0.383 mM limit of detection.

Vajedi and Dehghani had developed cobalt ferrite and graphene oxide based DNA biosensor (GO/$CoFe_2O_4$/ZnAl-LDH) for Etoposide (ETO) detection (Fig. 3b) [40]. They used graphene-based nanostructures due to specific surface area, high electron transfer, excellent conductivity, quantum-confinement effects, ease to handle, high bioactivity retention, and super biocompatibility. Cubic spinel structure, faster electron transfer kinetics, high surface-to-volume ratio, various redox states, super electrochemical stability, strong adsorption ability, and excellent conductivity are the reported characteristics of $CoFe_2O_4$ NPs. The electrophoretic deposition (EPD) technique was used to synthesise the $CoFe_2O_4$ nanoparticles and GO nanocomposite. The sensor had shown a 0.2–10 μM liner range and 0.0010 μM limit of detection. The sensor has shown 95% stability after 6–7 weeks.

Afkhami and coworkers fabricated nickel-zinc ferrite/graphene nanocomposite-based biosensors for omeprazole detection in real samples [41]. Low magnetic coercively, excellent magnetic properties, and high electrical resistivity are the main properties of Ni–Zn ferrite. Specific surface area, electrical conductivity, fast electron transfers, and low production cost are the key features of graphene. The composite was synthesised via the Hummers' method and hydrothermal method. High sensitivity, superior repeatability, super reproducibility, and simple process are the remarkable features of the sensor. The linear sensor response was 0.03–100.0 μmol L^{-1}, and the limit of detection was 0.015 μmol L^{-1}.

Madhura and coworkers had developed a non-enzymatic electrochemical biosensor for sensing hydrogen peroxide (H_2O_2). The rGO/$MnFe_2O_4$ nanocomposite modified glassy carbon electrode was used for the electrochemical reduction and detection of H_2O_2 (Fig. 4). The biosensor was used to determine H_2O_2 in real water samples [42].

3.2 Catalysis Application

Graphene-based composites also are being used in various catalysis based applications due to their large surface area per unit volume. These nano-sized composites catalysts enhance reaction and produce the desired result using a smaller amount of catalytic materials.

Zhang et al. had synthesised copper ferrite/graphene hybrid composite ($CuFe_2O_4$/G) as a catalyst to reduce nitroarenes [43]. They used $CuFe_2O_4$ because of its moisture intensity, high reactivity, high dispersion, easiness to separate using an external magnet, and environmental compatibility. Specific surface area, electrical conductivity, superior absorptivity, excellent thermal and chemical stability, and easy
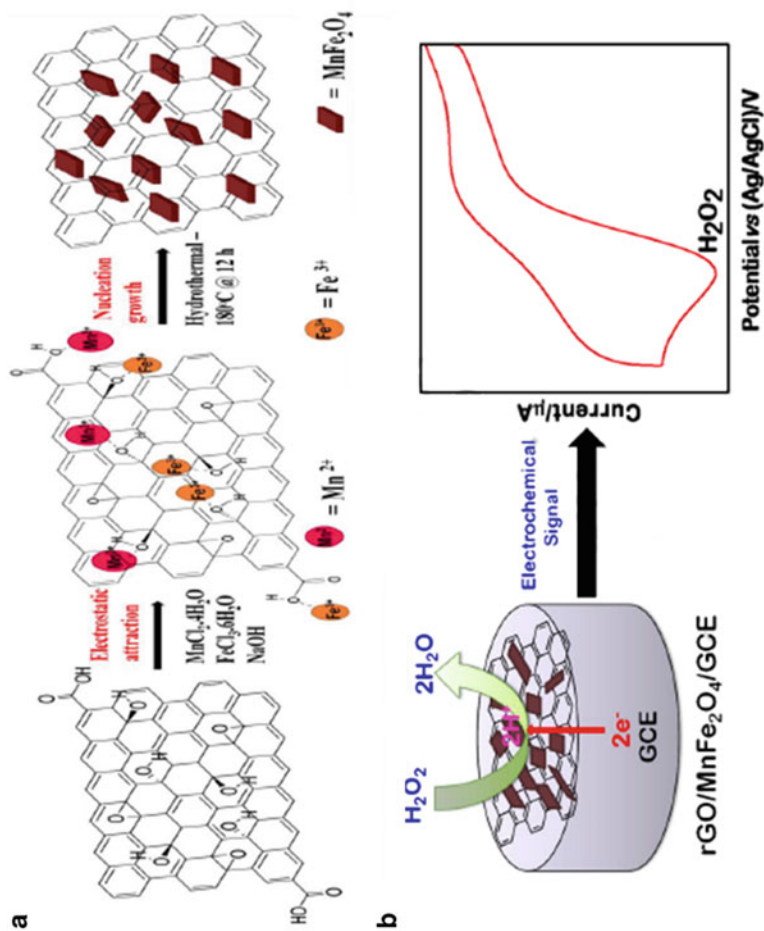
Fig. 4 **a** Schematic representation of the preparation of $MnFe_2O_4$ on rGO sheets, and **b** the electrocatalytic reduction of H_2O_2 at the rGO/$MnFe_2O_4$ nanocomposite modified GCE [42]

modification are the distinctive capabilities of graphene. The research group synthesised the copper ferrite-graphene hybrid composite using the hydrothermal method, and the synergetic effect of the composite facilitate the improvement of catalytic activities drastically, can easily isolate the catalyst using an external magnet, and the composite can be reused more than five consecutive cycles without any loss of catalytic activity.

Yao and coworkers had examined the catalytic activities of magnetic $CoFe_2O_4$-Graphene nanocomposite in phenol decomposition [44]. They had reported open porous structure, chemical stability, excellent electrical conductivity, and specific surface area as key characteristics of graphene. The research team synthesised the composite through the chemical deposition of $CoFe_2O_4$ NPs onto GO. The particle size of $CoFe_2O_4$ was 23.8 nm. They compared the catalytic activities of $CoFe_2O_4$-Graphene nanocomposite with $CoFe_2O_4$ nanoparticles, and they identified high activity exhibited $CoFe_2O_4$-Graphene nanocomposite than $CoFe_2O_4$ nanoparticles. The composite's activation energy was 15.8 kJ/mol, and environmental friendliness is another remarkable characteristic of the $CoFe_2O_4$-Graphene composite.

Kodasma and colleagues had investigated the catalytic activities of the copper ferrite-graphene oxide composite under UV light irradiation for Reactive Black 5 degradation [45]. They used $CuFe_2O_4$ because of its superior photochemical stability, high magnetic properties, light responsiveness, and low cost. After loading the catalyst, decolourisation and TOC removal efficiencies were reached 98.2% and 82.8%, respectively, within two hours.

3.3 Solar Cells and Photoelectrochemical Cells Applications

Fossil fuels still overcome present energy requirements. But, estimated data mentioned that fossil fuels could fill this energy requirement for almost the next century. Due to the increment of energy requirements in the future, fossil fuel will not be able to supply demands. Thus, there will be a global energy crisis in the future if the present world will not be succeeded in presenting appropriate substitutes to fulfil the energy requirements. Thus, the tendency of renewable energy requirement is increased. There are many renewable energy-based resources such as sunlight, wind, tides, waves, and geothermal heat, but these resources could only supply 19.3% of global energy consumptions. 8.9% is supplied through traditional biomass, 4.2% from heat energy such as geothermal, modern biogas, and solar heat, 3.9% from hydropower plant, and the remaining 2.2% from other renewable energy resources such as solar, wind, Ocean, and tidal wave, and other forms of biomass [46].

Pang and coworkers had developed solar cell using $CoFe_2O_4$/graphene composite [47]. They had developed this composite as a counter electrode of the dye-sensitised solar cell (Fig. 5a). They reported the ability to amplify electron transport rate and capture injected electrons as key characteristics of graphene and $CoFe_2O_4$ had identified as recyclable nanocatalysts, anode active materials, photocatalysts for the degradation of organics, and air cathode catalysts. The particle size of $CoFe_2O_4$ was 3 nm.
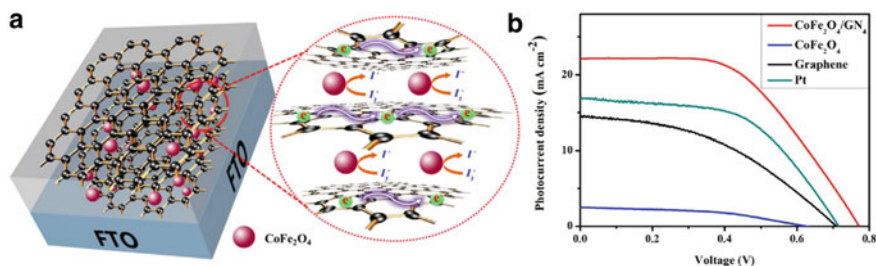
Fig. 5 a Schematic diagram of electrolyte regeneration reactions for the $CoFe_2O_4$/GN CE. **b** Current density–voltage (J–V) characteristic curves of DSSCs with different counter electrodes CEs (Pt, $CoFe_2O_4$, graphene, and $CoFe_2O_4$/GN composite) [47]

The synergistic effects of $CoFe_2O_4$/graphene have facilitated a large number of active reaction sites and low charge transfer resistance. The photoelectric conversion efficiency of $CoFe_2O_4$/GN was 9.04%. Highest current density–voltage (J–V) characteristic curve was obtained from DSSCs with $CoFe_2O_4$/GN counter electrodes CE (Fig. 5b).

Zheng and colleagues have developed $Bi_5FeTi_3O_{15}$ (BFTO) nanofibers and graphene (Gr) based nanocomposite for dye-sensitised solar cells [48]. BFTO nanofibers were synthesised using a sol–gel based electrospinning method, and their diameter was 40–100 nm. Excellent thermal conductivity and superior charge mobility specific surface area are the reported characteristics of graphene. BFTO is more prominent due to its chemical stability, non-toxicity, and direct bandgap as 2.13 eV. The composite's synergetic effect provides high catalytic activity, large surface area, and low charge transfer resistance for the cell. The maximum power conversion efficiency was 9.56%.

3.4 Application in Energy Storage Devices

In recent years, energy storage devices are highly demanded due to the regular increment in energy needs day by day. Thus, batteries and supercapacitors based research are increased and have opened tremendous amounts of funds and facilities. Many research articles are based on graphene-based supercapacitors applications can be seen in various fields during the last decade. The properties of various nanomaterial-based graphene nanocomposites have been increased, and those gain high demand for graphene-based supercapacitors and batteries.
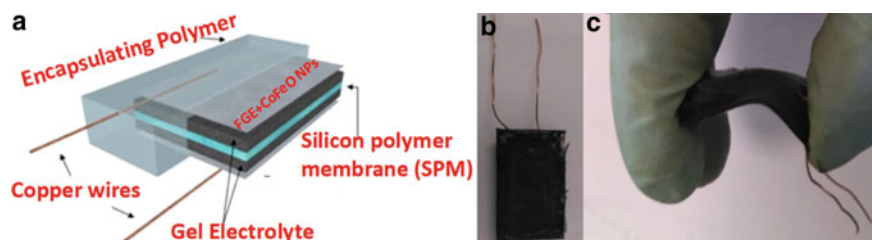
Fig. 6 **a** Schematic of a flexible supercapacitor, **b**, **c** flexible supercapacitor in the flat and bent state [50]

3.4.1 Supercapacitors

Supercapacitors, usually electrochemical-based capacitors, that provide high storage capacitance than conventional capacitors; usually several hundred times. Compared to batteries, capacitors have no chemical changes and possess unlimited cyclability.

Bashir and coworkers had fabricated copper substituted nickel ferrite NPs with graphene composite for electrodes of capacitors [30]. They decorated ferrite particles onto graphene sheets. The nanocomposite ($Ni_{0.9}Cu_{0.1}Fe_2O_4$/graphene) was synthesised using the ultra-sonication technique. Specific surface area, excellent chemical and mechanical properties, and super electron mobility are the highlighted properties of graphene. The composite was highly conductive and facilitated a relatively large surface area. The experiment results have shown nearly 85% of capacitance retention after 1000 cycles. The enhanced electrochemical capacitance was 735 F g^{-1} at 1.47 mA/g.

Wang et al. had synthesised $CoFe_2O_4$@graphene nanocomposites as a cathode material and Fe_3O_4@graphene nanocomposites as anode material for asymmetric supercapacitors [49]. The composites were synthesised via the facile hydrothermal method. The capacitor had shown high energy density, specific capacitance, and great cycling stability because of the synergetic effect. The asymmetric supercapacitor had performed 114.0 F g^{-1} specific capacitance, 45.5 Wh kg^{-1} energy density, and 91% capacitance retention after 5000 cycles.

Martnez-Vargas and colleagues had synthesised $CoFe_2O_4$ on flexible graphene electrodes for flexible solid-state supercapacitor applications (Fig. 6) [50]. The composite preparation was done through a thermal decomposition method. The specific capacitance of the supercapacitor was 337.1–835.7 F g^{-1} at 1.0 Ag^{-1} and the discharge time from 4957 to 21,969 s when the content of cobalt ferrite increases from 5 to 10 wt%.

3.4.2 Batteries

Li-ion batteries are now becoming more and better known in everyday life by popularizing mobile devices. Consequently, use of Li-ion batteries is highly requested.

Higher capacity and high magnification efficiency electrode materials are the key properties for lithium ion batteries of the next century. More and more researchers are concentrating on materials that are highly capable of providing high specific capacity and have sufficient resources for superior performance. Owing to their much higher capacity, metal oxides are promising candidates for energy storage. Significant progress is achieved through the use of nanoscale metal oxides, such as MnO_2 [51, 52], Co_3O_4 [53], Fe_2O_3 [54–56], in high-power anode materials. Nevertheless, transition metal ferrite, $NiFe_2O_4$ [57], owns an inverse spinel structure of $Fe^{3+}[Ni^{2+}, Fe^{3+}]O_4$ [58, 59], where Ni^{2+} and a half part of Fe^{3+} locate at octahedral sites, and the other Fe^{3+} occupy the tetrahedral sites. This structure helps the electron transport and could provide the required surface redox active sites for greater storage of lithium ions [58, 60].

Jiao et al. had developed $Ni_xCo_{1-x}Fe_2O_4$ and graphene-based composite for lithium-ion batteries [61]. They synthesised the composite through the hydrothermal co-precipitation method. The particle size was nearly 10 nm. Electrical conductivity, specific surface area, and super mechanical properties are the key characteristics of graphene. The composite leads to high capacity, rate performance, and cycling stability of the battery. The reversible capacity retention was 87%, and the battery's capacity was 1367.0 $mAhg^{-1}$ (Fig. 7).

Tong and coworkers had developed nickel ferrite nanocrystals wrapped by graphene (GNFO) composite for lithium-ion batteries [62]. According to their report, graphene may enhance the electric conductivity of pure transition metal oxides, volume changes, and drastic structural reorganisations under the electrochemical process. Hydrothermal process and facile solution mixing method had used to synthesised $NiFe_2O_4$ nanocrystals. The chemical reduction was used to coat the graphene on the $NiFe_2O_4$ nanocrystals. Specific capacity and excellent rate capability, and high capacity retention are the key characteristics of GNFO electrode. The reversible capacity was 937 mAh g^{-1} at 1 A g^{-1} after 250 cycles, and the specific capacity remains 312 mAh g^{-1} at 10.0 A g^{-1}.
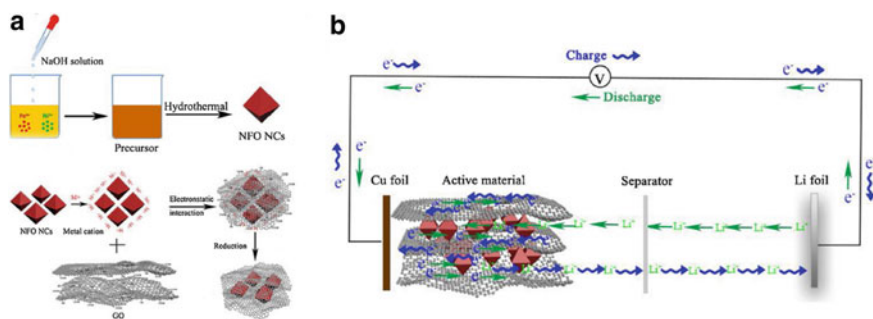
Fig. 7 **a** Schematic illustration of the typical synthetic process for the GNFO nanocomposites, **b** schematic of showing the working principle of GNFO electrode for lithium ion battery [62]

Table 1 Properties of graphene/ferrite nanocomposites in different applications

Application	Properties and examples	References
Biomedical applications (Biosensors, drug delivery, bioimaging)	Excellent ability to immobilise biomolecules Retain the biocatalytic activities Ease of preparations Good biocompatibility Large surface-area-to-volume ratio Offer high sensitivity though fast electron transfer	[40, 64–71]
Energy storage, production and conversion	Increase the current by fast Electron transferring Biocompatible Low toxicity Large surface area per volume Controllable particle size	[72–77]
Catalysis	Enhance electron-transfer kinetics Superior adsorption capability Facilitate high stability to the bioelectrode Facilitate appropriate platform for biomolecule immobilisation with proper directions High surface-to-volume ratio	[78–83]
Solar cells and photovoltaic devices	Excellent film-forming ability and solubility Biodegradability Non-toxicity Metal like electrical conductivity	[47, 84–86]

Yang et al. had developed $CoFe_2O_4$/graphene ($CoFe_2O_4$/G) nanocomposite for lithium-ion batteries (LIBs) [63]. The composite was synthesised through a facile one-pot strategy. The edge length of the $CoFe_2O_4$ was nearly 5–15 nm. High conductivity, large surface area, excellent thermal and chemical stability, and superior mechanical flexibility are the highlighted properties of $CoFe_2O_4$. The rate capability of the $CoFe_2O_4$/G electrode was 420 mAh g^{-1} at 5 A g^{-1}, and the cycling performance was 1109 mAhg^{-1} after 100 cycles at 0.2 Ag^{-1} (Table 1).

4 Concluding Remarks

As discussed in this chapter, graphene/ferrite nanocomposites have displayed some appealing properties in various applications. These dynamic materials have been applied in many areas of research; from engineering, medical science, physics, chemistry and biology. Throughout this chapter, the synthesis and use of graphene/ferrite comosite nanostructures and their distinct improvement in various fields have been well explored. However, absolute control over the fabrication of graphene/ferrite

nanocomposites remains a difficulty. Some of the main issues that require the attention of researchers involve, creating cost effective, more sustainable ways of manufacturing these composites and enabling a greater degree of control over the fabrication of the size and shape of the nanocomposite. The main properties of composites are crystalline structure, optoelectronic properties, magnetic properties, electrical conductivity, ability to modify their chemical composition, versatility for creating heterojunction and doped systems. Because of these properties, graphene/ferrite composites can be used for the future application of biomedical devices as biosensors, bioimaging, gas sensors; electronic devices such as memory devices, semiconductor devices; magnetic recording; energy devices such as solar cells, electrocatalytic and photocatalytic based chemical storages; and many other fields.

References

1. Zahid M, Nadeem N, Hanif MA, Bhatti IA, Bhatti HN, Mustafa G (2019) Metal ferrites and their graphene-based nanocomposites: synthesis, characterization, and applications in wastewater treatment
2. Kaur J, Kaur M (2019) Facile fabrication of ternary nanocomposite of MgFe 2 O 4 [sbnd]TiO 2 @GO for synergistic adsorption and photocatalytic degradation studies. Ceram Int 45(7):8646–8659. https://doi.org/10.1016/j.ceramint.2019.01.185
3. Biard PF et al (2016) Efficient catalytic ozonation by ruthenium nanoparticles supported on SiO2 or TiO2: towards the use of a non-woven fiber paper as original support. Chem Eng J 289:374–381. https://doi.org/10.1016/j.cej.2015.12.051
4. Dhal JP, Sahoo SK, Mishra BG, Hota G (2017) MgFe2O4-Fe2O3 heterostructured nanomaterials: synthesis and photocatalytic study. Mater Lett 196:95–99. https://doi.org/10.1016/j.matlet.2017.02.118
5. Shakir I, Sarfraz M, Ali Z, Aboud MFA, Agboola PO (2016) Magnetically separable and recyclable graphene-MgFe2O4 nanocomposites for enhanced photocatalytic applications. J Alloys Compd 660:450–455. https://doi.org/10.1016/j.jallcom.2015.11.055
6. Verma M, Singh AP, Sambyal P, Singh BP, Dhawan SK, Choudhary V (2015) Barium ferrite decorated reduced graphene oxide nanocomposite for effective electromagnetic interference shielding. Phys Chem Chem Phys 17(3):1610–1618. https://doi.org/10.1039/c4cp04284k
7. Singh K et al (2013) Nanostructured graphene/Fe3O4 incorporated polyaniline as a high performance shield against electromagnetic pollution. Nanoscale 5(6):2411–2420. https://doi.org/10.1039/c3nr33962a
8. Sun X et al (2013) Laminated magnetic graphene with enhanced electromagnetic wave absorption properties. J Mater Chem C 1(4):765–777. https://doi.org/10.1039/c2tc00159d
9. Karthik P, Vinesh V, Anpo M, Neppolian B (2020) Reduced graphene oxide (rGO)–supported mixed metal oxide catalysts for photocatalytic reactions. Elsevier Inc.
10. Bhattacharyya R et al (2019) Graphene oxide-ferrite hybrid framework as enhanced broadband absorption in gigahertz frequencies. Sci Rep 9(1):1–12. https://doi.org/10.1038/s41598-019-48487-5
11. Gupta B, Melvin AA (2017) TiO2/RGO composites: its achievement and factors involved in hydrogen production. Renew Sustain Energy Rev 76:1384–1392. https://doi.org/10.1016/j.rser.2017.03.123
12. Harzali H et al (2016) Structural and magnetic properties of nano-sized NiCuZn ferrites synthesized by co-precipitation method with ultrasound irradiation. J Magn Magn Mater 419:50–56. https://doi.org/10.1016/j.jmmm.2016.05.084

13. Zubair A et al (2017) Structural, morphological and magnetic properties of Eu-doped CoFe2O4 nano-ferrites. Results Phys 7:3203–3208. https://doi.org/10.1016/j.rinp.2017.08.035

14. Kefeni KK, Msagati TAM, Mamba BB (2017) Ferrite nanoparticles: synthesis, characterisation and applications in electronic device. Mater Sci Eng B Solid-State Mater Adv Technol 215:37–55. https://doi.org/10.1016/j.mseb.2016.11.002

15. Danks AE, Hall SR, Schnepp Z (2016) The evolution of 'sol-gel' chemistry as a technique for materials synthesis. Mater Horizons 3(2):91–112. https://doi.org/10.1039/c5mh00260e

16. Peng K, Fu L, Yang H, Ouyang J (2015) Perovskite LaFeO3/montmorillonite nanocomposites: synthesis, interface characteristics and enhanced photocatalytic activity. Sci Rep 6:1–10. https://doi.org/10.1038/srep19723

17. Orge CA, Soares OSGP, Ramalho PSF, Pereira MFR, Faria JL (2019) Magnetic nanoparticles for photocatalytic ozonation of organic pollutants. Catalysts 9(9). https://doi.org/10.3390/catal9090703

18. Sonu et al (2019) Review on augmentation in photocatalytic activity of CoFe2O4 via heterojunction formation for photocatalysis of organic pollutants in water. J Saudi Chem Soc 23(8):1119–1136. https://doi.org/10.1016/j.jscs.2019.07.003

19. Amara D, Felner I, Nowik I, Margel S (2009) Synthesis and characterization of Fe and Fe3O4 nanoparticles by thermal decomposition of triiron dodecacarbonyl. Colloids Surf. Physicochem Eng Asp 339(1–3):106–110. https://doi.org/10.1016/j.colsurfa.2009.02.003

20. Fantechi E, Innocenti C, Albino M, Lottini E, Sangregorio C (2015) Influence of cobalt doping on the hyperthermic efficiency of magnetite nanoparticles. J Magn Magn Mater 380:365–371. https://doi.org/10.1016/j.jmmm.2014.10.082

21. Meidanchi A, Akhavan O, Khoei S, Shokri AA, Hajikarimi Z, Khansari N (2015) ZnFe2O4 nanoparticles as radiosensitizers in radiotherapy of human prostate cancer cells. Mater Sci Eng C 46:394–399. https://doi.org/10.1016/j.msec.2014.10.062

22. Nemati A, Shadpour S, Khalafbeygi H, Barkhi M (2014) Hydrothermal synthesis and size control of Fe3O4 Nanoparticles in the Presence of 2,2,′2″,2‴-(ethane-1,2-diylbis(azanetriyl))tetraacetohydrazide. Synth React Inorganic Met Nano-Metal Chem 44(8):1161–1165. https://doi.org/10.1080/15533174.2013.797443

23. Atacan K (2019) CuFe2O4/reduced graphene oxide nanocomposite decorated with gold nanoparticles as a new electrochemical sensor material for L-cysteine detection. J Alloys Compd 791:391–401. https://doi.org/10.1016/j.jallcom.2019.03.303

24. Yuanchun Q, Yanbao Z, Zhishen W (2008) Preparation of cobalt oxide nanoparticles and cobalt powders by solvothermal process and their characterization. Mater Chem Phys 110(2–3):457–462. https://doi.org/10.1016/j.matchemphys.2008.03.001

25. Ameer S, Gul IH, Mujahid M (2015) Ultra low permittivity/loss CoFe2O4 and CoFe2O4-rGO nanohybrids by novel 1-hexanol assisted solvothermal process. J Alloys Compd 642:78–82. https://doi.org/10.1016/j.jallcom.2015.04.101

26. Hu L, Percheron A, Chaumont D, Brachais CH (2011) Microwave-assisted one-step hydrothermal synthesis of pure iron oxide nanoparticles: magnetite, maghemite and hematite. J Sol-Gel Sci Technol 60(2):198–205. https://doi.org/10.1007/s10971-011-2579-4

27. Konicki W, Sibera D, Mijowska E, Lendzion-Bieluń Z, Narkiewicz U (2013) Equilibrium and kinetic studies on acid dye Acid Red 88 adsorption by magnetic ZnFe2O4 spinel ferrite nanoparticles. J Colloid Interface Sci 398:152–160. https://doi.org/10.1016/j.jcis.2013.02.021

28. Marinca TF, Chicinaş I, Isnard O (2013) Structural and magnetic properties of the copper ferrite obtained by reactive milling and heat treatment. Ceram Int 39(4):4179–4186. https://doi.org/10.1016/j.ceramint.2012.10.274

29. Zhang Z, Yao G, Zhang X, Ma J, Lin H (2015) Synthesis and characterization of nickel ferrite nanoparticles via planetary ball milling assisted solid-state reaction. Ceram Int 41(3):4523–4530. https://doi.org/10.1016/j.ceramint.2014.11.147

30. Bashir B et al (2019) Copper substituted nickel ferrite nanoparticles anchored onto the graphene sheets as electrode materials for supercapacitors fabrication. Ceram Int 45(6):6759–6766. https://doi.org/10.1016/j.ceramint.2018.12.167

31. Rajapaksha RDAA, Hashim U, Afnan Uda MN, Fernando CAN, De Silva SNT (2017) Target ssDNA detection of E. coli O157: H7 through electrical based DNA biosensor. Microsyst Technol 23(12):5771–5780. https://doi.org/10.1007/s00542-017-3498-2

32. Rajapaksha RDAA, Hashim U, Gopinath SCB, Fernando CAN (2018) Sensitive pH detection on gold interdigitated electrodes as an electrochemical sensor. Microsyst Technol 24(4):1965–1974. https://doi.org/10.1007/s00542-017-3592-5

33. Parmin NA et al (2019) Voltammetric determination of human papillomavirus 16 DNA by using interdigitated electrodes modified with titanium dioxide nanoparticles. Microchim Acta 2:2–10

34. Letchumanan I, Md Arshad MK, Gopinath SCB, Rajapaksha RDAA, Balakrishnan SR (2020) Comparative analysis on dielectric gold and aluminium triangular junctions: impact of ionic strength and background electrolyte by pH variations. Sci Rep 10(1):6783. https://doi.org/10.1038/s41598-020-63831-w

35. Wang L et al (2019) Photovoltaic and antimicrobial potentials of electrodeposited copper nanoparticle. Biochem Eng J 97–104. https://doi.org/10.1016/j.bej.2018.10.009

36. Natasha NZ, Rajapaksha RDAA, Uda MNA, Hashim U (2017) Electrical DNA biosensor using aluminium interdigitated electrode for E. coli O157:H7 detection. AIP Conf Proc 020235:020235. https://doi.org/10.1063/1.5002429

37. Yahaya NAN, Rajapaksha RDAA, Uda MNA, Hashim U (2017) Ultra-low current biosensor output detection using portable electronic reader. AIP Conf Proc 1885. https://doi.org/10.1063/1.5002430

38. Rajapaksha RDAA, Hashim U, Natasha NZ, Uda MNA, Thivina V, Fernando CAN (2017) Gold nano-particle based Al interdigitated electrode electrical biosensor for specific ssDNA target detection. IEEE Reg Symp Micro Nanoelectron 191–194

39. Rajapaksha RDAA, Hashim U, Uda MNA, Fernando CAN (2018) High-performance electrical variable resistor sensor for E. coli. J Telecommun Electron Comput Eng 10(1):61–64

40. Sadat Vajedi F, Dehghani H (2020) A high-sensitive electrochemical DNA biosensor based on a novel ZnAl/layered double hydroxide modified cobalt ferrite-graphene oxide nanocomposite electrophoretically deposited onto FTO substrate for electroanalytical studies of etoposide. Talanta 208:120444. https://doi.org/10.1016/j.talanta.2019.120444

41. Afkhami A, Bahiraei A, Madrakian T (2017) Application of nickel zinc ferrite/graphene nanocomposite as a modifier for fabrication of a sensitive electrochemical sensor for determination of omeprazole in real samples. J Colloid Interface Sci 495:1–8. https://doi.org/10.1016/j.jcis.2017.01.116

42. Ravindran Madhura T, Viswanathan P, Gnana kumar G, Ramaraj, R (2017) Nanosheet-like manganese ferrite grown on reduced graphene oxide for non-enzymatic electrochemical sensing of hydrogen peroxide. J Electroanal Chem 792:15–22. https://doi.org/10.1016/10.1016/j.jelechem.2017.03.014

43. Zhang H, Gao S, Shang N, Wang C, Wang Z (2014) Copper ferrite-graphene hybrid: a highly efficient magnetic catalyst for chemoselective reduction of nitroarenes. RSC Adv 4(59):31328–31332. https://doi.org/10.1039/c4ra05059b

44. Yao Y, Yang Z, Zhang D, Peng W, Sun H, Wang S (2012) Magnetic CoFe2O4−graphene hybrids.pdf

45. Kodasma R, Palas B, Ersöz G, Atalay S (2020) Photocatalytic activity of copper ferrite graphene oxide particles for an efficient catalytic degradation of Reactive Black 5 in water. Ceram Int 46(5):6284–6292. https://doi.org/10.1016/j.ceramint.2019.11.100

46. Fernando CAN, Liyanaarachchi US, Rajapaksha RDAA (2013) Explanation of the photocurrent quantum efficiency (Φ) enhancements through the CAN's model equation for the p-CuI sensitized methylviolet-C 18 LB films in the photoelectrochemical cells (PECs) and Cu/n-Cu 2 O/M-C 18 /p-CuI solid-state photovoltaic cells. Semicond Sci Technol 28(4):045017. https://doi.org/10.1088/0268-1242/28/4/045017

47. Pang B et al (2019) Synthesis of CoFe2O4/graphene composite as a novel counter electrode for high performance dye-sensitized solar cells. Electrochim Acta 297:70–76. https://doi.org/10.1016/j.electacta.2018.11.170

48. Zheng HW et al (2017) Bi5FeTi3O15 nanofibers/graphene nanocomposites as an effective counter electrode for dye-sensitized solar cells. Nanoscale Res Lett 12(1). https://doi.org/10.1186/s11671-016-1799-5

49. Wang H, Song Y, Ye X, Wang H, Liu W, Yan L (2018) Asymmetric supercapacitors assembled by dual spinel ferrites@graphene nanocomposites as electrodes, vol 1, no 7

50. Martinez-Vargas S, Mtz-Enriquez AI, Flores-Zuñiga H, Encinas A, Oliva J (2020) Enhancing the capacitance and tailoring the discharge times of flexible graphene supercapacitors with cobalt ferrite nanoparticles. Synth Met 264:116384. https://doi.org/10.1016/j.synthmet.2020.116384

51. Ning P et al (2016) Facile synthesis of carbon nanofibers/MnO2 nanosheets as high-performance electrodes for asymmetric supercapacitors. Electrochim Acta. https://doi.org/10.1016/j.electacta.2016.05.214

52. Li L, Raji AO, Tour JM (2013) Graphene-wrapped MnO2–graphene nanoribbons as anode materials for high-performance lithium ion batteries, pp 1–5. https://doi.org/10.1002/adma.201302915

53. Xiong S, Chen JS, Lou XW, Zeng HC (2012) Mesoporous Co3O4 and CoO @ C topotactically transformed their lithium-storage properties, vol 5, pp 861–871. https://doi.org/10.1002/adfm.201102192

54. Reddy BMV et al (2007) a-Fe2O3 nanoflakes as an anode material for Li-ion batteries, pp 2792–2799. https://doi.org/10.1002/adfm.200601186

55. Zhu X, Zhu Y, Murali S, Stoller MD, Ruoff RS (2011) Nanostructured reduced graphene oxide/Fe2O3 composite as a high-performance anode material for lithium ion batteries, no 4, pp 3333–3338

56. Wu C, Yin P, Zhu X, Ouyang C, Xie Y (2006) Synthesis of hematite (r-Fe2O3) nanorods: diameter-size and shape effects on their applications in magnetism. Lithium Ion Battery Gas Sens 17806–17812. https://doi.org/10.1021/jp0633906

57. Wang N, Xu H, Chen L, Gu X, Yang J, Qian Y (2014) A general approach for MFe2O4 (M¼ZnCo, Ni) nanorods and their high performance as anode materials for lithium ion batteries. J Power Sources 247:163–169. https://doi.org/10.1016/j.jpowsour.2013.08.109

58. Han C, Mian Li LG, Xiong Y, Liu X, Bo X, Zhang Y (2015) Facile synthesis of electrospun MFe2O4 (M = Co, Ni, Cu, Mn) spinel nanofibers with excellent electrocatalytic properties for oxygen evolution and hydrogen peroxide reduction. Nanoscale 7:8920–8930. https://doi.org/10.1039/C4NR07243J

59. Zhu H, Zhang S, Huang Y, Wu L, Sun S (2013) Monodisperse M 4:3–7

60. Jianan Wang WY, Yang G, Wang L (2016) Synthesis of one-dimensional NiFe2O4 nanostructures: tunable morphology and high-performance anode materials for Li ion batteries. Mater Chem A 4:8620–8629. https://doi.org/10.1039/C6TA02655A

61. Jiao X, Cai L, Xia X, Lei W, Hao Q, Mandler D (2019) Novel spinel nanocomposites of Ni x Co 1–x Fe 2 O 4 nanoparticles with N-doped graphene for lithium ion batteries. Appl Surf Sci 481(February):200–208. https://doi.org/10.1016/j.apsusc.2019.03.063

62. Tong X et al (2017) High-index faceted nickel ferrite nanocrystals encapsulated by graphene with high performance for lithium-ion batteries. Electrochim Acta 257:99–108. https://doi.org/10.1016/j.electacta.2017.10.040

63. Yang Z, Huang Y, Hu J, Xiong L, Luo H, Wan Y (2018) Nanocubic CoFe2O4/graphene composite for superior lithium-ion battery anodes. Synth Met 242(May):92–98. https://doi.org/10.1016/j.synthmet.2018.05.010

64. Mousavi SM et al (2020) Development of graphene based nanocomposites towards medical and biological applications. Artif Cells Nanomed Biotechnol 48(1):1189–1205. https://doi.org/10.1080/21691401.2020.1817052

65. Peng E et al (2012) Synthesis of manganese ferrite/graphene oxide nanocomposites for biomedical applications. Small 8(23):3620–3630. https://doi.org/10.1002/smll.201201427

66. Kefeni KK, Msagati TAM, Nkambule TT, Mamba BB (2020) Spinel ferrite nanoparticles and nanocomposites for biomedical applications and their toxicity. Mater Sci Eng C 107:110314. https://doi.org/10.1016/j.msec.2019.110314

67. Wang G, Ma Y, Wei Z, Qi M (2016) Development of multifunctional cobalt ferrite/graphene oxide nanocomposites for magnetic resonance imaging and controlled drug delivery. Chem Eng J 289:150–160. https://doi.org/10.1016/j.cej.2015.12.072

68. Le AT et al (2016) Enhanced magnetic anisotropy and heating efficiency in multi-functional manganese ferrite/graphene oxide nanostructures. Nanotechnology 27(15). https://doi.org/10.1088/0957-4484/27/15/155707

69. Pourjavadi A, Mazaheri Tehrani Z, Jokar S (2015) Chitosan based supramolecular polypseudorotaxane as a pH-responsive polymer and their hybridization with mesoporous silica-coated magnetic graphene oxide for triggered anticancer drug delivery. Polymer (Guildf) 76:52–61. https://doi.org/10.1016/j.polymer.2015.08.050

70. Yang Y et al (2016) Graphene oxide/manganese ferrite nanohybrids for magnetic resonance imaging, photothermal therapy and drug delivery. J Biomater Appl 30(6):810–822. https://doi.org/10.1177/0885328215601926

71. Van Tran T, Nguyen DTC, Le HTN, Vo DVN, Nanda S, Nguyen TD (2020) Optimization, equilibrium, adsorption behavior and role of surface functional groups on graphene oxide-based nanocomposite towards diclofenac drug. J Environ Sci (China) 93(February):137–150. https://doi.org/10.1016/j.jes.2020.02.007

72. Mahmood N, Zhang C, Yin H, Hou Y (2014) Graphene-based nanocomposites for energy storage and conversion in lithium batteries, supercapacitors and fuel cells. J Mater Chem A 2(1):15–32. https://doi.org/10.1039/c3ta13033a

73. Li Z, Xiang Y, Lu S, Dong B, Ding S, Gao G (2018) Hierarchical hybrid ZnFe2O4 nanoparticles/reduced graphene oxide composite with long-term and high-rate performance for lithium ion batteries. J Alloys Compd 737:58–66. https://doi.org/10.1016/j.jallcom.2017.11.336

74. Su J, Cao M, Ren L, Hu C (2011) Fe3O4-graphene nanocomposites with improved lithium storage and magnetism properties. J Phys Chem C 115(30):14469–14477. https://doi.org/10.1021/jp201666s

75. Soam A et al (2019) Synthesis of nickel ferrite nanoparticles supported on graphene nanosheets as composite electrodes for high performance supercapacitor. Chem Select 4(34):9952–9958. https://doi.org/10.1002/slct.201901117

76. Xiong P, Huang H, Wang X (2014) Design and synthesis of ternary cobalt ferrite/graphene/polyaniline hierarchical nanocomposites for high-performance supercapacitors this work is dedicated to Professor MIN Enze on the occasion of his 90th birthday. J Power Sources 245:937–946. https://doi.org/10.1016/j.jpowsour.2013.07.064

77. Mousa MA, Khairy M, Shehab M (2017) Nanostructured ferrite/graphene/polyaniline using for supercapacitor to enhance the capacitive behavior. J Solid State Electrochem 21(4):995–1005. https://doi.org/10.1007/s10008-016-3446-6

78. Doustkhah E, Rostamnia S (2016) Covalently bonded sulfonic acid magnetic graphene oxide: Fe3O4@GO-Pr-SO3H as a powerful hybrid catalyst for synthesis of indazolophthalazinetriones. J Colloid Interface Sci 478:280–287. https://doi.org/10.1016/j.jcis.2016.06.020

79. Wu ZS, Yang S, Sun Y, Parvez K, Feng X, Müllen K (2012) 3D nitrogen-doped graphene aerogel-supported Fe3O4 nanoparticles as efficient electrocatalysts for the oxygen reduction reaction. J Am Chem Soc 134(22):9082–9085. https://doi.org/10.1021/ja3030565

80. Kumar A, Rout L, Achary LSK, Dhaka RS, Dash P (2017) Greener route for synthesis of aryl and alkyl-14H-dibenzo [a.j] xanthenes using graphene oxide-copper ferrite nanocomposite as a recyclable heterogeneous catalyst. Sci Rep 7. https://doi.org/10.1038/srep42975

81. Iftikhar A et al (2020) Erbium-substituted Ni0.4Co0.6Fe2O4 ferrite nanoparticles and their hybrids with reduced graphene oxide as magnetically separable powder photocatalyst. Ceram Int 46(1):1203–1210. https://doi.org/10.1016/j.ceramint.2019.08.176

82. Guo S, Zhang G, Guo Y, Yu JC (2013) Graphene oxide-Fe2O3 hybrid material as highly efficient heterogeneous catalyst for degradation of organic contaminants. Carbon NY 60:437–444. https://doi.org/10.1016/j.carbon.2013.04.058

83. Fatima S, Ali SI, Iqbal MZ (2020) Congo red dye degradation by graphene nanoplatelets/doped bismuth ferrite nanoparticle. Catalysts 10(4):367. https://doi.org/10.3390/catal10040367

84. El-Shafai NM et al (2020) Magnetite nano-spherical quantum dots decorated graphene oxide nano sheet (GO@Fe3O4): electrochemical properties and applications for removal heavy metals, pesticide and solar cell. Appl Surf Sci 506:144896. https://doi.org/10.1016/j.apsusc.2019.144896

85. Harnchana V, Chaiyachad S, Pimanpang S, Saiyasombat C, Srepusharawoot P, Amornkitbamrung V (2019) Hierarchical Fe3O4-reduced graphene oxide nanocomposite grown on NaCl crystals for triiodide reduction in dye-sensitized solar cells. Sci Rep 9(1):1–13. https://doi.org/10.1038/s41598-018-38050-z

86. El-Shafai NM et al (2020) Electrochemical property, antioxidant activities, water treatment and solar cell applications of titanium dioxide–zinc oxide hybrid nanocomposite based on graphene oxide nanosheet. Mater Sci Eng B Solid-State Mater Adv Technol 259: 114596. https://doi.org/10.1016/j.mseb.2020.114596